

METHODOLOGY FOR SEISMIC VULNERABILITY ASSESSMENT OF EXISTING MASONRY BUILDINGS IN URBAN CENTRES. APPLICATION TO THE *EIXAMPLE* DISTRICT IN BARCELONA

Doctoral Thesis by:
Sara Dimovska

Supervised by:
Pere Roca Fabregat
Luca Pelà

Doctoral programme in
Construction Engineering

Barcelona, March 2023



UNIVERSITAT POLITÈCNICA DE CATALUNYA
BARCELONATECH

Escola Tècnica Superior d'Enginyeria
de Camins, Canals i Ports de Barcelona





UNIVERSITAT POLITÈCNICA
DE CATALUNYA
BARCELONATECH

Methodology for seismic vulnerability assessment of existing masonry buildings in urban centres.

Application to the Eixample district in Barcelona

by

Sara Dimovska

ADVERTIMENT La consulta d'aquesta tesi queda condicionada a l'acceptació de les següents condicions d'ús: La difusió d'aquesta tesi per mitjà del repositori institucional UPCommons (<http://upcommons.upc.edu/tesis>) i el repositori cooperatiu TDX (<http://www.tdx.cat/>) ha estat autoritzada pels titulars dels drets de propietat intel·lectual **únicament per a usos privats** emmarcats en activitats d'investigació i docència. No s'autoritza la seva reproducció amb finalitats de lucre ni la seva difusió i posada a disposició des d'un lloc aliè al servei UPCommons o TDX. No s'autoritza la presentació del seu contingut en una finestra o marc aliè a UPCommons (*framing*). Aquesta reserva de drets afecta tant al resum de presentació de la tesi com als seus continguts. En la utilització o cita de parts de la tesi és obligat indicar el nom de la persona autora.

ADVERTENCIA La consulta de esta tesis queda condicionada a la aceptación de las siguientes condiciones de uso: La difusión de esta tesis por medio del repositorio institucional UPCommons (<http://upcommons.upc.edu/tesis>) y el repositorio cooperativo TDR (<http://www.tdx.cat/?locale-attribute=es>) ha sido autorizada por los titulares de los derechos de propiedad intelectual **únicamente para usos privados enmarcados** en actividades de investigación y docencia. No se autoriza su reproducción con finalidades de lucro ni su difusión y puesta a disposición desde un sitio ajeno al servicio UPCommons No se autoriza la presentación de su contenido en una ventana o marco ajeno a UPCommons (*framing*). Esta reserva de derechos afecta tanto al resumen de presentación de la tesis como a sus contenidos. En la utilización o cita de partes de la tesis es obligado indicar el nombre de la persona autora.

WARNING On having consulted this thesis you're accepting the following use conditions: Spreading this thesis by the institutional repository UPCommons (<http://upcommons.upc.edu/tesis>) and the cooperative repository TDX (<http://www.tdx.cat/?locale-attribute=en>) has been authorized by the titular of the intellectual property rights **only for private uses** placed in investigation and teaching activities. Reproduction with lucrative aims is not authorized neither its spreading nor availability from a site foreign to the UPCommons service. Introducing its content in a window or frame foreign to the UPCommons service is not authorized (*framing*). These rights affect to the presentation summary of the thesis as well as to its contents. In the using or citation of parts of the thesis it's obliged to indicate the name of the author.

*Methodology for seismic vulnerability assessment of
existing masonry buildings in urban centres.
Application to the Eixample district in Barcelona.*

Doctoral Thesis submitted in fulfilment of the requirements for the
Degree of Doctor of Philosophy in Construction Engineering

by

SARA DIMOVSKA

Thesis Supervisors:

Prof. Pere Roca Fabregat

Prof. Luca Pelà

Barcelona, March 2023



Universitat Politècnica de Catalunya

Departament d'Enginyeria Civil i Ambiental

Programa de Doctorat en Enginyeria de la Construcció

ACKNOWLEDGEMENTS

This thesis would have not been possible without the predoctoral grant provided by the AGAUR agency (*Agència de Gestió d'Ajuts Universitaris i de Recerca*) of the Generalitat de Catalunya and the financial support from the Ministry of Science, Innovation and Universities of the Spanish Government (MCIU), the State Agency of Research (AEI), as well as that of the ERDF (European Regional Development Fund) through the project SEVERUS (Multilevel evaluation of seismic vulnerability and risk mitigation of masonry buildings in resilient historical urban centres, ref. num. RTI2018-099589-B-I00).

I would like to gratefully acknowledge my supervisors Prof. Pere Roca and Prof. Luca Pelà for giving me this opportunity and accepting me as part of the research group. I am thankful for their continuous support, help and encouragement, for the very long and fruitful meetings, for the thorough revision of all my work and for sharing with me their profound knowledge and enthusiasm during all these years.

I would like to express my deep gratitude to Dr. Savvas Saloustros for supervising and being part of this research work, by giving invaluable guidance and very positive contributions. You have shared your great knowledge with me and helped me overcome many obstacles, as always with patience, humour, and encouragement.

I thank profusely Prof. Còssima Cornadó for sharing her research work, with all the extensive data collection and also her profound knowledge regarding the existing *Eixample* buildings.

I would also like to thank the master students, who I had the privilege of supervising or only helping and advising. Many of you have implemented, adapted and modified some of the numerical models, which are part of this research study. I learned a lot thanks to you and I would like to acknowledge that you were a great part of this research work.

A profound thank you goes to all my colleagues in the research group at UPC that welcomed me with open arms and shared this journey with me. Some of you I have met after starting this experience, having the chance to give back gladly the help that I received, and feeling especially grateful for all the love and support I obtained in return. You ended up being more than colleagues who work on similar research topics or friends that share many interests and become my second family in Barcelona. Thank you for bringing me so much happiness, love, and hope. I am very grateful for all the adventures and memories that we have shared together and I can only hope that our friendship and connection will continue growing. Even though now most of us are in different parts of the world, you have helped me enormously in many different ways. I would also like to sincerely thank all my friends that have been encouraging me through this very long journey. For those I met in Barcelona these past years, you have become a great part of my life.

I owe my deepest gratitude to my family, for their endless love, support, encouragement and keen interest in my academic achievements. Finally, I would like to dedicate this thesis to my mum, who is my role model in life and has always encouraged and helped me achieve all my dreams. All of this would have not been possible without you.

ABSTRACT

Unreinforced masonry buildings (URM), which prevail in many historic and urban centres, can be considered to be significantly vulnerable to seismic actions due to their peculiar constructive and structural features that could influence their seismic performance, even in low to moderate seismic hazard areas. These existing structures were usually designed considering only gravity loads without any seismic design requirements. Hence, they may endure severe consequences in the event of an earthquake due to the presence of many specific sources of structural vulnerability, such as the material's limited resistant capacity and ductility, the buildings' height, very slender load-bearing walls, semi-flexible horizontal diaphragms, irregular plan configurations, presence of vertical extensions, large façade openings, among other structural features.

The scientific literature currently offers a variety of methods for assessing seismic vulnerability of existing buildings on a large scale, as it is considered a challenging task. The selection of the appropriate approach is determined by several factors, including the purpose and nature of the study, the amount of data and resources available, the investigated building typologies, the level of analysis effort, and the cost required for the studies.

The aim of this research is to contribute to the seismic vulnerability assessment of existing masonry buildings of the *Eixample* district of Barcelona, though the derivation of a general methodology, intensively based on numerical simulation due to lack of seismic damage observations from past earthquakes. This approach could be applied to similar problems involving the vulnerability assessment of historic urban centres in low to moderate seismic regions, by applying the necessary modifications. The first step of the proposed methodology is elaborating a detailed building taxonomy of the masonry buildings of the *Eixample* district according to their structural, material and geometrical characteristics, relevant to their seismic behaviour and possible sources of vulnerability. The most representative building typologies are selected based on the aforementioned building taxonomy, by using available statistical data of structural features of the analysed building stock. The next step is developing sophisticated numerical models of the previously identified representative masonry buildings, by using an efficient and realistic simulation of their seismic response based on the Finite Element Method (FEM). Non-linear static (pushover) analysis are performed for both main directions (parallel and perpendicular to the façade) in order to better understand their global seismic behaviour in terms of capacity and failure mechanisms. Moreover, parametric analyses are carried out to investigate the influence of different structural parameters on the building's seismic performance. The N2 method is applied for the evaluation of the buildings' seismic performance for the seismic hazard scenarios in Barcelona. The final step is the proposal of new forms of the Vulnerability Index Method (VIM) for both main directions, by defining the classes and calibrating the weights of the specific vulnerability parameters. The methodology is applied eventually to the *Eixample* district of Barcelona's urban centre, by including two cases: a large number of existing masonry buildings and a typical urban block.

Keywords: Seismic Vulnerability, Masonry, Existing Buildings, Building Taxonomy, Finite Element Model, Pushover Analysis, N2 method, Vulnerability Index Method.

RESUMEN

Los edificios de obra de fábrica no armada (URM), abundantes en muchos centros urbanos históricos, resultan frecuentemente vulnerables ante las acciones sísmicas, incluso en zonas de baja o moderada peligrosidad sísmica, debido a sus características constructivas y estructurales. Por lo general, estas estructuras fueron diseñadas teniendo en cuenta únicamente las cargas gravitatorias y sin verificar su comportamiento sísmico. Ante un terremoto, dichas estructuras pueden sufrir graves consecuencias debido a varias fuentes específicas de vulnerabilidad estructural, entre las que cabe citar la limitada capacidad resistente y limitada ductilidad del material, la altura de los edificios, la presencia de muros de carga muy esbeltos, el carácter flexibles o semiflexible de los forjados en su plano, las configuraciones de planta, frecuentemente irregulares, la presencia de extensiones verticales (remontas) y la frecuente presencia de grandes aberturas de fachada, entre otras.

Como consecuencia del desafío que supone la evaluación de la vulnerabilidad sísmica de los edificios existentes a gran escala (es decir, a escala urbana o considerando múltiples edificios), en la literatura científica actual se han propuesto una gran variedad de métodos orientados hacia su caracterización. La selección del método más adecuado viene determinada por varios factores, entre los cuales se hallan el propósito y la naturaleza del estudio, la cantidad de datos y de recursos disponibles, las tipologías de los edificios investigados, el esfuerzo computacional requerido para el análisis y el coste de la investigación.

El objetivo del presente trabajo reside en contribuir a la evaluación de la vulnerabilidad sísmica de los edificios de obra de fábrica existentes en el distrito del *Eixample* de Barcelona. Ello se lleva a cabo mediante la elaboración de una metodología general basada principalmente en la simulación numérica debido a la ausencia de observaciones, en el caso investigado, relativas a daños sísmicos producidos terremotos ocurridos en el pasado. Esta metodología podría aplicarse, con las modificaciones necesarias, a casos similares relativos a la evaluación de la vulnerabilidad de centros urbanos históricos en regiones de sismicidad baja a moderada. El primer paso de la metodología propuesta consiste en elaborar una taxonomía detallada de los edificios de obra de fábrica del distrito del *Eixample* en función de las características estructurales, materiales y geométricas que resultan relevantes para la caracterización de comportamiento sísmico. Los tipos de edificios más representativos se han seleccionado en base a dicha taxonomía, utilizando para ello datos estadísticos disponibles sobre sus características estructurales. El siguiente paso ha consistido en desarrollar modelos numéricos avanzados de los edificios seleccionados. Para este fin se ha utilizado el Método de los Elementos Finitos (MEF) debido a que posibilita una simulación eficiente y realista de la respuesta sísmica. Se han realizado análisis estáticos no lineales (*pushover*) para las dos direcciones principales (paralela y perpendicular a la fachada) de los edificios con el fin de caracterizar con suficiente precisión su comportamiento sísmico global en términos de capacidad y mecanismos de fallo. Además, se han realizado análisis paramétricos con la finalidad de investigar la influencia de diferentes parámetros estructurales en el comportamiento sísmico. Se ha aplicado el método N2 para la evaluación del comportamiento sísmico de los edificios para distintos escenarios de peligrosidad sísmica en Barcelona. Finalmente, se han propuesto unos formularios modificados para la aplicación del Método del Índice de Vulnerabilidad (VIM) según las dos direcciones principales, de los edificios. Ello ha

comportado una definición de las clases de vulnerabilidad y la calibración de los pesos de los parámetros específicos de vulnerabilidad. La metodología se aplica finalmente al distrito del *Eixample* del centro urbano de Barcelona. Los métodos desarrollados han sido aplicados a dos casos particulares, consistentes en (1) un conjunto amplio de edificios de obra de fábrica existentes y (2) el caso específico de un bloque de edificios típico del entorno urbano investigado.

Palabras claves: Vulnerabilidad Sísmica, Obra de Fábrica, Edificios Existentes, Taxonomía de Edificios, Modelo de Elementos Finitos, Análisis *Pushover*, Método N2, Método del Índice de la Vulnerabilidad.

CONTENTS

ACKNOWLEDGEMENTS	I
ABSTRACT	II
RESUMEN	III
CONTENTS.....	V
LIST OF FIGURES	IX
LIST OF TABLES.....	XXV
LIST OF SYMBOLS	XXIX
LIST OF ACRONYMS	XXXII
Chapter 1. INTRODUCTION	1
1.1. Background and motivation	1
1.2. Scope and objectives	3
1.2.1. General objective	3
1.2.2. Specific objectives.....	4
1.3. Outline and organisation of the thesis.....	5
1.4. Research dissemination.....	7
Chapter 2. LITERATURE REVIEW	8
2.1. Introduction.....	8
2.2. Seismic risk analysis.....	8
2.3. Seismic vulnerability assessment	11
2.3.1. Seismic vulnerability methods	11
2.3.2. Vulnerability assessment at urban scale	21
2.4. Masonry mechanics and modelling techniques.....	24
2.4.1. Masonry main mechanical features	24
2.4.2. Numerical modelling approaches for masonry buildings	27
2.5. Seismic analysis methods for masonry buildings	31
2.5.1. Non-linear static (pushover) analysis.....	31
2.5.2. Non-linear dynamic analysis	32
2.6. Building taxonomies for seismic assessment of urban centres.....	33
2.7. Summary	41
Chapter 3. CASE STUDY – THE <i>EIXAMPLE</i> DISTRICT OF BARCELONA	42

3.1.	Introduction.....	42
3.2.	The city of Barcelona: location, demography and building stock.....	43
3.3.	History and urban development	47
3.4.	The <i>Eixample</i> district	49
3.5.	Construction typology of <i>Eixample</i> buildings	51
3.5.1.	Structural elements features	59
3.5.2.	Geometrical configuration of the <i>Eixample</i> buildings	67
3.6.	Seismicity.....	70
3.7.	Previous studies on seismic vulnerability assessment on unreinforced masonry buildings in Barcelona	74
3.8.	Previous studies on the experimental characterisation of masonry properties from buildings of Barcelona’s urban centre	87
3.9.	Summary	95
Chapter 4. BUILDING TAXONOMY OF REPRESENTATIVE TYPOLOGIES EXPOSED TO SEISMIC RISK IN THE <i>EIXAMPLE</i> DISTRICT		97
4.1.	Introduction.....	97
4.2.	Construction of a building taxonomy	98
4.2.1.	General building information	101
4.2.2.	Structural building system.....	101
4.2.3.	Structural elements and connections	103
4.2.4.	Configuration and irregularities	105
4.2.5.	Conservation state of the building	111
4.2.6.	Interaction and behaviour of the building within a block.....	111
4.3.	Statistical data extrapolation and generalisation of <i>Eixample</i> buildings’ construction characteristics	114
4.4.	Methodology adopted for selection of representative buildings.....	126
4.5.	Summary	132
Chapter 5. NUMERICAL MODELLING OF REPRESENTATIVE BUILDING TYPOLOGIES IN THE <i>EIXAMPLE</i> DISTRICT		134
5.1.	Introduction.....	134
5.2.	Numerical models of representative buildings of the <i>Eixample</i> district.....	135
5.2.1.	Geometrical modelling.....	136
5.2.2.	Material properties	142
5.2.3.	Modelling of one-way floor systems.....	144

5.3.	Variations of different parameters in the reference model	153
5.3.1.	Number of storeys	154
5.3.2.	Vertical extensions so-called " <i>remuntes</i> "	154
5.3.3.	Range of variations of material properties	159
5.3.4.	Thickness variation	160
5.3.5.	Horizontal diaphragms	161
5.3.6.	Façade openings on the ground floor	163
5.4.	Representative building typologies with different geometrical plan configurations	165
5.5.	Summary	169
Chapter 6.	SEISMIC ANALYSIS OF REPRESENTATIVE BUILDINGS IN THE <i>EIXAMPLE</i> DISTRICT	170
6.1.	Introduction	170
6.2.	Nonlinear static pushover analysis	170
6.2.1.	Seismic behaviour of the representative buildings in form of capacity curves	172
6.2.2.	Discussion of damage patterns and failure mechanisms	179
6.3.	Seismic performance of the existing buildings for the seismic hazard in Barcelona	183
6.3.1.	Application of the N2 method	183
6.4.	Summary	189
Chapter 7.	SEISMIC VULNERABILITY ASSESSMENT AT URBAN SCALE	191
7.1.	Introduction	191
7.2.	Methodology adopted for the seismic vulnerability assessment	191
7.3.	Calibration of the vulnerability index method using hybrid criteria	194
7.3.1.	Development of new forms for the vulnerability assessment	194
7.3.2.	Definitions of vulnerability classes	198
7.3.3.	Definition of weights for the vulnerability parameters	208
7.3.4.	Evaluation of the vulnerability index and damage grade	214
7.3.5.	Fragility curves	216
7.4.	Examples of application of the proposed methodology	224
7.4.1.	Application to a sample of buildings from the <i>Eixample</i> district	224
7.4.2.	Specific urban block of the <i>Eixample</i> district	227
7.5.	Summary	231
Chapter 8.	CONCLUSIONS	233
8.1.	Summary	233

8.2. Main conclusions and contributions	234
8.3. Suggestions for future work	236
BIBLIOGRAPHY	239
APPENDIX A	256
APPENDIX B	268
APPENDIX C	276

LIST OF FIGURES

Figure 2.1 - Seismic risk assessment definition.	10
Figure 2.2 - Graphical scheme for the different seismic vulnerability assessment methods (Lang, 2002).	12
Figure 2.3 - Vulnerability functions relating the damage factor (d) and PGA for different vulnerability indexes (Iv) (Guagenti and Petrini, 1989).	14
Figure 2.4 - Flow chart describing different components for evaluation analytical vulnerability curves and damage probability matrices (Calvi et al., 2006).	17
Figure 2.5 - Procedure for determining the performance point between the structure's capacity curve and the demand spectrum (HAZUS, 1999).	18
Figure 2.6 - Examples of different masonry typologies: a) Rubble stone masonry, b) ashlar stone masonry with dry joints, c) clay brick masonry, d) concrete block masonry (Segura Domingo, 2020).	24
Figure 2.7 - Failure modes and limit domains of masonry (a) at the scale of the material and (b) at the scale of the structure (Calderini et al., 2009).	26
Figure 2.8 - Typical failure modes of unreinforced masonry piers subjected to horizontal in-plane loading (from left to right): - Shear failure mechanism with sliding along bed joint; - Shear failure mechanism due to diagonal cracking; - Flexural failure mechanism due to rocking and toe crushing (Tomažević, 1999).	27
Figure 2.9 - Different numerical strategies for unreinforced masonry structures (D'Altri et al. 2019).	28
Figure 2.10 - Examples of FE numerical models of large-scale masonry structures: a) FE model of a section of Mallorca cathedral. FE mesh (left) and smeared damage model (right) (Roca et al., 2013) and b) Macro-mechanical model of a later nave in the church of the Poblet monastery. Left: FE discretisation with the demolished bay in green (left) and damage distribution at the end of the analysis (right) (Saloustros et al., 2015).	30
Figure 2.11 - (a) Example of macro-element modelling of masonry walls (Galasco et al., 2007); (b) Identification of the macro-element in a characteristic masonry wall with openings (Augenti and Parisi, 2010).	31
Figure 2.12 - Different steps for pushover analysis in the Capacity Spectrum Method (adapted from Najam 2018).	32
Figure 2.13 - GEM building taxonomy genome with different attributes (Brzev et al., 2013).	37
Figure 2.14 - Global Earthquake Model (GEM) building taxonomy, including all attributes and levels of details (Silva et al., 2022).	38
Figure 2.15 - Different survey forms: a) GNDT form for masonry buildings (GNDT, 2007); b) AeDES survey form (Baggio et al., 2007) and c) Survey form for masonry structures (Jiménez et al., 2018).	40

Figure 3.1 - Aerial view of a portion of the <i>Eixample</i> district (Maps, 2021).....	42
Figure 3.2 - Barcelona localisation and boundaries (Elaboration on a map from Plànol Barcelona, 2020).....	43
Figure 3.3 - Map of Barcelona with the territorial division of ten districts (adapted from Ajuntament de Barcelona 2005).....	44
Figure 3.4 - Density distribution map of the city of Barcelona (Ajuntament de Barcelona, 2011).	45
Figure 3.5 - Number of buildings constructed in Barcelona during the period from 1850 - 2005 (Aguilar Meléndez, 2011).....	46
Figure 3.6 - Plan of Ildefons Cerdà's project for the expansion of Barcelona (Corominas i Ayala, 2002).....	47
Figure 3.7 - a) Changes of the block sizes initially proposed by Cerda from 1859 to 1972 (Cerdà, 1860); b) Evolution of building's height.	48
Figure 3.8 - Part of Cerdà's plan for the <i>Eixample</i> district in 1859 (left) and its current state (right) (Pujades et al., 2012).	48
Figure 3.9 - The six neighbourhoods of the <i>Eixample</i> district.	49
Figure 3.10 - Typical urban layout of <i>Eixample</i> in accordance with the provisions of Cerdà's plan (Avila-Haro, 2021).	50
Figure 3.11 - Delimitation of the Special Complex, inside the dark grey border, and the Conservation Section of the <i>Eixample</i> , highlighted in black (Barcelona City Council 2002).	50
Figure 3.12 - RISK-UE project classification: a) Distribution of different building typologies: masonry buildings with wooden floors (M31), with masonry vaults (M32), with masonry vaults and steel beams (M33), and with floors of reinforced concrete beams and masonry vaults (M34); reinforced concrete buildings with irregular structural system, irregular infill, and soft/weak storey (RC32); steel buildings with moment frames, braced frames, and frames with unreinforced masonry infill walls (S1/S2/S3); steel and RC composite systems (S5); b) Age distribution of the building's construction periods based on the presence of seismic design recommendations (Barbat et al., 2006).	51
Figure 3.13 - Construction period of the buildings in <i>Eixample</i> (adapted from Cornadó Bardón, 2015).....	52
Figure 3.14 - Different structural systems (Paricio Casademunt, 2001): a) homogeneous system of slender walls; b) hybrid system – concrete columns and masonry walls; c) hybrid system – steel columns and masonry walls.	53
Figure 3.15 - Graphical representation of the ordinances' limits on the transversal section of a typical <i>Eixample</i> illa with changes by increasing (in red) and decreasing (in light grey) limits. The limits in height steadily increased until the 1970s, and the addition of <i>remuntes</i> started to be limited in terms of plot occupation and visibility from the street (Marafini et al., 2022).	54
Figure 3.16 - Distribution of the " <i>remuntes</i> " (shown in black) in the <i>Eixample</i> district of Barcelona (Colom, Cornadó Bardón, et al., 2016).....	55

Figure 3.17 - Example of a vertical section of an existing building with "remuntes" added on top of the original building's height in the <i>Eixample</i> district in Barcelona (adapted from Paricio Casademunt 2001).....	55
Figure 3.18 - Example of different vertical extensions (<i>remuntes</i>): a) remunta 1955, C. Wellington 15; b) remunta 1924, Passeig de Gràcia 91; (c) remunta 1960s, Aragó street 339 and Bailèn street 9 (adapted from Colom et al. 2016).....	56
Figure 3.19 - Development of the longitudinal section. (ARM = alçada reguladora municipal, municipal regulatory height, P.E. = profunditat edificada, building depth) (adapted from Colom 2014).....	56
Figure 3.20 - Three structural analysis units of <i>Eixample</i> 's building (Cornadó Bardón, 2015). ...	57
Figure 3.21 - Foundation types of the existing masonry buildings in <i>Eixample</i> district: a) continuous foundation under load-bearing masonry walls; b) foundation composed of masonry wells and brick arches under continuous masonry walls; c) isolated footing under concrete, masonry or cast-iron pillars (Paricio Casademunt, 2001).	57
Figure 3.22 - Front view of a traditional solid brick masonry wall in an existing building in the <i>Eixample</i> district (left) and a solid brick unit with dimensions 294 x 145 x 49 mm (right).	58
Figure 3.23 - Section of a typical existing <i>Eixample</i> building including all structural and non-structural elements (adapted from Paricio Casademunt 2001).	59
Figure 3.24 - Typical section of the façade wall in different construction periods (from left to right): without basements, with basement with masonry vaults below the ground level, with basement with flooring system on beams below ground level, and with porched system at the base level and different thicknesses and materials of the walls at the upper floor levels. On the right, a photograph with a side view of the front façade of an existing building in the <i>Eixample</i> district, in which it can be observed that the slenderness of the load-bearing masonry wall is increasing within the height of the building (Paricio Casademunt, 2001).	60
Figure 3.25 - Typical one-way flooring system with timber beams (left) or steel beams (right) and masonry vaults with flat ceramic tiles (Casanovas, Graus i Rovira, and Rosell 1993).....	61
Figure 3.26 - Use of different types of flooring system in Catalonia since 1850 (adapted from Casanovas, Graus i Rovira, and Rosell 1993).	61
Figure 3.27 - Different floor slab solutions during the construction periods of the <i>Eixample</i> buildings (Paricio Casademunt, 2001): a) timber beams connected with wood planks; b) timber beams with ceramic tile vaults; c) steel beams with ceramic tile vaults; d) metallic profile with concrete addition through round connectors; e) metal beams connected with a pavement of double row ceramic tiles; f) ceramic reinforced floor slab.	62
Figure 3.28 - Typical one-way floors in the <i>Eixample</i> district of Barcelona: a) timber beams with tile barrel vaults, and b) steel beams with tile barrel vaults (adapted from Paricio Casademunt 2001).....	62
Figure 3.29 - Presence of masonry columns ("pilastres") at the ground floor entrance of an existing masonry building in <i>Eixample</i> (Cornadó Bardón, 2015).....	63

Figure 3.30 - Circular section of a cast-iron pillar (left) and its connection to a steel beam (right) (Paricio Casademunt, 2001).	63
Figure 3.31 - Position and dimensions of the cast-iron pillars located at the ground floor of an existing masonry building in the <i>Eixample</i> district (Cornadó Bardón, 2015).	64
Figure 3.32 - Decorated cast-iron pillars in the existing historical buildings in <i>Eixample</i> district (Rigalt i Farriols, 1857).	64
Figure 3.33 - Steel beams typologies in the typical <i>Eixample</i> 's buildings. a) truss beams with rivetted grid; b) riveted beams with reinforced web; c) riveted beams with reinforced flanges; d) box beams with multiple reinforcements on the bottom flange and double reinforced web (Paricio Casademunt, 2001).	65
Figure 3.34 - Position of a steel beam at the ground floor and transmission of the load to a masonry column by a simple support (Paricio Casademunt, 2001).	65
Figure 3.35 - Simple supports of timber floor beams between two bricks on the load-bearing unreinforced masonry wall (Paricio Casademunt, 2001).	66
Figure 3.36 - Different solution for supporting the unidirectional floor system with timber beams and ceramic vaults on masonry resisting walls parallel to the floor's beams: placing a brick out of the masonry wall (left) or making a horizontal slot in the masonry wall for supporting the ceramic tile vault (right) (Paricio Casademunt, 2001).	66
Figure 3.37 - Detail of connection between riveted beam and column profiles (Paricio Casademunt, 2001).	66
Figure 3.38 - Different configurations of typical rectangular buildings in <i>Eixample</i> district: a) rectangular building with a central staircase and patio; b) wide rectangular building with a central part composed of two interior patios and a central staircase; c) wide irregular building with a central part composed of central staircase and patios, as well as lateral patios on each longitudinal load-bearing walls; d) wide irregular building with a central part composed of central staircase and patios, as well as two or more lateral patios on each longitudinal load-bearing walls; e) narrow building with a lateral staircase placed transversally along the building's plan and lateral patios; and f) narrow building with a lateral staircase placed longitudinally along the building's plan and lateral patios (Cornadó Bardón, 2015).	68
Figure 3.39 - Chamfer buildings' geometrical configurations located at each corner of the urban block: a) Chamfer buildings with radial structural distribution of the walls parallel to the façade; b) Chamfer buildings geometrically composed of two parts: "L" shape and a triangular part; c) Corner buildings that do not represent the typical chamfer characteristics (Cornadó Bardón, 2015).	69
Figure 3.40 - Position and number of central and lateral patios in plan (adapted from Cornadó Bardón 2015).	69
Figure 3.41 - a) Map of seismic intensities in the region of Catalonia and b) Map of earthquakes epicentres for the period between 1986-2000 (adapted from Institut Cartogràfic de Catalunya, 2001).	70
Figure 3.42 - Seismic zonation of Barcelona city by considering local soil effects. Zone 0 = Palaeozoic and Tertiary rock outcrops with different thickness of the tertiary substrate. Zone I =	

Holocene outcrops with soft soils. Zone II = Pleistocene outcrops with a tertiary substrate. Zone III = Pleistocene outcrops without a tertiary substrate (Cid et al., 2001).	71
Figure 3.43 - a) Map of the seismic zones in Catalonia with the location of deterministic scenario reference earthquakes – 1428 in Girona and 1448 earthquake in Cardedeu; b) Deterministic seismic acceleration response spectra for the city of Barcelona (RISK-UE, 2004).	72
Figure 3.44 - Maps of Barcelona with the location of the <i>Eixample</i> district for seismic intensities considering soil effects: a) Deterministic seismic scenario; b) Probabilistic seismic scenario (adapted from Lantada, 2007).	73
Figure 3.45 - Acceleration Displacement Response Spectra (ADRS) for Barcelona’s soil zones: a) Deterministic scenarios and b) Probabilistic scenario (adapted from Irizzary, 2004).	73
Figure 3.46 – Seismic vulnerability index evaluation using the GNDT forms: a) VI (0-382.5) b) normalised VI (0-100); c) Vulnerability index map of the case study <i>Eixample</i> (adapted from Yépez, Barbat, and Canas 1996).	75
Figure 3.47 - Mean vulnerability index evaluated for the unreinforced masonry buildings in the districts of Barcelona city (adapted from Mena 2002).	76
Figure 3.48 - Average vulnerability indices obtained with the Level I methodology for the unreinforced masonry buildings of Barcelona’s districts (Lantada, 2007).	77
Figure 3.49 - Damage grade obtained for the unreinforced masonry buildings in Barcelona (left) and in the <i>Eixample</i> district (right) (RISK-UE, 2004).	77
Figure 3.50 - Ten historical monuments with the highest mean damage grade (Irizzary 2004). ..	78
Figure 3.51 - Representation of the ELC system together with the vulnerability index (VI) for a street located in the <i>Eixample</i> district (a) and percentage of buildings with a given VI (Cara et al., 2018).	79
Figure 3.52 - Demand Spectra with bilinear capacity spectra for unreinforced masonry buildings for two different seismic scenarios deterministic (left) and probabilistic (right) (Barbat et al., 2008).	81
Figure 3.53 - Fragility curves for high-rise unreinforced masonry buildings for four damage state (Barbat et al., 2008).	81
Figure 3.54 - Damage grade maps for the districts in Barcelona from two different scenarios: a) deterministic scenario and b) probabilistic scenario buildings (Barbat et al., 2008).	82
Figure 3.55 - Schemes of the building modelled in previous studies. a) (Bonett Díaz, 2003); b) (Moreno-González and Bairán, 2011); c) (Pujades et al., 2012); d) (Avila-Haro et al., 2012); e) (Jiménez-Pacheco et al., 2020).	84
Figure 3.56 - Structural elements of the <i>Eixample</i> buildings: a) Typical one-way floor with timber beams (Pujades et al., 2012); b) Metallic girders and cast-iron pillars at the ground floor of the building (Gonzalez-Drigo et al., 2015).	85
Figure 3.57 - Existing unreinforced masonry buildings of Barcelona as part of different experimental campaigns executed at UPC: a) industrial complex; b) residential building located in	

the <i>Eixample</i> district; c) residential building located in the district of Ciutat Vella in Barcelona (Segura et al., 2019).....	89
Figure 3.58 - Interior masonry wall to be tested from an existing <i>Eixample</i> building (left) and in-situ core drilling (right) (Segura et al., 2019).	89
Figure 3.59 - Compressive stress-strain curves from an experimental campaign in a residential building located in the <i>Eixample</i> district: a) 150 mm cylinder core samples; b) 90 mm cylinder core samples (Segura et al., 2019).	90
Figure 3.60 - Histogram of the compressive strength's frequency distribution of the masonry samples extracted from the existing <i>Eixample</i> buildings (adapted from Cornadó Bardón 2015).	92
Figure 3.61 - Brick and mortar samples for compression tests (before and after): a) triple cylindrical brick sample (before compression test); b) triple cylindrical brick sample (after compression test); c) prismatic mortar sample (before compression test); d) prismatic mortar sample (after compression test) (adapted from Drougkas et al. 2016).	92
Figure 3.62 - Masonry prisms with a typical layout of LVDTs: a) vertical layout for displacement measurement in the unit and the composite and b) horizontal displacement for measurement of the Poisson's ratio (Drougkas et al., 2016).	93
Figure 3.63 - Stress displacement diagrams for masonry prisms with two types of mortars: a) aerial lime mortar prisms; b) hydraulic lime mortar prisms (Drougkas et al., 2016).	93
Figure 3.64 - Dimensions of two masonry samples: a) Running bond walls, b) Stack bond prisms. Common average thickness $t_s = 148$ mm (Segura et al., 2018).	94
Figure 3.65 - Stress vs. strain experimental curves until failure with monotonic loading for the two masonry specimens: a) running bond walls; b) stack bond prisms (Segura et al., 2018).	94
Figure 4.1 - Parameters for a specified building taxonomy.....	100
Figure 4.2 - Different structural systems for the rectangular shape buildings in the middle of the typical <i>Eixample</i> urban block: homogenous system of continuous slender walls (left) and hybrid system – steel/concrete frames on the ground floor and unreinforced masonry walls on the upper floors (right) (adapted from Paricio Casademunt 2001).	102
Figure 4.3 - Different height levels of existing masonry buildings in the <i>Eixample</i> district.	103
Figure 4.4 - Position and number of interior (in grey) and lateral (in yellow) patios in different plan configurations: a) building with lateral patios; b) building with interior central patio; c) building with interior patios near the central staircase and lateral patios on each side of the longitudinal masonry wall; d) buildings with interior central patios and two or more lateral patios on each side of the longitudinal masonry wall (adapted from Cornadó Bardón 2015).	107
Figure 4.5 - Position of the staircase: lateral staircase (left) and central staircase with interior patios (right) (adapted from Cornadó Bardón 2015).	108
Figure 4.6 - Distribution of walls in representative building typologies in <i>Eixample</i> district (adapted from Cornadó Bardón 2015).	109

Figure 4.7 - Different number of façade openings on the ground floor and the upper levels: a) narrow building with two openings on the ground floor and each of the upper levels; b) band building with three openings at the ground floor and three on each floor level; c) band building with three openings at the ground floor and four on each floor level. The drawings represent the number of opening on the upper floor levels depending on the width of the façade (Cornadó Bardón, 2015).	110
Figure 4.8 - Building's position within a typical <i>Eixample</i> block: 1) between buildings enclosed in a row; 2) at the corner of an urban block; 3) at the end of an aggregate.....	112
Figure 4.9 - Presence of staggered floors in a row of buildings in a typical example urban block (Castilla Marne, 2010).	112
Figure 4.10 - Structural and typological heterogeneities among band buildings in <i>Eixample</i> (Castilla Marne, 2010).	113
Figure 4.11 - Presence of different number of façade openings on the existing <i>Eixample</i> buildings (Modrego Casquero, 2011).	113
Figure 4.12 - Total sample of the analysed buildings built before 1940 in the <i>Eixample</i> district (Cornadó Bardón, 2015).....	114
Figure 4.13 - Parameters considered for the structural typological analysis of the existing unreinforced masonry buildings in <i>Eixample</i> district.	115
Figure 4.14 - Examples of structural plan distributions of the typical band buildings of the <i>Eixample</i> district composed of central part with the staircase and the lighting and ventilation patios, the front and rear bays, and the galleries at the back façade: a) band building with central stairwell and light patio; b) band building with central stairwell and lateral semi-patios, and c) narrow band building with lateral stairwell and lateral lighting patio (adapted from Cornadó Bardón 2015).	116
Figure 4.15 - Generator scheme of a typical floor plan of <i>Eixample's</i> band building. Seven types of core elements are identified based on the staircase position and the presence of lighting and ventilations patios. Each core element, in whichever direction, can be combined with a single or double front and rear bay (Cornadó Bardón, 2015).....	117
Figure 4.16 - Building typologies defined as in Cornadó's research (2015). "C" with Central stair (left), "L" with lateral stair, "V" corner building.....	118
Figure 4.17 - Frequency of the three building typologies.....	118
Figure 4.18 - Schematisation of subtypes for the building typology with central staircase 'C' (adapted from Cornadó Bardón 2015).	119
Figure 4.19 - Examples of floor section plans of existing <i>Eixample</i> buildings by representing the subtypes of the building typology 'C' (Cornadó Bardón, 2015).	120
Figure 4.20 - Frequency distribution of the building typology 'C'.	121
Figure 4.21 - Wall distribution and distances for a band building typology composed of a central part with addition of front and rear bays (adapted from Cornadó Bardón 2015).	122

Figure 4.22 - Different geometrical configurations of the central part of the structure with a central stairwell and continuous lateral walls (with or without lateral patios) or discontinuous lateral walls (presence of lateral patios) (adapted from Cornadó Bardón 2015).	122
Figure 4.23 - Geometrical configuration of the most common band building typology 'C22AB' composed of a central part and front and rear bays.	123
Figure 4.24 - Frequency of width of the most representative band building's façades.	124
Figure 4.25 - Frequency distribution of building's plot depth (type C22AB).	124
Figure 4.26 - Frequency distribution of the total number of floors for the band building typology 'C': a) without vertical additions (<i>remuntes</i>) and b) with vertical additions (<i>remuntes</i>).	125
Figure 4.27 - Frequency distribution of the following wall distances: a) Y1 distance between the front façade wall (W1) and the parallel interior wall (W5); b) Y2 distance between the back façade wall (W2) and the parallel interior wall (W6); c) Y3 distance between the interior walls W3 and W5 of the bay situated in front of the central part; d) Y4 distance between the interior walls W4 and W6 of the bay situated after the central part (see Figure 4.21 for the proper nomenclature of the walls and distances).	125
Figure 4.28 - Frequency distribution of the number of façade openings (a) and number of flats per floor (b).	126
Figure 4.29 - Flowchart of the methodology adopted for the definition of the most representative buildings.	127
Figure 4.30 - Frequency of all building typologies from the analysed sample of <i>Eixample</i> district.	128
Figure 4.31 - Frequency of building band typologies according to the geometrical configuration of the structure's central part with central staircase (50% criterion for selection of representative buildings).	129
Figure 4.32 - Frequency of building typology 'L'- narrow building with lateral staircase (50% criterion for selection of representative buildings).	129
Figure 4.33 - Frequency of building typology 'V' - corner buildings (50% criterion for selection of representative buildings).	130
Figure 5.1 - Numerical models of representative buildings and variation of different parameters.	136
Figure 5.2 - Selected reference building of the <i>Eixample</i> district: a) ground floor configuration; b) floor plan section (adapted from Cornadó Bardón 2015); c) front façade geometry (dimensions in metres).	137
Figure 5.3 - Finite numerical reference model of an existing building of the <i>Eixample</i> district: a) geometry of the front façade; b) 3D FE model of the building.	138
Figure 5.4 - Example of a typical ground floor of a rectangular shape building typology in the <i>Eixample</i> district (including unreinforced masonry walls, masonry columns, steel beams and cast-iron pillars).	139

Figure 5.5 - Geometrical configuration of an existing building typology in the *Eixample* district: a) plan of the ground floor with unreinforced masonry walls; b) plan of the ground floor of a hybrid steel-masonry system; c) typical floor plan for the rest of the storeys (dimensions in metres). . 140

Figure 5.6 - Finite element models of a representative building typology in the *Eixample* district: a) reference model and b) hybrid model. 141

Figure 5.7 - Section of the jack arch floor with steel beams and tile barrel vaults: Geometry (top) and finite element model (bottom) (dimensions in mm)..... 145

Figure 5.8 - Section of the jack arch floor with timber beams and tile barrel vaults: Geometry (top) and finite element model (bottom) (dimensions in mm)..... 145

Figure 5.9 - 3D solid finite element models of the floor system with tile vaults and: a) steel beams; b) timber beams (dimensions in metres). 146

Figure 5.10 - 2D equivalent shell model: a) floor model with steel beams; b) floor model with timber beams (dimensions in metres). 146

Figure 5.11 - Loading conditions for 3D solid floor model in order to obtain: a) Poisson's coefficients ν_{xi} with $i = y; z$; b) Poisson's coefficients ν_{yi} with $i = x; z$; c) Poisson's coefficients ν_{zi} with $i = y; x$ 149

Figure 5.12 - Flowchart of the numerical procedure used to compute the values of the shear moduli of the jack arch floors. 152

Figure 5.13 - Numerical models with different number of storeys: a) Building with three storeys (GF+3); b) Building with four storeys (GF+4); c) Building with five storeys (GF+5); d) Building with six storeys (GF+6). 154

Figure 5.14 - Existing buildings from the *Eixample* district with the most recurrent typologies of vertical extensions (*remuntes*): (a) type A), (b) type B and (c) type C (adapted from Colom, 2014). 155

Figure 5.15 - Schematic plans (top) and transversal (middle) and longitudinal (bottom) elevations of all four models, Reference and types A, B, C. The longitudinal elevation of the Reference model corresponds to the white portion of all three models (bottom row) (adapted from Marafini et al., 2022)..... 156

Figure 5.16 - Plan configuration of the reference model with the vertical extensions added in the models type A, B, and C (represented in blue, green and yellow, respectively). In the axonometric view, the URM building is divided into three structural units: 1) The vertical extensions-*remuntes*, 2) The upper floors, which vary in number but all feature a recurring plan configuration and elevation, and 3) The ground level, which has external linear structural elements and beams in place of the interior load-bearing walls. The red line refers to the changed structural alignment generated by the retracted façade of type B and type C (adapted from Marafini et al., 2022). 157

Figure 5.17 - Finite element models of the most common building typology and the three variations developed: a) Reference model b) type A, c) type B and d) type C..... 158

Figure 5.18 - Different horizontal diaphragms considering their in-plane stiffness: a) flexible floor system (timber beams and wooden planks); b) semi-flexible floor system (timber/steel beams and

ceramic tile vaults) and c) rigid floor system (reinforced concrete slab/ floor slab with ceramic blocks and a compressive layer of concrete).	161
Figure 5.19 - Geometry of the ground floor façade openings of the reference model: a) front façade and b) rear façade.	163
Figure 5.20 - Geometry of the ground floor façade openings of the two numerical models: a) Smaller façade openings and b) Bigger façade openings.	164
Figure 5.21 - Geometrical configuration of a representative narrow building model with central core without lateral patios (in metres): a) Floor plan section; b) Front façade geometry; c) 3D finite element model.	165
Figure 5.22 - Geometrical configuration of a representative wide building model with central staircase and two lateral patios (in metres): a) Floor plan section; b) Front façade geometry; c) 3D finite element model.	166
Figure 5.23 - Geometrical configuration of a representative narrow building model with lateral staircase and patios (in metres): a) Floor plan section; b) Front façade geometry; c) 3D finite element model.	167
Figure 6.1 - Graphical representation of pushover analysis to an URM building with different patterns for the load distributions.	171
Figure 6.2 - Pushover capacity curves of the reference model for pushover in X and Y direction.	173
Figure 6.3 - Pushover capacity curves of the reference and hybrid model: pushover in X direction (left) and pushover in Y direction (right).	174
Figure 6.4 - Capacity curves of the FE reference model with the two different composite floor systems composed of steel or timber beams and tile vaults: pushover in X direction (left) and pushover in Y direction (right).	174
Figure 6.5 - Capacity curves in terms of base shear and horizontal displacements of the <i>Example</i> building FEM model with the two different composite floor systems composed of steel or timber beams and tile vaults: pushover in X direction (left) and pushover in Y direction (right).	175
Figure 6.6 - Pushover capacity curves in terms of horizontal acceleration and displacements for the reference model and the three models with variation of number of storeys, in both X direction - parallel to the façade and Y direction - perpendicular to the façade.	175
Figure 6.7 - Pushover capacity curves of the reference model and the three model variations with vertical extensions, type A, B and C, in both X direction - parallel to the façade and Y direction - perpendicular to the façade.	176
Figure 6.8 - Pushover curves in terms of base shear and horizontal displacements of the Reference model and the three model variations with vertical extensions in both directions: X direction - parallel to the façade and Y direction - perpendicular to the façade.	177
Figure 6.9 - Contour of principal tensile strains for the maximum horizontal acceleration of the reference building model with homogeneous system of URM walls: a) Pushover loading parallel to the façade in X direction and b) Pushover loading orthogonal to the façade in Y direction.	179

Figure 6.10 - Contour of principal tensile strains for the maximum horizontal acceleration of the hybrid system: a) Pushover loading parallel to the façade in X direction and b) Pushover loading orthogonal to the façade in Y direction.	180
Figure 6.11 - Contour of maximum principal strains at maximum capacity for pushover analysis in X direction: a) building with composite floor system consisting of steel beams and ceramic tile vaults; b) building with composite floor system consisting of timber beams and ceramic tile vaults. 3D view at the top and view of the front façade at the bottom.....	181
Figure 6.12 - Contour of maximum principal strains at the maximum capacity for a pushover in Y direction: a) building with composite floor system of steel beams and tile vaults; b) building with composite floor system of timber beams and ceramic tile vaults. 3D view at the top and view of the lateral walls at the bottom.....	181
Figure 6.13 - Distribution of principal tensile strains for all numerical models at peak load for pushover analysis parallel to the façade (X direction): (a) Reference model, (b) type A, (c) type B and (d) type C.	182
Figure 6.14 - Distribution of principal tensile strains for all numerical models at peak load for pushover analysis perpendicular to the façade (Y direction): (a) Reference model, (b) type A, (c) type B and (d) type.	183
Figure 6.15 - Bilinear idealisation of the capacity curves for an equivalent SDOF system (MIT Ministero delle Infrastrutture e del Trasporti, 2019).....	184
Figure 6.16 - Reference point displacement according to the N2 method for: a) $T^* \geq T_c$ and b) $T^* < T_c$ (adapted from MIT Ministero delle Infrastrutture e del Trasporti 2019).	186
Figure 6.17 - Transformation of a pushover capacity curve from MDOF into a SDOF system of the reference building model and bilinear idealisation of the SDOF system (pushover in X direction).	187
Figure 6.18 - Graphical representation of the application of the N2 method with regards to the deterministic and probabilistic spectra for the bilinear curve of the reference model: a) Pushover in X direction and b) Pushover in Y direction.....	188
Figure 7.1 - Methodology adopted for the seismic vulnerability assessment of URM existing buildings.	193
Figure 7.2 - Definition of the ratio used to determine the effect of façade wall openings on the seismic behaviour of existing masonry building in relation to the direction of seismic loading (adapted from Ortega 2018).	197
Figure 7.3 - Specific structural attributes involved in the definition of the vulnerability classes for Parameter 1 “Seismic coefficient”, and relevant models elaborated to analyse the influence of structural attributes on the seismic capacity.	199
Figure 7.4 - Definition of classes for the vulnerability Parameter 1 “Seismic coefficient” according to the maximum capacity obtained from several numerical models.	199
Figure 7.5 - Definition of the four vulnerability classes (A, B,C and D) for the different parameters of the VIM forms: a) Number of floors (P2); b) Horizontal diaphragms (P3); c) Plan configuration	

(P4); d) Vertical irregularity (P5); e) Presence of patios (P6), and f) Façade openings on the ground floor (P7).....	200
Figure 7.6 - Definition of vulnerability classes for Parameter 2 “Number of floors”.....	201
Figure 7.7 - Definition of vulnerability classes for Parameter 3 “Horizontal diaphragms”.....	202
Figure 7.8 - Definition of vulnerability classes for Parameter 4 “Plan configuration” with examples of existing buildings plan configurations (adapted from Cornadó Bardón 2015).....	203
Figure 7.9 - Definition of vulnerability classes Parameter 5 “Vertical irregularity”.	204
Figure 7.10 - Definition of vulnerability classes for Parameter 6 “Presence of patios” (adapted from Cornadó Bardón 2015).....	204
Figure 7.11 - Definition of vulnerability classes for Parameter 10 “Presence of adjacent buildings with different height” (adapted from Formisano et al. 2015).....	206
Figure 7.12 - Definition of vulnerability classes for Parameter 11 “Position of the buildings in the aggregate” (adapted from Formisano et al. 2015).....	207
Figure 7.13 - Definition of vulnerability classes for Parameter 12 “Number of staggered floors” (adapted from Formisano et al. 2015).	207
Figure 7.14 - Definition of vulnerability classes for Parameter 13 “Effect of either structural or typological heterogeneity among adjacent structural units” (adapted from Formisano et al. 2015).	208
Figure 7.15 - Definition of vulnerability for Parameter 14 “Percentage difference of opening areas among adjacent façades” (adapted from Formisano et al. 2015).	208
Figure 7.16 - Correlation between the maximum capacity obtained from the pushover analysis in X direction (left) and Y direction (right) and the calculated vulnerability index for all the numerical models.....	215
Figure 7.17 - Definition of four limit states on the pushover capacity curve in X direction of Model 20.....	218
Figure 7.18 - Example of fragility curves for the subset of existing masonry buildings in the <i>Eixample</i> district for four different damage states (slight, moderate, extensive and complete), by plotting the spectral displacement for the reference model.....	223
Figure 7.19 - Vulnerability index distribution for both X and Y directions of the analysed building typologies in the <i>Eixample</i> district.....	225
Figure 7.20 - Frequency of calculated vulnerability index values: a) I_v for X direction and b) I_v for Y direction.....	225
Figure 7.21 - Vulnerability curves for the analysed building stock in the <i>Eixample</i> district.....	226
Figure 7.22 - Fragility curves obtained for the mean vulnerability index of the analysed building stock.....	226
Figure 7.23 - Discrete damage distribution histograms for the mean I_v value of the analysed building stock: a) $I_{EMS-98} = VI$; b) $I_{EMS-98} = VII$	227

Figure 7.24 - Geometrical configuration of the specific urban block with the main façade elevations of the existing buildings (Rago, 2022).	228
Figure 7.25 - 3D representation of the urban block (Rago, 2022).	228
Figure 7.26 - Vulnerability index map for the urban block for both loading directions X considering the aggregate effect (left) and Y (right) (adapted from Rago 2022).	231
Figure A.1 - Frequency of width of the band building's façades - type C21AB.	256
Figure A.2 - Frequency distribution of building's plot depth -type C21AB.	256
Figure A.3 - Frequency distribution of the total number of floors for the band building typology - type C21AB: a) without vertical additions (<i>remuntes</i>) and b) with vertical additions (<i>remuntes</i>).	257
Figure A.4 - Frequency distribution of the following wall distances for the band building typology - type C21AB: a) Y1 distance between the front façade wall (W1) and the parallel interior wall (W5); b) Y2 distance between the back façade wall (W2) and the parallel interior wall (W6); c) Y3 distance between the interior walls W3 and W5 of the bay situated in front of the central part; d) Y4 distance between the interior walls W4 and W6 of the bay situated after the central part.	257
Figure A.5 - Frequency distribution of the number of façade openings (a) and number of flats per floor (b).	258
Figure A.6 - Frequency of width of the most representative band building's façades - type C12AB.	258
Figure A.7 - Frequency distribution of building's plot depth - type C12AB.	259
Figure A.8 - Frequency distribution of the total number of floors for the band building typology - type C12AB: a) without vertical additions (<i>remuntes</i>) and b) with vertical additions (<i>remuntes</i>).	259
Figure A.9 - Frequency distribution of the following wall distances for the band building typology - type C12AB: a) Y1 distance between the front façade wall (W1) and the parallel interior wall (W5); b) Y2 distance between the back façade wall (W2) and the parallel interior wall (W6); c) Y3 distance between the interior walls W3 and W5 of the bay situated in front of the central part; d) Y4 distance between the interior walls W4 and W6 of the bay situated after the central part (see Figure 4.21 for the proper nomenclature of the walls and distances).	260
Figure A.10 - Frequency distribution of the number of façade openings (a) and number of flats per floor (b).	260
Figure A.11 - Schematisation of subtypes for the building typology with lateral staircase 'L' (adapted from Cornadó Bardón 2015).	261
Figure A.12 - Frequency of width of the most representative band building's façades for the narrow band building typology - type L22AB.	262
Figure A.13 - Frequency distribution of building's plot depth for the narrow band building typology - type L22AB.	262

Figure A.14 - Frequency distribution of the total number of floors for the narrow band building typology - type L22AB: a) without vertical additions (<i>remuntes</i>) and b) with vertical additions (<i>remuntes</i>).	263
Figure A.15 - Frequency distribution of the following wall distances for the narrow band building typology - type L22AB: a) Y1 distance between the front façade wall (W1) and the parallel interior wall (W5); b) Y2 distance between the back façade wall (W2) and the parallel interior wall (W6); c) Y3 distance between the interior walls W3 and W5 of the bay situated in front of the central part; d) Y4 distance between the interior walls W4 and W6 of the bay situated after the central part (see Figure 4.21 for the proper nomenclature of the walls and distances).	263
Figure A.16 - Frequency distribution of the number of façade openings (a) and number of flats per floor.	264
Figure A.17 - Frequency of width of the most representative band building's façades for the narrow band building typology - type L11A.	264
Figure A.18 - Frequency distribution of building's plot depth for the narrow band building typology - type L11A.	264
Figure A.19 - Frequency distribution of the total number of floors for the narrow band building typology - type L11A with vertical additions (<i>remuntes</i>).	265
Figure A.20 - Schematisation of subtypes for the corner building typology 'V' (adapted from Cornadó Bardón 2015).	265
Figure A.21 - Frequency distribution of the total number of floors for the corner building typology - type V1A: a) without vertical additions (<i>remuntes</i>) and b) with vertical additions (<i>remuntes</i>).	266
Figure A.22 - Frequency distribution of the following wall distances for the corner building typology - type V1A: a) Y1 distance between the front façade wall (W1) and the parallel interior wall (W5); b) Y2 distance between the back façade wall (W2) and the parallel interior wall (W6); c) Y3 distance between the interior walls W3 and W5 of the bay situated in front of the central part; d) Y4 distance between the interior walls W4 and W6 of the bay situated after the central part (see Figure 4.21 for the proper nomenclature of the walls and distances).	266
Figure A.23 - Frequency distribution of the total number of floors for the corner building typology - type V3: a) without vertical additions (<i>remuntes</i>) and b) with vertical additions (<i>remuntes</i>). ..	267
Figure A.24 - Frequency distribution of the following wall distances for the corner building typology - type V3: a) Y1 distance between the front façade wall (W1) and the parallel interior wall (W5); b) Y2 distance between the back façade wall (W2) and the parallel interior wall (W6); c) Y3 distance between the interior walls W3 and W5 of the bay situated in front of the central part; d) Y4 distance between the interior walls W4 and W6 of the bay situated after the central part (see Figure 4.21 for the proper nomenclature of the walls and distances).	267
Figure B.1 - Load-displacement curves derived from a compression test of the 3D solid floor models in X direction (perpendicular to the beams, left) and in Y direction (parallel to the beams, right).	268
Figure B.2 - Displacements in X direction of the 3D solid floor model with steel beams from a displacement load of 0.5 mm applied orthogonal to the beams.	269

Figure B.3 - Displacements in Y direction of the 3D solid floor model with steel beams from displacement load of 0.5 mm applied parallel to the beams.....	269
Figure B.4 - Load-displacement capacity curves obtained from in-plane shear tests of the 3D solid floor models in X direction (perpendicular to the beams, left) and in Y direction (parallel to the beams, right).....	270
Figure B.5 - Calibration of the elastic shear stiffness based on the comparison of the 3D solid and 2D shell floor models with steel beams (for both loading directions).....	270
Figure B.6 - Calibration of the elastic shear stiffness based on the comparison of the 3D solid and 2D shell floor models with timber beams (for both loading directions).	270
Figure B.7 - a) Displacements of the floors in the FEM building model from pushover in X direction; b) Displacements of the floors in the building model from pushover in Y direction (dimensions in meters). Red dashed lines illustrate the deformed shape at the maximum load capacity of the pushover analysis (deformation multiplied by 10).	271
Figure B.8 - Longitudinal and shear deformation modes: a) longitudinal deformation in X direction of the floors in the FEM building model; b) shear deformation of the floors in the FEM building model; c) longitudinal deformation in X direction of the 3D solid floor model; d) shear deformation of the 3D solid floor model.	272
Figure B.9 - Calibration of the effective shear stiffness of the 2D shell model in the 3D building model: a) floors with steel beams parallel to the loading direction; b) floors with steel beams perpendicular to the loading direction.....	273
Figure B.10 - Capacity curves from pushover analyses in X direction with different shear moduli for the one-way flexible floors: a) floors with steel beams; b) floors with timber beams.	274
Figure B.11 - Convergence of the values of the shear moduli of the 2D shell floors with steel beams.	274
Figure B.12 - Calibration of the effective shear stiffness of the 2D elastic shell model in the 3D building model: a) floors with timber beams parallel to the loading direction; b) floors with timber beams perpendicular to the loading direction.....	275
Figure B.13 - Convergence of the values for the shear moduli of the 2D shell floors with timber beams.....	275
Figure C.1 - Pushover capacity curves of the FE numerical models with the variation of the material properties: pushover in X direction (left) and pushover in Y direction (right).	276
Figure C.2 - Pushover capacity curves of the FE numerical models with the variation of the wall thickness: pushover in X direction (left) and pushover in Y direction (right).	276
Figure C.3 - Pushover capacity curves of the FE numerical models with the variation of the different horizontal diaphragms: pushover in X direction (left) and pushover in Y direction (right).	277
Figure C.4 - Pushover capacity curves of the FE numerical models with the variation of the façade openings on the ground floor: pushover in X direction (left) and pushover in Y direction (right).	277

Figure C.5 - Pushover capacity of the FE numerical models with the different geometrical configurations: pushover in X direction (left) and pushover in Y direction (right).277

LIST OF TABLES

Table 2.1 - Damage Probability Matrix proposed by Whitman et al (1973)	13
Table 2.2 - Vulnerability classes for different building typologies according to EMS-98 scale (Grünthal 1998).....	15
Table 2.3 - Attribution of vulnerability classes and vulnerability index values to different building typologies (Giovinazzi and Lagomarsino 2004).	16
Table 2.4 - Summary information for different vulnerability methods based on building system, seismic hazard, damage and vulnerability description (Giovinazzi 2005).....	20
Table 2.5 - Vulnerability index method formulation (Benedetti and Petrini 1984).....	21
Table 2.6 - Additional vulnerability parameters for the VIM form proposed for buildings in aggregate (Formisano et al. 2015).	23
Table 2.7 - Summary information of existing building taxonomies.....	34
Table 2.8 - EMS-98 and HAZUS building typology classification (Giovinazzi 2005).....	36
Table 3.1 - Distribution of number of inhabitants and buildings in the ten districts of Barcelona.	45
Table 3.2 - Number of cadastral buildings according to the year of construction (Ajuntament de Barcelona 2011).....	46
Table 3.3 - Summary information on available numerical models of typical URM buildings of the <i>Eixample</i> district studied in previous studies.	83
Table 3.4 - Summary of the material properties used in the 3D numerical models of the existing <i>Eixample</i> building from the previous studies.....	85
Table 3.5 - Summary of available data for the seismic performance of typical buildings located in <i>Eixample</i> district from previous research studies.	86
Table 3.6 - Masonry mechanical properties obtained with minor destructive testing on existing buildings in Barcelona's urban centre.	90
Table 3.7 - Mechanical properties obtained from laboratory testing on masonry specimens.	95
Table 4.1 - Summary table of the most recurrent subtypes of the vertical extensions.....	106
Table 5.1 - Loads used in the numerical models of the representative buildings.	141
Table 5.2 - Material properties of the unreinforced masonry walls in the numerical models.	142
Table 5.3 - Material properties of all the steel beams in the numerical models.	143
Table 5.4 - Material properties of the one-way diaphragm with steel beams and masonry vaults.	143
Table 5.5 - Material properties of the one-way diaphragm with timber beams and masonry vaults.	143

Table 5.6 - Material properties of the ceramic tile vaults, rubble, steel beams with corresponding interface elements, and timber beams with corresponding interface elements in the 3D solid numerical models of the jack arch floors.....	148
Table 5.7 - Values for the Poisson's coefficients used in the 2D shell floor models.	150
Table 5.8 - Values of the elastic properties of the floors obtained from the FEM analyses of isolated floor slab models.	151
Table 5.9 - Values obtained of the shear properties of the floor system with steel beams after the proposed iterative procedure.	153
Table 5.10 - Material properties used for the additional storeys.	159
Table 5.11 - Material properties of the unreinforced masonry walls used for the four numerical models.	160
Table 5.12 - Elastic properties for the modelling of the different horizontal diaphragms.....	162
Table 5.13 - Self-weight loads used in the numerical models for the different floor systems. ...	163
Table 5.14 - Size of the ground floor façade openings in the numerical models.	164
Table 5.15 - Summary information of all the numerical models of the representative <i>Example</i> buildings.	168
Table 6.1 - Summary of results obtained from the pushover analyses of the representative building models.	177
Table 6.2 - Characteristics of the equivalent SDOF system of the URM reference building.	187
Table 6.3 - Spectral and maximum displacements obtained for the SDOF and MDOF systems of the reference building for both deterministic and probabilistic spectra.	189
Table 7.1 - Vulnerability classes proposed for the Parameter 1 “Seismic coefficient” for both main directions (X and Y)	201
Table 7.2 - Vulnerability classes proposed for the Parameter 2 “Number of floors	201
Table 7.3 - Vulnerability classes proposed for the Parameter 3 “Horizontal diaphragms”	202
Table 7.4 - Vulnerability classes proposed for the Parameter 4 “Plan configuration”	202
Table 7.5 - Vulnerability classes proposed for the Parameter 5 “Vertical irregularity”	203
Table 7.6 - Vulnerability classes proposed for the Parameter 6 “Presence of patios”	204
Table 7.7 - Vulnerability classes proposed for the Parameter 7 “Façade openings at ground floor”	205
Table 7.8 - Vulnerability classes proposed for the Parameter 8 “Non-structural elements”	205
Table 7.9 - Vulnerability classes proposed for the Parameter 9 “General maintenance conditions”	205
Table 7.10 - Vulnerability classes proposed for the Parameter 10 “Presence of adjacent buildings with different height”	206

Table 7.11 - Vulnerability classes proposed for the Parameter 11 “Position of the buildings in the aggregate”	206
Table 7.12 - Vulnerability classes proposed for the Parameter 12 “Number of staggered floors”	207
Table 7.13 - Vulnerability classes proposed for the Parameter 13 “Effect of either structural or typological heterogeneity among adjacent structural units”	207
Table 7.14 - Vulnerability classes proposed for the Parameter 14 “Percentage difference of opening areas among adjacent façades”	208
Table 7.15 - Evaluation of the Random Consistency Index RI, according to (Saaty 1987)	209
Table 7.16 - The fundamental scale of the Analytic Hierarchy Process (AHP) (Saaty 1987)....	210
Table 7.17 - a) Description of the seven vulnerability parameters; b) Scale for the assignment of the importance of each parameter according to their absolute differences.....	211
Table 7.18 - Selection of numerical models for the calibration of each of the proposed vulnerability parameters for both loading directions: a) X direction and b) Y direction.	211
Table 7.19 - Numerical results of the maximum capacity (MC) for the definition of the parameters’ weights in X direction.....	212
Table 7.20 - Numerical results of the maximum capacity (MC) for the definition of the parameters’ weights in Y direction.....	213
Table 7.21 - Pairwise comparison matrix with the resulting priority vector for the weights for the seven vulnerability parameters considered in the VIM form for X loading direction.....	213
Table 7.22 - Pairwise comparison matrix with the resulting priority vector for the weights for the seven vulnerability parameters considered in the VIM form for Y loading direction.....	213
Table 7.23 - Vulnerability index form for X direction including the aggregate effect.....	214
Table 7.24 - Vulnerability index form for Y direction.....	215
Table 7.25 - Summary of the calculated vulnerability index (Iv) and the obtained maximum capacity for all the numerical models in both main X and Y directions.....	216
Table 7.26 - Tentative values of relative frequencies of instances for considered structural attributes in a subset of numerical models from the <i>Eixample</i> district based on expert judgement: a) material properties; b) horizontal diaphragms; c) façade openings; d) wall thickness; and e) presence of patios	221
Table 7.27 - Tentative evaluation of the frequencies of the assumed subset of numerical models based on expert judgement	221
Table 7.28 - S Weighted means S_d, d_s^* of spectral displacements for each damage threshold	222
Table 7.29 - Probability distribution of the expected damage states when fixing a 50% probability for each damage state: (1) slight, (2) moderate, (3) extensive and (4) complete, according to Giovinazzi (2005).	222

Table 7.30 - Parameters characterising the fragility curves for the selected subset of numerical models of the existing URM buildings223

Table 7.31 - Damage probability matrix for URM existing building in *Eixample* district for the performance point (P.P.) obtained for a probabilistic hazard scenario for the city of Barcelona.224

Table 7.32 - Summary information of the buildings' characteristics of the studied urban block (the buildings highlighted in grey are not evaluated) (Rago 2022).....229

Table 7.33 - Vulnerability index calculated for X and Y direction for the existing buildings from the specific urban block, with and without the aggregate effect.....230

Table B.1 - Values obtained of the shear properties of the floor system with timber beams after the proposed iterative procedure275

Table C.1 - Summary information of the characteristics of the SDOF systems of all the numerical models and the spectral displacements (P.P.) obtained with the application of the N2 method for both deterministic and probabilistic spectra.278

LIST OF SYMBOLS

R	Seismic risk
H	Hazard
V	Vulnerability
E	Exposure of the elements at risk
I_v	Seismic vulnerability index
V_{Imin}	Upper bound of the final vulnerability index value
V_{Imax}	Lower bound of the final vulnerability index value
V_I^-	Lower bound of the uncertainty range for the specific building type
V_I^+	Upper bound of the uncertainty range for the specific building type
$C_{v,i}$	Class scores
w_i	Weights to the vulnerability parameters
μ_D	Mean damage grade
d	Damage factor
I	Seismic intensity
Q	Ductility factor
$f(V, I)$	Function of the vulnerability and macroseismic intensity
P_k	Probability of a specific damage grade
D_k	Damage grade
$m-IPA$	Mass proportional
ϕ_i-IPA	i^{th} mode proportional
$\phi_i m-IPA$	i^{th} mode by mass distribution proportional
D_y	Displacements for the yield point
a_y	Accelerations for the yield point
D_u	Ultimate displacements
a_u	Ultimate accelerations
f_b	Bricks compressive strength
f_m	Mortar compressive strength
f_d	Compressive strength
E	Young's modulus
ν	Poisson's coefficients
L	Width of the floor slab
ΔL	Average change in width of the floor slab
H	Length of the floor slab
ΔH	Average change in length of the floor slab
t	Thickness of the floor slab
Δt	Average change in thickness of the floor slab
G	Shear modulus
$\delta_1-\delta_2$	Relative displacements of the floors
F_{bu}	Maximum capacity of the building (MDOF system)
F^*_{bu}	Maximum shear strength of the SDOF system
d^*_u	Ultimate displacement of the SDOF system
F^*	Forces of the equivalent SDOF system

d^*	Displacements of the equivalent SDOF system
F_b	Base shear force of the MDOF system
d_c	Control node displacement of the MDOF system
Γ	Modal participation factor
m_i	Mass of node i
Φ_i	Normalised displacement shape
F_{cr}^*	Cracking shear force of the SDOF system
k_e^*	Initial slope of the idealised bilinear curve - elastic stiffness
k_{cr}^*	Secant stiffness of the structure obtained for the first cracking
F_y^*	Yield strength of the SDOF system
d_y^*	Yield displacement of the SDOF system
A^*	Area below the idealised bilinear capacity curve
T^*	Elastic period of the equivalent SDOF system
m^*	Normalised mass of the SDOF system
k^*	Stiffness of the SDOF system
q^*	Ratio between the force of the elastic response and the yield force of the equivalent system
p_v	Verification plane
C_i	Seismic coefficient for X or Y direction
T_{uX}	Shear stress of the walls in the X direction
T_{uY}	Shear stress of the walls in the y direction
W_{pv}	Weight of the building at the verification plane
W_p	Total weight of the building above the verification plane
A_x	Total resistant area of the walls in the X direction
A_y	Total resistant area of the walls in the Y direction
τ_k	Specific shear resistance of the masonry
σ_0	Average normal stress
N	Number of floors
A_t	Average total floor area
h	Average inter-storey height of the floors
ρ_m	Average specific weight of the masonry
ρ_s	Average permanent load of the floors
C_{vi}	Vulnerability classes
w_i	Weights of the vulnerability parameters
$MC(g)_i$	Maximum capacity for each numerical model
$MC(g)_{max}$	Maximum value of the maximum capacities
A	Pairwise comparison matrix
w	Principal eigenvector values
λ_{max}	Principal eigenvalue of the pairwise comparison matrix
n	Number of analysed parameters for the AHP
$MC_{min}(g)$	Minimum value of the maximum capacities
$MC_{max}(g)$	Maximum value of the maximum capacities
$MC_{avg}(g)$	Average value of the maximum capacities
$MC_{mean}(g)$	Mean value of the average values of the maximum capacities
Φ	Standard normal cumulative distribution function

$\overline{S_{d,ds}}$	Median value of spectral displacements for a certain damage state ds
β_{ds}	Standard deviation of the natural logarithm of the spectral displacement of a <i>damage state</i>
β_C	lognormal standard deviation parameter that describes the variability of the capacity curve
β_D	lognormal standard deviation parameter that describes the variability of the demand spectrum
$\beta_{M(Sds)}$	lognormal standard deviation parameter that describes the uncertainty in the estimate of the median value of the threshold of the structural damage state
$\overline{S_{d,ds}^*}$	Weighted mean value of spectral displacements
$\rho_\beta(x)$	Beta probability distribution
a	Parameter of the beta distribution
b	Parameter of the beta distribution
t	Parameter of the beta distribution
r	Parameter representing a function between t and μ_D
D_k	Damage state
S_{d1}	Damage limit state 1
S_{d2}	Damage limit state 2
S_{d3}	Damage limit state 3
S_{d4}	Damage limit state 4

LIST OF ACRONYMS

URM	Unreinforced Masonry
VIM	Vulnerability Index Method
FEM	Finite Element Method
AHP	Analytical Hierarchy Process
PGA	Peak Ground Acceleration
DSHA	Deterministic Seismic Hazard Assessment
PSHA	Probabilistic Seismic Hazard Assessment
DPM	Damage Probability Matrices
GNDT	Gruppo Nazionale Difesa Terremoti
MCS	Mercalli-Cancani-Sieberg scale
MMI	Modified Mercalli scale
ATC	Applied Technology Council
EMS	European Macroseismic Scale
CSM	Capacity Spectrum Method
HAZUS	Hazard United States
NDOF	Number of Degrees of Freedom
DOF	Degree of Freedom
RC	Reinforced Concrete
EFM	Equivalent Frame Method
SVIVA	Seismic Vulnerability Index for Vernacular Architecture
SAVVAS	Seismic Assessment of the Vulnerability of Vernacular Architecture Structures
MPA	Multi-mode or Modal Pushover Analysis
APA	Adaptive Pushover Analysis
NDA	Nonlinear Dynamic Analysis
MDO	Multi Degree of Freedom
FEMA	Federal Emergency Management Agency
PAGER	Prompt Assessment of Global Earthquakes for Response
GEM	Global Earthquake Model
SYNER-G	Systematic Seismic Vulnerability and Risk Analysis for Buildings, Lifeline Networks and Infrastructure Safety Gain
FRM	Force Resisting Mechanism
FRMM	Force Resisting Mechanism Material
P	Plan regularity
E	Elevation regularity
C	Cladding
D	Detailing
FS	Floor System
RS	Roof System
H	Height level
CL	Code Level
ICC	Cartographic Institute of Catalonia
ADRS	Acceleration Displacement Response Spectra

VI	Vulnerability Index
GIS	Geographic Information System
MDT	Minor Destructive Technique
DPT	Double Punch Test
FE	Finite Element
UPC	Polytechnic University of Catalonia
PP	Performance Point
AHP	Analytical Hierarchy Process
MC	Maximum Capacity
CI	Consistency Index
RI	Random Consistency Index
PGV	Peak Ground Velocity
PDF	Probability Distribution Function

CHAPTER 1. INTRODUCTION

1.1. BACKGROUND AND MOTIVATION

Seismic events are one of the most destructive natural disasters known to humankind. During the last decades, major earthquakes have resulted in devastating human, structural and economic losses. In recent times, many regions around the world have been affected by high intensity earthquakes, such as Turkey and Syria in 2023, Afghanistan in 2022, Haiti in 2021, Albania in 2019, Indonesia in 2018, and Italy (in 2016, 2012 and 2009). The damage caused by earthquakes depends not only on the seismic hazard, but also on the vulnerability of the existing buildings and their exposure. As a result, seismic risk management strategies, aimed to increase the resilience of affected cities or regions, need to effectively integrate and consider the interaction among seismic hazard, structural vulnerability, and exposure. In this frame, the seismic vulnerability of existing buildings is associated with the probability of attaining a certain level of damage when subjected to a seismic event.

The majority of ancient historical centres and urban areas of European cities, as well as all over the world, consists mostly of load-bearing walls made of brick or stone masonry. Due to their significant contribution to the urban landscape and the identity of towns and cities, many of these buildings, and even those that are not officially recognised as cultural heritage, have unquestionable cultural and architectural value. Nevertheless, the seismic performance of such buildings is often unsatisfactory due to their peculiar constructive and structural features. Many existing unreinforced masonry (URM) buildings were often designed without considering any seismic design requirements, which may result in significant vulnerability even to moderate earthquakes.

Many geometrical and structural features can contribute to the seismic vulnerability of a typical URM building. Among these possible features are the material's limited resistant capacity and ductility, the buildings' height, the presence of very slender load-bearing walls, the irregular plan distribution, the vertical irregularity, the in-plane flexibility of the floor slabs, and the lack of efficient connections between the walls and the horizontal elements (Ortega, Saloustros and Roca 2021; Piazza, Baldessari, and Tomasi 2008). Existing URM structures are amongst the most vulnerable buildings in case of seismic events (Alex H. Barbat et al., 2008; Basaglia et al., 2020; Pujades et al., 2012; Stepinac et al., 2021). The 2011 earthquake in Lorca, Spain, revealed the buildings' high vulnerability through the significant damage caused to both residential buildings and architectural heritage.

Over the last few decades, the increasing interest in the study of the seismic risk in urban areas has resulted in various seismic vulnerability assessment methodologies. The application field of such methodologies ranges from individual buildings to large scale urban or geographical areas. The selection of the appropriate approach for seismic vulnerability assessment is determined by

several factors, including the purpose and nature of the study, the amount of data and resources available, the investigated different building typologies, the level of computational effort, and the cost required for the studies. Seismic vulnerability methods are classified into empirical, expert-judgment, analytical, and hybrid ones. On one hand, the empirical (indirect) and expert-judgment methods are based on the observation of damage after seismic events. They can be used to quickly and easily analyse seismic vulnerability at regional or urban scale. On the other hand, analytical (direct) methods employ sophisticated structural analyses. The hybrid methods combine the use of the previously mentioned methods, i.e. they combine empirically obtained data on post-earthquake damage with analytical results obtained from numerical modelling.

The scientific literature currently offers a variety of methods for assessing seismic vulnerability on a large scale (Kassem et al., 2020). The Vulnerability Index Method (VIM), originally proposed in Italy (Benedetti and Petrini, 1984; GNDT, 1986), has been widely used for assessing the seismic vulnerability of various types of masonry structures at large scale. This method evaluates a vulnerability index for individual buildings as a weighted sum of the most significant parameters influencing on the structure's seismic response and vulnerability. Each parameter is classified into four classes of increasing vulnerability (from A to D) with a relative score and specific weight, according to its overall influence on the seismic global behaviour. The scores and weights are assumed based on expert opinion evaluations of the observed damage after a past earthquake.

It must be noted, however, that in its original version, the VIM was based on the study of the effects on buildings of earthquakes occurred in Italy. Therefore, its accuracy could decrease when applied to structures with different structural features located in other geographical regions. The application of the method on different geographical regions, characterised by different building typologies, may require previous specific calibration or adaptation. Several authors have adapted the VIM method by changing or adding some parameters and/or by modifying the scores and weights in order to apply it to specific urban areas or regions (Basaglia et al., 2018; Ferreira et al., 2014; Ferreira et al., 2020; Formisano et al., 2015; Jiménez et al., 2021; Ortega et al., 2019; Palazzi et al., 2022; Vicente et al., 2011). Typically, the VIM has been used by associating it with macroseismic methods to estimate the degree of damage resulting from an earthquake of a certain intensity (Giovinazzi and Lagomarsino, 2004).

The calibration of the VIM can be done based on a large amount of data derived from post-earthquake surveys on damaged buildings. However, such data may not be available in many regions and cities due to different reasons. In specific, data on post-earthquake damage may be unavailable in regions subjected to low to moderate seismic hazard with no major earthquakes having occurred for long historical time. In these cases, numerical modelling and simulation may contribute successfully to predict seismic damage and therefore to evaluate the seismic vulnerability.

The seismic behaviour of individual buildings can be evaluated realistically by means of nonlinear static or dynamic analysis using advanced numerical models. However, a large-scale vulnerability analysis involving many buildings (as for large building aggregates of urban centres) is at the moment unfeasible due to the unaffordable computational effort it would require. Nevertheless, the application of vulnerability analysis at large scale can be made possible by adopting a hybrid approach and therefore combining available experience and observations with numerical analyses. The creation of a comprehensive building taxonomy of the common structural

typologies in a specific urban centre can help to identify the most representative building typologies and their possible sources of vulnerability. In the frame of a numerical or hybrid approach, the initial activity can optimise the number of detailed numerical models to be analysed. The Finite Element Method (FEM) can provide an acceptable approach for the numerical simulation of the seismic performance of masonry buildings through a nonlinear static (pushover) analysis. Furthermore, parametric analysis can be performed in order to evaluate their influence of different geometrical, mechanical and structural parameters on the seismic performance and vulnerability.

Several challenges have to be overcome in order to propose a seismic vulnerability assessment method for masonry buildings with specific characteristics. First, establishing a building taxonomy, which properly categorises the different structural typologies found in a specific urban area, is essential in order to identify the structural attributes and constructive characteristics relevant to their seismic behaviour. The second challenge is the identification of the most representative building typologies based on a statistical data evaluation. Identifying such representative buildings is necessary in order to limit the scope of the numerical simulation. A third challenge is found in the selection and application of a both efficient and realistic computational technique for the analysis of the seismic performance. The last challenge consists in calibrating the VIM by using the results obtained from the numerical simulations.

The aforementioned issues and challenges establish the main motivation of this doctoral thesis. This research will contribute to the current approaches on the study of seismic risk and vulnerability through the derivation of a general methodology, intensively based on numerical simulation, for the analysis of the seismic vulnerability of the masonry buildings of the *Eixample* district of Barcelona.

1.2. SCOPE AND OBJECTIVES

1.2.1. General objective

The present research aims to contribute to the seismic vulnerability assessment of the masonry buildings of the *Eixample* district of Barcelona. This aim faces two important challenges. On one hand, there is a lack of seismic damage observations that could be used as a database for the calibration of available seismic vulnerability assessment methods. Such lack of data is a consequence of the low to moderate seismic hazard experienced by the geographical zone investigated. On the other hand, the buildings of the *Eixample* district present very specific constructive and structural features (such as very slender load-bearing walls), some of which may confer a high seismic vulnerability level to them. In the present research, both challenges are addressed by resorting to an intensive use of numerical modelling and simulation as a way to obtain realistic predictions of the seismic performance and, specifically, of the expected damage and capacity.

The general approach developed for the study of the masonry buildings of the *Eixample* district can be regarded as a general methodology, strongly based on the possibilities of computational analysis, which could be applied, with the necessary modifications, to similar problems concerning seismic vulnerability assessment of historical urban centres in low to moderate seismic regions.

1.2.2. Specific objectives

The following specific objectives are going to be pursued in the doctoral thesis:

- Carrying out a critical review of the previous proposed methodologies and techniques for seismic risk assessment. In specific, investigating their merits and drawbacks regarding their application to different building typologies in urban centres. Analysing the differences and limitations of the methods proposed for the seismic vulnerability evaluation of buildings.
- Providing a building taxonomy to describe and classify the different structural typologies of the masonry buildings in the *Eixample* district. The taxonomy should categorise the buildings according to the structural attributes that are relevant for their seismic performance and vulnerability. Elaborating such taxonomy is an important first step for the later selection and analysis of the most representative building types.
- Selecting a numerical approach for the accurate modelling and simulation of the seismic performance of complex masonry load-bearing wall buildings. The approach selected should provide an optimal compromise between accuracy and computational cost. Numerically simulating and characterising the seismic response of the set of buildings chosen as representative building types. Systematically using numerical simulation for the characterisation of seismic capacity, damage and collapsing mechanisms.
- Adapting available methods (empirical and analytical) for the seismic vulnerability assessment for their application to the case of the masonry buildings of the *Eixample* district. In specific, and taking into consideration the features of the buildings in *Eixample*, the adapted methods must consider the case of buildings consisting of slender load bearing walls and the case of hybrid systems with load bearing walls supported on steel elements at the ground floors. One of the main features of the adapted methods will be the possibility of calibrating their parameters based on the damage predicted through numerical simulation instead of observed damage.

The following tasks have been considered in order to attain the mentioned specific objectives:

- Critical review of the state-of-the-art by carrying out a detailed study of the relevant scientific literature and by keeping abreast with all the novelties on seismic risk analysis and vulnerability assessment methodologies.
- Studying all structural features, at the level of structural elements and general structural organisation, of the representative buildings from the *Eixample* district. In specific, evaluating the ranges of the mechanical properties of their structural materials that compose by analysing the results of previous experimental campaigns.
- Elaborating a detailed building taxonomy of the masonry buildings of the *Eixample* district according to the geometrical, material and structural characteristics relevant for their seismic performance. Among the relevant attributes considered are the construction date, the seismic design level, the general geometry, the material properties, the lateral load-resisting system, the structural irregularities and the type of horizontal diaphragms.

- Based on the abovementioned building taxonomy, selecting the representative buildings on which to carry out numerical modelling and seismic analysis.
- Developing 3D detailed numerical models of the representative buildings by using an efficient and realistic simulation of the seismic response of the masonry structures based on the Finite Element Method. For that purpose, two reference models are elaborated corresponding to two different structural systems: the homogeneous system with slender URM walls and a hybrid one involving a combination of steel members at the ground floor and unreinforced masonry walls on the upper floor levels.
- Developing an accurate approach for the modelling of the typical jack-arch floors existing in the buildings of the *Eixample*. The approach is based on the modelling of the floor slabs as equivalent orthotropic solid slabs. Using this approach, modelling and incorporation of the floor slabs as flexible diaphragms in the building numerical models and studying their influence on their seismic response.
- Derivation of capacity curves using non-linear static (pushover) analyses along two main building directions (parallel and perpendicular to the façades) in order to simulate the stiffness and damage at different load levels, the failure mechanisms and the seismic capacity of the representative buildings. Carrying out detailed parametric analysis to investigate the influence of different material, geometrical and structural parameters on the building's seismic performance.
- Developing a methodology for seismic vulnerability assessment at urban level adapted to the case of the masonry buildings of the *Eixample* district. Proposal and calibration of new forms based on the Vulnerability Index Method. The forms will implement specific vulnerability parameters relevant for their seismic behaviour of the buildings analysed. Comparison between the vulnerability index calculated with the forms and the maximum capacity derived from the numerical analysis as a way to obtain an initial validation of the capacity for the proposed forms to characterize the seismic vulnerability.
- Tentative application of the proposed methodology to the *Eixample* district, by estimating the vulnerability of a sample of existing masonry buildings,

1.3. OUTLINE AND ORGANISATION OF THE THESIS

The thesis is organised in eight chapters. After the introductory chapter presenting the motivation and objectives, Chapter 2 reviews the state of the art on large-scale seismic risk assessment, including a literature study focusing on seismic vulnerability assessment methods for URM buildings and, in particular, on those aimed at large-scale urban assessment, such as the Vulnerability Index Method. The advantages and limitations of various methods are highlighted. Chapter 2 also provides an overview of the numerical simulation techniques for modelling masonry structures.

Chapter 3 includes a brief overview on the historic evolution of Barcelona city and in particular of the *Eixample* district. The geometrical and structural morphology of the case study is assessed through the knowledge of the historical background, the analyses of the materials used for the

construction of the buildings, and the study of urban organisation. Finally, the chapter presents a review on previous research studies done regarding the seismic vulnerability assessment and seismic performance of the existing typical buildings of *Eixample* district.

Chapter 4 presents a detailed building taxonomy prepared for the most representative masonry buildings of the *Eixample* district. This tool allows the classification of the different construction types according to their attributes (materials, properties, geometries, etc.), as well as the main types of heterogeneities, singularities and sources of seismic vulnerability. The detailed definition of a catalogue reporting different classes of masonry buildings characterised by similar parameters, and thus similar seismic behaviour, is essential for the definition of the proposed methodology for the seismic vulnerability assessment of historical urban centres. The methodology adopted for selection of representative buildings considers statistical data extrapolation of the buildings' structural features.

Chapter 5 describes the numerical models elaborated to describe the representative buildings of the *Eixample* district. The Finite Element Method has been used for the numerical simulation with proper material properties. Different numerical models have been prepared representing the different structural configurations and features that can influence the buildings' seismic global behaviour.

Chapter 6 presents the seismic analyses performed on the existing masonry buildings. Capacity curves using non-linear static (pushover) analyses for both main directions (parallel and perpendicular to the façades) have been derived in order to understand the typical failure mechanisms and the seismic capacity of the representative building typologies. The chapter presents a detailed discussion of the damage patterns and collapse mechanisms derived from the FEM models. The seismic performance of the buildings is estimated by applying the N2 Method and considering two seismic scenarios, i.e. deterministic and probabilistic.

Chapter 7 presents the adopted methodology for the assessment of the seismic vulnerability and the evaluation of the seismic risk at urban scale of existing masonry buildings. An adapted VIM form is provided for the seismic vulnerability assessment of the different building typologies at the urban scale. The definition of new seismic vulnerability classes is based on a parametric analysis oriented to obtain a better understanding of the influence of each of the parameters in the numerical model. The Analytical Hierarchy Process (AHP) has been used for the definition of the weights according to the variation of the maximum capacity of the specific numerical models for each VIM parameter. Finally, the developed procedure is applied and calibrated for the case study of the *Eixample* district. The vulnerability index and damage grades have been evaluated with the aim of plotting fragility curves considering the seismic hazard of the Catalonia region.

The final chapter provides an extended summary of the research work done, including the main contributions, findings and final conclusions reached. It also includes suggestions and recommendations for future improvements to the approach and the seismic vulnerability assessment method.

1.4. RESEARCH DISSEMINATION

The research included in this thesis has resulted in the following scientific publications at the moment of submission of the PhD thesis:

Articles in peer-reviewed international journals:

- Dimovska, S., Saloustros, S., Pelà, L., and Roca, P. (2022). Modelling of in-plane seismic behaviour of one-way steel or timber jack arch floors in existing buildings. Application to the *Eixample* district of Barcelona. *Engineering Structures*, 262, 114343. <https://doi.org/10.1016/j.engstruct.2022.114343>
- Marafini, F., Dimovska, S., Saloustros, S., Cornadó, C., and Roca, P. (2022). Historical Development and Seismic Performance of Unreinforced Masonry Buildings with Vertical Extensions in the City Centre of Barcelona. *International Journal of Architectural Heritage*, 00(00), 1–24. <https://doi.org/10.1080/15583058.2022.2096513>

Articles and presentations in international conferences:

- Dimovska, S., Saloustros, S., Pelà, L., and Roca, P. (2021). Seismic vulnerability assessment of representative building typologies from Barcelona's *Eixample* district. In P. Roca, L. Pelà, and C. Molins (Eds.), *Int. Conf. Struct. Anal. Hist. Constr., International Centre for Numerical Methods in Engineering*. CIMNE. <http://hdl.handle.net/2117/341820>
- Dimovska, S., Saloustros, S., Pelà, L., and Roca, P. (2022). Seismic performance of typical hybrid buildings in the urban centre of Barcelona. *9th Euro-American Congress REHABEND 2022-Construction Pathology, Rehabilitation Technology and Heritage Management, Granada, Spain*, 1122–1129. <http://hdl.handle.net/2117/372341>

CHAPTER 2. LITERATURE REVIEW

2.1. INTRODUCTION

Over the past few years, the research community has paid large attention to urban seismic risk assessment. The main objective of the vulnerability assessment methods is to indicate the likelihood of a damage level for a particular building typology as a result of a seismic event. Seismic risk models for large-scale assessment include various phases of analysis aimed at understanding and determining the vulnerability of the exposed area and elements at risk. A proper seismic risk assessment model is required in order to develop multiple risk studies, which include such aspects as calculating the socioeconomic effects of an earthquake, estimating the cost of repairs, and proposing strengthening solutions for the most vulnerable buildings in the studied urban area. It is a crucial tool for further seismic risk mitigation, for preparing different mitigation strategies, emergency management plans, reducing the seismic risk and enhancing the resilience of the city.

Assessing the vulnerability of existing buildings at the urban scale is a challenging task as it requires a global understanding of a wide range of building typologies with specific structural characteristics. This is a very complex study requiring a great time consumption, and thus, some simplified methodologies are needed. In order to be able to develop an improved methodology vulnerability assessment of an urban centre, a good understanding of the seismic risk analysis and available vulnerability assessment methodologies is needed.

This chapter provides an overview of the seismic vulnerability assessment methods that are frequently used in the estimation of possible effects of large earthquakes in populated areas. The fundamental ideas involved in seismic risk models are provided, followed by a comprehensive overview of the available methodologies established to address the challenge of risk estimation in large-scale applications. The concept of vulnerability assessment is then introduced, along with the development of the methodologies already in use for this purpose. In particular, the advancement of the Vulnerability Index Method (VIM) and the macroseismic vulnerability method towards hybrid techniques that include numerical evaluation are emphasised. Section 2.4 discusses the current numerical approaches for the evaluation of the seismic performance of masonry structures. Section 2.5 presents the seismic analysis methods for masonry buildings, such as the nonlinear static and dynamic analyses. Finally, a review of the existing building taxonomy approaches is presented, as a key step for the methodology of seismic vulnerability assessment in urban centres.

2.2. SEISMIC RISK ANALYSIS

Seismic risk assessment is a crucial step in the process for the risk mitigation and resilience enhancement of urban areas. Hence, it demands vulnerability assessment and damage evaluation

at the territorial scale in order to address earthquake emergency management and protection of the population, different existing structures, infrastructure, and built cultural heritage. The evaluation of the seismic risk of urban areas is associated to the level of seismic hazard of the region, building vulnerability and level of exposure.

Seismic risk analyses are performed in order to estimate and characterise the effects that a specific set of seismic events will have on a given geographic area (an urban area, city, or a region) over the duration of a specific time period. In particular, the consequences that must be anticipated include the number of fatalities, the damage of structures and infrastructure, financial losses due to direct and indirect economic effects, the loss of functionality of lifelines and essential facilities, known as social, economic and environmental effects (Giovinazzi, 2005).

Previous research studies have defined the principal concepts associated with the seismic risk analysis. The term "risk" is closely related to the anticipated number of lives lost, people injured, damage to property, and disruption of economic activity as results of a natural catastrophe, according to the Natural Disasters and Vulnerability Analysis report (UNDRO 1979). According to the glossary developed by the EERI Committee (1986), the seismic risk is defined as the likelihood that the social or economic consequences of earthquakes will exceed specified values at a single location, multiple locations, or an area during a specified exposure time.

According to past studies, such as those by Caicedo et al. (1994), Cardona (2001), Coburn and Spence (2002), McGuire (2004) and Barbat et al. (2010), absolute risk can be expressed as the result of a mathematical convolution between hazard, vulnerability and exposure. This concept can be expressed by mean of the following equation (2.1):

$$R_i = (H_i \times V_e) \times E \quad (2.1)$$

where R_i is the probability of exceeding a certain level of loss in an exposed element e , as a consequence of a seismic event of intensity i ; H is the probability of exceeding a certain level of seismic activity with intensity i ; V is vulnerability, defined as the intrinsic predisposition of an element to suffer damage from a seismic event of intensity i , and E is the exposure of the elements at risk, reflecting the value of the exposed elements.

The seismic risk (R) can be defined as a function of the hazard (H), vulnerability (V) and exposure (E) of elements at risk in specific region or city (Figure 2.1). The following definitions can be given for each of the quantities that are involved in the risk definition (EERI Committee, 1986):

Hazard is an external risk factor which can be expressed as the probability of occurrence of any physical phenomenon (e.g. ground shaking, ground failure) associated with an earthquake in a given area and in a certain time interval. It may produce severe adverse effects, by exceeding a certain threshold of intensity, magnitude or peak ground acceleration (PGA). The seismic hazard depends on the characteristics of a seismic event and the geological characteristics of the area where the event is manifested.

Vulnerability is defined as the degree of loss to a given element at risk (or set of elements) resulting from a given level of seismic hazard (earthquake of a given magnitude or intensity). The vulnerability expresses the probability that a structure of a certain type may suffer a certain level of damage when subjected to a seismic event of defined intensity.

Finally, the *Exposure* is the potential of economic loss to all or a certain subset of structures as a result of one or more earthquakes in an area. It is related to the elements at risk such as people, buildings, infrastructures or other systems, which can be subjected to potential losses nature, influenced directly or indirectly by a seismic event. This term evaluates the presence of assets in risk and therefore the possibility of damage (physical damage, casualties, economic damage).

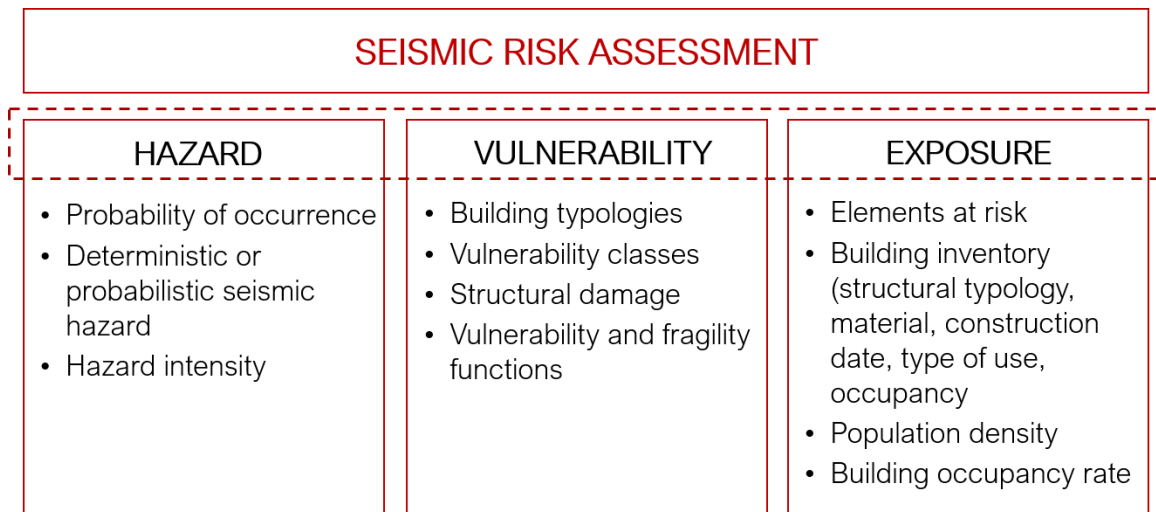


Figure 2.1 - Seismic risk assessment definition.

The first step in seismic risk assessment is to identify the hazard of the studied region or area. The seismic hazard represents the amount of ground motion that can be predicted in a certain area as a result of a seismic event. This includes an evaluation of the region's seismic activity, the likelihood of an earthquake occurring, and the magnitude and intensity of the earthquake. This data can be gathered from previous seismic activity in the area as well as from geological surveys. Two widely accepted approaches can be used in order to evaluate the seismic hazard: Deterministic Seismic Hazard Assessment (DSHA) and Probabilistic Seismic Hazard Assessment (PSHA). These analyses are valid for the seismic hazard assessment of both local or regional areas. The deterministic approach assumes that historical seismicity provides sufficient information to know the seismic hazard evaluation of the region. On the contrary, the probabilistic approach uses the seismicity and seismotectonics of a region to obtain seismic hazard associated to a certain probability of occurrence (Irizzary, 2004). The information required for the ground motion assessment is the same for both methods. Firstly, the potential sources must be identified and characterised in terms of location, geometry, activity, and potential energy and, secondly, the propagation of ground motion must be represented by a suitable predictive relationship considering the morphological and geological amplification effects (referred as site effects) (Giovinazzi, 2005). Seismic microzonation is another method for representing the hazard, as the process of dividing a potentially seismically prone region into zones with comparable geological and geophysical characteristics. It is typically based on dynamic soil characterisation by monitoring or recording ground acceleration amplitudes. These characteristics are frequently mapped into a grid of the study area that is closely spaced and divides the sub-areas into categories based on the main hazard (Gupta, 2002).

The next step in seismic risk assessment is to assess the vulnerability of an area. This involves an analysis of the physical characteristics of an area, such as the type of soil, the depth and quality

of foundation, and the type of buildings located in the area. This information can be obtained from data records, field surveys and inspections. The vulnerability assessment helps to determine the potential damage that could be caused by a possible earthquake. Subsequently, the exposed area is a very important element for the seismic risk assessment. This involves an analysis of the elements at risk such as population, buildings and other assets that could be affected by the seismic event. This information can be obtained from public census data, business directories, and public infrastructure records.

2.3. SEISMIC VULNERABILITY ASSESSMENT

The primary objective of the vulnerability assessment methods is to provide the likelihood of a damage level for a particular building typology as a result of a seismic event. In general, the seismic vulnerability of buildings can be assessed by doing an inspection of existing structures, using analytical numerical models, or laboratory experiments. It is necessary to distinguish between observed vulnerability, which is obtained from post-earthquake damage observation and statistical analysis from some defined structural typology, and calculated vulnerability, which is obtained from numerical analysis models or experimental laboratory models (Herrera et al., 2013). The choice of a seismic vulnerability assessment methodology should consider the nature, function, and structural typology of the buildings to be assessed, as well as the scale of the assessment (single building or urban areas).

2.3.1. Seismic vulnerability methods

Several vulnerability assessment methods have been developed and proposed in the past few years. In the literature, different classifications for the available seismic vulnerability methods designed for various types of analysis with different objectives are provided (Calvi et al., 2006; Corsanego and Petrini, 1994; Dolce et al., 1994; Herrera et al., 2013; Panagiotis and Vagelis, 2015; Pitilakis et al., 2014). Therefore, a detailed review of all the methodologies proposed and their categorisation for the vulnerability assessment will be done in the following sections, including a discussion differences and limitations of the methods are presented.

Seismic vulnerability methods can also be classified based on the scope of the study, the level of detail and the required input data (Vicente, 2008). First-level approaches rely on qualitative inputs with a limited number of parameters such as the building type, construction age and height, which can be easily obtained through an inspection. They are especially well suited for large-scale vulnerability assessments. Second-level approaches necessitate more detailed information about the geometrical configuration and structural features, as well as material properties of the analysed buildings. Third-level approaches include sophisticated analytical procedures and require detailed data collection for modelling of individual buildings. Hence, these approaches are not practical for large-scale assessments due to their high computational time and cost.

Figure 2.2 illustrates the different methods for the seismic vulnerability assessment, which can differ based on the on the approach adopted to obtain information, the level of application and computational effort depending on the available data and technology (Lang, 2002).

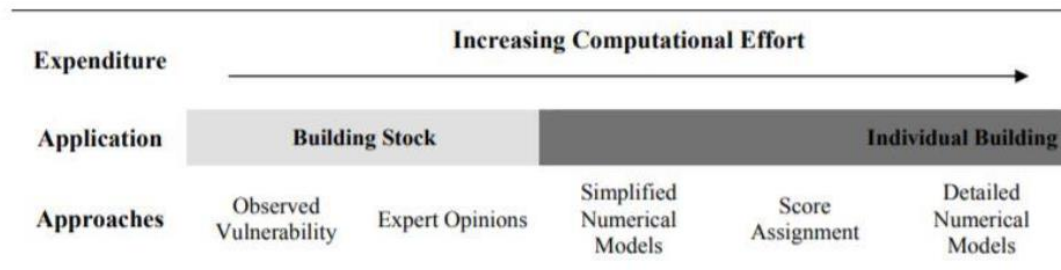


Figure 2.2 - Graphical scheme for the different seismic vulnerability assessment methods (Lang, 2002).

The methods used for the seismic vulnerability assessment can be classified as: a) empirical approaches (also known as observed vulnerability methods methods), which are based on statistical observations of recorded damage data from previous seismic events as a function of their intensity; b) expert judgement methods based on experts' opinions; c) analytical methods, which are based on mechanical calculations of the structure's seismic response; and d) hybrid methods as a combination between the previously discussed methods. It should be noted that some authors consider the empirical and expert-judgment methods in one category since they share similarities and can complement each other.

2.3.1.1. Empirical methods

The most common and simplest of the vulnerability assessment methods is the empirical approach, also known as observed vulnerability methods. They are based primarily on collected data from post-earthquake damage observation. According to Calvi et al. (2006), these methods provide a correlation between the observed damage on different building typologies and a given ground motion intensity in a macro seismic scale. In the literature, different types of correlations can be used such as the damage probability matrices (DPM) and vulnerability functions, both based on observed damage after earthquakes. The DPM are formulated in a discrete form by expressing the probability that a specific structural typology has of reaching a given damage state as a result of a ground motion intensity. Whitman et al (1973) were among the first to generate DPM of various building types based on a damage survey from 1600 reinforced concrete buildings caused by the San Fernando earthquake that struck on February 9, 1971. Table 2.1 presents the basic format of the proposed damage probability matrix. Each number in the matrix indicates the probability that a building of a specific class will survive a certain level of damage as a result of certain earthquake intensity (Whitman et al., 1973).

Table 2.1 - Damage Probability Matrix proposed by Whitman et al (1973).

Damage State	Structural Damage	Non-structural Damage	Damage Ratio (%)	Intensity of Earthquake				
				V	VI	VII	VIII	IX
0	None	None	0-0.05	10.4	-	-	-	-
1	None	Minor	0.05-0.3	16.4	0.5	-	-	-
2	None	Localised	0.3-1.25	40.0	22.5	-	-	-
3	Not noticeable	Widespread	1.25-3.5	20.0	30.0	2.7	-	-
4	Minor	Substantial	3.5-4.5	13.2	47.1	92.3	58.8	14.7
5	Substantial	Extensive	7.5-20	-	0.2	5.0	41.2	83.0
6	Major	Nearly total	20-65	-	-	-	-	2.3
7	Building condemned		100	-	-	-	-	-
8	Collapse		100	-	-	-	-	-

The DPM format has become widely used to define the likely distribution of damage, and it has been applied and adapted after different earthquakes. Corsanego and Petrini (1994) proposed the GNDT I level approach, which is an example of a DPM-based method, with three classes of vulnerability ranging from A to C, each with its own DPM. Furthermore, Braga, Dolce, and Liberatore (1982) used statistical data from the 1980 Irpinia earthquake in order to update the DPM approach for the European building stock. It should be noted that the GNDT damage probability matrix refers to Mercalli-Cancani-Sieberg (MCS) scale intensity rather than the Modified Mercalli (MMI), which was used in Whitman et al (1973).

Moreover, the vulnerability functions express the likelihood of exceeding a specific damage state by an earthquake of a given intensity (Calvi et al., 2006). Coburn and Spence (1992) proposed the use of vulnerability functions in order to describe the damage-ground motion relationship. They are based on information gathered during various case studies of earthquake damage from a variety of different countries, by considering five different damage grades. The scatter of the intensity at which each individual structure building exceeds a specific damage threshold is normally distributed for each building type. The damage distribution is graphically presented by the probability of exceeding a specific damage grade given the seismic input in terms of a parameter-less intensity scale (Giovinazzi, 2005).

In general, empirical methods are considered to be the most cost-effective ones for large scale assessments, even though they require a large set of post-earthquake damage data, which is not always available. Therefore, these methods are of relatively easy application, but are limited in accuracy, as the empirical collected data may not be relevant to the analysed building stock.

2.3.1.2. Expert judgment methods

The methods based on expert judgment are similar to the empirical methods, since they are based on empirical data collection. These methods were developed due to the lack of post-earthquake damage data for various building typologies and the high costs associated with analytical approaches. They are as well considered as indirect methods according to the classification proposed by Corsanego and Petrini (1994).

The Applied Technology Council (ATC 1985) introduced the first systematic attempt to provide a probability matrix based on expert judgement, which was summarised in the ATC-13 (1987) report. ATC-13 derived damage probability matrix for 36 different building classes in order to estimate the expected percentage of damage and loss for a specific structural type subjected to a given intensity.

The Italian National Group of Defense from Earthquakes (GNDT, 1993) provided the GNDT II level approach, known as Vulnerability Index Method (VIM), for the vulnerability assessment and damage estimation of existing masonry and reinforced concrete buildings, at large scale. This approach is based on calculating a seismic vulnerability index (I_v) by evaluating 11 different parameters as the most significant ones for the assessment of the possible seismic damage: structural system organisation, structural system quality, conventional strength, building position and foundations, horizontal diaphragms, plan configuration, configuration in elevation, maximum distance between walls, roof type, non-structural elements, and general maintenance conditions (see Table 2.5). The vulnerability curves used for the formulation of this vulnerability method were calibrated after data from the 1976 Friuli and 1984 Abruzzo earthquakes, in Italy (see Figure 2.3). The use of PGA to express the intensity of the ground motion allows using a continuous parameter instead of a discrete one, such as the macroseismic intensity. Following a visual inspection to identify the building's primary structural system and significant seismic structural features, a vulnerability index I_v is estimated for each individual building.

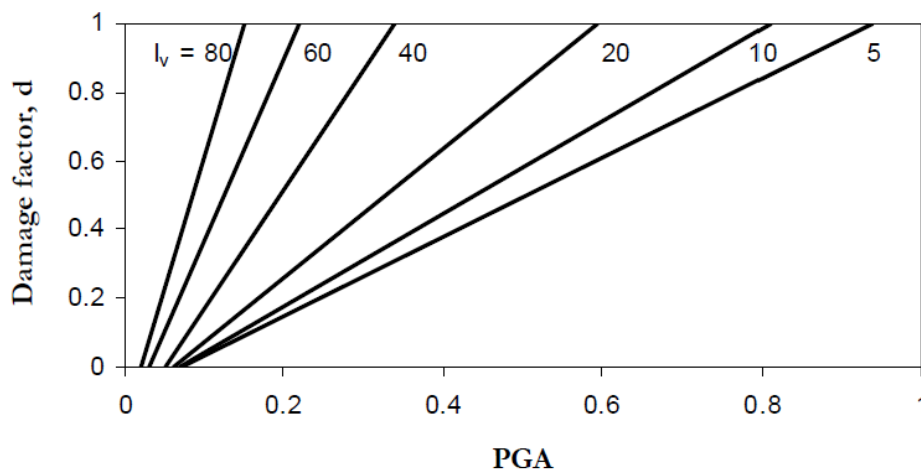


Figure 2.3 - Vulnerability functions relating the damage factor (d) and PGA for different vulnerability indexes (I_v) (Guagenti and Petrini, 1989).

Giovinazzi and Lagomarsino (2004) suggested a macroseismic method that allows for the definition of damage probability functions based on the European Macroseismic Scale (EMS-98) defined by Grünthal (1998). The EMS-98 scale establishes qualitative definitions of "Few," "Many," and "Most" for five damage grades for intensity levels spanning from V to XII for six distinct classes of vulnerability from A to F, being "A" the most vulnerable and "F" the least vulnerable class, based on expert judgment. Table 2.2 presents the EMS-98 vulnerability classes for different building typologies assigns based primarily on its structural typology and construction material. The connection between vulnerability class and building typology is essentially probabilistic, with the dominant class being explicated as most likely (referred to as "most likely vulnerability class") in comparison to the adjacent classes considered probable ("Probable") and less probable ("less

probable" or "exceptional"). Additionally, the EMS-98 scale provides a damage classification for masonry and reinforced concrete buildings individually, by including five seismic damage grades (D1, D2, D3, D4 and D5) from negligible/slight damage to complete destruction.

Table 2.2 - Vulnerability classes for different building typologies according to EMS-98 scale (Grünthal, 1998).

Type of structure		Vulnerability Class					
		A	B	C	D	E	F
MASONRY	rubble stone, fieldstone	○					
	adobe (earth brick)	○	—				
	simple stone	—	○				
	massive stone			—	○	—	
	unreinforced, with manufactured stone units	—	○	—			
	unreinforced, with RC floors			—	○	—	
	reinforced or confined				—	○	—
REINFORCED CONCRETE	frame without ERD (earthquake-resistant design)	—	—	○	—		
	frame with moderate level of ERD		—	—	○	—	
	frame with high level of ERD			—	—	○	—
	walls without ERD	—	○	—			
	walls with moderate level of ERD		—	—	○	—	
	wall with high level of ERD			—	—	○	—
STEEL	steel structures			—	—	○	—
WOOD	timber structures	—	—	○	—		

LEGEND:
 ○ most likely vulnerability class
 — probable range;
 --- range of less probable, exceptional cases

The macroseismic method was designed to address the EMS-98 DPM's problems of qualitative description and incompleteness. This approach makes use of probability theory, presuming a beta distribution for the possible damage in the existing buildings. The fuzzy set theory (Dubois and Parade, 1980), which mathematically explains the overlapping ranges of the linguistic definitions in terms of membership functions, is used to resolve the imprecision of the correlation between intensity and damage (Ortega, 2018). Moreover, a vulnerability index (V) was introduced, ranging from 0 to 1, which was initially based on the EMS-98 vulnerability classes table. Within the application of the fuzzy set theory, the vulnerability classes were converted into vulnerability indices on a numerical scale. Table 2.3 represents the attribution of the vulnerability classes and defines the values for the vulnerability index, where V_{Imin} and V_{Imax} correspond to the upper and lower bounds of the possible values of the final vulnerability index value, and V_I^- and V_I^+ , which were evaluated by a 0.5-cut of the membership function, represent the bounds of the uncertainty range of, for the specific building type. Moreover, the vulnerability index could be influenced by vulnerability modifier factors by considering specific characteristics of different building stock (Giovinazzi and Lagomarsino, 2004).

Table 2.3 - Attribution of vulnerability classes and vulnerability index values to different building typologies (Giovinazzi and Lagomarsino, 2004).

Typologies		Building type	Vulnerability Classes						Vulnerability Classes				
			A	B	C	D	E	F	V_{Imin}	V_I^-	V_I^+	V_I^+	V_{Imax}
Masonry	M1	Rubble stone	■	■					0.62	0.81	0.873	0.98	1.02
	M2	Adobe (earth bricks)	■	■					0.62	0.687	0.84	$0.98V_I^+$	1.02
	M3	Simple stone	■	■	■				0.46	0.65	0.74	0.83	1.02
	M4	Massive stone	■	■	■	■			0.3	0.49	0.616	0.793	0.86
	M5	Unreinforced M (old bricks)	■	■	■	■	■		0.46	0.65	0.74	0.83	1.02
	M6	Unreinforced M with r.c. floors	■	■	■	■	■	■	0.3	0.49	0.616	0.79	0.86
	M7	Reinforced or confined masonry	■	■	■	■	■	■	0.14	0.33	0.451	0.633	0.7
Reinforced concrete	RC1	Frame in r.c. (without E.R.D.)	■	■	■	■	■		0.3	0.49	0.644	0.8	1.02
	RC2	Frame in r.c. (moderate E.R.D.)	■	■	■	■	■	■	0.14	0.33	0.484	0.64	0.86
	RC3	Frame in r.c. (high E.R.D.)	■	■	■	■	■	■	-0.02	0.17	0.324	0.48	0.7
	RC4	Shear walls (without E.R.D.)	■	■	■	■	■	■	0.3	0.367	0.544	0.467	0.86
	RC5	Shear walls (moderate E.R.D.)	■	■	■	■	■	■	0.14	0.21	0.384	0.51	0.7
	RC6	Shear walls (high E.R.D.)	■	■	■	■	■	■	-0.02	0.047	0.224	0.35	0.54
Steel	S	Steel structures	■	■	■	■	■	■	-0.02	0.17	0.324	0.48	0.7
Timber	W	Timber structures	■	■	■	■	■	■	0.14	0.207	0.447	0.64	0.86

Situations: ■ Most Likely; ■ Probable; ■ Less Probable (exceptional cases)

The primary benefit of these vulnerability index methods is that the vulnerability definition is not based solely on the building typology, and different vulnerability characteristics of the building are taken under consideration using score assignments. It enables updating the specific vulnerability in response to modifications or alterations done to the structure, by carrying out a vulnerability assessment for damage probability functions based purely on damage observations or expert judgements. In earthquake prone regions like Italy, Albania, Greece, Turkey, New Zealand, California, the importance and requirement for vulnerability assessment on existing buildings has been recognised and used by many researchers. However, these methodologies still require for the use of expert judgement when evaluating the structural response of the buildings, and there is a degree of uncertainty while estimating the parameters' coefficients and weights used for the calculation of the vulnerability index. A brief overview of the application of this Vulnerability Index Method (VM) is given below in section 2.3.2, as one of the most used method for the vulnerability assessment in different regions and urban centres.

2.3.1.3. Analytical methods

Analytical methods, also referred as direct methods, are based on a numerical evaluation of the structure's global seismic behaviour, by using complex structural analysis. The expected damage experienced by a typological class is determined by the interaction between the structure's seismic behaviour (identified, for example, by capacity curves) and the seismic demand (identified, for example, by response spectra). There are numerous methods that vary in complexity depending on the type of model used to simulate the structure and the analytical procedure used to perform the analysis. Due to the substantial amount of input data and the length of time required for the analyses, these techniques are very accurate but require high computation time and cost. As a result, they are not adequate to be used on large-scale analyses involving areas with diverse construction characteristics.

The assessment of a building's response during a seismic event necessitates the characterisation of building systems and the estimation of possible ground motions. Numerical models are used to conduct various analyses, such as nonlinear static or dynamic analysis, in

relation to determine the structure's seismic vulnerability, by previously defining various damage limit states and representative set of earthquakes. The data is then statistically processed to determine the likelihood of various types of damage, validating and contrasting the data with actual observed damage from previous earthquakes or with experimental data. The fundamental components needed to analytically determine vulnerability curves or damage probability matrices are presented in Figure 2.4.

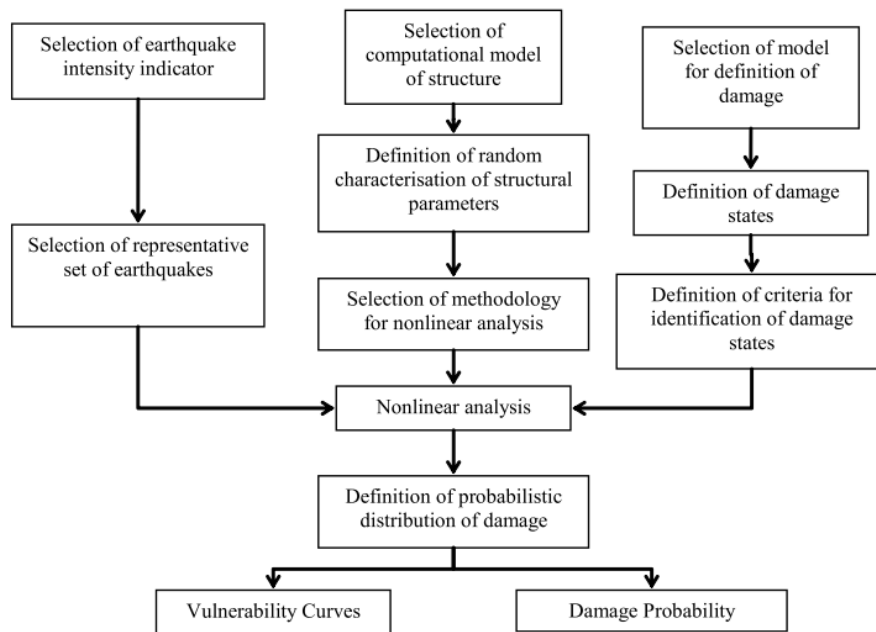


Figure 2.4 - Flow chart describing different components for evaluation analytical vulnerability curves and damage probability matrices (Calvi et al., 2006).

Nowadays, the most recent trends in the field of vulnerability assessment with the use of simplified mechanical models, are essentially based on the Capacity Spectrum Method (Freeman, 1998; HAZUS, 1999). The Capacity Spectrum Method (CSM), as a performance-based seismic analysis technique, can be used for a variety of purposes such as rapid evaluation of a large inventory of buildings, design verification for new structures, evaluation of an existing structure to identify damage states, and correlation of damage states of buildings to various amplitudes of ground motion (see Figure 2.5). HAZUS (1999) developed a methodology specifically for the built environment in the United States to estimate the potential losses of an earthquake at urban scale (FEMA 2003, Kircher et al. 2006). The methodology is founded on three fundamental concepts of the CSM: the capacity curve, the performance point, and the fragility curve.

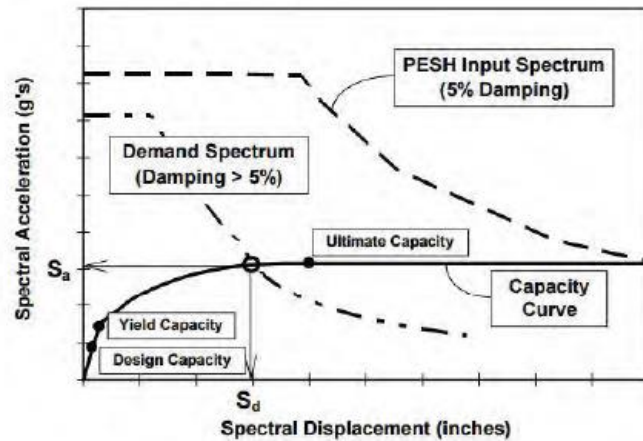


Figure 2.5 - Procedure for determining the performance point between the structure's capacity curve and the demand spectrum (HAZUS, 1999).

The methodology considers 36 different types of building typologies, for which a corresponding capacity curve can be determined. Moreover, the HAZUS manual presents the process for generating fragility curves that allow representing the probability of reaching or exceeding a specific damage limit state. After determining the spectral response, fragility curves and discrete damage distributions can be defined by calculating the conditional cumulative probabilities of reaching or exceeding a certain damage state (FEMA 2003). Damage is represented and distributed by fragility curves in five different threshold states: no damage, light damage, moderate damage, heavy damage, and collapse.

Other proposals for simplified analytical methods allude to displacement-based approaches as opposed to force-based approaches. Calvi (1999) evaluated the displacement demand resulting from a displacement spectrum and the displacement capacity corresponding to various limit states of a structure. The process employed the direct method based on a displacement format, where a structure with many degrees of freedom (NDOF) is modelled as a structure with a single degree of freedom (DOF), using various displacement profiles related to the mechanism of collapse while considering the geometry and material properties of the building. In this method, four limit states are considered. For each type of building structure and limit state, a structural model is specified in terms of secant stiffness corresponding to the maximum displacement of the limit state under consideration, from which the equivalent period of vibration is derived, and a displacement demand reduction factor (Giovinazzi, 2005).

Within the framework of significant European projects like GEM (D'Ayala et al., 2014), PERPETUATE (Lagomarsino and Cattari, 2015), and SYNER-G (Pitilakis et al., 2014), significant work has been done around the application of capacity spectrum-based approaches. Masi (2003) uses an analytical method to describe the seismic behaviour of reinforced concrete (RC) frame structural systems, which constitute the primary structural typology of Italian buildings built after the 1960s, and highlights their vulnerability with the EMS-98 Scale (Grünthal, 1998). Similar to this, Rossetto and Elnashai (2005) studied a variety of European RC structures, as Dumova-Jovanoska (2000) constructed vulnerability curves and damage probability matrices for RC structures in the city of Skopje, Macedonia.

The ability of numerical models to accurately predict the structure's real response, the accuracy in converting numerical damage indices into actual damage to real structures, the capability of accounting for human errors in building design and construction, being the primary causes of catastrophic collapses, are some of the many unresolved issues that need to be addressed when using analytical/mechanical methods for vulnerability assessment (Calvi et al., 2006). Nevertheless, they can be employed successfully to carry out sensitivity or typological studies on a small group of representative buildings in an urban centre. This analytical technique can be very useful when there is lack of information on post-earthquake damage for the specific region and building typologies, and can therefore enable the calibration of empirical or expert judgment vulnerability methods.

2.3.1.4. *Hybrid methods*

Hybrid methods, in general, combine the benefits of analytical, empirical and expert-judgment approaches. In these methods, the analytical results help to make up for the absence of observational damaged data or to calibrate empirical approaches by using some analytical simulations of specific building typologies. Hence, this method integrates the statistical building damage data from the empirical methods, and the results obtained from the mechanical (simplified or more sophisticated) models of the studied building typology, to create DPMs and vulnerability or fragility curves.

This method is especially helpful for calibrating empirical vulnerability approaches for regions with low seismic hazard, and therefore lacking post-earthquake damage observations. This is very common for the region of Spain, since the seismic hazard is considered to be low to medium and there is scarce data information from previous past earthquakes. Barbat et al. (1996) provided an example of hybrid methods by comparing and calibrating vulnerability curves obtained from an empirical vulnerability assessment of a building stock of Barcelona city with capacity/demand ratios of models sharing the same characteristics as the construction typology under study.

The hybrid methods have a wide range of applications because they are adapted to the particular needs of the assessment. There are a number of techniques that use various material models, types of analysis, and probabilistic models that can be found in the literature. Based on the PGA and spectral displacement, Kappos et al. (2006) created vulnerability curves for a number of existing reinforced concrete and URM structures in Greece by calibrating the pushover curves with the statistical damage database from the Thessaloniki earthquake in 1978. Most recently, Kappos (2016) made a significant contribution for the systematic application of hybrid methods to determine the seismic vulnerability of RC and masonry structures, combining results from nonlinear analysis of representative structural models with empirical databases of earthquake damage.

Other approaches, such as FAMIVE (D'Ayala and Speranza, 2003) and VULNUS (Bernardini et al., 1990), can be regarded as hybrid methods as well (not just analytical) because they integrate analytical assessments of the structures with aspects of vulnerability index methodology. In this regard, the use of these techniques is appropriate for masonry aggregate vulnerability assessments in historical centres. They have been widely applied to several case studies of old city centres, (D'Ayala and Speranza, 2004; Formisano et al., 2013; Munari et al., 2009; Novelli

et al., 2015; MR Valluzzi et al., 2009), where the information relates only to external onsite inspections. Nevertheless, the use of methods like VULNUS and FaMIVE is limited for loss assessments, since they cannot clearly define the correlation between the structural capacity with the seismic demand to evaluate the probability of exceeding specific limit states or damage (Romis, 2020).

The primary challenge in using hybrid methods is presumably related to the calibration of the two different data acquired with different techniques (empirical and analytical). given that the two vulnerability curves include different sources of uncertainty and are thus not directly comparable (Calvi et al., 2006).

- Summary of the previous vulnerability methods

Finally, the vulnerability method, the physical condition of the built system, or directly losses could be used to express the negative impact of the seismic event. Damage Probability Matrices, Vulnerability Curves, and Vulnerability Scores provide a direct assessment of physical damage, whereas fragility Curves may provide loss results. Table 2.4 shows a summary information of the previously classified seismic vulnerability methods based on the building description system, seismic hazard input, damage and the output for the building vulnerability description, adopted from Giovinazzi (2005).

Table 2.4 - Summary information for different vulnerability methods based on building system, seismic hazard, damage and vulnerability description (adapted from Giovinazzi 2005).

Vulnerability methods		Building System Description	Hazard	Damage	Vulnerability Description
Empirical	GNDT - I Level	Vulnerability Classes	MCS intensity	Damage	DPM
	Coburn and Spence (1992)	Building Typologies	PSI scale	Damage	Fragility Curves
Expert	ATC13	Building Typologies	MMI Intensity	Losses	Fragility Curves
	ATC21	Single Building	PGA	Safety Criterion	Vulnerability Score
	GNDT - II Level	Single Building		Losses	Vulnerability Score/ Fragility Curves
	Macroseismic Giovinazzi and Lagomarsino (2004)	Vulnerability Classes	EMS-98 Macroseismic Intensity	Losses	Vulnerability Score/ Fragility Curves
Analytical	HAZUS (1999)	Building Typologies	ADRS	Damage	Capacity Curve
	Calvi (1999)	Building Categories	DS	Damage	Structural Parameters
Hybrid	VULVUS	Single Building/ Set of Building	PGA	Safety Criterion	Collapse Multiplier
	FAMIVE	Single Building	PGA	Safety Criterion	Collapse Multiplier

where ADRS = Acceleration Displacement Response Spectra and DS = Displacement Spectra.

2.3.2. Vulnerability assessment at urban scale

The seismic Vulnerability Index Method (VIM) (Benedetti and Petrini, 1984; GNDT, 1993) is an extremely useful method for the comprehensive evaluation of buildings in urban centres that are vulnerable to certain seismic hazard. Several researchers have applied this indirect method based on post-earthquake observations and expert opinions, in different historical centres located in different European countries. As aforementioned, it enables the assessment of seismic vulnerability from a set of parameters representative of the sources of vulnerability in the building stock. VIM is considered to be an empirical/expert judgement method, also called indirect method, for evaluating a structure's seismic vulnerability that considers both its structural and non-structural elements. It establishes a relationship between seismic action and structural response using a vulnerability index. The method is based on field surveys that were carried out to determine which attributes, such as plan configuration, foundation type, structural and non-structural elements, typology and material quality, etc., have the greatest impact on structural vulnerability. This method scores different vulnerability parameters using a weighting system, with each parameter having a different weight based on its importance. This weighting method is used to determine the building's total vulnerability index, which can be compared to other buildings or used to determine the vulnerability of an individual building. There are 11 parameters, and each one is assigned one of the four qualifying classes (from A - least vulnerable to D - worst condition) (see Table 2.5). The vulnerability index is calculated by assigning class scores $C_{v,i}$ and weights w_i to the vulnerability parameters relating to the individual building's structural features in accordance with the following equation:

$$I_V^* = \sum_{i=1}^{11} c_{v,i} \cdot w_i \quad (2.2)$$

Table 2.5 - Vulnerability index method formulation (Benedetti and Petrini 1984).

PARAMETERS		CLASSES				WEIGHTS	VULNERABILITY INDEX
		$C_{v,i}$				w_i	
		A	B	C	D	p_i	
1	Type and organisation of resisting system	0	5	20	45	1.00	$I_V^* = \sum_{i=1}^{11} c_{v,i} \cdot w_i$
2	Quality of resisting system	0	5	25	45	0.25	
3	Conventional strength	0	5	25	45	1.50	
4	Building position and foundations	0	5	15	45	0.75	
5	Horizontal diaphragms	0	5	25	45	variable	
6	Plan configuration	0	5	25	45	0.5	Normalisation: $0 \leq I_V \leq 100$
7	In height configuration	0	5	25	45	variable	
8	Maximum distance between walls	0	5	25	45	0.2	
9	Roof	0	15	25	45	variable	
10	Non-structural elements	0	0	25	45	0.25	
11	General maintenance conditions	0	5	25	45	1.00	

The vulnerability index is initially in the range from 0 to 382.5, but it is normalised within the range of 0-100. The minimum vulnerability is indicated by the value 0 and the maximum vulnerability is indicated by the value 100. It is crucial to note that the vulnerability index is not, by itself, a damage predictor because neither damage scales nor seismic indicators are included in its computation. To determine the level of building damage, following correlations between the relative vulnerability index and the earthquake hazard of a specific location are necessary.

In recent years, various variations of the VIM technique have been created with the intention of incorporating new evaluation parameters or even calibrating new forms for other structural typologies (Basaglia et al., 2018; Cara et al., 2018; Ferreira et al., 2015; Formisano et al., 2015; Jiménez et al., 2021; Ortega, 2018; Vicente et al., 2011).

Vicente et al. (2011) adapted the Italian GDNT form for its application to the Portuguese masonry buildings with some modification to the chosen parameters and their assign weights. The new added parameters are the following: number of floors, aggregate position and interaction and wall façade openings and alignments. As previously mentioned, the macroseismic method gives the variation of the mean damage grade (μ_D) as a function of the EMS-98 macroseismic intensity, whereas the VIM relates variations of the damage factor (d) as a function of the PGA (see Figure 2.3). The expression suggested by Vicente et al. (2011) gives an analytical correlation between the vulnerability indices of the two methods (VIM and macroseismic):

$$V = 0.592 + 0.0057 \cdot I_V \quad (2.3)$$

To obtain the structural damage and the economic damage indicator, a correlation between vulnerability index I_V and vulnerability scale was used as provided by the GNDT-II method (GNDT, 1993), in order to use analytical (A. Bernardini et al., 2007; Giovinazzi and Lagomarsino, 2004), which correlate the seismic hazard with damage grade μ_D according to equations (2.4) and (2.5):

$$\mu_D = \left[2.5 + 3 \cdot \tanh \left(\frac{I + 6.25 \cdot V - 13.1}{Q} \right) \right] \cdot f(V, I) \quad 0 \leq \mu_D \leq 5 \quad (2.4)$$

$$f(V, I) = \begin{cases} e^{\frac{V}{2}(I-7)} & I \leq 7 \\ 1 & I > 7 \end{cases} \quad (2.5)$$

Where I is the seismic hazard (expressed in terms of macro-seismic intensity), V is the vulnerability indicator according to the GNDT-II methods, Q is a ductility factor (typically assumed equal to 2.3 for unreinforced masonry buildings), and $f(V, I)$ is a function of the vulnerability and macroseismic intensity. This last parameter assumes different values in function of the value of I .

The mean damage grade μ_D can be also expressed by equation (2.6):

$$\mu_D = \sum_{k=0}^5 P_K \cdot D_K \quad (2.6)$$

Where P_k is the probability associated to a specific damage grade D_k , with k from 0 to 5 for each damage grade. The mean damage grade is a continuous parameter representing the distribution of the possible damage to analysed buildings, following the proposed EMS-98 damage grades.

In historical urban centres, it is difficult to analyse a building as an independent structure, because mainly it shares the same boundary walls with other buildings. Therefore, the interaction of the structural units under seismic action raises the need to analyse the seismic behaviour of building aggregates. The VIM technique was recently upgraded by Formisano et al. (2015) to consider the assessment of masonry structures in structural aggregates. Five additional parameters were introduced to the previous GNDT vulnerability form (see Table 2.6): the presence of adjacent building with different heights, the position of the structural unit in the aggregate, the presence of staggered slabs, the structural difference between adjacent buildings and the percentage difference of openings among adjacent façades. The scores and weights given to each new parameter were calibrated by creating simplified numerical models using the Equivalent Frame Method (EFM) and performing non-linear static analysis with the application of the N2 method (Fajfar, 2000). The proposed method represents the structural features of the construction typologies in the urban centre of Sessa Aurunca, in South Italy.

Table 2.6 - Additional vulnerability parameters for the VIM form proposed for buildings in aggregate (Formisano et al., 2015).

Parameter	Class score (s)				Weight (w)
	A	B	C	D	
1. Organization of vertical structures	0	5	20	45	1
2. Nature of vertical structures	0	5	25	45	0.25
3. Location of the building and type of foundation	0	5	25	45	0.75
4. Distribution of plan resisting elements	0	5	25	45	1.5
5. In-plane regularity	0	5	25	45	0.5
6. Vertical regularity	0	5	25	45	0.5-1
7. Type of floor	0	5	15	45	0.75-1
8. Roofing	0	15	25	45	0.75
9. Details	0	0	25	45	0.25
10. Physical conditions	0	5	25	45	1
11. Presence of adjacent buildings with different height	-20	0	15	45	1
12. Position of the building in the aggregate	-45	-25	-15	0	1.5
13. Number of staggered floors	0	15	25	45	0.5
14. Structural or typological heterogeneity among adjacent structural units	-15	-10	0	45	1.2
15. Percentage difference of opening areas among adjacent façades	-20	0	25	45	1

There are several benefits to using the VIM for seismic assessment such as its simple and easy application, making it appropriate for use in emergency risk management. The weights given to each parameter can be adjusted depending on the given information of the studied area, giving this assessment procedure more flexibility. The VI method is a useful tool for decision-making because it can be used to compare various building typologies or determine the vulnerability of a particular building. The weights assigned to each parameter are determined by expert judgements and may be susceptible to subjectivity, and it does not account for all variables that might impact a building's seismic vulnerability. As a result, the VIM needs to be correctly calibrated in order to be used in different regions, and account for the distinctive geometrical configurations, structural peculiarities or a combination of structural resisting systems of the studied existing buildings. Previous researchers have considered this issue and managed to improve the VIM by adding appropriate guidelines for building inspection, new evaluation criteria, and new vulnerability forms for different construction typologies.

Ortega (2018) proposed the development of two seismic vulnerability assessment methods for vernacular architecture, by carrying out an extensive numerical FE modelling campaign by performing pushover analysis. The first method, known as the Seismic Vulnerability Index for Vernacular Architecture (SVIVA) method, adapts the current previously described vulnerability index methods to the characteristics of the vernacular architecture by determining the classes and weights of the chosen vulnerability parameters on the basis of numerical and statistical analysis. The second method, called the Seismic Assessment of the Vulnerability of Vernacular Architecture Structures (SAVVAS) method, proposes a new formulation that allows correlating the seismic vulnerability assessment parameters with the seismic capacity of the building expressed in terms of load factors defining various structural limit states (Ortega et al., 2019).

Different authors have employed the VIM to specific urban centres with different building typologies. Hence, they have managed to adapt and improve this empirical-expert base method, by modifying some of the specific vulnerability parameters and proposing new weights for each selected parameter based on expert opinions of previously observed post-earthquake damage, numerical analysis and different statistical methods (Ferreira et al., 2012; Ferreira et al., 2014; Ferreira et al., 2017; Jiménez et al., 2021; Maio et al., 2015, 2020; Palazzi et al., 2022; Romis et al., 2021; Vicente et al., 2014).

An overview of the previous studies for the application of the different vulnerability assessment methods for urban centres of Barcelona city is given in Chapter 3, section 3.7.

2.4. MASONRY MECHANICS AND MODELLING TECHNIQUES

2.4.1. Masonry main mechanical features

Masonry is a composite material constructed by arranging units that are either dry-laid or bound together with mortar. There are various alternatives for possible unit-mortar combinations, which together form the composite masonry material. Masonry can consist of units such as stone blocks, bricks, adobes, or irregular stone mixed with mortars of clay, bitumen, chalk, lime or cement base, or other mortar components. Different masonry typologies exist depending on the geometry and arrangement of the units and mortars (see Figure 2.6).

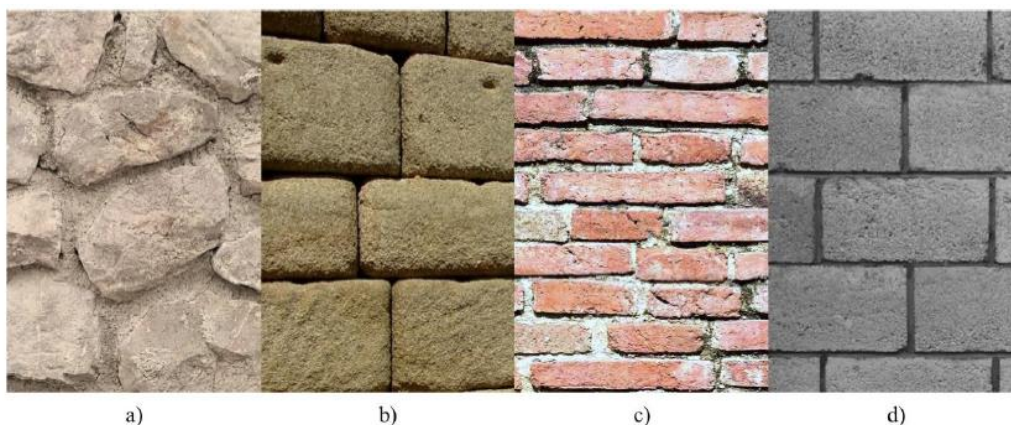


Figure 2.6 - Examples of different masonry typologies: a) Rubble stone masonry, b) ashlar stone masonry with dry joints, c) clay brick masonry, d) concrete block masonry (Segura Domingo, 2020).

Masonry is considered an anisotropic material and due to its composite nature and geometrical organisation. Masonry exhibits an extremely complex mechanical behaviour, which is influenced by the material properties of the units and the mortar, the bond between them, their relative dimensions and the placement of the pieces (Hendry, 1998). Masonry's behaviour is highly nonlinear due to the nonlinearities of the components and the source of weakness represented by the bond interface between the two components (D'Altri et al., 2019).

The most important characteristic of masonry is its ability to endure compression, as opposed to a very limited, or even non-existent, capacity in tension. The amount of historical masonry constructions built many centuries ago demonstrate the material's durability and resistance (Roca et al., 2019). Another characteristic of masonry is its shear strength, which is influenced by a number of factors, including the geometry and boundary conditions of the structural component, the arrangement of the masonry, the acting axial force, and the mechanical characteristics of the constituents (Calderini et al., 2009). Masonry members also need to withstand shear in addition to compression in different scenarios such as seismic events, soil settlement or wind loads. Due to the severe consequences that could be caused by an earthquake in terms of structural damage and loss of life, the resistance to in-plane loading is of the highest concern.

According to Lourenço (2009), masonry exhibits a generalised brittle mechanical behaviour that is defined by low tensile and shear strength as well as low ductility. The compressive behaviour exhibits higher values of strength and fracture energy than the tensile one. The bonding between the units and mortar joints is often very weak, with a cohesive-frictional response in shear and a cohesive response in tension. Cohesion softening is observed in the shear and tensile responses (Hendry, 1998). The masonry material can be anisotropic in the elastic range, in the strength properties, and in its post-peak brittle response (D'Altri et al., 2019). The mechanical behaviour of masonry can be interpreted using different scales, usually the material scale (Page, 1983, 1981) and the structural element scale (Magenes and Calvi, 1997). Both situations require a broad definition of the mechanical behaviour in terms of stiffness, strength, and ductility. Figure 2.7 depicts the masonry strength domain at the scale of the material and at the scale of the masonry pier.

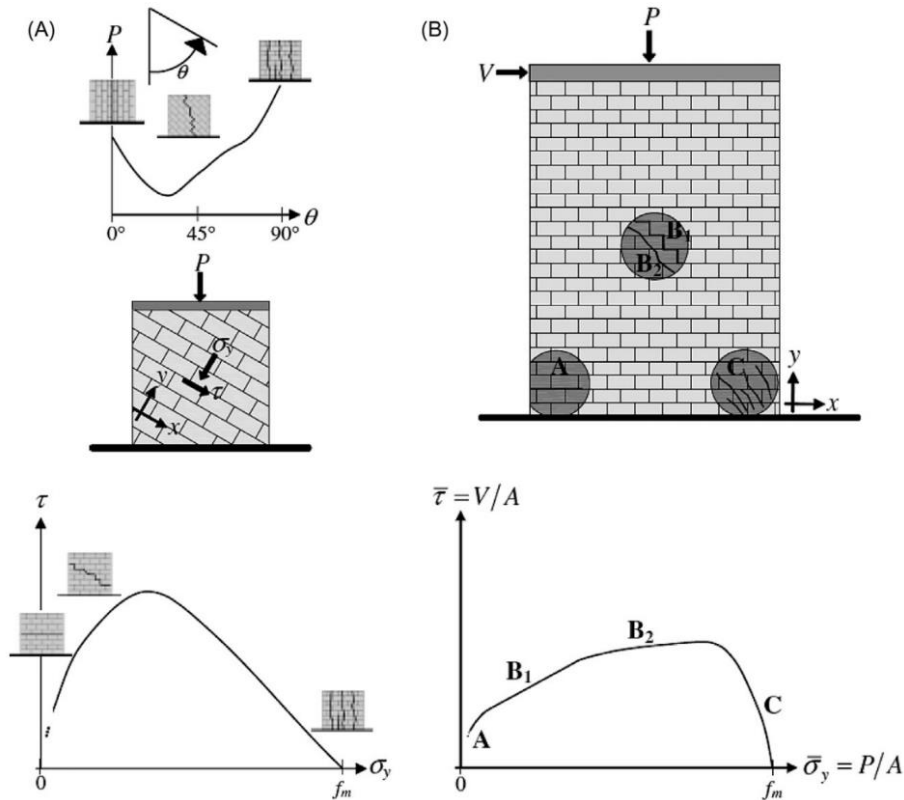


Figure 2.7 - Failure modes and limit domains of masonry (a) at the scale of the material and (b) at the scale of the structure (Calderini et al., 2009).

Basic structural resisting models (or schemes) can be envisaged to describe the response of the structure (notwithstanding its complexity) and to foresee possible collapsing mechanism. The seismic behaviour of unreinforced masonry buildings is defined by box-behaviour, and two possible collapse mechanisms control its resistance, namely the in-plane and the out-of-plane mechanisms of structural walls. The geometry of the piers, spandrels, and openings, the materials properties, the boundary conditions, and the loading conditions acting on the walls are only a few factors that affect the in-plane and out-of-plane behaviour of load bearing masonry walls.

Figure 2.8 illustrates the types of failure modes of unreinforced masonry piers subjected to in-plane loading. The main types of failure mechanisms as explained as follows:

- Sliding shear failure mechanism is associated with the formation of horizontal or diagonal cracks when horizontal stresses in the piers are greater than the shear strength of the bed joints.
- Diagonal shear cracking is linked to the exceeding of the masonry's tensile strength, which leads to cracks with stair-stepped patterns or diagonal cracks that go through both units and mortar. This depends of the unit-mortar interaction and their shear and tensile strength.
- Flexural failure mechanism is commonly related with simultaneous crushing of the compressed corner around which the wall experiences rigid body rotation better known as rocking, or crushing of the corner due to high compression forces, also called toe-crushing.

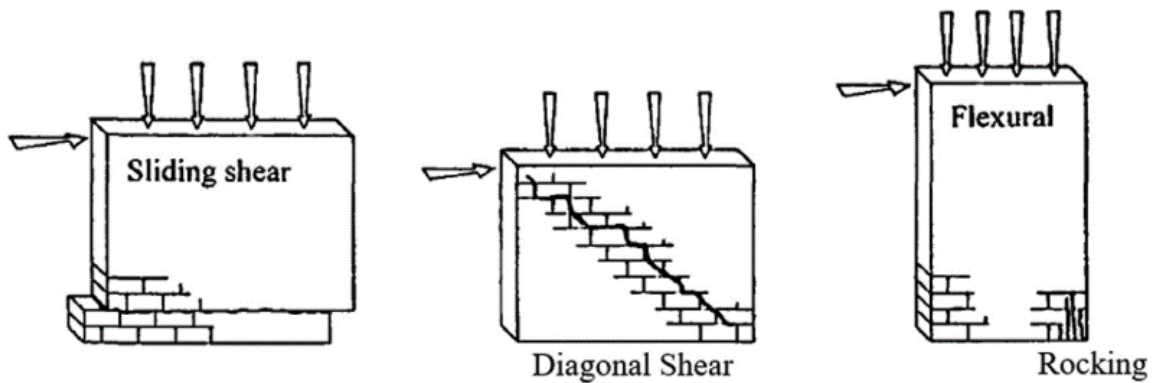


Figure 2.8 - Typical failure modes of unreinforced masonry piers subjected to horizontal in-plane loading (from left to right): - Shear failure mechanism with sliding along bed joint; - Shear failure mechanism due to diagonal cracking; - Flexural failure mechanism due to rocking and toe crushing (Tomažević, 1999).

Unreinforced masonry walls' seismic behaviour is a complex phenomenon that is dependent on the connection between the load-bearing masonry walls and the connection between the walls and floors. The type of a masonry building's horizontal elements, which are either rigid or flexible floor diaphragms with adequate or poor connections to the vertical elements, actually serves as the primary indicator of a possible seismic behaviour. The building experiences a global behaviour with lower stiffness and strength when there is a weak connection between flexible floors and walls. As a result, there are two types of masonry structures: those with box behaviour and those without it. Box behaviour is defined as the joint response of vertical and horizontal elements as opposed to the independent and out of phase behaviour of the structural elements, which results in significant out-of-plane damage. This characteristic provides the structure with certain ductility, or inelastic displacement capacity, to better withstand significant ground accelerations.

2.4.2. Numerical modelling approaches for masonry buildings

Over the past few decades, numerical modelling techniques have evolved into a well-established tool for the evaluation of the structural behaviour of different building typologies. An overall summary into different approaches is provided in previous research studies (D'Altri et al., 2019; Lourenço, 2002; Roca et al., 2010). D'Altri et al. (2019) proposed to classify the numerical modelling strategies for masonry structures into four different categories (see Figure 2.9): a) Block-based models, where the actual arrangement of masonry is accounted by considering the blocks either rigid or deformable; b) Continuum models, where masonry is modelled as a continuum deformable body, with no distinction between the masonry components; c) Macroelement models, where the structure is idealised into structural members such as piers and spandrels and d) Geometry-based models, where the structure is modelled as a combination of rigid bodies and the equilibrium is investigated by means of limit analysis-based solutions.

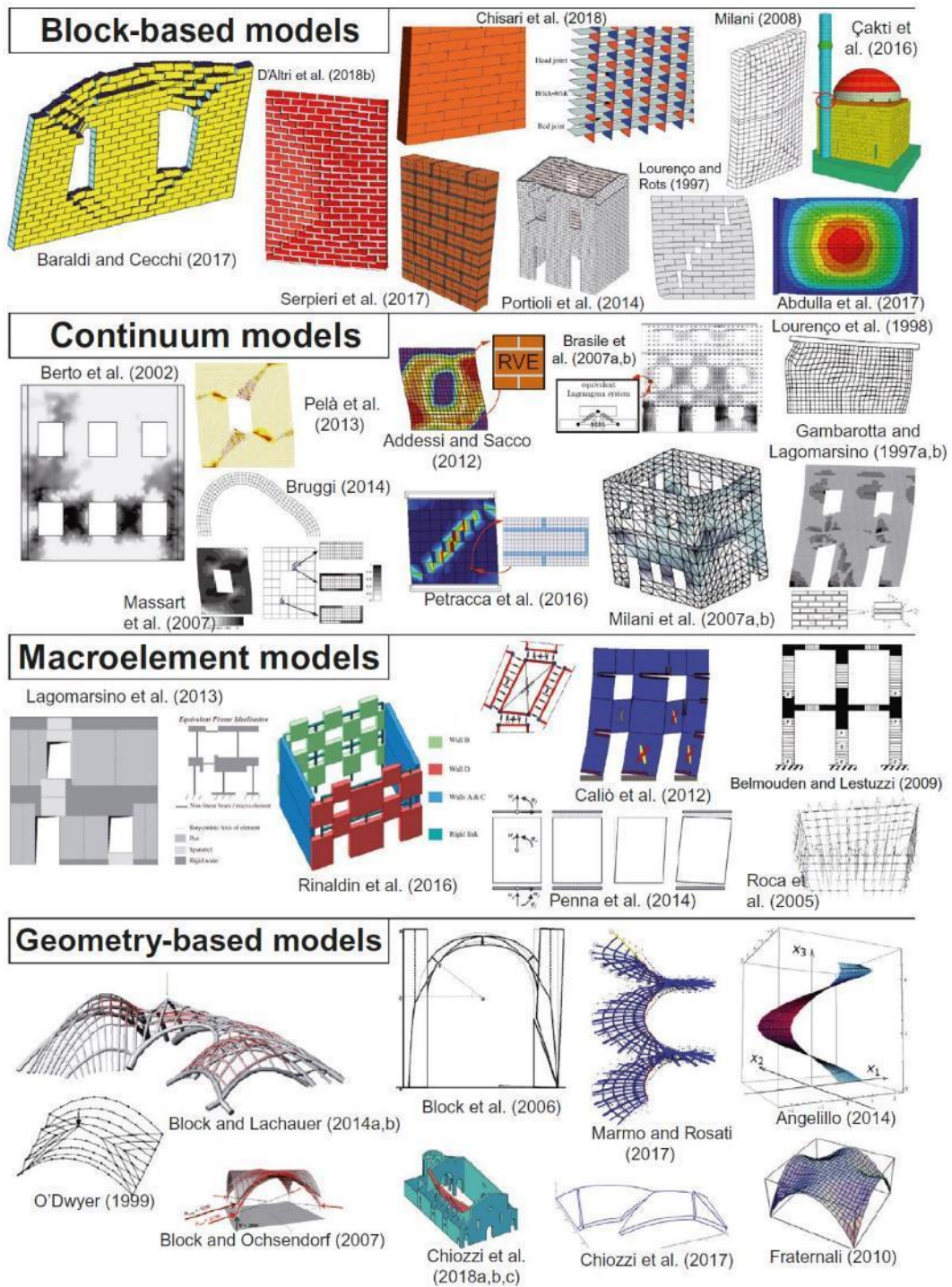


Figure 2.9 - Different numerical strategies for unreinforced masonry structures (D'Altri et al. 2019).

In this study a brief description is given for some of the numerical approaches used in the modelling of masonry structures. The development of various approaches offers different levels of detail regarding the modelling of composite materials such as masonry in terms of component typology and their geometrical arrangement. There is currently no perfect solution for the simulation of masonry, since it can depend on various factors such as the goals of the structural analysis, the complexity and scale of the structure, and the available resources (Saloustros, 2017).

According to the level of detail in the material description, the numerical FE methods used in the analysis of masonry structures can be divided into the following categories: (i) micro-mechanical, (ii) multi-scale, (iii) dis-continuous, (iv) macro-element (continuous), and (v) macro-mechanical approaches.

Micro-mechanical methods use a unique modelling of the masonry components. The varying mechanical characteristics and constitutive laws for each component can be considered when using this method. Various micro-mechanical systems for representing the composite nature of masonry have been proposed in the literature, each with a different level of detail such as (a) Detailed micro-model, (b) Simplified micro-model with mortar and unit/mortar behaviour lumped in interface elements, (c) Simplified micro-model with additional interfaces for vertical cracking in bricks, (d) Continuous micro-model with modelling of units and mortar with continuum elements (Saloustros, 2017).

Several discontinuity approaches have been proposed that simulate strong discontinuities between the various blocks or parts of a structure by distributing non-linear interfaces within the structure in a selective manner, as opposed to adopting a detailed description of the masonry's texture, as in micro-modelling and multi-scale approaches. This category of FE methods was developed based on the observation that structural collapse in masonry is defined by the development of global or local mechanisms, triggered by the separation of various structural components as a result of crack propagation (Saloustros, 2017).

The complex structural behaviour of masonry has a significant impact on how its structural response evolves. Therefore, drawing a connection between the impact of micro-structure and the need to anticipate macroscopic behaviour is a challenging aim. This challenge is made all the more difficult by the fact that strain and damage are typically localised primarily at the micro-level, leading to dissipative processes at the structural scale and requiring the use of multi-scale approaches to be solved (Petracca et al., 2016). The resolution of two Boundary Value Problems (BVP) in two distinct scales is used in multi-scale approaches (macro-scale and micro-scale). In this instance, a Representative Volume Element (RVE), a technique frequently used in regular brick typologies, is used. The assumption is made that the masonry is a composite substance on a large scale (Saloustros, 2017). When compared to micro-mechanical models, multi-scale models are more effective, particularly in terms of model construction. This is because only the RVE's geometry must adhere to the chosen masonry's design. Despite the fact these multi-scale models have advantages over micro-scale models, they still have high computational time and cost. Hence, the application of multi-scale methods for large-scale buildings is very limited (Petracca et al., 2016)

Macro modelling techniques consider masonry as a homogeneous material with average properties and therefore without differentiating between brick units and mortar joints. All elements of the FE model are assigned a single material model that accounts for both linear and nonlinear ranges of the behaviour. Macro-modelling approaches are frequently used for the numerical simulation of large-scale masonry structures in order to assess their global structural behaviour (Figure 2.10).

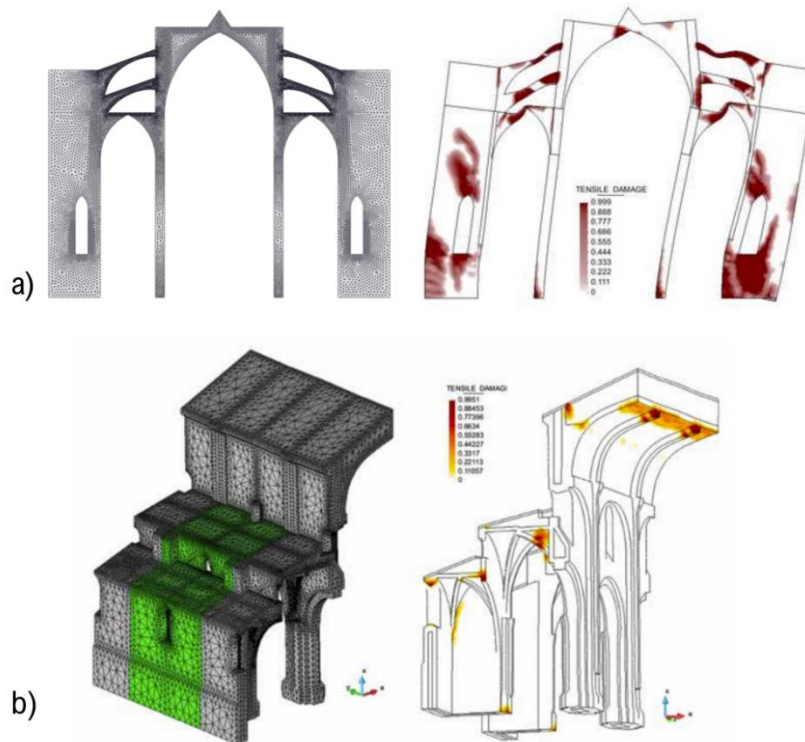


Figure 2.10 - Examples of FE numerical models of large-scale masonry structures: a) FE model of a section of Mallorca cathedral. FE mesh (left) and smeared damage model (right) (Roca et al., 2013) and b) Macro-mechanical model of a later nave in the church of the Poblet monastery. Left: FE discretisation with the demolished bay in green (left) and damage distribution at the end of the analysis (right) (Saloustros et al., 2015).

The geometrical modelling of masonry structures is simplified in macro modelling techniques because no specific masonry bond needs to be defined in the finite element models. The continuous domain is discretized by a mesh made up of elements linked by nodes in the Finite Element Method (FEM). The FEM has a variety of 1D, 2D, and 3D element types that can be used to model structural members, such as beams, shells, and solid elements. The anisotropic behaviour of the masonry can be considered with appropriate constitutive laws. The constitutive law in a realistic macro-mechanical model should at the very least be able to reflect the differing behaviour of brickwork under tensile and compressive loads (Saloustros, 2017). Static and dynamic responses can be analysed using this technique. Strategies for nonlinear analyses can be used to model geometric nonlinearity or the nonlinear behaviour of the materials. Several commercialised software programs are available for FE macro modelling, which finds a widespread application in the construction industry, such as DIANA-FEA, ANSYS or Abaqus Unified FEATM.

Macro-element approaches are a simplified technique for the study of masonry structures based on discretizing them as an arrangement of rigid and deformable macro-elements. They describe the geometric configuration and discretize the structural elements in a simplified way. The goal of these simplified approaches is to provide not only an assessment of the structure's ultimate strength, but also a sufficient detailed description of its nonlinear behaviour through simplified discretization of the structural layout. As a result, the engineering industry has showed a significant interest in the development of such simplified techniques, which are aimed at reducing the high computational cost associated with the analysis of large-scale structures.

The structural components included in a regular masonry building, such as the piers, walls, spandrels, and lintels are easily identifiable. The Equivalent Frame Method (EFM) was developed according to a simplified structural idealisation of the structure as a frame system composed of vertical elements, which represent the piers or walls, and horizontal elements for modelling the spandrels or lintels above the openings (Figure 2.11). Using rigid connectors, these vertical and horizontal components are joined together.

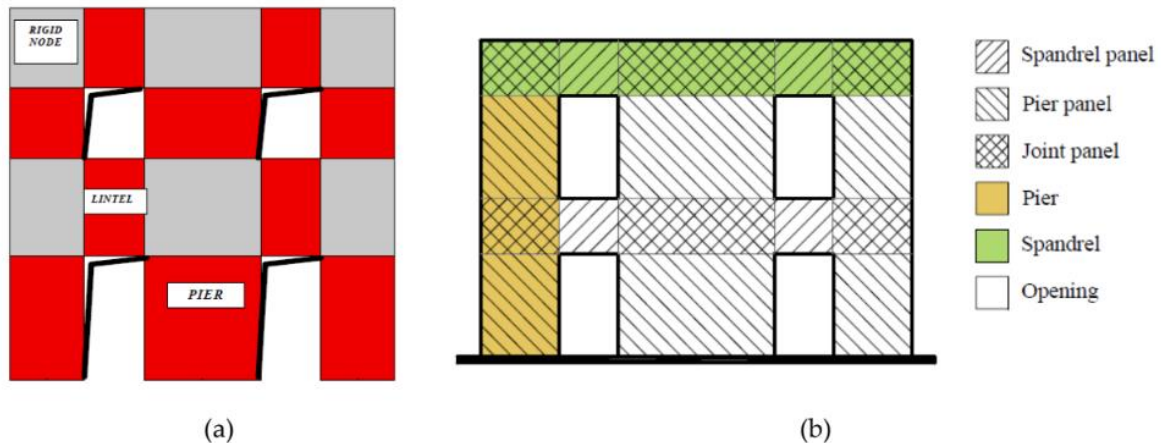


Figure 2.11 - (a) Example of macro-element modelling of masonry walls (Galasco et al., 2007); (b) Identification of the macro-element in a characteristic masonry wall with openings (Augenti and Parisi, 2010).

2.5. SEISMIC ANALYSIS METHODS FOR MASONRY BUILDINGS

Different types of analysis can be carried out to analyse the seismic response of existing masonry buildings using the previously described numerical modelling strategies. The following five fundamental categories of structural analysis are highlighted: limit analysis, linear static analysis, nonlinear static (pushover) analysis, and nonlinear dynamic analysis with time integration. In the following section only the non-linear static and dynamic iterative procedures are briefly discussed.

2.5.1. Non-linear static (pushover) analysis

The nonlinear static analysis (pushover analysis) is frequently used in the assessment of the seismic performance of existing masonry structures. Pushover analysis is a nonlinear static analysis method in which the structure is subjected to a pattern of lateral forces that increases monotonically until it reaches collapse or some predetermined analysis threshold. This tool is used for determining the global seismic behaviour of a structure and the possible damage produced by an earthquake.

Endo (2015) reported a classification of different pushover analysis: Invariant-force Pushover Analysis (IPA); Multi-mode or Modal Pushover Analysis (MPA); and Adaptive Pushover Analysis (APA). The load patterns in the IPAs, where the seismic force is idealised as a static and constant load in the later direction, can be as follows: mass proportional (m-IPA); i_{th} mode proportional (Φ_i -IPA); and i_{th} mode by mass distribution proportional ($\Phi_i m$ -IPA), as a combination of the first two patterns. Since the effects of higher order modes in complex aggregates cannot be represented

by the m-IPA, the last two patterns typically have weaker estimation capacities than the mass proportional pattern. However, m-IPA provides a good approximation of the results in terms of shear demand when compared to nonlinear dynamic analysis (NDA), even though this approach is still a more accurate technique for complex structures (Endo, Pelà, et al., 2017b). Subsequently, the mass proportional pushover load pattern, which is regarded as the most convenient compromise between accuracy and efficiency, is still the most frequently used for masonry structures that are not overly complex.

Simple nonlinear static analysis procedures are commonly used for evaluating the structure's global seismic response by means of the Capacity Spectrum Method (ATC 40, 1996), the Displacement Coefficient Method (FEMA 2000), or the N2 method (Fajfar, 2000). The N2 method consists of the application of the traditional force-based pushover analysis approach. This approach merges the response spectrum analysis of an equivalent Single Degree Of Freedom (SDOF) system with the pushover analysis of a Multi Degree Of Freedom (MDOF) model (see Figure 2.12). The N2 method aims to identify a performance point (target displacement) of the structure as the point of intersection between the capacity (pushover) curve and the inelastic demand spectra (as described in detailed in Chapter 6).

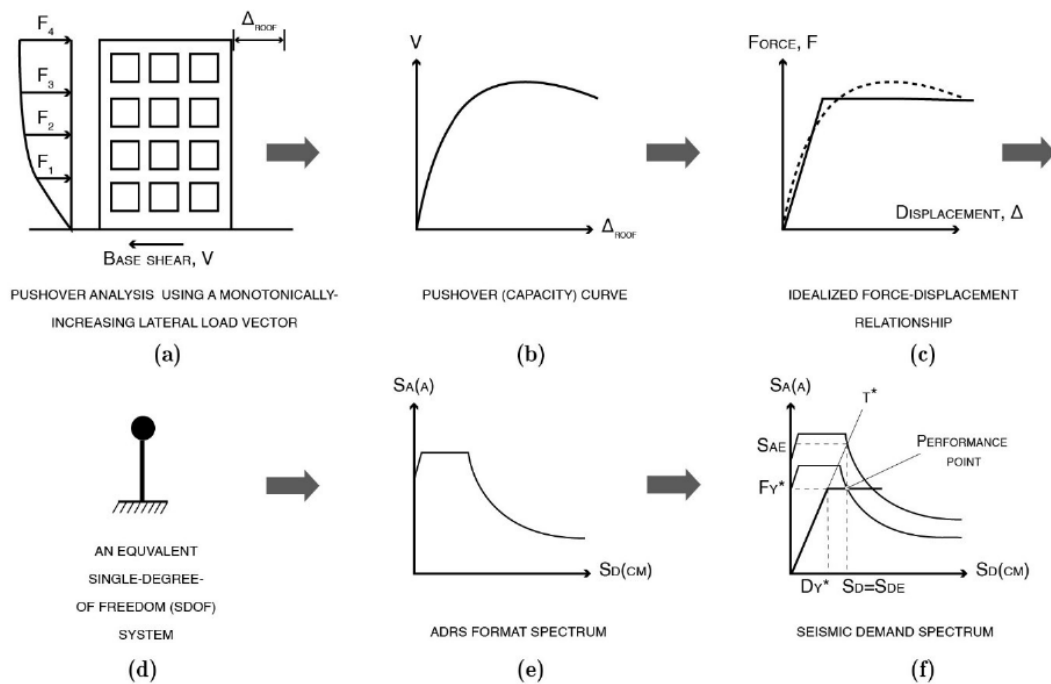


Figure 2.12 - Different steps for pushover analysis in the Capacity Spectrum Method (adapted from Najam 2018).

2.5.2. Non-linear dynamic analysis

The non-linear dynamic analysis (known as time history analysis) is the most accurate approach for determining the non-linear behaviour of a structure subjected to an earthquake ground motion. The structure is gradually subjected to time-dependent actions in the frame of a nonlinear time history analysis, also known as transient nonlinear analysis, and the structural

response develops in real time while also taking damping and inertial effects into consideration (D'Altri et al., 2020). The response of structures is strongly dependent on the earthquake motion input (set of ground peak records) used in the dynamic analysis. Additionally, there is a lack of consistent verification techniques, which makes it difficult to assess a building's seismic response based on the results of dynamic analysis. The computing cost and time required for a nonlinear dynamic analysis are determined by the analysed structure's size and the duration and demand of the ground motion.

The effects of dynamic events (such as earthquakes, impacts, explosions, etc.) on masonry buildings can be simulated using nonlinear time history analyses. The main advantages of this method include the ability to model a wide range of non-linear material behaviours, pounding building behaviour, and higher mode effects in tall buildings, which can only be simulated precisely with the non-linear dynamic procedure. Nevertheless, this type of analysis continues to face some challenges and drawbacks such as high computational cost, lack of readily available supercomputers to perform the analysis, and requiring a large number of ground motions (Kassem et al., 2020).

2.6. BUILDING TAXONOMIES FOR SEISMIC ASSESSMENT OF URBAN CENTRES

As aforementioned, there are various approaches available for assessing seismic vulnerability, as part of the seismic risk analysis. Nevertheless, the accuracy of these methods depends on how reliable the information is in the relevant databases. The clear categorisation of buildings is the main foundation for this reliability. The structural typologies that will uniformly encompass the numerous structural attributes must be chosen in order to provide a consistent classification of buildings and accurately characterise the building stock.

Buildings and other vulnerable elements must be grouped together into homogeneous groups that exhibit as much comparable response characteristics to ground shaking, as a first step in the general seismic risk assessment. As a result, the development of appropriate fragility curves for any form of structure totally depends on the development of an extensive taxonomy that can categorise the many types of buildings and infrastructures in any system. Any taxonomy should be a compromise between simplicity and thoroughness (Brzev et al., 2013; Pitilakis et al., 2014).

This section presents a summary of different existing building taxonomies used for the seismic vulnerability assessment in different regions. The building taxonomy identifies and groups different building typologies according to structural characteristics, so called attributes, that are significant for structure's seismic behaviour, such as load-resisting systems, material properties, age, height, etc. Hence, buildings in each class have common structural attributes and are thus expected to exhibit similar behaviour during a seismic event. Various building taxonomies have been created for application on a regional and international scale. The vulnerability assessment models based on these taxonomies are frequently estimated by combining reliable data (such as census data) with expert opinion, or by doing a proper field survey (Nicodemo et al., 2020). These taxonomies primarily categorise and describe buildings based on their structural response and performance to horizontal actions.

The main structural resisting system was the only structural parameter employed in the first developed taxonomies, such as ATC-13 (ATC-13, 1985), HAZUS (FEMA, 2003) or European Macroseismic Scale (EMS-98) (Grünthal, 1998). Hence, the chosen building typologies were relatively generic and could not be used for structures with specific characteristics. More recent building taxonomies (Brzev et al., 2013; Jaiswal and Wald, 2008; Pitilakis et al., 2014) include the proper data and knowledge of several structural and non-structural features, which can more precisely describe the global seismic behaviour of a specific building typology.

Over the last few decades, several building taxonomies have been developed, including ATC-13 (ATC-13, 1985), HAZUS (FEMA, 2003), EMS-98 (Grünthal, 1998), PAGER-STR (Jaiswal and Wald, 2008), RISK-UE (Milutinovic and Trendafiloski, 2003), GEM building taxonomy (Brzev et al., 2013), SYNER-G project (Pitilakis et al., 2014) etc. Table 2.7 presents a summary of the building taxonomies that have been used in the past 30 years in different parts of the world.

Table 2.7 - Summary information of existing building taxonomies.

Name	Reference	Taxonomy type	Classification	Use
ATC-13	(ATC-13, 1985)	Risk-oriented building taxonomy	78 classes of structures (40 are buildings and 38 are other structure types such as bridges, storage tanks, towers etc.)	USA
FEMA 154	(FEMA, 1988)	Risk-oriented building taxonomy	15 structural types (2 classes for wood buildings, 5 classes for steel buildings, 3 classes for reinforced concrete, 2 classes for precast concrete, and 3 classes for masonry buildings)	USA
HAZUS	(FEMA, 2003)	Risk-oriented building taxonomy	36 structural categories, including 9 with three height ranges	USA
EMS-98	(Grünthal, 1998)	Building taxonomy for assessment of macroseismic intensity earthquakes	15 structural typologies (7 for masonry building, 6 for reinforced concrete, 1 for steel and 1 for timber buildings)	Europe
PAGER-STR	(Jaiswal and Wald, 2008)	Risk-oriented building taxonomy	103 building classes based on lateral-load resisting system, wall material, height, and seismic code compliance.	Worldwide
RISK-UE	(Milutinovic and Trendafiloski, 2003)	Building taxonomy	23 building classes of different structural type and materials (10 are for unreinforced masonry buildings, 7 for reinforced concrete, 5 for metallic structure and 1 class for timber structure)	European countries
GEM	(Brzev et al., 2013)	Faced building taxonomy	13 attributes and three level of details	Global
SYNER-G	(Pitilakis et al., 2014)	Faced building taxonomy (non-hierarchical)	Modular structure of 10 categories with sub-categories	Global

These taxonomies were created to describe and categorise building typologies according to their structural and seismic behaviour, with the main focus on the most significant structural features. Specific risk-oriented taxonomies, such as the HAZUS taxonomy (FEMA, 2003), European Macroseismic Scale (Grünthal, 1998) or PAGER-STR taxonomy (Jaiswal and Wald, 2008), are typically used for large-scale seismic risk assessments. Building taxonomies produced in the United States are primarily concerned with regional design and construction techniques (for example, ATC-13, FEMA 154, and HAZUS).

The Applied Technology Council (ATC) created the first seismic assessment methodology in 1985 for the evaluation of the seismic damage specific to the building stock of California, in the United States (ATC-13, 1985). The ATC-13 taxonomy offers a thorough classification of 78 classes of structures, including 40 different types of residential or commercial buildings, and 38 different industrial, utility, and transportation structures in California. Several key attributes were considered in developing this pioneering classification for the different structures, including construction materials, soil conditions, foundation, height, structural framing system, configuration, structural continuity, design and construction quality, age, and proximity to other structures. This taxonomy is not collapsible since it is based on specific assumptions for the structures in California.

FEMA 154 (FEMA, 1988) building classification is focused on the US building stock. Buildings were divided into 15 general structural classes, including 5 classes for reinforced and precast concrete structures, 3 classes for masonry structures, 5 classes for steel structures, and 2 classes for timber structures. Most classes solely include the vertical structural system as the key parameter for the classification, and only for the masonry buildings the type of horizontal diaphragms (rigid or flexible) was considered.

The HAZUS taxonomy (FEMA, 2003) was developed as part of an extensive methodology originally proposed by the Federal Emergency Management Agency (FEMA) objectively evaluate the effects of natural disasters (earthquakes, hurricanes and floods) on buildings in the United States. This taxonomy was established based on the building classes suggested within the framework of a rapid visual inspection of buildings conducted to evaluate their use, safety, and occupancy. There are 36 building typologies included in the HAZUS taxonomy (see Table 2.8), mostly defined by various lateral-load-resisting systems, with 4 levels of seismic code compliance.

Table 2.8 - EMS-98 and HAZUS building typology classification (Giovinazzi, 2005).

EMS 98 Classification	HAZUS Classification
Unreinforced Masonry	Masonry Typologies
Rubble stone Adobe (earth bricks) Simple stone Massive stone U Masonry (old bricks) U Masonry - r.c. floors	Unreinforced Masonry Bearing Walls (URM)
Reinforced /confined masonry	Reinforced /confined masonry
Reinforced/confined masonry	RM Bearing walls with wood or metal deck diaphragms RM Bearing walls with precast concrete diaphragms
Reinforced Concrete	Reinforced Concrete
Frame in Reinforce Concrete Shear walls	Concrete Moment Frame Concrete Shear Walls Concrete Frame with U. Masonry Infill Walls
Steel Typologies	Steel Typologies
Steel structures	Steel Moment Frame Low-Rise Steel Braced Frame Steel Light Frame Steel Frame with Cast-in-Place Concrete Shear Walls Steel Frame with Unreinforced Masonry Infill Walls
Timber Typologies	Timber Typologies
Timber structures	Wood, Light Frame Wood, Commercial and Industrial
...	Pre Cast Typologies
	Precast Concrete Tilt-Up Walls Precast Concrete Frames with Concrete Shear Walls
...	Mobile Homes

The European Macroseismic Scale (EMS-98) (Grünthal, 1998) provides a uniform framework for defining vulnerability and evaluating damage to masonry and concrete structures. The EMS-98 scale is the most recent revision of the macroseismic scales that may explain the observable consequences of earthquake shaking on the environment, people, and built environment, as an improvement to the Mercalli-Cancani-Sieberg scale. Subsequently, the EMS-98 provides fifteen different building classes (see Table 2.8), primarily accounting for different materials of the load-bearing system but also considering the levels of earthquake-resistant design. The estimated range of physical vulnerability for each building typology is specified on a six-level scale from "A" to "F" (with "A" denoting the most vulnerable and "F" denoting the least vulnerable). These classes are typical of the building stock in European cities, however, this scale is widely used all over the world.

The RISK-UE building classification matrix summarises the various characteristics of the inventory of buildings constructed in different European countries (Milutinovic and Trendafiloski, 2003). This classification scheme is based on a number of building parameters such as load-bearing system, material, height, seismic design level, and non-structural elements, all of which influence the structure's seismic performance and degree of damage. The building typologies are divided into 23 classes for different construction materials (of which ten are for unreinforced masonry buildings, seven for reinforced concrete, five for metallic structure and one class for timber structure). Moreover, three sub-groups of different height were established such as low-rise, mid-rise and high-rise for each building class. For further classification, a building design code

and a performance level (pre-code, low-code, moderate-code, and high-code) were given to all the building typologies.

The Prompt Assessment of Global Earthquakes for Response (PAGER) programme created a global catalogue of construction types, so called PAGER-STR taxonomy, which was based on the processing of varied data with varying levels of uncertainty, quantity, and quality from several countries worldwide (K. S. Jaiswal and Wald, 2008). Several pre-existing taxonomies were combined for its creation and moreover, it was expanded with different building typologies found in several regions. A detailed approach was employed to integrate multiple databases and extrapolate for missing inventory data, which is subsequently used for immediate estimation of post-earthquake damage (Jaiswal et al. 2011). This is the most comprehensive risk-oriented taxonomy, which contains a total of 103 classes. The PAGER-STR classification scheme includes the primary critical structural attributes that influence seismic performance, such as the material and type of load-bearing structure, the lateral resisting system, the horizontal diaphragm, and the height of the structure. The taxonomy is simple and collapsible, and it aims to cover globally a variety of structural types. However, the number of existing classes for local studies at a specific region or city level is substantially less. Moreover, the influence of the different key parameters on the structure's seismic performance is not specifically ranked in this classification scheme.

A faceted taxonomy is a collection of taxonomies that each describe the domain of interest from a different perspective (Tzitzikas, 2009). The properties of this taxonomy type that have been recognised as lacking in risk-oriented taxonomies are conceptual clarity, compactness, and scalability (Pittore et al., 2018). More recent building taxonomies such as GEM and SYNER-G (Brzev et al. 2013; Pitilakis et al. 2014) are considered to be faceted taxonomies, including several structural and non-structural features of various building taxonomies, so called facets or attributes.

The Global Earthquake Model (GEM) introduced a comprehensive detailed taxonomy for a description and categorisation of structures at global scale, being independent of the geographic area and the specific hazard (Brzev et al., 2013). The GEM building taxonomy is created as a unique code for a building typology, like a genome, which is defined by several attributes corresponding to a specific structural characteristic (see Figure 2.13). This taxonomy scheme is adaptable, allowing for the addition and modification of attributes based on the amount of information necessary, as well as for the new knowledge acquired during the data collection (Brzev et al., 2013).

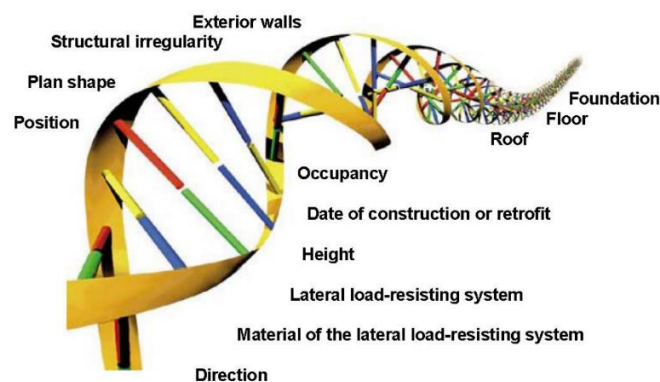


Figure 2.13 - GEM building taxonomy genome with different attributes (Brzev et al., 2013).

This more recent faceted taxonomy proposed 13 different types of attributes adaptable to various building typologies, which potentially affect their seismic performance (Figure 2.14): (1) building direction; (2) lateral load-resisting system material; (3) lateral load-resisting system; (4) height; (5) date of construction or retrofit; (6) occupancy; (7) building position within a block; (8) shape of the building plan; (9) structural irregularity; (10) exterior walls; (11) roof; (12) floor; and (13) foundation system. These features are grouped in four different areas such as the structural system, building's information, exterior attributes, and roof, floor and foundation system. Each attribute relates to a distinct feature of a single building or a building typology, allowing for their identification and classification into specific building classes. It should be noted that some attributes offer data relevant to other natural hazards. Moreover, the chosen attributes can be defined by up to three levels of detail, depending on the data available and the level of detail that is needed (see Figure 2.14). Therefore, some features are complemented by first, second and third-level attributes, such as the material of the lateral load-resisting system, height, structural irregularity, etc. For instance, Level 1 determines the type of irregularity (Plan or Vertical), Level 2 the Primary Irregularity, and Level 3 the Secondary Irregularity for the attribute Structural Irregularity (Silva et al., 2022).

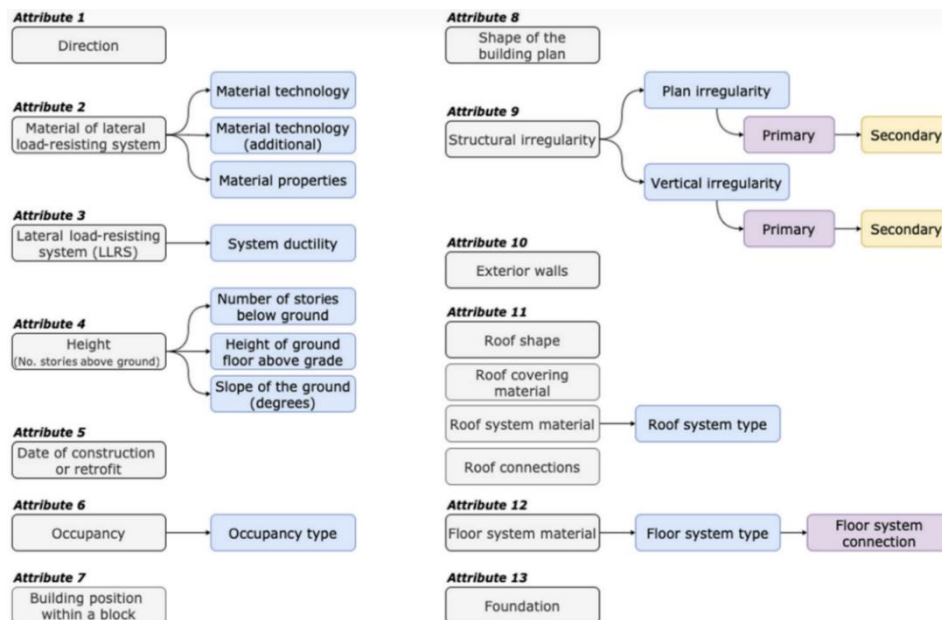


Figure 2.14 - Global Earthquake Model (GEM) building taxonomy, including all attributes and levels of details (Silva et al., 2022).

The GEM taxonomy comprises well-defined and specific attributes, being a very efficient tool for describing a variety of building typologies. However, in practise, it is hard to collect all the data for the creation of earthquake exposure models. Therefore, using this taxonomy for a large-scale risk assessment is more challenging (Pavić et al., 2020).

The SYNER-G project identified the main typologies and presented the classification of the systems and their sub-components, so called SYNER-G taxonomies, for buildings, utility networks, transportation infrastructures and critical facilities (Pitilakis et al., 2014). A faceted building taxonomy based on lists of specific attributes, has been proposed for the description of the European buildings. This taxonomy was used as a guide for the revision and development of fragility models for each component, with a focus on European specific traits, as well as for the

modelling of the systems. The SYNER-G proposed classification scheme for structures is divided into ten primary categories: force resisting mechanism (FRM), force resisting mechanism material (FRMM), plan regularity (P), elevation regularity (E), cladding (C), detailing (D), floor system (FS), roof system (RS), height level (H), and code level (CL). A more thorough categorisation and sub-classification is related to some of the described categories. Its objective is to enable users to categorise European building typologies using the same fundamental classification scheme. This taxonomy is very complete and able to describe different building typologies. Its flexibility is considered as the main advantage comparing to the other existing taxonomies, since more attributes can be added in order to apprehend different vulnerability parameters.

Reviewing these taxonomies was essential for determining each taxonomy's key advantages and, more significantly, for identifying any potential structural and non-structural attributes that should be used in order to provide a comprehensive classification. The presented information in this section has helped for the generation of a detailed building taxonomy for existing URM buildings of an historical urban centre with specific structural features.

Detailed survey activity is necessary in order to get a better understanding of the existing building stock and moreover, define a reliable and exhaustive taxonomy (Jiménez et al., 2018). There are many available survey forms for gathering information for individual buildings, which can be used for the further steps of the seismic vulnerability assessment.

GNDT (2007) proposed two types of survey forms (for masonry buildings, see Figure 2.15a and reinforced concrete buildings), for a simplified evaluation of each parameter considered in the VIM. The eleven vulnerability parameters related to different structural features for masonry buildings have been previously discussed in section 2.3.2 (see Table 2.5).

The Rapid Visual Screening of Buildings for Potential Seismic Hazards (FEMA, 2015) suggested a simple data-collection form to obtain details regarding the building's typology, occupancy, type of soil and potential hazards, as part of the methodology for seismic vulnerability analysis.

The AeDES field manual for post-earthquake damage assessment provides forms for collecting several information for the evaluation of post-earthquake damage data (Baggio et al., 2007). These forms include a set of parameters related to the seismic vulnerability of the buildings (Figure 2.15b). The AeDES survey form is composed of nine sections listed as: building identification, building description, building typology, damage to structural and non-structural elements, external danger, soil and foundations, usability judgment reports, and other observations.

Monteiro et al. (2016) suggested two building survey forms (a more technical for practitioners and a simpler form for the inexpert population), as part of the SASPARM 2.0 project for the definition of fragility curves for the building structural typologies of the city of Nablus in Palestine. The expert forms are divided into six sections by including the identification of the building, building's description, structural information, regularity, geomorphological information, and notes.

Jiménez et al. (2018) proposed four survey forms for on-field inspections, allowing the systematic collection of set of structural parameters required for the second level seismic vulnerability assessment. Masonry, reinforced concrete, steel/iron, and timber constructions were considered as different structural materials for the forms' development. Moreover, the most

representative characteristics and typologies were contemplated in each case. These forms consist of the following seven sections: (1) general information, (2) building typology, (3) structural regularity, (4) soil and foundations conditions, (5) non-structural elements, (6) damage condition, and (7) current condition of conservation. These forms were applied to the study of 111 existing structural typologies found in the historical centre of Valparaíso, Chile, such as masonry, RC, timber frame and mixed iron-RC buildings. Figure 2.15c shows an example of the proposed forms for the identification of the main lateral load resistant system of masonry structures.

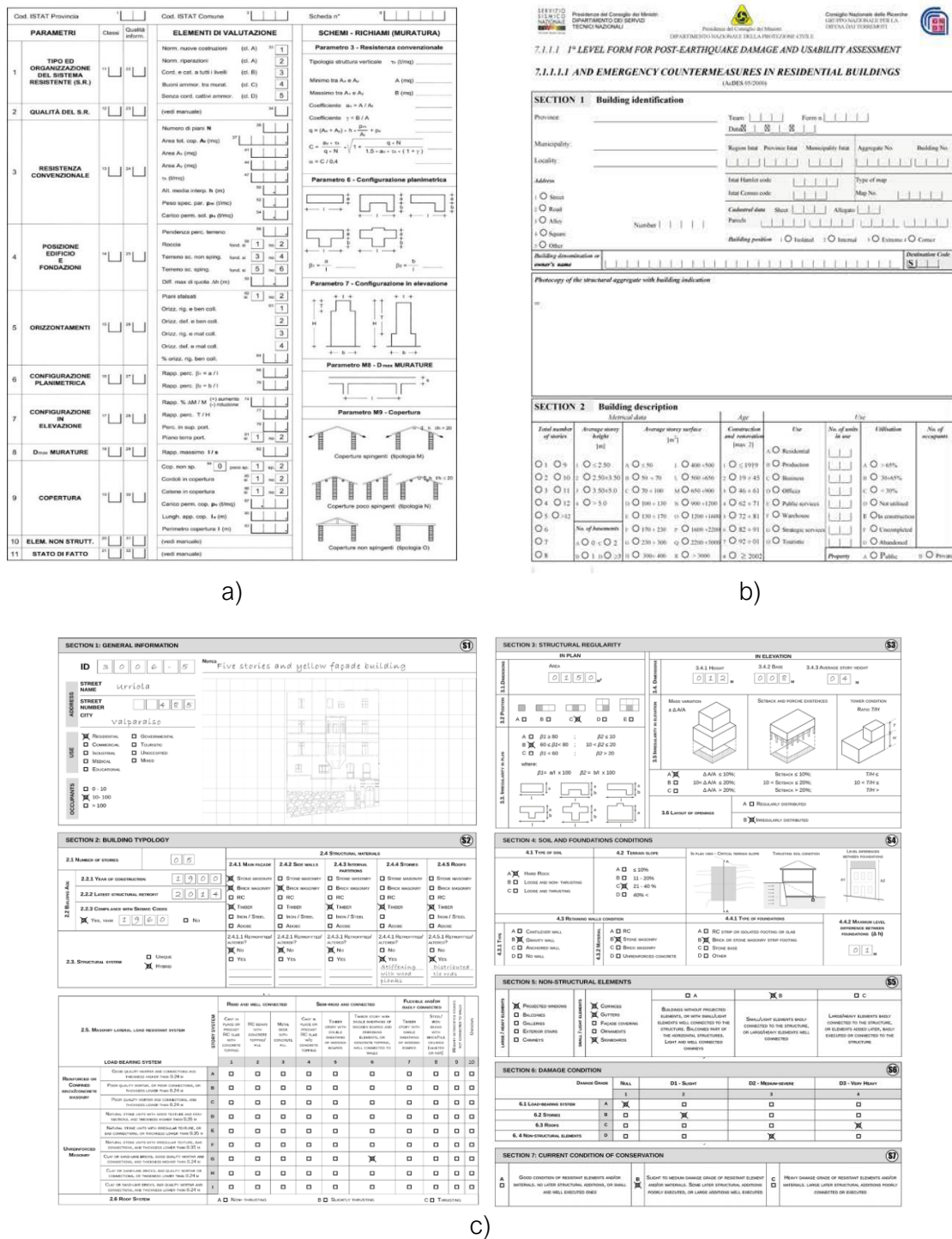


Figure 2.15 - Different survey forms: a) GNDT form for masonry buildings (GNDT, 2007); b) AeDES survey form (Baggio et al., 2007) and c) Survey form for masonry structures (Jiménez et al., 2018).

2.7. SUMMARY

This chapter elaborates and discusses the theoretical background and context of this research study. Different topics have been addressed starting from the general overview of the seismic risk assessment analysis and providing some definitions in order to better understand the fundamental concepts. The purpose of seismic risk assessment models is to quantitatively predict and prevent economic and social losses from a possible seismic event.

The following section focuses on the vulnerability assessment methods as the foundation for seismic risk analyses. Among different available vulnerability assessment methods, it is very crucial to consider several factors before their selection and adaptation to a specific case study. The main factor should be the purpose of the assessment, followed by the size of the studied urban centre, the amount of data and resources available, the possible classification of different building typologies and specifically, the computational effort and cost. Therefore, the vulnerability methods have been classified in four groups as: empirical, expert-judgment, analytical and hybrid. A brief review is given for all different methods categories in order to assess their suitability for analysing various risk scenarios, emphasising their key benefits, drawbacks, and prerequisites. The Vulnerability Index Method (VIM) by Benedetti and Petrini (1984) was used as an indirect assessment of the buildings' vulnerability by several researchers in the scientific community, with some proper modifications and adaptation to the chosen case studies.

Additionally, a brief state-of-the-art is introduced about the masonry mechanics and the several numerical strategies for the modelling of existing unreinforced masonry buildings. Special attention has been given to the continuum FE modelling, as the chosen numerical modelling technique for the existing masonry buildings. Furthermore, the most common non-linear seismic analyses have been discussed briefly.

The last section has presented an overview of the available building taxonomies over the past 30 years. This review has been considered for the proper creation of a specific building taxonomy for the *Example* district as the case study of this thesis. This building taxonomy is presented in Chapter 4 and it is the basis for the developed methodology for the vulnerability assessment of URM existing buildings.

CHAPTER 3. CASE STUDY – THE *EIXAMPLE* DISTRICT OF BARCELONA

3.1. INTRODUCTION

The *Eixample* district is the second oldest historical district of the city of Barcelona, as well as the most populated one. The name *Eixample* means expansion or enlargement in Catalan, which refers to the exact reason why this area of the city was planned: to expand the ancient town and establish a connection with all the adjacent smaller urban agglomerations. This part of Barcelona is very well known for its distinguished architecture and specific urbanism.

Built during the 19th and the beginning of the 20th century and previously designed by the engineer Ildefons Cerdà, the *Eixample* district is a symbol of Barcelona, with its distinctive network of large urban blocks (Figure 3.1). The historical and cultural value of this district is recognised by including many UNESCO World Heritage Sites like the *Sagrada Família*, *Casa Mila*, and *Casa Batlló*, which are work of the acclaimed Spanish architect Antoni Gaudi and the famous works by the architect Lluís Domènech i Montaner, such as the *Palau de la Música Catalana* and the *Hospital de Sant Pau*.



Figure 3.1 - Aerial view of a portion of the *Eixample* district (Maps, 2021).

Most of the *Eixample* buildings are unreinforced masonry ones with semi-flexible diaphragms and were designed for gravitational loads only, without considering any seismic requirements. Despite Barcelona being a region with a low to moderate seismic hazard, the seismic evaluation of this type of existing buildings is especially important, considering the high population density of this part of the city. They present a high vulnerability given their slender load-bearing masonry walls and an average height of six storeys. Hence, this specific part of the city has been chosen as an application case of the methodologies developed in this work.

This chapter describes the historic evolution of Barcelona and focuses on the development of the *Eixample* district as a specific area of the city. Moreover, a contextualisation, including information on the *Eixample*'s location, population distribution and building stock. The historical evolution of this specific area of the Barcelona city will be explained, addressing the key milestones of its origin and development. The information available regarding the seismic hazard of this area are provided, as a starting point for the vulnerability assessment. Subsequently, this chapter also includes a detailed description of the structural features of the typical *Eixample* buildings, including the used materials and construction techniques. Furthermore, a review on previous research studies regarding the seismic vulnerability assessment and seismic performance of the existing typical buildings of the *Eixample* district is presented. Finally, the last section includes the experimental characterisation of the masonry's mechanical properties of existing buildings located in Barcelona's urban centre.

3.2. THE CITY OF BARCELONA: LOCATION, DEMOGRAPHY AND BUILDING STOCK

Barcelona is the political and economic capital of Catalonia and the second largest city in Spain, after Madrid, in terms of population. The city of Barcelona is located in the NE of the Iberian Peninsula, extending along the Mediterranean coast. Currently Barcelona is enclosed between the *Llobregat* river on the South, the *Besòs* river on the North, the *Collserola* mountain range on the West and the Mediterranean Sea on the East (Figure 3.2). These geographical boundaries clearly limit the city's potential growth, leaving the rehabilitation of existing historical, industrial or abandoned areas, as the only alternative solution for the demographic growth pressure (Modrego Casquero, 2011).



Figure 3.2 - Barcelona localisation and boundaries (Elaboration on a map from *Plànol Barcelona*, 2020).

Currently, the municipal district of Barcelona extends over an area of 10,190 hectares with a population of 1,639,981 inhabitants according to the municipal census of January 2022 (Ajuntament de Barcelona, 2022). The city of Barcelona is composed of ten districts (Figure 3.3): *Ciutat Vella*, *Eixample*, *Sants-Montjuïc*, *Les Corts*, *Sarrià-Sant Gervasi*, *Gràcia*, *Horta-Guinardó*, *Nou Barris*, *Sant Andreu* and *Sant Martí*. This corresponding division of Barcelona city into administrative districts is part of the history, evolution and growth of the city. The *Eixample* district is the second oldest one and stands out as the main residential area of Barcelona.

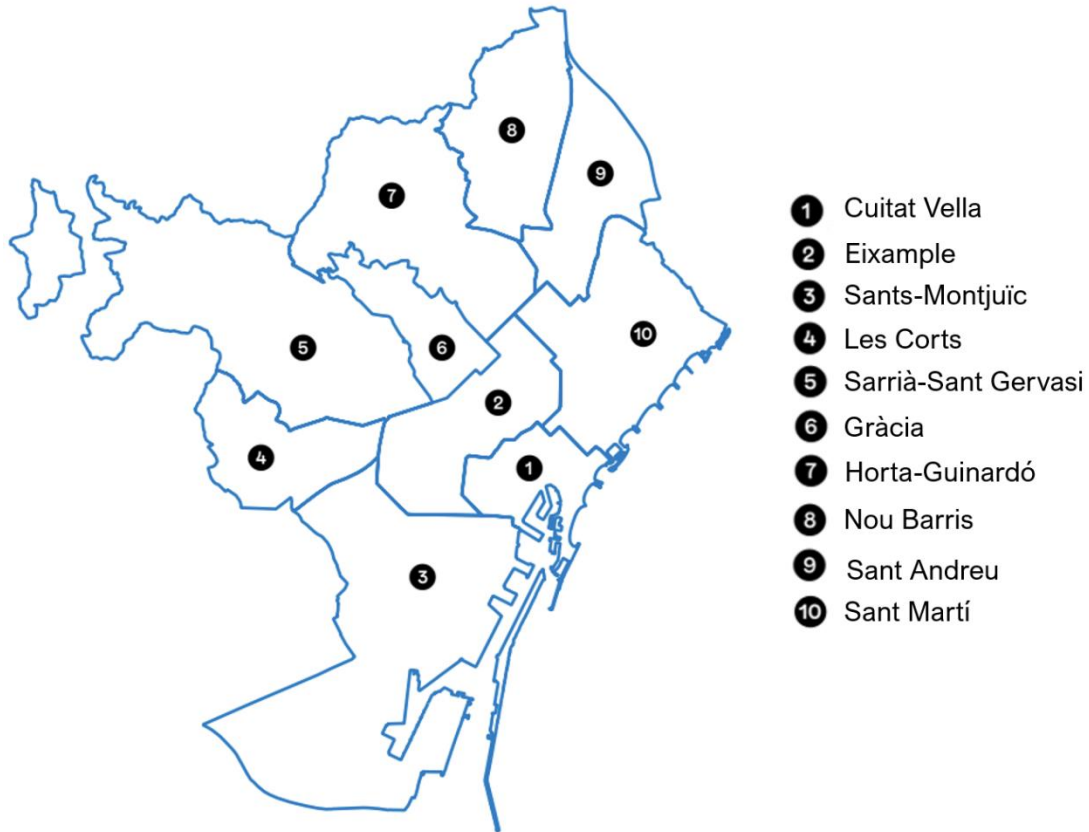


Figure 3.3 - Map of Barcelona with the territorial division of ten districts (adapted from Ajuntament de Barcelona 2005).

Table 3.1 shows the population of each city district. The area of the *Eixample* district is currently the largest and most densely populated part of Barcelona, and it constitutes a significant urban centre for all the activity in the city. Additionally, it has the biggest proportion of foreigners in the Barcelona region. As of the 1 of January 2022, the *Eixample* district had 266,857 inhabitants (Table 3.1), the 16.3% of the entire population of Barcelona (Ajuntament de Barcelona, 2022).

According to the 2011 census (Ajuntament de Barcelona, 2021), the *Eixample* comprises 7780 buildings, of which 97.5% are intended wholly or primarily for housing. Another indicator of the *Eixample*'s high population density is the district's housing unit count, which is 162,237 housing units, the highest of all ten Barcelona districts. It is conceivable to think of a net density of 712 hab/ha in relation to the 371.9 hectares of residential area (Ajuntament de Barcelona, 2021).

Table 3.1 - Distribution of number of inhabitants and buildings in the ten districts of Barcelona (Ajuntament de Barcelona, 2011).

District	Population	Buildings
Ciutat Vella	106,028	5,462
<i>Eixample</i>	266,857	7,780
Sants-Montjuïc	183,770	6,916
Les Corts	81,074	2,456
Sarrià-Sant Gervasi	148,201	8,252
Gràcia	121,915	7,413
Horta-Guinardó	172,109	9,951
Nou Barris	170,736	7,090
Sant Andreu	149,826	7,068
Sant Martí	239,465	7,442
Total	1,639,981	69,830

The *Eixample* district in Barcelona has the highest population density at 35,452 inhabitants per km², according to the data presented in Figure 3.4. The two *Eixample*'s neighbourhoods with the highest population density are *Sagrada Família* and *Sant Antoni*, with corresponding densities of 51,538 and 48,579 inhabitants per km² (Aguilar Meléndez, 2011).

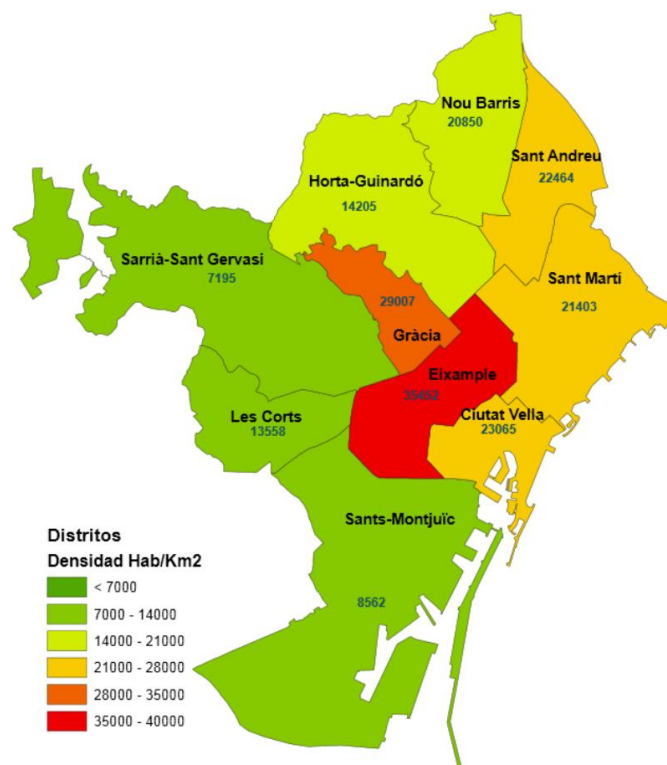


Figure 3.4 - Density distribution map of the city of Barcelona (Ajuntament de Barcelona, 2011).

A complex database covering nearly the entire building stock of Barcelona has been created over the past 15 years. It includes details on the geometry, floor plan, height, age, construction typology, kind of use, and status of conservation of the city's structures. Most buildings of *Ciutat Vella* were constructed in average around the year 1900, making this area the oldest in the city, according to information on the year of construction of the buildings (Table 3.2).

Table 3.2 - Number of cadastral buildings according to the year of construction (Ajuntament de Barcelona, 2011).

Number of cadastral buildings according to years of construction													
District	Total	Before 1901	1901 1940	1941 1950	1951 1960	1961 1970	1971 1980	1981 1990	1991 2000	2001 2005	2006 2010	2011 2019	Average age (years)
Ciutat Vella	7427	4288	1637	191	182	264	174	114	274	183	84	36	113.9
Eixample	13569	3103	4287	575	783	1612	1388	583	543	444	181	70	78.5
Sants-Montjuïc	10189	1485	3046	368	756	1358	1167	568	645	471	237	88	70.0
Les Corts	3807	97	598	242	341	777	857	338	240	155	107	55	54.6
Sarrià-Sant Gervasi	11290	635	2124	1004	1615	2076	1684	563	625	543	304	117	59.8
Gràcia	9208	1596	2446	521	780	1370	1116	374	442	320	168	75	72.8
Horta-Guinardó	12819	451	2068	885	2374	3345	1596	486	697	563	235	119	58.0
Nou Barris	9187	88	1100	341	1762	3042	1525	308	394	348	223	56	54.5
Sant Andreu	9287	1014	1750	440	1024	1778	1149	484	542	745	270	91	61.5
Sant Martí	10059	1188	2481	301	833	1522	1001	375	753	1082	369	154	63.1
BARCELONA	96842	13945	21537	4868	10450	17144	11657	4193	5155	4854	2178	861	68.4

The main pick periods in which most of the buildings have been built in Barcelona can be observed from Figure 3.5. A construction boom is thought to have occurred at one of these times, which is close to the year 1850 (1858–1868), around the time that the city's walls were demolished (Lantada, 2007). The high rise in the number of buildings around the year 1900 is related with the subsequent years after the start of the annexation in 1885 of Barcelona with the other municipalities such as *Sants*, *Gràcia*, *Sant Gervasi*, *Sant Martí de Provençals*, *Les Corts* and *Sant Andreu*. However, it is believed that the most significant construction activity occurred between the years 1940 and 1980 (Lantada, 2007).

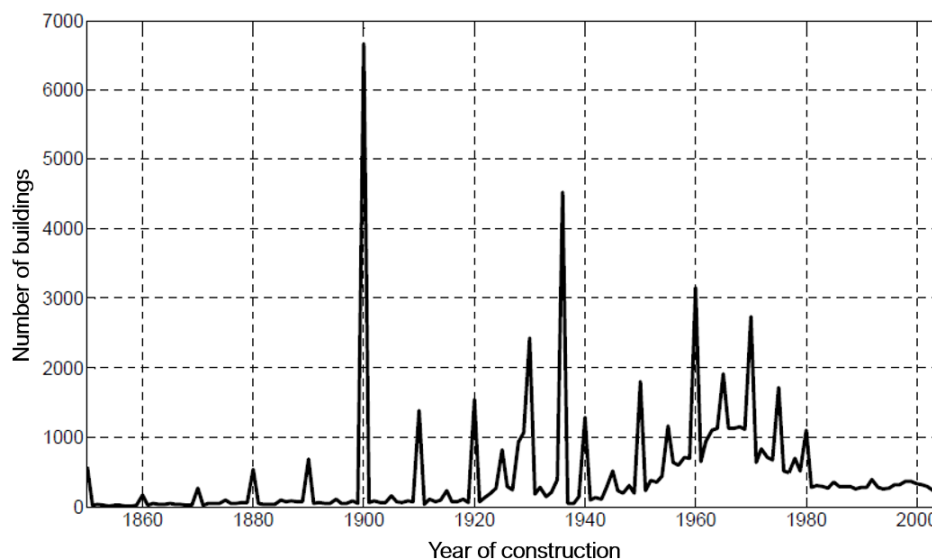


Figure 3.5 - Number of buildings constructed in Barcelona during the period from 1850 - 2005 (Aguilar Meléndez, 2011).

The district with the highest concentration of structures with more than seven storeys is *Eixample*. Contrary to the older *Ciutat Vella* district, which concentrates the largest number of

buildings in states of bad or deficient conservation (linked to the time of construction of the majority of the buildings), the state of conservation of *Eixample* buildings is above the average for the city (Avila-Haro, 2021).

3.3. HISTORY AND URBAN DEVELOPMENT

The historical development of Barcelona city has seen various periods of prosperity, destruction and reconstruction through the centuries, dating back to its foundation around 230 BC. Before the mid-nineteenth century, Barcelona was a small city (approximately 190 hectares) confined by walls, which prevented its potential growth (Barbat et al., 2010). Due to its strategic location, close to the sea and the good connection with central Europe, Barcelona had an enormous potential for further expansion and extension (Corominas i Ayala, 2002). During this period, Barcelona began to be influenced by the significant changes brought about by the Industrial Revolution. Due to the migration from rural to urban regions brought on by this Revolution, along with the XVIII century building ban and military rule, the city suffered from a housing shortage. The city's poor sanitary and hygienic conditions would led to a significant social pressure to demolish the walls that were preventing the city's growth (Avila-Haro, 2021).

The City Council of Barcelona started submitting petitions to the government in 1838, asking for permission to move forward with the city's expansion. The Barcelona City Council conducted a competitive public tendering for the project to expand the city. Meanwhile, Ildefons Cerdà, a civil engineer with a background in urbanism, was hired directly by the Spanish central government to design the new urban development, which was enforced in 1859 (Pujades et al., 2012). The plan created by Cerdà (Figure 3.6) aimed to link the old, walled city of Barcelona with previous municipalities like *Sants*, *Gràcia*, *Sant Gervasi*, *Sant Martí de Provençals*, *Les Corts* and *Sant Andreu*, among others (Lantada, 2007).



Figure 3.6 - Plan of Ildefons Cerdà's project for the expansion of Barcelona (Corominas i Ayala, 2002).

The *Eixample* district underwent constant changes since its original design, modifying its urban arrangement in the direction of a higher density (Colom, Cornadó, and Díaz 2016). In the beginning, it was decided that only half of the plot space would be used for construction, and that the blocks would only be enclosed on two sides (Cerdá, 1860). Furthermore, buildings were expected to be no taller than 20 m and no deeper than 15-20 m. The goal was to build blocks that were accessible to natural light, ventilated, and green. The purpose of this distribution was to reduce the social distance and inequality that dominated this era (Torner, 2009). As the development and political pressure increased, the original concept would ultimately be modified (see Figure 3.7). The blocks were designed to be oriented from north to east, with identical specifications and intersecting streets that were normally 20 metres wide.

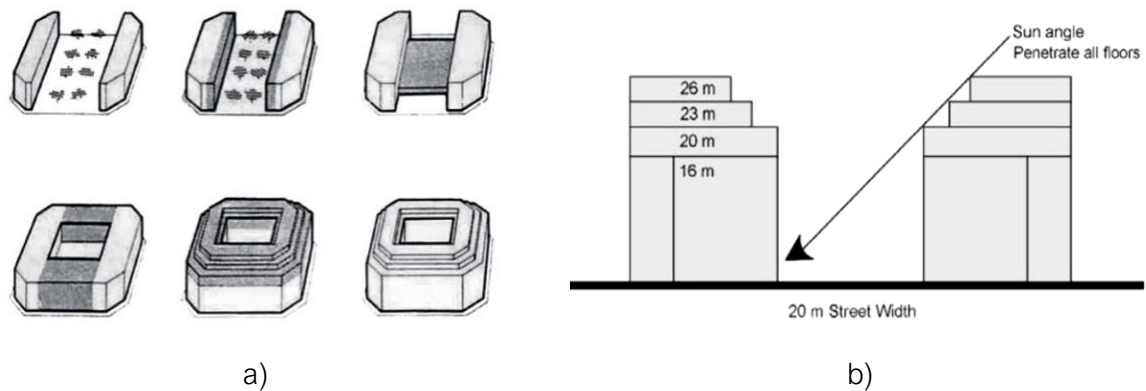


Figure 3.7 - a) Changes of the block sizes initially proposed by Cerdá from 1859 to 1972 (Cerdá, 1860); b) Evolution of building's height.

In general, four key elements can be identified that had a significant impact on the district's development: demographic increase, urban planning and management and the progressive definition of the city (Colom, 2014). Nowadays, the city of Barcelona, a dense, dynamic, and diverse metropolis, has become the standard for modern sustainable city plans (Torner, 2009). Figure 3.8 shows the difference between the original plan and the current situation of this specific area of the city.

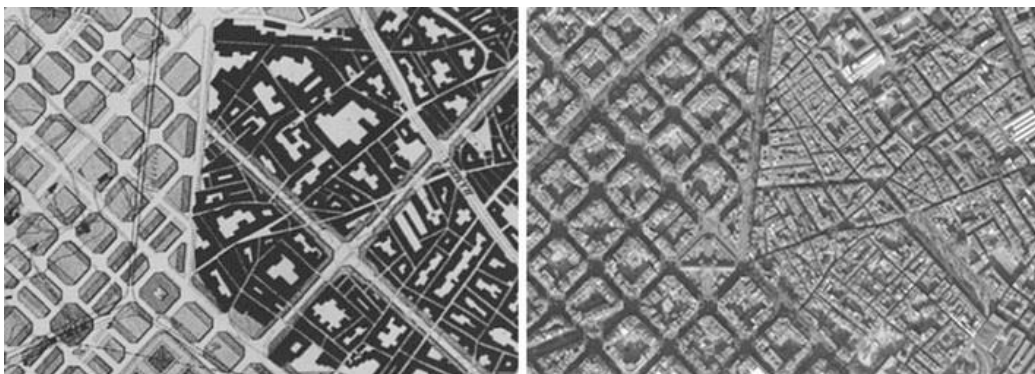


Figure 3.8 - Part of Cerdà's plan for the *Eixample* district in 1859 (left) and its current state (right) (Pujades et al., 2012).

3.4. THE *EIXAMPLE* DISTRICT

The *Eixample* district, located in the heart of Barcelona (see Figure 3.3), is currently the most populated district in Spain, with 266,857 inhabitants, covering an area of 748 square kilometres with more than 9000 buildings. The district is subdivided in six administrative neighbourhoods (see Figure 3.9): Sant Antoni, Nova Esquerra de l'*Eixample*, Antiga Esquerra de l'*Eixample*, Dreta de l'*Eixample*, Sagrada Família and Fort Pienc (Ajuntament de Barcelona, 2021).



Figure 3.9 - The six neighbourhoods of the *Eixample* district.

The average age of the *Eixample* constructions is 78,5 years, which is the second-highest age in the city (after Ciutat Vella, the Old City). Some of the original buildings have been replaced by more recent reinforced concrete (RC) structures (Moreno-González and Bairán, 2011). More than half of the buildings in the *Eixample* district, up to 70% (Pujades et al., 2012), are unreinforced masonry structures and this building stock was built before the 1960s, when concrete was first used in city construction.

The district's distinctive buildings were constructed in the late nineteenth and early twentieth century, and they have largely remained unaltered ever since. The majority of the structures built during this period of expansion were unreinforced masonry buildings, which formed aggregates that later became common building blocks, so called "*illes*" in Catalan (Paricio Casademunt, 2001). Each block was nearly the same size of around 113 x 113 m² and chamfered by 20 m at the corners (Figure 3.10). There are roughly 520 blocks in all, with 25 buildings each block on average. Their position is N-E to S-W to maximise solar exposure. In order to create squared blocks that are symmetrical, this pattern is repeated in a squared grid divided with 20 metres wide avenues. The blocks are composed of rectangular buildings lining the streets and pentagonal buildings at the chamfered corners. The specific number of buildings, whose façade's widths match the size of the typical *illes* is one of the secrets to the architectonic and urbanistic success of the *Eixample* district.

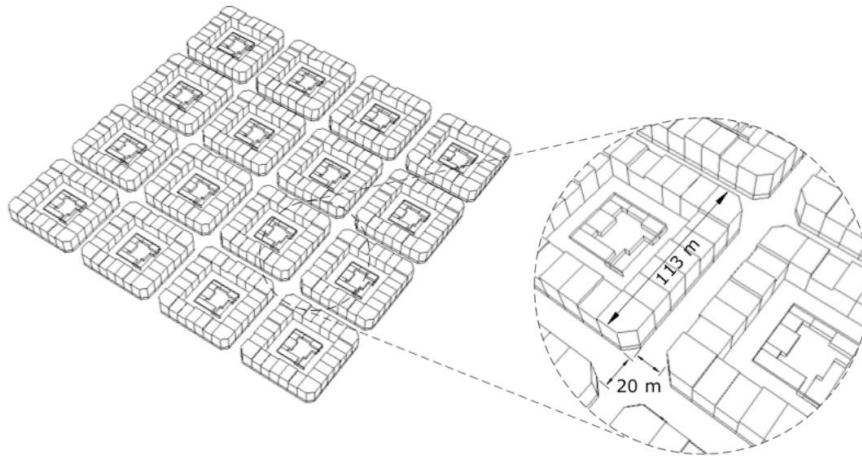


Figure 3.10 - Typical urban layout of Eixample in accordance with the provisions of Cerdà's plan (Avila-Haro, 2021).

The legislation from 1991 on the protection of the historical and artistic architectural heritage of the city of Barcelona limits and regulates architectural interventions in the *Eixample* neighbourhood (Barcelona City Council, 1991). For the historic structures in the *Eixample* district, this ordinance defines three levels of protection. "El Conjunt Especial", the special complex, defines the first level, in which constraints and limitations are set on the interventions permitted in terms of height and volumetric enlargement, as well as on the façades and their protrusions. Furthermore, a higher level of protection is established within the special complex's "El Sector de Conservació," the conservation sector, by a ban on demolition under certain circumstances (buildings constructed before the 1932 ordinance, not in a state of declared ruin, or appropriate to the *Eixample* typology (see Figure 3.11). The structures recognised as Monuments of National or provincial interest, on which any interventions for demolition, rebuilding, refurbishment, or repair work are prohibited, are the only ones that receive the highest level of protection (Cornadó Bardón, 2015).

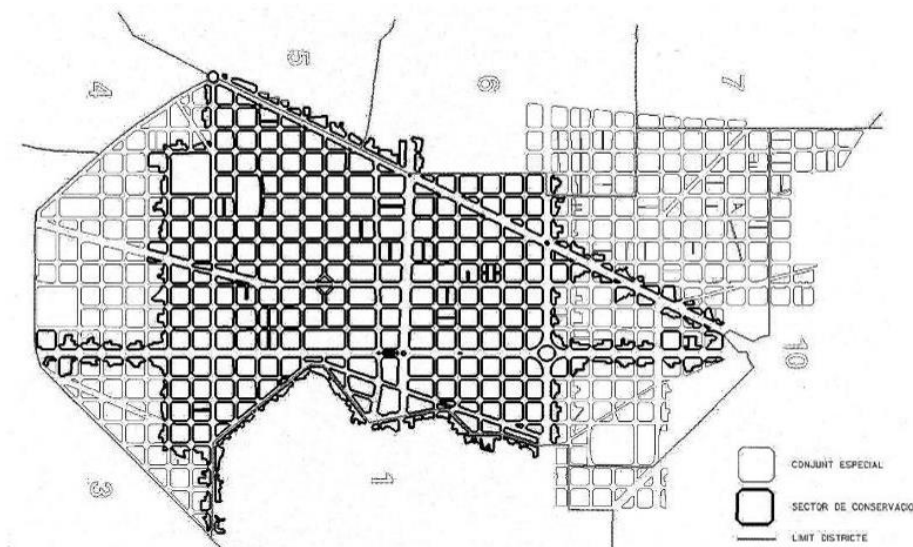


Figure 3.11 - Delimitation of the Special Complex, inside the dark grey border, and the Conservation Section of the Eixample, highlighted in black (Barcelona City Council 2002).

3.5. CONSTRUCTION TYPOLOGY OF *EIXAMPLE* BUILDINGS

Since the urban development of the *Eixample* district took place over a period of about 80 years, the original structures that were constructed featured numerous contributions from various architects and master builders (Bonett Díaz, 2003). The typical urban block was originally composed of predominantly URM buildings arranged in large aggregates, even though it can be frequently found a more recent concrete building built between two masonry ones, or even, a steel construction (Moreno González and Bairán García, 2012). According to many previous studies, despite the low to moderate seismic hazard in this area, these existing unreinforced masonry typologies are especially vulnerable to horizontal actions (Barbat et al., 2006); (Avila-Haro et al., 2012); (González and Bairán, 2015).

According to the Risk-UE project (Milutinovic and Trendafiloski, 2003), the load-bearing system of the existing buildings in Barcelona's urban centre is composed of unreinforced masonry, specifically for 79% of the buildings, while only 18% are RC structures (Figure 3.12b), approximately 80% of Barcelona's building stock was constructed prior to the adoption of the first Spanish Seismic Code in 1969. Moreover, Barcelona's existing buildings have been grouped in six construction periods, by considering the different Spanish construction regulations and their real application. The first period before 1940, known as Period I, is characterised by a lack of regulations and a complete disregard for seismic actions. The structural typologies from this period are the buildings with load-bearing walls, which were designed only for gravity loads. Period II, which covers the years 1940 to 1962, is distinguished by the use of some seismic-resistant techniques in the buildings' construction, despite the fact that no Spanish seismic-resistant regulations were in place at the time. Period III begins in 1963, the year in which the recommendation standard for considering the seismic action was published (MV-101, 1963). Period IV (1969–1974) is defined by the introduction of first Spanish seismic regulation (PGS-1, 1968). Period V, between 1975 and 1994, follows the seismic standard (PDS-1, 1974), which addressed in a more systematic way the calculation of structures under horizontal actions. The final period (1995-1996) is characterised with the application of the Spanish Standard for seismic resistant construction, NCSE-94 (1994), which establishes both calculation and design parameters that ensure proper global structural behaviour from horizontal loading (Lantada, 2007).

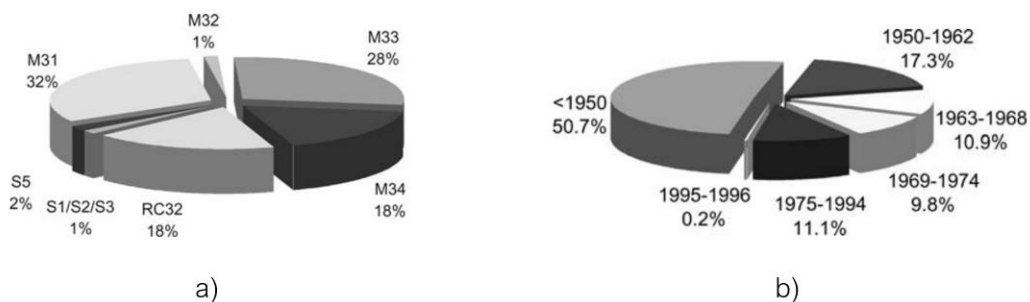


Figure 3.12 - RISK-UE project classification: a) Distribution of different building typologies: masonry buildings with wooden floors (M31), with masonry vaults (M32), with masonry vaults and steel beams (M33), and with floors of reinforced concrete beams and masonry vaults (M34); reinforced concrete buildings with irregular structural system, irregular infill, and soft/weak storey (RC32); steel buildings with moment frames, braced frames, and frames with unreinforced masonry infill walls (S1/S2/S3); steel and RC composite systems (S5); b) Age distribution of the building's construction periods based on the presence of seismic design recommendations (Barbat et al., 2006).

The buildings of the "*Eixample*" can be classified into four construction periods. The first period, so called pre-modernism (1860-1900), includes approximately 45% of the *Eixample* buildings. The height of the storeys decreases as the floor's levels rise. Particularly, in this period, cast iron *pillars* were added at the ground floor, allowing for much larger used space. The architectural style of these buildings is very minimalist with limited decoration to few elements. Modernism refers to the *Eixample*'s second construction period (1888-1915), which includes approximately 13% of the existing buildings. This period, designed primarily by the first generation of architects from Barcelona, is distinguished by its free forms, as opposed to the simplicity of the first period's architecture. The third period, known as post-modernism (1910-1936), includes approximately 20% of the existing masonry buildings in *Eixample* district. This period is characterised by the return to the simplification of the shapes and decorations as in the first period (Ajuntament de Barcelona, 1993). The most common building material in the first three periods is unreinforced masonry for the structural system of load-bearing walls. The last period is defined in the beginning of the 1960s, when the use of reinforced concrete as a construction system in buildings started to become significant, giving rise to the beginning of contemporary architecture (Paricio Casademunt, 2001). These structural typologies consist of columns with infill masonry walls and one-way slabs with precast joists.

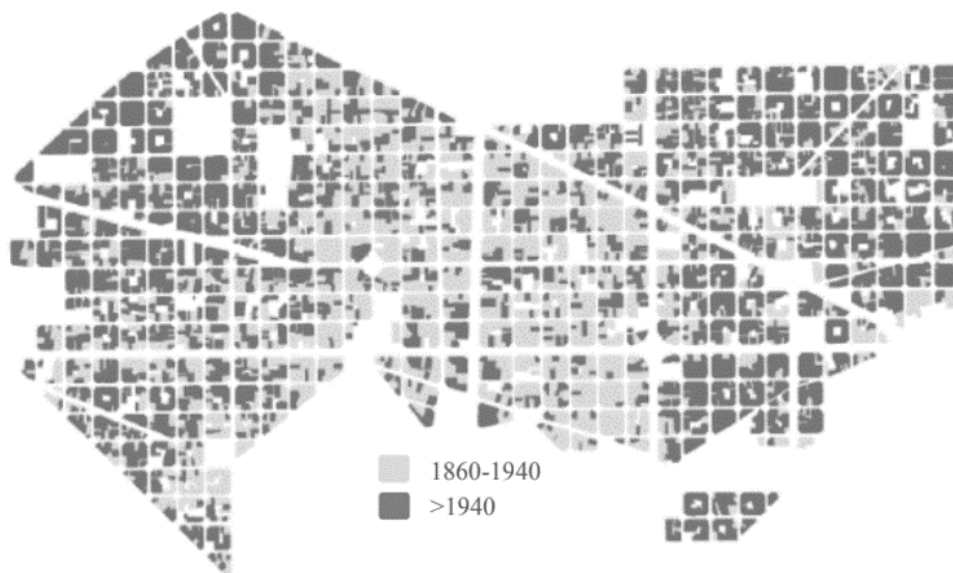


Figure 3.13 - Construction period of the buildings in *Eixample* (adapted from Cornadó Bardón, 2015).

The large number of revisions to the city planning requirements that came after the original design provoked further evolutions in terms of typology, morphology, and implementation. After the first ten years, a constructive process set in, producing a group of buildings with nearly identical shapes and designs that could be considered to be the standard model of *Eixample*. Hence, the construction system was evidently a repeated scheme, particularly when referring to historical existing buildings built between 1860 and 1940 (Figure 3.13). These structures were only designed to withstand gravitational loads and account for roughly half of the total building stock in this urban area. As a result, the existing buildings constructed during this time period should be regarded as the most representative typology (Cornadó Bardón, 2015).

The *Eixample* unreinforced masonry buildings can be categorised into two generations. The first generation of buildings have a continuous and uniform structural system, made of unreinforced masonry walls starting from the base and going throughout the entire height of the structure (Figure 3.14a). Buildings of the second generation have a hybrid structural system, including a frame system made of cast-iron *pillars* and metallic beams in order to provide a big open space at the ground floor (Figure 3.14b). The rest of the structure is one continuous structural system of unreinforced masonry walls. This hybrid system, which is frequently constructed of steel or in some cases of concrete (depending on the year of construction), typically appears at the corner structures that can have different geometrical configurations (Figure 3.14c) (Paricio Casademunt, 2001).

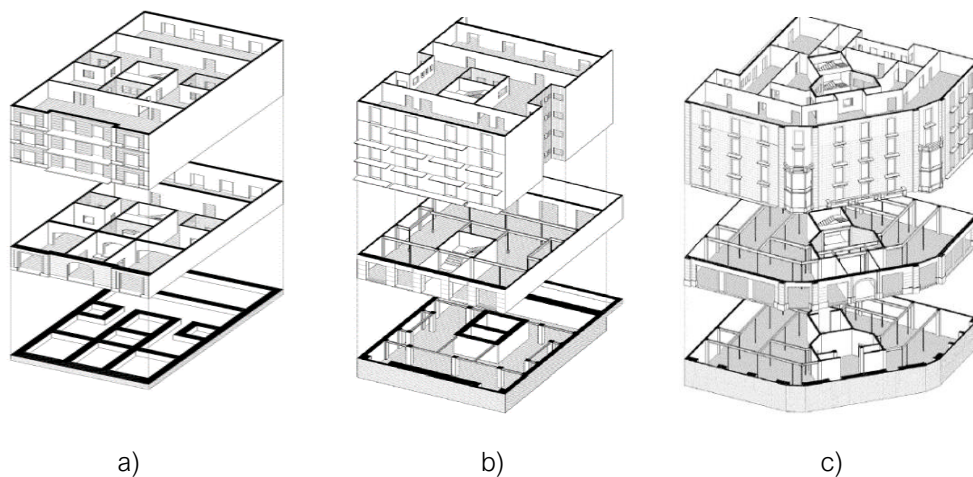


Figure 3.14 - Different structural systems (Paricio Casademunt, 2001): a) homogeneous system of slender walls; b) hybrid system – concrete columns and masonry walls; c) hybrid system – steel columns and masonry walls.

The number of floors of the *Eixample* typical buildings can generally vary between 4 and 7 floor levels. The average number of storeys is 5 to 6 storeys according to the statistical data provided from the Ajuntament de Barcelona (2021). Each building has three distinct height levels: the ground floor, the mezzanine floor, and the upper levels, which are identical up to the rooftop. The ground floor of these buildings has a higher height than any other level of the same building, around 4 - 4.5 m high, and the rest of the storeys have a constant height of between 3 and 3.2 m. This is due to the fact that these lower floors were intended for commercial activities, which is why they required a more versatile space than a residential unit. Therefore, in the basement and the ground floor, the presence of *pillars* of cast iron and steel beams is very common, which are used for supporting the load-bearing walls of the rest storeys. This construction solution allows large open space permitting the ground floors to be used for trading activities and office or administrative spaces in the mezzanine floors. However, it also provides with the systematic soft-storey behaviour in most of the structures, which are built as a mix of two typologies (steel/concrete frame system and unreinforced masonry walls). This suggests a reduction in the stiffness of the ground floor of the buildings, which, when combined with the lack of seismic-resistant structural elements, leads to a preliminary conclusion that the seismic vulnerability of these structures is considerable.

For many years, regulations have imposed height limits on buildings, preventing the number from exceeding a certain level. The specific criteria that had to be followed during the construction were gradually altered by a long series of municipal ordinances, which frequently revised the configuration of the building type. These regulations specified the building parameters, including the height and depth of the structures, the number of storeys, the built volume, and even the occupation of the urban block plot. Figure 3.15 illustrates a visual representation of the volumetric configurations of the municipal ordinances' rules.

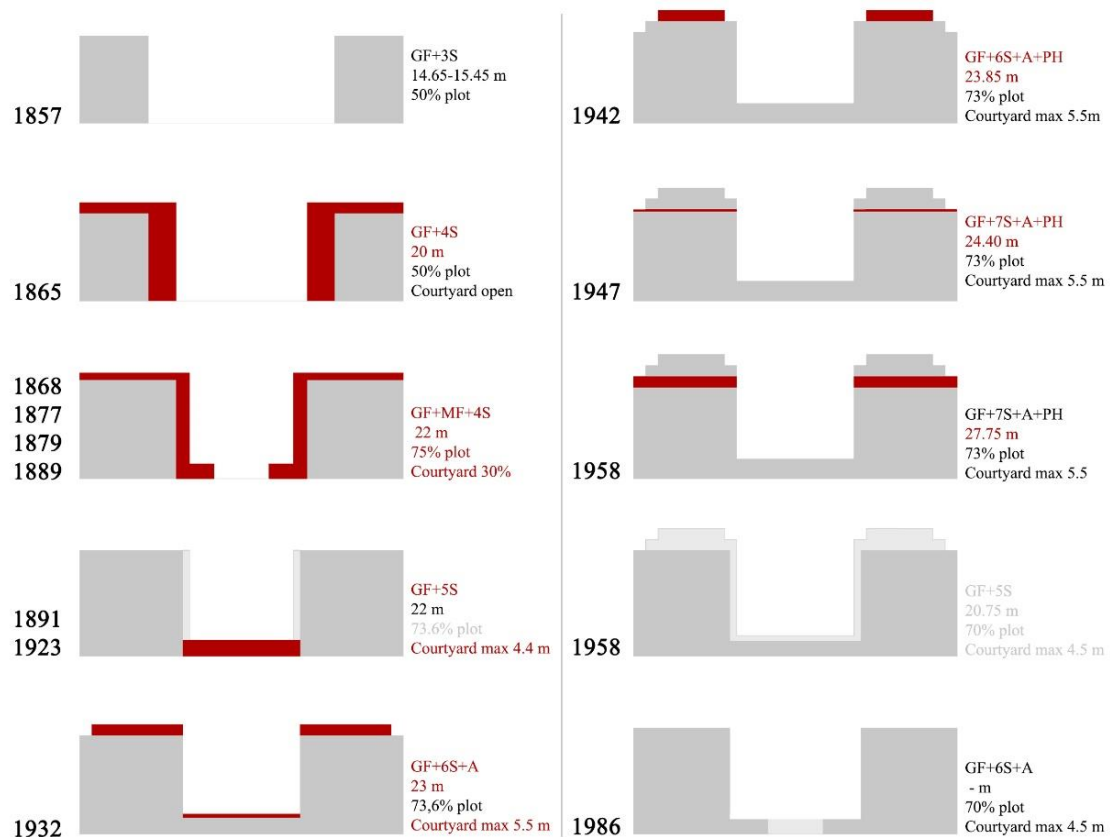


Figure 3.15 - Graphical representation of the ordinances' limits on the transversal section of a typical *Eixample illa* with changes by increasing (in red) and decreasing (in light grey) limits. The limits in height steadily increased until the 1970s, and the addition of *remuntes* started to be limited in terms of plot occupation and visibility from the street (Marafini et al., 2022).

According to the evolution of the ordinances, the maximum height limit was changed during the years and thus, many existing buildings have additional storeys on top of the original buildings, known in Catalan as *remuntes*. The majority of the *remuntes* found in the *Eixample* district date from the early 19th century until 1976, when the General Metropolitan Plan regulations put an end to subjective construction in the central urban area of Barcelona city by limiting the number of storeys and the allowed building height (Colom et al., 2016).

The *remuntes* are additional storeys added as vertical extensions to the existing *Eixample* buildings. The structural and construction features of the *remuntes* were influenced by external factors, such as the evolution of construction techniques, the different use of materials, the building regulations, and the interests of private ownership decision-making. The configurations that remain prevalent today differ in terms of architectural design, alignment, the number of storeys, the covered space and other characteristics. Around half of the old existing historical

buildings in the *Eixample* district have *remuntes*, according to the most recent typological classification (Colom, 2014). These vertical extensions are found mainly in the urban area close to the Old City (see Figure 3.16).



Figure 3.16 - Distribution of the "remuntes" (shown in black) in the *Eixample* district of Barcelona (Colom, Cornadó Bardón, et al., 2016).

The additional storeys represent a vertical irregularity for the existing buildings (see Figure 3.17). Hence, the *remuntes* have been evaluated as a specific parameter for the vulnerability assessment and the different configurations are specifically described in section 5.3.2 of the following Chapter 5.

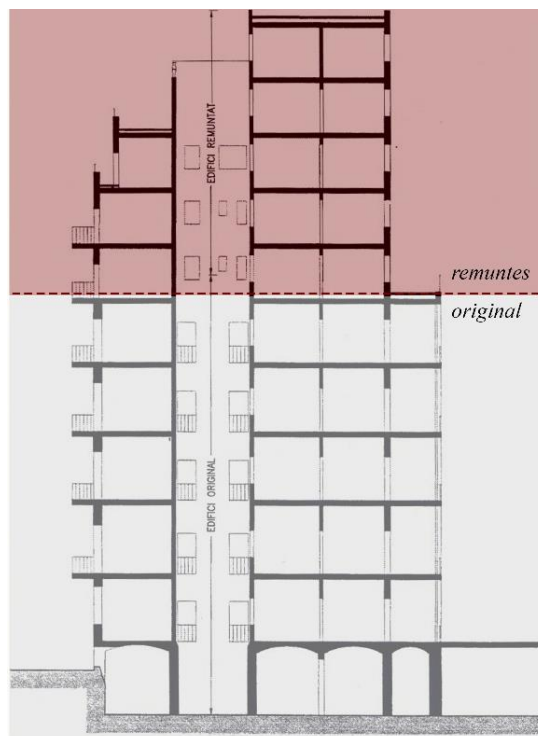


Figure 3.17 - Example of a vertical section of an existing building with "remuntes" added on top of the original building's height in the *Eixample* district in Barcelona (adapted from Paricio Casademunt 2001).

Initially, the vertical extensions followed the style of the existing buildings, employing chromatic analogy and avoiding the use of specific ornamental elements (see Figure 3.18a). Later with the Catalan modernism, decorative motives and additional elements were introduced, which can still be seen today in the most eclectic *Eixample* façades. In a few cases, the additions exceeded the municipal regulatory height with expedient of including superpositions, domes, or other elements, which also added to the building's monumental character (see Figure 3.18b). Finally, by the second half of the twentieth century, stylistic configurations had become more diverse, adapting to a modern style with larger built volumes and variability (see Figure 3.18c).

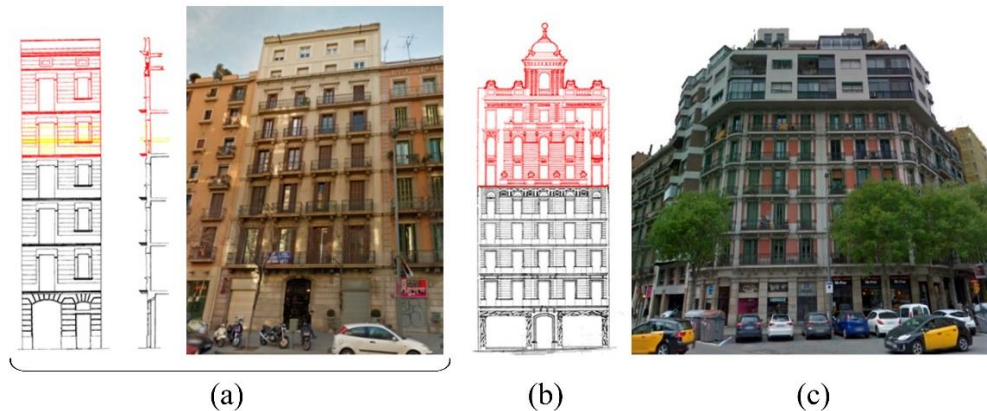


Figure 3.18 - Example of different vertical extensions (*remuntes*): a) *remunta* 1955, C. Wellington 15; b) *remunta* 1924, Passeig de Gràcia 91; c) *remunta* 1960s, Aragó street 339 and Bailèn street 9 (adapted from Colom et al. 2016).

Initially, the ordinances prohibited visible roofing from the street level, but later they only restricted its geometry in terms of inclination. With the addition of the attic, new configurations of vertical extensions emerged. In terms of both depth and inclination, the additional floors were constructed either within, at, or above the regulatory limits. The *remuntes* were often retracted in regards to the front façade (Colom et al., 2016). Figure 3.19 illustrates the most frequent configuration in terms of longitudinal section for the *Eixample* buildings, where the vertical extensions are retracted on the front façade and aligned on the rear façade.

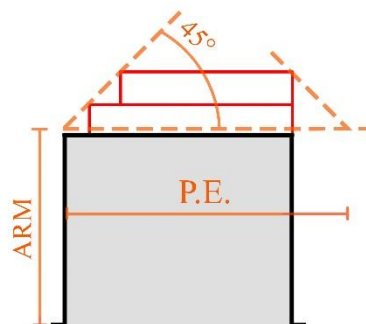


Figure 3.19 - Development of the longitudinal section. (ARM = *alçada reguladora municipal*, municipal regulatory height, P.E. = *profunditat edificada*, building depth) (adapted from Colom 2014).

The majority of the buildings in the *Eixample* district follow the same structural pattern, with front and back façades and a second interior wall, which is parallel to the street in order to define rooms with wider spans. The bottom floor, the upper levels, and the vertical extensions are the three structural components that make up the typical building (see Figure 3.20). Each of these

components contributes to the building's structural response based on its morphological and constructive features (Cornadó Bardón, 2015).

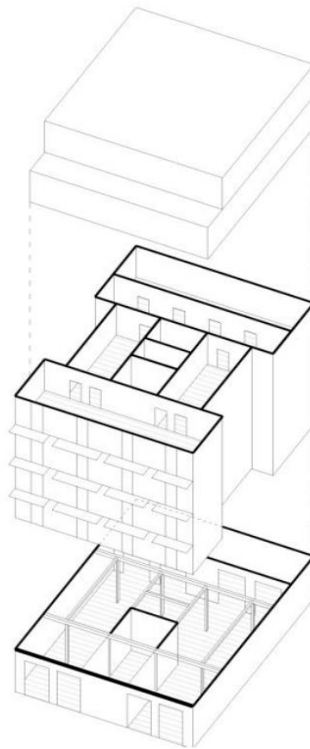


Figure 3.20 - Three structural analysis units of Eixample's building (Cornadó Bardón, 2015).

The foundations for the masonry buildings in the *Eixample* district are considered to be shallow foundations under the entire length of the bearing masonry walls, or in the case of newer buildings, isolated footings were placed under concrete, masonry or cast-iron pillars (Figure 3.21) (Paricio Casademunt, 2001).

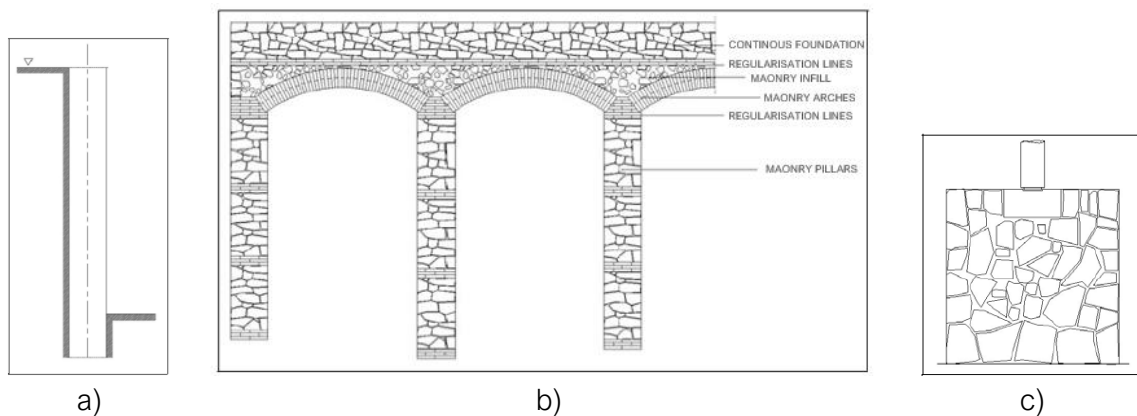


Figure 3.21 - Foundation types of the existing masonry buildings in Eixample district: a) continuous foundation under load-bearing masonry walls; b) foundation composed of masonry wells and brick arches under continuous masonry walls; c) isolated footing under concrete, masonry or cast-iron pillars (Paricio Casademunt, 2001).

The primary construction material used in the *Eixample* buildings is masonry, composed of solid clay ceramic bricks and lime mortar. This composite material is used not only for the load-bearing

walls, but also for the partition walls, columns, staircases, foundations, and for decorative elements. Initially, until 1925, the bricks were made with traditional techniques, cooked in ovens and manually moulded in shape, presenting many heterogeneities, coarse grain, and high porosity (see Figure 3.22). Later on, during the industrialisation period, solid brick units made with Hoffman kilns began to be manufactured, having a more regular shape and more homogeneous characteristics than those used previously. The standard brick is typically made of solid fired clay and has dimensions of approximately 300 x 150 mm, with or without holes (Paricio Casademunt, 2001).



Figure 3.22 - Front view of a traditional solid brick masonry wall in an existing building in the *Eixample* district (left) and a solid brick unit with dimensions 294 x 145 x 49 mm (right).

The mortars are the result of the elaboration process during the specific construction period. As a result, they can be primarily composed of aerial lime, hydraulic lime, slow cement, or Portland cement (Paricio Casademunt, 2001). The most commonly used mortar is the hydraulic lime mortar. The mechanical properties of the brick units and the used lime mortar, as well of the masonry as composite material, have been described in section 3.8 obtained from experimental studies on specimens extracted from unreinforced buildings located in Barcelona's urban centre.

Before 1920, ashlar stone (usually Montjuïc sandstone) was used for the ground floor of some buildings' front façades, as well as for the foundations. This stone was also used as a decorative element on the main façades, particularly around the openings such as doors and windows.

During the 19th century, wood was used as a structural material for the beam elements used in the one-way floor systems. Wooden lintels were also used to provide extra support for small openings (Paricio Casademunt, 2001). In the beginning of the 20th century, the industrialisation period brought the introduction of the metal, which was used for the replacement of the timber beams with steel beams in the one-way floors, as well as the lintels above the openings. The presence of the metal as a material is found at the ground floor of some existing buildings, where steel beams and cast-iron *pillars* are placed for having a large open space for commercial activities.

Figure 3.23 illustrates a section of a typical building in the *Eixample* district, with a load bearing system composed of masonry walls on the upper levels and a hybrid system (masonry walls, masonry columns, cast-iron *pillars* and steel truss beams) at the ground floor level. All the structural and non-structural elements are shown, starting from the foundations, then the ground floor level and continuing throughout the rest of the storeys.

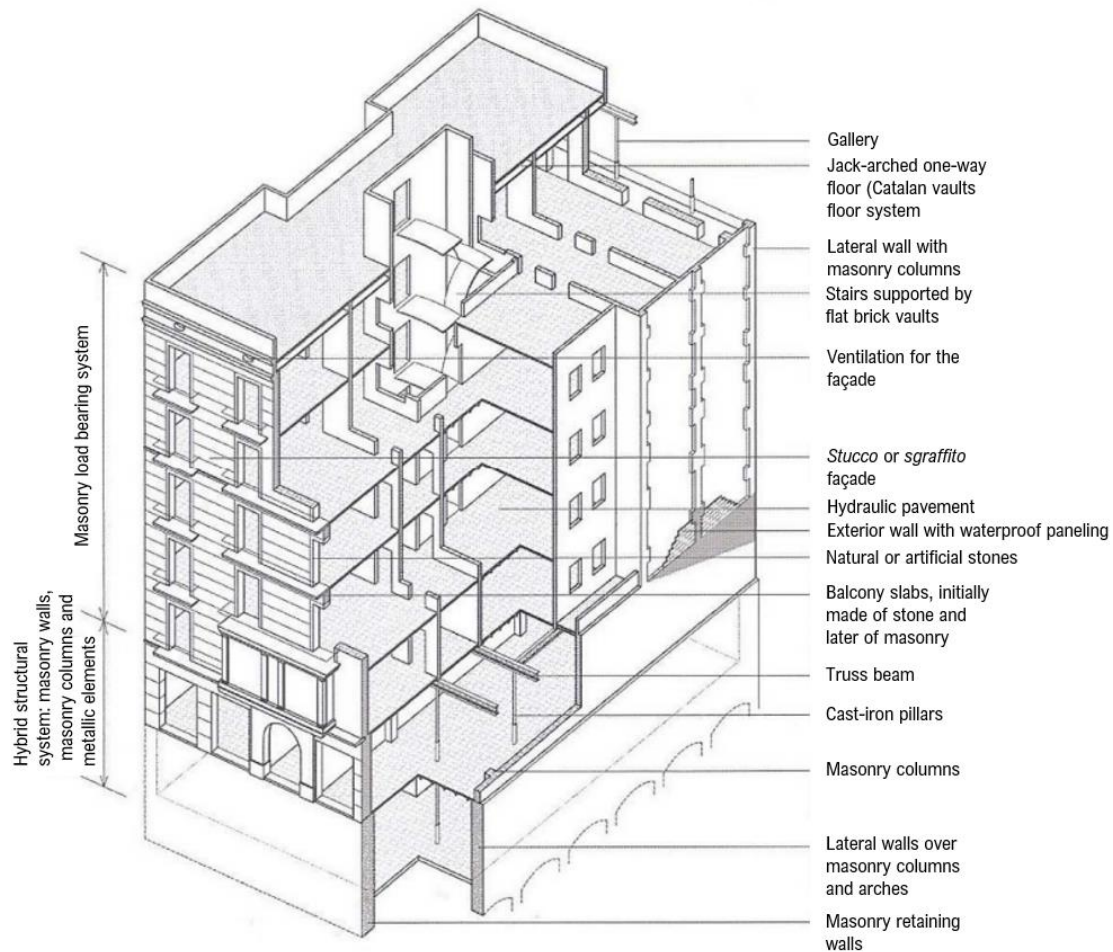


Figure 3.23 - Section of a typical existing *Eixample* building including all structural and non-structural elements (adapted from Paricio Casademunt 2001).

3.5.1. Structural elements features

The structural resisting system of the *Eixample* buildings can be composed of different structural elements such as: load-bearing masonry walls, horizontal flooring system, masonry columns, cast-iron *pillars* and the steel truss beams at the ground floor level. The detailed description of all the construction features of each of the structural elements and their connections is presented in the following sections.

- Masonry walls

The primary load-bearing walls are the front and rear façade, the interior walls parallel to the façade, the walls forming the stairwell and patio, and the lateral walls between buildings, also known as intermediate walls (Cornadó Bardón, 2015). These unreinforced masonry walls can have a variety of thicknesses.

In general, the façade walls are typically 0.30 m thick, with large openings and balconies on the street side. In some existing buildings the thickness of the façade walls varies according to the floor level, where the thickness at the base level can be 0.45 m, with a reduction to 0.30 m at the upper floor levels. The wall thickness at ground level can be greater than on the upper floor levels,

by ranging from 0.20 m in the staircase walls to 0.60 m at the façades (Pujades et al. 2012). The central core of the building typically has a continuous thickness of 0.15 m across all storeys, where the staircase and interior patios are typically located. The lateral walls are the ones perpendicular to the façades and divide the buildings parcels for the rectangular band buildings. They are approximately 0.30 m thick on the ground floor and 0.15 m thick on the upper floors. Moreover, the division walls are 0.05 m thick and they are not structural, but only provide separation and acoustic insulation without any proper connection to the façades and lateral walls (Gonzalez-Drigo et al. 2015). The brickwork and wall organisation of these walls were completed using traditional construction techniques. Figure 3.24 illustrates different constructive solutions for the ground level façade and flooring system. Overall, the load-bearing walls have an increasing slenderness in height across the various configurations of the lower levels, which can extend to basement levels.

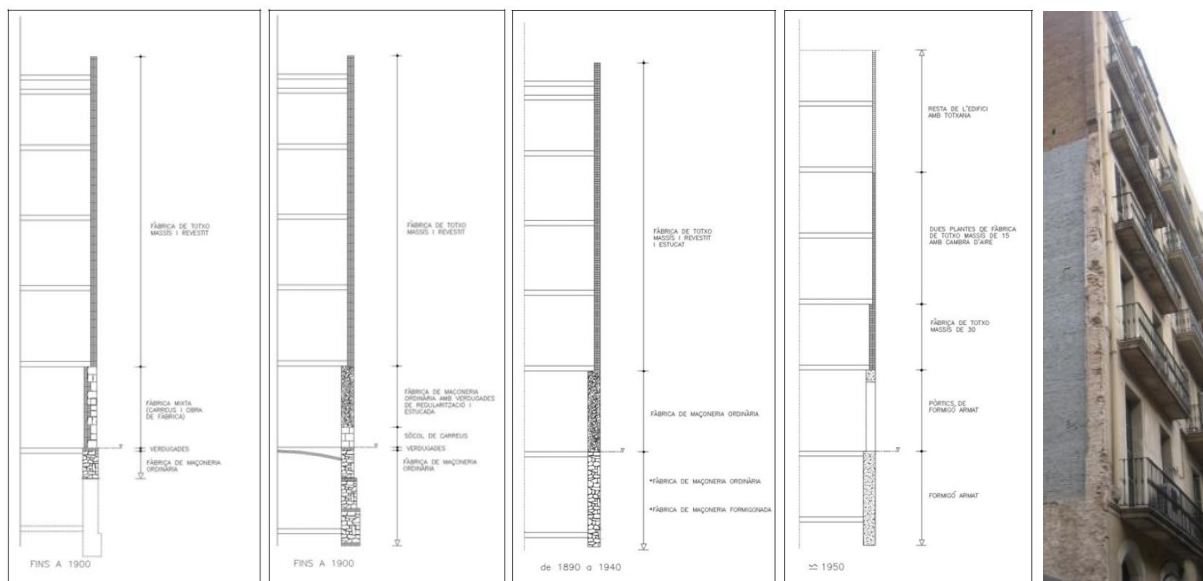


Figure 3.24 - Typical section of the façade wall in different construction periods (from left to right): without basements, with basement with masonry vaults below the ground level, with basement with flooring system on beams below ground level, and with porched system at the base level and different thicknesses and materials of the walls at the upper floor levels. On the right, a photograph with a side view of the front façade of an existing building in the *Eixample* district, in which it can be observed that the slenderness of the load-bearing masonry wall is increasing within the height of the building (Paricio Casademunt, 2001).

Furthermore, there are openings for doors, windows, or balconies and above each opening, steel lintels of varying sizes are present. The wall sections over the lintels can be unstable, with visible cracks caused by differential displacements (Cornadó Bardón, 2015).

- The horizontal floor system

The typical *Eixample* buildings' one-way slabs are distinguished by beams made of wood, steel, or concrete that are connected by small ceramic barrel vaults. The material used for the beams is determined by the building's construction period. Before 1890, timber beams with wood plank pavements were used in the construction of the *Eixample* buildings (Paricio Casademunt, 2001). Later, and until the middle of the 20th century, horizontal timber structures known as jack arch floors (*forjados de bovedilla* in Spanish) were popular along Spain's Mediterranean coast (Diodato et al., 2013).



Figure 3.25 - Typical one-way flooring system with timber beams (left) or steel beams (right) and masonry vaults with flat ceramic tiles (Casanovas, Graus i Rovira, and Rosell 1993).

The introduction of new materials and industrialisation resulted in the replacement of timber beams as a horizontal structural system by metallic beam elements (see Figure 3.25) (Diodato et al., 2015). Although steel beams with tile vaults were gradually introduced in the last decade of the nineteenth century, timber floor systems were still used during a nearly 30-year transition period. Due to a metal shortage caused by the Spanish Civil War, reinforced concrete beams were used instead of steel beams (Gonzalez-Drigo et al., 2015).

Figure 3.26 represents the evolution of various flooring system solutions in Catalonia, Spain, over the last 150 years.

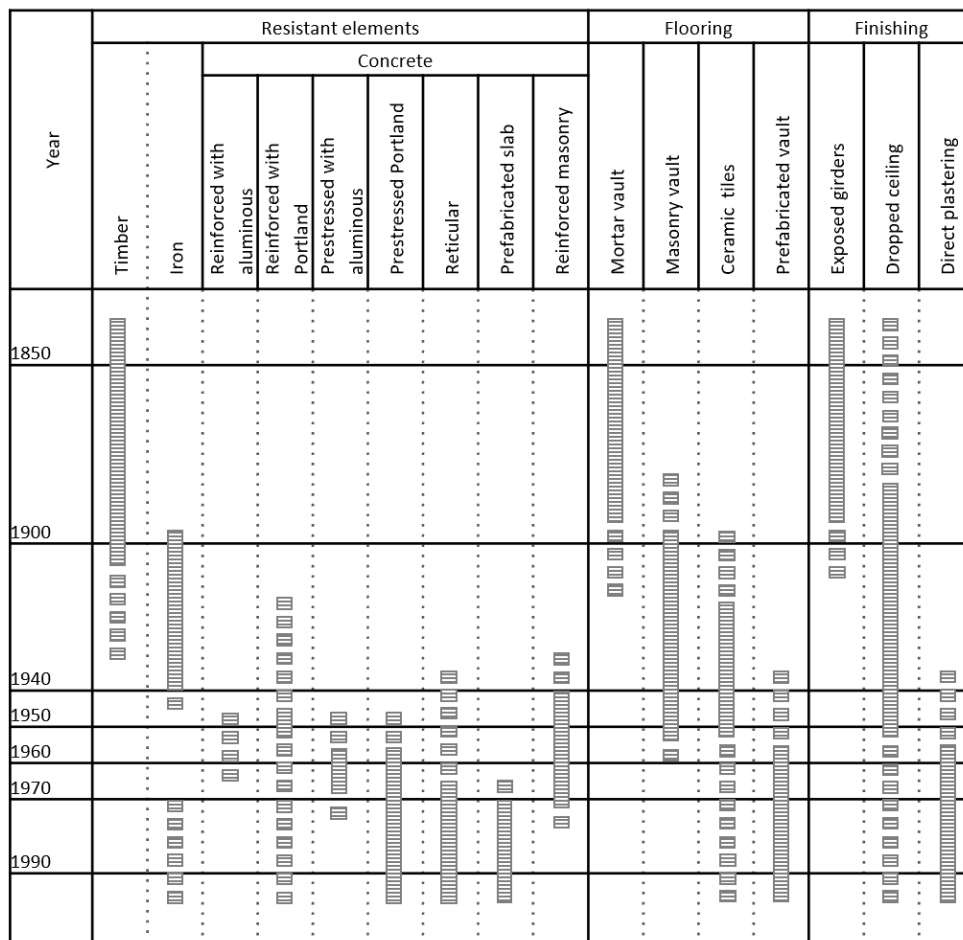


Figure 3.26 - Use of different types of flooring system in Catalonia since 1850 (adapted from Casanovas, Graus i Rovira, and Rosell 1993).

During the construction periods of the *Eixample* buildings, different horizontal flooring systems were used, depending on the materials available and the applied construction techniques (see Figure 3.27): a) timber beams connected with wood planks; b) timber beams with ceramic tile vaults; c) steel beams with ceramic tile vaults; d) metallic profiles with concrete addition through round connectors; e) metal beams connected with a pavement of double row of ceramic tiles; f) ceramic reinforced floor slab.

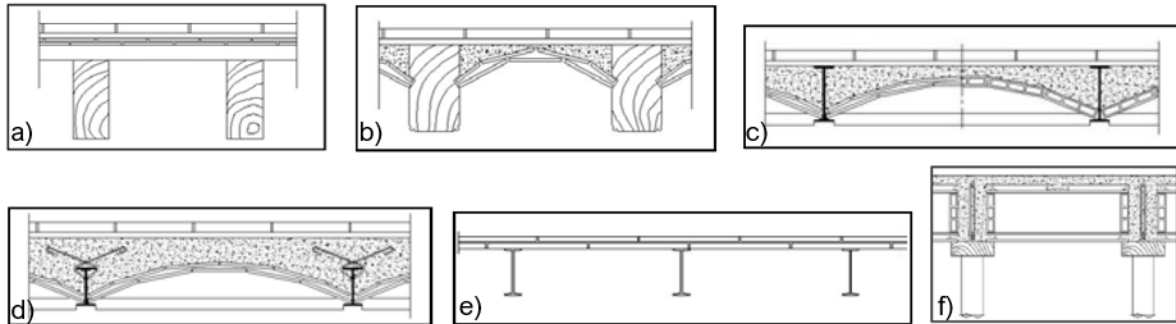


Figure 3.27 - Different floor slab solutions during the construction periods of the *Eixample* buildings (Paricio Casademunt, 2001): a) timber beams connected with wood planks; b) timber beams with ceramic tile vaults; c) steel beams with ceramic tile vaults; d) metallic profile with concrete addition through round connectors; e) metal beams connected with a pavement of double row ceramic tiles; f) ceramic reinforced floor slab.

The typical design of this flooring system, when steel is used in place of timber, consists of steel beam girders and masonry vaults covered in flat ceramic tiles (applied in one or two layers) or hollow bricks. The beams have an I-shaped cross section and can range in height from 140 to 240 mm (ITEC, 1994). The spacing between them can be between 600 and 1000 mm. The thickness of the floors can range between 150 and 200 mm (Gonzalez-Drigo et al., 2015). Floor beams are typically supported by load-bearing masonry walls with a support length of about one-third the wall thickness.

The most common floor system in the *Eixample* district's existing buildings is the one-way floor slab composed of the following elements (Figure 3.28): 1) one-way timber or steel beams; 2) tile barrel vaults supported by the beams; 3) an infill layer of rubble or lime mortar over the vaults; and 4) an upper layer finished with a pavement on top.

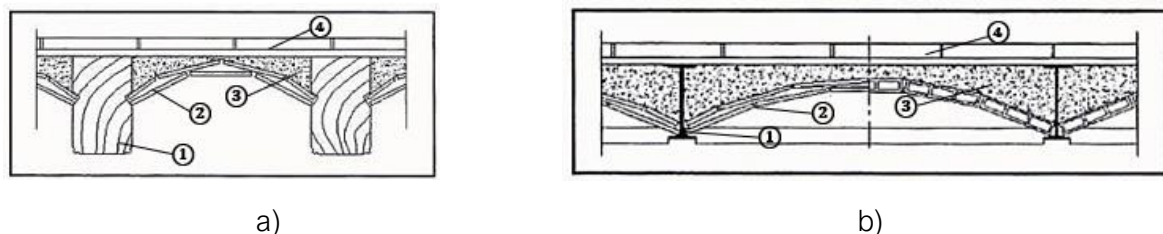


Figure 3.28 - Typical one-way floors in the *Eixample* district of Barcelona: a) timber beams with tile barrel vaults, and b) steel beams with tile barrel vaults (adapted from Paricio Casademunt 2001).

- Masonry columns and cast-iron pillars

The columns and *pillars* are the structural elements only found on the ground floor. They serve a structural purpose by supporting the beams that bear the load of the upper floors' URM walls.

These elements are either attached to the side partition walls, in solid clay brick masonry, where they add stability to the slenderness or they are placed in the centre of the building's plan, as cast-iron *pillars* (Cornadó Bardón, 2015).

The masonry columns (known as '*pilastres*' in Catalan) are constructed as extension to the lateral walls and they support the steel beams in order to have a bigger open space for the commercial activities (Figure 3.29). These columns can vary greatly in size, potentially causing a point loading effect on the wall separating adjacent buildings. Normally, they are square columns with dimensions of 0.45 m by 0.45 m and are typically embedded at regular intervals of 3.5 m to 5 m. They play a crucial role at the ground floors by supporting the primary and additional metallic beams needed for the hybrid structural system, since there are no interior walls.



Figure 3.29 - Presence of masonry columns ("*pilastres*") at the ground floor entrance of an existing masonry building in Eixample (Cornadó Bardón, 2015).

The cast-iron pillars that comprise the hybrid building systems can be found in either circular cross sections or other diverse profiles. The cases of circular pillars were initially fabricated as solid members, but a common solution was a hollow section with eccentricity by having a non-constant crown thickness (Figure 3.30). Cast-iron was typically used for these pillars as it was a popular material from the 18th to the 20th centuries. Cast-iron pillars could be found at the ground floor used for commercial activities and at the galleries on the back façades (Figure 3.31).

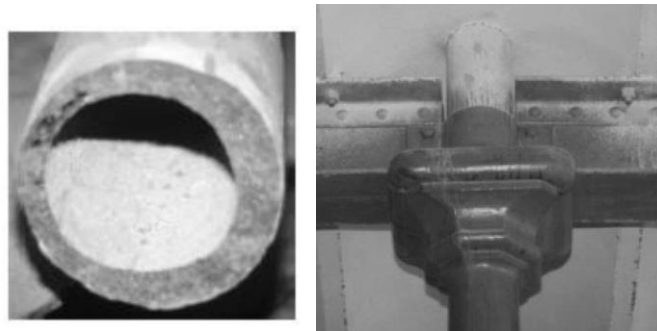


Figure 3.30 - Circular section of a cast-iron pillar (left) and its connection to a steel beam (right) (Paricio Casademunt, 2001).



Figure 3.31 - Position and dimensions of the cast-iron pillars located at the ground floor of an existing masonry building in the Eixample district (Cornadó Bardón, 2015).

In most cases, these cast iron columns offer a decorative purpose to the buildings in addition to their structural role. In most cases, they are decorated with geometrical patterns that run the length of their height (see Figure 3.32). The majority of these cast-iron pillars are found in buildings constructed between 1915 and 1930 (Paricio Casademunt, 2001).



Figure 3.32 - Decorated cast-iron pillars in the existing historical buildings in Eixample district (Rigalt i Fariols, 1857).

- Steel beams

The beams are the structural elements that are present in the existing buildings in *Eixample* district since the beginning of their construction. Different materials and construction techniques were used depending on the construction period (Paricio Casademunt, 2001).

Metallic profiles were used as a construction solution for the beams (*jässeres* in Catalan), since there was the need of having a big open space at the ground floor. These beams support the interior walls from the upper levels, which are parallel to the façades as well as the horizontal flooring system. The spans that these beams had to cover were frequently greater than 5 m, while the height available on the market of prefabricated beams was up to 300 mm. The different

geometrical and structural configurations of the metallic beams depended on the strength requirements that they had to provide. Initially, when higher resistance was required in buildings, beams with composite geometries were chosen, whereas in subsequent years, the final price was the primary factor in determining the appropriate type of beam to be used.

According to Paricio Casademunt (2001), the main types of metallic beams present in existing buildings in the *Eixample* district are:

- Truss beams (*Jàsseres amb gelosia*): The resistance section of these beams is made up of four "L" profiles, two of which are placed in the upper part and two in the lower part (Figure 3.33a).

- Riveted beams (*Jàsseres de palastre*): Beams with four flange angles, two at the bottom and two at the top, riveted together (Figure 3.33b).

- Reinforced riveted beams (*Jàsseres de palastre reforçades*): beams with the same properties as the aforementioned riveted ones but with the addition of reinforcement plate in the lower part, aiming to increase the beam's moment of inertia (Figure 3.33c).

- Box beams (*Jàssera de caixó*): A configuration of two joined simple beams that are secured at right angles to form what appears to be a long, hollow box (Figure 3.33d).

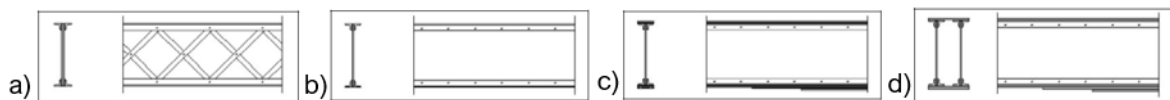


Figure 3.33 - Steel beams typologies in the typical *Eixample's* buildings. a) truss beams with rivetted grid; b) riveted beams with reinforced web; c) riveted beams with reinforced flanges; d) box beams with multiple reinforcements on the bottom flange and double reinforced web (Paricio Casademunt, 2001).

The beams were used as part of the structural solution together with the masonry columns embedded in the lateral walls, and thus, specific solutions for load transmission were frequently implemented (Figure 3.34).



Figure 3.34 - Position of a steel beam at the ground floor and transmission of the load to a masonry column by a simple support (Paricio Casademunt, 2001).

- Connections between structural elements

The primary connection is between the orthogonal load-bearing walls, depending on their interlocking. The secondary connection is between different types of structural elements and materials, such as the connection between the masonry walls and the horizontal diaphragms. Additionally, a number of solutions can be found for the connections between these structural elements that can either increase a building's capacity (in the case of adequate connections) or

result in a decrease in capacity where the elements connections are inadequate, such as when they are not perfectly clamped, etc.

The connection between the timber beams of the one-way floor slab and the unreinforced masonry walls was realised though a simple support by placing the beams between two bricks on the lateral walls (Figure 3.35).

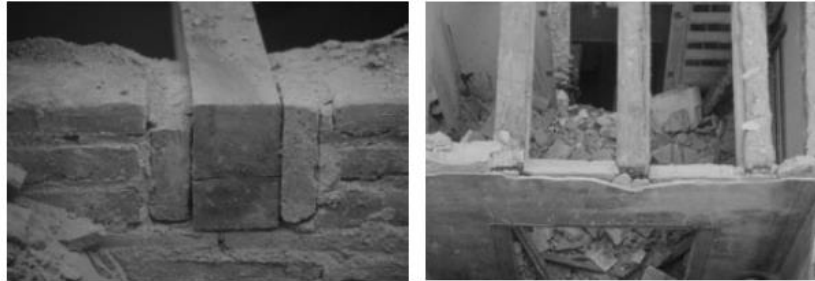


Figure 3.35 - Simple supports of timber floor beams between two bricks on the load-bearing unreinforced masonry wall (Paricio Casademunt, 2001).

Figure 3.36 illustrates two different supporting solutions for the unidirectional floor system with timber beams and ceramic vaults on the masonry resisting walls parallel to the timber floor beams (Paricio Casademunt, 2001).

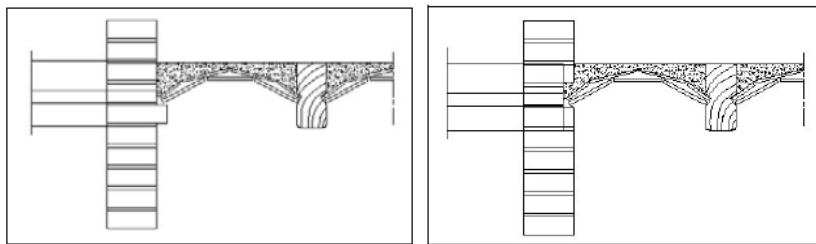


Figure 3.36 - Different solution for supporting the unidirectional floor system with timber beams and ceramic vaults on masonry resisting walls parallel to the floor's beams: placing a brick out of the masonry wall (left) or making a horizontal slot in the masonry wall for supporting the ceramic tile vault (right) (Paricio Casademunt, 2001).

The connections between the primary elements such as the cast-iron *pillars* and the steel truss beams had to be determined beforehand as they were delivered to the construction site as prefabricated elements. Therefore, the most typical connections were usually made by using box and nail joints or screwed joints (Figure 3.37).

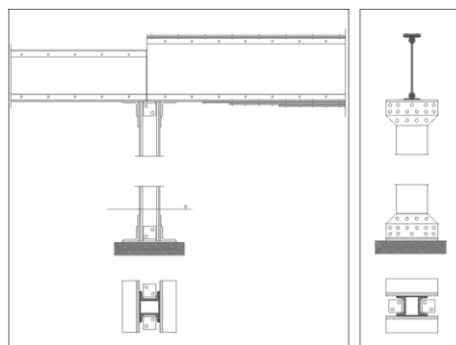


Figure 3.37 - Detail of connection between riveted beam and column profiles (Paricio Casademunt, 2001).

3.5.2. Geometrical configuration of the *Eixample* buildings

The configuration of the *Eixample*'s buildings can be described with some typical characteristics such as the width and depth of the building's plan, the number of walls (parallel to the façades and parallel to the lateral walls), the distance between walls, the position and number of patios (central and lateral), the type, position and size of the stairwell and number of bays (with beams perpendicular to the façade or to the lateral walls). There are two main types of building plans: the rectangular plan, with a ratio of the width of the façade to the building depth of 1:2 or more, positioned on the sides of the urban blocks for the so-called band buildings, and the pentagonal plan for the corner buildings, which follow the geometry of the chamfered corners of the typical *block*. The width of the buildings' façades can vary between 9 and 17 m and the buildings' depth is normally between 18 and 27 m for the rectangular wide band buildings (Cornadó Bardón, 2015).

The configuration of the typical rectangular buildings is composed of a central part (where the staircase and patios are located) and bays (parts of the structure before and after the central part, formed of masonry walls and one-way floor slabs with beams perpendicular to the façades) (Cornadó Bardón, 2015). According to this geometrical configuration, the following typical building typologies can be recognised (see Figure 3.38):

- Wide regular buildings composed of a central part (with a central staircase, interior patio and bays around them with beams perpendicular to the lateral walls) without any lateral patios and one or two bay spans before and after the central part, with floor beams perpendicular to the façades.
- Wide regular buildings composed of a central part (with a central staircase, interior patio and bays around them with beams perpendicular to the lateral walls interrupted with one/two/three lateral patios) and bays before and after the central part, with floor beams perpendicular to the façades.
- Wide irregular buildings composed of a central part (with a central staircase, interior patio and bays around them with beams perpendicular to the lateral walls interrupted continuously with one patio) and bays before and after the central part, with floor beams perpendicular to the façades.
- Wide irregular buildings composed of a central part (with a central staircase, interior patio and bays around them with beams perpendicular to the lateral walls interrupted not continuously with one patio) and bays before and after the central part, with floor beams perpendicular to the façades.
- Narrow buildings with a lateral staircase and patio placed transversally regarding the building's plot, and front and rear bays, with floor beams parallel to the façade walls.
- Narrow buildings with a lateral staircase and patio placed longitudinally regarding the building's plot, and front and rear bays, with floor beams perpendicular to the façade walls.

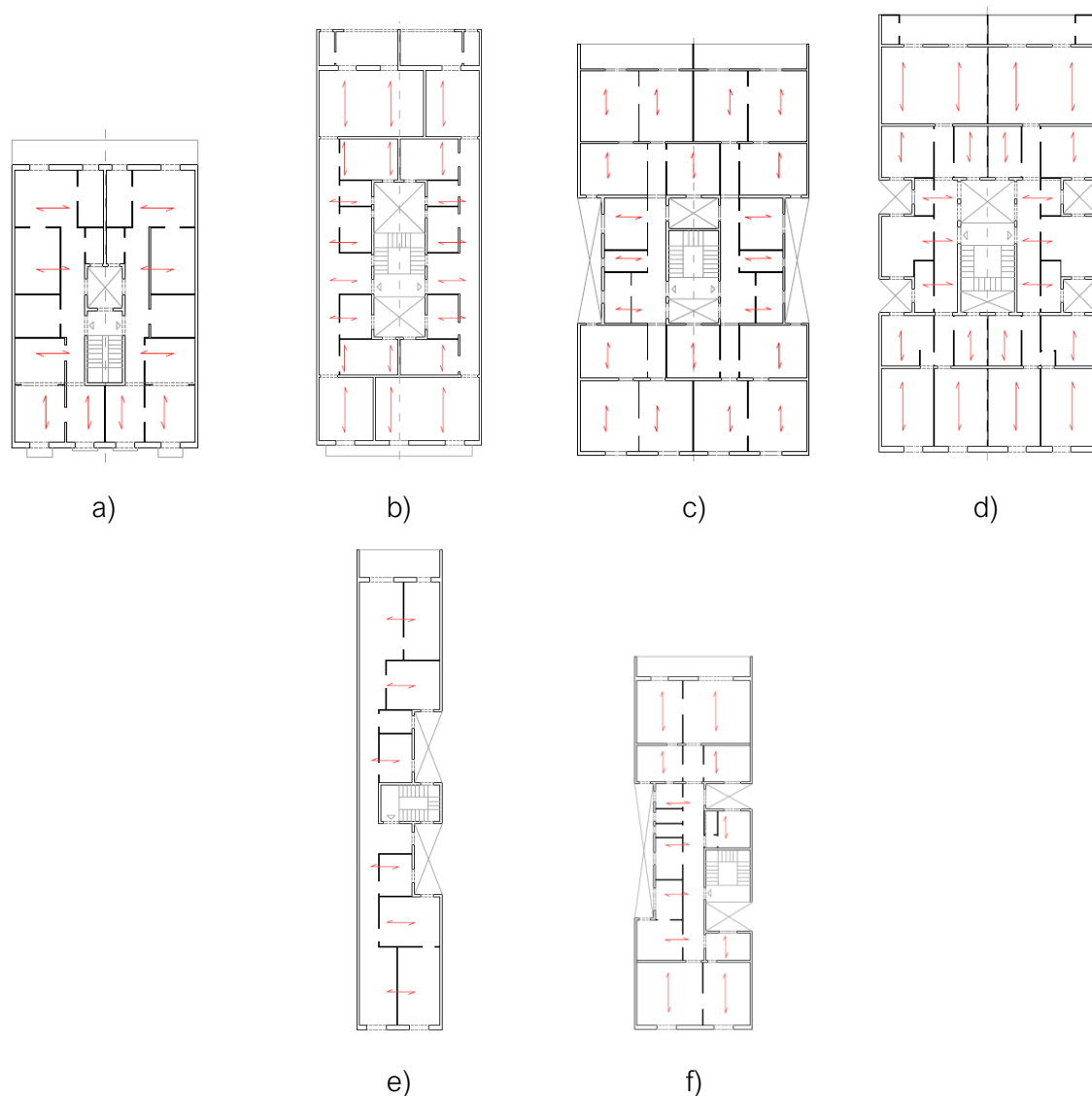


Figure 3.38 - Different configurations of typical rectangular buildings in Eixample district: a) rectangular building with a central staircase and patio; b) wide rectangular building with a central part composed of two interior patios and a central staircase; c) wide irregular building with a central part composed of central staircase and patios, as well as lateral patios on each longitudinal load-bearing walls; d) wide irregular building with a central part composed of central staircase and patios, as well as two or more lateral patios on each longitudinal load-bearing walls; e) narrow building with a lateral staircase placed transversally along the building's plan and lateral patios; and f) narrow building with a lateral staircase placed longitudinally along the building's plan and lateral patios (Cornadó Bardón, 2015).

The buildings located at the corner of the urban block, generally having a pentagonal shape, can be divided by their geometrical configuration into the following typologies (Cornadó Bardón, 2015):

- Chamfer buildings with radial structural distribution of the walls parallel to the façade and with floor beams perpendicular to the facades or perpendicular to the walls of the patios (Figure 3.39a).

- Chamfer buildings geometrically composed of two parts: a triangular part that forms the chamfer which consist of one/two bays with beams perpendicular to the façade and the staircase box; and a part with "L" shape which plots are perpendicular to the streets and have a structural configuration similar to the middle buildings in the block (with or without patios) (Figure 3.39b).

- Corner buildings that do not represent the specific chamfer characteristics provided in Cerdà's plan and they are located on the streets that intersect the typical orthogonal *Eixample* grid (Figure 3.39c).



Figure 3.39 - Chamfer buildings' geometrical configurations located at each corner of the urban block: a) Chamfer buildings with radial structural distribution of the walls parallel to the façade; b) Chamfer buildings geometrically composed of two parts: "L" shape and a triangular part; c) Corner buildings that do not represent the typical chamfer characteristics (Cornadó Bardón, 2015).

The existence of patios, as ventilation and lightening shafts, is very common for the typical *Eixample* buildings. The number and position (central and lateral) of patios depends on the different plan configurations, previously described. Therefore, the central part of the structure can consist of one or two interior patios, close to the staircase, as well as one or more lateral patios, which interrupt the continuity of the lateral load-bearing walls (see Figure 3.40).

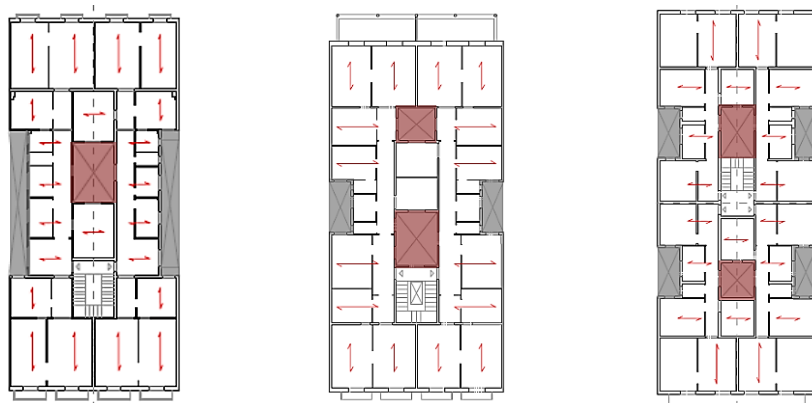


Figure 3.40 - Position and number of central and lateral patios in plan (adapted from Cornadó Bardón 2015).

Another typological feature of the *Eixample* buildings is the presence of large openings for doors and windows in the façades, which are distributed in different widths and at variable heights at each storey. Normally, the façade openings have a vertical scheme, with sizes ranging from 1 - 1.45 m wide, being 1.2 m the most typical value for door openings on the main façade (Vila, 1989). The façade openings at the ground floor are greater in size (with a width from 2 - 3.5 m) and they are frequently misaligned with those on the upper floor levels. This particular feature can cause discontinuities of the masonry walls and thus, it is considered as vulnerability parameter

(presented in Chapter 4). The number of façade openings depends on the façade's width and can vary between two and five openings. Moreover, it determines the functional configuration of the floor plan. Façades with two and four openings reflect symmetrical floor plan configuration, whereas façades with three openings reflect asymmetrical distribution, one with two rooms facing the street and one facing the patio, and the other with one facing the street and two facing the patio. According to the type of central body structure of the building, the openings frequently resemble the same pattern of openings on the back façade as well (Cornadó Bardón, 2015).

Furthermore, all the structural characteristics previously described, such as the height, width, depth, number of storeys, position of patios and percentage of façade openings are significant structural parameters that can influence the seismic behaviour of the existing *Eixample* buildings. Therefore, all these parameters are included in the building taxonomy presented in chapter 4.

3.6. SEISMICITY

The seismicity of the Catalonia region is moderate when compared to other regions in the Mediterranean Sea, such as Italy or Greece. The seismic intensity expected in Barcelona is between VI "Slightly damaging" and VII "Damaging" grades MSK, according to the EMS-98 scale (Grünthal, 1998), as indicated by the probabilistic seismic hazard map linked with a return period of 500 years (Secanell et al., 2004). Peak Ground Acceleration (PGA) is defined as 0.04 g for a return period of 500 years in the current Spanish seismic code (NCSE-02, 2002). However, the seismic risk is significantly amplified by the exposure of historic buildings with high vulnerability, the high population density and the existence of certain soil characteristics.

The map provided from the Cartographic Institute of Catalonia (ICC, 1997) (see Figure 3.41a), shows an intensity of VI to VII for this region, with a potential value of VII when considering the amplifying effects of the soil. Figure 3.41b shows the epicentres of all the recent earthquakes that have taken place in the region of Catalonia from 1986-2000. Many of them are located in the Pyrenees and also close to Barcelona city.

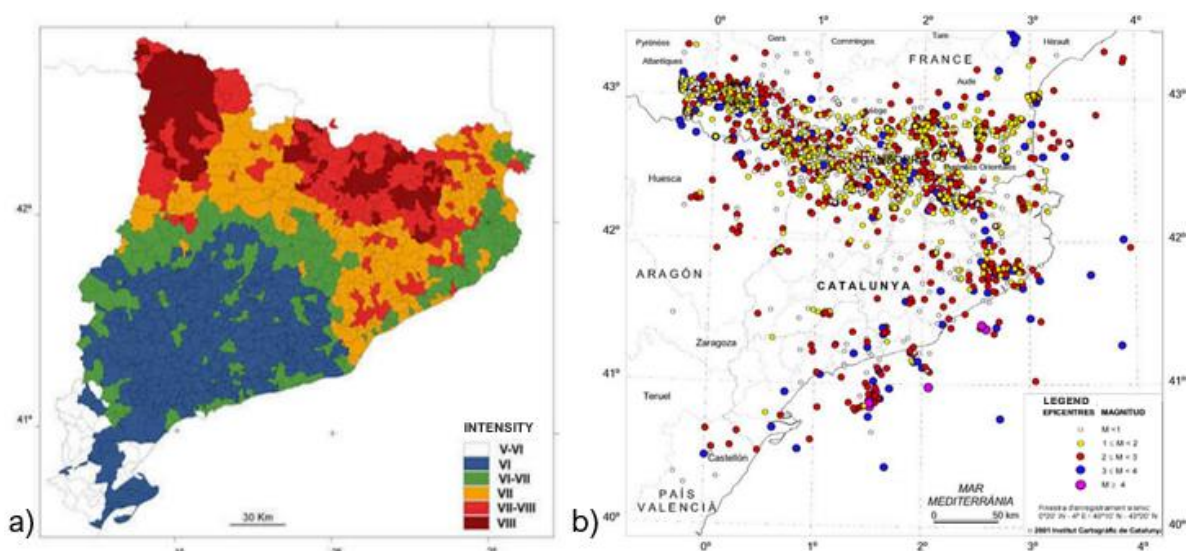


Figure 3.41 - a) Map of seismic intensities in the region of Catalonia and b) Map of earthquakes epicentres for the period between 1986-2000 (adapted from Institut Cartogràfic de Catalunya, 2001).

Barcelona is situated on two geomorphological units: the mountainous relief of the *Collserola's* range and the plain between the relief and the sea. Moreover, the Barcelona plain is divided into two main units: the pediment plain, where the city centre was built, formed by Pleistocene materials, and the deltaic deposits of the *Besós* and the *Llobregat* rivers, formed by Holocene materials (Cid et al., 2001).

In recent years, a number of studies were conducted to determine the seismic hazard in Catalonia (Cid, 1998; Cid et al., 2001; Irizzary, 2004; Secanell, 1999; Secanell et al., 2004). Hence, four zones in the city of Barcelona were identified, allowing the classification of various soil types according to local geological conditions and amplifying effects (see Figure 3.42). According to Cid et al. 2001, the *Eixample* district almost entirely encompasses Zone II when it comes to the four different soil types.

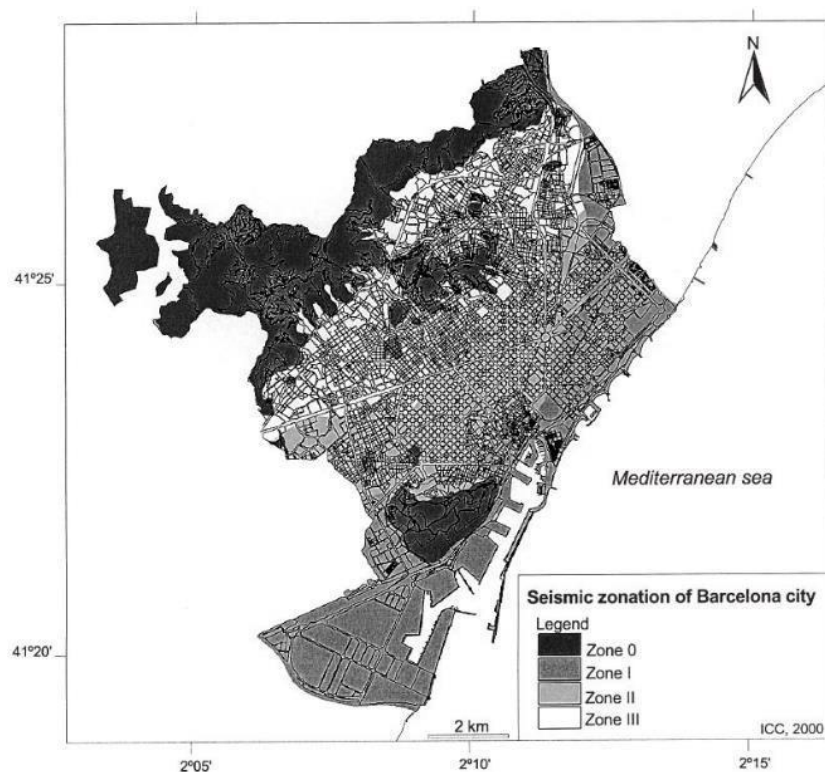


Figure 3.42 - Seismic zonation of Barcelona city by considering local soil effects. Zone 0 = Palaeozoic and Tertiary rock outcrops with different thickness of the tertiary substrate. Zone I = Holocene outcrops with soft soils. Zone II = Pleistocene outcrops with a tertiary substrate. Zone III = Pleistocene outcrops without a tertiary substrate (Cid et al., 2001).

The seismic activity recorded in Catalonia between the 14th and 15th centuries was exceptionally higher, and several earthquakes damaged a number of buildings in Barcelona. On February 2, 1428, an earthquake in the Pyrenees with a local magnitude of 6.5 and an epicentral distance of 90 km damaged some churches located in Barcelona city centre. In 1448, another earthquake with a local magnitude of 5.5 caused damages in many castles in Barcelona province (RISK-UE, 2004). During the 20th century, a few earthquakes have been felt in the city with a maximum intensity of IV degrees in the MSK intensity scale.

Both deterministic and probabilistic methods, as well as site effects, were used in the RISK-UE project to assess the seismic risk for the city of Barcelona. The deterministic seismic hazard was

assessed using historical earthquake data from Barcelona. The historical seismic events with an epicentre in the Pyrenees (Camprodon) in 1428 (I=IX) and in Cardedeu in 1448 (I=VIII) were chosen as reference earthquakes (see Figure 3.43). Additionally, the probabilistic scenario is established using the law of Ambrasseys attenuation (Ambrasseys et al., 1996) and regional parameters discovered by Secanell et al. 2004, which are consistent with records of seismic movement with a 10% probability of occurrence in 50 years. The EMS-98 intensity, as well as spectral values and response spectra, was used to define both of these scenarios. Seismic microzoning, which considers the various types of soil in the city, is also taken into consideration in addition to these basic demand scenarios (Lantada, 2007). Therefore, the deterministic scenario provides the highest seismic intensity that can be reasonably expected to occur in the city, but the probabilistic scenario corresponds to an earthquake with a 10% chance of occurring in 50 years, which is comparable to an earthquake with a return period of 475 years (Irizarry, 2004).

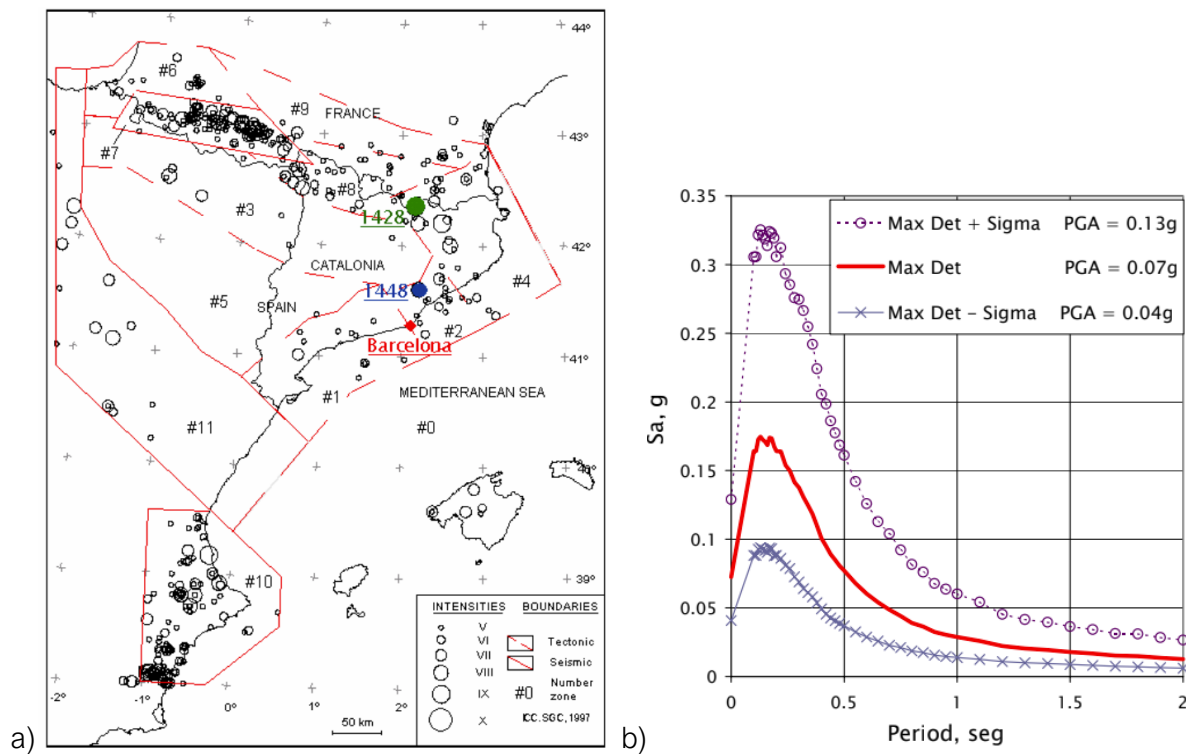


Figure 3.43 - a) Map of the seismic zones in Catalonia with the location of deterministic scenario reference earthquakes – 1428 in Girona and 1448 earthquake in Cardedeu; b) Deterministic seismic acceleration response spectra for the city of Barcelona (RISK-UE, 2004).

Figure 3.44 presents seismic intensities considering soil effects for both deterministic and probabilistic scenarios for the city of Barcelona. It can be observed that the *Eixample* district has an intensity of 7.0 MSK according to the EMS-98 scale and a small part of the district has an intensity of 6.5 MSK. Figure 3.45 shows the corresponding Acceleration Displacement Response Spectra (ADRS) for all four Barcelona’s soil zones. In this research, both the deterministic and probabilistic scenarios have been used for the seismic risk assessment.

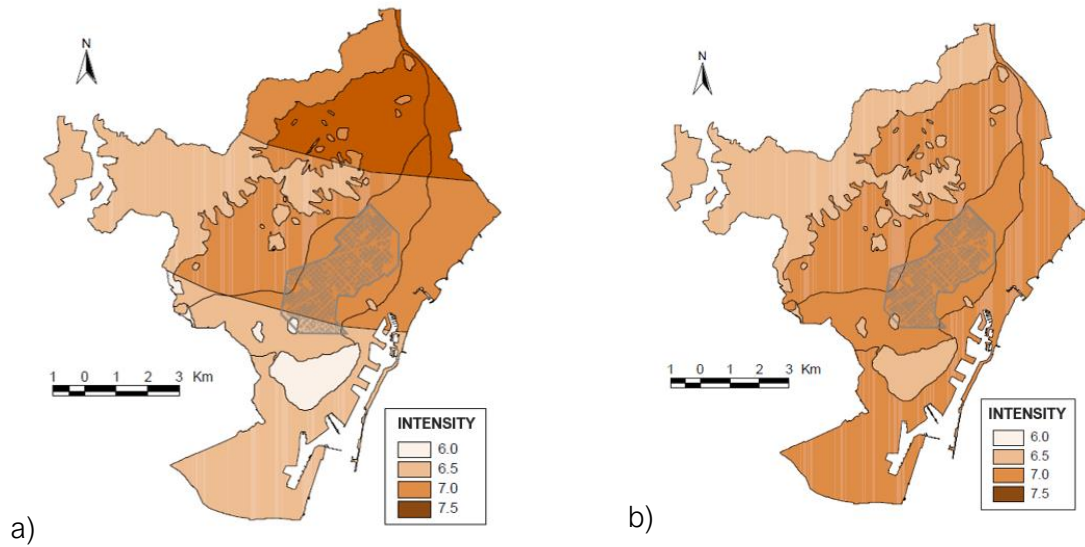


Figure 3.44 - Maps of Barcelona with the location of the Eixample district for seismic intensities considering soil effects: a) Deterministic seismic scenario; b) Probabilistic seismic scenario (adapted from Lantada, 2007).

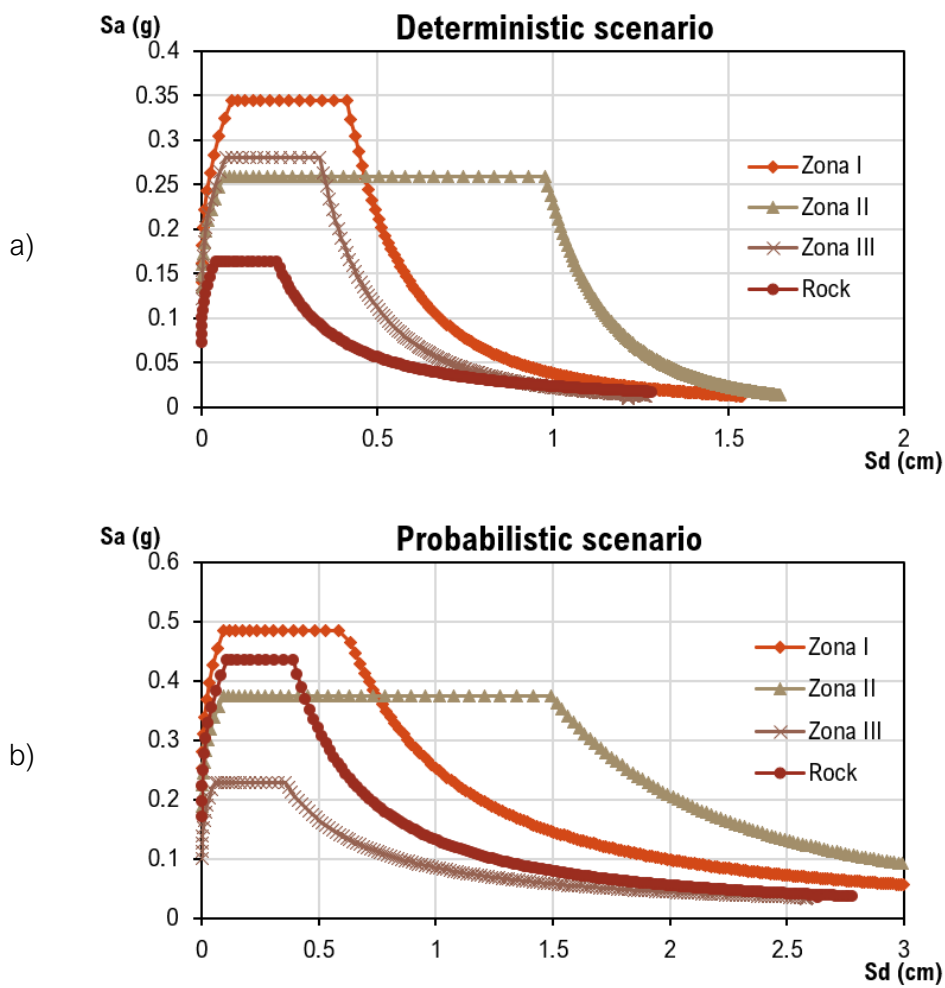


Figure 3.45 - Acceleration Displacement Response Spectra (ADRS) for Barcelona's soil zones: a) Deterministic scenarios and b) Probabilistic scenario (adapted from Irizarry, 2004).

3.7. PREVIOUS STUDIES ON SEISMIC VULNERABILITY ASSESSMENT ON UNREINFORCED MASONRY BUILDINGS IN BARCELONA

Numerous historical and scientific studies, covering from urban planning to conservation to structural performance analysis, have been conducted for the city of Barcelona and especially the *Eixample* district. From studies conducted in the early part of the 1990s until the present, a synthetic chronology of prior research conducted regarding the existing buildings in the *Eixample* district is prepared. All contributions to the current understanding of this topic, including mostly journal articles, significant projects involving several institutions, some conference papers, as well as many doctoral theses, have been taken into consideration. The studies conducted by the same research group on similar topics have been compiled together and they have been discussed in a chronological order. The previous research studies are divided in two different sections: i) Seismic vulnerability studies of the existing *Eixample* buildings using empirical methods; and ii) Seismic vulnerability studies of the existing *Eixample* buildings using analytical methods. Additionally, the structural modelling and seismic performance of the *Eixample* buildings from previous studies is discussed.

- **Seismic vulnerability studies of the *Eixample* buildings using empirical methods**

Over the past 25 years, numerous seismic risk studies have been conducted on the city of Barcelona. These studies produced results regarding the seismic vulnerability through the application of empirical vulnerability methods (described in Chapter 2). It is significant to note that the URM buildings of Barcelona's *Eixample* urban centre were found to be classified between class A and B (as the most vulnerable classes) of the EMS-98 scale in terms of seismic vulnerability (Grünthal, 1998). Each of the following described research studies assessed and evaluated the seismic vulnerability by calculating a specific vulnerability index (VI) and by estimating the expected caused damage.

During the 90s, Caicedo et al. (1994), Yopez (1996) and Barbat et al. (1998) adopted Benedetti and Petrini's (1984) methodology (GNDT, 1986) for the seismic assessment of Barcelona city, by defining the vulnerability indices and damage functions specific to the existing buildings of this urban centre. The Vulnerability Index Method (VIM) proposed in Italy (GNDT, 1986) was used, in which the building's vulnerability is defined by a vulnerability index ranging from 0 to 382.5 and the seismic action by the MSK macroseismic intensity (Caicedo et al., 1994).

Figure 3.46 presents the range of the calculated vulnerability index (VI) values using the GNDT forms for a specific percentage of buildings evaluated in the *Eixample* district as the most representative urban centre of Barcelona city. As it can be seen, almost 40% of the buildings have a normalised VI between 39 and 46, and around 30% of them present a more severe vulnerability (VI=46-52). With this first study, the increased vulnerability of the existing URM buildings in *Eixample* district is confirmed. However, it should be noted that the forms for calculating the vulnerability index were proposed and calibrated from observed damage in typical low-rise unreinforced masonry buildings in Italy, and might not be applicable to the *Eixample* typical buildings due to their peculiar structural features.

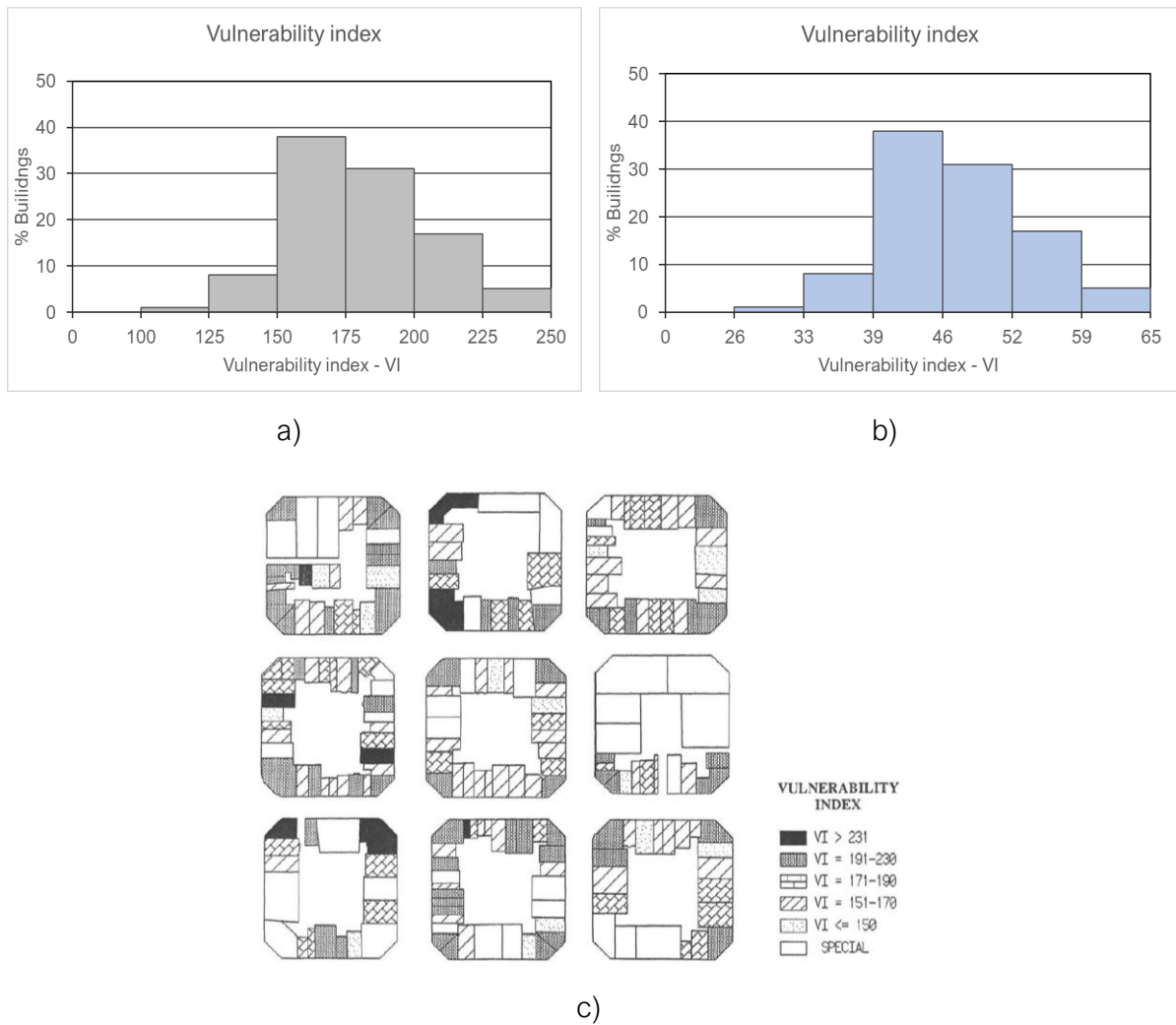


Figure 3.46 – Seismic vulnerability index evaluation using the GNDT forms: a) VI (0-382.5) b) normalised VI (0-100); c) Vulnerability index map of the case study Eixample (adapted from Yépez, Barbat, and Canas 1996).

Additionally, empirical functions that connect a damage index to the intensity were used to estimate the damage. These studies proposed a method for the evaluation of the seismic risk in regions with moderate seismicity, where damage data is limited or not available, as in the case study of Barcelona city. The seismic damage was estimated using empirical functions that relate a damage index to the intensity. In the research study by Yépez, Barbat, and Canas (1996), damage functions were developed for masonry and reinforced concrete buildings. They were derived from damage seen in two earthquakes that occurred in Almeria (southern Spain), on December 23, 1993 and January 4, 1994, and were related to unreinforced masonry buildings with intensity VII. Yépez, Barbat, and Canas (1996) also developed damage curves for reinforced concrete buildings, although by using only simulations. Vulnerability and damage maps were plotted for the studied buildings in the central part of Barcelona. Seismic vulnerability functions were obtained of the representative typologies in terms of damage index versus the probability of damage exceedance (Barbat et al., 1998).

Mena (2002) developed the first global study for obtaining the seismic vulnerability and seismic damage scenarios of Barcelona city. In this study, as in the previous ones, the VIM (GNDT, 1986)

was employed for the evaluation of the vulnerability index (ranging from 0 - 100) of the existing buildings of Barcelona city. Detailed information was collected for the buildings studied, which was necessary for the calculation of the vulnerability index. This extended database was managed using Geographic Information System (GIS). Seismic damage scenarios were obtained for different degrees of MSK intensity (grades VI, VII, VIII and IX). Additionally, the seismic damage was expressed in terms of a damage index, ranging between 0 and 100. Seismic vulnerability and damage maps were obtained for all the neighbourhoods and districts of Barcelona (Pujades et al., 2000). Figure 3.47 illustrates a seismic vulnerability map of the districts of Barcelona city by plotting the average calculated vulnerability index. As it can be observed, the unreinforced masonry buildings of *Eixample* district have a high mean vulnerability ranging from 50 to 60.

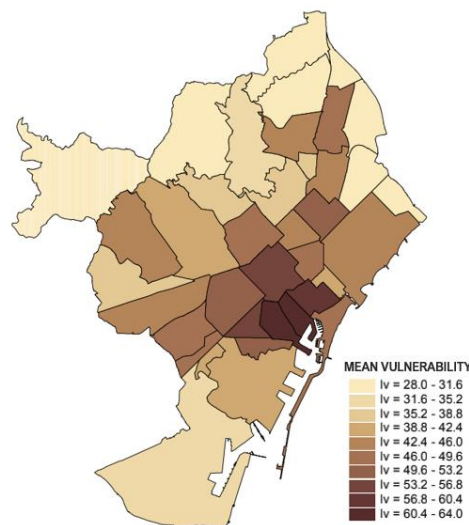


Figure 3.47 - Mean vulnerability index evaluated for the unreinforced masonry buildings in the districts of Barcelona city (adapted from Mena 2002).

The research project RISK-UE (Mouroux and Le Brun, 2006) was carried out with the purpose of developing and standardising advanced seismic risk assessment methodologies for the existing buildings and infrastructures in Europe. As a result, the seismic risk associated with various European cities was estimated by evaluating their seismic hazard and vulnerability, including Barcelona city among them. The two proposed methodologies Level I and Level II were created as part of the Risk-UE project (Milutinovic and Trendafiloski, 2003), and they are previously discussed in chapter 2. The methods and techniques used during the project's implementation were applied to the city of Barcelona with the goal of evaluating the direct physical damage expected in residential buildings and analysing other relevant aspects of seismic risk, such as the expected effects on the population and the economic cost (Lantada, 2007).

The Level I methodology includes the definition of vulnerability classes, vulnerability indices and development of damage probability matrices. The vulnerability of both existing buildings and monumental structures was evaluated, as well as expected damages were estimated for all the studied building stock (Milutinovic and Trendafiloski, 2003). These studies employ the Vulnerability Index Method (VIM), also known as level I in the Risk-UE project, which considers five non-null damage states, where the building's vulnerability is defined by calculating a vulnerability index from 0 to 1 (see Figure 3.48) and the seismic action is characterized in terms of macroseismic intensity.

Moreover, the expected degree of damage is influenced by semi-empirical functions that are dependent on the intensity and the vulnerability index. The mean damage grade varies from 0 to 5 (see Figure 3.49). The probabilities of damage states were calculated using a probability distribution with a binomial or beta distribution.

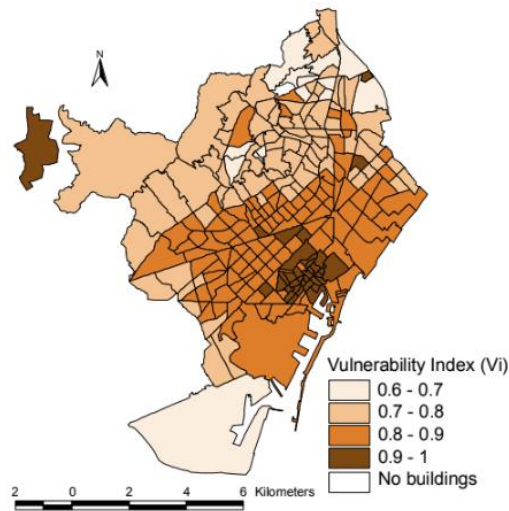


Figure 3.48 - Average vulnerability indices obtained with the Level I methodology for the unreinforced masonry buildings of Barcelona’s districts (Lantada, 2007).

The papers published from 2004 to 2010 (Lantada, Pujades, and Barbat 2004; Barbat et al. 2006; Barbat, Pujades, and Lantada 2008; Lantada et al. 2010) have followed the same methodology proposed in the RISK-UE project and have estimated different risk scenarios for Barcelona. Geographic information systems were used to facilitate the estimation processes of seismic vulnerability, and thus, the seismic risk of buildings in Barcelona. These studies investigated the application of the proposed vulnerability index method followed with the generation of damage scenarios for the two most frequent building typologies in Barcelona. Figure 3.49 shows the damage map by representing five different damage states obtained for the city of Barcelona and the *Eixample* district for the evaluated unreinforced masonry buildings.

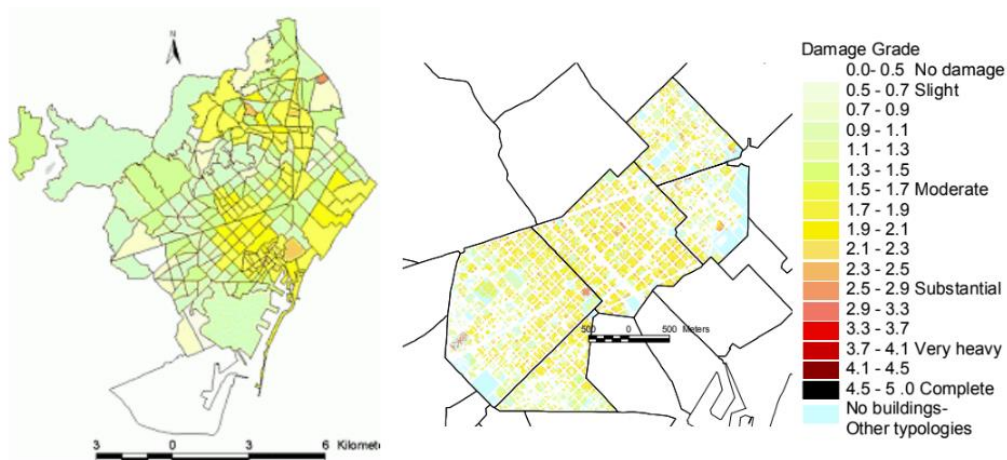


Figure 3.49 - Damage grade obtained for the unreinforced masonry buildings in Barcelona (left) and in the *Eixample* district (right) (RISK-UE, 2004).

Irizarry (2004) continued with the application of the methodologies defined within the Risk-UE project for the vulnerability evaluation of the historical monuments of Barcelona city. Firstly, this research involved a seismic hazard assessment for Catalonia and Barcelona city in particular, together with a global exposure analysis. Two distinct seismic scenarios were evaluated, one deterministic and the other probabilistic, both of which were quantified in macroseismic and spectral terms. The deterministic scenario corresponds to a historical earthquake that occurred 25 kilometres north of the city, whereas the probabilistic one corresponds to an earthquake with a 10% chance of occurrence in 50 years, or, equivalently, an earthquake with a 475-year recurrence period (Irizarry, 2004).

Secondly, Irizarry (2004) employs the Vulnerability Index Method and the Capacity Spectrum Method, as the two-level methodologies developed in the Risk-UE Project. The vulnerability index was evaluated for the principal 68 monuments and historical buildings of Barcelona city that have been designated as Cultural Heritage. Moreover, the vulnerability of Santa Maria del Mar Church, as a representative monument was assessed using the second level methodology. The vulnerability index was assigned to each monument as function of a given typology, and it was modified regarding the structure's specific characteristics. Subsequently, damage distributions were obtained using upper and lower limits of the obtained vulnerability index in order to evaluate the expected damage. Figure 3.50 illustrates the ten monuments with the highest mean damage grade. Some of them obtained a value close to 3, indicating an expected moderate damage for these structures. This vulnerability assessment was used in order to determine which monuments are the most vulnerable, as well as to provide seismic enhancement action plans to prevent possible seismic damage to the city. Finally, a global exposure analysis was performed for Barcelona's urban system based on the different elements considered at risk (Irizarry et al., 2011).

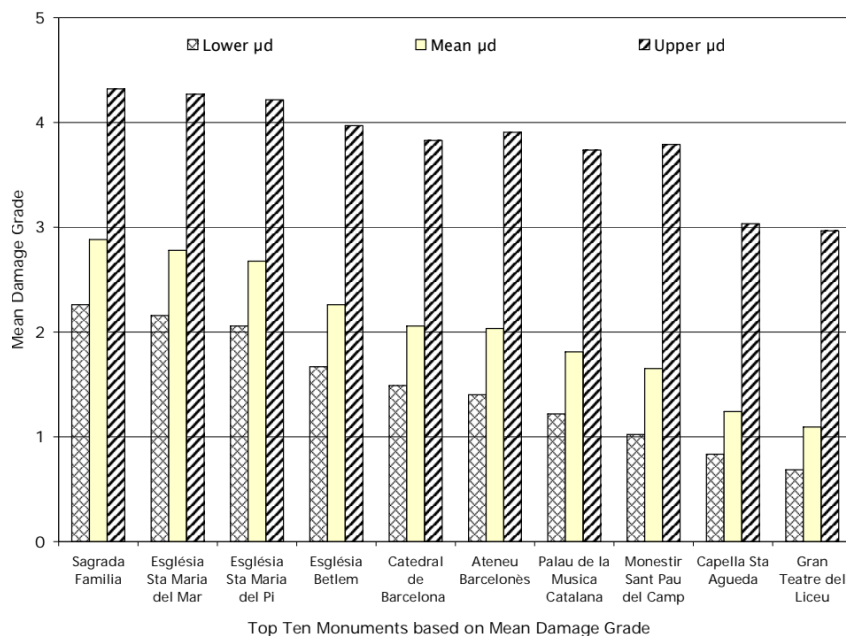


Figure 3.50 - Ten historical monuments with the highest mean damage grade (Irizarry 2004).

Furthermore, the research of Aguilar et al. (2009) used a probabilistic methodology in order to obtain an actualized estimation of the seismic risk of Barcelona. The developed methodology considered important uncertainties that are present in the main elements which are used to

estimate the seismic risk of buildings. The proposed methodology in Aguilar Meléndez (2011), which has as a starting point the Level I methodology of the RISK-UE project (Milutinovic and Trendafiloski, 2003), also allows representing uncertainty related to the seismic risk results. This assessment included the following two steps: the probabilistic seismic hazard assessment of Barcelona and the seismic vulnerability assessment of the buildings of Barcelona. Moreover, seismic vulnerability curves are obtained for different stages on the future life of a building (Aguilar-Meléndez, García-Elías et al., 2012).

More recent study was carried out for assessing and mitigating the seismic risk in large-scale urban systems (Cara et al., 2018). It proposed a quick method for evaluating how the potential collapse of important or interfering structures would affect the usability of key urban routes in the event of an earthquake. A performance-based approach was based on the concept of urban Emergency Limit Condition. The GIS system was used to gather all the available information and for simulations of possible risk scenarios. The proposed methodology was applied to the neighbourhood “*Antiga Esquerra de l’Eixample*” of Barcelona in order to evaluate the effect on the serviceability of strategic routes of the potential collapse of strategic structures (Cara et al., 2018). The seismic vulnerability of 43 interfering buildings was evaluated according to the vulnerability index methodology proposed by GNDT (GNDT, 1986). This research has also confirmed the higher levels of seismic vulnerability (see Figure 3.51) and expected damage of the existing buildings, even for a moderate earthquake scenario.

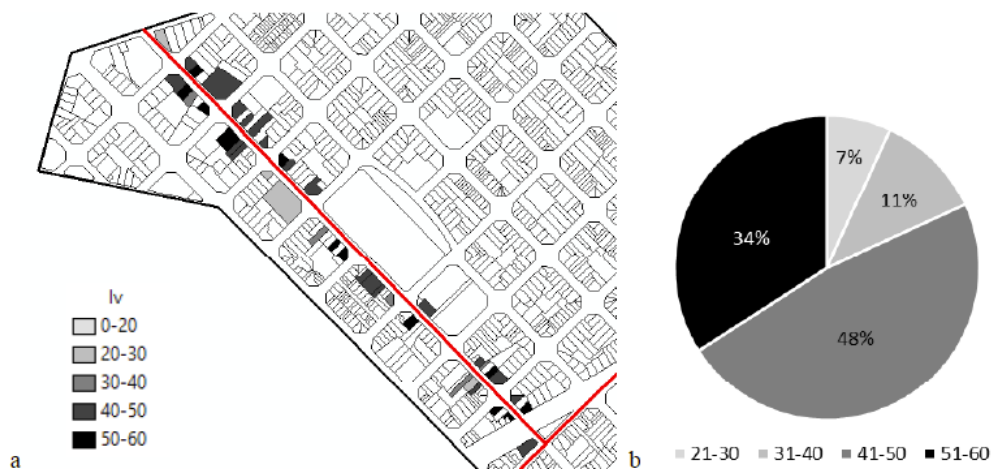


Figure 3.51 - Representation of the ELC system together with the vulnerability index (VI) for a street located in the Eixample district (a) and percentage of buildings with a given VI (Cara et al., 2018).

- **Seismic vulnerability studies of the *Eixample* buildings using analytical methods**

In the following section, the previous studies on the seismic performance of the existing *Eixample* buildings using analytical methods are presented and discussed in a chronological order. The aim of each research study, followed by a short description is included, by highlighting the main objectives achieved. Furthermore, a summary of all the numerical models, regarding their geometrical configurations, material properties used, and the results obtained from the non-linear static (pushover) analysis is provided in different tables (Table 3.3 - Table 3.5).

The second applied methodology from the RISK-UE project (Milutinovic and Trendafiloski, 2003) involves a Capacity Spectrum Method by considering four non-null damage states, where

the seismic action is represented in terms of response spectra and the building's vulnerability by means of its capacity curve. Hence, the damage functions are estimated using analytical vulnerability models. Particularly, fragility curves are obtained for estimating the probability that a damage state will be exceeded. These fragility curves are expressed in terms of the conditional probability of overcoming a state of damage versus the structure's spectral displacement. Many of the following described research studies adopted the same methodology for the evaluation of the seismic performance of existing buildings and obtaining the expected damage scenarios.

The focus of Bonett's (2003) doctoral thesis is on the evaluation of the seismic performance and vulnerability of buildings in urban centres. The proposed methodology was applied to the unreinforced masonry buildings of the city of Barcelona. A non-linear static analysis was performed on an existing unreinforced masonry building of the *Eixample* district by using the software TreMuri and applying the simplified equivalent frame method (see Figure 3.55a). Three numerical models were developed from the same building by changing the number of floor levels (with four, five and six storeys). The seismic demand was considered for three different scenarios, referenced as: case NCSE-02 (Spanish seismic code NCSE-02 2002), and deterministic and probabilistic cases (Institut Cartografic de Catalunya, 2001). Additionally, the N2 method was used for obtaining the performance point for each of the seismic scenarios. The thresholds for the damage states were defined according to the proposed formulation by Lagormasino et al. (2002) in order to determine the level of seismic performance of these models. The seismic vulnerability of buildings was assessed by fragility curves, which are generated from a lognormal distribution function. The corresponding fragility curves were used to calculate the probabilities of occurrence for each of the four damage states using the values of the spectral displacements obtained for the three models. Finally, seismic damage scenarios for the unreinforced masonry buildings of the *Eixample* district were generated. Bonett (2003) discusses that the probabilistic scenario is the most unfavourable for the *Eixample* buildings, by producing moderate damage very close to the severe damage state. In this work, it was concluded that the seismic performance and vulnerability of these existing buildings is sensitive to many uncertainties such as the structural parameters, the demand spectral parameters and the damage thresholds, because any small variations in these parameters can easily modify the expected damage.

The previous mentioned studies (Barbat et al. 2006; Lantada 2007; Barbat et al. 2008) followed as well the Level II methodology of the RISK-UE project. A seismic risk assessment was carried out, beginning with the Capacity Spectrum Method and proceeding to the construction of fragility curves and damage probability matrices. Finally, three different levels (districts, neighbourhoods and census zones) of seismic risk scenarios were simulated and presented as maps (see Figure 3.54). In these studies, three different models were developed for each building typology: a low-rise building with two stories, a mid-rise building with four stories, and a high-rise building with six stories. Architectural and structural plans were used to model the existing buildings representative of each of the building typologies considered (Lantada, 2007). Pushover analysis was used in the software TreMuri to produce capacity curves of typical unreinforced masonry and reinforced buildings located in the *Eixample* district. The seismic demand was evaluated using deterministic and probabilistic scenarios and modelled using 5% damped elastic response spectra in ADRS format. Figure 3.52 represents the demand spectra for each seismic zone together with the bilinear capacity curves obtained from the numerical models of the unreinforced masonry buildings with different number of storeys. It should be remarked that the low-rise building model presents

a much higher stiffness and strength than the mid-rise and high-rise building models (see Figure 3.52). However, this low-rise building typology is not very common in the *Eixample* district. Moreover, the capacity of the existing masonry buildings decreases with the increase of their total height.

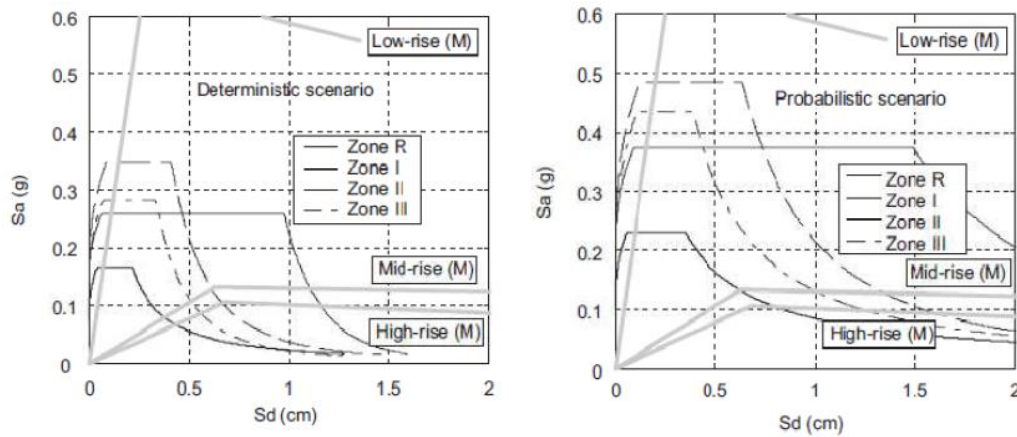


Figure 3.52 - Demand Spectra with bilinear capacity spectra for unreinforced masonry buildings for two different seismic scenarios deterministic (left) and probabilistic (right) (Barbat et al., 2008).

Fragility curves were obtained for each building typology in a simplified way previously proposed in the Risk-UE project, starting from the bilinear representation of the capacity curves. Figure 3.53 shows the generated fragility curves for high-rise masonry buildings, as the most vulnerable building typology in the *Eixample* district.

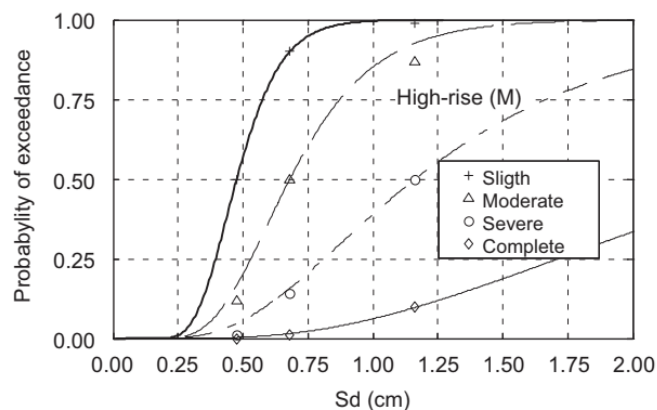


Figure 3.53 - Fragility curves for high-rise unreinforced masonry buildings for four damage state (Barbat et al., 2008).

Furthermore, the damage probability matrices for all of the considered building typologies were obtained by combining the corresponding fragility curves with the spectral displacement obtained from the performance point as the intersection of the capacity curve and the demand spectra (Lantada, 2007). Figure 3.54 illustrates the damage grade maps (from 0 - 4) for the districts of Barcelona city, obtained from the application of the Capacity Spectrum Method from the Level II methodology for the two different seismic scenarios: a) deterministic and b) probabilistic. As it can be noticed, the average damage grade for the existing masonry buildings in the *Eixample* district is 1.16 for the deterministic scenario and 1.90 for the probabilistic one. In conclusion, the possible

damage produced from a given earthquake with a lower intensity (VI according to the EMS-98 scale) can be from slight to moderate due to the high vulnerability of these building typologies.

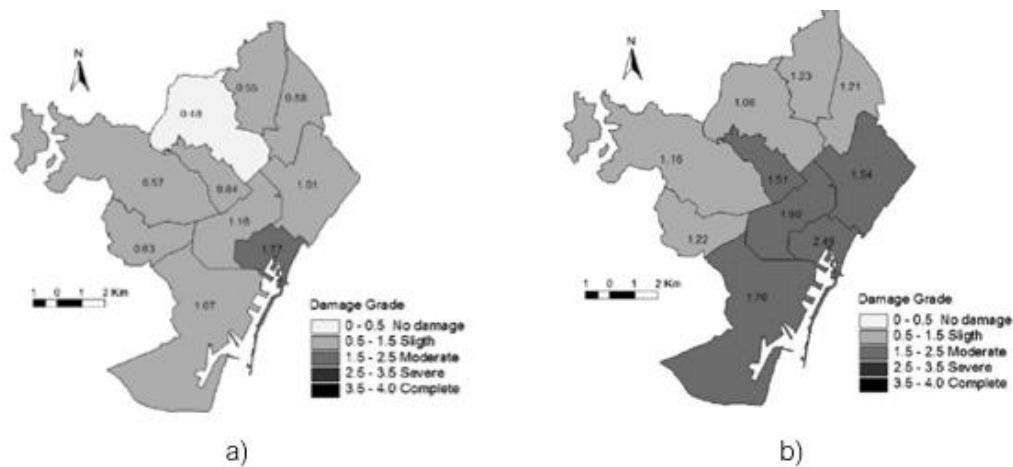


Figure 3.54 - Damage grade maps for the districts in Barcelona from two different scenarios: a) deterministic scenario and b) probabilistic scenario buildings (Barbat et al., 2008).

The evaluation of the seismic performance of typical URM structures of Barcelona continued with more published journal articles during the period of 2008 - 2012. The equivalent frame approach by using the software TreMuri was applied and a nonlinear static analysis was carried out for the evaluation of the seismic of representative structural typologies of Barcelona (Moreno-González et al., 2008). A seismic scenario defined by the Spanish seismic standard NCSE-02 and Eurocode 8 with a basic seismic acceleration for Barcelona of 0.04 g was considered to study expected seismic damage in these building types. Capacity curves were acquired from buildings with different geometries and they were compared with the demand spectra in order to obtain the performance points. Finally, fragility curves and damage probability matrices were estimated considering different seismic scenarios (Moreno González and Bairán García, 2012).

Another seismic performance assessment on typical existing buildings of the *Eixample* was carried out in 2012. In contrast to the previous research studies, in this one the typical *Eixample* buildings were considered as individual and as a group by forming an aggregate (Pujades et al., 2012). Standard pushover analyses by using the TreMuri software lead to evaluate their seismic performance by means of capacity and fragility curves (Avila-Haro et al., 2012). Additionally, a Capacity Spectrum Method was employed to study the seismic behaviour of the existing masonry buildings by considering two earthquake scenarios (deterministic and probabilistic). Moreover, different papers were published by the same research group, where a more detailed study of the structural elements of the existing buildings was presented (Gonzalez-Drigo et al., 2015).

The doctoral thesis of Jiménez-Pacheco (2016) studied seismic performance of unreinforced masonry buildings considering the flexibility of the floor through nonlinear static analysis of a 6-story typological building of the *Eixample* (Figure 3.55e). The building was modelled with macro-elements as one-dimensional spring elements. Furthermore, the influence of the stiffening of the floor system in the global seismic performance for this type of buildings was investigated by applying the Capacity Spectrum Method. The seismic response was estimated in terms of modal parameters, capacity curves, and deformed shapes of the floors (Jiménez-Pacheco et al., 2020).

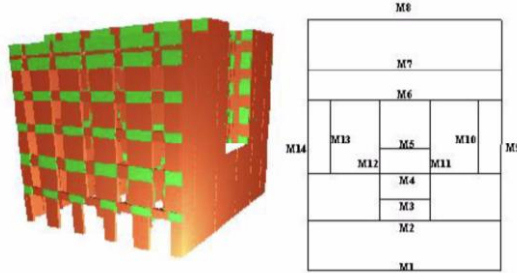
- **Structural modelling and seismic performance of the *Eixample* buildings**

The primary characteristics of the analysed existing structures from the previous studies for the seismic performance analysis, such as the type (band or corner building), number of storeys, and dimensions, are summarized and presented in Table 3.3. Figure 3.55 shows the reported plan configurations, elevations or 3D views (if available) of each of the modelled existing buildings. This information is condensed in order to compare previously analysed buildings with those that will be used in the current research study. It is important to highlight that all previous studies have considered existing real buildings in the *Eixample* district, with generic considerations on their representativeness of the larger district but have never done a detailed and comprehensive typological or statistical analysis. Hence, they can be referred to as typical buildings rather than representative ones.

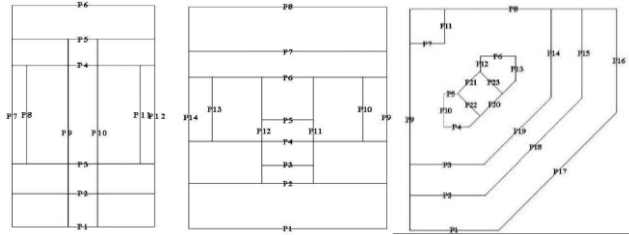
Table 3.3 - Summary information on available numerical models of typical URM buildings of the Eixample district studied in previous studies.

Research study	Model	Building type	Number of storeys ¹	Dimensions	
				Width [m]	Depth [m]
Bonett Díaz (2003)	M.1	Band	4 (GF+3)	18.9	24.5
	M.2	Band	5 (GF+4)	18.9	24.5
	M.3	Band	6 (GF+5)	18.9	24.5
Barbat et al. (2006); Barbat et al. (2008)	M33L	Band	2 (GF+1)	7.3	9.3
	M33M	Band	4 (GF+3)	18.9	24.5
	M33H	Band	6 (GF+5)	18.9	24.5
Moreno-González and Bairán, (2011)	Casti	Band	6 (GF+5)	12.65	27.00
	Pelai	Band	7 (GF+6)	18.40	23.70
	Angolo	Corner	8 (GF+7)	22.40	
Pujades et al. (2012)	C1	Band	5 (GF+MF+4)	17.65	23.65
	C2	Band	5 (GF+5)	11.5	26.57
	E	Corner	5 (GF+5)	24.80	24.65
Avila-Haro et al. (2012); Gonzalez-Drigo et al. (2015)	M01	Band	7 (GF+6)	16	27.85
Avila-Haro and Máca (2015)		Band	7 (GF+6)	12.7	17.75
Jiménez-Pacheco et al. (2020)		Band	6 (GF + 5)	12.90	23.90

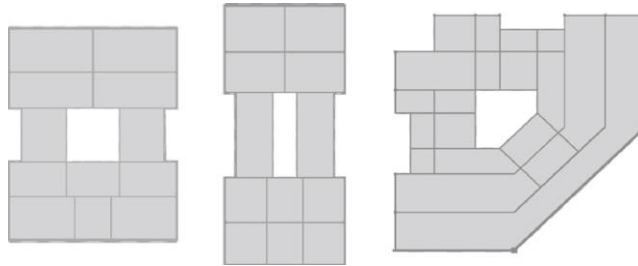
¹ GF - ground floor, MF - mezzanine floor.



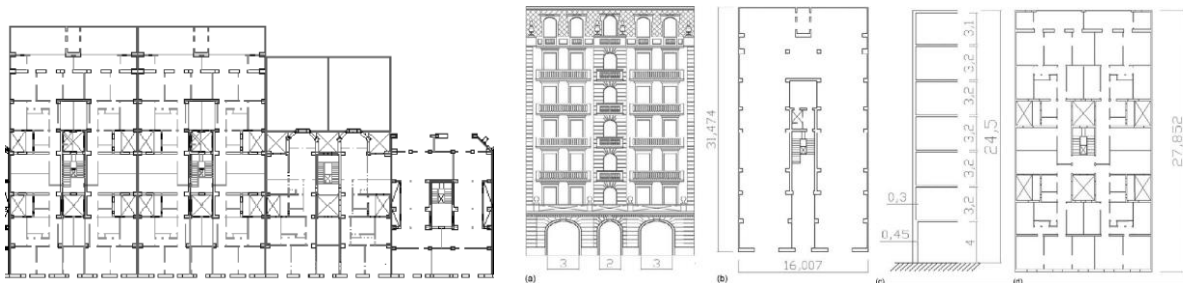
a) 3D model of a band building with 6 storeys



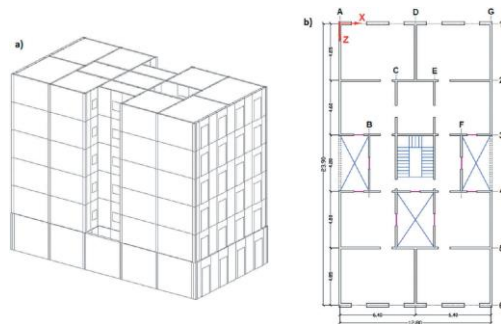
b) Casti, Pelai, Angolo



c) C1, C2, band buildings, E corner building and AGG the combination of the three in the aggregate



d) M155, A155, M157, M159 and a focus on M155



e) Typical band building

Figure 3.55 - Schemes of the building modelled in previous studies. a) (Bonett Díaz, 2003); b) (Moreno-González and Bairán, 2011); c) (Pujades et al., 2012); d) (Avila-Haro et al., 2012); e) (Jiménez-Pacheco et al., 2020).

Table 3.4 presents the material properties adopted in the different numerical models of typical *Eixample* buildings as reported in the previous studies. The compressive strength of the masonry material was assumed varying from 2.95 to 4.00 MPa, and the corresponding Young's modulus had a range between 1800 and 2650 MPa. The selection of compressive strength and elastic modulus values lacks a consistent criterion, as various authors chose widely diverse values.

Table 3.4 - Summary of the material properties used in the 3D numerical models of the existing *Eixample* building from the previous studies.

Material properties		(Bonett Díaz, 2003)	(Moreno-González and Bairán, 2011)	(Pujades et al., 2012)	(Gonzalez-Drigo et al., 2015)
Masonry	Units				
Young's modulus - E	MPa	2100	1800	1800	2650
Shear modulus - G	MPa	700	300	300	590
Mass density - γ	kg/m ³	1800	1800	1800	1800
Compressive strength - f_c	MPa		4.0	1.8	2.95
Shear strength - τ_k	MPa	0.10	0.12	0.20	0.0795
Steel beams					
Young's modulus	MPa	210000	210000		
Mass density	kg/m ³	7850	7850		
One-way floor slabs with timber beams and ceramic vaults					
Young's modulus – E ₁	MPa	4200	4000	958	
Young's modulus – E ₂	MPa	42	40		
Shear modulus - G	MPa	400	100	25040	

The Young's modulus for the one-way floors with timber beams and ceramic vaults was calculated for two directions, where E₁ is the direction of the beams and E₂ is the perpendicular direction. The proper values were obtained according to the TreMuri software, by assuming a floor slab with an equivalent thickness of 40 mm. Figure 3.56 presents the typical one-way floors with timber beams and ceramic vaults, as well as the metallic elements used on the ground floor of some buildings, which represent the previously mentioned hybrid structural typology.

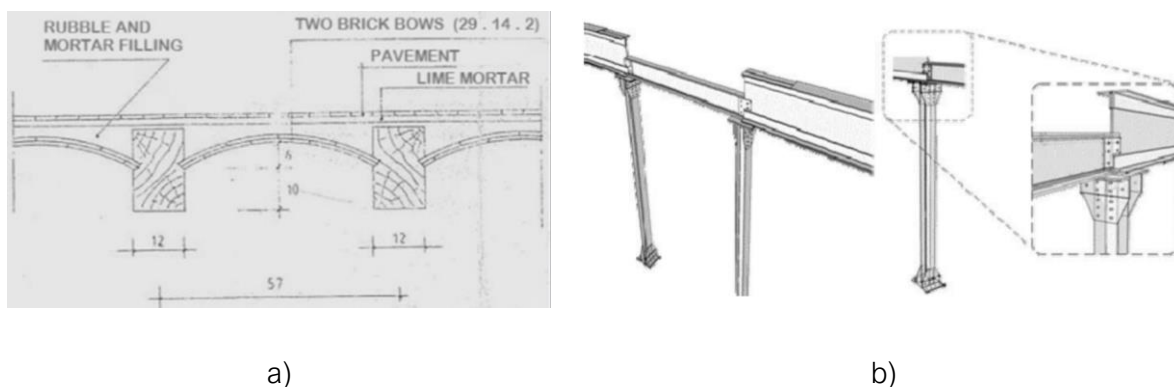


Figure 3.56 - Structural elements of the *Eixample* buildings: a) Typical one-way floor with timber beams (Pujades et al., 2012); b) Metallic girders and cast-iron pillars at the ground floor of the building (Gonzalez-Drigo et al., 2015).

Table 3.5 presents a summary of the obtained results from the seismic performance of existing *Eixample* buildings, in terms of the estimated displacements and accelerations for the yield (D_y , a_y) and ultimate (D_u , a_u) points of the bilinear capacity curves. The direction X represents the loading direction parallel to the façade, while the direction Y is the loading direction perpendicular to the façade.

Table 3.5 - Summary of available data for the seismic performance of typical buildings located in *Eixample* district from previous research studies.

Reference study	Pushover direction	Building	Yield point		Ultimate point	
			D_y (cm)	a_y (g)	D_u (cm)	a_u (g)
Bonett Díaz (2003)	Y	M.1 ²	0.63	0.132	2.91	0.123
		M.2 ³	0.64	0.116	2.82	0.111
		M.3 ⁴	0.69	0.105	2.61	0.100
Barbat et al. (2008)	-	M33L ⁵	0.27	0.65	1.36	0.56
		M33M ⁶	0.63	0.13	2.91	0.12
		M33H ⁷	0.68	0.11	2.61	0.08
Moreno-González and Bairán, (2011)	X	Casti	1.50	0.19	7.10	0.20
		Pelai	2.50	0.12	17.0	0.10
		Angolo	1.10	0.12	1.51	0.12
Pujades et al. (2012)	X	C1	0.22	0.05	4.52	0.05
		C2	0.19	0.02	5.17	0.02
		E	0.91	0.12	2.55	0.11
		AGG	0.49	0.09	3.23	0.08
	Y	C1	0.52	0.11	1.65	0.11
		C2	0.50	0.11	0.77	0.12
		E	0.37	0.15	1.67	0.14
		AGG	0.49	0.15	1.82	0.14
Avila-Haro et al. (2012)	X	M155	5.06	0.078	9.35	0.077
		A155	4.21	0.087	6.18	0.072
		M157	8.12	0.058	10.51	0.062
		M159	1.67	0.052	2.24	0.060
	Y	M155	2.90	0.138	4.86	0.137
		A155	4.69	0.132	6.51	0.134
		M157	2.34	0.143	3.56	0.135
		M159	2.40	0.077	3.76	0.115

A quick review of the findings in Table 3.5 reveals that, as should be expected, mid-rise URM structures have higher seismic capacity than high-rise structures (Milutinovic and Trendafiloski, 2003). The capacity of all the analysed typologies is lower in the X direction (parallel to the façade)

² URM buildings with four storeys.

³ URM buildings with five storeys.

⁴ URM buildings with six storeys.

⁵ URM buildings with composite slabs, low-rise.

⁶ URM buildings with composite slabs, mid-rise.

⁷ URM buildings with composite slabs, high-rise.

than the Y direction (perpendicular to the façade) (Moreno-González and Bairán, 2011), and the capacity of band buildings appears to increase when they are included in an aggregate (Pujades et al., 2012). Due to the increased degree of irregularity, corner buildings are reported to have lower seismic capacity (Avila-Haro et al., 2012; Pujades et al., 2012).

The seismic vulnerability assessment and structural analysis under horizontal actions, presented in the previous studies, demonstrate and confirm the high vulnerability of these existing buildings, even for moderate earthquakes. The expected damage in these structures is anticipated to be mostly moderate with some exceedance likelihood connected to the severe damage state, highlighting the necessity of seriously considering the option of retrofitting and upgrading (Gonzalez-Drigo et al., 2015; Moreno-González and Bairán, 2011). The results of the studies presented in this section will be used as a term of comparison for the analysis and interpretation of the results of this work presented in Chapter 6.

3.8. PREVIOUS STUDIES ON THE EXPERIMENTAL CHARACTERISATION OF MASONRY PROPERTIES FROM BUILDINGS OF BARCELONA'S URBAN CENTRE

The ATEM (Analysis and Technology of Structures and Materials) research group of the Department of Civil and Environmental Engineering of the UPC executed several experimental campaigns regarding the material characterisation of historical buildings constructed between 1840 and 1952 in the urban centre of Barcelona. The samples extracted in-situ were all tested in the Laboratory of Technology of Structures and Materials (LATEM) of the UPC. A large part of the studied existing buildings was located in the *Eixample* district. Experimental programs in these buildings provided representative ranges of brick masonry mechanical properties. These same ranges will be considered as the reference values to be adopted in the numerical models described in Chapter 5.

As previously discussed, a significant part of *Eixample*'s building stock consists of structural elements such as unreinforced masonry load-bearing walls, masonry columns and ceramic tile vaults for the one-way floors. Masonry is the main material used for the construction of these existing buildings and its mechanical characterisation is of paramount importance for this research.

Masonry is a composite material made of an arrangement of units that are bond with mortar. Its complex mechanical behaviour depends on the individual properties of each of the components (units and mortar), such as the tensile and compressive strength, as well as their geometry and arrangement, the interaction among the components, and the loading conditions. Additionally, the union between the units and mortar, stress direction, loading conditions and local effects can also greatly influence the masonry's behaviour as a composite material (Molins i Borrell, 1996). The properties of the masonry material are also influenced by a variety of factors, such as the heterogeneities in the bricks caused by differences or deficiencies in the cooking process, heterogeneities in the joints caused by the use of different dosages or types of mortars, the quality of the work, the degree of curing, etc.

The detailed characterisation of existing historical buildings' mechanical properties is critical for proper structural evaluation by using numerical modelling. The complex and heterogeneous

behaviour of this composite material, however, poses significant challenges to the characterisation of the mechanical properties of existing masonry (Segura et al. 2018). Among the most influential parameters of the mechanical behaviour of masonry as a composite material are the compressive strength and the Young's modulus. Therefore, their characterisation is essential in order to better understand structural behaviour of the existing masonry buildings (Segura et al., 2019).

The experimental characterisation of masonry's mechanical properties in existing buildings is a complex task presenting some difficulties in the extraction of sufficiently unaltered composite samples in order to be tested in the laboratory. Many experimental campaigns and laboratory testing on masonry core specimens were executed at UPC during the last 10 years: (Pelà et al. 2016), (Pelà, Roca, and Benedetti 2016), (Drougkas, Roca, and Molins 2016), (Pelà, Kasioumi, and Roca 2017), (Pelà et al., 2018), (Segura et al., 2018), (Segura et al., 2019), (Segura, Bernat, et al., 2021), and (Cabané et al., 2022).

In-situ sampling, followed by laboratory testing of masonry specimens, provide an adequate approach for the estimation of the mechanical parameters, such as the compressive strength and elastic modulus. However, due to the composite nature of masonry, sufficiently large samples are required in order to be able to accurately depict the complexity of the material (including both units and mortar joints). Furthermore, seeing as historical buildings have cultural heritage value, the extraction of samples from existing walls should always be reduced to a minimum, presenting some significant challenges (Segura et al., 2019). Therefore, a minor destructive technique (MDT) was used for extracting masonry core samples from the existing buildings and then testing them in the laboratory. The MDT consisted in core drilling of cylinders with a diameter of 150 mm including four brick segments, with two horizontal and one vertical mortar joints. Recent studies showed that the failures obtained by this method can represent the complex interaction between the masonry's components, providing accurate estimations of the actual compressive strength (Pelà et al. 2016; Pelà, Roca, and Benedetti 2016).

The research study of Segura et al. (2019) presents results of an experimental campaign evaluating the size effect on the compressive behaviour of cylindrical samples (with diameters of 150 mm and 90 mm) extracted from masonry walls of existing historical buildings. The studied existing unreinforced masonry buildings are mostly residential ones from the Barcelona's urban centre, as well as some industrial and educational historical buildings (see Figure 3.57). The construction date of the analysed buildings is before 1940, as this is the period when most of Barcelona building stock was built using unreinforced masonry material. As mentioned previously in this Chapter, the residential buildings located in the *Eixample* district were constructed between 1880 and 1930.

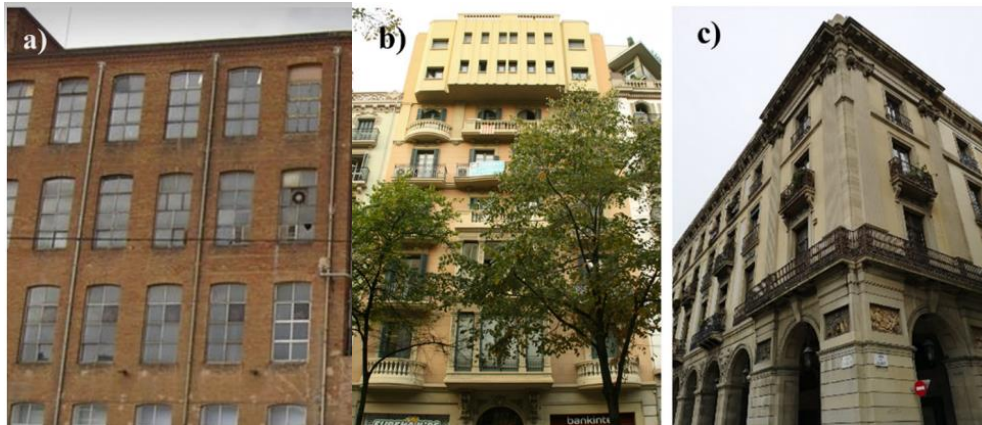


Figure 3.57 - Existing unreinforced masonry buildings of Barcelona as part of different experimental campaigns executed at UPC: a) industrial complex; b) residential building located in the *Eixample* district; c) residential building located in the district of *Ciutat Vella* in Barcelona (Segura et al., 2019).

The cylinders were extracted from masonry walls that were to be demolished as part of the ongoing renovation work. Previously, a structural assessment of the unreinforced masonry structures was completed before the start of some renovation works. In order to characterise the mechanical properties of the masonry, inspection tasks were included in the assessment. The different stages of the experimental campaign are explained in the research study of Segura et al. (2019).

Figure 3.58 shows an interior single leaf masonry wall of 145 mm thickness from an existing building of *Eixample* district, from which masonry specimens were extracted with in-situ core drilling. Moreover, the extracted specimens of the different experimental campaigns were regularized with mortar caps and tested in compression. The compressive stresses acting on the specimens were calculated as the ratio between the load and the cross section determined by the width of the mortar caps (Segura et al., 2019). Figure 3.59 illustrates the compressive stress-strain curves for both 150 mm and 90 mm core samples extracted from a residential building located in the *Eixample* district.



Figure 3.58 - Interior masonry wall to be tested from an existing *Eixample* building (left) and in-situ core drilling (right) (Segura et al., 2019).

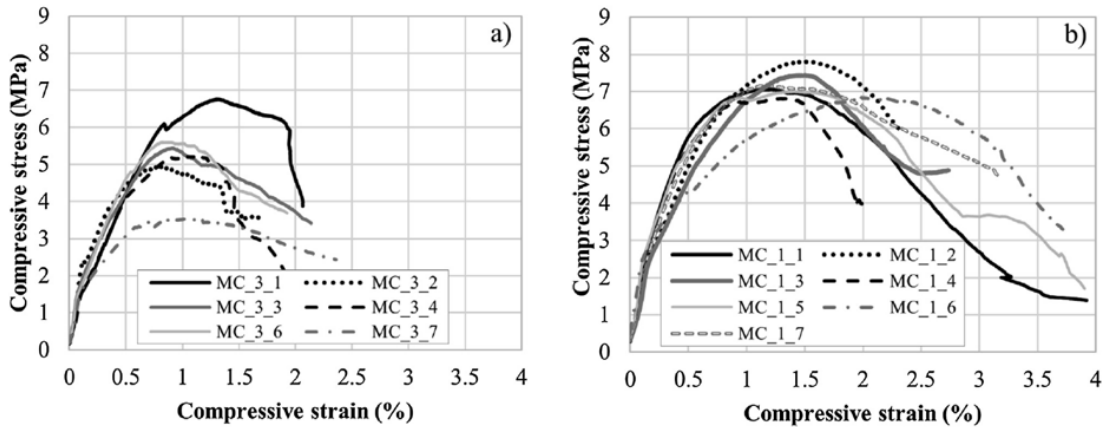


Figure 3.59 - Compressive stress-strain curves from an experimental campaign in a residential building located in the Eixample district: a) 150 mm cylinder core samples; b) 90 mm cylinder core samples (Segura et al., 2019).

Table 3.6 presents a summary of the estimated mechanical properties of the masonry components (brick and mortar), and of the masonry as composite material. The results are obtained from different experimental campaigns on existing historical buildings in Barcelona’s urban centre, whose tests were executed at the LATTEM laboratory of the UPC. The bricks compressive strength (f_b) was calculated on a set of bricks, which were cut into pieces with dimensions of 100 x 100 mm². Moreover, the mortar samples with approximate dimensions of 50 x 50 mm² were tested using the double punch test (DPT) for the estimation of the mortar compressive strength (f_m). The presented masonry mechanical properties were obtained from cylinders specimens with diameter of 150 mm (including one vertical and two horizontal mortar joints), by considering the mortar cap area (150 x 100 mm²).

Table 3.6 - Masonry mechanical properties obtained with minor destructive testing on existing buildings in Barcelona’s urban centre.

Existing masonry buildings	Brick compressive strength - f_b (MPa)			Mortar compressive strength - f_m (MPa)			Masonry compressive strength - f_d (MPa)			Young’s modulus - E (MPa)		
	min	max	mean	min	max	mean	min	max	mean	min	max	mean
Residential building (1)	8.38	13.55	10.5	0.45	1.65	1.06	3.55	6.76	5.28	1,291	1,830	1,569
Residential building (2)	9.24	13.21	11.4	0.34	2.95	2.47	-	-	-	-	-	-
Residential building (3)	11.4	21.12	16.8	0.2	0.81	0.4	3.29	8.61	5.64	-	-	-
Residential building (4)	20.9	44.9	32.3	0.54	6.23	2.2	6.7	13.04	9.4	1,783	4,258	3,448
Industrial building	-	-	21.2	-	-	0.75	3.14	6.04	4.64	1,301	2,932	2,018
Industrial building	-	-	-	0.34	0.57	0.43	5.6	10.74	7.83	1,663	2,902	2,304
Educational building	-	-	19.7	-	-	1.92	6.12	10.04	8.16	9,405	14,966	12,193

The values for the compressive strength (f_d) and the Young's modulus (E) are among the most crucial ones for the characterisation of the masonry material. For each of the properties a minimum, maximum and an average value has been presented. As it was previously discussed, the compressive strength of each of the masonry's components has a great influence on the mechanical behaviour of the masonry as a composite material. Therefore, the values of the brick's compressive strength vary between 8.38 and 44.9 MPa, with an average value of 18.7 MPa. The obtained average value of the compressive strength of the mortar is 1.3 MPa, varying from 0.2 to 6.23 MPa, as tested from extracted masonry specimens of different existing buildings. The experimental masonry compressive strength has an average value of 6.8 MPa considering all the data presented in Table 3.6. The Young's modulus was evaluated as well by means of compression tests of the masonry core samples. Its values range between 1291 and 4258 MPa, with an average value of 2590 MPa, excluding the values obtained for the educational existing building, which are significantly higher than the rest. In conclusion, the most representative data for this research study, regarding the masonry's compressive strength and Young's modulus are the results of the existing residential building (1), dating from 1930 and located in the *Eixample* district.

In Cornadó's (2015) doctoral thesis, results from experimental studies (1995 - 2013) carried out on core prismatic samples extracted from unreinforced masonry walls, provided by the laboratory of materials in the Barcelona School of Building Construction of the UPC, provided an overview of the possible range of the masonry's compressive strength in a large sample of buildings. The tests were carried out on more than 60 existing unreinforced masonry buildings in Barcelona city, of which only 15 buildings (with a total of 37 samples), were chosen according to their year of construction and location in the *Eixample* district. However, the dispersion in the size and slenderness of the test samples resulted as a limitation of the results from these tests. The values obtained from the experimental campaign cannot be directly compared due to these variations in slenderness. Therefore, a linear regression analysis was implemented in order to relate the decrease of the compressive strength with the increase of the slenderness of the tested specimens. Finally, the obtained data for the different sizes of the samples was converted to an equivalent compressive strength for a reference specimen with slenderness of 4 (Cornadó Bardón, 2015). Figure 3.60 illustrates the frequency distribution of the compressive strength obtained from the different samples of the existing buildings. The masonry's compressive strength of the analysed samples shows a vast dispersion, with values between 2.15 MPa as minimum and 16.25 MPa as maximum. In Cornadó's (2015) research, a value of 3.6 MPa was chosen as a characteristic compressive strength representing, in average, the entire set of masonry buildings.

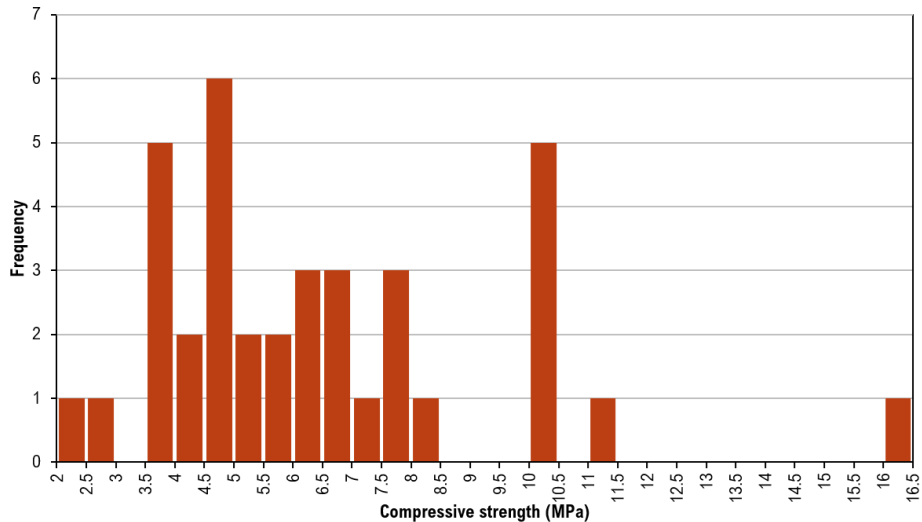


Figure 3.60 - Histogram of the compressive strength's frequency distribution of the masonry samples extracted from the existing Eixample buildings (adapted from Cornadó Bardón 2015).

Furthermore, different experimental campaigns were carried out on masonry specimens built and tested at the LATEM Laboratory of the UPC. Drougkas et al. (2016) mechanically characterised a variety of masonry materials commonly found in historical structures, including fired clay bricks, aerial calcium mortar, and hydraulic calcium mortar. The bricks compressive strength was estimated from cylindrical core brick samples with a diameter of 45.25 mm (see Figure 3.61a). The mortars prismatic samples measuring at $160 \times 40 \times 40 \text{ mm}^3$ were prepared for each mortar type (aerial calcium and hydraulic calcium mortar) and they were subjected to flexural and compressive tests (see Figure 3.61c).

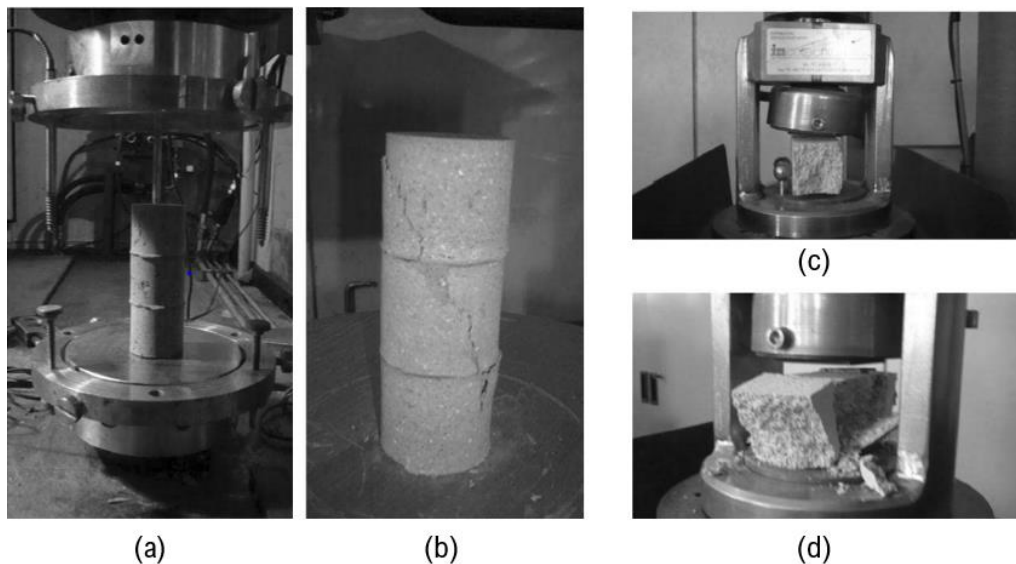


Figure 3.61 - Brick and mortar samples for compression tests (before and after): a) triple cylindrical brick sample (before compression test); b) triple cylindrical brick sample (after compression test); c) prismatic mortar sample (before compression test); d) prismatic mortar sample (after compression test) (adapted from Drougkas et al. 2016).

Masonry prisms consisted of five bricks and four mortar bed joints of 10 mm thickness, resulting in overall nominal dimensions of $290 \times 140 \times 290 \text{ mm}^3$ were constructed using the handmade

bricks and the two types of mortars, and they were tested in compression with a typical layout of LVDTs (Figure 3.62).



Figure 3.62 - Masonry prisms with a typical layout of LVDTs: a) vertical layout for displacement measurement in the unit and the composite and b) horizontal displacement for measurement of the Poisson's ratio (Drougkas et al., 2016).

Figure 3.63 illustrates the stress displacement diagrams for the three masonry prisms with two different types of mortars: a) aerial lime mortar and b) hydraulic lime mortar. The hydraulic lime mortar prisms showed a higher capacity and global stiffness than the aerial lime mortar prisms. This research study demonstrated that using conventional lime mortars and moderately strong units, relatively high masonry strength can be consistently achieved. In particular, a masonry strength nearly ten times greater than the mortar's compressive strength was achieved (Drougkas et al., 2016).

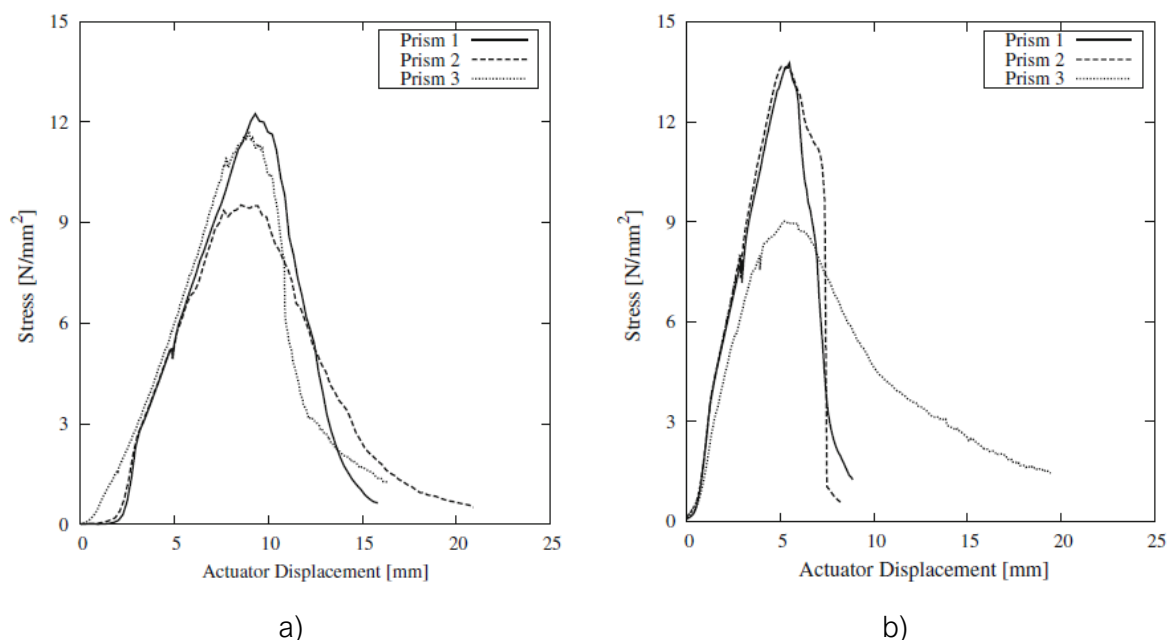


Figure 3.63 - Stress displacement diagrams for masonry prisms with two types of mortars: a) aerial lime mortar prisms; b) hydraulic lime mortar prisms (Drougkas et al., 2016).

Segura et al. (2018) presents a research regarding the mechanical characterisation of handmade clay brick and hydraulic lime mortar masonry under compression. In this experimental

programme, compression tests on two distinct types of specimens (running bond walls and stack bond prisms, see Figure 3.64) were performed under monotonic and cyclic loading.

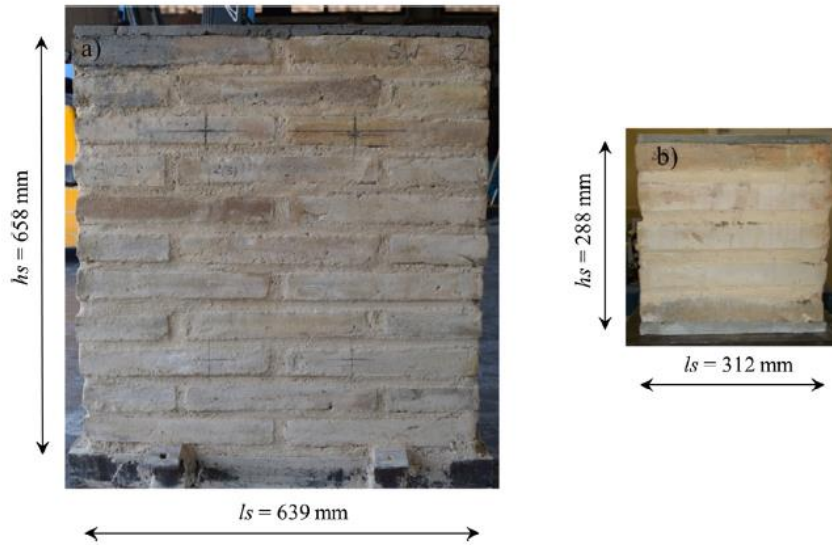


Figure 3.64 - Dimensions of two masonry samples: a) Running bond walls, b) Stack bond prisms. Common average thickness $t_s = 148$ mm (Segura et al., 2018).

Figure 3.65 shows the experimental stress-strain curves for the different masonry specimens under monotonic loading. Moreover, the compressive strength and elastic modulus of the masonry were evaluated for each of the masonry specimens under both monotonic and cyclic loading and they were compared with the values yielded by available predictive equations. The average compressive strength obtained for monotonically loaded stack bonded prisms and running bond walls was very similar, equal to 6.49 MPa and 6.51 MPa, respectively (Segura et al., 2018).

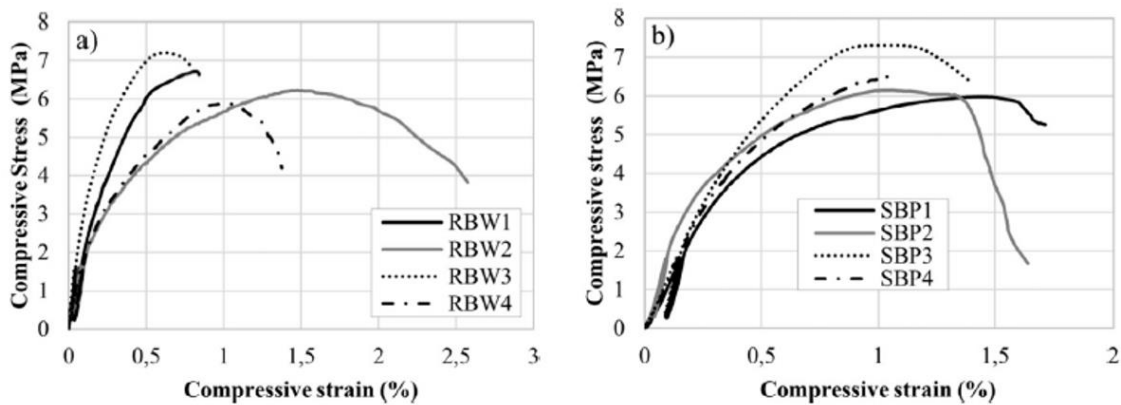


Figure 3.65 - Stress vs. strain experimental curves until failure with monotonic loading for the two masonry specimens: a) running bond walls; b) stack bond prisms (Segura et al., 2018).

From the aforementioned experimental campaigns executed at LATEM of the UPC, the characteristic values of each series of core samples from masonry walls have been calculated. Table 3.7 presents the average of the characteristic values of the mechanical properties obtained from different laboratory compression tests on masonry core samples with a diameter of 150 mm,

composed of handmade clay bricks and lime mortar. In addition, Table 3.7 presents the masonry mean tensile strength due to shear as measured during an experimental program at LATEM executed by (Segura et al. 2021) and consisting of diagonal compression testing of masonry walls with handmade units and hydraulic lime mortar. These values reported in Table 3.7 can be used as reference values for modelling the non-linear mechanical behaviour of the masonry as a composite material.

Table 3.7 - Mechanical properties obtained from laboratory testing on masonry specimens.

Mechanical parameters of masonry from laboratory testing		
Brick mean compressive strength	17.99	MPa
Mortar mean compressive strength	2.19	MPa
Masonry characteristic compressive strength	5.42	MPa
Masonry mean tensile strength due to shear	0.20	MPa
Masonry mean elastic modulus	2318	MPa

3.9. SUMMARY

This chapter presented a complete description of the buildings of the *Eixample* district, which is the most representative urban centre of Barcelona city and the case study of this doctoral thesis. This district of Barcelona was built during the 19th and the beginning of the 20th century, and it is famous for its unique architecture and urban design. The name *Eixample* means "expansion or enlargement" in Catalan, referring to the expansion of the ancient town by establishing a connection with the surrounding smaller urban areas.

In the first part of this chapter, a historical overview and urban evolution of the city of Barcelona has been provided in order to better understand the development of the *Eixample* district as a specific area of the city. Moreover, the specific construction features and construction techniques of its historical existing buildings have been presented.

Unreinforced masonry buildings account for roughly 70% of the existing buildings in Barcelona's *Eixample* district. They have a significant historical, economic, and cultural value. The buildings of this district are organised into blocks of 113 x 113 m², with chamfers in the corners and an average of 25 buildings per block. The majority of the buildings were designed and built using the same structural resisting model without considering seismic resistant requirements. The existing *Eixample* buildings are of exceptional historical and cultural value, not only because they are a symbol of modernism architecture, but also because of the particularities recognised in their construction and structural features. As previously mentioned, these constructions have a complex architectural and structural configuration that has been studied and analysed by many researchers.

The main characteristics and structural elements of the buildings of the Example district have been described in terms of geometric and constructive features, as well as with regard to the construction materials used for these structures. Different structural building systems can be

found in this historical urban centre; however, the most prevalent and representative type is the URM building with traditional one-way floor slabs.

The seismic hazard of Barcelona city is considered to be moderate when compared to other regions in the Mediterranean Sea. In the RISK-UE project, deterministic and probabilistic approaches, considering soil effects, were used to assess the seismic risk for the city of Barcelona. Furthermore, the acceleration-displacement response spectra (ADRS) for both seismic scenarios and for the different soil zones were developed and used in the previous studies for the seismic vulnerability assessment. Even though, the seismicity of this region is low to moderate, the existing masonry buildings of the *Eixample* district present significant seismic vulnerability and require an evaluation of their seismic performance.

The previous studies of the seismic risk of Barcelona that have been mentioned in this chapter are examples of the valuable information available about the city. The state-of-the-art research on seismic vulnerability assessment on existing buildings from Barcelona's urban centre has been presented and discussed. The previous research studies carried out in the last two decades have been summarized in a chronological order. They are based on the use of empirical and analytical vulnerability methods. Many seismic vulnerability studies were carried out for the existing buildings of Barcelona's urban centre by applying the Vulnerability Index Method (VIM) proposed in Italy (GNDT, 1986). The vulnerability index calculation forms were proposed for existing masonry buildings in Italy and were calibrated based on observed damage. Hence, these forms are not fully representative of the typical *Eixample* buildings and they should be updated accordingly. The previous researches for the seismic vulnerability assessment of existing buildings in Barcelona have not provided a proper building taxonomy. However, an accurate building taxonomy will help in the definition of building typologies and the identification of representative buildings with respect to seismic performance.

Previous research studies regarding the seismic performance through structural non-linear modelling have been also presented. Nonlinear static (pushover) analysis has been extensively used in the past for the evaluation of the seismic performance of existing buildings of Barcelona's urban centre. The results from the structural modelling of the existing *Eixample* buildings have been compiled in order to better understand their seismic behaviour. Nonetheless, in all these studies a simplified modelling strategy such as EFM was employed for some existing buildings not previously categorised as representative ones. Hence, a more detailed study of the seismic behaviour is necessary based on an accurate modelling of previously selected representative building typologies. The previous studies will be used as a basis for comparison with the seismic analysis results obtained from the present research.

Previous studies carried out on the experimental characterisation of masonry properties are presented for Barcelona's building stock. Results of different experimental campaigns executed at LATEM (UPC) assessing the masonry compressive strength and Young's modulus from cylindrical samples extracted from existing masonry buildings have been summarized. These results have been used as reference ones for the preparation of the numerical models of the representative buildings, presented in Chapter 5. The proper definition of these mechanical properties is of paramount importance for the buildings' seismic behaviour, since the main structural system is consisted of load-bearing unreinforced masonry walls.

CHAPTER 4. BUILDING TAXONOMY OF REPRESENTATIVE TYPOLOGIES EXPOSED TO SEISMIC RISK IN THE *EIXAMPLE* DISTRICT

4.1. INTRODUCTION

Taxonomy is the classification of objects in an orderly system that represents their relationships. The building taxonomy outlines the characteristics of a single building or a group of buildings with similar features, which is referred to as a building typology (Brzev et al., 2013). The creation of a building taxonomy for existing buildings is crucial for understanding their structural system and architectural configuration relevant to their seismic behaviour. This typology classification will contribute in the empirical assessment of the buildings' vulnerability, as well as serve as the basis for developing numerical models of representative building typologies for the analysis of its nonlinear seismic performance.

The classification of a city's or region's building stock is one of the most difficult challenges when conducting a seismic risk assessment at the urban scale. The primary goal of any building taxonomy is to classify and group building typologies that have comparable overall performance during an earthquake shaking because they have similar vulnerabilities. As a result, it is absolutely necessary to classify buildings using various building attributes that describe a specific characteristic of an individual building or group of buildings that may affect their seismic behaviour. Typical typology parameters considered for a building taxonomy are the following ones: geometry, material properties, lateral load-resisting system, construction date, seismic design level, structural irregularities, and foundation details. The main parameters influencing structural vulnerability are the building's load resisting system and the materials used in construction. Secondary classification parameters include overall building height, construction period, building plan shape, foundation, irregularities, and so on. Certain criteria based on data gathered from field surveys related to the previously mentioned parameters should be used in the classification scheme. Another reason for this type of categorisation is to establish a common terminology in order to document differences in building design and construction around the world (Brzev et al., 2013).

The demand for a building taxonomy is due to the fact that it is practically impossible to consider each building with its specific structural and non-structural characteristics in a city or region with a great amount of individual buildings. As a result, grouping the buildings will result in a more feasible and cost-effective study while still ensuring the accuracy of the obtained results for the entire building stock. Subsequently, the seismic risk assessment will undoubtedly be simpler to carry out if a specific number of building typology classes are defined based on their expected vulnerability during an earthquake motion. Any building typology class should include typologies

that are similar in terms of each parameter that could influence the seismic response of the building (structural system, construction materials used, building size and shape, irregularities, and etc). This typology classification will allow a better understanding of the building's global behaviour and response to a natural hazard, and also defining retrofit techniques for reducing a building's seismic vulnerability.

Many building taxonomies have been developed over the last 30 years, including ATC-13 (ATC-13, 1985), HAZUS (FEMA, 2003), EMS-98 (Grünthal, 1998), GEM building taxonomy (Brzev et al., 2013), PAGER-STR (Jaiswal and Wald, 2008), RISK-UE taxonomy (Lagomarsino and Giovinazzi, 2006), and the SYNER-G project (Pitilakis et al., 2014). These taxonomies are created for the most common existing building types in different regions in the world. As a result, for each region, city, or country, a more detailed classification (including specific building attributes) should be completed in accordance with the existing general taxonomies.

This chapter includes an in-depth description of the specific building taxonomy of the typical *Eixample* buildings. The classification of their construction system and features has been done, considering their influence on the structures' seismic performance. Moreover, a statistical extrapolation of *Eixample* buildings' construction features is presented from an extensive field survey and data collection, which was previously done in another research study (Cornadó Bardón, 2015) and it was used as a base data for the generalisation of the buildings' characteristics and for the definition of the most representative ones. Finally, the methodology adopted for the selection of the representative buildings, which are the basis for the creation of the mechanical models in this doctoral thesis is explained.

4.2. CONSTRUCTION OF A BUILDING TAXONOMY

A consistent and comprehensive classification system, also known as taxonomy is essential for identifying classes of buildings with consistent behaviour, as it is frequently a significant step in a large-scale vulnerability assessment (Brzev et al., 2013). A proper building taxonomy describes and classifies various construction types based on features relevant for the structure's seismic performance. These characteristics are included in the taxonomy since they can influence the likelihood of damage in buildings caused by seismic hazard events (Silva et al., 2022). Hence, each building can be assigned to a particular typological class once the taxonomy is established.

Several studies in Europe have defined taxonomies, beginning with the EMS-98 (Grünthal, 1998), which defined building and vulnerability classes, and then with the Risk-UE project (Lagomarsino and Giovinazzi, 2006), which implemented the EMS-98 classes by adding some specifications for each city or region. The construction of a building taxonomy by including all the main characteristics of the studied building stock, along with identifying the most common typological classes of a specific city or region, are crucial challenges needed to be implemented for accurate vulnerability assessment at large scale. This simplified procedure is necessary since the evaluation of all individual buildings is a time-consuming and costly process. Individual evaluations are only appropriate for strategic buildings, such as hospitals, schools or other relevant buildings that play a critical role in the emergency post-earthquake planning (Diana et al., 2019). Moreover, the classification of building typologies assists in providing a basis for numerical

modelling and performing non-linear analysis in order to evaluate the seismic performance of representative buildings and assess their vulnerability.

The studies on the seismic vulnerability of urban areas are strongly connected with the gathering of available information of existing buildings. The detailed survey activity is essential for defining a reliable taxonomy for existing buildings in urban centres. Sometimes there is a lack of historical records or technical documentation and thus, for the completion of the database, it is necessary a field survey of the existing buildings. However, in large urban areas with inhabited buildings, comprehensive inspections of every structure are hardly practical and very time consuming (Jiménez et al., 2018). Therefore, there is a need of a proper methodology for the generation of a taxonomy used for the definition of most representative classes of existing building that cover the area of research. This step is very important for determining the seismic vulnerability of each building in an urban centre.

Many taxonomy systems that are both globally applicable (Coburn and Spence 2002, Jaiswal and Wald 2008, Brzev et al. 2013) and regionally relevant (ATC-13 1985, Grünthal 1998, FEMA 2003, Lagomarsino and Giovinazzi 2006) are available in the literature and previously summarised in Chapter 2. In these taxonomies, existing buildings are commonly classified based on several structural and non-structural parameters that are assumed for the evaluation of the structure's response to seismic actions. However, existing taxonomies appear to exclude some specific structural characteristics such as different geometrical configurations in plan, presence of additional storeys, percentage area of façade openings and their distribution, which could be used to identify different building typologies of a city or an urban centre. For the seismic evaluation and vulnerability assessment of particular building classes, a detailed classification system with all the specific structural attributes should be completed in line with the existing generic taxonomies.

The first step for developing a building taxonomy is analysing all the specific structural features of the existing buildings located in the *Eixample* district. Previously, existing taxonomies have been reviewed in order to confirm if any of them could satisfy the classification of the *Eixample* representative building typologies and to assist with the selection of the parameters affecting the buildings' seismic performance. It has been anticipated that no previously available taxonomy describes comprehensively all the structural and non-structural parameters that could influence the global seismic behaviour of these existing buildings. The existing *Eixample* buildings present several construction characteristics (described in Chapter 3), such as the different geometrical configurations (presence of patios), soft-storey effect, presence of vertical extensions, big façade openings on the ground floor, which should be included in a specific building classification for seismic vulnerability assessment. Therefore, a methodology has been proposed, which involves the generation of a detailed building taxonomy for a specific urban centre including all the structural and non-structural features. After analysing all the structural features of a number of buildings, a new building taxonomy has been created for the existing *Eixample* buildings. This taxonomy can be changed and updated for the use of similar building typologies of historical urban centres by following the same proposed methodology.

The specific building taxonomy has been created for the definition of most significant structural parameters and for the identification of the most representative buildings, necessary for the seismic vulnerability assessment at large scale, by using numerical methods. As a result, the

building classification has been completed by considering the influence of the most important characteristics on the seismic performance of the buildings. An extensive database of *Eixample* buildings from a detailed survey conducted by Cornadó Bardón (2015) was used to prepare the building taxonomy, as well as some building plans obtained from the public archives of Barcelona City municipality (Cara et al., 2018).

Many parameters for the seismic vulnerability assessment methodologies are established from the data available regarding the existing buildings. For this case study, different parameters have been considered in order to define a specific and adequate taxonomy, which will represent most of the building stock of the *Eixample* district (see Figure 2.1). The studied parameters are grouped into the following sections: general building information, structural building system, structural elements and connections, configuration and irregularities, conservation state of the building, and interaction and behaviour of the building within a block. A detailed description on all available parameters, which can effectively impact on a structure's behaviour and possible damage, is presented below. The most recurrent parameters are considered as part of the Vulnerability Index Method, which is explained in Chapter 7.

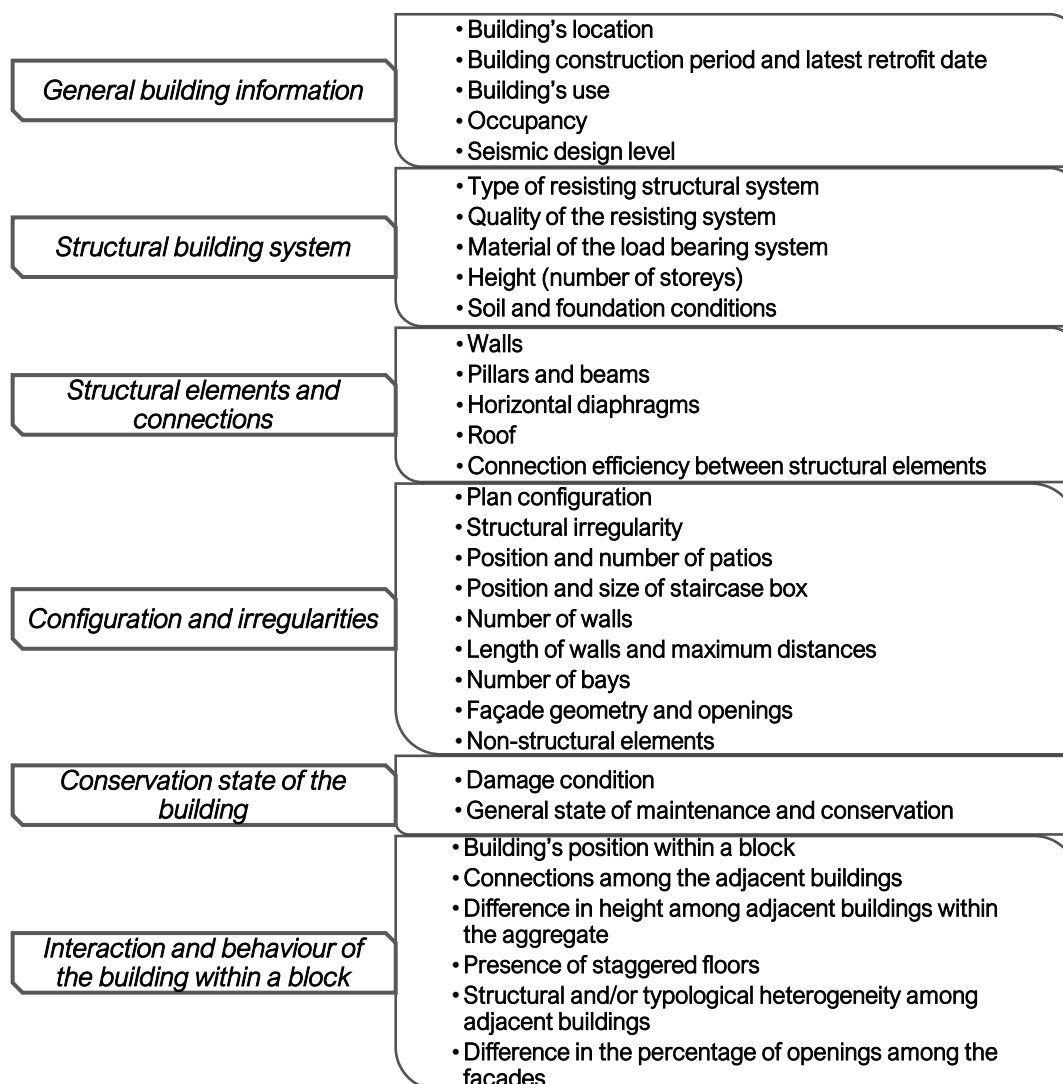


Figure 4.1 - Parameters for a specified building taxonomy.

4.2.1. General building information

The first part of the building taxonomy includes some general information about the buildings, including the date of construction, the number of occupants, the use of the building, and the seismic design level (necessary for the further risk analysis, primarily for the damage losses).

The date of the building's construction is crucial since it essentially provides more details about the building's typology, the materials and construction practises used, and the consideration of any earthquake-resistant design criteria. Generally, the building's construction period can be divided into four periods: pre-modernism (1860-1900), modernism (1888-1915), postmodernism (1910-1936), and the last period, which began in the 1960s. The specific architectural and structural characteristics of each period are previously described in Chapter 3. The historical unreinforced masonry buildings, built between 1860 and 1940, were designed only for vertical static loads, without considering any seismic resistance requirements. These structures account for roughly half of the total building stock in this urban area. After 1960, reinforced concrete buildings were constructed, with application of some seismic design requirements after the implementation of the first Spanish seismic code in 1968.

According to previously done taxonomies such as the GEM taxonomy (Brzev et al., 2013), the number of occupants, the use of the building and the seismic code level are attributes needed for the general information regarding these buildings. The seismic code level is important and has to be defined properly in the case of older existing masonry buildings, which were usually designed without any seismic requirements. Therefore, the seismic code level can be defined as No code, Low code, Medium code and High Code Level (Milutinovic and Trendafiloski, 2003). In the case of Barcelona's historical centre, all masonry building typologies will be defined with No code level, indicating that they are not earthquake-resistant, since these structures were designed only for vertical loads and without any consideration for seismic actions. As previously mentioned, the majority of *Eixample*'s building stock was constructed between the 1860s and the 1940s, prior to the adoption of Spain's first seismic code in 1968 (PGS-1, 1968). Moreover, in order to study buildings built between the 1960s and 1970s, such as the reinforced concrete structures, it has to be assumed that horizontal seismic loading was considered in accordance with the regulations in that time period and they can be classified as having Low code level.

4.2.2. Structural building system

The building's load resisting system and the used construction materials are considered as the primary parameters in a building taxonomy for better understanding of the buildings' seismic behaviour and structural vulnerability. As described in Chapter 3, the existing *Eixample* masonry buildings can be categorised in the following typologies regarding the resisting load-bearing system (Figure 4.2):

- Homogenous structural system with continuous load-bearing masonry walls throughout the full height of the building;
- Hybrid structural system of steel/concrete columns at the ground floor and unreinforced masonry walls on the upper floor levels.

The second structural typology is very common because it allows for a great open space at the ground floor, which is usually used for commercial or administrative purposes. The hybrid structural system presents different seismic performance than the homogeneous one due to the reduction of stiffness at the ground floor. The disadvantage of this hybrid structural system is that it has poor seismic performance, as the slender piers at the ground floor facilitate the development of a soft-storey mechanism.

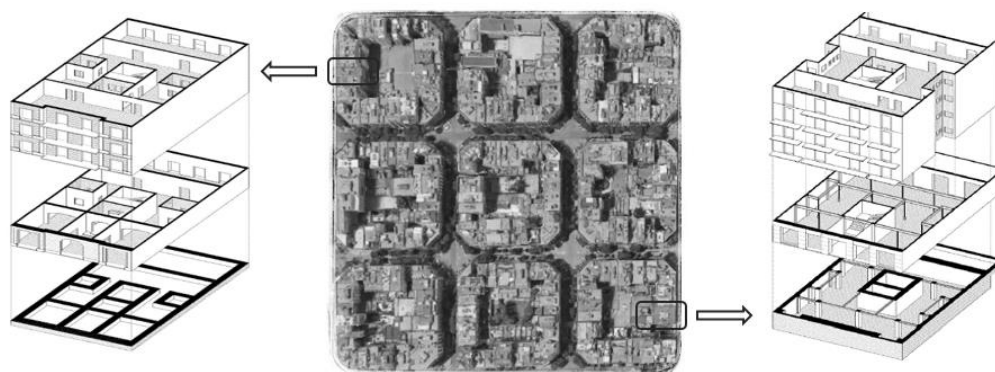


Figure 4.2 - Different structural systems for the rectangular shape buildings in the middle of the typical *Eixample* urban block: homogenous system of continuous slender walls (left) and hybrid system – steel/concrete frames on the ground floor and unreinforced masonry walls on the upper floors (right) (adapted from Paricio Casademunt 2001).

The material properties used for each of the structural elements has a great influence on the seismic performance and vulnerability of the buildings. As mentioned in Chapter 3, different materials were used in different construction periods. The quality of the masonry as the main material used for the resisting structural system is a crucial parameter of the vulnerability assessment. Depending on the type of masonry, the shape and size of the constituent elements, the homogeneity of the material, and most importantly the resistance characteristics, the following different classes can be defined (GNDT, 1986): - Good quality masonry with high resistance made of clay or sand-lime blocks with good quality mortar; - Regular quality masonry made of clay or sand-lime blocks with good quality mortar; - Poor quality unreinforced masonry made of clay or sand-lime blocks with poor quality mortar. Most of the existing building stock in the *Eixample* district can be classified as buildings with regular or poor-quality masonry, made of clay brick masonry with hydraulic lime mortar. The specific material properties for the bricks and mortars, as well as of the masonry as composite material, have been previously presented and analysed in section 3.8.

The height of a building, represented by the number of storeys, is one of the attributes that determines the building's vibration period, which can have a significant influence for the overall earthquake forces and basal shear of the buildings as well as for their seismic vulnerability. The number of floor levels in the existing *Eixample* building typologies can range between 4 and 7. According to the evolution of the ordinances, described in Chapter 3, additional storeys - *remuntes* were constructed above the original height of some existing buildings, resulting in another important parameter that greatly influences the seismic behaviour of the structure.

The existing masonry *Eixample* buildings can be divided in three classes based on their height variation including the existence of vertical extensions (*remuntes*) (Figure 4.3):

- Low-rise: buildings of low height with four or less floor levels (\leq GF+4);
- Mid-rise: buildings of medium height, between five and six floor levels (GF+5, GF+6);
- High-rise: buildings of high height with seven or more floors for unreinforced masonry buildings including the existence of *remuntes* (\geq GF+7+R).



Figure 4.3 - Different height levels of existing masonry buildings in the Eixample district.

Additionally, the type of foundation system, as well as the soil characteristics, may influence the seismic performance of a building and thus, they are considered as a secondary parameter in the existing building taxonomies. The typical foundation system, described in the previous chapter 3, depends on the structural building system and can be characterised as shallow continuous foundation under the load-bearing walls and isolated footings under the columns. The type of soil is a key factor for the choice of foundation system as well as it influences the seismic intensity at the given location. As previously mentioned (in section 3.6), the *Eixample* district is located in Zone II, according to the identification of the four different soil types. Therefore, the parameter regarding the location of the buildings and their foundation system will not be considered as part of the proposed form for the seismic vulnerability assessment.

4.2.3. Structural elements and connections

The masonry load-bearing walls, the horizontal flooring system, the masonry columns, cast-iron *pillars* and the steel truss beams at the base level are the different structural elements composing the structural resisting system. In Chapter 3, each of these elements was described in detail, regarding the different structural typologies, material and construction techniques.

These structural elements play an important role in the structural behaviour of the existing *Eixample* buildings, thus they should be included in the detailed building taxonomy. The dimensions, position and material of the structural elements should be studied previously in order to understand the resisting building system. The structural elements and their different typologies in terms of dimensions or materials, have a great influence on the seismic performance of the buildings and thus, they may induce some existing vulnerabilities.

As described in Chapter 3, the masonry resisting walls have a variety of different thicknesses, from 0.15 to 0.45 m. Moreover, the thickness of these load-bearing walls can change along the height of the building, having thicker walls on the ground floor and decreasing the thickness for the walls at the upper levels. Therefore, the variation of thickness in the load-bearing masonry walls is a necessary attribute for the seismic vulnerability assessment, since it affects the resisting area of these vertical elements and their slenderness.

Moreover, structural elements such as the masonry columns (extensions of the masonry walls), cast-iron *pillars* and steel truss beams are located only at the ground floor of some *Eixample* buildings. As it was mentioned previously, they are part of the hybrid structural system, by forming a more flexible ground floor than the rest of the storeys, and might induce in a soft-storey collapsing mechanism. The presence of these structural elements at the ground floor of the existing buildings can affect strongly the structure's seismic capacity and therefore its vulnerability.

- The horizontal floor system

The horizontal system is a necessary vulnerability parameter for the preparation of the building taxonomy, since it can affect the structural behaviour of the buildings under seismic actions, both in terms of mass and stiffness. These horizontal structures are required to distribute the seismic horizontal forces to the resisting vertical elements. Therefore, the flexibility of the floors can play an important role in the seismic performance of URM buildings. This parameter considers the in-plane stiffness of floors and their connections with the vertical resisting elements.

According to the existing building taxonomies (Brzev et al. 2013, Pitilakis et al. 2014) the floor systems can be differentiated as flexible, semi-flexible and rigid, depending on their stiffness and distribution of the lateral loads to the resisting vertical elements. Due to their flexibility, flexible horizontal structures tend to have a load distribution proportional to the influence area of each masonry wall. Moreover, they are unable to have any restraints between walls that are parallel and orthogonal to the seismic force. Semi-flexible horizontal diaphragms allow the distribution of lateral forces among the load-bearing walls based on their stiffness, but they do not present a box behaviour. Finally, rigid diaphragms distribute the lateral forces to the vertical resisting elements in direct proportion to their stiffness, acting as an effective confinement between them, resulting into a proper box behaviour. Buildings with rigid diaphragms present higher seismic resistance than buildings with flexible horizontal diaphragms. However, the rigid floors are normally heavier and they can increase the horizontal seismic actions, which can lead to a worse seismic behaviour.

The different floor typologies are described in Chapter 3, regarding the use of different materials and construction techniques in different time periods. In the typical *Eixample* buildings, flexible floor slabs are constructed from wooden beams with a single or double layer of wood planks (Figure 3.27a). Semi-flexible slabs are usually made of timber or steel beams with flat arch vaults and a layer of rubble material above (Figure 3.28). Rigid slabs are made of steel or reinforced concrete joists with hollow clay brick, or prefabricated hollow clay bricks with longitudinal reinforcement (Figure 3.27f).

- Roof system

The roof system can influence the seismic behaviour of the building by considering its roof typology, possible thrusting actions and the applied weight. The roof system in these existing

buildings is a flat one, which is usually used as a huge terrace space for all the residents of the building. In these building typologies it is not common to have a pitched roof formed of timber trusses. Therefore, this vulnerability parameter will not be included in the new developed form for the vulnerability assessment.

- Connections between structural elements

The connections between the structural elements (walls, floor slabs, beams and columns) have an especially important role in the structural performance of the structures and can greatly increase the building's vulnerability. The proper box behaviour depends on the type and quality of the interlocking connection between the orthogonal load-bearing walls. Buildings in *Eixample* have a variety of configurations, establishing various types of connections that can be achieved between the vertical and horizontal structural elements (presented in section 3.5.1). Different types of connections such as wall-to wall or floor-to-wall connections (previously discussed in Chapter 3) can produce significantly different results in terms of strength, stiffness, and capacity. Hence, these connections should be properly studied as they could increase the structure's seismic vulnerability.

This parameter is based on relative stiffness and quality of the connection between the vertical and horizontal structural elements. Therefore, the proper connections found in the existing buildings can be classified as: poor (damaged) connections presenting imperfect interlocking between the orthogonal masonry walls and with the horizontal diaphragms; and efficient (not damaged) connections with good interlocking between the masonry walls, ascertaining the typical box-behaviour.

4.2.4. Configuration and irregularities

In the detailed building taxonomy, it is crucial to describe the most common geometrical configuration of the buildings (rectangular and pentagonal) and the structural irregularities (in plan and in elevation). The *Eixample* buildings present many irregularities, which are an important attribute for the evaluation of the seismic performance of the structure, as well as its vulnerability.

Plan configuration irregularities are essential in seismic vulnerability assessments because asymmetrical shapes can cause torsional effects. This attribute concerns the geometrical plane configuration, the mass of the seismic resistant elements and their stiffness distribution. Therefore, the buildings can be classified depending on the ratio between the width and length of the buildings with a rectangular shape plan. The different geometrical configurations were presented in the previous chapter (section 3.5.2). Moreover, the plan irregularities such as some additions or subtractions to a rectangular building shape, which interrupt the continuity of the load-bearing walls, have to be considered for the vulnerability class definition of the existing buildings. The building classes according to the plan irregularity are defined according to the different shape and eccentricity. The latter is obtained as the distance between the centre of rigidity and the centre of mass.

The vertical regularity is another parameter included in the building taxonomy, considering the mass change between floor levels and potential discontinuities in the placement of vertical




seismic-resistant systems. As explained in Chapter 3, the vertical extensions (*remuntes*), which were constructed as additional storeys to the existing buildings, are considered in the vertical irregularity parameter by adding mass on the upper levels. The vertical extensions can be grouped into five categories based on prior research. The main distinguishing feature is the façade alignment between the new vertical additions and the original structure (Colom, 2014). The classification groups are as follows:

- "Aligned," the new façades are aligned with the original building.
- "Partially aligned," the new façades are only partially aligned with the original structure.
- "Retracted," the additional façades are retracted with a reference to the original façade.
- "Combination of partially aligned and retracted" means that the façades are both partially aligned and retracted in relation to the original façade.
- "Extruding," finally, the façade of the vertical extension protrudes from the plane of the original façade.

The existing buildings in the *Eixample* district can have combinations of these five groups of different alignments between the vertical extensions and the original existing building. Table 4.1 shows the three most common combinations, denoted as types A, B, and C.

Table 4.1 - Summary table of the most recurrent subtypes of the vertical extensions.

Type	Number of elements observed	Description	Scheme	Period	Opening percentage	Materials
A	(158/756) 20,9 %	one additional aligned storey (base +1)		Up to the 1940s	Homogeneous 29,2% (front), 26,3% (rear)	Solid bricks (walls) steel beams with ceramic vaulted structure (floors)
B	(115/756) 15,2 %	one aligned storey and one additional retracted storey (base +2)		1950s - 60s -70s	Homogeneous 28,8% (front), 26,3% (rear)	Ceramic hollow bricks (walls) RC (floors)
C	(87/756) 11,5 %	one additional aligned storey, two additional retracted storeys in scale (base +3)		1950s - 60s - 70sx	Nonhomogeneous 32,3% (front), 26,6% (rear)	Ceramic hollow bricks (walls) RC (floors)

-  1st *remunta*
-  2nd *remunta* - attic
-  3rd *remunta* - penthouse

The existence of a soft story in an existing building is included as a vertical irregularity in the prepared building taxonomy, because it is a critical source of seismic vulnerability. The soft ground story is a structural weakness, as it is significantly more flexible or weak in lateral load resistance than the stories above it. This is a very common seismic vulnerability, resulting in a significant reduction in the stiffness and resisting area of the vertical elements. As it was previously mentioned, some existing *Eixample* buildings with hybrid structural system have steel or concrete columns at the ground floor and masonry load-bearing walls for the upper ones, resulting in a soft story behaviour.

In relation to the vertical irregularity as a vulnerability parameter, the following building typologies in the *Eixample* district can be considered:

- Buildings without any vertical extensions;
- Buildings with vertical extensions (one or more additional storeys);
- Buildings with hybrid structural system (ground soft-story);
- Presence of patios

The position and number of patios, as well as the size and position of the stairway box are important characteristics to consider for the building taxonomy of *Eixample* buildings. Patios are typically located in the centre of buildings (close to the staircase), or on the sides, and can be found in a variety of positions, depending on the geometrical configuration of the building (presented in Chapter 3). This attribute presents an irregularity in the building's plan configuration and can reduce the structure's stiffness. Patios can have a significant seismic impact because they represent an interruption in the length of the building's lateral walls and their ability to function as continuous walls.



Figure 4.4 - Position and number of interior (in grey) and lateral (in yellow) patios in different plan configurations: a) building with lateral patios; b) building with interior central patio; c) building with interior patios near the central staircase and lateral patios on each side of the longitudinal masonry wall; d) buildings with interior central patios and two or more lateral patios on each side of the longitudinal masonry wall (adapted from Cornadó Bardón 2015).

As a result, based on the various geometrical configurations of the types of patios presented in Chapter 3, the following classification is proposed (see Figure 3.40): a) narrow band buildings with lateral patios on each side; b) rectangular band buildings with one or two interior patios in the central part (without any lateral patios); c) wide band buildings with interior patios near the central staircase and lateral patios interrupting the continuity of the longitudinal load-bearing walls; and d) buildings with central interior patios and two or more smaller lateral patios interrupting the continuity of the longitudinal load-bearing walls.

The stairwell, along with the interior patios, function as a core that contributes to the stiffness of the structure because they are typically positioned in the geometric centre of the building's plan. Moreover, there are also present a smaller number of buildings with lateral stairwell and patios, located close to the longitudinal walls (Figure 4.5). Therefore, the position of the staircase (central or lateral), contributing for a symmetrical or asymmetrical building plan based on the distribution of mass and stiffness along each storey, affects considerably the structure's seismic performance. These structural features can also change the stiffness of the structure at its base for the hybrid structural system, as the staircase starts at the ground floor or basement while the patios appear from the first story.

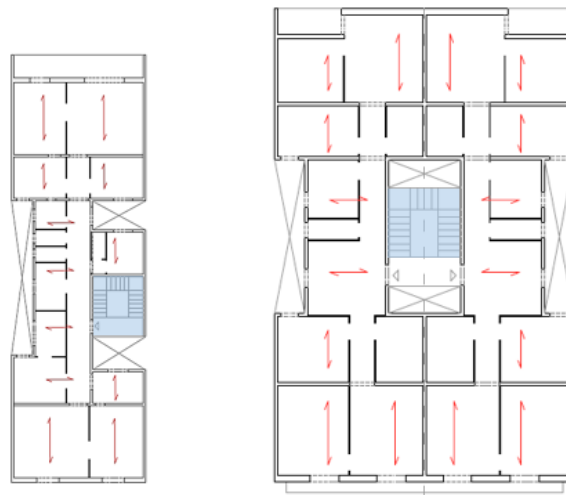


Figure 4.5 - Position of the staircase: lateral staircase (left) and central staircase with interior patios (right) (adapted from Cornadó Bardón 2015).

- Distribution of load-bearing masonry walls

The distribution of the load-bearing masonry walls is considered as another important parameter for the detailed building taxonomy of the *Eixample* buildings. This parameter considers the presence of main resisting structural walls (disregarding partition walls), which are positioned at specific distances, as well as intercepted by the transverse walls.

As previously described, the building typologies in the *Eixample* district are composed of front and rear façade walls, interior walls parallel to the façades, lateral walls perpendicular to the façade, and interior walls around the core formed of the stairwell and interior patios (Figure 4.6). The distribution of the main façades is along the street, which form the typical grid of the *Eixample* district. The lateral walls are intermediate masonry walls between the buildings positioned in a row and they act as load-bearing walls for the area of lateral patios. The interior walls parallel to the

façades are forming bays with smaller spans where the floor beams of the one-way floor slabs are positioned perpendicular to the main façade. The interior walls parallel to the lateral ones can also act as load-bearing masonry walls around the interior patios containing the stairwells.

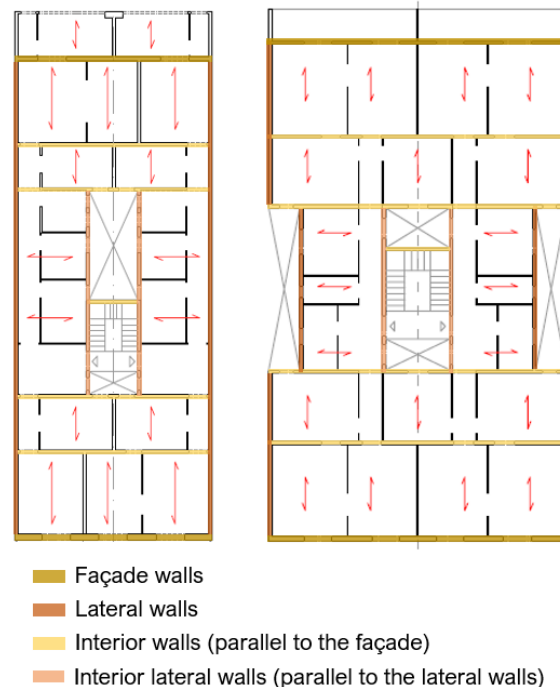


Figure 4.6 - Distribution of walls in representative building typologies in Eixample district (adapted from Cornadó Bardón 2015).

The distances between the façade and interior load-bearing masonry walls are part of this building taxonomy as a specific parameter, which has been evaluated as a part of the statistical analyses (presented in the section 4.3). This parameter defines the geometrical configuration of the front and rear bays of the structure, as well as the spans that have to cover the timber or steel floor beams of the unidirectional diaphragms.

- Façade openings

In seismic resistant masonry walls, the presence of wall openings perpetually affects their in-plane resistance and can decrease the structure's seismic capacity. Therefore, the distribution of façade openings, regarding their dimensions and position, is another critical parameter as part of the building taxonomy, which is necessary for the seismic vulnerability assessment.

The number of façade openings of the rectangular shape buildings in *Eixample* can vary between two to five openings on each of the upper floor levels. Figure 4.7 shows three different band buildings with different number of openings on the ground floor and upper levels, with respectively two, three or four openings on the upper levels and two or three façade openings at the ground floor. The most common ones are the wide buildings with three or four façade openings (see Figure 4.7b and c).

In terms of the size and location of the openings on the façade walls, they are usually aligned except for the ground floor, where there can be the same amount or less openings than on the

upper levels. Moreover, the façade openings on the ground floor are significantly bigger than the ones on the rest of the storeys, since the ground level is generally used for commercial purposes. The size of these openings can vary between 2 - 3.5 m in width and 2.5 - 3.5 m in height. As it was described in section 3.5.2, the most typical size of the upper façade openings is 1.2 m.



Figure 4.7 - Different number of façade openings on the ground floor and the upper levels: a) narrow building with two openings on the ground floor and each of the upper levels; b) band building with three openings at the ground floor and three on each floor level; c) band building with three openings at the ground floor and four on each floor level. The drawings represent the number of opening on the upper floor levels depending on the width of the façade (Cornadó Bardón, 2015).

The openings on the façades, as windows or doors for balconies, are always smaller at higher levels and larger at the ground floor and, if present, at the mezzanine floor. Therefore, the variation of the dimensions of the ground façade openings and the rest of the façade openings influences the building's global structural behaviour under seismic actions and has to be considered for the vulnerability assessment. The buildings can be classified according to the percentage of façade openings obtained as the ratio between the area of wall openings and the total area of the wall.

- Non-structural elements

The building taxonomy considers the presence of non-structural elements such as balconies, statues, façade decorations, additions, ceilings, and etc., whose collapse could cause damage, blockage on the streets, or injury to people. Therefore, the definition of this secondary attribute for the seismic vulnerability assessment is based on their presence, dimensions, heaviness and connection to the resisting structural elements. The buildings can be classified as: buildings with

well-connected or without any external non-structural elements; buildings with non-structural elements not very well-connected to existing elements due to poor execution or deterioration of the materials; and buildings with presence of non-structural elements that are poorly connected to the vertical elements.

4.2.5. Conservation state of the building

The conservation state of the building is included in this building taxonomy as it considers the structure's current state and the overall condition of the structural elements, by focusing on any visible damage. Many existing unreinforced masonry structures suffer from poor maintenance, which can cause advanced material deterioration and frequently leaves previous structural damage unrepaired, like widespread wall cracking. Therefore, the conservation condition depends on the presence of deterioration phenomena, cracking patterns or any damage on the structural elements of the existing building.

In order to define the general conservation state of the building some aspects should be examined such as the crack pattern on load-bearing masonry walls (width and direction of the cracks), the degree of degradation of the material, any visible damage on the structural elements (walls, beams, columns, floors), previous maintenance interventions and the presence of strengthening elements. Later retrofit interventions must be carefully evaluated because they may seriously impact the building's capacity and overall seismic behaviour. Unfavourable interventions include structural additions such as upper floors or poorly connected enlargements (Jiménez et al., 2018). Prior visible damage may vary from extensive material degradation and extensive cracking to walls. Specific areas of the structure are more vulnerable and susceptible to failure due to existing cracks (Ortega, 2018). Thus, this parameter is important for the seismic vulnerability assessment since it focuses on the state of damage of the structure's load bearing walls.

Regarding the maintenance and conservation state of the buildings, the buildings can be classified as follows: Buildings in very good condition, without any visible cracks; Buildings with presence of minor cracks on the masonry load bearing walls; Buildings with medium cracks on the masonry load-bearing walls, which can reduce the masonry's strength due to bad preservation of walls; and Buildings with severe damage (cracks and deformations) produced from past earthquakes or from other previous conditions.

4.2.6. Interaction and behaviour of the building within a block

The *Eixample* district is composed of around 520 octagonal blocks, with an average of 25 buildings per block, which present one of the aforementioned layouts. In order to study the aggregate effect, some interactions between the buildings within the urban block should be considered for the evaluation of their global seismic behaviour. Formisano et al. (2015) proposed some parameters that should be considered for the seismic vulnerability assessment of unreinforced masonry buildings in aggregates (explained in more detail in Chapter 7). A brief

description of these parameters is given in the following paragraphs, by considering the aggregate effect as part of the building taxonomy for *Eixample* buildings.

- Building's position within a block

The position of the buildings within an aggregate has a great influence for the evaluation of the in-plane interaction of the buildings. In the typical *Eixample illes*, the buildings can be located in the following positions (see Figure 4.8): ① in the middle between two buildings enclosed in a row, ② in a corner position of the urban block, or ③ at the end of the aggregate, in the case of the presence of a passage separating the urban block in half.



Figure 4.8 - Building's position within a typical *Eixample* block: 1) between buildings enclosed in a row; 2) at the corner of an urban block; 3) at the end of an aggregate.

- Difference in height among adjacent buildings within the aggregate

The interaction of adjacent buildings with different height has a significant influence on the buildings' seismic response. Therefore, it is important to be considered if the studied building is enclosed between two taller buildings, two buildings of the same height or between building with different height.

- Presence of staggered floors

The presence of staggered floors is a result of the different story height of adjacent buildings (Figure 4.9). This parameter can influence the vulnerability of the building, which can increase with the number of staggered floors (Formisano et al., 2015).



Figure 4.9 - Presence of staggered floors in a row of buildings in a typical example urban block (Castilla Marne, 2010).

- Structural and/or typological heterogeneity among adjacent buildings

In the *Eixample* district, a structural and typological heterogeneity can be found among adjacent buildings. According to Pujades et al. (2012), around 70% of the existing buildings are unreinforced masonry ones built before 1940. However, with the introduction of concrete as a construction material, in 1960, reinforced concrete buildings were built, which nowadays represent around 18% of Barcelona's building stock (Barbat et al., 2006). Additionally, a small number of metallic structures are present as well in some of the typical *Eixample* urban blocks. Figure 4.10 shows the presence of a more modern reinforced concrete building between existing unreinforced masonry buildings.



Figure 4.10 - Structural and typological heterogeneities among band buildings in Eixample (Castilla Marne, 2010).

- Difference in the percentage of openings among the facades

The percentage difference of opening areas among adjacent structural units should be estimated as another parameter for the seismic vulnerability assessment proposed by Formisano et al. (2015). The front façades of *Eixample* buildings can have different number and size of openings (see Figure 4.11), which could reduce the in-plane resistance of load-bearing walls and impact on the structure's seismic response.



Figure 4.11 - Presence of different number of façade openings on the existing Eixample buildings (Modrego Casquero, 2011).

4.3. STATISTICAL DATA EXTRAPOLATION AND GENERALISATION OF *EIXAMPLE* BUILDINGS' CONSTRUCTION CHARACTERISTICS

The first part of this section is based on a previous research study of Cornadó Bardón (2015) that was done on the historical unreinforced masonry buildings in the *Eixample* district. A brief summary of Cornadó's (2015) research has been presented, focusing on the statistical data obtained from the existing *Eixample* buildings by considering different structural features. The second part of this work is considered as a continuation of Cornadó's previous research. The extrapolated data have been applied to the identification of representative buildings for seismic vulnerability assessment, based on the criteria defined in the proposed methodology in section 4.4.

- **Statistical data extrapolation of existing building in the *Eixample* district**

For the creation of the proper building taxonomy, a sample of 175 buildings (built between 1860 and 1940) presented in Figure 4.12 was analysed as part of Cornadó Bardón's research (2015). In order to identify the frequency of occurrence of specific building typologies, the following parameters have been considered: the width and length of the building, the number and location of internal patios, the position of the staircase and the relationship between the building morphology and the plot global size. Hence, a statistical typological analysis was performed for obtaining the representative building models.



Figure 4.12 - Total sample of the analysed buildings built before 1940 in the *Eixample* district (Cornadó Bardón, 2015).

According to the statistical information available, the total number of existing buildings in *Eixample* can be categorised into two groups: Buildings constructed before 1940 (5162 buildings representing 52%) and Buildings constructed after 1940 (4768 buildings representing 48%). As it was previously discussed the buildings built before 1940 are the most representative building typologies of masonry buildings with unreinforced load-bearing walls. Therefore, the distribution of the 5162 buildings constructed prior to 1940, are classified based on their location within the urban block, as follows: 4254 buildings (82.4%) are located in a band with rectangular or parallelepiped shape; 843 buildings are positioned in a chamfer (16.3%) with pentagonal shape,

and 65 buildings (1.3%) are located in a passage, i.e. buildings with plots in an interior passage of the urban block (Cornadó Bardón, 2015).

Cornadó's (2015) accomplished the identification of different structural typology schemes for *Eixample's* buildings. The following structural features were analysed to create the structural typology and identify the different types (see Figure 4.13): (i) the width and length of the buildings' plan, (ii) number of storeys (with or without *remuntes*), (iii) the distribution of front and rear bays added to the central part, (iv) the number of load-bearing walls (either parallel or perpendicular to the façade), (v) the geometrical configuration of the central part (composed of the stairwell and interior patios), (vi) the position and dimensions of the staircase, (vii) the presence and position (central or lateral) of ventilation patios or lighting shafts, (viii) and the number of façade openings as well as the number and distribution of flats per floor of each building. All of these parameters can greatly influence the structure's seismic performance and its seismic vulnerability and thus, they have been considered as part of the previously described building typology.

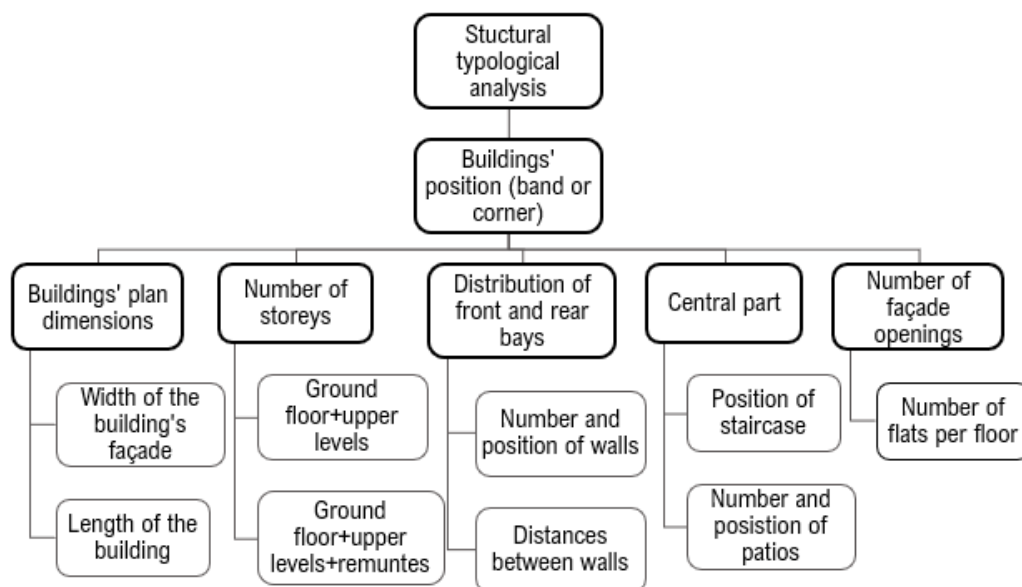


Figure 4.13 - Parameters considered for the structural typological analysis of the existing unreinforced masonry buildings in *Eixample* district.

The classification of the buildings established in the statistical analysis was done according to their geometrical and structural configuration's morphology, which is directly influenced the building's position in the typical block (Cornadó Bardón, 2015). Thus, two structural configurations can be distinguished: band (rectangular) and chamfered (pentagonal) buildings. The width and length of the building's plan were analysed, as principal characteristics for the geometrical configuration. The central part of structure consists of the stairwell and the interior and lateral patios (Figure 4.14). Their location can either be in the centre (type C) or linked to a lateral wall (type L). Moreover, the distribution of the other structural walls is influenced by the position of the staircase. The presence and position of patios is an important structural feature for the existing *Eixample* buildings, which is not typically present in previous building classifications. The patios improve the lighting and ventilation of the building's central part, and also play an important role for the stiffness of the structure.



Figure 4.14 - Examples of structural plan distributions of the typical band buildings of the Eixample district composed of central part with the staircase and the lighting and ventilation patios, the front and rear bays, and the galleries at the back façade: a) band building with central stairwell and light patio; b) band building with central stairwell and lateral semi-patios, and c) narrow band building with lateral stairwell and lateral lighting patio (adapted from Cornadó Bardón 2015).

Nowadays, two main types of building plans can be distinguished very clearly: the rectangular plan, which is placed on the side of the block and has a ratio of at least 1:2 between the width of the façade and the building's depth for so-called in row or band buildings, and the pentagonal or quasi-triangular building's plan shape, which fits the corners with chamfered edges, for corner buildings (see Figure 4.16). The rectangular buildings dominate at each of the block's four sides, with varying façade widths, while the pentagonal structures are typically located at each of the block's four corners.

The result of Cornadó's (2015) structural typological analysis was the generation of a standard floor plan of the most representative band building of the *Eixample* district. Figure 4.15 illustrates the layout of the typical floor plan of the typical *Eixample* band building, where the structure is

determined by the type of the central part to which the front and rear bays are added. There are seven types of different configurations for the central core element by differencing the number and position of the interior and lateral patios.

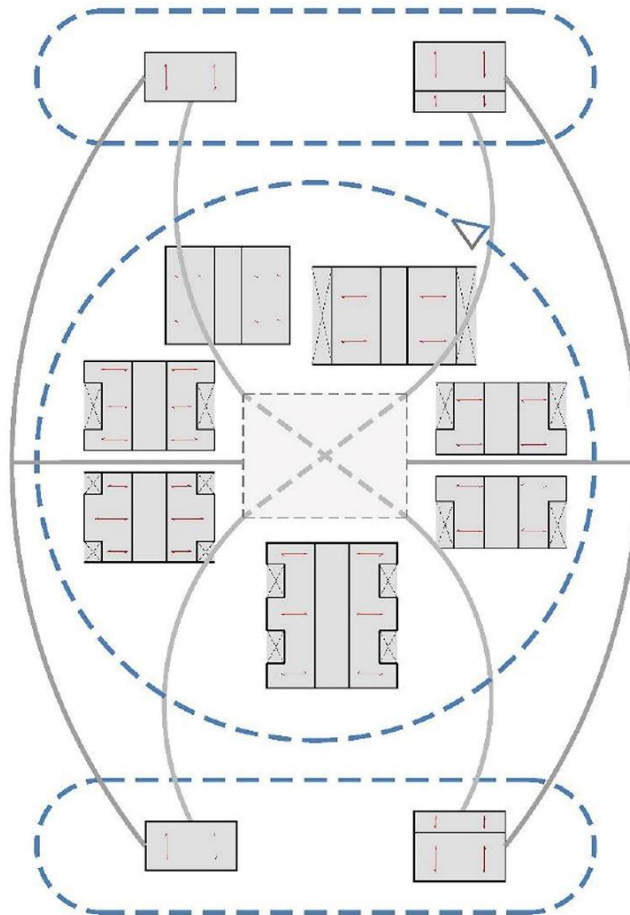


Figure 4.15 - Generator scheme of a typical floor plan of Eixample's band building. Seven types of core elements are identified based on the staircase position and the presence of lighting and ventilations patios. Each core element, in whichever direction, can be combined with a single or double front and rear bay (Cornadó Bardón, 2015).

The data collected from extensive field surveys has been used to determine the frequency of occurrence of the building types in the analysed sample. According to the geometrical configuration, the building typologies can be defined as wider band buildings with central staircase box and patios, narrow band building with lateral staircase box and patios and a chamfer (pentagonal) building located in the corner of the typical building block (see Figure 4.16). The total number of analysed buildings is 175, of which 112 are band wide buildings, 23 are narrow band buildings and 39 are corner buildings.

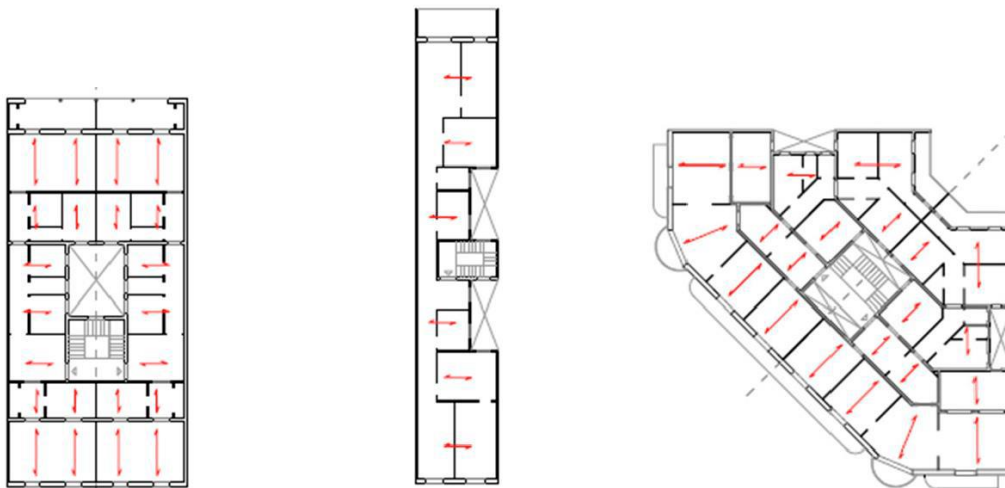


Figure 4.16 - Building typologies defined as in Cornadó's research (2015). "C" with Central stair (left), "L" with lateral stair, "V" corner building.

Figure 4.17 presents the frequency of the three building typologies from the total sample of studied buildings. The most frequent typology is the band building with central staircase and patios, by representing 64.4% from the total sample. The building typology with lateral staircase and patios (narrow building) represent around 13% and finally, the chamfered building typology shows a frequency of 22% of the total number of analysed buildings.

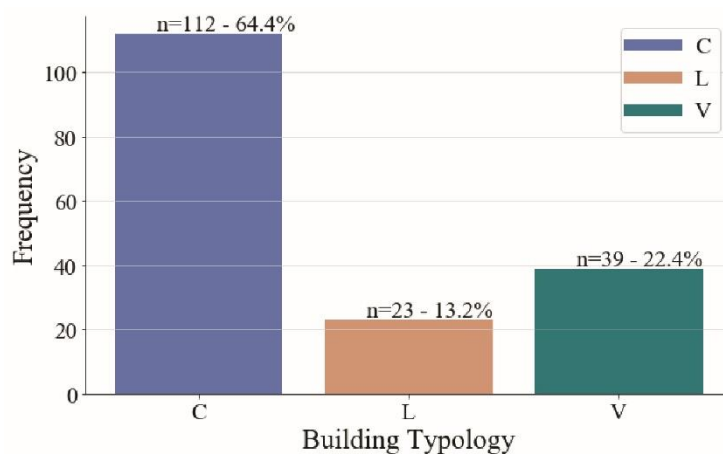


Figure 4.17 - Frequency of the three building typologies.

Each building typology has been analysed separately by considering several geometrical features such as the building's plot width and length, number of storeys (with and without *remuntes*), walls distribution and corresponding distances.

The first distinction between the band buildings was done regarding the position of the stairwell: buildings with a central staircase ('C' building typology) and buildings with a lateral staircase ('L' building typology). Cornadó's (2015) building data sample was primarily systematised by utilising the width and length of the building's plot. The subtypes were defined according to the number and location of patios, the number of bays, and the direction in which the load was transmitted from the floors to the walls.

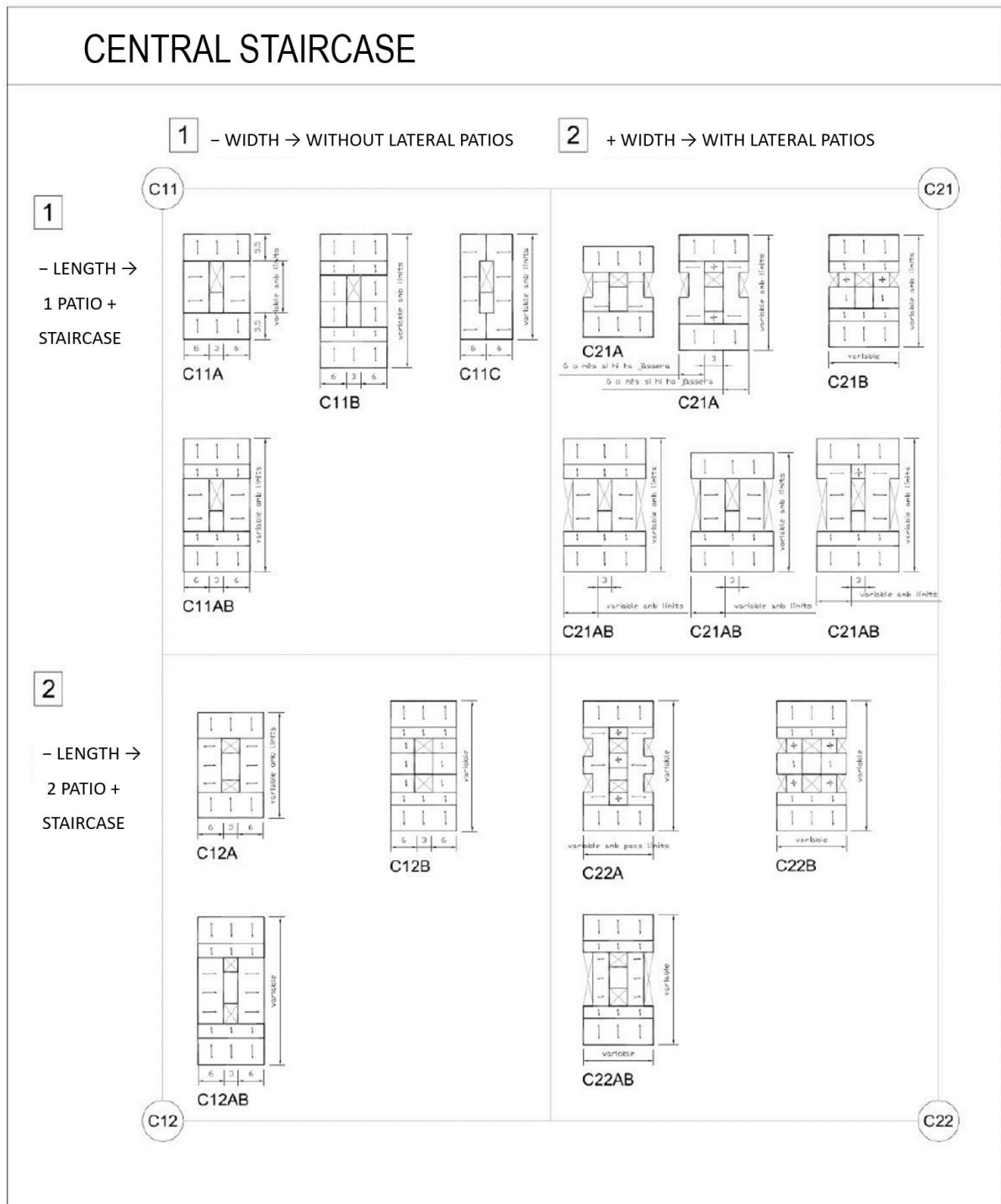


Figure 4.18 - Schematisation of subtypes for the building typology with central staircase 'C' (adapted from Cornadó Bardón 2015).

The main parameters for the characterisation of the subtypes of the most representative building typology with central part (formed of stairwell and patios) are the width and length of the building, which influence on the number of central and lateral patios. According to Cornadó (2015), the schematisation of the subtypes for the 'C' building typology is the following (see Figure 4.18): the subtype C11 considers narrower buildings without lateral patios and with a central staircase and one central patio; the subtype C12 includes more narrow buildings without lateral

patios and with two central patios in front and after the central staircase; the subtype C21 is characterised by a wider building plot with a central staircase and patio, as well as lateral patios on each side; and the subtype C22 comprises buildings constructed on a larger plot (in width and length), with a central part containing the stairwell and two central patios, as well as one or more patios on each lateral wall. The number of bays in front and behind the central part of the building can vary depending on the length of the building. There are existing buildings with one or two bays with one-way floor slabs, where the beams are perpendicular to the façade. Figure 4.19 shows an example of representative rectangular band buildings with a central staircase for each of the subtypes of the building typology 'C'.

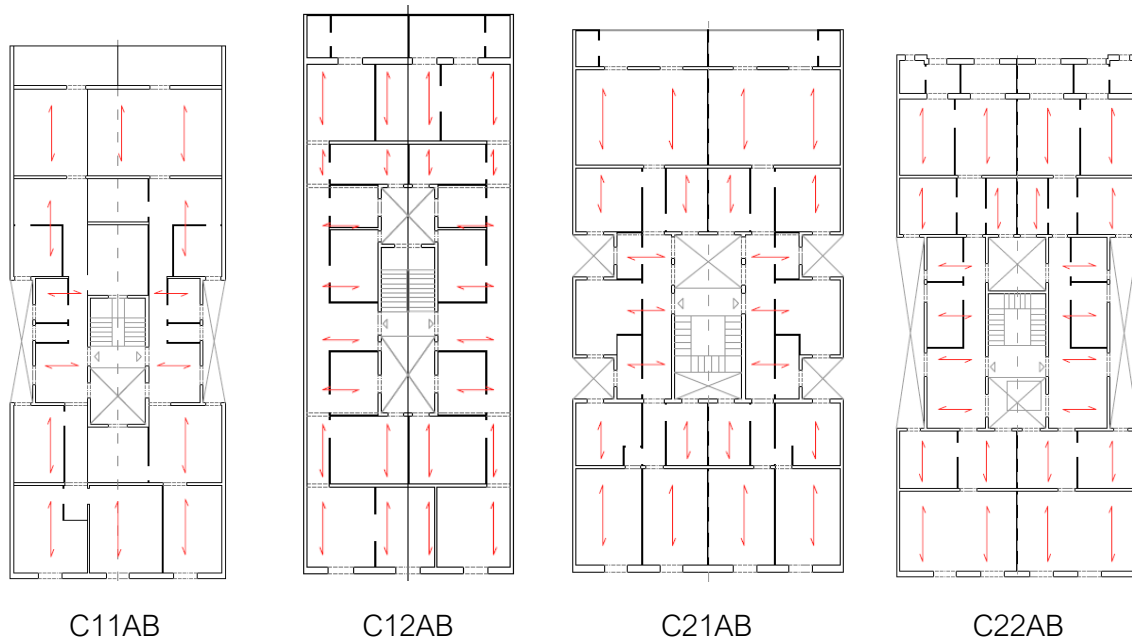


Figure 4.19 - Examples of floor section plans of existing Eixample buildings by representing the subtypes of the building typology 'C' (Cornadó Bardón, 2015).

Buildings constructed before 1890 have greater variation in their size and proportions than those constructed after that time. The first plot ordinances allowed for greater dispersion of building sizes and proportions, since a percentage of the plot was fixed. However, beginning in 1891, the architectural type of the buildings was defined and fixed progressively, by when establishing a maximum building's length with the subsequent ordinances. There is more variation in plot sizes for the buildings in the sample that are of type C. The most common dimensional range appears to be of building plot sizes between 8 and 18 metres wide and built-up lengths of between 21 and 28 metres (Cornadó Bardón, 2015).

According to Cornadó's research (2015), the most common plan configuration in the existing buildings of the Eixample district are those of type C22AB and C21AB, accounting for 39.6% of both subtypes (Figure 4.20). The structural configurations with two bays perpendicular to the main and rear facades (type AB) are more abundant, followed by those with a single bay span perpendicular to the facades (type A).

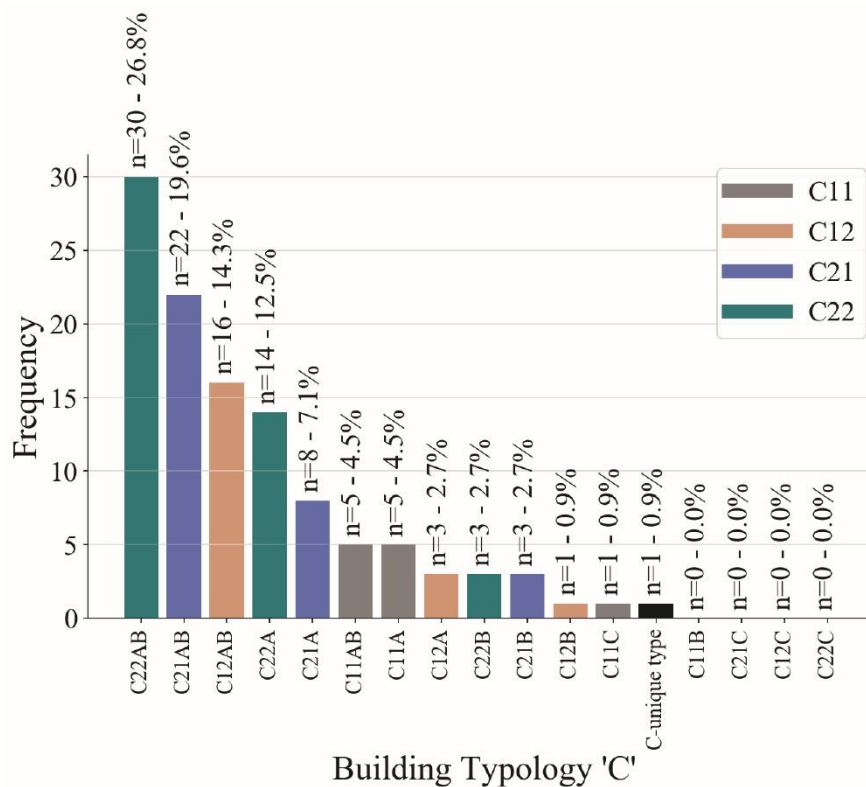


Figure 4.20 - Frequency distribution of the building typology 'C'.

The most recurrent building typology in the *Eixample* district is the band building composed of a central part containing a central stairwell with interior patios, and an addition of front and rear bays (see Figure 4.21) (Cornadó Bardón, 2015). These bays are formed by the front and back façade load bearing walls together with the parallel interior walls. The interior walls W5 and W6 exist, when the distance between the façade walls (main W1 or back W2) and the walls comprising the central part (W3 and W4) is superior than the recommended span of the bays. These interior walls parallel to the façades are load-bearing ones with a thickness of 0.15 m. Normally, the spans of the front and rear bays (Y1 and Y2 distances), formed by the façades are wider than the spans of the bays closer to the central part of the structure (Y3 and Y4 distances).

The central part of the structure is the area influenced by the presence of the staircase and patios. The central core element is generally composed by two bays on either side of the staircase, where the loading distribution of the one-way floor slabs is perpendicular to the lateral load bearing. Different geometrical configurations of the structure's central part can be found in existing *Eixample* buildings: central part - type 1 composed of continuous lateral walls (with or without lateral patios) and central part - type 2 with discontinuous lateral load-bearing walls, where there is a presence of lateral patios interrupting their continuity (see Figure 4.22). According to the statistical data of Cornadó's research (2015), more than half of the 128 buildings (54.7%) of building types 1 and 2 have interior walls (W3 and W4) parallel to the façades at the ends of the central body part.

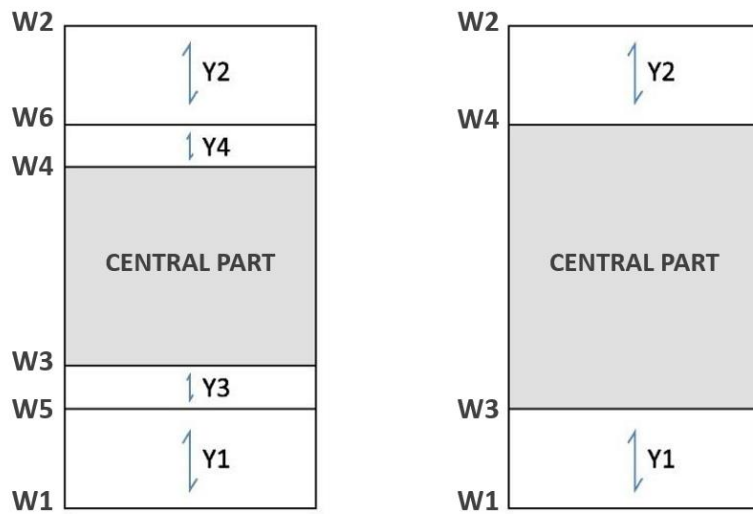


Figure 4.21 - Wall distribution and distances for a band building typology composed of a central part with addition of front and rear bays (adapted from Cornadó Bardón 2015).

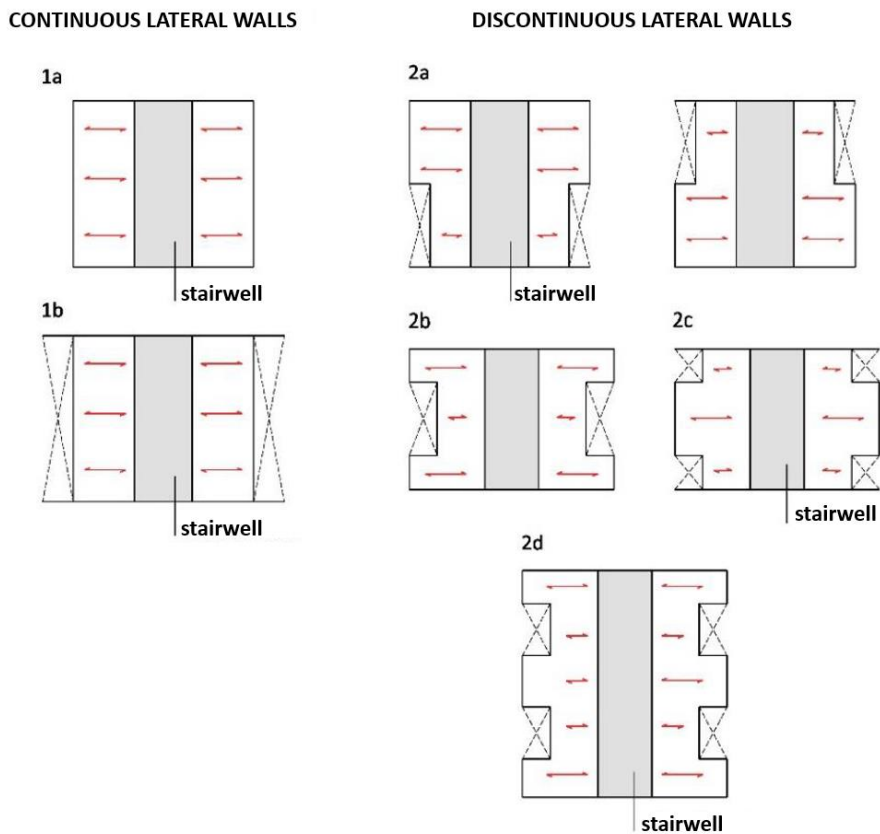


Figure 4.22 - Different geometrical configurations of the central part of the structure with a central stairwell and continuous lateral walls (with or without lateral patios) or discontinuous lateral walls (presence of lateral patios) (adapted from Cornadó Bardón 2015).

- Identification of most recurrent building typologies in the *Eixample* district

The data collected from field surveys is a crucial part of the proposed methodology for the selection of the most representative buildings, necessary for the seismic vulnerability assessment of existing buildings. In the following paragraphs, the frequency distributions for each of the previously mentioned geometrical features have been presented for the most common band building with a central part 'C'. The statistical data obtained for the other two building typologies ('L' - narrow buildings with lateral staircase and patios and 'V' - corner buildings), with the frequency distributions of the general geometrical characteristics, is presented in APPENDIX A

According to the presented statistical data (Figure 4.20), the most frequent building typology with a central staircase is the one with two interior and two lateral patios as part of the structure's central part (Type 1b), with an addition of two front and two rear bays – 'C22AB' (see Figure 4.23). This building typology represents around 27% of the wide rectangular band buildings and has been chosen as the most representative one.

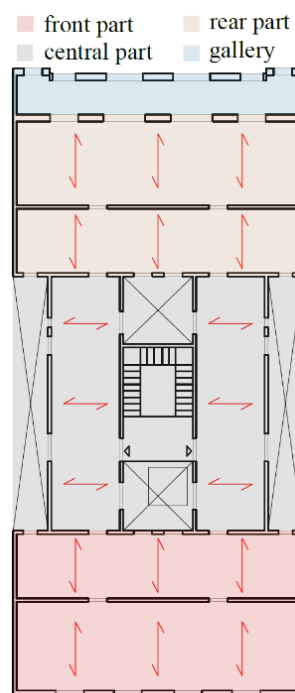


Figure 4.23 - Geometrical configuration of the most common band building typology 'C22AB' composed of a central part and front and rear bays.

The main geometrical characteristics are the width of the building's façade and the length/depth of the building. These dimensions have been assessed from the data set available for each building type, obtaining the mean, median and the most common value for each of the types. Figure 4.24 and Figure 4.25 illustrate the frequency distributions of the band buildings' width and length, respectively. There is a variability of different façade's width sizes between 8 and 19 m. The most common value for the façade's width is 11.7 m and the most frequent one is between 12 and 13 m.

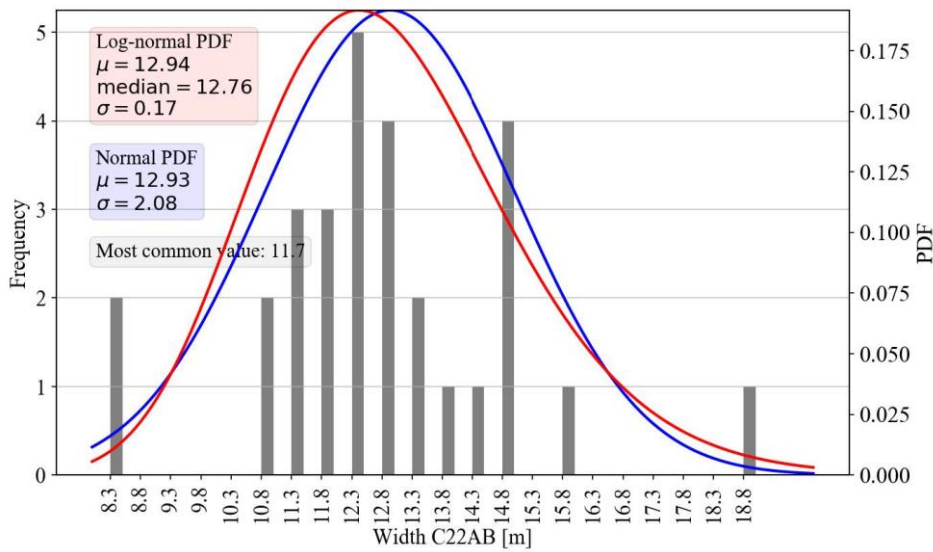


Figure 4.24 - Frequency of width of the most representative band building's façades.

The variation of building's length is between 19 and 35 m, much greater than the ones of the building's width. The mean value for the length of the longitudinal walls is around 27 m. The most common value for the building's length is 28 m.

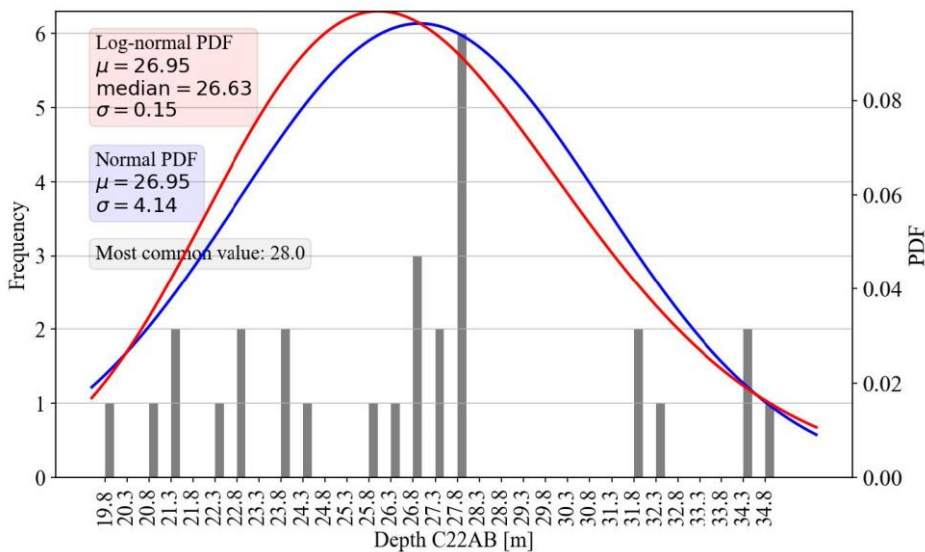


Figure 4.25 - Frequency distribution of building's plot depth (type C22AB).

The frequency distribution of the total number of floors is presented without or with vertical additions (*remuntes*). Therefore, the total number of storeys without vertical extensions can vary between 4 and 6 storeys above the ground floor (Figure 4.26a). The statistical data shows that a building with a total of five storeys (GF+5) is the most common one. In the case of presence of vertical extensions, existing buildings with one, two or even three vertical additions can be found from the analysed sample. The total number of floors with vertical extensions can vary from 4 to 8 storeys, and 6 storeys is the most common value (GF+5+R) (Figure 4.26b).

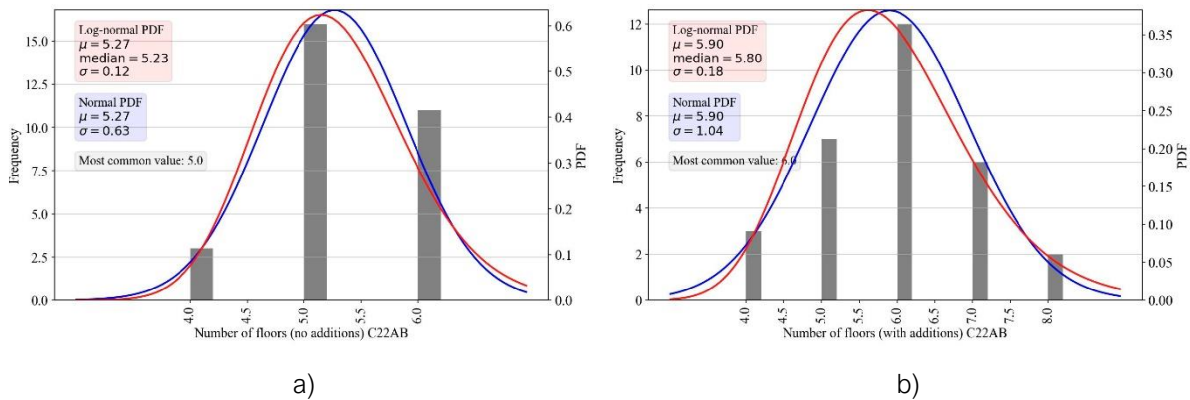


Figure 4.26 - Frequency distribution of the total number of floors for the band building typology 'C': a) without vertical additions (remuntes) and b) with vertical additions (remuntes).

Another geometrical parameter that has been evaluated from Cornadó's typological analysis is the distances between the load bearing walls parallel to the façades (see Figure 4.21). As it was previously discussed, the distance Y1 and Y2 are greater and can vary between 3 and 5.50 m, with a median value of 4.2 m. Moreover, the most common Y1 and Y2 values are 4.4 and 4.6 m, respectively (see Figure 4.27a and b).

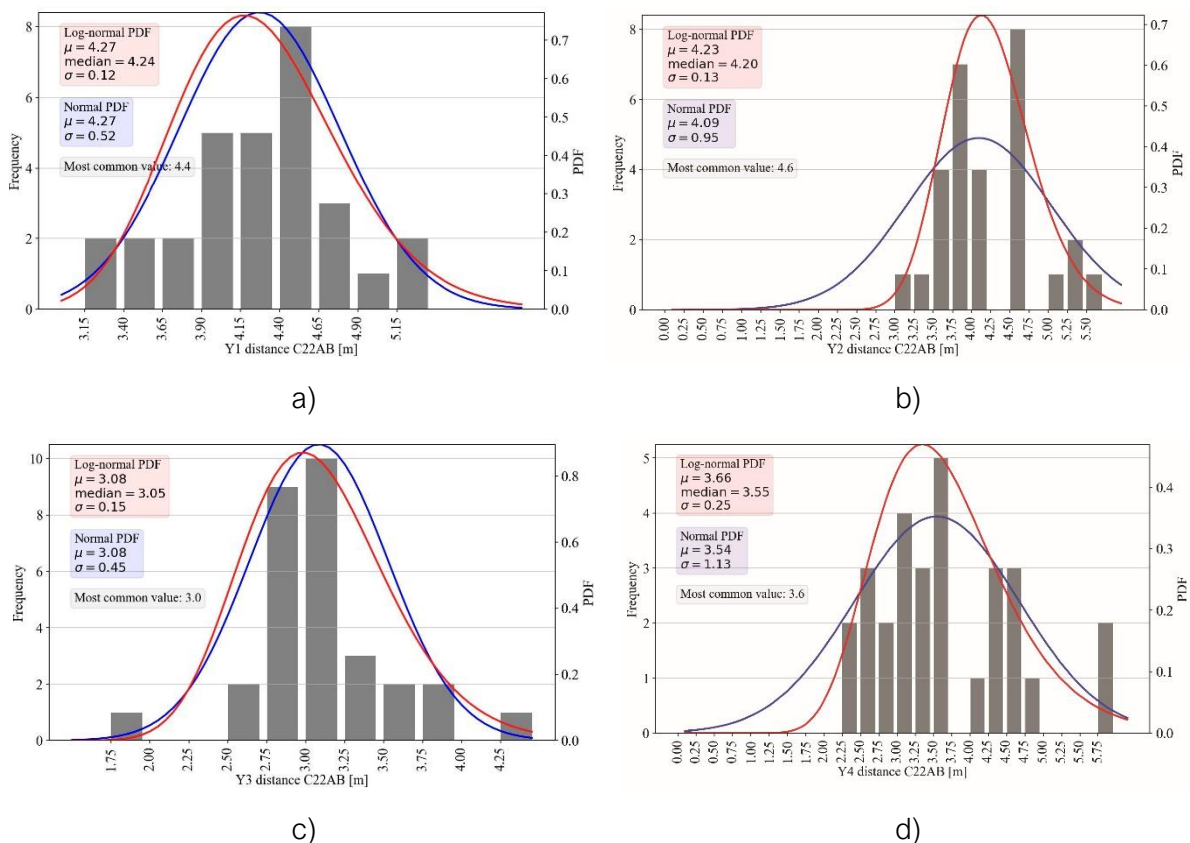


Figure 4.27 - Frequency distribution of the following wall distances: a) Y1 distance between the front façade wall (W1) and the parallel interior wall (W5); b) Y2 distance between the back façade wall (W2) and the parallel interior wall (W6); c) Y3 distance between the interior walls W3 and W5 of the bay situated in front of the central part; d) Y4 distance between the interior walls W4 and W6 of the bay situated after the central part (see Figure 4.21 for the proper nomenclature of the walls and distances).

The smaller distances (Y3 and Y4), in front and behind the structure's central part, can have a greater variation of different values between 1.75 and 5.75 m (see Figure 4.27c and d). Normally, the distance Y3, which represents the span of the bay in front of the central part, is around 3 m as the most common value. The distance Y4 is slightly greater, with a most common value of 3.6 m. The statistical data has showed that the distances of the walls composing the rear bays close to the back façade are greater than the ones close to the front façade. In some cases, the buildings are symmetrical and the distances Y1 and Y2, as well as Y3 and Y4 have the same values.

The number of façade openings is another attribute considered for the statistical analysis of the existing *Eixample* buildings (Figure 4.28a). This representative building typology has typically four façade openings on each floor level and three openings on the ground floor. Additionally, the number of flats per floor level has been included as it depends on the division of the building's floor plan. There can be two or four apartments on each floor level (Figure 4.28b).

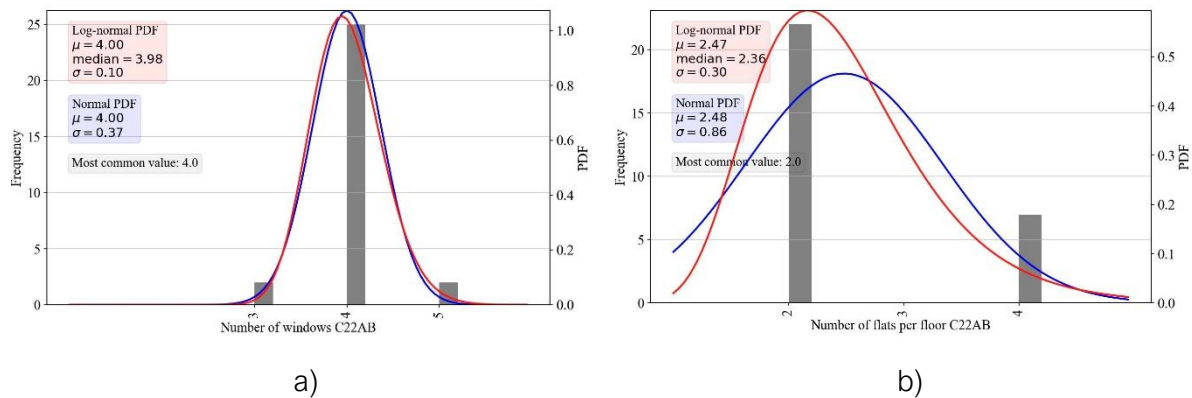


Figure 4.28 - Frequency distribution of the number of façade openings (a) and number of flats per floor (b).

The statistical data of these geometrical features has been used as part of the proposed methodology for the definition and selection of the most representative buildings in the *Eixample* district. Moreover, some of these attributes have been selected for the empirical method of the seismic vulnerability assessment of masonry buildings.

4.4. METHODOLOGY ADOPTED FOR SELECTION OF REPRESENTATIVE BUILDINGS

The methodology adopted for the selection of representative buildings from a specific urban centre (*Eixample* district) is divided into the following primary work tasks: i) definition of a detailed building taxonomy; ii) statistical distribution analysis regarding the geometrical and structural morphology of the buildings; iii) selection and assignment of the most representative building typologies, which are used for the numerical modelling. This methodology has been established in a way that a reasonable number of detailed FE models (in the order of 20 models) of the representative buildings with a variation of different structural parameters have to be analysed. Moreover, the representative buildings that have been analysed, which are based on the

taxonomy and the previous statistical extrapolation study carried out, correspond to real existing buildings.

Figure 4.29 illustrates a flowchart of the proposed methodology starting from the generation of the detailed building taxonomy until the selection and definition of representative existing buildings, necessary for the seismic vulnerability assessment by implementing numerical modelling.

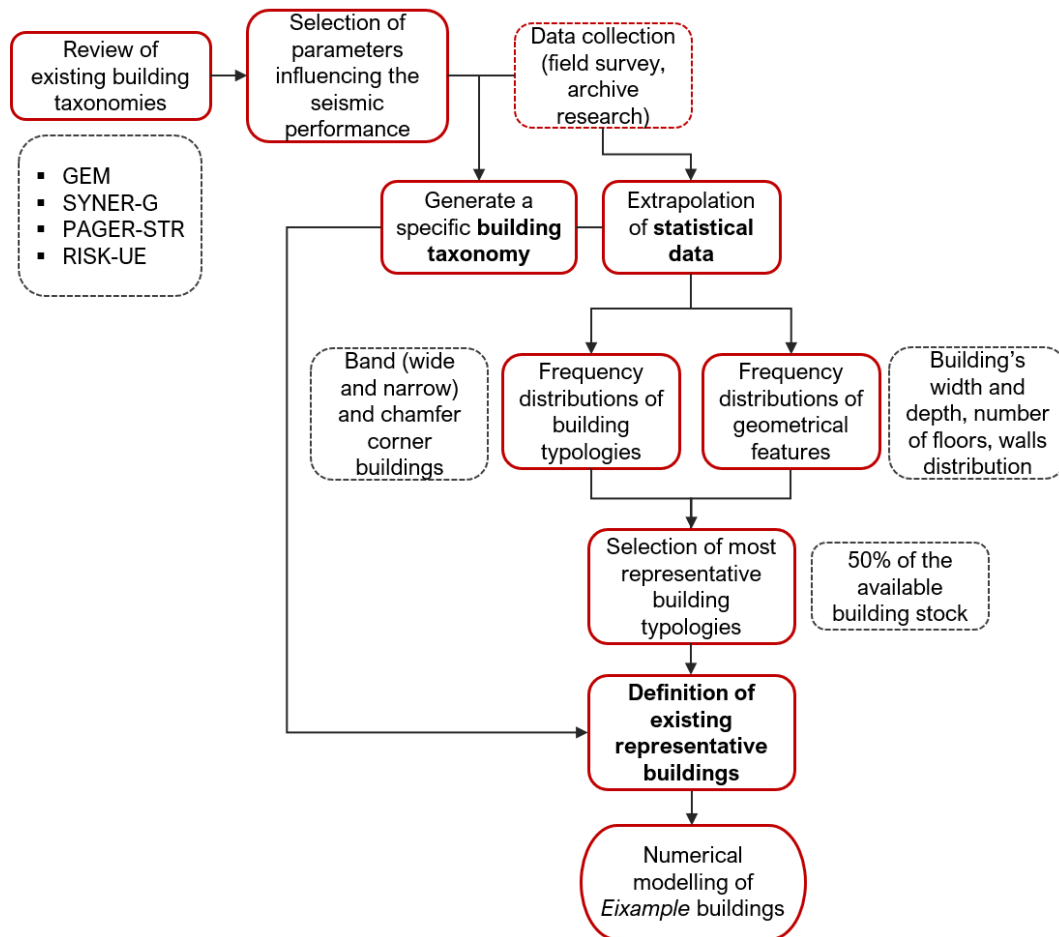


Figure 4.29 - Flowchart of the methodology adopted for the definition of the most representative buildings.

The first step of the proposed methodology for structural classification of existing masonry buildings is to establish a consistent and detailed taxonomy that will allow suitable representative buildings to be identified in the building stock from the urban centre studied. As a result, a review of critical parameters from existing global taxonomies (GEM taxonomy, SYNER-G, PAGER-STR, RISK-UE), combined with a detailed survey of a sample of buildings from previous research studies, has been used to identify the parameters and their attributes, which will be essential for the grouping of the buildings with similar characteristics in order to identify the most representative *Example* buildings. The process for the creation of the building taxonomy is previously explained, by identifying and describing each of the structural parameters relevant for the seismic performance of the existing *Example* buildings.

Secondly, a comprehensive database containing construction and vulnerability information on the most common structural typologies can help for the development of the classification system.

The creation of such a database allows for the identification of similarities and differences in geometry, resisting systems, materials, structural elements and other attributes that influence the vulnerability of existing masonry buildings. Furthermore, the study of such parameters can assist in the development of vulnerability functions for each structural typology, by implementing hybrid methods for the seismic vulnerability assessment.

Additionally, the extrapolation of the statistical data has been used for the definition of the frequency distribution of each building typology regarding their position in the typical urban block and the frequency distribution of the most recurrent geometrical characteristics. Finally, the selection of the most representative building typology has been done by an application of a 50% criterion of the analysed buildings stock, by always considering the most crucial parameters from the building taxonomy that mostly could affect the structure’s seismic performance and vulnerability.

It is crucial to define representative buildings for each typology of the building stock, when assessing the seismic vulnerability of buildings in urban centres. The selected representative buildings have specific attributes that influence their global seismic behaviour, which have been previously defined. This assumption allows detailed numerical modelling and analysis of only the selected representative buildings to represent the seismic performance of most of the building stock. This procedure can save a lot of the computational time and resources.

According to the previously described methodology, a criterion of 50% from all the building typologies available in the data sample has been considered for the pre-selection of the representative buildings (Figure 4.30). Following this criterion, a total of six building typologies had to be chosen as the most representative ones of the 175 analysed buildings. However, it has been decided to evaluate each of the most common building typologies separately as described in Cornadó’s research (2015), according to their frequency distribution in the entire building stock of *Eixample* district. The selection of buildings has to be done by considering the variation of the parameters, which influence the building’s vulnerability, according to the available statistical data and detailed building taxonomy.

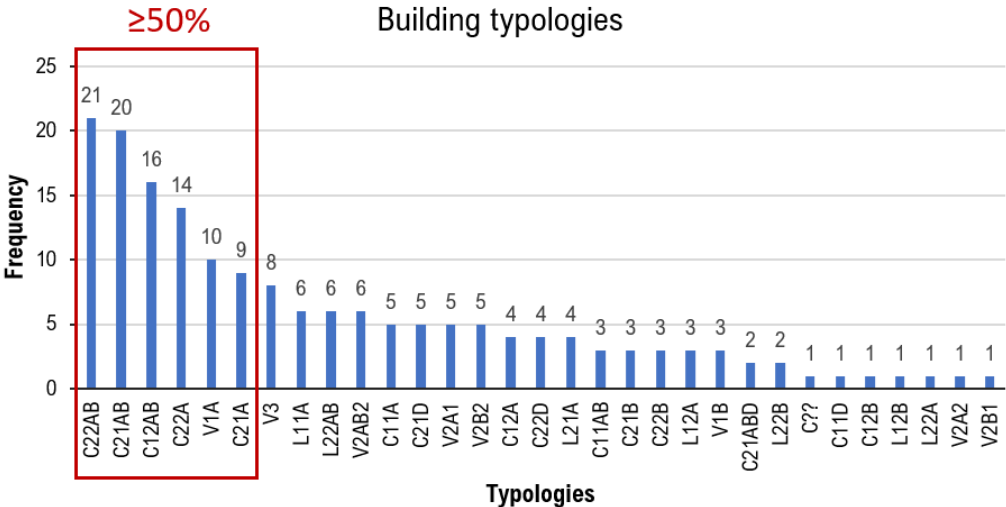


Figure 4.30 - Frequency of all building typologies from the analysed sample of Eixample district.

As it was mentioned previously, the building typology 'C', also referenced as the building typology with a central part of type 1b, is the most frequent typology within the three different building typologies regarding their geometrical characteristics and position in the urban block. Figure 4.31 shows the frequency distribution of the most common building typologies with a different geometrical configurations of the structure's central part. The most frequent typology is the one with continuous lateral patios in the central part of the structure, by representing around 48% of the total sample of analysed buildings with a central staircase. The second most recurrent typology according to the geometrical configuration is the narrow band building with a central part type 1a - composed of a central staircase and interior patios around it, but without any lateral patios at the longitudinal walls. These two building typologies have been chosen as the basis for the selection of the representative buildings, as they represent 66.1% of the analysed building stock.

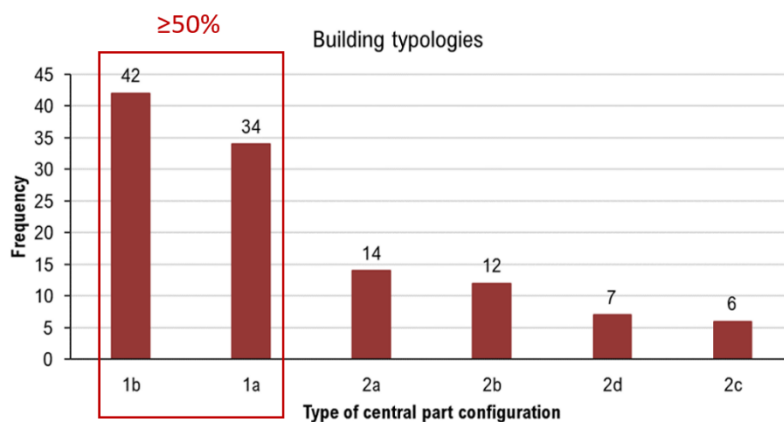


Figure 4.31 - Frequency of building band typologies according to the geometrical configuration of the structure's central part with central staircase (50% criterion for selection of representative buildings).

Additionally, the same criterion of 50% has been adopted for the other two building typologies: 'L' narrow buildings with lateral staircase and 'V' shaped corner buildings (Figure 4.32 and Figure 4.33). According to the applied criterion, two typologies can be considered as the most representative ones of each building typology.

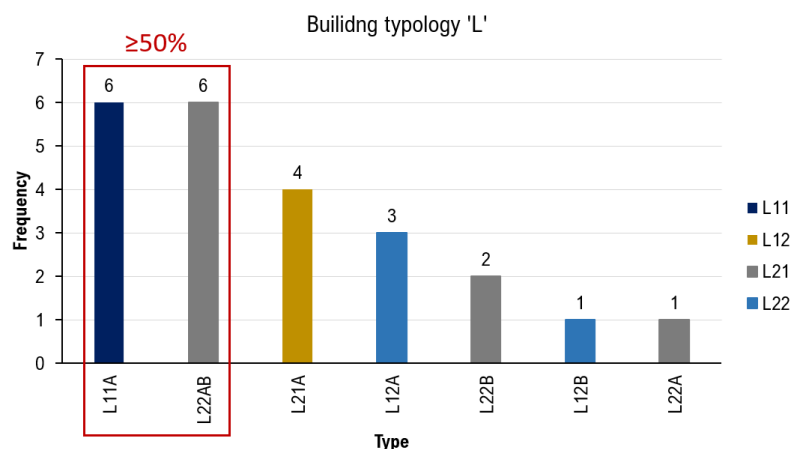


Figure 4.32 - Frequency of building typology 'L' - narrow building with lateral staircase (50% criterion for selection of representative buildings).

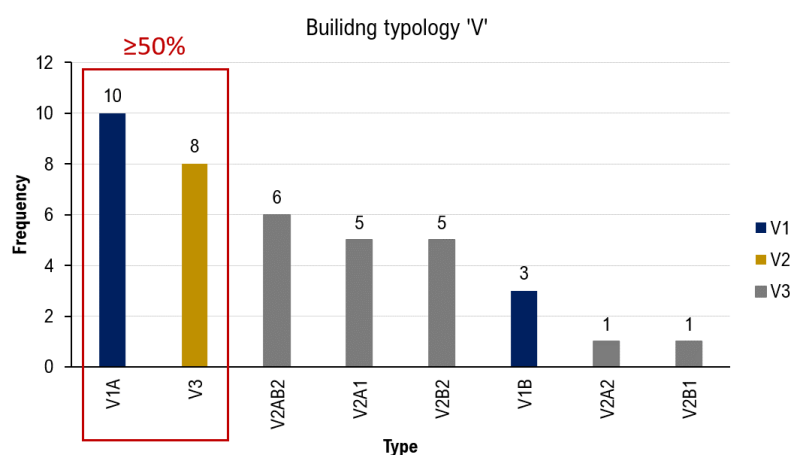


Figure 4.33 - Frequency of building typology 'V' - corner buildings (50% criterion for selection of representative buildings).

The main parameters considered for selection are the width of the building's façade, the total length of the building, as well as the distances between the load bearing walls parallel to the façades. Normally, a reference idealised model is defined as a benchmark, where the chosen dimensions for the geometrical configuration are some average values of the available data. In this study, the representative building typologies correspond very well with real case studies. Hence, existing real buildings with its exact dimensions obtained from a previous in situ survey (Cornadó Bardón, 2015) have been selected from the most recurrent subtypes. This decision was taken in due to the fact that many of the existing buildings in the *Eixample* district have a repeated geometric configuration, and there is a great knowledge of the buildings' structural characteristics and their materials.

Finally, the representative buildings have been chosen after detailed analysis of the statistical data available of each subtype that defines the selection of more than 50% of the proper building typology. After evaluating the frequency distribution of each of the previously mentioned parameters, a specific existing building has been selected, which includes the most common values of the studied parameters.

The chosen existing masonry building with a central part of type 1b (Figure 4.23) is the most representative one of that specific building typology and represents more than 36% of the analysed band buildings. The selection of the proper existing *Eixample* building from this specific typology has been done by following the frequency distribution for the buildings' width and length and number of storeys. Therefore, the geometrical dimensions of the selected building fit within the range of the most recurrent once of the analysed sample of this building typology. Moreover, different parameters from the detailed building taxonomy have been attributed to the most representative existing building, which has been considered as a base model. The variation of the parameters, such as the number of storeys, the existence of vertical extensions, the different thickness of the load-bearing walls, horizontal diaphragms, the different percentage of façade openings, has been implemented into the numerical modelling of the representative building, as part of the seismic vulnerability assessment.

The second most representative existing building is the one with a central part type 1a, composed of a central core (staircase + patios) and without any lateral patios, having continuity in the lateral load-bearing walls. This building typology represents around 30% of the studied wide rectangular buildings with different structural configurations of the structure's central part. These existing buildings have a frequent range of the façade's width between 9 and 11 m and the most recurrent building's depth is between 24 and 26 m. The selected existing masonry building presents geometrical characteristics within the most frequent range of values.

The presence of patios is considered to be an important geometrical characteristic for the *Eixample* buildings. Thus, for the accurate representation of this parameter, a specific building typology apart of the most representative ones has been chosen by having more than one lateral patios on each side of the structure's central part - type 2d (Figure 4.22).

Each *Eixample* block is composed of around 20 - 22 buildings, from which only four of them are chamfer ones (18%) and usually, around two to four band buildings (9-18%) of the typical block are narrow with two façade openings on each floor level. The rest of the buildings are wide band buildings with a central staircase and patios, representing more than 60% of the one urban block. The building typology 'L' - narrow buildings with lateral staircase and patios and the building typology 'V' - chamfer buildings represent only a small amount of the total studied building stock of the *Eixample* district, with 13.2% and 22.4% respectively. Hence, only the most recurrent building typology of the narrow and chamfer buildings has been chosen as part of the representative buildings for the further detailed numerical modelling due to time limit and computational cost.

A much reasonable number of detailed FE models (in the order of 20 models) of the representative buildings with a variation of different structural parameters has been chosen for the seismic analysis due to the computational time and cost. The chosen representative buildings have been used for developing numerical models used for evaluating their global seismic behaviour and understanding the possible failure mechanisms that could exist under horizontal loading. The geometrical configuration of each of the chosen building typologies and the variation of the parameters considered for the seismic vulnerability assessment are described in the next Chapter 5.

This methodology could be maintained in the future, expanding the number of models. These are some variables of the proposed methodology that can be modified in order to obtain a larger number of models, such as: - expanding the percentage of the sample selection (50%) as a criterion for the identification of the most representative buildings to a larger one (for example 70%); - including more parameters for the identification of the representative buildings; - including more statistical data for each evaluated parameter; or considering a wider range of the frequency distribution of the structural characteristics previously studied. Therefore, the modified methodology will increase the total number of numerical models, if at some point in the future computers will allow the analysis of a greater number of buildings with a lower computational cost.

4.5. SUMMARY

The building taxonomy is a crucial step in the seismic vulnerability assessment for the accurate identification all of the parameters that may influence the seismic performance and vulnerability of the exposed building stock. For the seismic evaluation of a residential building stock in an urban region or a city, it is generally required to have a more general typological classes that are representative of the seismic behaviour of other buildings with similar characteristics. The seismic resistance characteristics of an overall structural system should be reflected in the classification systems used to construct the building taxonomy. This can be accomplished by identifying the potentially vulnerable elements according to pre-established taxonomies for which specific characteristics, such as load-bearing resisting system, materials used, height, geometrical configuration, different structural and non-structural elements, are taken into consideration. Therefore, buildings are classified into categories based on their expected performance and similar vulnerability when subjected to earthquakes.

An exhaustive knowledge of the existing buildings and its structural features is necessary for the preparation of the building taxonomy and definition of representative buildings as part of the methodology for seismic vulnerability assessment of an urban centre. The classification scheme employs specific criteria based on data collected from field surveys and archives, which are related to the geometric characteristics of the building, the structural system of the building, the materials and construction techniques used, the different structural, and etc. Several existing taxonomic systems have been reviewed, and this information has been used for the determination of all the crucial parameters necessary for a detailed building taxonomy, which affect the buildings' seismic performance and vulnerability.

The new proposed methodology described in this chapter is oriented for the case study in which there is lack or no evidence of previous seismic damage and thus, it is necessary to work with complex numerical FE models. It focuses on two crucial components in the analysis of the seismic behaviour of an existing building stock: the development of an appropriate taxonomy system and the definition of representative buildings, which are used as the base numerical models for the vulnerability assessment. The first step in developing the taxonomy is to identify and describe all the attributes required to represent the selected building stock from the Barcelona's urban centre. Secondly, the building typologies have been classified based on the previously chosen structural attributes. Additionally, statistical analysis has been used to select representative typologies of the studied building stock by considering the frequency distribution of specific geometrical characteristics. The selected existing building are the basis for the numerical models used to better understand the global seismic behaviour of these structures. The methodology allows the number of models to be reduced to a reasonable amount.

This building taxonomy enabled us to define the most common building typologies in order to assess their expected vulnerability during an earthquake. Additionally, the identification of the most common building typologies and representative buildings that share common characteristics can help reduce the amount of modelling and computational time, when performing seismic risk analysis at urban scale. Subsequently, the previously described methodology is used for a detailed FE numerical modelling and seismic analysis of only the chosen existing representative buildings, which can represent the seismic response of more than half of the studied building stock. The total

number of numerical models for the existing buildings can be easily modified, if the computational calculation allows it to be increases.

In conclusion, the detailed building taxonomy has been designed as a significant precondition for the seismic vulnerability assessment of the existing unreinforced masonry buildings in the *Eixample* district. Moreover, this taxonomy can be extrapolated to existing buildings in other cities in Spain or in other countries, following the same methodology for the construction of a specific taxonomy by defining all the parameters that can influence the buildings' seismic behaviour. The final goal is to evaluate the vulnerability of existing buildings from a certain urban region and to generate fragility curves for each building typology in order to assess the likelihood of damage occurring as a result of a specific seismic action.

CHAPTER 5. NUMERICAL MODELLING OF REPRESENTATIVE BUILDING TYPOLOGIES IN THE *EIXAMPLE* DISTRICT

5.1. INTRODUCTION

Numerical modelling is a specifically prevalent procedure for determining the seismic vulnerability of existing masonry buildings since it enables it to predict the structural capacity of the building as well as both its global and local failures due to seismic action. The numerical simulation of existing masonry building is not always a straightforward procedure and can represent some important challenges. It can be addressed using different modelling strategies depending on the complexity of the structural typologies and the scope and aim of the study.

Analytical and hybrid methods for seismic vulnerability assessment usually employ numerical models by performing structural analysis in order to generate damage data and to assess and estimate the seismic capacity of the structures, as explained in Chapter 2. There are various approaches with different levels of complexity depending on the type of model used for the numerical simulation of the structure and the adopted analytical procedure for seismic analysis.

Many previous studies use the equivalent frame model (Lagomarsino et al., 2013) as a simplified approach to simulated the behaviour of masonry walls, combined with nonlinear static or dynamic analyses for the seismic assessment of existing masonry buildings. Another more complex approach is the finite element (FE) macro-modelling, where masonry is considered as a homogeneous material by using the appropriate constitutive laws to represent the nonlinear response under compression and tension.

The lack of post-earthquake damage observations can be solved using analytical methods, by numerically simulating the seismic performance of existing buildings. These approaches should be used for a specified number of numerical models with different geometrical configurations and construction features, since they can be extremely time consuming and require a high computational cost for large scale assessments. Additionally, using advanced numerical modelling also makes it possible to account for the impact of structural and material properties that are often not considered by empirical approaches, making it a suitable tool for parametric studies (Ortega, 2018).

The objective of the present thesis is the use of a hybrid method such as the Vulnerability Index method for the seismic vulnerability assessment at large urban scale, where both analytical and empirical methods are combined together. Subsequently, the numerical FE models are used for

the calibration of the different parameters proposed in the empirical forms. Typically, these methods have been supported by statistical studies of post-earthquake damage information and they solely rely on the engineering expert opinion. In this case, the detailed numerical models, which have been developed using the macro-modelling strategy, are the basis for the representation of the expected damage and collapse mechanisms in existing structures even for a low to moderate seismic hazard.

This chapter presents the description and characterisation of the geometrical and structural characteristics of the developed numerical models of the representative buildings of the *Eixample* district. The Finite Element Method (FEM) has been used for the numerical simulation of the most recurrent structural systems and geometrical configurations. Moreover, the proper material properties used for the numerical models are described in detail for each structural element. A numerical procedure for the modelling of the in-plane seismic behaviour of the one-way floor slabs, as the most common horizontal diaphragm in these buildings, is presented, since it can greatly influence the structure's seismic capacity. Finally, the variations of different parameters on the reference building model, such as the number of storeys, presence of vertical extensions, material properties, change of walls' thickness, horizontal diaphragms, different plan configurations, and façade openings, are described and explained. These parameters have a large influence on the seismic performance and vulnerability assessment of existing unreinforced masonry buildings.

5.2. NUMERICAL MODELS OF REPRESENTATIVE BUILDINGS OF THE *EIXAMPLE* DISTRICT

As aforementioned, the representative buildings have been chosen from the specific building taxonomy of *Eixample* district (presented in Chapter 4), which are the basis for the numerical models used to better understand the global seismic behaviour of these structures. Moreover, different parameters have been selected as influential on the seismic performance of the existing buildings and they have been used for the definition of the reference building model's variations. The numerical analysis has been based on a detailed FE modelling, followed with non-linear static (pushover) analysis. The developed numerical models help for evaluating the seismic performance and recognising the different failure mechanisms in the structures with different geometry configurations. Additionally, these FE models have been used for studying the impact of the most significant parameters of the building taxonomy for the seismic vulnerability assessment.

Figure 2.1 illustrates the different numerical models of the most representative *Eixample* buildings together with the variation of parameters, which are significant for the seismic vulnerability assessment. As established in Chapter 4, the most recurrent building typology is a rectangular band building with a central part composed of interior patio and central staircase, and lateral patios, which are interrupting the continuity of the lateral load-bearing masonry walls. The variations of the selected parameters have been implemented to this building typology considered as the reference one. Additionally, four building typologies with different geometrical configurations have been modelled, which were selected according to the presented statistical data in Chapter 4. In the following sections, a detail description of the geometry, the FE modelling, material properties and load conditions has been explained for the developed numerical models.

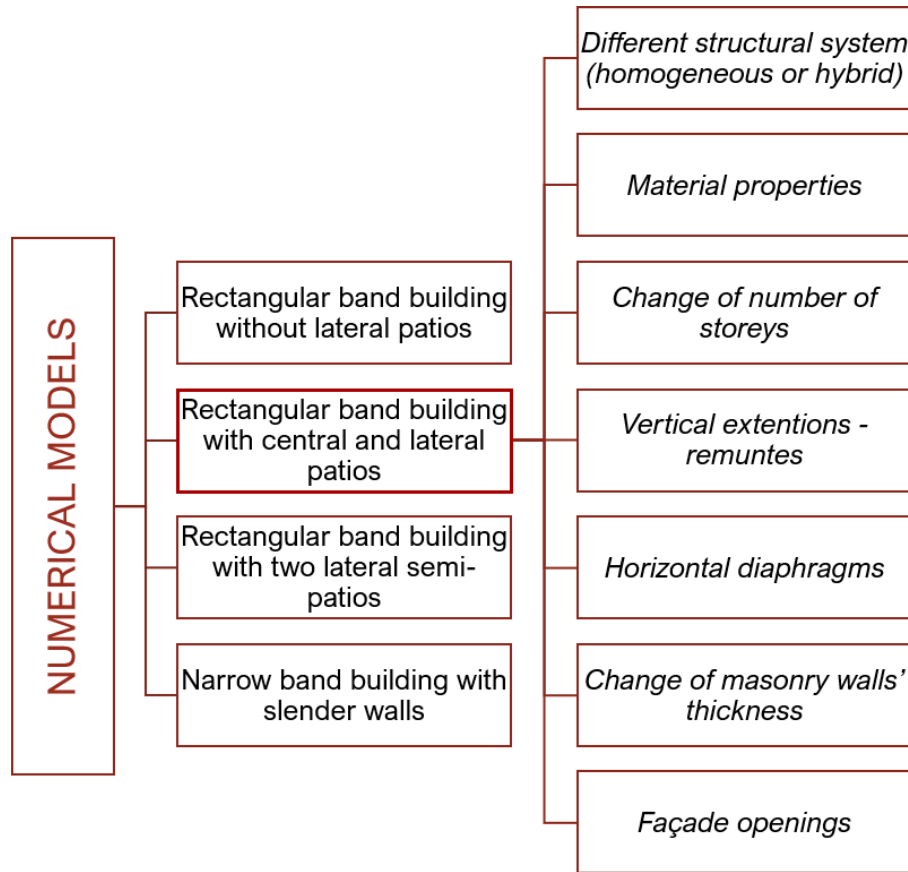


Figure 5.1 - Numerical models of representative buildings and variation of different parameters.

5.2.1. Geometrical modelling

The numerical modelling of the representative building typologies has been presented as the basis for the seismic vulnerability assessment at urban scale. These typologies have been chosen by considering the specific information provided in Chapter 4 regarding the building taxonomy and the statistical data analysis of the studied building stock in the *Eixample* district. The detailed geometrical modelling is presented for the two following structural typologies regarding the resisting load-bearing system (as described in Chapter 3): 1) Homogeneous structural system with continuous load-bearing masonry walls throughout the full height of the building; and 2) Hybrid structural system with steel frames at the ground floor and unreinforced masonry walls on the upper floor levels.

5.2.1.1. Homogeneous system with slender masonry walls

Based on the previous information, the most recurrent URM building typology is a rectangular band building composed of a central part containing a central stairwell with interior patios, and an addition of front and rear bays (Figure 5.2b). Existing real buildings with exact dimensions obtained from a previous in situ survey (Cornadó Bardón 2015) have been selected from the most common subtypes of the representative typologies, as explained in the new proposed methodology in

Chapter 4. The chosen existing URM building was built in 1891 and is located on *Entença Street* in the neighbourhood of *La Nova Esquerra de l'Eixample* of Barcelona. Figure 5.2 presents a view of the façade and floor plans of the selected existing building, chosen as reference one. All the information related with the geometry and the structural characteristics is based on the detailed inspection carried out by Cornadó (Cornadó Bardón, 2015).

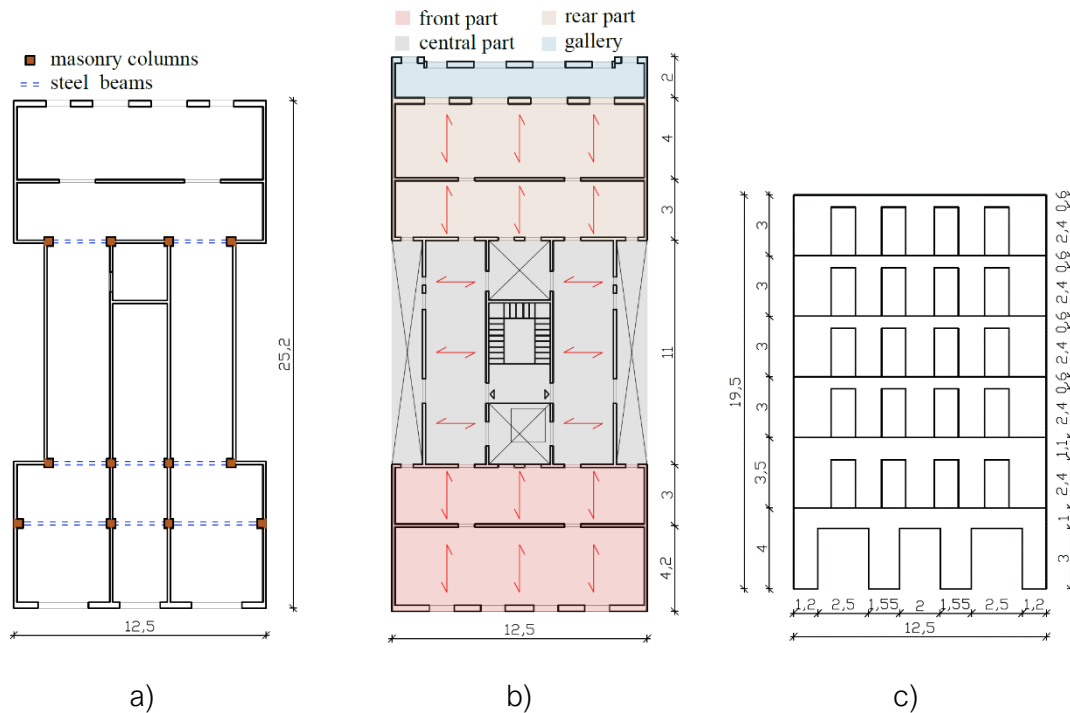


Figure 5.2 - Selected reference building of the Eixample district: a) ground floor configuration; b) floor plan section (adapted from Cornadó Bardón 2015); c) front façade geometry (dimensions in metres).

The architectural plan of the building has a rectangular shape of $12.50 \times 27.15 \text{ m}^2$. The geometrical configuration consists of a central core connecting two symmetrically shaped bays. The central part of the structure consists of an interior patio, a staircase box and two exterior semi-patios (Figure 5.2b). The building has six storeys (GF+5), with the first two floor levels having different height comparing to the rest of them. The ground floor is 4 m high, the mezzanine floor 3.50 m high and the top four storeys are 3.00 m high. The overall height of the building is 19.50 m.

The façade walls have a thickness of 300 mm, while the lateral and interior structural walls have a thickness of 150 mm. Masonry square pilasters of $450 \times 450 \text{ mm}^2$ are constructed as part of the lateral walls in order to support the steel truss beams on the ground floor, used to create a large open space for commercial activities (Figure 5.2a). These steel truss beams are commonly composed of several steel profiles (box beams), as explained in Chapter 3 (section 3.5.1).

The main façade has a well-defined arrangement of four $1.20 \times 2.40 \text{ m}^2$ door openings at each level, with the exception of the front façade of the ground floor, which has three larger size openings since this level was intended for commercial activities (Figure 5.2c). The percentage of openings on the façades is notable, with 32.3% at the front façade and 36.2% at the back façade. Steel beams have been used as lintels for all of the openings in the model.

The building's structural and seismic behaviour has been numerically investigated using continuum Finite Element models. Figure 5.3 illustrates a frontal view of the front façade, as well as a generic view of the 3D FE reference model, which includes all the structural elements, namely load bearing walls and pillars, steel beams and trusses and floors. The galleries located at the exterior of the rear façade (see Figure 5.2b) have not been considered as part of the numerical model, as due to their large openings, they are not expected to contribute to the structural performance. Nonetheless, their mass has been applied to the back-façade wall.

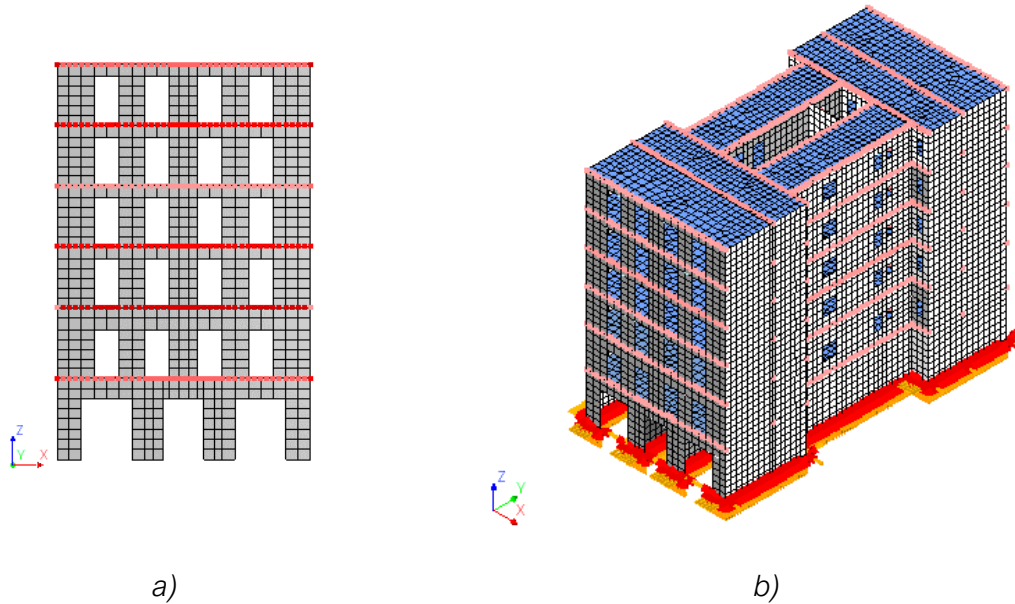


Figure 5.3 - Finite numerical reference model of an existing building of the Eixample district: a) geometry of the front façade; b) 3D FE model of the building.

The FEM model has been prepared using the software DIANA-FEA (DIANA FEA BV, 2020). Quadratic shell elements have been used to model the masonry walls and the one-way floor slabs. The used quadratic shell elements (CQ40S) have eight nodes and five degrees of freedom (three translations and two rotations) per each node. The integration scheme consists of a 3×3 Gauss integration over the element's plane, and a Simpson integration scheme with seven points through the thickness of the elements. The ground floor steel beams and lintels above all the openings have been modelled using the 3D beam element CL18B (composed of three nodes and six degrees of freedom for each node). The movement of the rotational degree of freedom in Z direction (see Figure 5.3 for the used axes convention) of the 3D steel elements has been restrained in order to ensure compatibility between beam and shell elements.

The dimensions of the beam elements used in the lintels correspond to steel profiles of IPN240 for the façade openings at the ground floor and IPN140 for the rest of the openings, while the section of the steel profiles at the basement has been manually defined to match the inertia properties of the original steel truss profiles. The FE numerical model is composed of 17,596 shell elements (10,949 shell elements for the URM walls and 6,647 shell elements for the floors), 805 3D beam elements and 3,052 one-node translational mass elements used to provide the loads of the diaphragms. The total number of nodes is 52,155. The final mesh size (with an average

element size of 0.5 m), as well as the type of elements and integration scheme, have been selected following a mesh convergence study. The boundary conditions at the base of the building have been assigned as totally fixed by restricting both translational and rotational movements.

The floors have been modelled as one-way diaphragms using quadrilateral (CQ40S) and triangular (CT30S) shell elements. The corresponding permanent and live loads of the floors have been lumped to the walls supporting the floor beams. The longitudinal axis of the floor beams is orthogonal to the façade walls for the floors located in the front and rear bays, and it is parallel to the façade for the beams of the floors located in the central part (Figure 5.2b). The roof has the same one-way slab construction of the floors, which provides regularity to the structure, and has facilitated the addition of storeys at the top in many buildings in *Eixample*. In this work, wall-to-floor connections are assumed as fixed, as focus is given on the evaluation of the effect of the in-plane stiffness of the one-way floors. Therefore, any local failures due to sliding between the floor beams and walls are not considered.

5.2.1.2. Hybrid system – steel columns and masonry load-bearing walls

The typical ground floor of an existing *Eixample* building with a hybrid system consists of the following structural elements (Figure 5.4): unreinforced masonry walls, masonry columns (as extension of the masonry walls), steel truss beams and circular cast-iron pillars. The main load-bearing walls, such as the front and back façade, lateral exterior walls, interior walls (parallel to the façades) and walls surrounding the staircase box and inner courtyards, are made of unreinforced masonry and can have a varying thickness from 0.15 to 0.45 m.

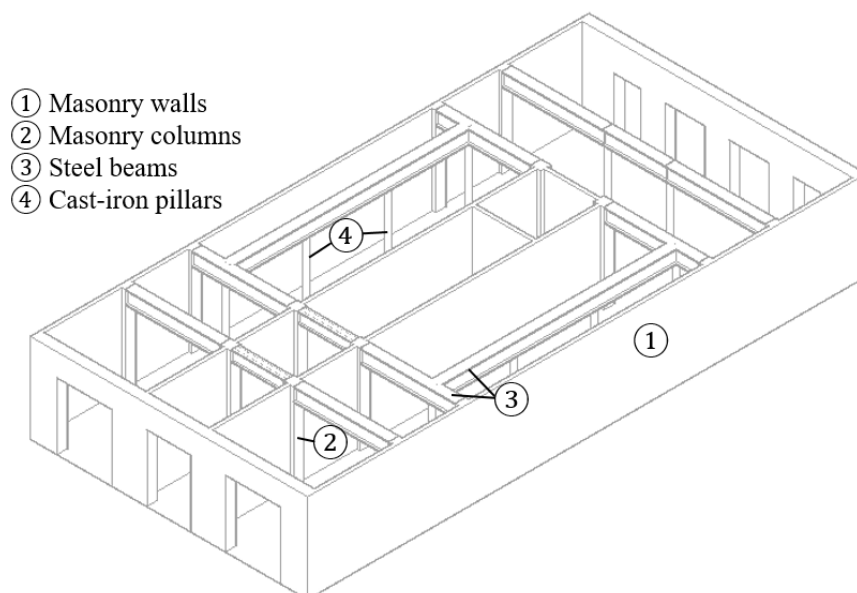


Figure 5.4 - Example of a typical ground floor of a rectangular shape building typology in the *Eixample* district (including unreinforced masonry walls, masonry columns, steel beams and cast-iron pillars).

As it was described in Chapter 3, masonry columns (known as ‘pilasters’ in Catalan) can be found at the ground floor of these existing buildings. They are typically constructed as an extension of the lateral walls and support the steel truss beams in order to provide a bigger open space for

the commercial activities. The beams and pillars were formed basically from industrial metallic elements, which for most of the cases were prefabricated (Paricio Casademunt, 2001). In these buildings, different types of beams with composite geometries (such as truss beams, riveted beams or box beams) can be found in order to support the upper floors and interior walls. The pillars usually were made of cast-iron with circular cross section.

The 3D FE model for the hybrid structural system has been developed by changing the geometrical configuration of the ground floor of the reference building model. In this model, the plan configuration of the ground floor differs from that of the upper floors in the location of the semi-patios. Therefore, the continuity of the semi-patios is disturbed at the ground floor and this relative space can be used by introducing cast-iron pillars and steel beams for supporting the above semi-patio walls (see Figure 5.5b and Figure 5.6b). The interior wall located at the rear part of the structure on the ground floor has also been removed and replaced with steel beams and two circular cast-iron pillars. Figure 5.5 presents the difference between the ground floor plan for the reference building with homogenous structural system and hybrid system. The dimensions of all the structural elements have been considered to be the same among both models.

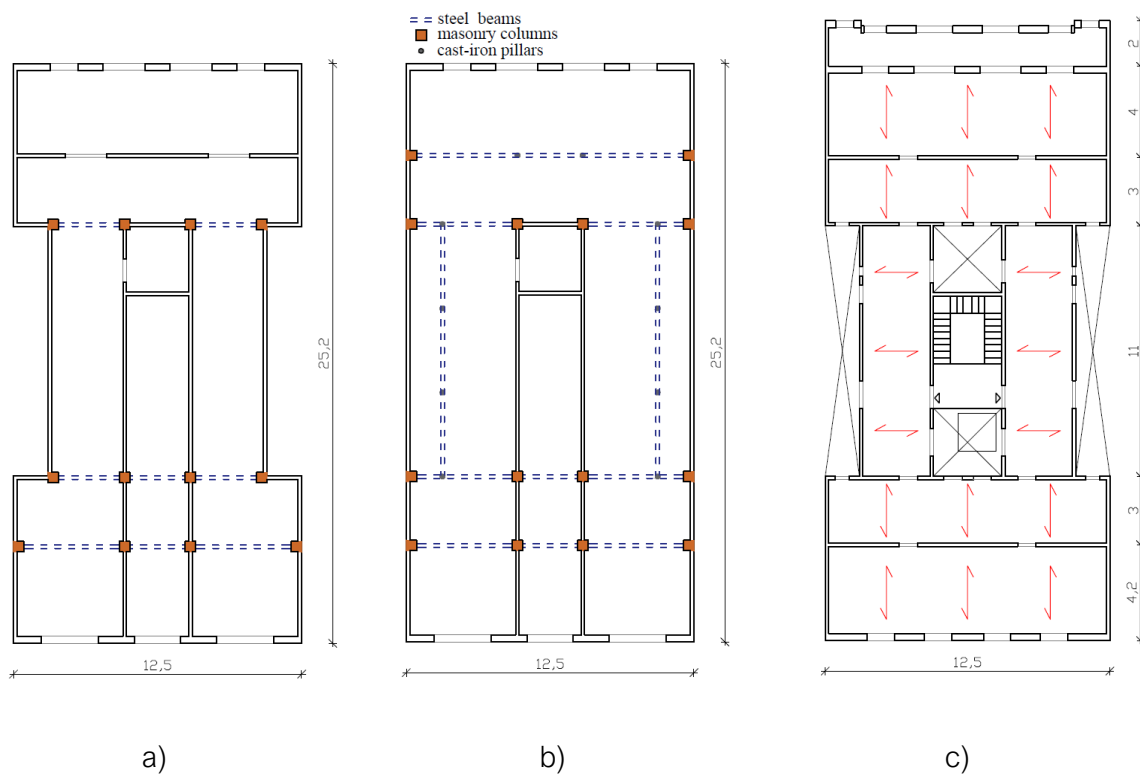


Figure 5.5 - Geometrical configuration of an existing building typology in the Eixample district: a) plan of the ground floor with unreinforced masonry walls; b) plan of the ground floor of a hybrid steel-masonry system; c) typical floor plan for the rest of the storeys (dimensions in metres).

As aforementioned, the reference model is considered to be the building typology with continuous unreinforced masonry walls across the whole height of the building (Figure 5.6a). Figure 5.6b illustrates the 3D FE hybrid model with a different ground floor plan. The same characteristics for the numerical modelling have been adopted as previously discussed.

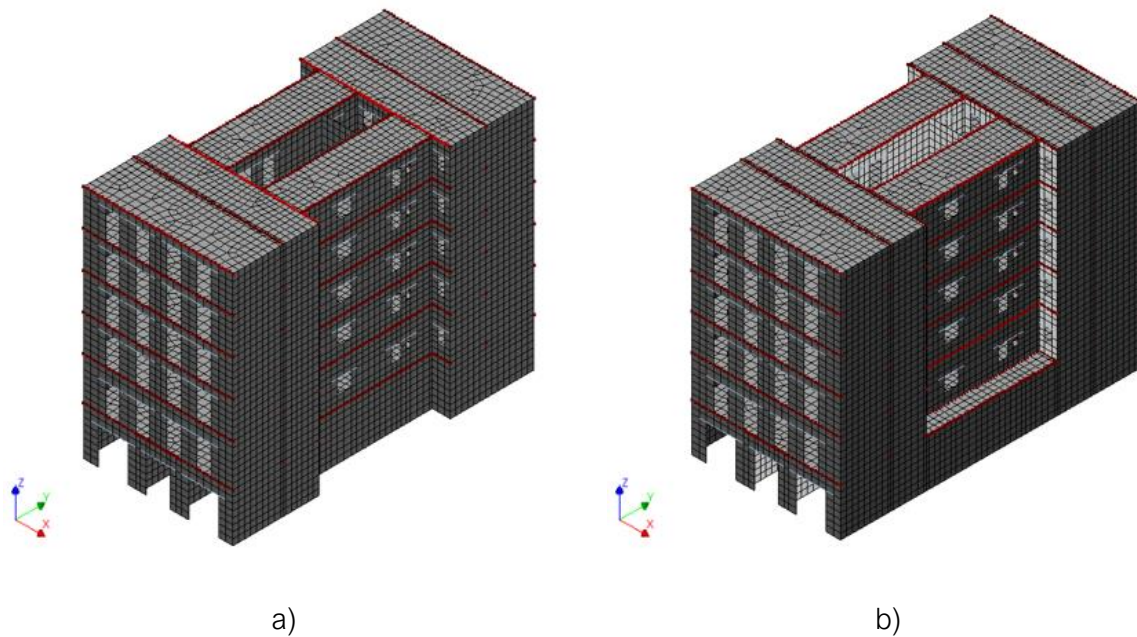


Figure 5.6 - Finite element models of a representative building typology in the Eixample district: a) reference model and b) hybrid model.

- Loading conditions

Table 5.1 shows the loads acting on the structure have been defined according to the provisions of the Spanish norm (CTE_DB-SE-AE, 2009). The dead load of the floor diaphragms includes the weight of the beams (steel or timber), the rubble infill and the pavement, according to NRE-AEOR-93 (ITEC, 1994). In addition to the live load of 2 kN/m², a load of 1 kN/m² has been added to the floors, corresponding to the division walls and the potential addition of new pavements, which is common in *Eixample* buildings following past rehabilitation works. The weight considered during the seismic event has been defined as the entire self-weight load and 30% of the live load applied to the typical one-way floors (CTE_DB-SE-AE, 2009). As aforementioned, in order to simulate correctly the loading conditions given by the one-way floor systems, the load of the floors has been applied as a concentrated mass to the nodes at the edge where the beams of each floor are connected with the lateral walls.

Table 5.1 - Loads used in the numerical models of the representative buildings.

Load	[kN/m ²]
Floor structural system (steel beams and masonry vaults)	2.45
Floor structural system (timber beams and masonry vaults)	1.25
Pavement	1
Division walls	1
Live load	2

5.2.2. Material properties

Masonry is simulated as a continuum material with properties corresponding to the average response of the composite material. Its nonlinear behaviour is considered through the use of the Total Strain Fixed Crack model implemented in DIANA-FEA software (DIANA FEA BV, 2020). This constitutive model has been commonly used in the literature to simulate the nonlinear response of unreinforced masonry (Aşıkoğlu et al., 2020; Chieffo et al., 2021; Mendes and Lourenço, 2014; Pereira et al., 2021). A parabolic softening curve has been used under compression and an exponential softening curve under tension. The shear behaviour after cracking has been described through a constant shear stiffness reduction with a shear retention factor of 0.01. Table 5.2 presents the mechanical properties used for the URM walls in all the simulations.

Table 5.2 - Material properties of the unreinforced masonry walls in the numerical models.

Masonry walls		
Young's modulus	1800	MPa
Poisson's ratio	0.2	[-]
Mass density	1800	kg/m ³
Compressive strength	4.0	MPa
Compressive fracture energy	6400	N/m
Tensile strength	0.08	MPa
Tensile fracture energy	50	N/m

As discussed in Chapter 3 (see section 3.7), different values ranging between 1.8 MPa and 4.0 MPa have been reported by previous studies for the compressive strength of the masonry walls in existing buildings located in the *Eixample* district of Barcelona (Pujades et al. 2012; Gonzalez-Drigo et al. 2015). This work considers the values for the Young's modulus and the compressive strength derived from the experimental tests done at the Polytechnic University of Catalonia (UPC) on specimens extracted from existing buildings in Barcelona (Segura et al., 2019), which are presented in section 3.8. The chosen values correspond to the upper bound of the values given by the Italian Code for solid brick masonry (MIT Ministero delle Infrastrutture e del Transporti, 2019). The value of the mass density has been selected according to the recommendations of the Italian code for solid brick masonry (MIT Ministero delle Infrastrutture e del Transporti, 2019).

The tensile strength corresponds to 2% of the compressive strength. This value is lower than the one given as a function of the shear strength as $ft=1.5\tau_0$ (Turnsek and Sheppard, 1980) considering a shear strength of $\tau_0=0.12\text{ MPa}$ according to Moreno-González and Bairán, (2011). According to previous experience, it has been considered to model a masonry material with a lower tensile strength, as being more representative for the existing *Eixample* buildings.

The value of the compressive fracture energy has been defined as a function of the compressive strength according to Lourenço (2008):

$$G_f^c = d f_c \quad (5.7)$$

where $d = 1.6$ mm. For the tensile fracture energy, after performing some sensitivity analysis, a value of 50 N/m has been adopted in order to obtain more stable numerical results. This value is approximately four times the value obtained using the following equation (Lourenço, 2009):

$$G_f^t = 0.025 \left(\frac{f_c}{10} \right)^{0.7} \quad (5.8)$$

The mechanical properties for the steel beams have been defined according to Moreno-González and Bairán, (2011), and have been used for the steel beams in the ground floor, as well as for the lintels in the numerical models of the representative buildings (Table 5.3).

Table 5.3 - Material properties of all the steel beams in the numerical models.

Steel beams		
Young's modulus	210000	MPa
Poisson's ratio	0.3	[-]
Mass density	7850	kg/m ³

The one-way floors have been simulated as an orthotropic elastic material. The elastic properties are presented in Table 5.4 and Table 5.5 for steel and timber beam one-way floors, respectively. The procedure for the derivation of these orthotropic elastic properties of one-way floors is presented in the following section 5.2.3.

Table 5.4 - Material properties of the one-way diaphragm with steel beams and masonry vaults.

One-way diaphragm with steel beams and masonry vaults		
E_x (perpendicular to the beams)	1000	MPa
E_y (parallel to the beams)	7800	MPa
$G_{xy\perp}$ (perpendicular to the beams)	27	MPa
$G_{xy\parallel}$ (parallel to the beams)	110	MPa
ν_{xy}	0.06	[-]

Table 5.5 - Material properties of the one-way diaphragm with timber beams and masonry vaults.

One-way diaphragm with timber beams and masonry vaults		
E_x (perpendicular to the beams)	1100	MPa
E_y (parallel to the beams)	4000	MPa
$G_{xy\perp}$ (perpendicular to the beams)	27	MPa
$G_{xy\parallel}$ (parallel to the beams)	46	MPa
ν_{xy}	0.10	[-]

5.2.3. Modelling of one-way floor systems

This section investigates the modelling of the in-plane stiffness of typical one-way floors in order to assess its effect on the seismic behaviour of *Eixample* URM buildings. The response of unreinforced masonry (URM) structures under horizontal loading depends significantly on the in-plane stiffness of the diaphragms (Senaldi et al., 2014; Senaldi et al., 2020; Vintzileou et al., 2015). Because the horizontal diaphragms are crucial in the distribution of horizontal forces among the walls during an earthquake (Tomažević et al. 1991). The existence of a flexible diaphragm may result in a lack of a box behaviour and in an increase of the seismic vulnerability (Diaferio et al., 2014). The efficiency of the wall-to-floor connection as well as the in-plane stiffness of the floor slabs have a substantial impact on the structure's seismic response, among the various parameters that affect the resistance of existing URM buildings (Piazza et al. 2008). This point highlights the importance of estimating and considering in a realistic way the in-plane stiffness of floors in the seismic assessment of existing URM buildings.

The influence of deformable wooden floors on the seismic performance of unreinforced masonry buildings has been investigated both at experimental and numerical level (Brignola et al., 2009; Giongo, 2013; Lourenço et al., 2011; Ortega et al., 2021; Valluzzi et al., 2010). Additionally, international guidelines on seismic rehabilitation of buildings (ASCE/SEI 41-17, 2017) provide some reference values for the shear stiffness of different flexible timber floors, and propose some analytical procedures for the evaluation of their in-plane stiffness (NZSEE, 2006). However, there is scarce information regarding the in-plane behaviour of floor systems composed of timber beams (with round or squared section) or steel beams and ceramic vaults. These one-way floor slabs, called jack arch floors, are very common in many historical and existing buildings of the Mediterranean countries, and especially in the eastern coast of Spain (M Diodato et al., 2015; Paricio Casademunt, 2001). Only a few studies, focusing on Iranian masonry or steel buildings, have contributed to the evaluation of the shear stiffness and the seismic behaviour of this type of floor slabs (Maheri and Rahmani, 2003; Maheri and Rahmani, 2004; Shakib et al., 2015; Zahrai et al., 2006; Zahrai, 2015).

The numerical procedure for a simplified modelling of jack arch one-way floors with tile vaults and steel or timber beams is presented in the following sections. The adopted simplified floor modelling consists of considering 2D shell elements with orthotropic elastic homogeneous material. In order to properly model the behaviour of the jack arch floors, a detailed 3D solid FE model and a simplified 2D shell FE model have been prepared for computing the elastic orthotropic properties of the composite floor system, by matching their effective stiffness with an iterative procedure. After estimating the floors' orthotropic properties, they can be implemented in the global FEM model of the existing URM building to assess its seismic performance using a pushover analysis.

- Geometry and FE mesh

This section presents the *detailed 3D solid* and the *simplified 2D shell* finite element models that have been used to evaluate the in-plane stiffness of one-way jack arch floors. Two one-way floors with steel or timber beams have been selected as the most representative ones, from all the variety of possible floor slabs found in the existing *Eixample* buildings, as presented in Chapter 3.

Figure 5.7 and Figure 5.8 illustrate these typical floors that can be found in the URM buildings. The vaults in both cases are made of thin clay tiles and a compression layer of rubble material. Different materials are used for the one-way beams, namely steel and timber. The geometry of the jack arch floors has been defined according to previous research studies related with the structural elements in the representative building typologies of *Eixample* (Paricio Casademunt, 2001). This information was supported by reports of rehabilitation works carried out on existing buildings, and by original design plans of buildings found in the public archive of Barcelona.

The first model consists of steel beams spaced at a distance of 700 mm and the second model has timber beams spaced at a distance of 550 mm. In both cases, the vaults are composed of a double layer of thin clay tiles, and the compression layer on top of them is a rubble material. Figure 5.7 and Figure 5.8 present the geometrical characteristics of the steel and timber jack floors, respectively.

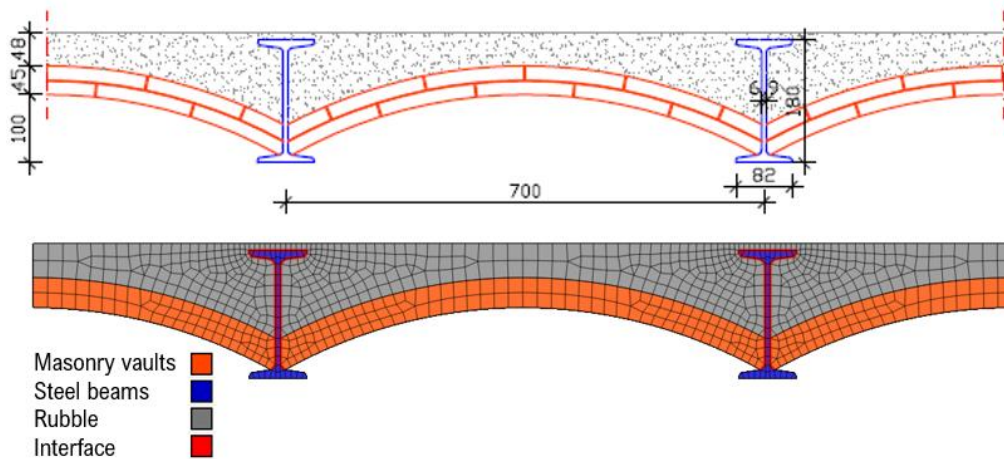


Figure 5.7 - Section of the jack arch floor with steel beams and tile barrel vaults: Geometry (top) and finite element model (bottom) (dimensions in mm).

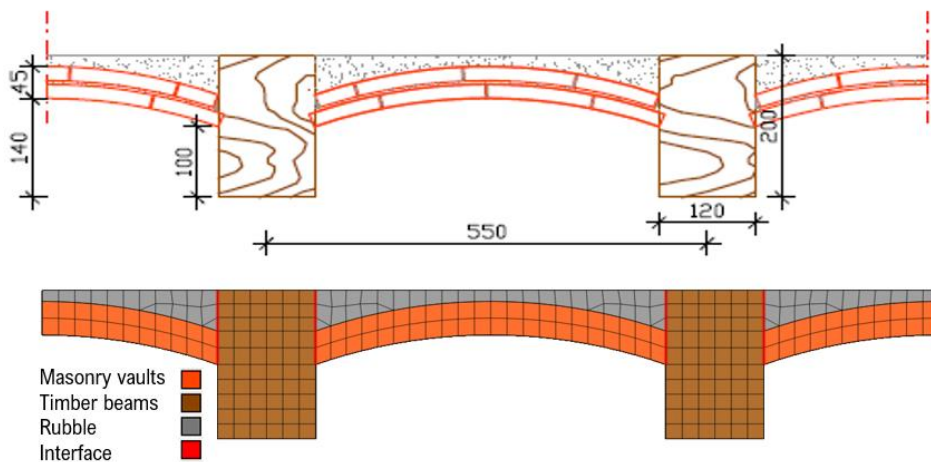


Figure 5.8 - Section of the jack arch floor with timber beams and tile barrel vaults: Geometry (top) and finite element model (bottom) (dimensions in mm).

The 3D finite element models of the two floors (referred hereafter as *3D solid floor model*) have been prepared using DIANA-FEA software (DIANA FEA BV, 2020). The models consider a full vault and two halves at each side with overall dimensions 1.40 m × 4.00 m for the floor with steel beams, and 1.10 m × 4.00 m for the floor with timber beams (see Figure 5.9). The length of the floor models is assumed to be 4.00 m as this is the most typical dimension for the one-way floors of *Eixample* buildings. The finite element meshes consist of eight-node (HX24L) and six-node (TP18L) solid brick elements, based on linear interpolation and standard Gauss integration. Interface elements (Q24IF) have been used to define the interface between the beams and the vaults and between the rubble material and the beams.

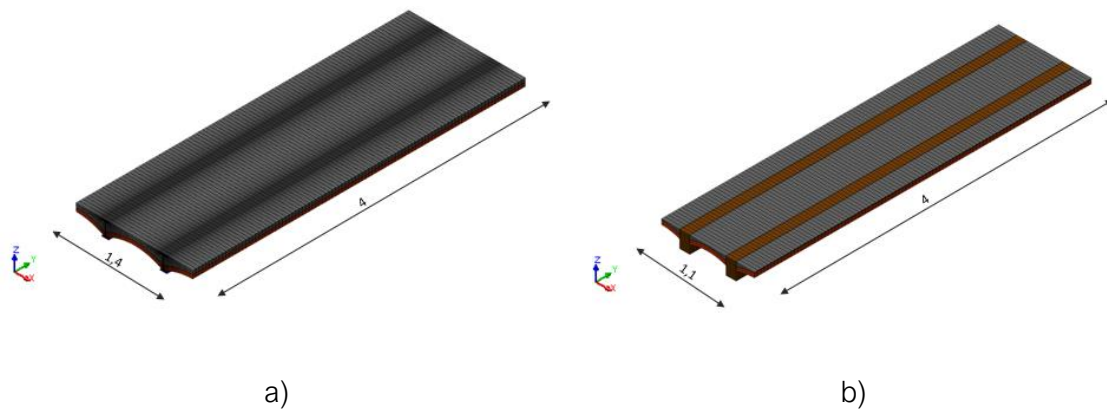


Figure 5.9 - 3D solid finite element models of the floor system with tile vaults and: a) steel beams; b) timber beams (dimensions in metres).

The simplified 2D shell models (referred hereafter as *2D shell floor model*) follow the same modelling approach used for the simulation of the floors in the models of the whole buildings. The 2D shell floor model is made of the quadratic shell elements (CQ40S) by considering an orthotropic elastic behaviour. The 2D shell models for the two floors have the same length, width and volume with their corresponding 3D solid models (Figure 5.10). Their thickness is constant and defined in such a way that the sections orthogonal to the longitudinal axis of the beams are equal in terms of area to those of the detailed 3D models. This results to an equivalent thickness of 121.4 mm for the floor with steel beams and 100.8 mm for the floor with timber beams.

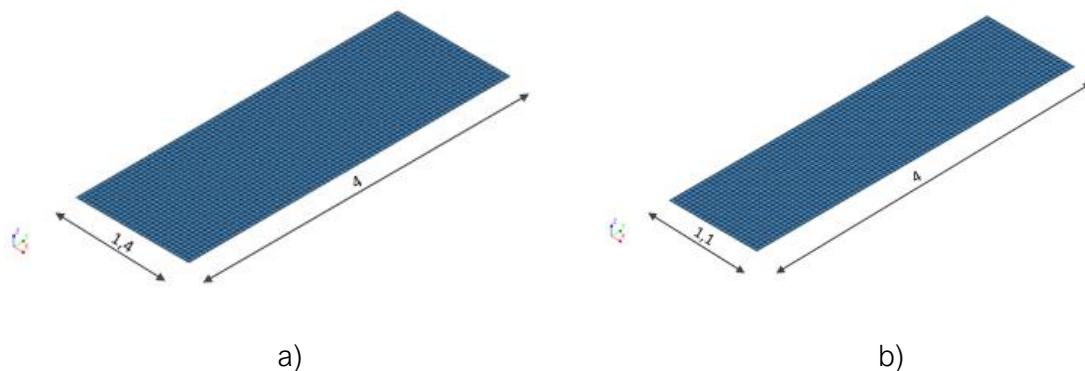


Figure 5.10 - 2D equivalent shell model: a) floor model with steel beams; b) floor model with timber beams (dimensions in metres).

- Material properties for the 3D solid FE floor models

Similar to the masonry walls of the 3D existing building models, the mechanical behaviour of both masonry and the rubble material has been simulated with the Total Strain Fixed Cracking model of the DIANA-FEA software (DIANA FEA BV, 2020). The tensile response has been characterized by a linear behaviour up to the tensile strength followed by an exponential softening. The compressive response has been represented by a parabolic hardening and softening. The shear behaviour has been assumed as constant with a shear retention factor of 0.01. In both cases, the stress-strain curves have been regularized considering the fracture energy and the characteristic length of the material. A linear elastic behaviour has been adopted for the steel and timber elements. This modelling approach has been used successfully in the past for simulating masonry vaults with steel elements in historical buildings of Barcelona (Endo, Llorens, et al., 2017).

Table 5.6 presents the material properties used in the 3D solid models of the typical jack arch floors. The masonry vaults have been modelled with the same material properties as the masonry walls in the reference numerical model of the most recurrent building typology (see section 5.2.2). The properties of the rubble material have been defined according to the experimental results in Segura et al. (2018) and the selected values are also in line with the lower bound for rubble masonry in the Italian guidelines (MIT Ministero delle Infrastrutture e del Trasporti, 2019). The value for the compressive fracture energy has been obtained following the recommendations from Lourenço (2008), as explained in the section 5.2.2. A value of 20 N/m has been defined for the tensile fracture energy.

The mechanical properties for the steel beams are the same as the ones used for the steel lintels as presented in Table 5.6. A Coulomb friction model has been used for the simulation of the interface between beams and bricks and rubble. The values for the normal and shear stiffness have been defined according to Endo (2015) and Endo et al. (2017). Since the information in the literature regarding the frictional behaviour between steel and masonry or rubble materials is very limited, the frictional parameters have been considered equal to the ones used in the literature for describing a contact surface between steel and concrete. A value of 0.1 MPa has been chosen for the cohesion as used in Campione et al. (2017) for the simulation of frictional effects in structural behaviour of no-end-connected steel-jacketed reinforced concrete columns. This value corresponds to an upper bound value for an interface between concrete and steel according to Adam and Ivorra (2007). The frictional angle is 26.5° ($\tan\phi = 0.5$), corresponding to a value for an interface between steel and concrete according to PCI Industry Handbook Committee (2004).

The last part of Table 5.6 presents the material properties for the timber and the interface elements used in the 3D solid model of the one-way flexible floor with timber beams and masonry vaults. In most of the buildings with timber floors in the *Eixample* district, the timber beams are made out of Pine wood (*Pinus sylvestris*), which can be easily found in the Pyrenees (Paricio Casademunt, 2001). The Young's modulus of this type of timber is defined as equal to one of the lower resistance class C16 in the Spanish code for construction with timber (CTE-DB-SE-M. Código Técnico de la Edificación, 2007). The density and Poisson's coefficient have been chosen according to the physical properties of Pine wood (de la Fuente-Leon et al., 2014). Due to the lack of information for the cohesive properties between timber and masonry materials, the properties of the interface elements are conservatively chosen the same as in the floor model with steel

beams. The value for the frictional angle has been obtained according to a static frictional coefficient $\tan\varphi=0.6$ (frictional angle of 30.96°) between timber and brick (Aira et al., 2014).

Table 5.6 - Material properties of the ceramic tile vaults, rubble, steel beams with corresponding interface elements, and timber beams with corresponding interface elements in the 3D solid numerical models of the jack arch floors.

Material properties		
Masonry vaults		
Young's modulus	1800	MPa
Poisson's ratio	0.2	[-]
Mass density	1800	kg/m ³
Compressive strength	4.0	MPa
Compressive fracture energy	6400	N/m
Tensile strength	0.08	MPa
Tensile fracture energy	50	N/m
Rubble		
Young's modulus	690	MPa
Poisson's ratio	0.2	[-]
Mass density	1900	kg/m ³
Compressive strength	1.0	MPa
Compressive fracture energy	1600	N/m
Tensile strength	0.02	MPa
Tensile fracture energy	20	N/m
Steel beams		
Young's modulus	210000	MPa
Poisson's ratio	0.3	[-]
Mass density	7850	kg/m ³
Normal Stiffness	200	N/mm ³
Shear stiffness	100	N/mm ³
Cohesion	0.1	MPa
Frictional angle	26.5	°
Timber beams		
Young's modulus	8000	MPa
Poisson's ratio	0.3	[-]
Mass density	520	kg/m ³
Interface elements between timber and masonry		
Normal Stiffness	200	N/mm ³
Shear stiffness	100	N/mm ³
Cohesion	0.1	MPa
Frictional angle	30.96	°

5.2.3.1. Numerical procedure for evaluation of the elastic properties

This section presents the numerical procedure used for the estimation of the orthotropic elastic properties of the two types of jack arch floors that are necessary for their simplified modelling using shell elements in FEM models of URM buildings. It has not been possible to validate the numerical analyses by comparison with experiments, because experimental data at structural level on the floor slab system have not been so far carried out. Therefore, numerical simulations are used as a virtual laboratory to obtain the desired orthotropic properties of the floors. In the following section parts, the necessary parameters for the definition of the orthotropic elastic behaviour are computed, namely three Young's moduli, three shear moduli and three Poisson's coefficients.

- Evaluation of the Poisson's coefficients

The Poisson's coefficients of the 3D solid floor model have been computed by performing three linear elastic analyses. In particular, for each of these analyses a compressive distributed load is applied at one of the faces (Figure 5.11) and the ratio between transversal and axial deformation has been computed, as shown in equations (5.9) - (5.11).

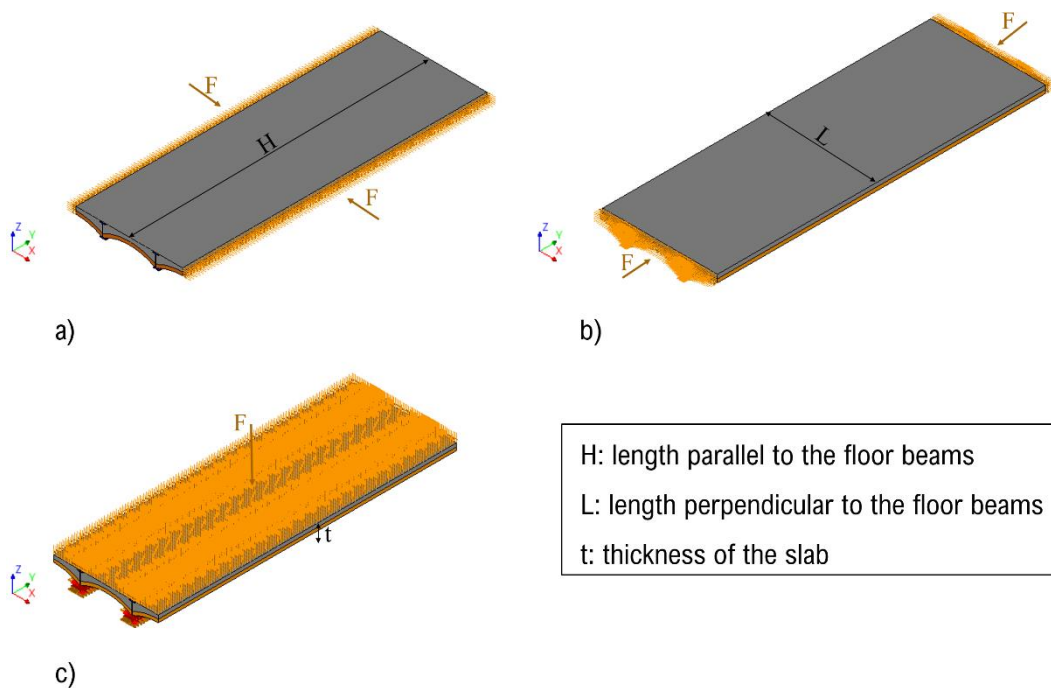


Figure 5.11 - Loading conditions for 3D solid floor model in order to obtain: a) Poisson's coefficients ν_{xi} with $i = y; z$; b) Poisson's coefficients ν_{yi} with $i = x; z$; c) Poisson's coefficients ν_{zi} with $i = y; x$.

$$\varepsilon_x = \frac{\Delta L}{L} \quad (5.9)$$

$$\varepsilon_y = \frac{\Delta H}{H} \quad (5.10)$$

$$\varepsilon_z = \frac{\Delta t}{t} \quad (5.11)$$

In the above equations, ΔL , ΔH and Δt correspond to the average change in the width (L), length (H) and thickness (t) of the floor, after the application of the load. The following equations (5.12) - (5.14) have been used to estimate the Poisson's coefficients (ν_{xy} , ν_{yz} and ν_{xz}), which are required for the elastic orthotropic material in DIANA-FEA software (DIANA FEA BV, 2020). The other three Poisson's coefficients are calculated considering the symmetry of the orthotropic stiffness matrix.

$$\nu_{xy} = -\frac{\varepsilon_y}{\varepsilon_x} \quad (5.12)$$

$$\nu_{yz} = -\frac{\varepsilon_z}{\varepsilon_y} \quad (5.13)$$

$$\nu_{xz} = -\frac{\varepsilon_z}{\varepsilon_x} \quad (5.14)$$

Table 5.7 - Values for the Poisson's coefficients used in the 2D shell floor models.

Poisson's coefficients	Floor system with steel beams	Floor system with timber beams
ν_{xy}	0.06	0.10
ν_{yz}	0.14	0.17
ν_{xz}	0.23	0.20

Table 5.7 presents the computed values of the Poisson's coefficients, which are used later in the numerical model of the representative *Eixample* buildings. The computed values satisfy the conditions (5.15) and (5.16) for an orthotropic material (DIANA FEA BV, 2020; LEMPRIERE, 1968):

$$\nu_{xy}^2 < \frac{E_x}{E_y}, \nu_{yz}^2 < \frac{E_y}{E_z}, \nu_{xz}^2 < \frac{E_x}{E_z} \quad (5.15)$$

$$2\nu_{xy}\nu_{yz}\nu_{xz}\frac{E_z}{E_x} < 1 - \nu_{xy}^2\frac{E_y}{E_x} - \nu_{yz}^2\frac{E_z}{E_y} - \nu_{xz}^2\frac{E_z}{E_x} \leq 1 \quad (5.16)$$

- Evaluation of the Young's and shear moduli

The evaluation of the Young's and shear moduli of the orthotropic material used to simulate the floors in the building model has been made through the direct comparison of the in-plane response under uniaxial and shear loading of the 3D solid model of the floors and 2D shell model of each floor type with elastic orthotropic properties. The same loading conditions have been applied to both 3D solid and 2D shell floor slab models in order to allow the estimation of their axial and shear stiffness. The values of the Young's moduli for the elastic orthotropic material of the 2D shell models have been computed along the local in-plane axes X and Y by matching the elastic axial stiffness of the 3D solid floor models. Accordingly, a set of two analyses per floor type have been

carried out with the 3D solid floor models in order to evaluate the axial stiffness of the two floors by applying a compressive load along the two axes of orthotropy, i.e parallel and orthogonal to the beams. Moreover, the shear modulus G_{xy} of the 2D shell models has been computed by matching the elastic shear stiffness of the 3D solid floor models. Thus, two analyses have been performed using the 3D solid model for each floor system and inducing a shear deformation of the floor by applying a horizontal displacement at one end of the floor (restraining the vertical displacement) and keeping the opposite end fixed. The corresponding load-displacement curves from the compression and in-plane shear tests are presented in APPENDIX B of this doctoral thesis.

Table 5.8 presents the corresponding estimated values for each floor system. These values confirm the orthotropic behaviour of the jack arch floors in the two principal loading directions (parallel and perpendicular to the beams). The Young's modulus E_z has been assumed equal to the Young's modulus E_y . The shear moduli in the other two planes (G_{yz} , G_{xz}) have been considered equal to G_{xy} . The elastic orthotropic properties obtained from the floor models are different in both floor systems depending on the loading direction.

Table 5.8 - Values of the elastic properties of the floors obtained from the FEM analyses of isolated floor slab models.

Type of floor	Elastic orthotropic properties			
	E_x (MPa)	E_y (MPa)	$G_{xy\perp}$ (MPa)	$G_{xy\parallel}$ (MPa)
Floor with steel beams and tile vaults	1000	7800	290	430
Floor with timber beams and tile vaults	1100	4000	320	500

These estimated values of the Young's and shear moduli have been based on FEM nonlinear analyses on isolated detailed 3D solid models of the floor slabs. Such values can be adopted for the simplified 2D shell modelling of the floors under the assumption of elastic behaviour only if the strain/stress admissibility is guaranteed. This check has been performed through a nonlinear seismic analysis of the global FEM model of the selected URM building, including the simplified 2D shell modelling of the floors. The procedure consists in checking if the deformation levels of the 2D shell models of the floor slabs remain in the elastic field during the seismic loading of the entire building, simulated with nonlinear FEM pushover analysis. If the level of deformation experienced by the floors of the building model corresponds to the elastic deformation as identified by the axial and shear tests of the 3D solid floor models, then the selection of the elastic properties for both models is valid. Contrariwise, if the level of deformation reached by the 2D shell floors in the FEM building model corresponds to a nonlinear behaviour of the 3D solid floor models, then the values of the Young's and shear moduli for the elastic orthotropic material of the floors are updated accordingly (see Figure 5.12).

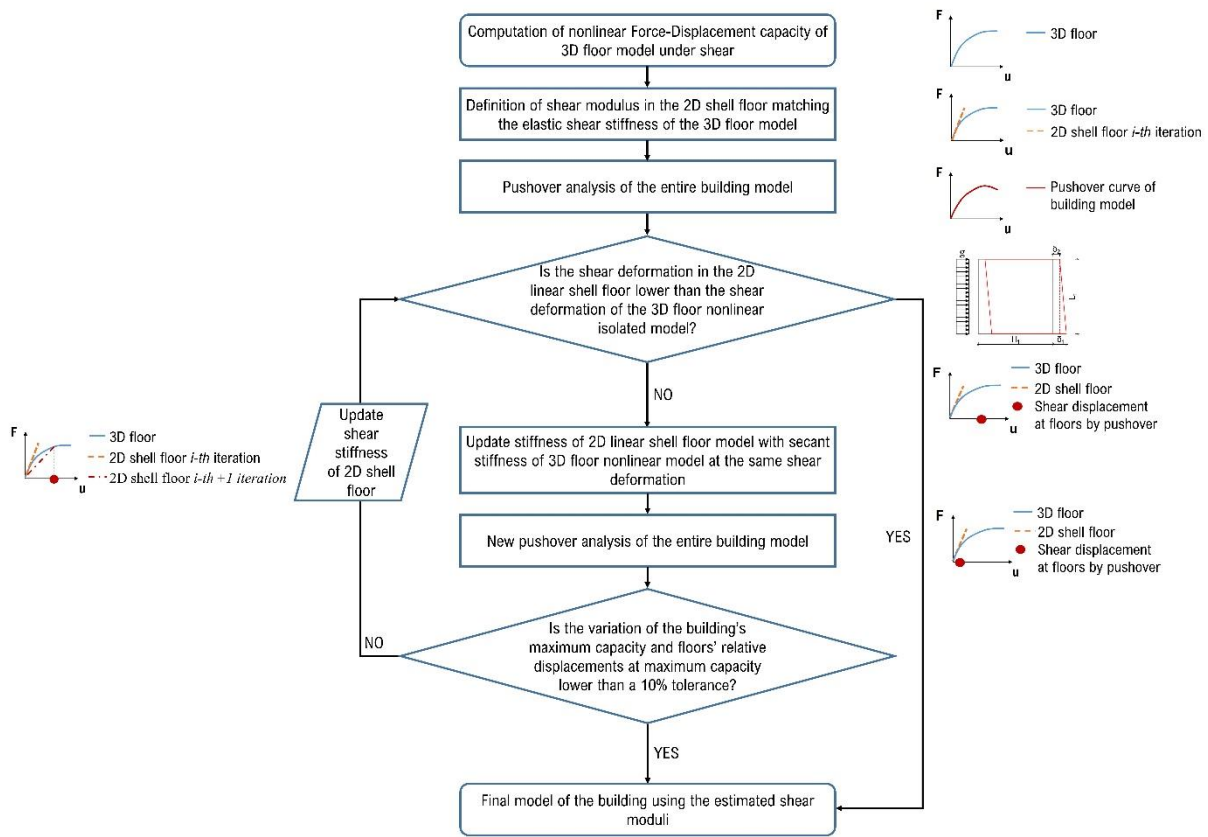


Figure 5.12 - Flowchart of the numerical procedure used to compute the values of the shear moduli of the jack arch floors.

The steps to compute the new values of this effective floor stiffness are the following: i) computation of the equivalent shear deformation of the 3D solid floor slab model corresponding to the shear deformation calculated in the 2D shell floors of the building model; ii) computation of the secant stiffness of the 3D solid floor model corresponding to the computed shear deformations of the 2D shell floors of the building model; iii) update of the shear modulus of the 2D shell model so that its effective shear stiffness matches the secant stiffness computed for the nonlinear 3D solid floor model; and iv) execution of a new pushover analysis and computation of shear deformation at maximum capacity. After the execution of the new pushover analysis, a check has been carried out considering two factors (Table 5.9): i) change of maximum capacity from the pushover analysis in X direction, and ii) change of relative displacements ($\delta_1 - \delta_2$) in the floors (with beams parallel and perpendicular to the loading direction) corresponding to the maximum capacity of the building model. The iterative procedure has been finalized when the changes are below 10% (based on previous experience) between two successive iterations. Figure 5.12 shows a visual summary of the entire procedure.

The application of the seismic loading to the building models has been simulated through pushover analysis. The iterative procedure has been followed only for loading in the X direction, which is the case producing shear deformation to the floors due to the torsional response of the building. At each iteration, the deformation levels have been checked and the shear moduli have been updated, if necessary, for both floors with beams parallel and orthogonal to the loading direction.

Table 5.9 summarizes the values of the monitored parameters during the iterative procedure. The difference in the values of the shear moduli between the first iteration and the second one is around 143% in the floor with beams aligned with the X direction ($G_{xy\parallel}$), and around 87% in the floor with beams aligned with Y direction ($G_{xy\perp}$). The same difference between the second and the third iteration is smaller, around 56% for $G_{xy\perp}$ and 34% for $G_{xy\parallel}$. Lastly, the values of the shear moduli of the fourth iteration have converged, with an identical value for $G_{xy\perp}$ and around 9% difference for $G_{xy\parallel}$.

Table 5.9 - Values obtained of the shear properties of the floor system with steel beams after the proposed iterative procedure.

Convergence of the shear properties for the floors with steel beams				
Properties	Iteration 1	Iteration 2	Iteration 3	Iteration 4
$G_{xy\perp}$ (MPa)	290	48	27	27
$G_{xy\parallel}$ (MPa)	430	170	120	110
Maximum capacity (g)	0.137	0.126	0.126	0.123
Displacement \perp (m)	0.003	0.0064	0.0067	0.0071
Displacement \parallel (m)	0.0012	0.0031	0.0039	0.0039

The same methodology has been applied for the calculation of the shear moduli of the one-way floors with timber beams and ceramic tile vaults. The procedure of the numerical modelling of one-way floor slabs is explained in detail in our research paper Dimovska et al. (2022) and the proper calculations and results are presented in APPENDIX B of this doctoral thesis.

5.3. VARIATIONS OF DIFFERENT PARAMETERS IN THE REFERENCE MODEL

Various structural parameters are significant for the seismic vulnerability assessment of the existing URM buildings, as previously discussed in the detailed building taxonomy in Chapter 4. Only the parameters that mostly influence the structures' seismic performance, which can be numerically simulated, have been chosen for developing different FE models, considering the high computational time and cost. Hence, the numerical models are categorized according to the most significant parameters such as: the number of storeys, presence of vertical extensions-*remuntes*, material properties, masonry walls' thickness variation, horizontal diaphragms, and façade openings. These parameters are included as part of the proposed Vulnerability Index Method in Chapter 7.

The variations of the selected parameters have been implemented to the previously described reference model. Approximately four models (including the reference one) have been developed for the variations of each analysed parameter. As explained previously in section 5.2.1, all the numerical models have been developed using the software DIANA-FEA (DIANA FEA BV, 2020) with the same eight-node quadratic shell elements (CQ40S) for the masonry walls and columns, and 3D beam elements (CL18B) for the metallic beams and pillars. The loads have been applied

as masses (PT3T) at the nodes of each floor edge, according to the direction of the one-way floor diaphragms.

5.3.1. Number of storeys

The number of storeys is a very significant parameter that influences the buildings' seismic behaviour. The buildings with higher number of storeys tend to be more vulnerable to seismic actions and prone to a higher expected damage than the lower buildings. The number of floor levels in the existing *Eixample* building typologies can range between 4 and 7. There is a very small number of buildings with less than three storeys or more than eight. Therefore, according to the prepared building taxonomy, four building models have been developed in order to represent the different existing heights of buildings. Figure 5.13 illustrates the numerical models of the reference building typology with different number of storeys: a) Building with three storeys (GF+3); b) Building with four storeys (GF+4); c) Building with five storeys (GF+5); d) Building with six storeys (GF+6). The reference building model used for the numerical simulation is the previously described existing *Eixample* building with slender masonry walls. The most common height for this building typology is of five storeys (GF+5). All four FE models have the same geometrical configuration and material properties, and the only variation is the number of storeys from three to six storeys, excluding the ground floor, which is used for the commercial activities.

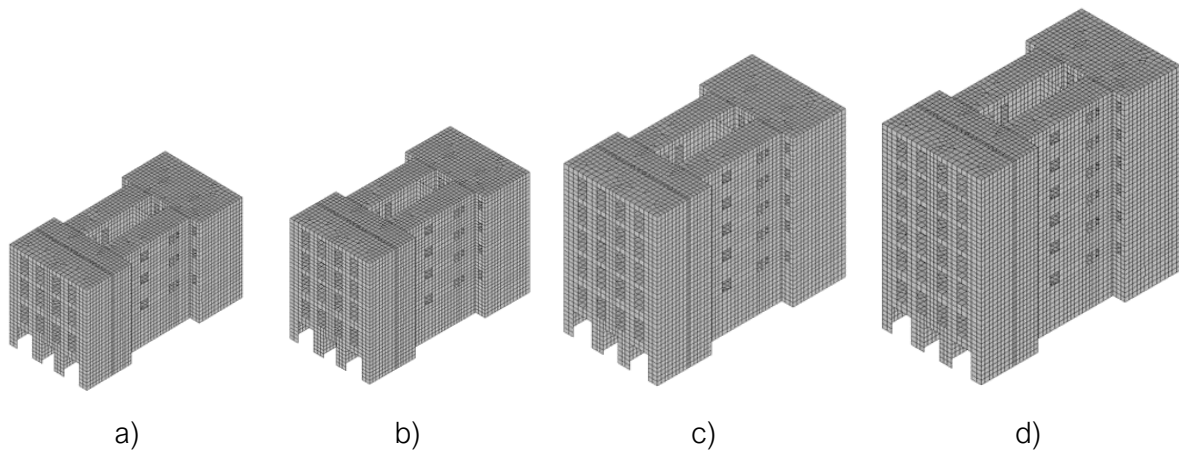


Figure 5.13 - Numerical models with different number of storeys: a) Building with three storeys (GF+3); b) Building with four storeys (GF+4); c) Building with five storeys (GF+5); d) Building with six storeys (GF+6).

5.3.2. Vertical extensions so-called "remuntes"

The vertical extensions are considered as another significant parameter implemented in the building taxonomy (presented in Chapter 4), which can impact the seismic performance of existing URM buildings in the *Eixample* district. The numerical modelling of this structural parameter is considered as part of the vulnerability assessment, since it results in structural irregularities both in height and in plan configuration. Eccentricities and a concentration of loads on the rear façade were caused by new additional façades, which are not in alignment with the existing ones of the original structure. Furthermore, the juxtaposition of dissimilar materials and elements of varying stiffness could compromise the overall structural regularity of the structure.

Three different types of vertical extensions have been chosen as the most recurrent combinations found in the existing URM buildings of the *Eixample* district, which have been presented and defined in Chapter 4 section 4.2.4. The main differences between the three typologies is the number of additional storeys, the homogeneity of the façade, front façade alignment (aligned or retracted), the construction period and used materials. The nomenclature of the defined numerical models is the following: Type A - totally aligned façades of the additional storey; Type B - one aligned and another retracted additional storey; and Type C - one aligned and two additional retracted storeys. Figure 5.14 shows real case examples of the geometric configurations of the vertical extensions.

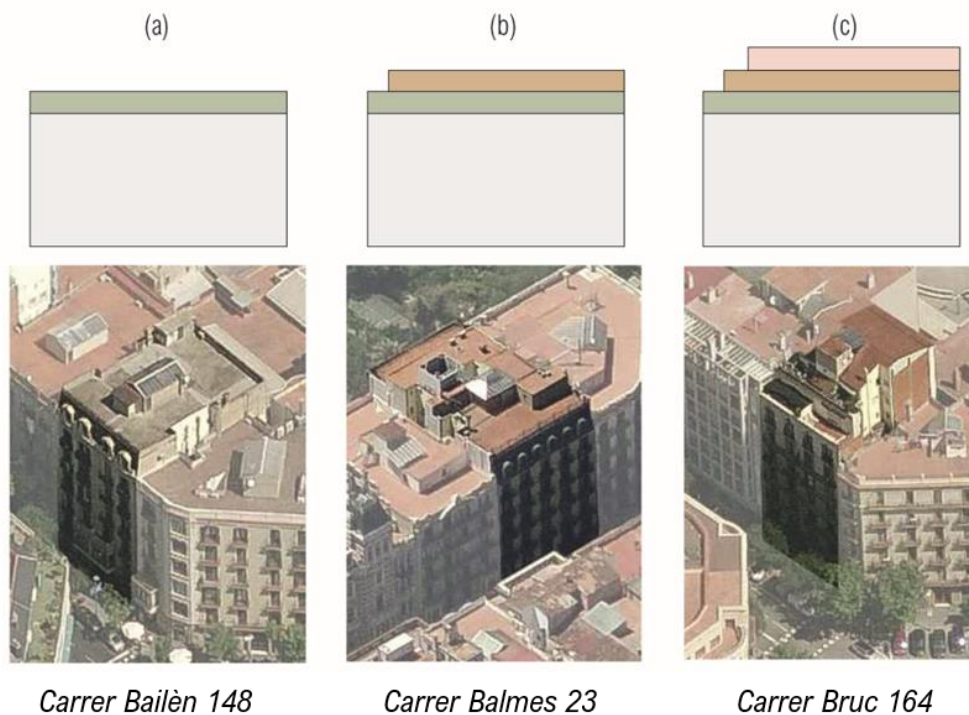


Figure 5.14 - Existing buildings from the *Eixample* district with the most recurrent typologies of vertical extensions (*remuntes*): (a) type A), (b) type B and (c) type C (adapted from Colom, 2014).

The attic for type B and the penthouse for type C are the two out of the three configurations that feature additionally retracted floors (see Figure 5.14). To comply with the ordinances, the retracted alignment had to be positioned so that the top corner of the front façade was aligned at 45° with the top corner of the storey immediately below, as already discussed in Chapter 3. The same requirement applied to the floors that were added on top of the attic, resulting in confined areas with only a single room apartment.

The configurations previously defined do not refer to specific existing buildings in the district. They are contemplated as representative variations of vertical extensions applied to the reference building model. Figure 5.15 shows the geometrical configuration of the numerical models herein considered. The reference model has the same structural configuration as the most recurrent building typology with a rectangular shape plan of 14 x 22 m². For a total height of 19,5 m, or a six-story existing building, the ground floor is 4 m high, the mezzanine floor is 3,5 m high, and the

top four storeys are 3 m high. The structural composition of the reference model is the same as explained in section 5.2.1.1.

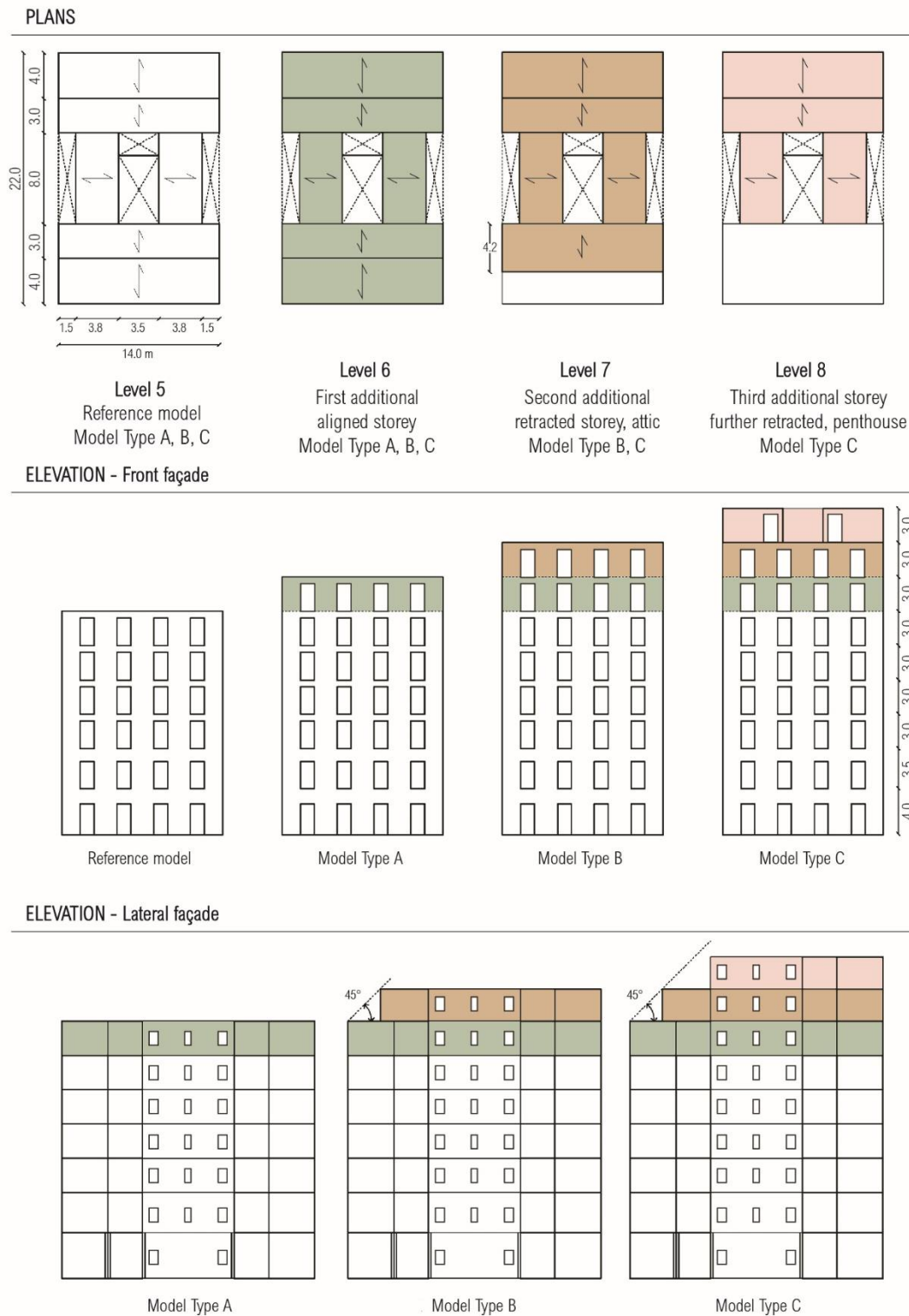


Figure 5.15 - Schematic plans (top) and transversal (middle) and longitudinal (bottom) elevations of all four models, Reference and types A, B, C. The longitudinal elevation of the Reference model corresponds to the white portion of all three models (bottom row) (adapted from Marafini et al., 2022).

Models A, B, and C have been defined with the reference model as a base plus vertical extensions. The additional storey of the model type A is designed in the same way as the reference model's last storey level. For types B and C, the front façade of the attic storey is moved back by 3 m, but the original rear façade is maintained. The vertical extensions cause asymmetries in the volumetric distribution in height as well as the loading conditions along the X axis (parallel to the façade). In terms of symmetry, the Y axis remains unchanged (see the elevations in Figure 5.15). Figure 5.16 illustrates an axonometric view of the plan configuration of the reference model with the different types of vertical extensions presented in different colours.

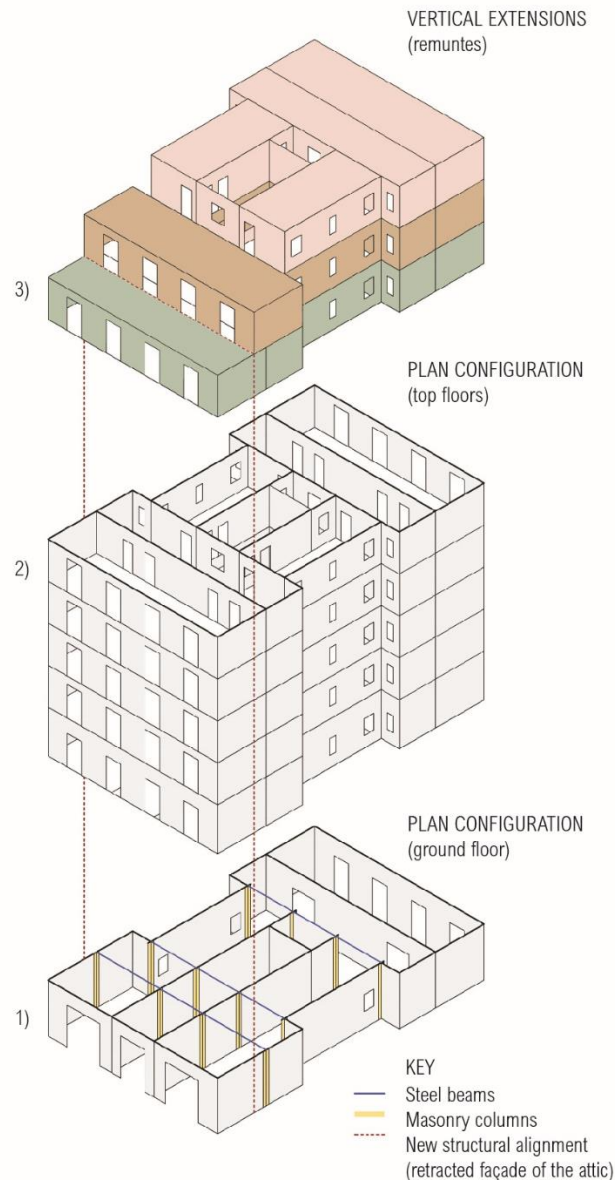


Figure 5.16 - Plan configuration of the reference model with the vertical extensions added in the models type A, B, and C (represented in blue, green and yellow, respectively). In the axonometric view, the URM building is divided into three structural units: 1) The vertical extensions-remuntes, 2) The upper floors, which vary in number but all feature a recurring plan configuration and elevation, and 3) The ground level, which has external linear structural elements and beams in place of the interior load-bearing walls. The red

line refers to the changed structural alignment generated by the retracted façade of type B and type C (adapted from Marafini et al., 2022).

Figure 5.17 illustrates the four 3D FE models: a) Reference model b) type A, c) type B and d) type C. The same quadratic shell and beam elements with an average size of 0.5 m have been used for all the models. The four FE models consist of a number of elements ranging from 21.450 to 30.017 (number of nodes 52.359 to 73.206).

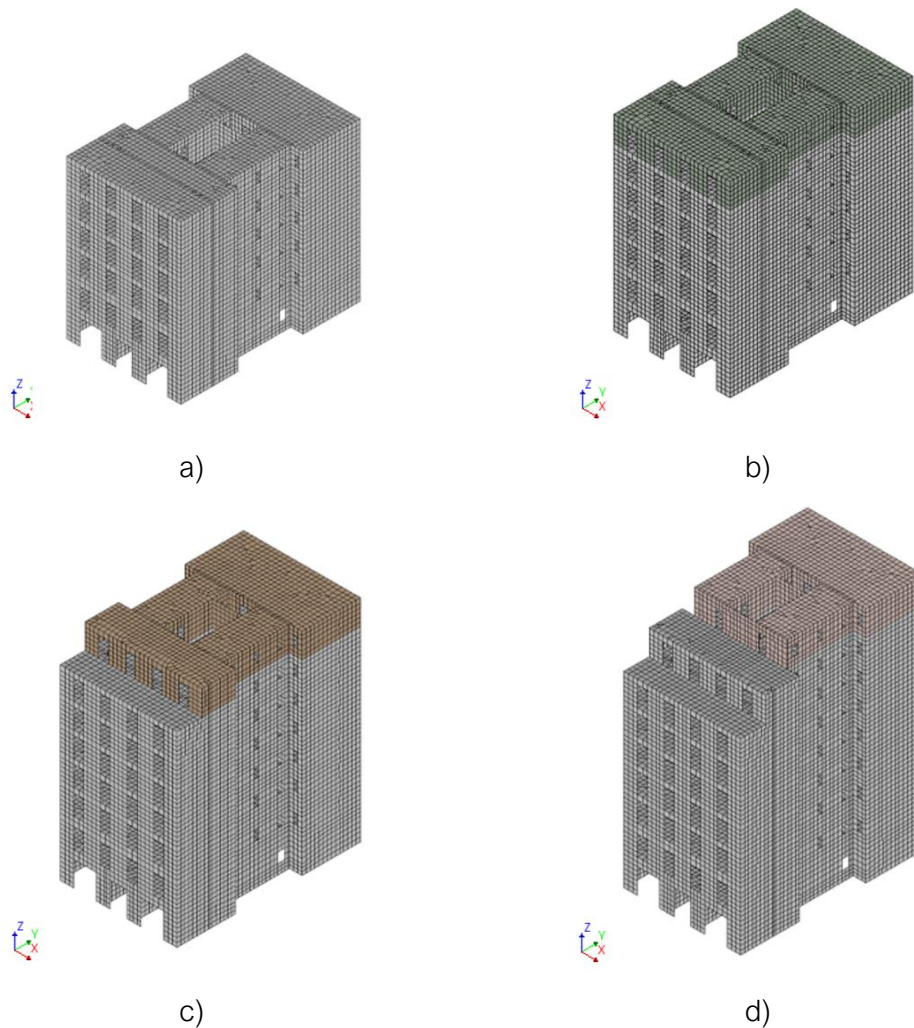


Figure 5.17 - Finite element models of the most common building typology and the three variations developed: a) Reference model b) type A, c) type B and d) type C.

The loads and material properties have been applied as explained beforehand for the reference building model (see Section 5.2.2). Different materials were used depending on the construction period of the additional storeys. Since the retracted *remuntes* date from the second half of the 20th century, the load-bearing walls were no longer built with solid brickwork. From the outside to the inside, they presented a multilayer configuration consisting of a layer of ceramic hollow bricks, a cavity, and a layer of solid brick. Therefore, ceramic hollow bricks have been used as a different material for the vertical extensions of the models type B and C. The properties have been established using historical normative values for the compressive strength (Instituto de la Construcción y del Cemento 'Eduardo Torroja', 1970) and proportional values for the Young's

modulus and the tensile strength. The compressive fracture energy and the tensile fracture energy have been defined using the suitable analytical formulations, using equations (5.7) and (5.8) ('CEB-FIP MODEL CODE 1990', 1993). Table 5.10 presents the material properties used for the solid brick masonry walls, which are the same as the ones in the reference model, and the properties for the vertical extensions made of ceramic hollow bricks.

Table 5.10 - Material properties used for the additional storeys.

Material properties for the numerical models		
Solid brick masonry walls		
Young's modulus - E	1800	MPa
Poisson's ratio	0,2	[]
Mass density	1800	kg/m ³
Compressive strength - f_c	4	MPa
Compressive fracture energy - G_f^c	6400	N/m
Tensile strength - f_t	0,08	MPa
Tensile fracture energy - G_f^t	50	N/m
Ceramic hollow blocks masonry walls		
Young's modulus - E	900	MPa
Poisson's ratio	0,2	[]
Mass density	1500	kg/m ³
Compressive strength - f_c	2	MPa
Compressive fracture energy - G_f^c	3200	N/m
Tensile strength - f_t	0,1	MPa
Tensile fracture energy - G_f^t	8,1	N/m

The original flooring system of steel beams and ceramic vaults was only used in the aligned typologies. Following its widespread use for the creation of floor slabs, reinforced concrete was used later. The floors in all the numerical models have been modelled as one-way jack-arch floor systems assigning the appropriate in-plane stiffness as explained in the section 5.2.3.

5.3.3. Range of variations of material properties

The mechanical properties of unreinforced masonry have been extensively researched and experimentally characterized in previous studies. The variation of the masonry's material properties has been done regarding the compressive strength as it is one of the most influential parameters that represents its mechanical behaviour of as a composite material. Three numerical models have been determined for the range of variation of the material properties of the unreinforced masonry walls, where the geometrical configuration and material properties of the

other structural elements have been considered to be the same as the ones in the reference building model.

As described in Chapter 3 (section 3.8), the results that were obtained from different experimental campaigns done on historical existing buildings show a variation of the compressive strength from 2.15 to 13.04 MPa. According to the Italian standard (MIT Ministero delle Infrastrutture e del Trasporti, 2019), the compressive strength can vary between 2.6 and 4.3 MPa for this specific type of regular masonry composed of handmade bricks and lime mortar with density of 1800 kg/m³. Hence, three specific values of the compressive strength have been decided as 2, 3 and 5 MPa, being $f_c=4$ MPa for the reference model, according to the values obtained from the previously explained experimental campaigns (section 3.8). The values of the Young's modulus and the Poisson's ratio have been maintained as the ones for the reference model. The same criterion and assumptions explained for the reference model in section 5.2.2 have been used to derive proportionally the compressive and tensile parameters. Table 5.11 provides all the input values of the three models, together with the reference one, for the mechanical characteristics of the unreinforced masonry walls.

Table 5.11 - Material properties of the unreinforced masonry walls used for the four numerical models.

Material properties	Model 1	Model 2	Reference model	Model 3
Young's modulus (MPa)	1800	1800	1800	1800
Poisson's ratio	0.2	0.2	0.2	0.2
Mass density (kg/m ³)	1800	1800	1800	1800
Compressive strength (MPa)	2.0	3.0	4.0	5.0
Compressive fracture energy (N/m)	3200	4800	6400	8000
Tensile strength (MPa)	0.04	0.06	0.08	0.1
Tensile fracture energy (N/m)	30	40	50	60

5.3.4. Thickness variation

The overall stability of the structure may be impacted by the variation of thickness for the outer façade and lateral masonry walls on the ground level of the building in comparison to the above storeys. In the literature, different thicknesses have been found for these load-bearing walls from 0.60 to 0.15 m, with possible reduction of the walls' thickness along their height. Therefore, another numerical model has been developed by changing the thickness of load bearing masonry walls at the ground. The thickness of the façade walls at the ground floor has been assumed to be 0.45 m and 0.30 m for the load bearing lateral walls. The rest of the masonry walls have the same geometrical properties as previously discussed.

5.3.5. Horizontal diaphragms

The horizontal diaphragms play an important role in transferring lateral seismic loads to the structure's vertical resisting elements, such as walls and pillars. They can have an impact on the structural behaviour of buildings during seismic events, both in terms of mass and stiffness. As a result, the seismic performance of URM structures may be significantly influenced by the flexibility of the floors. As previously mentioned in Chapter 4, the floor systems can be differentiated as flexible, semi-flexible and rigid, depending on their stiffness and distribution of the lateral loads to the resisting vertical elements. Hence, different horizontal diaphragms considering their in-plane stiffness have been defined such as (see Figure 5.18) flexible floor system (timber beams and wooden planks); semi-flexible floor system (timber/steel beams and ceramic tile vaults) and rigid floor system (reinforced concrete slab and floor slab with ceramic blocks and a compressive layer of concrete).

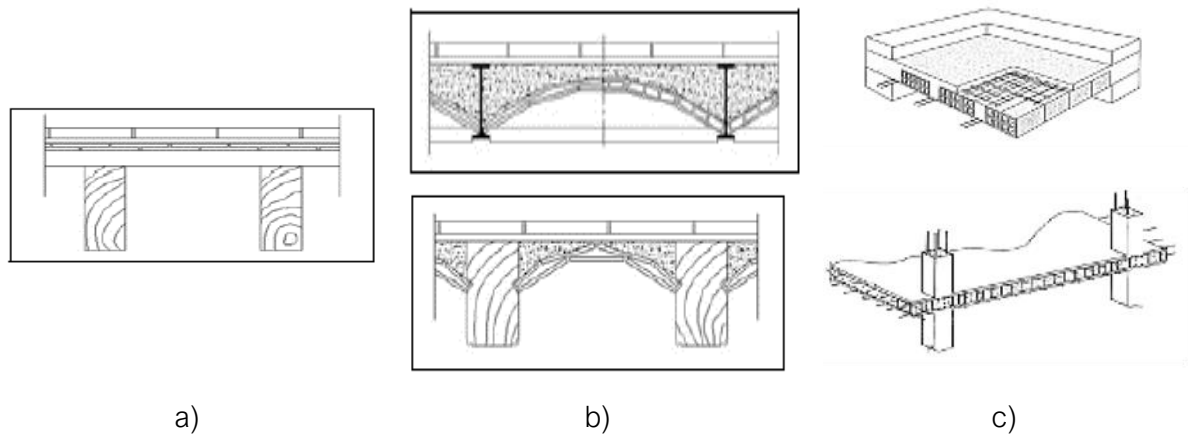


Figure 5.18 - Different horizontal diaphragms considering their in-plane stiffness: a) flexible floor system (timber beams and wooden planks); b) semi-flexible floor system (timber/steel beams and ceramic tile vaults) and c) rigid floor system (reinforced concrete slab/ floor slab with ceramic blocks and a compressive layer of concrete).

The material properties such as the elastic and shear modulus are the ones that define the in-plane stiffness of the horizontal diaphragms. The numerical procedure explained in section 5.2.3, which was used to compute the material properties of the jack arch floors, has been considered for the numerical modelling of the flexible diaphragm composed of timber beams and wooden planks. The rigid diaphragm, depending on its weight, has been defined as a weighted reinforced concrete slab and a light floor slab of ceramic reinforced blocks and concrete topping.

Table 5.12 presents the elastic properties used for the modelling of the different horizontal diaphragms regarding their in-plane stiffness.

Table 5.12 - Elastic properties for the modelling of the different horizontal diaphragms.

Elastic properties		
Flexible floor - timber beams and wooden planks		
E_x (perpendicular to the beams)	75	MPa
E_y (parallel to the beams)	5000	MPa
$G_{xy\perp}$ (perpendicular to the beams)	25	MPa
$G_{xy\parallel}$ (parallel to the beams)	30	MPa
ν_{xy}	0.07	[-]
Semi-flexible floor - steel beams and ceramic tile vaults		
E_x (perpendicular to the beams)	1000	MPa
E_y (parallel to the beams)	7800	MPa
$G_{xy\perp}$ (perpendicular to the beams)	27	MPa
$G_{xy\parallel}$ (parallel to the beams)	110	MPa
ν_{xy}	0.06	[-]
Semi-flexible floor - timber beams and ceramic tile vaults		
E_x (perpendicular to the beams)	1100	MPa
E_y (parallel to the beams)	4000	MPa
$G_{xy\perp}$ (perpendicular to the beams)	27	MPa
$G_{xy\parallel}$ (parallel to the beams)	46	MPa
ν_{xy}	0.10	[-]
Rigid light floor - hollow concrete slab with ceramic blocks and concrete topping.		
E_x (perpendicular to the T section)	30000	MPa
E_y (parallel to the T section)	54000	MPa
G_{xy}	12500	MPa
ν_{xy}	0.15	[-]
Rigid weighted floor - reinforced concrete slab		
E - Young modulus	30000	MPa
ν - Poisson's ratio	0.2	[-]
Density	2400	kg/m ³

The self-weight load of the floor structural systems has been considered following the suggestions of the specific standard for rehabilitation and structural works on floor systems of residential buildings NRE-AEOR-93 (ITEC, 1994) (see Table 5.13).

Table 5.13 - Self-weight loads used in the numerical models for the different floor systems.

Load	[kg/m ²]
Flexible floor (timer beams and wooden planks)	70
Semi-flexible floor (steel beams and masonry vaults)	250
Semi-flexible floor (timber beams and masonry vaults)	127
Rigid light floor (reinforced ceramic blocks with concrete topping)	200
Rigid weighted floor (reinforced concrete slab)	300

5.3.6. Façade openings on the ground floor

As previously indicated in Chapter 4, the number and size of openings in a structure's facades significantly affects the load capacity of its load-bearing walls, and a greater percentage of openings on the ground floor weakens the facade's stability against overturning collapse mechanisms. Façade openings can often reduce the in-plane resistance of the masonry resistant walls. The size of the openings and their misalignment, can influence the collapse mechanisms either in the plane of the wall or out of the plane.

Two numerical models have also been created with altered façade openings on the front and back façades of the ground floor. As a result, when compared to the reference model, one model has greater openings while the other one has smaller openings. Figure 5.19 and Figure 5.20 show the updated geometry of the ground floor façades for the two numerical models with smaller and bigger openings. The front façade has three bigger openings on the ground floor of which the middle one is the entrance in the residential building and the two other openings are the entrances to different commercial stores or restaurants. The openings at the back façade can vary in size and number since it mainly depends on the commercial activities that take place at the buildings' ground floor.

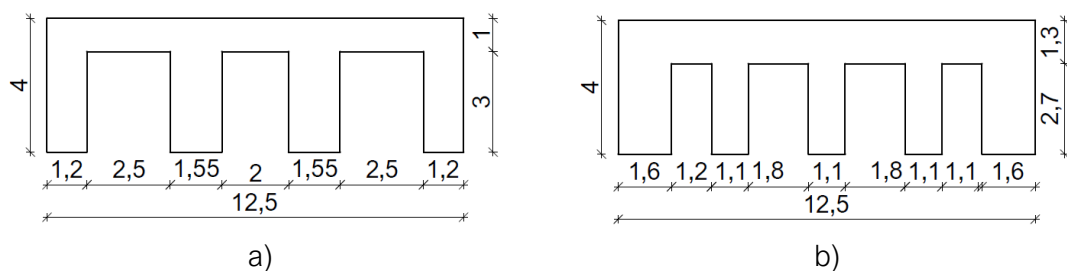


Figure 5.19 - Geometry of the ground floor façade openings of the reference model: a) front façade and b) rear façade.

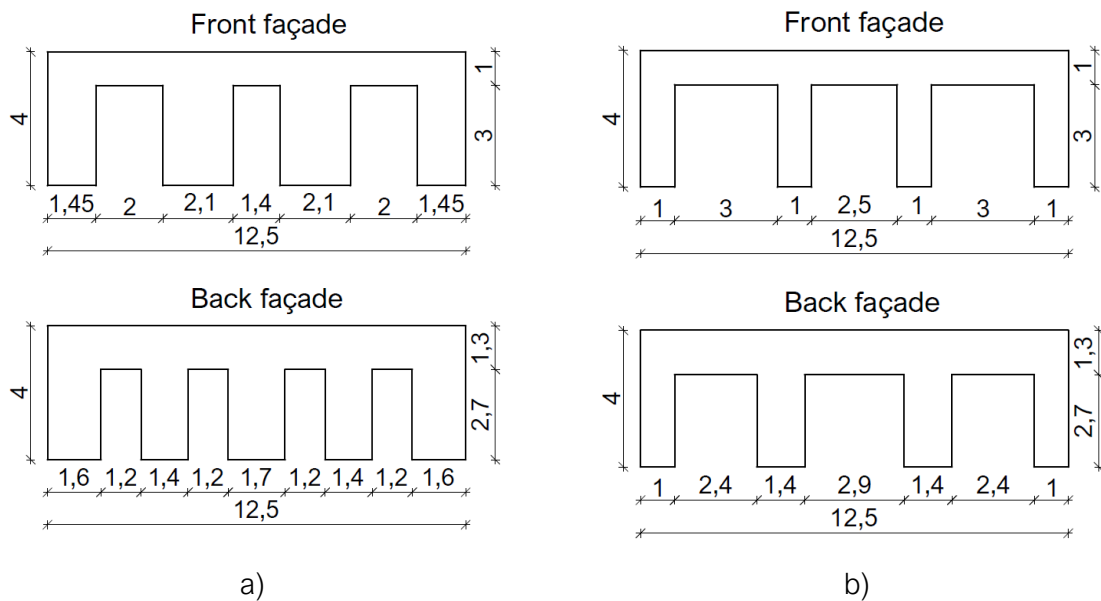


Figure 5.20 - Geometry of the ground floor façade openings of the two numerical models: a) Smaller façade openings and b) Bigger façade openings.

Table 5.14 provides a description of the proposed percentage values for the further models under analysis. A difference of 9 - 10% of the façade openings at the ground floor between all numerical models has been considered for the analysis. For a better comparison of the results, all other geometrical and mechanical properties for each structural element in the comparative models have been remained constant with those used in the reference building model, which have been described in section 5.2.2.

Table 5.14 - Size of the ground floor façade openings in the numerical models.

Numerical models	Total area of the ground floor façades (m ²)	Area of the openings of the ground floor front façade (m ²)	Area of the openings of the ground floor rear façade (m ²)	Ground floor openings (%)
Reference model	100	21.00	16.20	37%
Smaller openings	100	25.50	20.79	47%
Bigger openings	100	16.20	12.96	28%

These numerical models have been used for the definition and calibration of the parameter evaluating the percentage difference of the façade openings for the vulnerability assessment of the existing buildings in the *Eixample* district. All parameters of the new proposed forms for the vulnerability assessment of the existing masonry buildings are explained specifically in the Chapter 7.

5.4. REPRESENTATIVE BUILDING TYPOLOGIES WITH DIFFERENT GEOMETRICAL PLAN CONFIGURATIONS

In Chapter 4, the most representative building typologies have been defined by a detailed analysis of the statistical data available for each subtype. Following an evaluation of the frequency distribution of each of the parameters regarding the geometrical configurations such as the buildings' width and depth, specific existing buildings with the most common values of the studied parameters have been chosen.

The second most recurrent building typology has a central part type 1a (see Figure 4.22), consisting of a central core (staircase + patios), with continuity in the lateral load-bearing walls. This building typology accounts for approximately 30% of the studied wide rectangular buildings with various central core structural configurations. The chosen existing building was built in 1913 and is located on *Vilamarí Street* in the neighbourhood of *La Nova Esquerra de l'Eixample* of Barcelona. This representative six storey building has a rectangular shape with plan dimensions of 9.2 x 24.6 m². For comparison purposes, the height of this building model as well with the other ones has been assumed to be the same as the most representative building with a total of 19.5 m, since this is the most common height found in these existing masonry buildings. The load-bearing walls' thicknesses, as well as the masonry columns dimensions are the same as in the reference building. The geometry of the front façade is composed of three bigger openings for the ground floor (2.0 x 3.0 m²) and three smaller ones (1.2 x 2.4 m²) for the rest of the floor levels. Figure 5.21 illustrates the geometrical configuration plan and 3D model of the representative building with a central staircase box and interior patio.

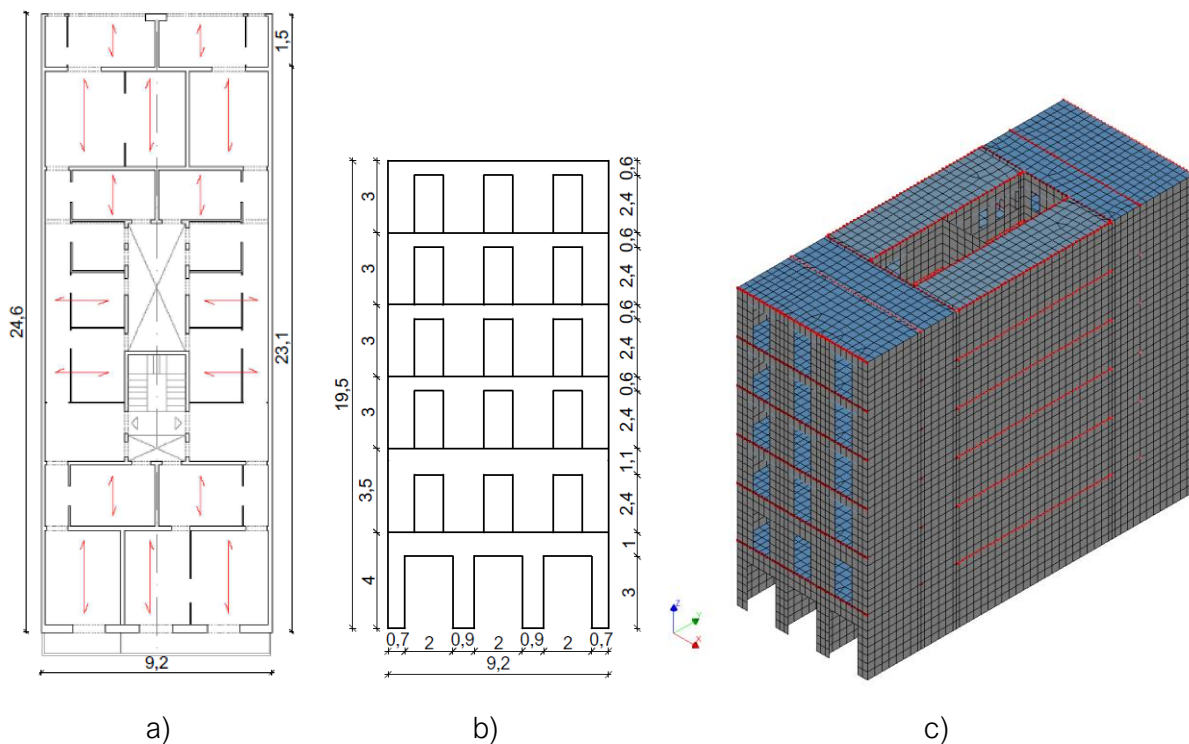


Figure 5.21 - Geometrical configuration of a representative narrow building model with central core without lateral patios (in metres): a) Floor plan section; b) Front façade geometry; c) 3D finite element model.

since the ground floor is composed of masonry columns, cast-iron pillars and steel beams in order to have that larger open space. The front façade has two openings on each storey, where the ones on the ground floor are bigger with dimensions of $2.0 \times 3.0 \text{ m}^2$, since they are the entrance to the residential building and to a commercial store as well.

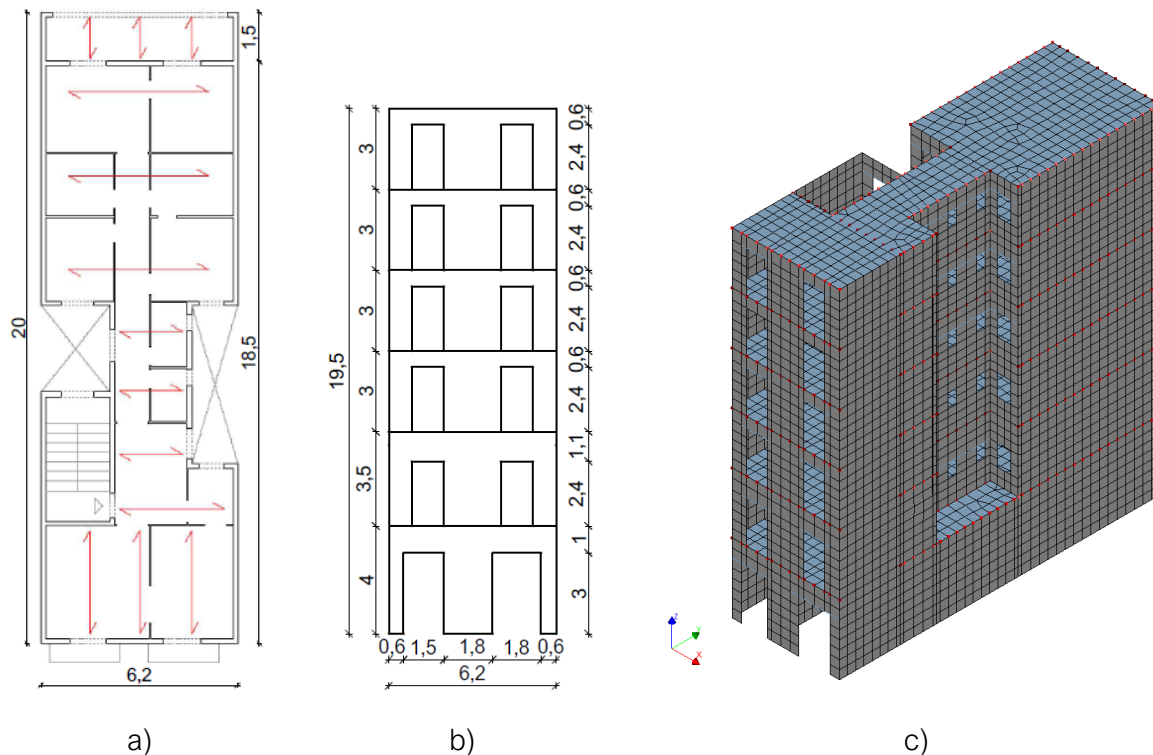


Figure 5.23 - Geometrical configuration of a representative narrow building model with lateral staircase and patios (in metres): a) Floor plan section; b) Front façade geometry; c) 3D finite element model.

Finally, a summary with information regarding the different building types, number of storeys and plan dimensions has been presented. Table 5.15 shows this summary information of all the FE models of the representative building typologies of the *Eixample* district. A total of 23 FE models have been developed for this research study. The first model is the reference one as the most recurrent building typology found in the *Eixample* district according to the statistical data presented in Chapter 4. The second hybrid model consists of a different structural system at the ground floor of the reference URM building model. The following developed numerical models represent the variations of different parameters in the reference model that mostly influence the structures' seismic performance such as the number of storeys, presence of vertical extensions, material properties, thickness variation, horizontal diaphragms, and façade openings. The last four models are the representative buildings with different plan configurations, defined in Chapter 4.

Table 5.15 - Summary information of all the numerical models of the representative Eixample buildings.

Model	Building type	Number of storeys ⁸	Dimensions	
			Width [m]	Depth [m]
Model 1	Reference model - Band building with URM walls and one-way floor slabs (steel beams and tile vaults)	GF+5	12.5	25.2
Model 2	Hybrid model - Band building with URM walls and steel frame on the GF, one-way floor slabs (steel beams and tile vaults)	GF+5	12.5	25.2
Model 3	Band building with URM walls and one-way floor slabs (steel beams and tile vaults)	GF+3	12.5	25.2
Model 4	Band building with URM walls and one-way floor slabs (steel beams and tile vaults)	GF+4	12.5	25.2
Model 5	Band building with URM walls and one-way floor slabs (steel beams and tile vaults)	GF+6	12.5	25.2
Model 6	Reference model - Band building with URM walls, one-way floors (steel beams and tile vaults), without vertical extensions	GF+5	14	22
Model 7	Band building with URM walls, one-way floors (steel beams and tile vaults), with one vertical extension - Type A	GF+5+R	14	22
Model 8	Band building with URM walls, one-way floors (steel beams and tile vaults), with two vertical extension - Type B	GF+5+2R	14	22
Model 9	Band building with URM walls, one-way floors (steel beams and tile vaults), with three vertical extension - Type C	GF+5+3R	14	22
Model 10	Band building with URM walls, one-way floors (steel beams and tile vaults), with low compressive strength (2 MPa)	GF+5	12.5	25.2
Model 11	Band building with URM walls, one-way floors (steel beams and tile vaults), with average compressive strength (3 MPa)	GF+5	12.5	25.2
Model 12	Band building with URM walls, one-way floors (steel beams and tile vaults), with greater compressive strength (5 MPa)	GF+5	12.5	25.2
Model 13	Band building with URM walls, one-way floors (steel beams and tile vaults), with varying wall thickness	GF+5	12.5	25.2
Model 14	Band building with URM walls, with flexible floor (timber beams and planks)	GF+5	12.5	25.2
Model 15	Band building with URM walls, with semi-flexible one-way floor (timber beams and tile vaults)	GF+5	12.5	25.2
Model 16	Band building with URM walls, with rigid light floor (ceramic reinforced blocks and concrete topping)	GF+5	12.5	25.2
Model 17	Band building with URM walls, with rigid weighted floor (reinforced concrete floor)	GF+5	12.5	25.2
Model 18	Band building with URM walls, one-way floors (steel beams and tile vaults) with smaller façade openings	GF+5	12.5	25.2
Model 19	Band building with URM walls, one-way floors (steel beams and tile vaults) with greater façade openings	GF+5	12.5	25.2
Model 20	Band narrow building with URM walls, one-way floors (steel beams and tile vaults), without lateral patios	GF+5	9.2	24.6
Model 21	Band wide building with URM walls, one-way floors (steel beams and tile vaults), with two lateral patios	GF+5	12.9	24
Model 22	Band narrow building with URM walls, one-way floors (steel beams and tile vaults), with lateral staircase and patio	GF+5	6.2	18.5

⁸ GF - ground floor, R - vertical extensions (*remuntes*)

5.5. SUMMARY

Numerical simulation methods are a very useful tool in order to better understand the seismic behaviour of a specific existing masonry structures. This chapter elaborates and discusses the numerical modelling of the buildings of the *Eixample* district chosen as more representative for the purpose of the seismic vulnerability analysis. The continuum Finite Element (FE) approach has been adopted for the numerical simulation of the seismic response of the existing unreinforced buildings using the software DIANA-FEA. This contributes to a better understanding of the seismic behaviour and collapse mechanisms of unreinforced masonry buildings with varying structural system, materials, geometrical configuration and structural elements.

The numerical models have been defined according to the previously described building taxonomy and the statistical extrapolation data of the existing *Eixample* buildings. Therefore, the most recurrent building typology has been chosen as a reference one, by representing the two different structural systems: homogeneous system with slender URM walls and a hybrid system with steel frames at the ground floor and URM walls on the upper storeys. The numerical modelling of all the structural elements has been defined with a detailed description of the material properties and loads applied. The numerical procedure for the modelling of the in-plane stiffness of the one-way jack arch floor system, which is the most typical one for the *Eixample* existing buildings, has been established by providing indicative values for the proper modelling of these particular floor slabs. Moreover, this methodology can be applicable for the numerical simulation of any other one-way floor system.

Additionally, several numerical models have been developed by implementing the variations of the parameters that significantly influence the buildings' seismic performance and vulnerability. The number of storeys, presence of vertical extensions, different material properties, masonry walls' thickness variation, horizontal diaphragms, façade openings are the chosen parameters that mostly affect the seismic capacity of the structures and thus, their variations have been implemented in the numerical models. Accordingly, for each parameter a few numerical models by modifying the reference model have been prepared in order to represent the most recurrent variations. Moreover, numerical models of existing buildings with different geometrical plan configurations have been described, which have been selected according to the methodology proposed in Chapter 4. A brief description of the geometrical and structural characteristics of all the numerical models is given. These FE models will be used for the definition and classification of the seismic vulnerability classes for the most significant parameters in the Vulnerability Index Method.

CHAPTER 6. SEISMIC ANALYSIS OF REPRESENTATIVE BUILDINGS IN THE *EIXAMPLE* DISTRICT

6.1. INTRODUCTION

Nonlinear static procedures, also known as pushover analysis (NSP), are commonly used to assess the seismic performance of masonry existing buildings (Pelà et al. 2009, Lourenço et al. 2011, Lagomarsino et al. 2013). Numerous types of nonlinear static procedures have been developed and widely used for seismic analysis (as aforementioned in chapter 2), as a simplified alternative to nonlinear dynamic analysis. The N2 method proposed by Fajfar (2000) is one of the procedures used to determine the target displacement of the investigated building using nonlinear pushover analysis. The applicability and reliability of nonlinear static procedures on URM structures are still being questioned and discussed in the scientific community, particularly when applied to high-rise and irregular structures (Marino et al., 2019), (Azizi-bondarabadi et al., 2021).

This chapter presents the seismic analysis performed on the developed numerical models of the representative buildings of the *Eixample* district. These analyses can contribute to obtain a better and quantitative understanding of the influence of the different parameters on the seismic performance of URM existing buildings. Nonlinear static analysis has been carried out using the DIANA-FEA software to estimate the maximum capacity and to determine the global failures of the building models. Mass-proportional loading distribution has been applied in the two main directions (parallel and perpendicular to the façade) of the existing buildings in order to evaluate the influence of the seismic actions. The results have been represented graphically by load-displacement capacity curves and also by indicating the relevant collapse mechanisms. Moreover, the seismic performance of all the numerical models has been evaluated through the application of the N2 method (Fajfar, 2000) by considering both deterministic and probabilistic seismic hazard. The performance point, which representing the inelastic displacement of the structure has been obtained by the intersection between the bilinear capacity curve and the demand spectrum. The obtained spectral displacements can provide information for estimating the damage of the representative existing masonry buildings.

6.2. NONLINEAR STATIC PUSHOVER ANALYSIS

The nonlinear static analysis approach has been used in various research studies in the recent years, being included in both the Eurocode 8 (EN 1998-1, 2004) and the Italian code (MIT Ministero delle Infrastrutture e del Transporti, 2019), both for structural design and seismic assessment. The NSP analysis method together with the FE macro modelling have already been widely and successfully applied to analyse the global seismic behaviour of existing masonry

structures (Betti et al., 2015), (Lourenço et al., 2011), (Ortega, 2018), (Saloustros et al., 2019), (Aşikoğlu et al., 2020). The principal objective of this type of analysis is to obtain information about a structure's global stiffness, strength, displacement capacity, and collapse mechanism when subjected to seismic action (Saloustros et al., 2020), (A. M. D'Altri et al., 2019), (Endo, Pelà, et al., 2017a), (Lagomarsino and Cattari, 2015).

Pushover analysis is a nonlinear static analysis technique in which the structure is subjected to a monotonically increasing pattern of lateral forces, which simulate a simplified distribution of seismic action, until it reaches collapse or some predetermined analysis threshold. The main purpose is to assess the structure's stiffness, global lateral strength, displacement ductility, and failure mechanisms. The nonlinear behaviour of the materials as well as the geometrical nonlinearity of the structure is considered during the analysis procedure. Subsequently, a capacity curve is generated as a relationship between the horizontal acceleration or base shear forces and the roof top displacements from the studied building. The seismic loading can be simulated by applying horizontal static forces uniformly with respect to the structure's height (mass proportional) or proportional to the main translational modal shape (mode proportional) (see Figure 2.1).

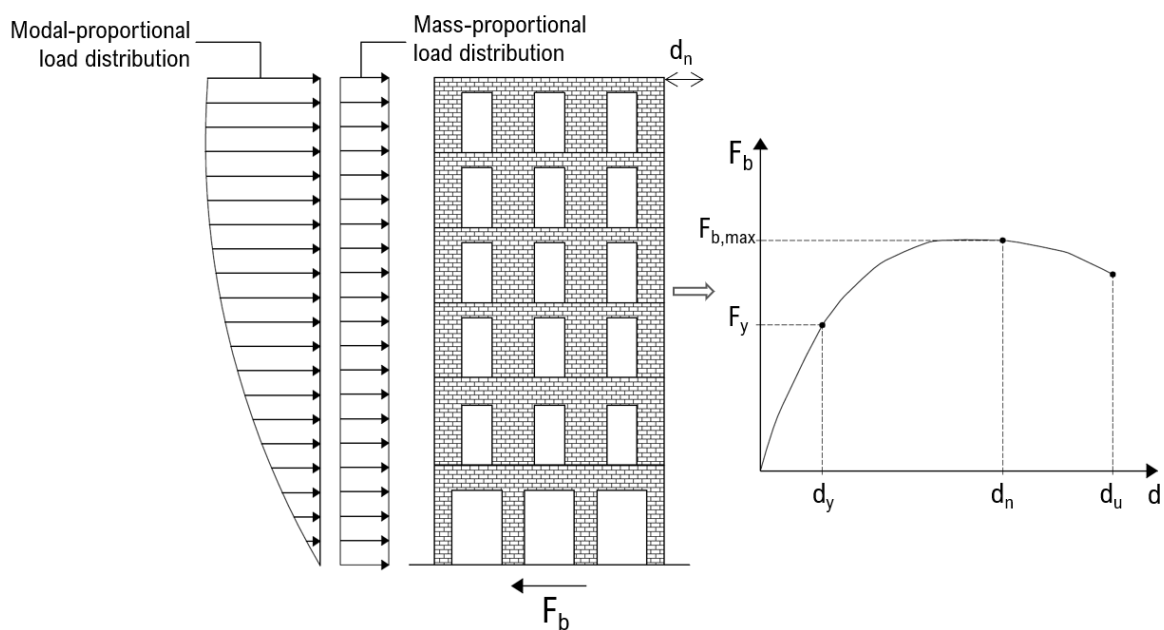


Figure 6.1 - Graphical representation of pushover analysis to an URM building with different patterns for the load distributions.

According to Lourenço et al. (2011) the mass proportional load pattern can be used for the seismic assessment of existing masonry buildings without box behaviour. As a result, a nonlinear force-displacement curve for each loading direction is generated, so-called pushover capacity curve, which shows the progression of base shear force against displacement of a control point (at the roof top). The form of the capacity curve represents the structure's global seismic behaviour and it is determined by the formation of cracks and failure mechanisms that occur in the analysed structure.

Pushover analysis is an effective method to evaluate the structure's seismic behaviour since it requires less computational time than other, more complex nonlinear dynamic analysis. Despite its limitations, this type of analysis can give insights into the seismic capacity and the expected damage, as well as identifying the most vulnerable parts of the structure (Saloustros et al., 2019). Hence, pushover analyses have been performed to all the previously described FE models using the software DIANA-FEA (DIANA FEA BV, 2020), with the purpose of obtaining information on the seismic capacity of the existing URM buildings of the *Eixample* district and their variations according to the previously specified building taxonomy.

6.2.1. Seismic behaviour of the representative buildings in form of capacity curves

Pushover analyses have been carried out on all numerical models (previously described in Chapter 5). The seismic analysis consisted of applying horizontal loads in two directions: parallel to the façade (X-direction) and perpendicular to the façade (Y-direction). A mass equivalent distribution has been used to simulate the horizontal loads of a possible earthquake. The adopted methodology consisted of two steps: first, the application of self-weight, and second, the gradual increase of horizontal seismic forces proportional to the structure's mass.

A Newton-Raphson regular iteration method has been used for solving the nonlinear system of algebraic equations, complemented with the arc-length control method. The main advantage of this method is that it has quadratic convergence, which implies that it converges to the final solution in a relatively smaller number of iterations, despite being quite time consuming and with a high computational cost. The total Lagrange formulation has been used to introduce geometrical and physical nonlinearity. The maximum number of iterations and the size of the steps in the different numerical model have been chosen depending on the seismic behaviour of the existing buildings. The convergence has been checked using the energy criteria, with a convergence tolerance of 1‰.

The response of the structure is given by the capacity curves, which represent the building's lateral load resistance versus its characteristic lateral top displacement. The presented pushover capacity curves are generated as a relationship between the load factor (base shear coefficient) or the applied horizontal acceleration and the displacements obtained at a control point. The chosen control point is normally a corner of the roof top of the numerical models, being the point with the greatest displacements. Moreover, capacity curves in terms of base shear and horizontal displacements have been presented, where the horizontal acceleration (load factor) is multiplied with the structure's self-weight.

As described in Chapter 5, several variations of different parameters selected from the specific building taxonomy have been implemented on the reference building model and thus, the influence of each parameter has been evaluated by applying nonlinear static analysis. The capacity curves of the reference model for both main directions are presented and discussed below. Moreover, they are compared with the results obtained from some of the numerical models with different parameters' variations.

Figure 6.2 represents the seismic behaviour of the reference building typology of the *Eixample* district in a form of capacity curves for both pushover loading directions, by plotting the horizontal acceleration against the top horizontal displacements. The reference FEM model presents a linear behaviour until a sudden loss of stiffness, associated with the development of a soft-storey mechanism at the ground floor for the pushover analysis in the X direction. This soft-storey mechanism does not appear in the pushover analysis in the Y direction due to the presence of the transverse shear masonry walls, which are continuous along the whole height of the building. This difference makes the studied building more vulnerable in the X direction, showing lower strength capacity, whereas a similar deformation capacity is obtained for both loading directions.

The seismic response in the X direction (parallel to the façade) differs significantly to the one in Y direction (orthogonal to the façade). The analysed existing reference building is more flexible in the loading direction parallel to the façade (X direction) due to the presence of large openings in the façades and the lack of interior walls at the ground floor parallel to the loading direction. On the contrary, the reference building presents greater stiffness in the direction perpendicular to the façade (Y-direction) due to the presence of the lateral and interior load bearing walls act as shear walls.

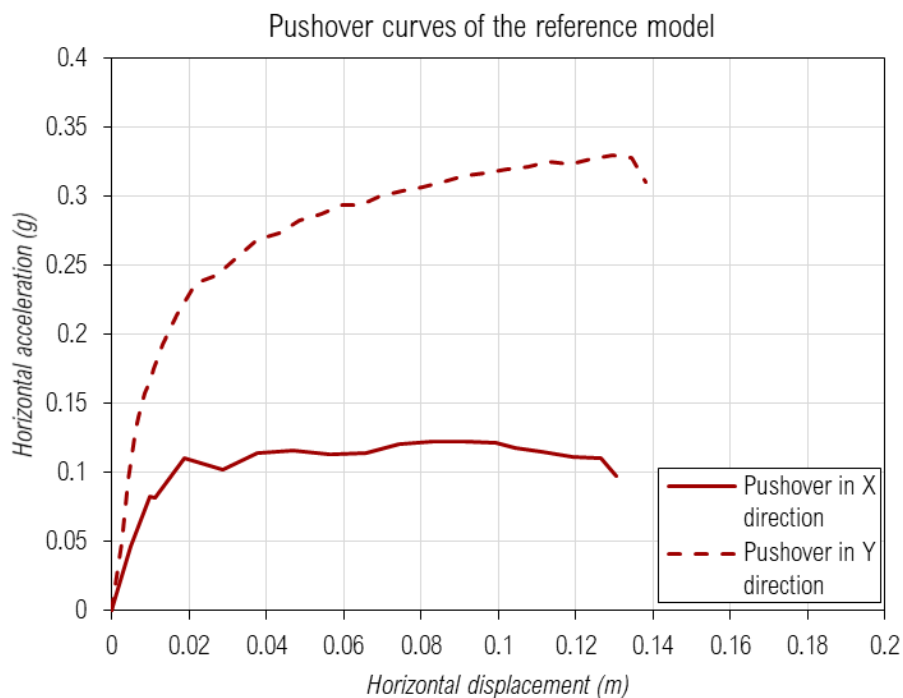


Figure 6.2 - Pushover capacity curves of the reference model for pushover in X and Y direction.

Additionally, this reference model has been compared with a hybrid structural system model with steel beams and pillars on the ground floor. Figure 6.3 presents, for the models of these two buildings, the pushover capacity curves in terms of horizontal acceleration against horizontal displacement at the roof level for both directions. As it can be observed, the substitution of the unreinforced masonry walls with slender pillars in the ground floor reduces the strength by 16.52% for a loading parallel to the façade (X direction). For a loading direction orthogonal to the façade (Y direction), the hybrid model presents a higher maximum capacity, with an increment of 3.43%. This slightly higher capacity is attributed to the continuity of the lateral walls in the hybrid building,

in which the semi-patios are part of the geometrical configuration of the ground floor. In terms of maximum displacement capacity, the hybrid model presents notably lower level of displacements in the X direction, while the results are very similar when the pushover load is applied in the Y direction.

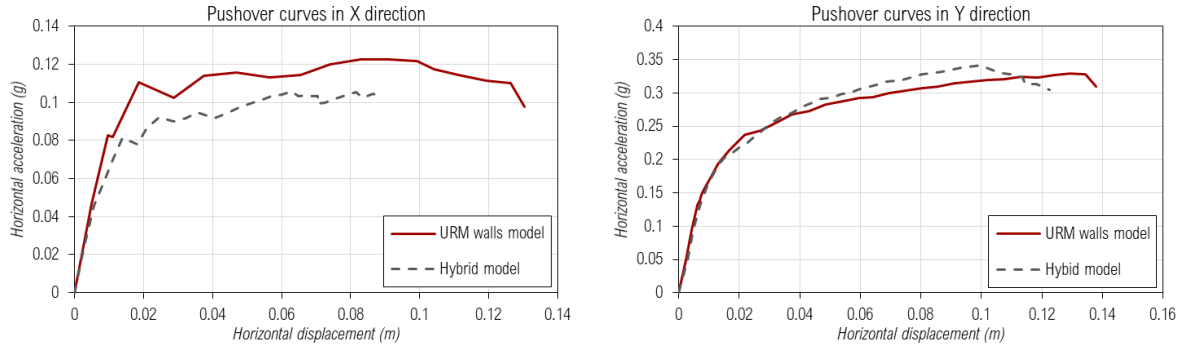


Figure 6.3 - Pushover capacity curves of the reference and hybrid model: pushover in X direction (left) and pushover in Y direction (right).

Additionally, the pushover analysis performed on the reference building model by changing the configuration of the one-way floor slab (steel/timber beams and ceramic tile vaults) is presented. Figure 6.4 shows the capacity curves of the static pushover analyses in terms of horizontal acceleration and displacement for the two analysed cases. The shape of the capacity curve is very similar for both cases. The maximum capacity in terms of the applied horizontal acceleration is very similar in both floor typologies for the pushover in the X direction. However, there is a difference of 8.3% for the maximum capacity of the pushover in the Y direction. A big difference exists in the deformation capacity, with the displacement reached at the last converged step of the analyses of the building with floors of steel beams being 33.5% and 29.5% lower than the one of timber beams for loading in X and Y directions, respectively. This shows a less ductile behaviour for the model with one-way floors of steel beams and tile ceramic vaults.

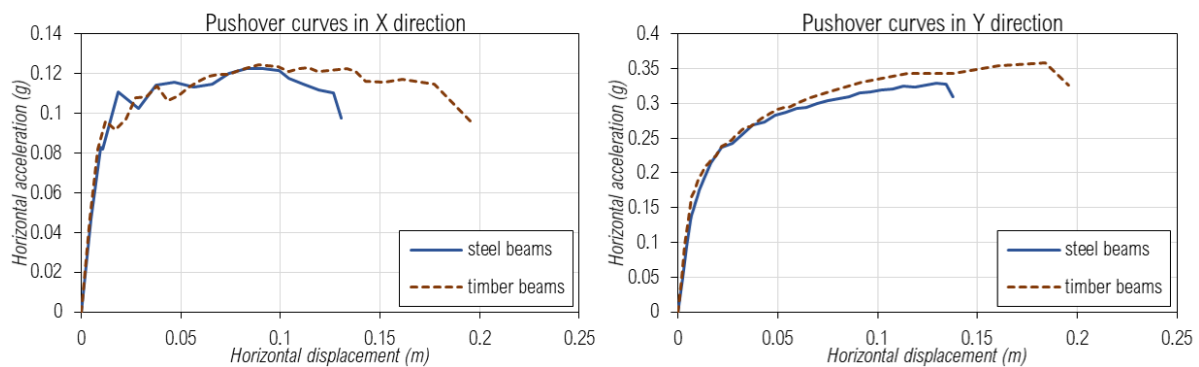


Figure 6.4 - Capacity curves of the FE reference model with the two different composite floor systems composed of steel or timber beams and tile vaults: pushover in X direction (left) and pushover in Y direction (right).

Figure 6.5 shows the capacity curves of the static pushover analyses in terms of base shear and horizontal displacement for the two floor systems with steel and timber beams, in the X and Y directions. As it can be seen from the graphs, there is no significant difference in stiffness between the two models with different floor systems. The total mass of the existing building with one-way

floors of steel beams and masonry vaults is 1,572,300 kg and 1,369,500 kg for the model with floor system of timber beams and masonry vaults. Accordingly, the base shear capacity is higher in the model with floor systems composed of steel beams and masonry vaults than the model with timber beams, due to the difference in the mass of the floor systems.

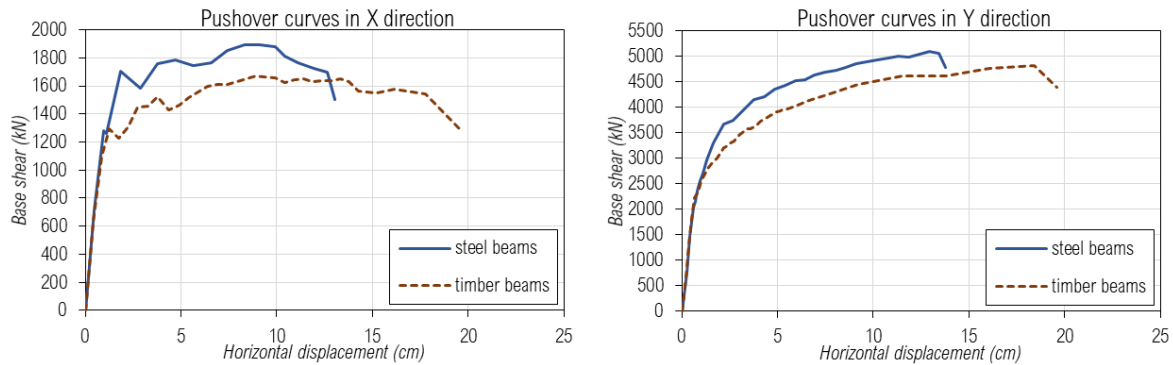


Figure 6.5 - Capacity curves in terms of base shear and horizontal displacements of the Eixample building FEM model with the two different composite floor systems composed of steel or timber beams and tile vaults: pushover in X direction (left) and pushover in Y direction (right).

A parametric analysis has been carried out to evaluate the different seismic response of the reference building by varying the number of storeys in height (changing the total height of the building). The performed pushover analysis contributes to a better understanding on how the different height of the buildings can influence the global seismic behaviour and thus, their seismic vulnerability. Figure 6.6 illustrates the capacity curves of the reference building model with a ground floor and 5 storeys (GF+5), together with the three FE models representing the variation of the number of storeys, between three and six storeys.

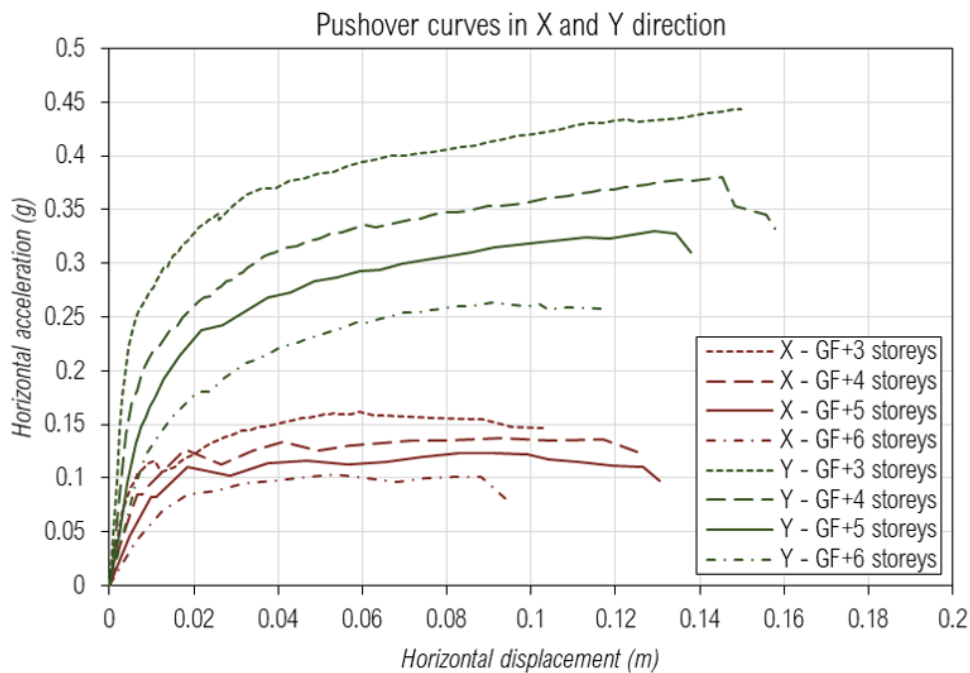


Figure 6.6 - Pushover capacity curves in terms of horizontal acceleration and displacements for the reference model and the three models with variation of number of storeys, in both X direction - parallel to the façade and Y direction - perpendicular to the façade.

As already mentioned, the difference in the horizontal stiffness observed between the X and Y axes of the building is attributed to the presence of big openings in the façades, while there is a small percentage of openings in the lateral walls and the lateral sides of the central core. As anticipated, there is a significant drop of stiffness between the model with GF+3 storeys and the one with GF+6 storeys, in both pushover loading directions. Moreover, the seismic capacity has decreased with the increase of the total number of storeys. The difference between the maximum capacity of the models of 3 and 6 storeys for the pushover loading directions parallel to the façade (X direction) and perpendicular to the façade (Y direction), is 43% and 51% respectively.

Figure 6.7 shows the obtained capacity curves describing the seismic behaviour of the numerical models with vertical extensions. The reference horizontal displacement is set up at the top right corner of the fifth floor for all analysed numerical models. As expected, the seismic response of the building differs significantly according to the pushover loading direction. By comparing the capacity curves of all analysed models, the same seismic behaviour identified for the reference model, concerning the difference between the response in the two loading directions (parallel and perpendicular to the façade), is also confirmed for the other three model variations. Furthermore, a clear decrease in terms of maximum acceleration capacity can be observed with the addition of subsequent stories (see Figure 6.7). For model types A, B and C, the reduction of capacity is of 17,6%, 26,4% and 35,5% respectively for loading parallel to the façade, and 16,1%, 29,2% and 45,8% respectively for the loading perpendicular to it.

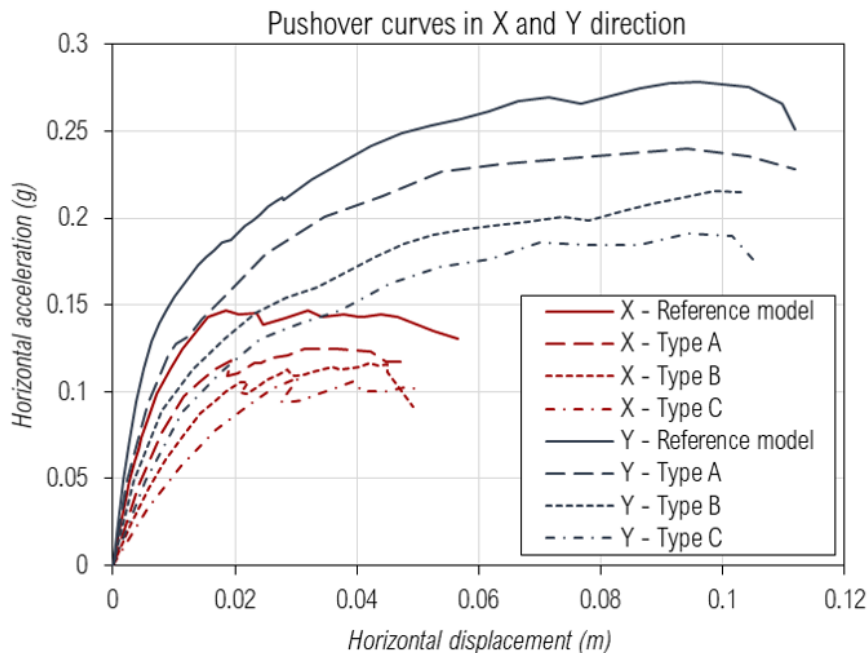


Figure 6.7 - Pushover capacity curves of the reference model and the three model variations with vertical extensions, type A, B and C, in both X direction - parallel to the façade and Y direction - perpendicular to the façade.

Figure 6.8 shows the capacity curves in terms of base shear and horizontal displacements for the reference building and the different models with vertical extensions for both X and Y direction. It is evident from the graphs that there is a noticeable difference in the displacement corresponding to the same load level among the models. The addition of one, two or three vertical extensions,

with proportional increase of load and mass, correspond to a higher level of displacement reached with each new addition. Furthermore, the additions correspond also to a slight drop in stiffness, since cracking at the lateral walls occurs earlier during the analysis.

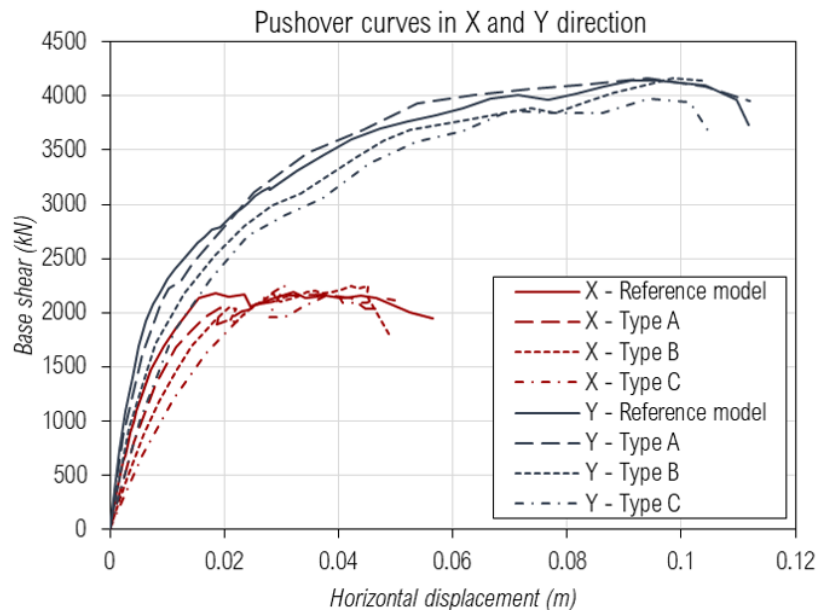


Figure 6.8 - Pushover curves in terms of base shear and horizontal displacements of the Reference model and the three model variations with vertical extensions in both directions: X direction - parallel to the façade and Y direction - perpendicular to the façade.

The capacity curves obtained for the rest of the numerical models for both pushover directions (parallel and perpendicular to the façade) are presented in the APPENDIX C. Table 6.1 shows a summary of the numerical results from the pushover analysis in X and Y direction of all the FE models, in terms of maximum acceleration capacity, corresponding value of displacement, and the ultimate displacement reached at the end of the analysis. The geometrical and structural configurations of all the numerical models was summarized in Chapter 5 (see Table 5.15).

Table 6.1 - Summary of results obtained from the pushover analyses of the representative building models.

Model	Pushover direction	Maximum acceleration capacity	Displacement (at peak) [m]	Ultimate Displacement [m]
Model 1	+ X	0.12g	0.09	0.13
	+ Y	0.32g	0.12	0.14
Model 2	+ X	0.11g	0.06	0.09
	+ Y	0.34g	0.10	0.12
Model 3	+ X	0.16g	0.11	0.12
	+ Y	0.44g	0.15	0.15
Model 4	+ X	0.14g	0.09	0.13
	+ Y	0.38g	0.15	0.16
Model 5	+ X	0.10g	0.05	0.10
	+ Y	0.26g	0.09	0.12

Table 6.1 - (Continued).

Model	Pushover direction	Maximum acceleration capacity	Displacement (at peak) [m]	Ultimate Displacement [m]
Model 6	+ X	0.15g	0.03	0.06
	+ Y	0.28g	0.10	0.11
Model 7	+ X	0.12g	0.04	0.05
	+ Y	0.24g	0.09	0.11
Model 8	+ X	0.12g	0.04	0.05
	+ Y	0.22g	0.10	0.10
Model 9	+ X	0.11g	0.03	0.05
	+ Y	0.19g	0.09	0.10
Model 10	+ X	0.07g	0.02	0.05
	+ Y	0.22g	0.04	0.05
Model 11	+ X	0.10g	0.07	0.08
	+ Y	0.29g	0.08	0.10
Model 12	+ X	0.14g	0.05	0.15
	+ Y	0.36g	0.18	0.21
Model 13	+ X	0.16g	0.08	0.10
	+ Y	0.36g	0.15	0.15
Model 14	+ X	0.11g	0.02	0.21
	+ Y	0.27g	0.14	0.16
Model 15	+ X	0.12g	0.09	0.20
	+ Y	0.36g	0.18	0.20
Model 16	+ X	0.15g	0.05	0.06
	+ Y	0.40g	0.08	0.10
Model 17	+ X	0.15g	0.03	0.05
	+ Y	0.41g	0.09	0.11
Model 18	+ X	0.13g	0.10	0.18
	+ Y	0.40g	0.10	0.16
Model 19	+ X	0.13g	0.09	0.09
	+ Y	0.22g	0.06	0.07
Model 20	+ X	0.10g	0.13	0.17
	+ Y	0.37g	0.19	0.20
Model 21	+ X	0.15g	0.06	0.07
	+ Y	0.32g	0.10	0.12
Model 22	+ X	0.12g	0.05	0.09
	+ Y	0.31g	0.11	0.13

6.2.2. Discussion of damage patterns and failure mechanisms

The damage patterns are a fundamental aspect for a better understanding of the structure's seismic behaviour, as well as for the localising the collapse mechanisms. The different steps of the nonlinear static analysis contribute to illustrate the progress of the damage cracking in the masonry load-bearing structural elements and interpreting the possible failures.

Figure 6.9 illustrates the damage localisation simulated by the FE reference model of the reference building model in terms of maximum principal strains for the maximum horizontal acceleration of the pushover analysis in X and Y direction, respectively. With regard to the pushover in the X direction, the damage pattern shows a formation of diagonal cracks in the piers of the front façade of the ground floors, which further leads to a shear failure (see Figure 6.11a). This type of mechanism is commonly known as soft-storey behaviour. The distribution of the tensile damage at the maximum capacity of the pushover analysis indicates a collapse mechanism of the piers of the front façade at the ground floor. Additionally, shear cracking appears in the other interior parts parallel to the façade and the lintels over the openings. Due to the absence of the interior walls at the ground floor in the frontal part of the structure and their replacement with steel beams, a local mechanism of overturning occurs at the lateral wall perpendicular to the seismic action. The level of the ground floor is seen as the weakest part of the structure because of the great change in the in-plane stiffness of the resisting elements.

The non-symmetrical distribution of openings between the front and rear façades has as important role in the seismic performance, producing a torsional response when the structure is loaded towards the X direction (see Figure 6.9a). On the contrary, no torsional response is observed when loading along the Y direction, due to the symmetrical distribution of walls and openings in the Y axis of the building (see Figure 6.9b).

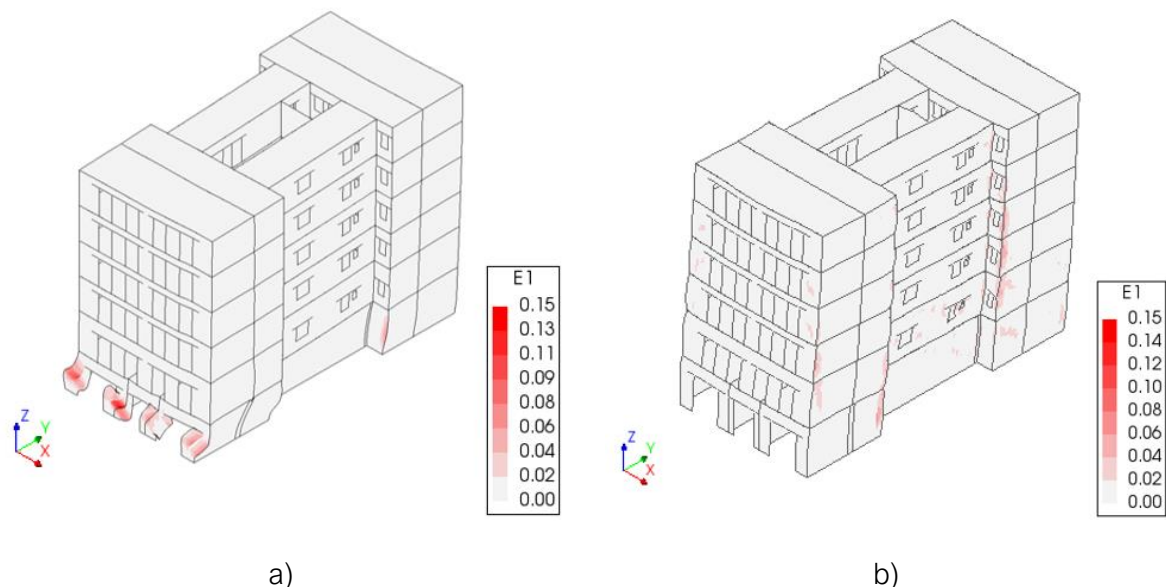


Figure 6.9 - Contour of principal tensile strains for the maximum horizontal acceleration of the reference building model with homogeneous system of URM walls: a) Pushover loading parallel to the façade in X direction and b) Pushover loading orthogonal to the façade in Y direction.

The pushover analysis in Y direction shows a damage pattern symmetrical with respect to the Y-axis, due to the symmetrical distribution of the resisting structural elements. Diagonal shear cracks appear on the lateral walls, starting from the lowest floor level, where the highest axial load exists, and progressing throughout the walls (see Figure 6.11b). Additionally, high levels of damage are observed in the corners of the semi-patios, which have resulted in a vertical separation of the walls as a local failure mechanism. Therefore, the structural irregularity introduced by the patios can be considered as a source of seismic vulnerability.

Figure 6.10 shows the damage localisation in the FE model in terms of principal tensile strains for the pushover analysis of the hybrid model for both loading directions. For the pushover applied parallel to the façade, concentration of damage is observed in the unreinforced masonry piers of the front façade at the ground floor level, which fail under shear. The presence of the large openings in the façade and the slender columns at the ground floor interrupt the stiffness continuity across the floors and lead to the development of a soft-storey behaviour. A significant difference between the reference model with homogeneous system (URM walls) and the hybrid model has been observed at the propagation of the damage at the rear part of the structure, where the hybrid model shows shear cracks also at the piers of the rear façade, unlike the reference one. This is due to the fact that the interior wall in the rear part of the structure has been replaced by two cast-iron pillars and steel beams. With regard to the pushover in Y direction, cracks appear at the lateral load bearing walls parallel to the loading direction. Diagonal shear cracks appear on the lateral walls starting from the lower floor level. Moreover, high levels of damage are observed at the corners of the lateral semi-patios, which can result in a vertical separation of the walls. In this case, the damage pattern is very similar for both models (reference and hybrid) because the area of the lateral load-bearing walls is the same for this loading direction (see Figure 6.10b and Figure 6.11b).

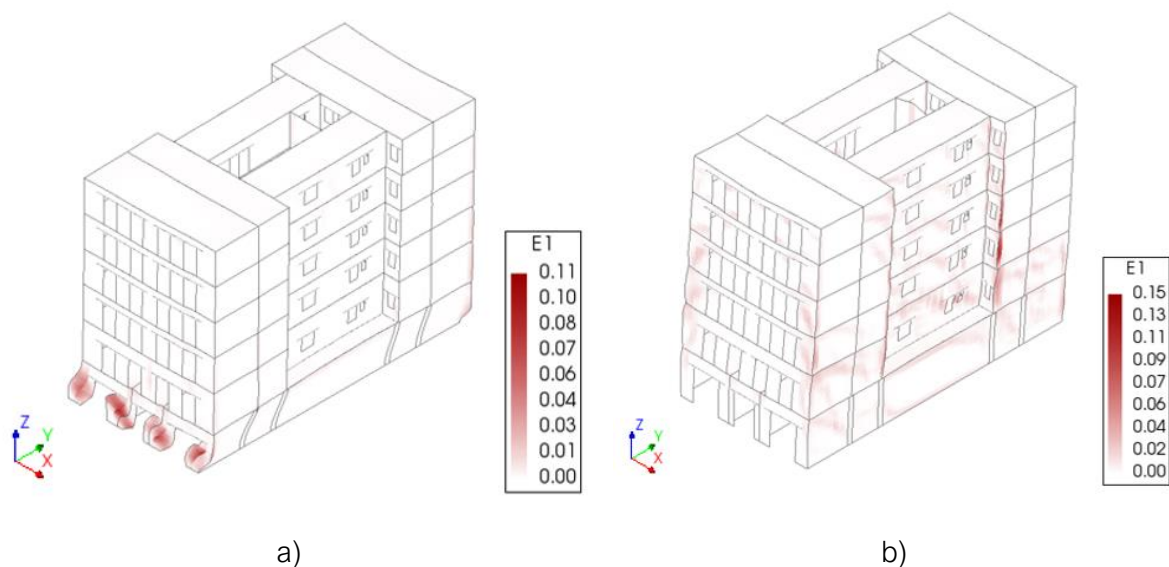


Figure 6.10 - Contour of principal tensile strains for the maximum horizontal acceleration of the hybrid system: a) Pushover loading parallel to the façade in X direction and b) Pushover loading orthogonal to the façade in Y direction.

Additionally, the damage pattern is very similar for the reference models with different floor slabs (steel/timber beams and ceramic tile vaults), for the pushover loading direction parallel to

the façade. The collapse mechanism is the same for both types of floors, following the evolution of a soft-storey in the pushover in X direction and a shear failure of the lateral walls for the pushover in Y direction (see Figure 6.11 and Figure 6.12). The principal tensile strains obtained at the maximum horizontal acceleration for both pushover directions are slightly higher for the model with one-way floor slab of timber beams and tile vaults than the reference model (with one-way floor of steel beams and tile vaults). In conclusion, both models with the typical one-way floor system provide a very seismic response for the two main pushover loading directions (X and Y directions).

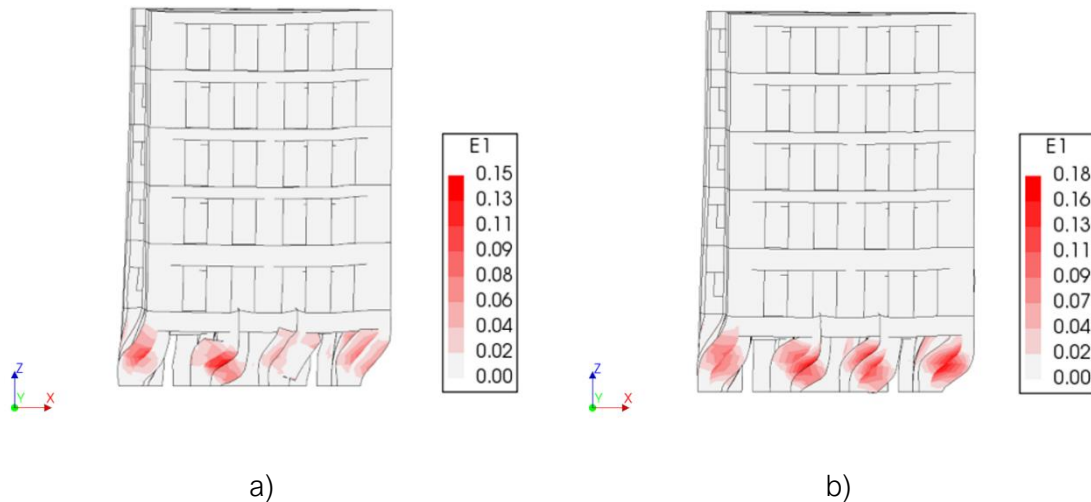


Figure 6.11 - Contour of maximum principal strains at maximum capacity for pushover analysis in X direction: a) building with composite floor system consisting of steel beams and ceramic tile vaults; b) building with composite floor system consisting of timber beams and ceramic tile vaults. 3D view at the top and view of the front façade at the bottom.

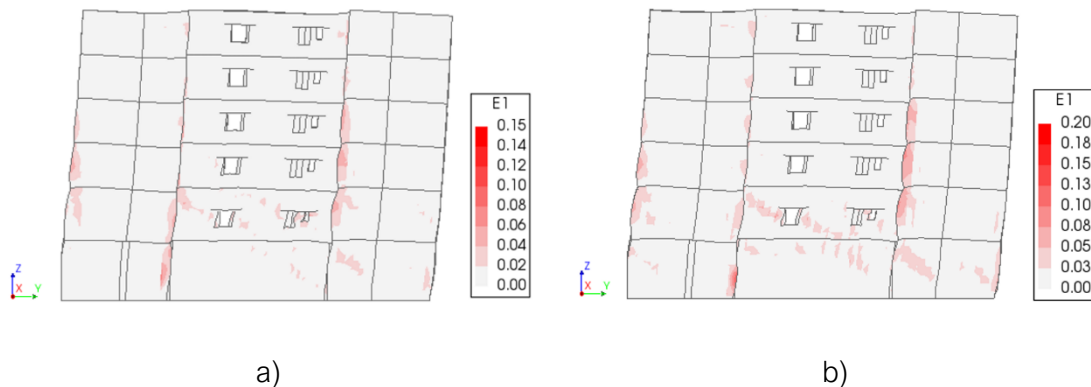


Figure 6.12 - Contour of maximum principal strains at the maximum capacity for a pushover in Y direction: a) building with composite floor system of steel beams and tile vaults; b) building with composite floor system of timber beams and ceramic tile vaults. 3D view at the top and view of the lateral walls at the bottom.

Figure 6.13 and Figure 6.14 indicate the distribution of the damage for the numerical models with vertical extensions in terms of principal tensile strains for both loading directions. For the loading direction parallel to the façade, the damage pattern is remarkably similar in all FE models with or without vertical extensions. The damage affects mostly the piers of the front at the ground

floor, which show diagonal shear cracks (see Figure 6.13). The same soft-storey collapse mechanism is observed in the reference model and all three models with vertical extensions, with shear cracking occurring in the piers on each side of the openings. The sudden drop in the analysis in the X direction is related to the formation of these cracks (see Figure 6.7). Shear cracks also form close to the openings in front façade, along the height, for the model type A (see Figure 6.13(b)), and on the corners of the façades of the additional storeys (attics) in the models type B and C (see Figure 6.13(c) and (d)). Hence, the additional mass and the discontinuities in the placement of vertical extensions are a possible source of seismic vulnerability for these existing URM buildings.

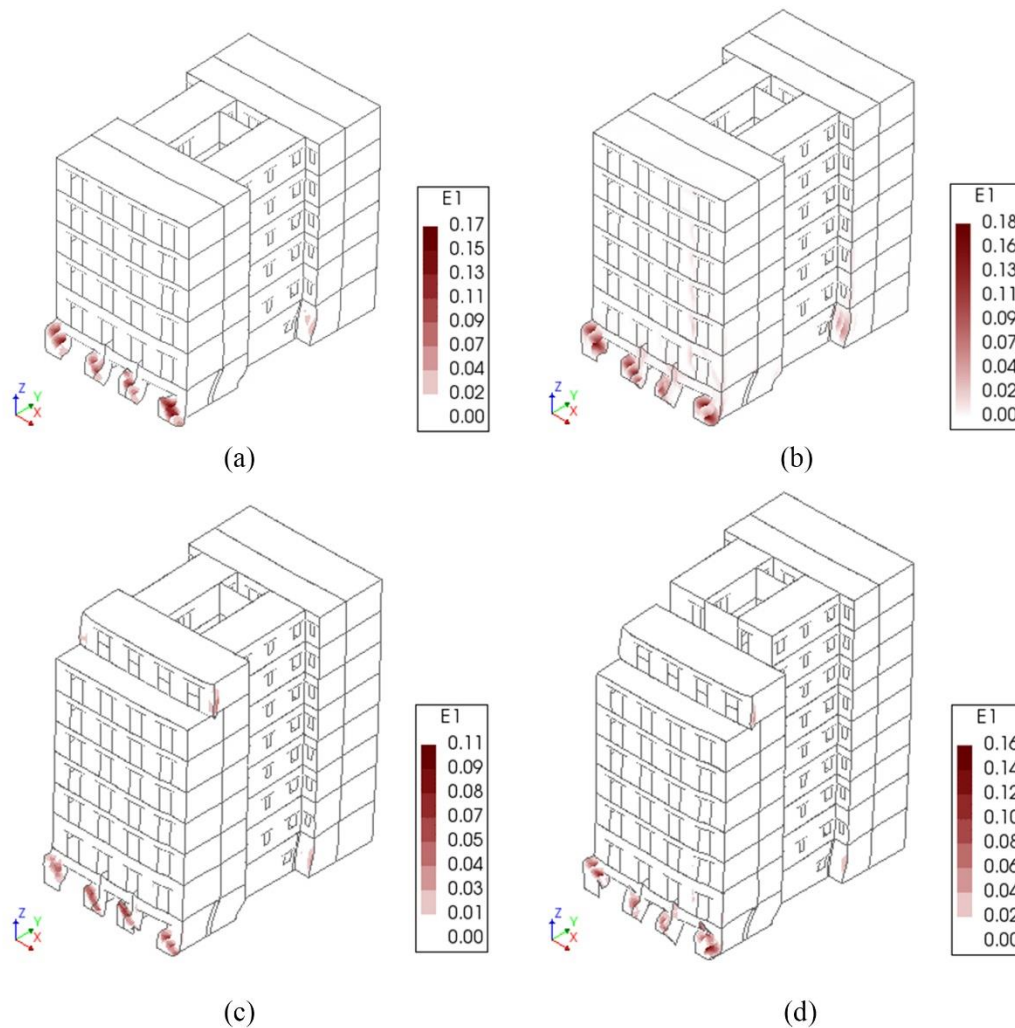


Figure 6.13 - Distribution of principal tensile strains for all numerical models at peak load for pushover analysis parallel to the façade (X direction): (a) Reference model, (b) type A, (c) type B and (d) type C.

In the Y-direction, diagonal shear cracks appear in the lateral shear walls and in the interior walls perpendicular to the façade (see Figure 6.14), as it was previously mentioned for the other models. Moreover, significant levels of damage are observed in the interior corners of the semi-patio. Damage is always present around these patios, especially in the Y direction. Overall, in the Y-direction the damage pattern is similar for all numerical models, when analysing the effect of the vertical extensions, starting with the appearance of diagonal cracks from the lower floors and progressing to the upper levels. The same local collapse mechanism can be observed in all

models, with the appearance of vertical cracks in the outer corners of the building that could lead to out-of-plane detachment.

In conclusion, the numerical approach adopted, by performing seismic analysis, has allowed the characterisation of the seismic response of the different building models of the existing *Eixample* buildings, investigated both in terms of capacity and damage.

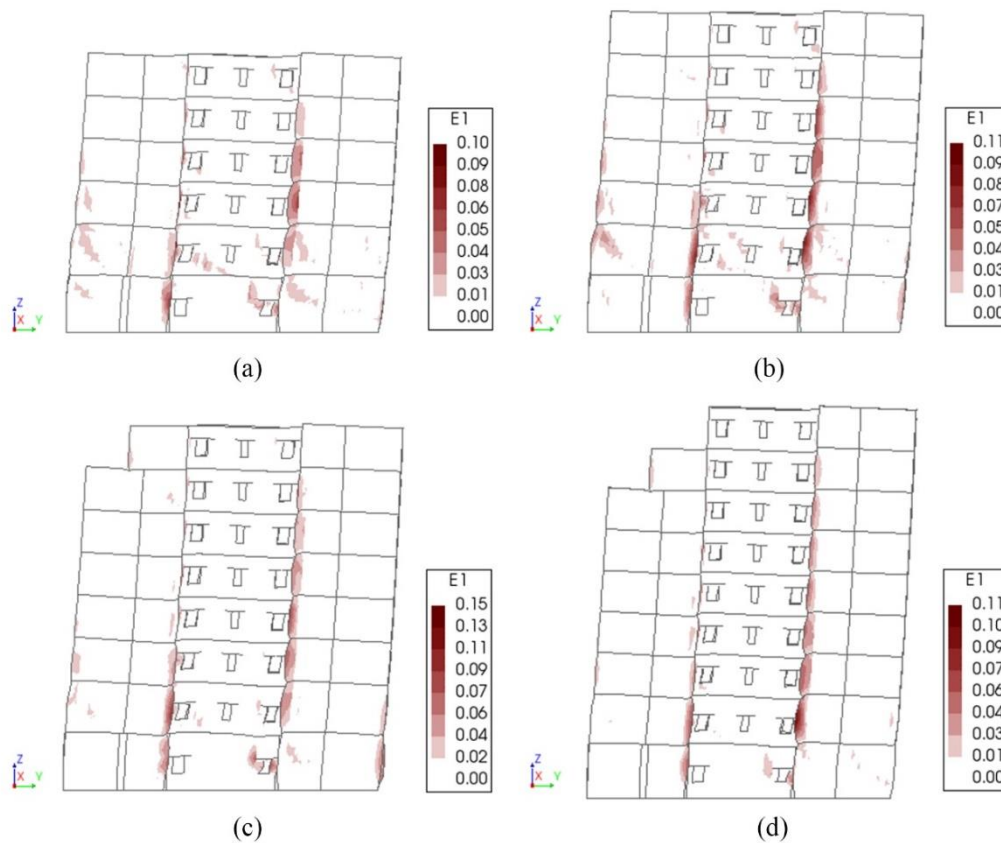


Figure 6.14 - Distribution of principal tensile strains for all numerical models at peak load for pushover analysis perpendicular to the façade (Y direction): (a) Reference model, (b) type A, (c) type B and (d) type.

6.3. SEISMIC PERFORMANCE OF THE EXISTING BUILDINGS FOR THE SEISMIC HAZARD IN BARCELONA

6.3.1. Application of the N2 method

The seismic performance of the existing URM buildings of the *Eixample* district has been evaluated by applying the N2 Method (Fajfar, 2000), as considered in the Italian standard (MIT Ministero delle Infrastrutture e del Trasporti, 2019). The fundamental N2 method is based on the application of traditional force-based pushover analysis approach, which indicates that the lateral loads are applied to the structure incrementally, in accordance with a predetermined pattern. This method combines the pushover analysis of a Multi Degree Of Freedom (MDOF) model with the response spectrum analysis of an equivalent Single Degree Of Freedom (SDOF) system (Fajfar, 2000).

The N2 method aims to identify a performance point (target displacement) of the structure as the point of intersection between the capacity (pushover) curve and the inelastic demand spectra. The evaluation of the performance point (PP) of the structure is possible by following the method based on the identification of the inelastic demand through the principle of equal energies. The obtained PP determines the estimated spectral displacement endured by the structure when subjected to a seismic scenario, which is represented by the demand curve.

The first step is the transformation of the capacity curve of the MDOF system, which represents the relationship between the base shear force and control node displacement, to an equivalent SDOF system that should be idealised. The basic assumption of this transformation is to equalise areas (dissipation energies) under the SDOF capacity curve and the idealised bilinear curve. Figure 6.15 illustrates bilinear idealisation of the capacity curves for an equivalent SDOF system, as proposed by the Italian standard (MIT Ministero delle Infrastrutture e del Trasporti, 2019).

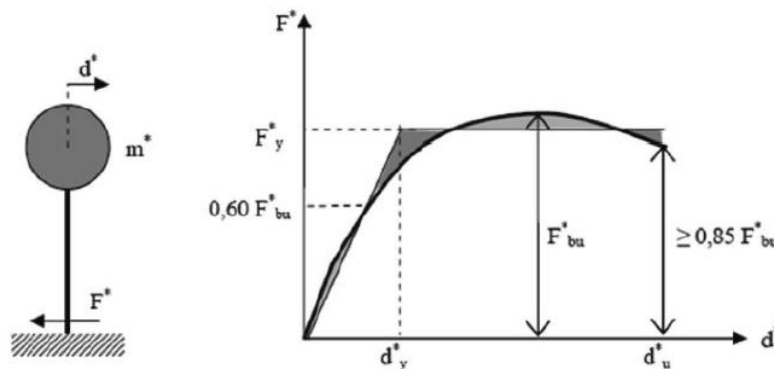


Figure 6.15 - Bilinear idealisation of the capacity curves for an equivalent SDOF system (MIT Ministero delle Infrastrutture e del Trasporti, 2019).

The nonlinear static (pushover) analysis allows the determination of the capacity curve of the structure, expressed by the base shear-displacement relation. The equivalent SDOF capacity curve is simplified to an idealised bilinear curve by considering first an elastic range followed by a perfectly-plastic branch (see Figure 6.15). The maximum capacity of the building (MDOF system) is represented by F_{bu} , and F^*_{bu} is the capacity of the SDOF idealised system, by using the equation (6.1). The N2 procedure is predicated on the assumption that the displacement corresponding to a 20% reduction of the maximum shear strength (F^*_{bu}) is the ultimate displacement d^*_u . As a result, the post-peak part of the capacity curve should be equal or greater than 80% of the maximum strength.

The following equations have been used for the transformation from MDOF to a SDOF system by calculating the forces (F^*) and displacements (d^*) of the equivalent SDOF system:

$$F^* = \frac{F_b}{\Gamma} \quad (6.1)$$

$$d^* = \frac{d_c}{\Gamma} \quad (6.2)$$

where F_b is the base shear force and d_c is the control node displacement of the MDOF system. Γ is the modal participation factor, which controls the transformation from the MDOF to the SDOF system and vice-versa, given by the following equation (6.3):

$$\Gamma = \frac{\Phi^T M \mathbf{1}}{\Phi^T M \Phi} = \frac{\sum m_i \phi_i}{\sum m_i \phi_i^2} = \frac{m^*}{\sum m_i \phi_i^2} \quad (6.3)$$

$$m^* = \sum m_i \phi_i \quad (6.4)$$

where, m_i is the mass of node i (for a MDOF masonry structure), ϕ_i is an assumed normalised displacement shape so that the value at the building top is equal to 1 and m^* is the normalised mass for the SDOF system. In order to make a distinction between the parameters of the equivalent SDOF system and those of the MDOF system, the symbol "*" is used.

The process of bilinearisation is based on the principles of energy equivalence, imposing that the areas below the capacity and bilinear curve ($F^* - d^*$) are equal. Firstly, it should be defined the structure's initial yielding point (minor cracking), where the bilinear idealised curve intersects the pushover capacity curve of the SDOF system. According to this procedure, the cracking shear force (F_{cr}^*) should be equal to 60% of the maximum shear strength (F_{bu}^*). The corresponding displacement is then derived from the capacity curve.

The initial slope of the idealised bilinear curve - elastic stiffness (k_e^*) is equal to the secant stiffness of the structure obtained for the point representing the first cracking (k_{cr}^*), which is estimated as:

$$k_{cr}^* = \frac{F_{cr}^*}{d_{cr}^*} \quad (6.5)$$

Additionally, the yield strength (F_y^*) and displacement (d_y^*) have been calculated by following the equal energy criterion, where the areas below both capacity and bilinear curves are equal. The proper values have been obtained by solving the set of equations and (6.6) and (6.7):

$$F_y^* = k_e^* \cdot d_y^* \quad (6.6)$$

$$F_y^* = \frac{A^*}{(d_u^* - 0.5d_y^*)} \quad (6.7)$$

Where A^* is the area below the idealised bilinear capacity curve, which equal to the area below the capacity curve of the SDOF system.

Moreover, the elastic period of the equivalent SDOF system (T^*) can be calculated as follows:

$$T^* = 2\pi \sqrt{\frac{m^*}{k^*}} = 2\pi \sqrt{\frac{m^* d_y^*}{F_y^*}} \quad (6.8)$$

Where m^* is calculated using equation (6.4) and k^* is the stiffness of the SDOF system obtained from the elastic branch of the bilinear curve.

The following equation (6.10) is used for the calculation of the horizontal spectral acceleration (S_a) in order to obtain a capacity diagram (spectral acceleration versus spectral displacement):

$$S_a = \frac{F^*}{m^*} \quad (6.9)$$

In the case where $T^* \geq T_C$, the inelastic displacement demand is equal to the elastic displacement demand S_{De} (see Figure 6.16a):

$$d_{max}^* = d_{e,max}^* = S_{De}(T^*) \quad (6.10)$$

If the elastic period of the SDOF system is smaller than T_C ($T^* < T_C$), the displacement demand is greater than the one of the elastic displacement demand spectra (see Figure 6.16b), and it is calculated with the following equation:

$$d_{max}^* = \frac{d_{e,max}^*}{q^*} \left[1 + (q^* - 1) \frac{T_C}{T^*} \right] \geq d_{e,max}^* \quad (6.11)$$

Where q^* is the ratio between the force of the elastic response and the yield force of the equivalent system

$$q^* = \frac{S_e(T^*)m^*}{F_y^*} \quad (6.12)$$

If $q^* \leq 1$ then:

$$d_{max}^* = d_{e,max}^* = S_{De}(T^*) \quad (6.13)$$

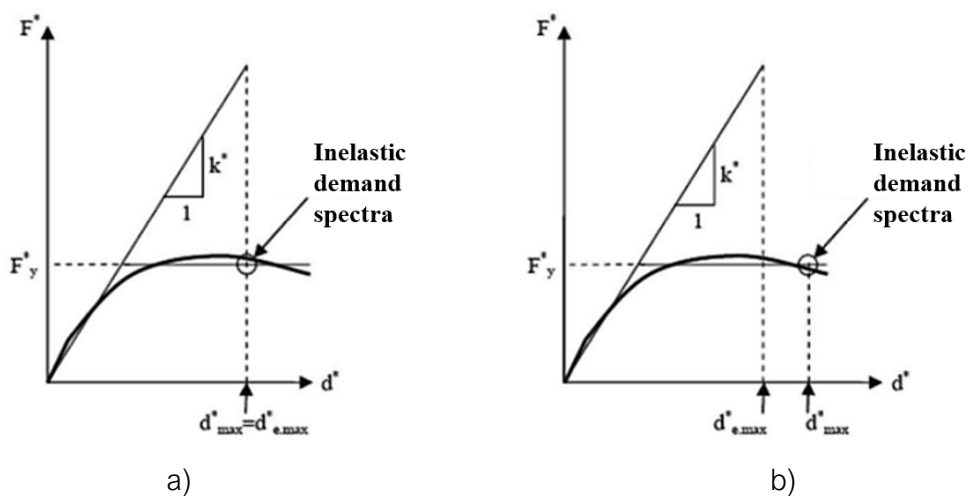


Figure 6.16 - Reference point displacement according to the N2 method for: a) $T^* \geq T_C$ and b) $T^* < T_C$ (adapted from MIT Ministero delle Infrastrutture e del Trasporti 2019).

The target displacement of the performance point for the MDOF system is calculated by the equation (6.14):

$$D_{max} = \Gamma d_{max}^* \quad (6.14)$$

Figure 6.17 illustrates the transformation of the capacity curve from MDOF into a SDOF system of the reference building model and bilinear idealisation of the SDOF system, for a pushover loading in X direction.

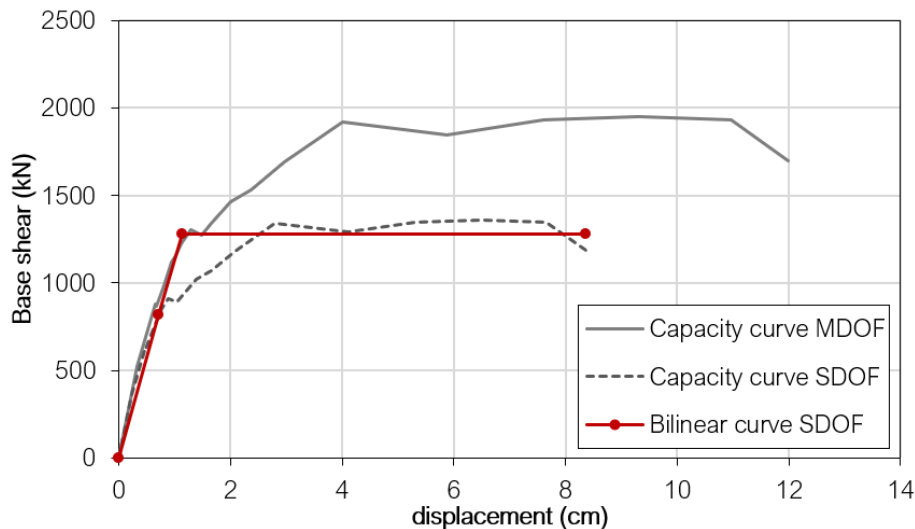


Figure 6.17 - Transformation of a pushover capacity curve from MDOF into a SDOF system of the reference building model and bilinear idealisation of the SDOF system (pushover in X direction).

The characteristics of the SDOF system have been obtained independently for each horizontal loading direction (parallel and perpendicular to the building's façade, since the seismic behaviour in both directions is completely different). Table 6.2 presents the characteristics of the idealised SDOF system of the reference building model for both loading directions. Hereafter, only the results of the reference model are presented, since it represents more than 30% of the studied building stock.

Table 6.2 - Characteristics of the equivalent SDOF system of the URM reference building.

URM reference building model	Pushover direction	
	X	Y
m^* [t]	925.65	862.42
F_y [kN]	1281.71	2077.05
d_y [m]	0.0072	0.0091
T^* [s]	0.57	0.39
Γ	1.43	1.46

Figure 6.18 illustrates the application of the N2 method to the reference building, for both deterministic and probabilistic demand spectra, and by considering the X and Y pushover loading directions. The seismic demand of Barcelona city is defined by considering two different spectra, with a deterministic and a probabilistic seismic scenario (see section 3.6 of Chapter 3).

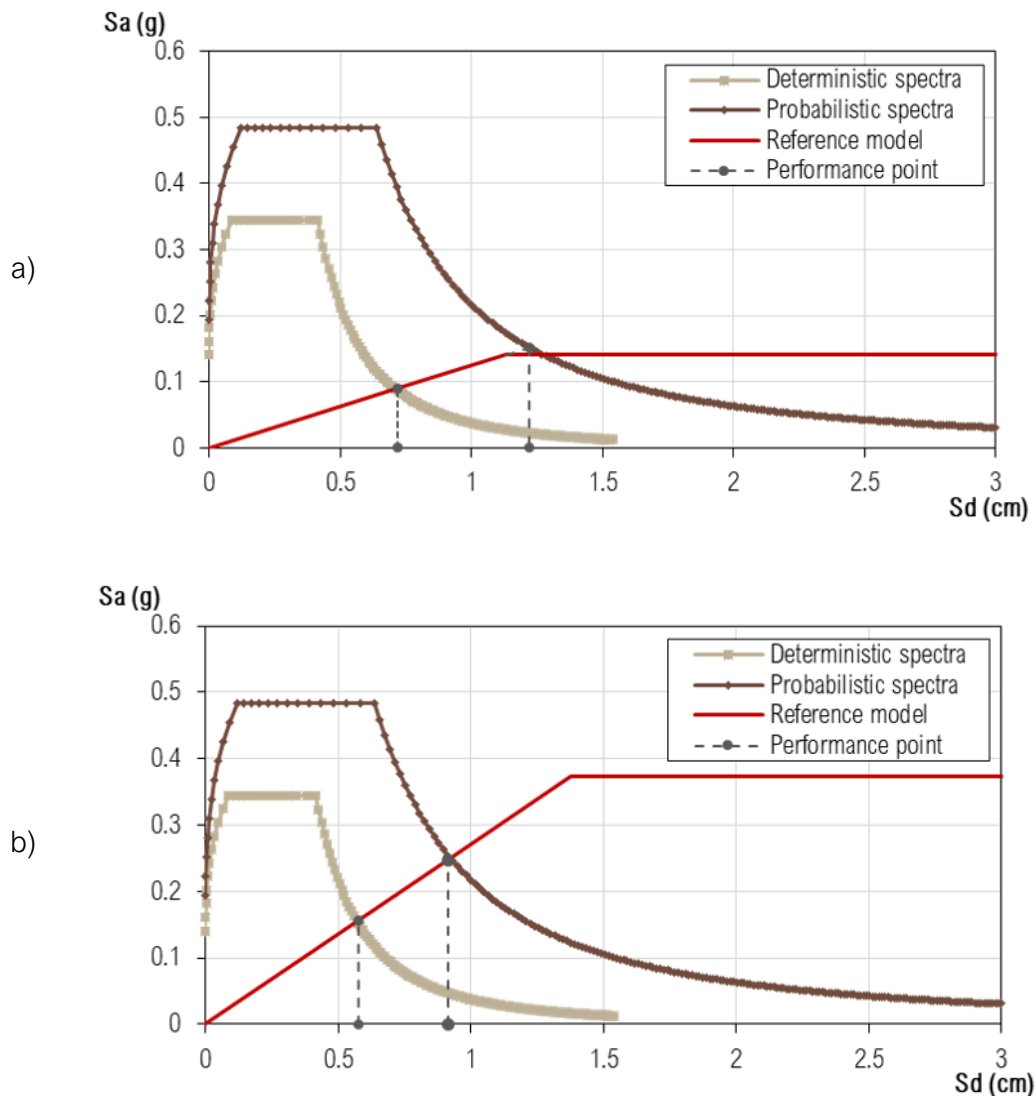


Figure 6.18 - Graphical representation of the application of the N2 method with regards to the deterministic and probabilistic spectra for the bilinear curve of the reference model: a) Pushover in X direction and b) Pushover in Y direction.

The key point of the N2 procedure is obtaining the performance point (spectral displacement), by crossing the demand spectra and capacity curve. The performance point of the representative building model for the pushover in X direction is in the elastic range for the deterministic spectra and in the plastic range for the probabilistic demand spectra. This means that the building may have a higher probability of damage for the probabilistic seismic scenario than for the deterministic one. Moreover, the performance point of the reference building model for the pushover in Y direction is in the elastic range for both seismic scenarios, since this model presents a better seismic behaviour for the pushover loading in Y (perpendicular to the façade), as discussed in section 6.2.1.

The expected damage can be potentially estimated from the numerical analysis performed on the FE models for the obtained target displacement for the MDOF system. Table 6.3 presents the values for the target displacements of the SDOF and MDOF systems, which have been obtained for both loading directions and for the two seismic scenarios. Furthermore, these results have been used for estimating the probability of damage to the models by generating the fragility curves, as explained in Chapter 7.

Table 6.3 - Spectral and maximum displacements obtained for the SDOF and MDOF systems of the reference building for both deterministic and probabilistic spectra.

URM reference building	Deterministic demand spectra		Probabilistic demand spectra	
	X	Y	X	Y
S_{de} (SDOF) [m]	0.0072	0.0062	0.0122	0.0091
D_{max} (MDOF) [m]	0.01032	0.00898	0.01752	0.01333

A summary of the results obtained from the application of the N2 method to all previously analysed numerical models is presented in APPENDIX C. Furthermore, these results have been used for estimating the probability of damage to a subset of numerical models by generating fragility curves, as explained in Chapter 7.

6.4. SUMMARY

This chapter presents the nonlinear static pushover (NSP) analysis on the representative *Eixample* buildings and discusses the obtained results in terms of capacity curves and failure mechanisms. NSP analyses have been performed in the two main directions (X-parallel to the façade and Y-perpendicular to the façade) of the all previously described FE models by applying a loading pattern with horizontal forces proportional to the mass distribution of the buildings. Additionally, these seismic analyses have allowed the estimation of the seismic performance of typical *Eixample* buildings and the understanding of the influence that the various investigated structural characteristics have on the structures' seismic capacity and vulnerability.

Finite element modelling combined with pushover analysis can contribute to a better understanding of the seismic performance of existing masonry building typologies. Considering the necessary compromise between computational cost and desired output, the pushover analysis has provided a satisfactory approach to correlate the typological and structural features with the seismic response. Comparisons have been made between the reference building model and different modified FE models obtained by changing various parameters as specified in the building taxonomy (presented in chapter 4).

The buildings of the *Eixample* district present a very different response according to the loading direction. The presence of large open spaces at the ground floor and a large number of openings in the front façade, makes the structure more vulnerable for loading in the direction parallel to the façade. The collapse mechanism in X direction is related to the appearance of the soft-story effect at the ground level, while the collapse mechanism in Y direction is connected to the local in-plane

shear failure of the lateral load-bearing walls. The maximum level of displacements is different for both directions depending on the structural system, type of horizontal diaphragms, number of storeys and vertical extensions, and other structural characteristics.

The hybrid building typology showed a higher seismic vulnerability than the building with homogeneous structural system in the loading direction parallel to the façade due to the substitution of the internal walls with slender piers and beams. In the direction orthogonal to the façade, the structure shows a better seismic performance due to the larger resisting area provided by the lateral shear walls.

The numerical analyses confirmed the influence of the slender URM walls, large façade openings, the irregularities introduced by the lateral patios, the vertical extensions and the different plan configuration on the ground floor. Realistic damage patterns and collapse mechanisms have been recognised in each of the different models analysed for both loading directions applied parallel and perpendicular to the façade. It was possible to clearly identify the soft-storey behaviour in the direction parallel to the façade and shear and vertical cracking in the orthogonal walls around the semi-patios in the direction perpendicular to the façade. While this vulnerability is expected to be reduced due to the construction of these buildings in aggregates, the global behaviour is not expected to change as all structures share the same structural characteristics with the presence of a soft-storey at the ground floor. Hence, the obtained results have allowed predictions on the seismic response and the influence of the building's structural system and characteristics.

Moreover, the seismic performance of the buildings has been assessed by applying the N2 Method for two different seismic demand spectra, i.e. the deterministic and probabilistic one. The performance point has been obtained by intersecting the bilinear capacity curve and the demand response spectra. The reference model demonstrated a better seismic performance in the Y direction, where the performance point remained in the elastic range for both seismic (deterministic and probabilistic) scenarios. In the X direction, the target displacement resulted slightly higher than the yield displacement for the probabilistic demand spectra, which confirms the lower obtained capacity and the higher probability of damage. Moreover, the results obtained regarding the spectral displacements will be used for the generation of the fragility curves in Chapter 7.

CHAPTER 7. SEISMIC VULNERABILITY ASSESSMENT AT URBAN SCALE

7.1. INTRODUCTION

A hybrid seismic vulnerability methodology is developed in order to improve and adapt the Vulnerability Index Method (VIM) for evaluating existing masonry buildings with peculiar structural characteristics in urban centres (discussed in Chapter 3). The proposed methodology considers the calibration of a new vulnerability index form based on a sensitivity analysis derived from numerical simulations, due to the impossibility of calibrating the VIM based on post-earthquake observed damage. The new VIM form aims to evaluate the seismic vulnerability of the *Eixample* urban area. However, this methodology could be extended to be applied to specific building typologies from different urban centres.

This chapter is focused on presenting the methodology developed and adopted for the seismic vulnerability assessment of existing URM buildings. A brief description is given of the parameters chosen for the new proposed VIM form, whose selection is based on the previously discussed literature review of the existing vulnerability methods and mainly on the detailed building taxonomy for the building typologies from the *Eixample* district. Moreover, the definition of the vulnerability classes for each parameter is described according to the parametric studies done on the developed numerical FE models with the variations of the chosen vulnerability parameters. The assigned weights for each parameter have been determined using the Analytical Hierarchy Process (AHP), by using the variation of the maximum capacity obtained of the individual numerical models. The vulnerability index for all the numerical models is estimated and used for the further estimation of the damage grade. Fragility curves have been developed for the representative building typologies, corresponding to the spectral displacements obtained from the application of the N2 method, as a variable that characterises the seismic action. The proposed methodology for the seismic vulnerability assessment is applied to the sample of 176 buildings of the *Eixample* building stock, collected by Cornadó Bardón (2015). Additionally, a specific urban block from the neighbourhood of *Eixample* district with the greatest amount of URM buildings has been selected for the vulnerability evaluation considering the aggregate effect.

7.2. METHODOLOGY ADOPTED FOR THE SEISMIC VULNERABILITY ASSESSMENT

This section discusses the methodology adopted for the seismic vulnerability assessment of existing URM buildings. The first part of the new proposed methodology has been explained in Chapter 4, regarding the preparation of a specific building taxonomy and the selection of

representative building typologies, used for numerical modelling. First, a consistent and detailed building taxonomy has been established that allows the identification of the parameters influencing the structures' seismic performance. This is supported and combined with a comprehensive database containing detailed geometrical and structural information of the most common building typologies of the studied urban centre. Furthermore, the frequency distribution of each studied building typology has been defined using extrapolation of the statistical data. Following the previous steps, the most representative building typologies have been identified by applying a 50% criterion to the studied building stock, by considering the most significant parameters that could possibly impact the seismic performance and vulnerability of the structure.

Subsequently, numerical models of the most representative building typologies have been developed using the FEM. Several parameters that significantly influence the buildings' seismic performance and vulnerability have been selected from the detailed building taxonomy, such as the number of storeys, presence of vertical extensions, different material properties, masonry walls' thickness variation, horizontal diaphragms, and façade openings. Accordingly, the variations of these parameters have been implemented to the most common building typology, called reference model. Nonlinear static analyses have been performed for both main directions (parallel and perpendicular to the façades) on all the numerical models. Moreover, the seismic behaviour of the existing buildings has been evaluated through capacity pushover curves, which allowed for a better understanding of the structures' typical failure mechanisms. Moreover, the N2 method has been applied for the evaluation of the buildings' seismic performance for the seismic hazard in Barcelona.

The proposed method for the vulnerability assessment is an adaptation of the Vulnerability Index Method-VIM (GNDT, 1986), which was followed by Vicente et al. (2008), Formisano et al. (2011), as presented in Chapter 2. The proposed VIM has been validated to be used for existing URM buildings with specific structural features as part of an historic urban centre. A new and more specific VIM form has been established for evaluating the seismic vulnerability of various building typologies by previously defining their specific characteristics, which could actually impact their seismic response. The seismic vulnerability assessment parameters are weighted to calculate the vulnerability index (I_v). The seismic vulnerability classes for the key parameters are defined using parametric studies in order to better comprehend the influence of each parameter. The vulnerability index was calculated using the same proposed scores as in the GNDT forms (GNDT, 1986). Weights for VIM parameters are commonly assigned based on expert opinion and post-earthquake observed damage. Due to the absence of observed damage from previous earthquakes in our case study, numerical simulations have been used to identify the typical failure mechanisms and define the seismic vulnerability that these structural typologies present. The Analytical Hierarchy Process (AHP) has been adopted to define the weights for each parameter of the vulnerability index method based on the variation of the maximum capacity of the specific numerical models. Furthermore, the weights have been normalised by using the same sum of weights for the parameters used in previous empirical studies for individual building evaluation. Finally, the vulnerability index has been calculated to allow a damage estimation of the analysed building stock. Fragility curves have been generated in a tentative way according to the spectral displacements obtained from the application of the N2 method.

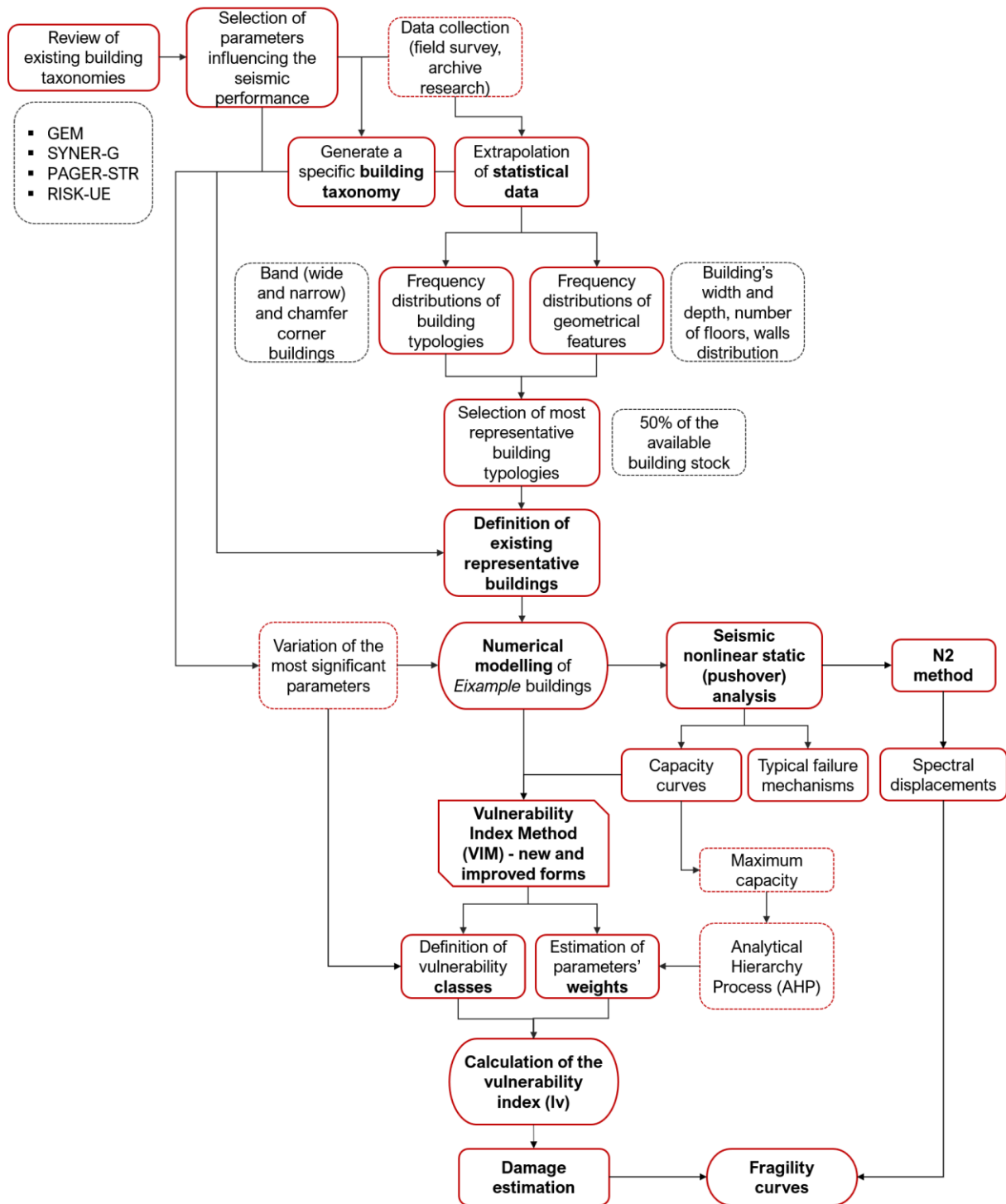


Figure 7.1 - Methodology adopted for the seismic vulnerability assessment of URM existing buildings.

The steps required for the creation of this methodology are summarized as follows (Figure 2.1): 1) reviewing previously existing building taxonomies and selecting parameters that influence the structures' seismic performance from a comprehensive data collection (field survey and archive research); 2) generating a specific building taxonomy for the historic urban centre; 3) frequency distribution of the different building typologies by using the extrapolation of the statistical data collection; 4) selection of most representative typologies; 5) identifying real existing URM buildings according to the building taxonomy and the provided database; 6) numerical modelling of the

existing buildings with variation of key parameters from the building taxonomy; 7) seismic nonlinear static (pushover) analysis, by generating capacity curves and defining the typical failure mechanisms; 8) adapting the Vulnerability Index Method (VIM) by generating new and improved VIM forms; 9) definition of the four vulnerability classes for each selected parameter; 10) estimation of the weights for each parameter; 11) calculation of the vulnerability index (I_v), and 12) damage estimation.

7.3. CALIBRATION OF THE VULNERABILITY INDEX METHOD USING HYBRID CRITERIA

This section describes the calibration of the hybrid criteria for the seismic vulnerability assessment, consisting in evaluating a vulnerability index following an empirical/expert judgment approach, i.e. the vulnerability index method, based on the extensive use of numerical simulations of previously defined representative building typologies.

7.3.1. Development of new forms for the vulnerability assessment

A new set of vulnerability parameters is proposed for the adapted Vulnerability Index Method on the basis of the literature review of prior research studies on various vulnerability methodologies (see Chapter 2) and the creation of a specific building taxonomy as a first step of the seismic risk assessment at a large scale (see Chapter 4). The initial focus of the study was on unreinforced masonry (URM) buildings with distinctive features from the *Example* district, whose structural system generally consists of load-bearing masonry walls that are typically connected with one-way floor systems. The most important attributes that affect the seismic performance and consequently the seismic vulnerability of the representative *Example* building typologies are chosen from the previously described comprehensive building taxonomy.

Some of the original vulnerability parameters for masonry structures are included in the new proposed VIM form, such as conventional strength, plan configuration, vertical irregularity, non-structural elements and general maintenance conditions (Benedetti and Petrini, 1984; GNDT, 1993). The last two parameters regarding the non-structural elements and general maintenance conditions have not been specifically modelled and calibrated. They have been considered as proposed in the original VIM form following the expert opinions for their influence on the buildings' seismic vulnerability. It should be noted that other parameters from the original VIM form, regarding the type and organisation of resisting system, the quality of resisting system, the maximum distance between walls and the roof typology have not been considered as part of the new proposed VIM form. This is because the analysed buildings share some constant features, as the lack of a proper box-behaviour, the fact of having been designed without any seismic regulations, the fact of having been constructed mainly with regular masonry of brick units and lime mortar, the recurrent presence of a flat roof type.

Additionally, the five parameters suggested by Formisano et al. (2015) have been adopted for the vulnerability assessment in the X direction (parallel to the façade) to account the effect of aggregate structural conditions on the seismic vulnerability of the buildings. The scores and

weights for these last parameters have not been modified or calibrated due to the high computational time and prohibitive cost required for the simulation of the aggregates with the level of detail invested in the numerical models elaborated for the representative *Example* buildings. However, the aggregate effects could be investigated by means of more simplified methods, such as the equivalent frame method. The application of this last possibility is presented as a possible future development of the research.

In Chapter 5, several models have been defined in order to better understand the influence of each structural attribute and their variation on the global seismic behaviour of the URM buildings. It should be highlighted that two different VIM forms have been proposed, depending on the seismic loading action (X and Y direction), since the significant different behaviour of each numerical model for main both directions (parallel and perpendicular to the façade) has been emphasised (see Chapter 6). The VIM form for X direction (seismic loading parallel to the façade) is composed of nine parameters, expanded with five more parameters considering the aggregate influence conditions in this direction. The VIM form for Y direction (seismic loading perpendicular to the façade) has only eight parameters, as it does not consider any aggregate effects. A very brief description of all the chosen vulnerability parameters is given below. They have been described and evaluated into detail in the prepared building taxonomy in Chapter 4.

Parameter 1 - Seismic coefficient. This parameter evaluates the seismic resistance of the building considering the ultimate shear forces of the load-bearing masonry walls. The "Conventional strength" parameter in the GNDT II level form considers only the minimum value of the ultimate shear forces among those resulting from both directions of the load-bearing walls in the verification plane (p_v). More precisely, it evaluates the seismic coefficient "C" as the ratio between the minimum shear resisting force and the total weight of the building. This parameter should consider the resistance area of the load-bearing walls depending on the seismic loading direction (X and Y direction). The seismic coefficient is calculated for both directions using the following equations:

$$C_X = \frac{T_{u,pv}^X}{W_{pv}^*} \qquad C_Y = \frac{T_{u,pv}^Y}{W_{pv}^*} \qquad (7.1)$$

$$T_{u,p}^X = \sum_{ix} T_{u,ix} = \sum_{ix} A_{ix} \cdot \tau_{k,p} \cdot \sqrt{1 + \frac{\sigma_{0,p}}{1,5 \cdot \tau_{k,p}}} = A_{X,p} \cdot \tau_{k,p} \cdot \sqrt{1 + \frac{\sigma_{0,p}}{1,5 \cdot \tau_{k,p}}}; \qquad (7.2)$$

$$T_{u,p}^Y = \sum_{jy} T_{u,jy} = \sum_{jy} A_{jy} \cdot \tau_{k,p} \cdot \sqrt{1 + \frac{\sigma_{0,p}}{1,5 \cdot \tau_{k,p}}} = A_{Y,p} \cdot \tau_{k,p} \cdot \sqrt{1 + \frac{\sigma_{0,p}}{1,5 \cdot \tau_{k,p}}}; \qquad (7.3)$$

$$C = \frac{T_{u,pv}^{X,Y}}{W_{pv}^*} = \frac{A_{X,Y} \cdot \tau_{k,pv} \cdot \sqrt{1 + \frac{\sigma_{0,pv}}{1,5 \cdot \tau_{k,pv}}}}{q \cdot N \cdot A_t} \qquad (7.4)$$

$$\sigma_{0,pv} = \frac{W_p}{(A_X + A_Y)} \qquad (7.5)$$

$$W_{pv} = q \cdot N \cdot A_t \qquad (7.6)$$

$$q = \frac{(A_x + A_y) \cdot h \cdot p_m}{A_t} + p_s \quad (7.7)$$

Where:

C_i - Seismic coefficient for X or Y direction

T_u^X - Shear stress of the walls in the X direction

T_u^Y - Shear stress of the walls in the y direction

W_{pv} - Weight of the building at the verification plane

W_p - Total weight of the building above the verification plane

A_x - Total resistant area of the walls in the X direction

A_y - Total resistant area of the walls in the Y direction

τ_k - Specific shear resistance of the masonry

σ_0 - Average normal stress;

N - Number of floors;

A_t - Average total floor area

h - Average inter-storey height of the floors

ρ_m - Average specific weight of the masonry

ρ_s - Average permanent load of the floors

Parameter 2 - Number of floors. This parameter considers the total number of storeys of the existing building. Moreover, the vertical extensions which have been added should also be considered in the total storey number.

Parameter 3 - Horizontal diaphragms. This parameter depends on the type and quality of the horizontal structural system, their in-plane stiffness as well as their connections with the vertical seismic resistant systems.

Parameter 4 - Plan configuration. This parameter appraises the geometrical configuration of the building in plan, the mass of the seismic resistant elements, their stiffness distribution and the existing eccentricity between the centre of rigidity and the centre of mass.

Parameter 5 - Vertical irregularity. This parameter assesses whether the vertical load-bearing system presents irregularities brought on, respectively, by the presence of soft-storeys, vertical extensions, galleries, cantilevers etc. It considers possible discontinuities when introducing different vertical seismic-resistant systems as well as the mass change between floor levels.

Parameter 6 - Presence of patios. The presence of patios is a specific vulnerability parameter for these existing building typologies, as it represents a plan irregularity in the geometrical shape plan of the building that can reduce the structure's stiffness.

Parameter 7 - Façade openings at ground floor. This parameter evaluates the percentage of façade openings only at the ground floor for both front and back façades of the building. The amount of wall openings is a geometrical parameter that can be measured as the ratio between the area of facade openings and the total area of both façades in terms of percentage (see Figure 7.2). This parameter is calculated only for the X direction (parallel to the façade).

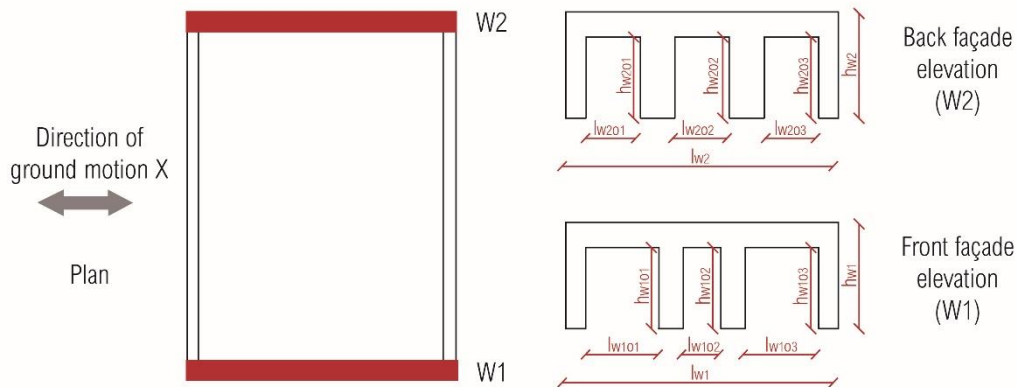


Figure 7.2 - Definition of the ratio used to determine the effect of façade wall openings on the seismic behaviour of existing masonry building in relation to the direction of seismic loading (adapted from Ortega 2018).

$$IP_x = \frac{(h_{w101} \times l_{w101}) + (h_{w102} \times l_{w102}) + (h_{w103} \times l_{w103}) + (h_{w201} \times l_{w201}) + (h_{w202} \times l_{w202}) + (h_{w203} \times l_{w203})}{(h_{w1} \times l_{w1}) + (h_{w2} \times l_{w2})} \quad (7.8)$$

Parameter 8 - Non-structural elements. This parameter classifies non-structural external elements such as balconies, statues, façade decorations, additions, ceilings, and etc., which may partially or totally collapse and cause damage to structures, infrastructure or injury to people in case of fall. The definition of this parameter is based on their presence, dimensions, heaviness and connection to the resisting structural elements.

Parameter 9 - General maintenance conditions. This parameter takes into account the state of conservation of the building and mainly focuses on the existing damage that can be observed, such as the crack pattern on load-bearing masonry walls, any visible damage on the structural elements, or the degree of degradation of the material, which can affect the stability of the structural elements of the building.

Parameter 10 - Presence of adjacent buildings with different height. This parameter evaluates the influence of adjacent buildings with different heights on the structural vulnerability of the building of study.

Parameter 11 - Position of the buildings in the aggregate.: This parameter assesses the in-plan influence of the position of the buildings within a structural aggregate.

Parameter 12 - Number of staggered floors. This parameter studies the influence of staggered storeys among aggregate buildings.

Parameter 13 - Effect of either structural or typological heterogeneity among adjacent structural units. The following parameter evaluates the structural or typological heterogeneity among adjacent structural units.

Parameter 14 - Percentage difference of opening areas among adjacent facades. This parameter evaluates the percentage difference of opening areas among adjacent structural units in an urban block.

7.3.2. Definitions of vulnerability classes

The vulnerability index (I_v), which is computed as the weighted sum of the seismic vulnerability assessment parameters, has been described previously in Chapter 2 (Table 2.2) as part of the VIM method proposed by GNDT (1994). The vulnerability class given amount (C_{vi}) is multiplied by the weights (w_i), which represent the relative significance of each parameter in determining the overall building's seismic vulnerability. The VIM method is regarded as an expert-judgment vulnerability method because the weights of the parameters are usually decided based on expert opinions. The use of numerical results to define parameters classes and weights was implemented first by Ortega (2018) in order to propose an application to vernacular buildings. A similar procedure is herein developed for the calibration of the new VIM forms that will later applied to the study of the *Eixample* district.

The nonlinear pushover analyses on different FE numerical models with varying geometrical, structural, material and other peculiar structural characteristics, as described in detail in Chapter 5 and 6, have been employed for the definition and calibration of the vulnerability classes and weights of the VIM forms. Four different classes have been identified for each parameter, identified from A to D, (being A the least vulnerable class and D the most vulnerable one), by using the parametric study carried out on the set of analysed numerical models. The structural response of the FE models is compared in terms of the maximum capacity obtained from the pushover curves for both main directions (parallel and perpendicular to the façade). The values for the maximum capacity (horizontal acceleration) of the various models are compared in order to obtain a better knowledge of the variation of the building's capacity as a result of the variations defined for each key parameter.

The definition for classes of the other vulnerability parameters has been done following a similar approach by considering the maximum horizontal acceleration as suggested by Ortega (2018). The horizontal acceleration (load factor) is calculated as the ratio between the base shear forces and the self-weight of the structure. The maximum horizontal acceleration obtained for each building model is associated to the structure's maximum capacity strength according to the pushover curve. The variation of the maximum capacity (MC) is expressed in percentage in order to normalize the values obtained for each numerical model following equation (7.8).

$$MC(\%) = \frac{MC(g)_i}{MC(g)_{max}} \quad (7.9)$$

Where $MC(g)_i$ is the maximum capacity for each numerical model and $MC(g)_{max}$ is the maximum value of the maximum capacities of the numerical models used for the definition of each parameter.

The maximum capacity reached by a numerical model is the result of several structural attributes that influence the seismic behaviour, such as the geometrical configuration, the structural system, the number of floors, the material properties, the walls' thickness, and the size of façade openings). A set of numerical models has been analysed to study the influence of each of the previously mentioned attributes on the seismic capacity in order to relate them with the vulnerability classes of the Parameter 1 "Seismic Coefficient", see (Figure 7.3).

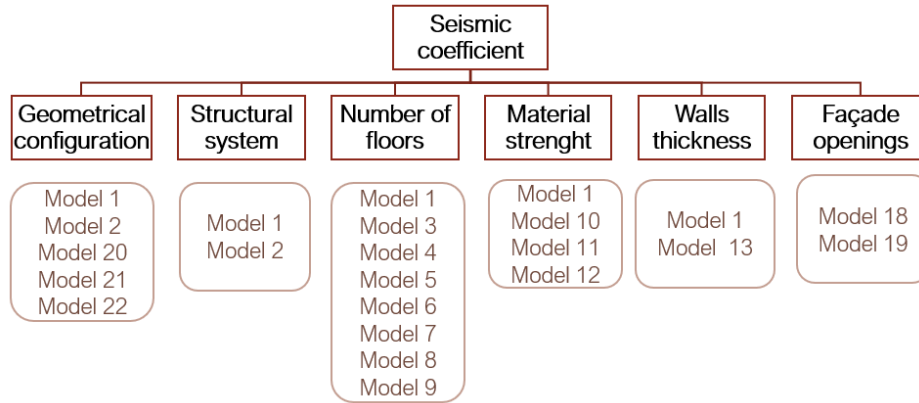


Figure 7.3 - Specific structural attributes involved in the definition of the vulnerability classes for Parameter 1 “Seismic coefficient”, and relevant models elaborated to analyse the influence of structural attributes on the seismic capacity.

The vulnerability classes of the Parameter 1 are related with the maximum seismic capacities obtained in the different models, and have been assessed according to the following procedure. First, the maximum capacity (understood as the peak value obtained for each pushover curve) of all the selected numerical models has been normalised according to the maximum value obtained for the entire set, according to Equation (7.9). Second, a diagram has been obtained (Figure 7.4) relating the maximum capacity of each model with the corresponding calculated seismic coefficient derived from Equations (7.1)-(7.7). The total range of variation between the model with the lowest and highest seismic coefficients is divided into four equal parts, which are assigned to the increasing vulnerability classes A, B, C and D of Parameter 1. The following range of variation is obtained for the definition of the four classes (Figure 7.4): a) Class A for a seismic coefficient equal or higher than 0.271; b) Class B for a seismic coefficient equal or higher than 0.211 but smaller than 0.271; c) Class C for a seismic coefficient equal or higher than 0.141 but smaller than 0.271 and d) Class D for a seismic coefficient smaller than 0.141.

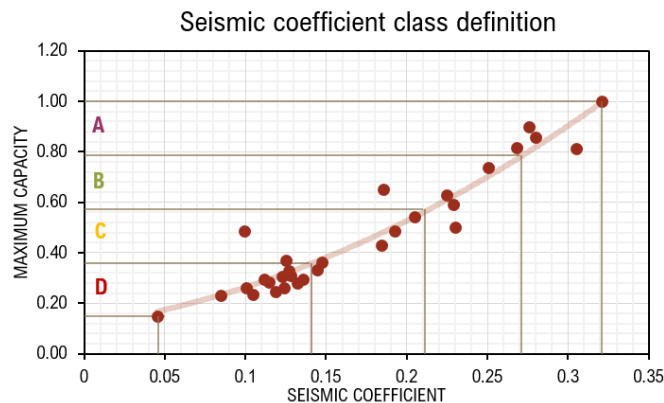
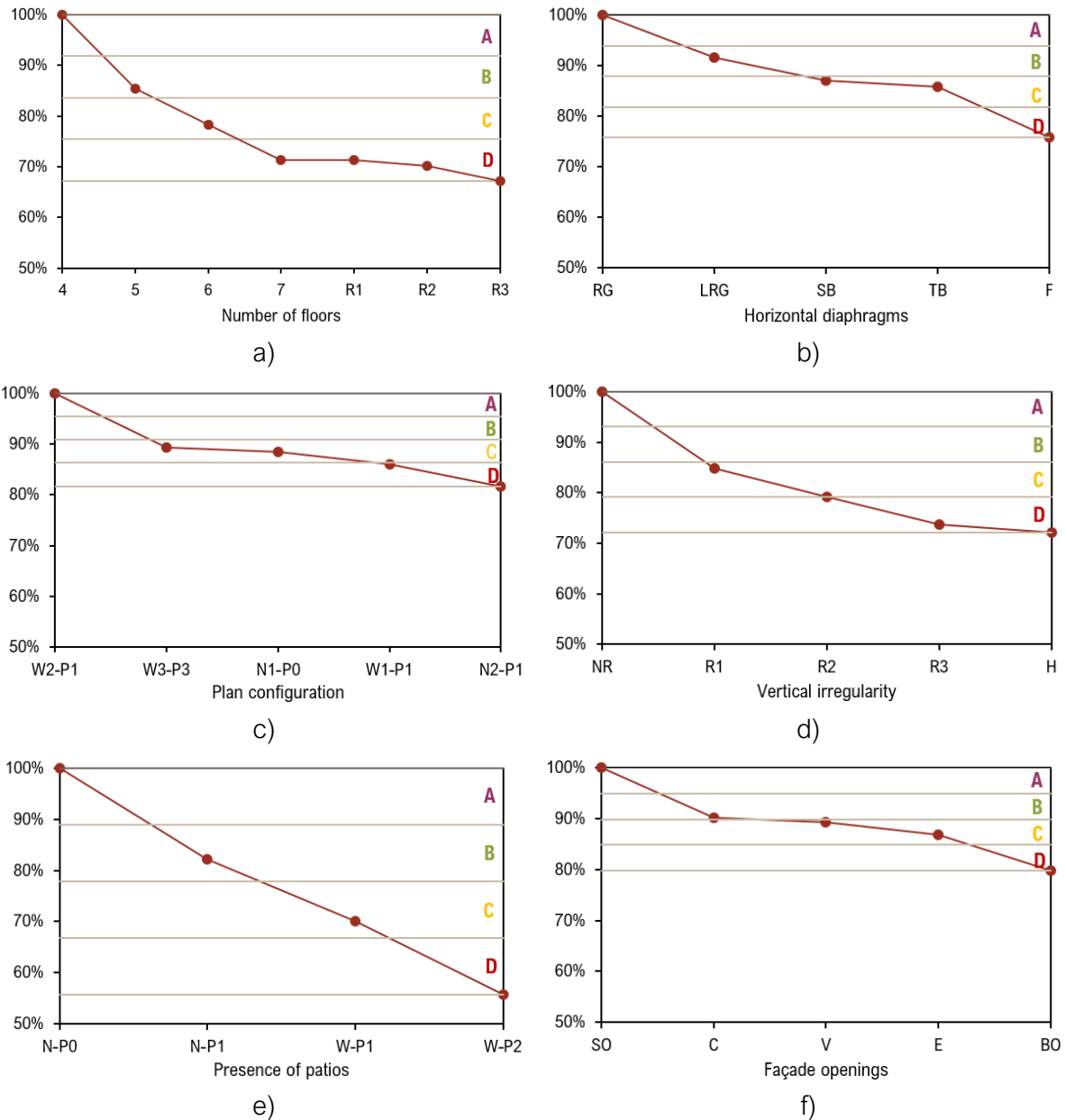


Figure 7.4 - Definition of classes for the vulnerability Parameter 1 “Seismic coefficient” according to the maximum capacity obtained from several numerical models.

It should be noted that the number of developed numerical models could be increased, by modifying the selection criteria of the representative building typologies and their possible variations (as mentioned in Chapter 4). Hence, the previously defined ranges for the definition of the vulnerability classes can be modified and easily adapted for a different selection of building typologies.

The definition of the vulnerability classes for the other parameters is done by dividing the total range of variation $MC(\%)_{max} - MC(\%)_{min}$ into four equal parts (see Figure 7.5). A summary of the definition of the vulnerability classes for all the vulnerability parameters considered for the new proposed VIM forms is given in Table 7.1-Table 7.14.



Legend: R1-one vertical extension-remunta; R2-two remuntes; R3-three remuntes; RG-rigid floor; LRG-light weighted rigid floor; SB-one-way floor with steel beams and tile vaults; TB-one-way floor with timber beams and tile vaults; F-flexible floor with timber beams and planks; W1-P1-wide shape plan with one lateral patio; W2-P1-wide shape plan with one lateral patio; W3-P2-wide shape plan with two lateral patios; N1-P0-narrow shape plan without lateral patios; N2-P1-narrow shape plan with lateral patios; NR-no remuntes; H-hybrid system; SO-small openings (41%); C-Casanova (58%); V-Villaroel (48%); E-Entença (52%); BO-big openings (65%).

Figure 7.5 - Definition of the four vulnerability classes (A, B,C and D) for the different parameters of the VIM forms: a) Number of floors (P2); b) Horizontal diaphragms (P3); c) Plan configuration (P4); d) Vertical irregularity (P5); e) Presence of patios (P6), and f) Façade openings on the ground floor (P7).

Table 7.1 - Vulnerability classes proposed for the Parameter 1 “Seismic coefficient” for both main directions (X and Y).

Parameter 1 - Seismic coefficient for X and Y direction

- Class A** $C \geq 0.271$
- Class B** $0.211 \leq C < 0.271$
- Class C** $0.141 \leq C < 0.211$
- Class D** $C < 0.141$

Table 7.1 shows the proposed ranges for the definition of the vulnerability classes for the seismic coefficient for both main directions X (parallel to street façade) and Y. The calculation of the seismic coefficient should be done carefully using the previously described equations (7.1) - (7.7).

Table 7.2 - Vulnerability classes proposed for the Parameter 2 “Number of floors”.

Parameter 2 - Number of floors

- Class A** Buildings with four or less storeys (GR+3)
- Class B** Buildings with five storeys (GR+4)
- Class C** Buildings with six storeys (GR+5)
- Class D** Buildings with more than seven storeys (GR+6); Buildings with two or three vertical extensions-remuntes (GR+5+2R) (GR+6+3R)

Table 7.2 presents the definition of the vulnerability classes for the Parameter 2 “Number of floors”. Figure 7.6 illustrates the building typologies used for the definition of the four classes regarding the number of floors.

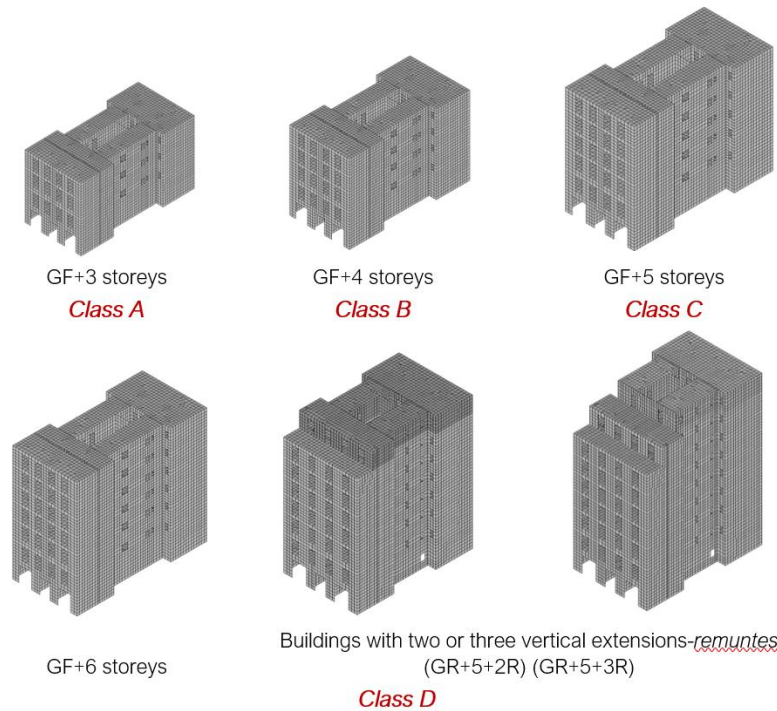


Figure 7.6 - Definition of vulnerability classes for Parameter 2 “Number of floors”.

Table 7.3 - Vulnerability classes proposed for the Parameter 3 "Horizontal diaphragms".

Parameter 3 - Horizontal diaphragms	
Class A	Light rigid floors
Class B	Weighted rigid floors
Class C	Semi-flexible floors (steel or timber beams and tile vaults)
Class D	Flexible floors (timber beams and timber planks)

Table 7.3 shows the definition of the vulnerability classes, according to the different horizontal diaphragms. Figure 7.7 shows the definition of the vulnerability classes for the different horizontal diaphragms depending on their type, material and quality, as well as their in-plane stiffness.

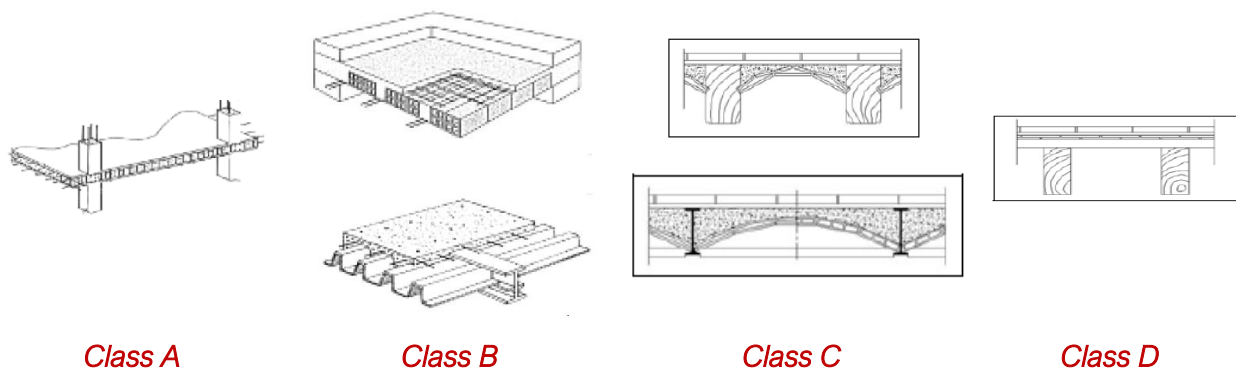


Figure 7.7 - Definition of vulnerability classes for Parameter 3 "Horizontal diaphragms".

Table 7.4 - Vulnerability classes proposed for the Parameter 4 "Plan configuration".

Parameter 4 - Plan configuration	
Class A	Buildings with a regular shape (centred staircase and patios) $\beta=a/l \geq 75$; Building with an eccentricity (difference between the centre of rigidity and centre of mass) less than 10% of the greater dimension in plan
Class B	Buildings with a regular shape (centred staircase and patios) $55 \leq \beta=a/l < 75$; Building with an eccentricity (difference between the centre of rigidity and centre of mass) between 10% and 20% of the greater dimension in plan
Class C	Buildings with a regular shape (centred staircase and patios) $35 \leq \beta=a/l < 55$; Building with an eccentricity (difference between the centre of rigidity and centre of mass) between 20% and 30% of the greater dimension in plan
Class D	Building with an irregular plan (lateral staircase and patios) $\beta=a/l < 35$; Building with an eccentricity (difference between the centre of rigidity and centre of mass) greater than 30% of the larger dimension in plan

Table 7.4 presents the vulnerability classes for the different plan configurations. Figure 7.8 presents examples of possible classification of the different geometrical configurations of existing buildings into four vulnerability classes.



Figure 7.8 - Definition of vulnerability classes for Parameter 4 "Plan configuration" with examples of existing buildings plan configurations (adapted from Cornadó Bardón 2015).

Table 7.5 - Vulnerability classes proposed for the Parameter 5 "Vertical irregularity".

Parameter 5 - Vertical irregularity

- Class A** Building without vertical extension
- Class B** Building with one vertical extension (aligned with the front façade)
- Class C** Building with two vertical extensions (aligned and retracted from the front façade)
- Class D** Building with three vertical extensions (one aligned and two retracted from the front façade)
- Building with a hybrid system (load bearing walls over a steel frame on the ground floor)

Table 7.5 and Figure 7.9 describe the different vulnerability classes for the vertical irregularity with the presence of vertical extensions.

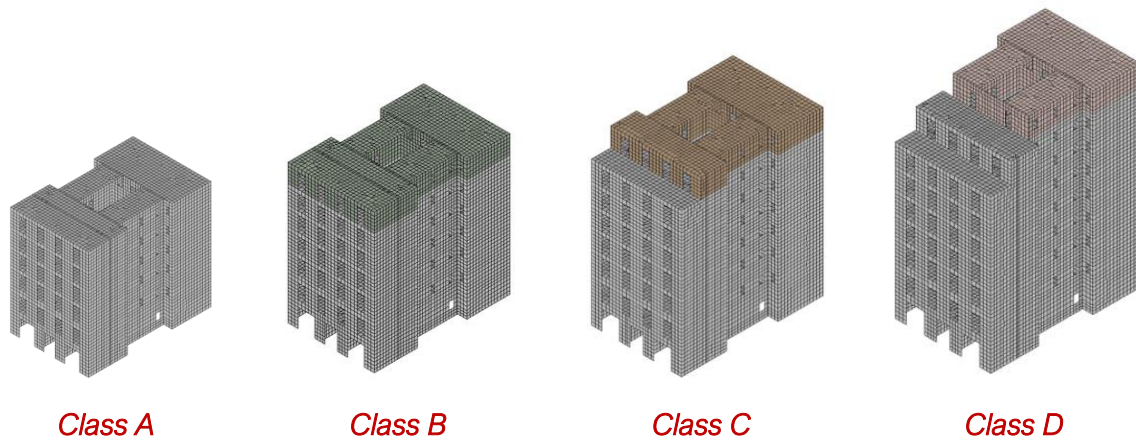


Figure 7.9 - Definition of vulnerability classes Parameter 5 “Vertical irregularity”.

Table 7.6 - Vulnerability classes proposed for the Parameter 6 “Presence of patios”.

Parameter 6 - Presence of patios

- Class A** Building with no lateral patios
- Class B** Building with one lateral patio on each side
- Class C** Building with two smaller lateral patios on each side
- Class D** Building with three or more lateral patios on each side

Table 7.6 describes the vulnerability classes regarding the presence of patios in the existing buildings. Figure 7.10 shows examples of different geometrical configurations of existing *Example* buildings for the possible classification of the vulnerability classes regarding the presence of patios.

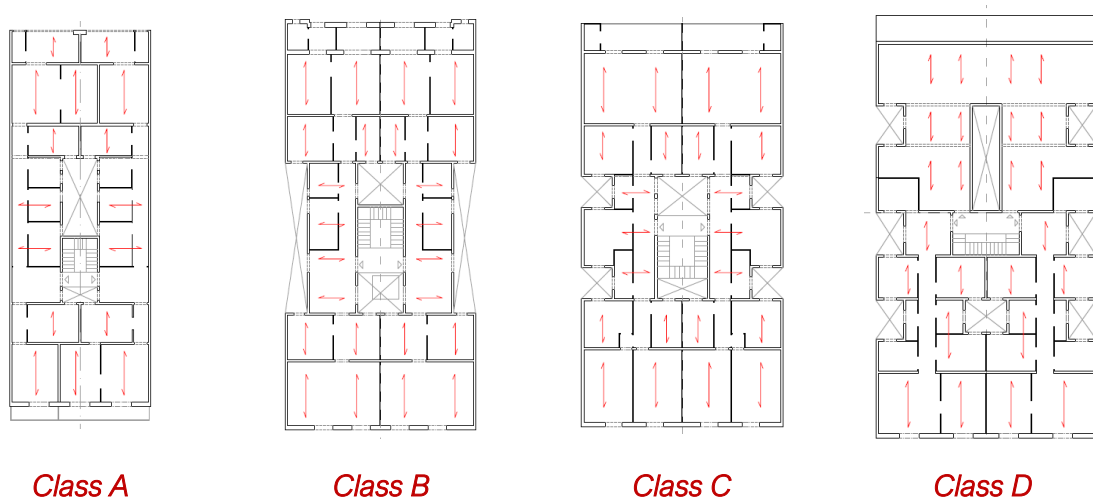


Figure 7.10 - Definition of vulnerability classes for Parameter 6 “Presence of patios” (adapted from Cornadó Bardón 2015).

*Table 7.7 - Vulnerability classes proposed for the Parameter 7 "Façade openings at ground floor".***Parameter 7 - Façade openings at the ground floor**

- Class A** Percentage of façade openings on the ground floor smaller than 30%
- Class B** Percentage of façade openings on the ground floor between 30% and 37%
- Class C** Percentage of façade openings on the ground floor between 37% and 45%
- Class D** Percentage of façade openings on the ground floor equal or higher than 45%

Table 7.7 defines the vulnerability classes for the façade openings at the ground floor. The percentage of façade openings is calculated with the equation (see Figure 7.2) as the ratio between the area of all facade openings and the total area of both front and back façade on the ground floor for the loading direction parallel to the façade. Hence, this parameter is excluded from the VIM form for the Y direction (perpendicular to the façade).

*Table 7.8 - Vulnerability classes proposed for the Parameter 8 "Non-structural elements".***Parameter 8 - Non-structural elements**

- Class A** Buildings with no non-structural elements
- Class B** Buildings with only small and light non-structural elements, which are well-connected to the structural elements; Buildings with exterior large/heavy elements well-connected to the resistant systems, and well-connected internal false ceilings
- Class C** Buildings with large/heavy elements poorly connected to structural elements due to bad execution or deterioration of the connections; Buildings with external small/light accessory elements badly connected to the structural elements
- Class D** Buildings with exterior large/heavy elements poorly or badly connected to the structural elements; Buildings with projected elements subsequently added to the main structural system

*Table 7.9 - Vulnerability classes proposed for the Parameter 9 "General maintenance conditions".***Parameter 9 - General maintenance conditions**

- Class A** The building is in a good condition and there are no visible cracks
- Class B** Some structural load bearing walls present small hairline cracks that are not widespread and are not caused due to earthquake
- Class C** Structural load bearing walls present a poor state of conservation showing moderate cracks and/or slight signs of deformation in the structural elements
- Class D** Structural load bearing walls are characterised by severe deterioration of materials with widespread damage (cracks or deformations or material degradation)

Table 7.8 and Table 7.9 describes the different vulnerability classes for the non-structural elements and general maintenance conditions, as proposed by (GNDT, 2007).

The next five parameters are regarding the influence of the aggregate effect on the buildings' seismic vulnerability as proposed by Formisano et al. (2015). The same vulnerability classes have been adopted for the vulnerability assessment in the X direction (parallel to the façade).

Table 7.10 - Vulnerability classes proposed for the Parameter 10 "Presence of adjacent buildings with different height".

Parameter 10 - Presence of adjacent buildings with different height

- Class A** The building is enclosed between two buildings of the same height
- Class B** The building is adjacent to a building with the same height and a taller one; The building is enclosed between two taller adjacent buildings
- Class C** The building is enclosed between one building of the same height and a shorter one; The building is located between a taller and a shorter building
- Class D** The building is enclosed between two shorter buildings

Table 7.10 defines the vulnerability classes for Parameter 10, as proposed by proposed by Formisano et al. (2015). Figure 7.11 represents definition of the vulnerability classes for the presence of adjacent buildings with different heights.

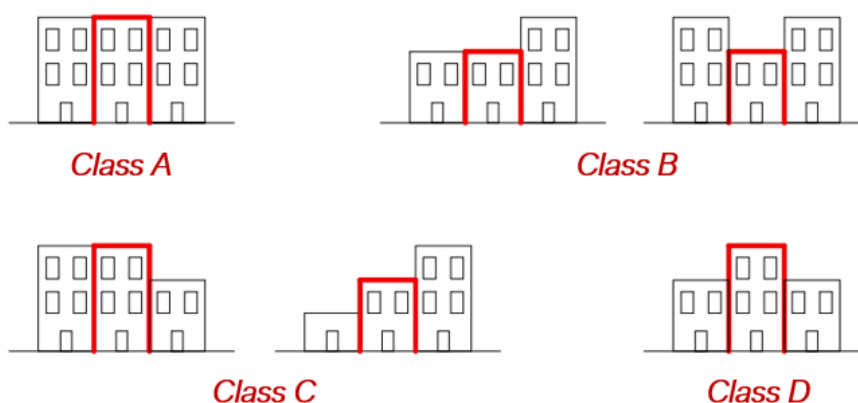


Figure 7.11 - Definition of vulnerability classes for Parameter 10 "Presence of adjacent buildings with different height" (adapted from Formisano et al. 2015).

Table 7.11 - Vulnerability classes proposed for the Parameter 11 "Position of the buildings in the aggregate".

Parameter 11 - Position of the buildings in the aggregate

- Class A** Building within a structural aggregate
- Class B** Building between two buildings enclosed in row
- Class C** Building in a corner position within a structural aggregate
- Class D** Building in a corner position within an in-row structural aggregate

Table 7.11 describes the different vulnerability classes regarding the position of the building in an aggregate, proposed by proposed by Formisano et al. (2015). Figure 7.12 shows the definition of the four classes depending on the position of the structural unit in an urban block.

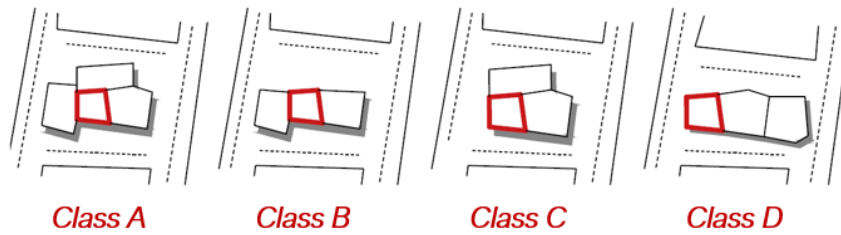


Figure 7.12 - Definition of vulnerability classes for Parameter 11 "Position of the buildings in the aggregate" (adapted from Formisano et al. 2015).

Table 7.12 - Vulnerability classes proposed for the Parameter 12 "Number of staggered floors".

Parameter 12 - Number of staggered floors

- Class A** No staggered storeys
- Class B** Presence of two staggered storeys
- Class C** Presence of four staggered storeys
- Class D** Presence of more than four staggered storeys

Table 7.12 defines the vulnerability classes for Parameter 12, proposed by Formisano et al. (2015). Figure 7.13 illustrates the different vulnerability classes regarding the different number of staggered floors among adjacent buildings.

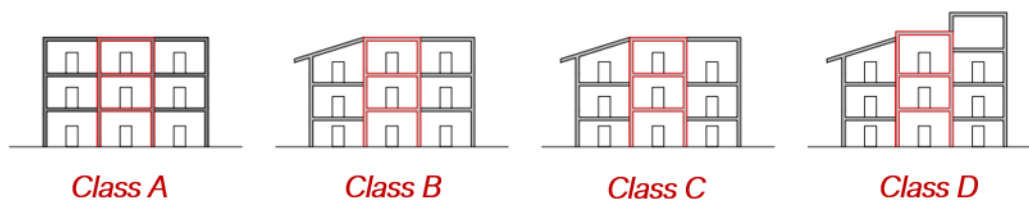


Figure 7.13 - Definition of vulnerability classes for Parameter 12 "Number of staggered floors" (adapted from Formisano et al. 2015).

Table 7.13 - Vulnerability classes proposed for the Parameter 13 "Effect of either structural or typological heterogeneity among adjacent structural units".

Parameter 13 - Effect of either structural or typological heterogeneity among adjacent structural units

- Class A** The studied building is adjacent to buildings with a very different structural typology (e.g. a masonry building adjacent to a reinforced concrete building)
- Class B** The studied building is adjacent to buildings made of the same material but built with a construction technique worse than the examined one
- Class C** The building is homogeneous with the adjacent buildings from both the typological and the structural viewpoint
- Class D** The studied building is next to buildings made of the same material but having greater strength than the examined one

Table 7.13 defines the vulnerability classes for the Parameter 13, proposed by Formisano et al. (2015). Figure 7.14 represents the four vulnerability classes by considering the effect of structural typological heterogeneity among adjacent buildings.

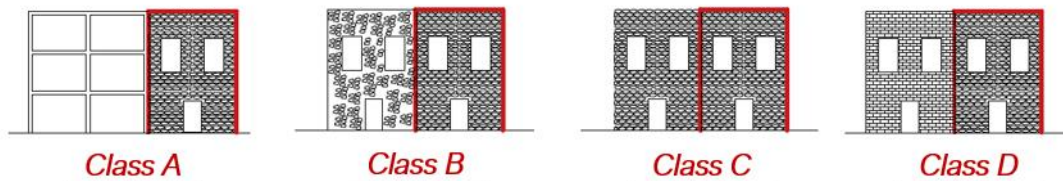


Figure 7.14 - Definition of vulnerability classes for Parameter 13 “Effect of either structural or typological heterogeneity among adjacent structural units” (adapted from Formisano et al. 2015).

Table 7.14 - Vulnerability classes proposed for the Parameter 14 “Percentage difference of opening areas among adjacent façades”.

Parameter 14 - Percentage difference of opening areas among adjacent façades

Class A	Equal opening percentage between the studied structural unit and the adjacent buildings
Class B	Between 5% and 10% of opening differences between the studied structural unit and the adjacent buildings
Class C	Between 10% and 20% of opening differences between the studied structural unit and the adjacent buildings
Class D	More than 20% of opening differences between the studied structural unit and the adjacent buildings

Table 7.14 describes the different vulnerability classes for the Parameter 14, considering the percentage difference of façade openings. Figure 7.15 illustrates a graphical description of the different vulnerability classes for this parameter proposed by Formisano et al. (2015).

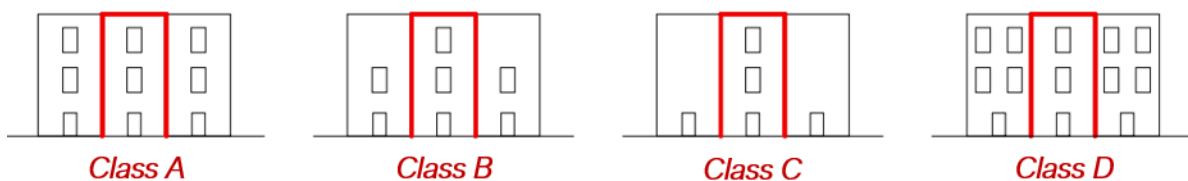


Figure 7.15 - Definition of vulnerability for Parameter 14 “Percentage difference of opening areas among adjacent façades” (adapted from Formisano et al. 2015).

7.3.3. Definition of weights for the vulnerability parameters

The definition of the parameters’ weights in previous proposals of the vulnerability index methods was based on the judgement of professionals. It must be noted that very significant differences can be seen between the weights adopted by the GNDT in the original VIM form and the ones proposed by other authors (Ferreira et al., 2017; GNDT, 2007; Maio et al., 2020; Ortega et al., 2019; Romis et al., 2021; Vicente et al., 2008; Vicente et al., 2011). These differences

highlight the difficulty involved in the definition of the appropriate weights purely based on experts' opinions and post-earthquake damage observation.

More recent research proposals have been partially or fully based on numerical simulation for the calibration of the weights required to complete the proposed VIM form. According to this approach, the weights are proposed to account for the relative significance of all the parameters and they can be numerically evaluated in terms of their impact on the seismic performance on the set of buildings analysed.

The Analytic Hierarchy Process (AHP) introduced by Saaty (1987) has been widely used to calibrate various weights and scores with the aim to decrease the procedure's subjectivity and obtain reasonable results. The AHP is a method oriented to decision-making involving various attributes (Makoond et al., 2021). It enables the hierarchy-based decomposition of a specific problem, ensuring that both its qualitative and quantitative aspects are considered in the evaluation process. This procedure enables an analyst to assign the weights in a logical and mathematically effective way. Normally, this process is performed by collecting information from experts, who give certain evaluation on some parameters by using pair-wise comparisons which are compiled into a decision matrix (A).

The AHP enables the estimation of the principal eigenvector (w) values by solving an eigenvalue problem, with the following equation:

$$Aw = \lambda_{max}w \tag{7.10}$$

Where λ_{max} is the principal eigenvalue of the pairwise comparison matrix A .

The AHP is considered to be an adequate procedure for the judgement of the relative importance of variables having different nature and the calculation of their relative weights. One advantage of this method is its ability to verify the consistency of the comparison matrix by calculating its eigenvalues and a consistency index, with the following equation:

$$CI = \frac{\lambda_{max} - n}{n - 1} \tag{7.11}$$

Where n is the number of analysed parameters.

Due to possible judgement errors, Saaty (1987) proposes the Consistency Ratio (CR), in order to evaluate the level of consistency of the matrix A . The ratio CR is calculated by comparing the consistency index CI (defined below) with the appropriate one of the following set of values of the Random Consistency Index (RI), shown in Table 7.15 (Saaty, 1987), as follows:

$$CR = \frac{CI}{RI} \leq 0.1 \tag{7.12}$$

Table 7.15 - Evaluation of the Random Consistency Index RI , according to (Saaty, 1987).

n	1	2	3	4	5	6	7	8	9	10
RI	0	0	0.58	0.9	1.12	1.24	1.32	1.41	1.45	1.49

According to Saaty (1987), a good precision is assured for small consistency ratios with $CR < 0.1$ in which case the judgments are considered acceptable.

The AHP method provides a fundamental scale from 1 to 9 in order to compare the relative importance of the evaluated parameters. Table 7.16 shows the different intensities of importance in the AHP scale with their definition and detailed description, where 1 denotes equal significance for both parameters and 9 denotes a significantly greater importance for one parameter compared to another. The purpose of this technique is to specify an order of magnitude for the weights' value and to identify the parameters that are more important. For the collection of data for the AHP method, different authors have used questionnaire surveys (Ortega, 2018; Romis, 2020).

Table 7.16 - The fundamental scale of the Analytic Hierarchy Process (AHP) (Saaty 1987).

Intensity of importance	Definition	Explanation
1	Equal importance	Two parameters contribute equally to the objective
3	Moderate importance of one over another	Experience and judgment slightly favour one parameter over another
5	Essential or strong importance	Experience and judgment strongly favour one parameter over another
7	Very strong importance	A parameter is strongly favoured and its dominance demonstrated in practice
9	Extreme importance	The evidence favouring one parameter over another is of the highest possible order of affirmation
2, 4, 6, 8	Intermediate values between two adjacent judgments	When compromise is needed

In this work, instead of using expert judgments for the evaluation of the importance of each of the seven vulnerability parameters (see Table 7.17a), the variation of the numerical results obtained from the performed pushover analyses on the previously described FE models (see Chapter 6) have been used as basic data for the objective application of the AHP method. The first step has been to select the numerical models that represent the specific vulnerability parameter and can contribute on the definition of its weight or relative importance for the overall building's seismic vulnerability (see Table 7.18). For each of the models, the maximum capacity has been chosen as the parameter representing the global seismic behaviour and therefore usable for the calibration of the parameters' weights. The same procedure has been done for both main directions (X and Y) using the numerical results of the pushover parametric study. In order to properly assign the importance for each parameter, a difference range has been proposed for each scale factor from 1 to 9 (see Table 7.17b). The provided scale has been used for the definition of the importance between two parameters by considering the differences in absolute values between the maximum capacities obtained from the selected numerical models for each of the vulnerability parameters (see Table 7.18).

Table 7.17 - a) Description of the seven vulnerability parameters; b) Scale for the assignment of the importance of each parameter according to their absolute differences.

a)		b)	
P1	Seismic coefficient	Difference range	Scale
P2	Number of floors	0	1
P3	Horizontal diaphragms	$0 < X \leq 0.14$	2
P4	Plan configuration	$0.14 < X \leq 0.29$	3
P5	Vertical regularity	$0.29 < X \leq 0.43$	4
P6	Presence of patios	$0.43 < X \leq 0.57$	5
P7	Façade openings	$0.57 < X \leq 0.71$	6
		$0.71 < X \leq 0.86$	7
		$0.86 < X \leq 1$	8
		1	9

Table 7.18 - Selection of numerical models for the calibration of each of the proposed vulnerability parameters for both loading directions: a) X direction and b) Y direction.

a)								b)						
FE Models	P1	P2	P3	P4	P5	P6	P7	FE Models	P1	P2	P3	P4	P5	P6
Model 1								Model 1						
Model 2								Model 2						
Model 3								Model 3						
Model 4								Model 4						
Model 5								Model 5						
Model 6								Model 6						
Model 7								Model 7						
Model 8								Model 8						
Model 9								Model 9						
Model 10								Model 10						
Model 11								Model 11						
Model 12								Model 12						
Model 13								Model 13						
Model 14								Model 14						
Model 15								Model 15						
Model 16								Model 16						
Model 17								Model 17						
Model 18								Model 18						
Model 19								Model 19						
Model 20								Model 20						
Model 21								Model 21						
Model 22								Model 22						

The variation of the maximum capacities obtained from the pushover curves for each of the 22 numerical models, as presented in the previous matrix in Table 7.18, has been considered for the estimation of the influence of each parameter on the building's seismic vulnerability. For example, almost all FE models have been considered for the Parameter 1 "Seismic coefficient", which depends on various structural attributes as previously mentioned (see Figure 7.3). The influence of the Parameter 1 has been assessed based on a single typology of diaphragm, i.e. avoiding models 14-17 as shown in Table 7.18, in order to keep the same magnitude of the masses at the storeys of the building in the comparison amongst the numerical models. The influence of the Parameter 2 "Number of floors" has been investigated by only considering the numerical models with the variations of number of storeys and presence of vertical extensions. Only the numerical models with the variation of the type of floor system have been accounted for the calibration of the Parameter 3 "Horizontal diaphragms", and so on.

Subsequently, the numerical results on the maximum capacity (MC) for each model have been arranged and their minimum ($MC_{min}(g)$), maximum ($MC_{max}(g)$) and average ($MC_{avg}(g)$) values from all the selected models have been calculated. Table 7.19 and Table 7.20 show the summary results of the maximum capacities and the calculation of their variation as a ratio between the difference of the $MC_{max}(g)$ and $MC_{min}(g)$ values and the $MC_{mean}(g)$ value, in order to normalise them. The values $MC_{mean}(g)$ is obtained as the mean value of the $MC_{avg}(g)$ values obtained for the group of selected models for each parameter. Moreover, the difference in absolute values between each of the parameters has been calculated. This difference is used for the assignment of the pairwise comparisons using the scale previously defined in Table 7.17b.

Table 7.19 - Numerical results of the maximum capacity (MC) for the definition of the parameters' weights in X direction.

Maximum capacity (MC)	P1	P2	P3	P4	P5	P6	P7
$MC_{min}(g)$	0.065	0.103	0.110	0.106	0.106	0.126	0.116
$MC_{max}(g)$	0.164	0.161	0.145	0.147	0.147	0.147	0.145
$MC_{avg}(g)$	0.115	0.132	0.128	0.126	0.126	0.137	0.131
$\frac{MC_{max}(g) - MC_{min}(g)}{MC_{mean}(g)}$	0.776	0.453	0.274	0.321	0.321	0.161	0.229
Difference in absolute values		0.323	0.502	0.456	0.456	0.615	0.547
			0.179	0.133	0.133	0.292	0.224
				0.046	0.046	0.113	0.045
					0.000	0.159	0.091
						0.159	0.091
							0.068

Table 7.20 - Numerical results of the maximum capacity (MC) for the definition of the parameters' weights in Y direction.

Maximum capacity (MC)	P1	P2	P3	P4	P5	P6	P7
$MC_{min} (g)$	0.191	0.191	0.274	0.222	0.191	0.222	0.306
$MC_{max} (g)$	0.443	0.443	0.410	0.398	0.341	0.398	0.327
$MC_{avg} (g)$	0.317	0.317	0.342	0.310	0.266	0.310	0.317
$\frac{MC_{max} (g) - MC_{min} (g)}{MC_{mean} (g)}$	0.811	0.811	0.436	0.566	0.482	0.566	0.067
Absolute differences		0.000	0.375	0.244	0.329	0.244	0.743
			0.375	0.244	0.329	0.244	0.743
				0.131	0.046	0.131	0.368
					0.084	0.000	0.499
						0.084	0.415
							0.499

Table 7.21 - Pairwise comparison matrix with the resulting priority vector for the weights for the seven vulnerability parameters considered in the VIM form for X loading direction.

	P1	P2	P3	P4	P5	P6	P7	Priority vector (weights)
P1	1	4	5	5	5	6	5	43.3%
P2	1/4	1	3	2	2	4	3	17.7%
P3	1/5	1/3	1	1/2	1/2	2	2	7.3%
P4	1/5	1/2	2	1	1	3	2	10.8%
P5	1/5	1/2	2	1	1	3	2	10.8%
P6	1/6	1/4	1/2	1/3	1/3	1	1/2	4.1%
P7	1/5	1/3	1/2	1/2	1/2	2	1	6.0%

Table 7.22 - Pairwise comparison matrix with the resulting priority vector for the weights for the seven vulnerability parameters considered in the VIM form for Y loading direction.

	P1	P2	P3	P4	P5	P6	Priority vector (weights)
P1	1	1	5	4	4	4	33.3%
P2	1	1	5	4	4	4	33.3%
P3	1/5	1/5	1	1/3	1/2	1/3	4.7%
P4	1/4	1/4	3	1	2	1	10.8%
P5	1/4	1/4	2	1/2	1	1/2	7.1%
P6	1/4	1/4	3	1	2	1	10.8%

Table 7.21 and Table 7.22 show the pairwise comparison matrix, which has been obtained from the comparison of the parameters according to the absolute differences of the maximum

capacities obtained from the numerical models, with the resulting priority vector indicating the parameters' weights. These estimated weights represent the relative importance of each parameter in the calculation of the corresponding vulnerability index. These principal eigenvectors (w_i) obtained using the previous equation (7.10) are normalised according to the sum of the original weights used in the VIM form. The final weights are shown in Table 7.23 and Table 7.24.

7.3.4. Evaluation of the vulnerability index and damage grade

The new proposed VIM forms for both main directions (X and Y) with the calibrated and normalised weights are presented in Table 7.23 and Table 7.24. The parameters treated according to the method herein presented are indicated in red.

Table 7.23 - Vulnerability index form for X direction including the aggregate effect.

PARAMETERS		CLASSES $C_{v,i}$				WEIGHTS
		A	B	C	D	w_i
1	Seismic coefficient	0	5	25	45	2.90
2	Number of floors	0	5	25	45	1.20
3	Horizontal diaphragms	0	5	15	45	0.50
4	Plan configuration	0	5	25	45	0.75
5	Height regularity	0	5	25	45	0.75
6	Presence of patios	0	5	25	45	0.30
7	Façade openings at ground floor	0	5	25	45	0.40
8	Non-structural elements	0	0	25	45	0.25
9	General maintenance conditions	0	5	25	45	1.00
10	Presence of adjacent buildings with different height	-20	0	15	45	1.00
11	Position of the building in the aggregate	-45	-25	-15	0	1.50
12	Number of staggered floors	0	15	25	45	0.50
13	Structural or typological heterogeneity among adjacent structural units	-15	-10	0	45	1.20
14	Percentage difference of openings among adjacent facades	-20	0	25	45	1.00

As aforementioned, the VIM form for the X direction includes the seven proposed structural parameters, which have been considered as the most significant for the seismic vulnerability assessment, according to the detailed building taxonomy. Additionally, the two parameters regarding the general maintenance conditions and the non-structural elements are added for both forms, with the same weight as proposed by previous authors (GNDT, 1993; Vicente, 2008). Finally, the five parameters including the aggregate effect of a structural unit in an urban block

have been added for the X direction (parallel to the façade), as proposed by Formisano et al. (2015). The same scores for each of the four vulnerability classes (A, B, C and D) have been considered as in the original GNDT forms, plus the additional parameters for the aggregates. The VIM form for the Y loading direction includes only six calibrated vulnerability parameters (indicated in red) (see Table 7.24). In the following form, the parameter regarding the façade openings on the ground floor is disregarded.

Table 7.24 - Vulnerability index form for Y direction.

PARAMETERS		CLASSES $C_{v,i}$				WEIGHTS
		A	B	C	D	w_i
1	Seismic coefficient	0	5	25	45	2.25
2	Number of floors	0	5	25	45	2.25
3	Horizontal diaphragms	0	5	15	45	0.30
4	Plan configuration	0	5	25	45	0.75
5	Height regularity	0	5	25	45	0.50
6	Presence of patios	0	5	25	45	0.75
7	Non-structural elements	0	0	25	45	0.25
8	General maintenance conditions	0	5	25	45	1.00

The vulnerability index has been calculated for all the numerical models in both main directions (X and Y) by using the new proposed VIM forms with only the calibrated parameters, i.e. parameters 1-7 for X direction and 1-6 for Y direction (see Table 7.25). In fact, the numerical models do not include non-structural elements and do not represent any specific maintenance condition. Moreover, the 22 FEM models represent individual buildings not located within any aggregate. Figure 7.16 illustrates the relationship between the maximum capacity obtained from the pushover analysis and the estimation of the vulnerability index for all the numerical models for the loading X and Y directions.

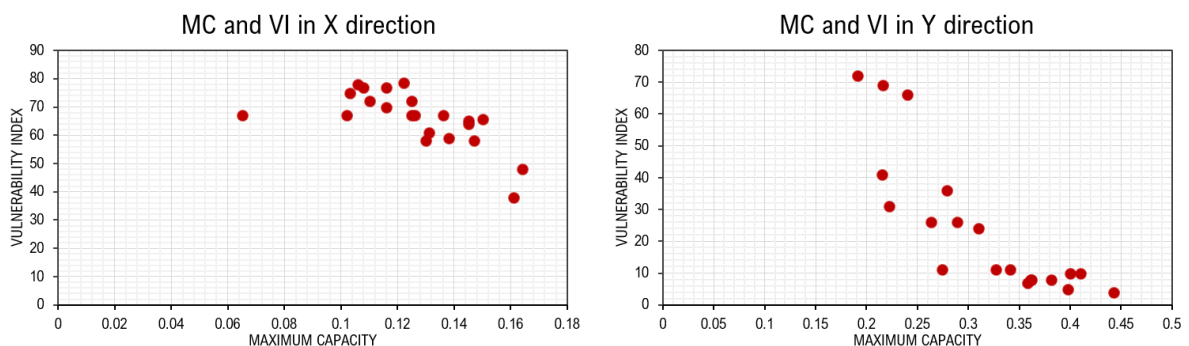


Figure 7.16 - Correlation between the maximum capacity obtained from the pushover analysis in X direction (left) and Y direction (right) and the calculated vulnerability index for all the numerical models.

Table 7.25 - Summary of the calculated vulnerability index (*I_v*) and the obtained maximum capacity for all the numerical models in both main X and Y directions.

Models	<i>I_v</i> (X direction)	<i>I_v</i> (Y direction)	Maximum capacity P _X	Maximum capacity P _Y
Model 1	67	11	0.12g	0.32g
Model 2	78	11	0.11g	0.34g
Model 3	38	4	0.16g	0.44g
Model 4	59	8	0.14g	0.38g
Model 5	75	26	0.10g	0.26g
Model 6	58	36	0.15g	0.28g
Model 7	72	66	0.12g	0.24g
Model 8	77	69	0.12g	0.22g
Model 9	77	72	0.11g	0.19g
Model 10	67	41	0.07g	0.22g
Model 11	67	26	0.10g	0.29g
Model 12	67	8	0.14g	0.36g
Model 13	48	8	0.16g	0.36g
Model 14	72	11	0.11g	0.27g
Model 15	67	7	0.12g	0.36g
Model 16	66	10	0.15g	0.40g
Model 17	65	10	0.15g	0.41g
Model 18	64	-	0.15g	0.40g
Model 19	70	-	0.13g	0.22g
Model 20	58	5	0.13g	0.37g
Model 21	61	31	0.15g	0.22g
Model 22	79	24	0.12g	0.31g

This test has been done in order to check the validity of the calibrated weights and the proper definition of the vulnerability classes according to the obtained numerical results. The obtained correlation can be considered as acceptable since the calculated vulnerability index is increasing consistently with the decrease of the maximum capacity obtained from the pushover analysis of the FE models.

7.3.5. Fragility curves

A fragility curve is the graphical representation of the cumulative distribution function of the probability of reaching or exceeding a specific damage or limit state, given a structural response to a given seismic action (FEMA, 2003). The fragility curves can be established as a function of a variable that characterises the seismic action, such as the effective peak acceleration (PGA), effective peak velocity (PGV), spectral displacement (S_d), or spectral acceleration (S_a). Different definitions have been proposed by several authors for the evaluation of the damage limit states to be considered in the generation of the fragility curves.

According to the HAZUS methodology (HAZUS 1999; FEMA 2003;), the construction of fragility curves is based on the assumption that the probability of reaching or exceeding a given damage state follows a cumulative lognormal distribution. Therefore, for a spectral displacement S_d , the probability of being in or exceeding a damage state, ds , is modelled as:

$$P[ds|S_d] = \Phi \left[\frac{1}{\beta_{ds}} \ln \left(\frac{S_d}{\overline{S_{d,ds}}} \right) \right] \quad (7.13)$$

where: Φ is the standard normal cumulative distribution function;

S_d is the spectral displacement,

$\overline{S_{d,ds}}$ is the median value of spectral displacement at which the structure reaches a certain threshold of the damage state, ds ,

and β_{ds} is the standard deviation of the natural logarithm of the spectral displacement of a damage state ds .

All fragility curves are plotted for an average value of the spectral displacement corresponding to the damage state threshold, considering the variability and uncertainty associated with capacity curve definition, damage states, and seismic action.

The parameter β_{ds} can be obtained by the following equation proposed in HAZUS (1999):

$$\beta_{ds} = \sqrt{[CONV(\beta_C \beta_D)]^2 + (\beta_{M(sds)})^2} \quad (7.14)$$

where: β_{ds} is the lognormal standard deviation that describes the total variability for structural damage state, ds ,

β_C is the lognormal standard deviation parameter that describes the variability of the capacity curve,

β_D is the lognormal standard deviation parameter that describes the variability of the demand spectrum,

$\beta_{M(sds)}$ is the lognormal standard deviation parameter that describes the uncertainty in the estimate of the median value of the threshold of the structural damage state ds .

The methodology used for the construction of the fragility curves and therefore the determination of the damage state probabilities is explained in the following paragraphs. A similar procedure to that proposed by the RISK-UE project (Giovinazzi and Lagomarsino, 2004; Milutinovic and Trendafiloski, 2003) is adopted. According to the RISK-UE project, it is assumed that the probability of damage follows a certain probability distribution (binomial or beta distribution), allowing for the calculation of the expected probabilities and the adjustment of the fragility curves.

The parameters $\overline{S_{d,ds}}$, and β_{ds} have to be defined for each damage state in order to calculate the probabilities from the distribution function Φ of Equation (7.13). As previously discussed in Chapter 6 (see section 6.3), the N2 method has been used for the definition of the bilinear capacity curves represented by the corresponding yield point coordinates (d_y , a_y) and the ultimate capacity

point coordinates (d_u , a_u) and furthermore, for establishing the performance point of each analysed building model. The so-called performance point represents the demand of strength and displacement and is obtained by intersecting the capacity curve with the seismic demand spectrum. Thus, this point is expressed in terms of spectral acceleration (S_a) and displacement (S_d), which are parameters used to generate the fragility curves and estimate the damage probability matrices.

Additionally, four limit states have been considered in order to correlate the seismic behaviour of the building with the damage obtained from a horizontal loading. In this research, the assignment of these limits states differ with the definition by previous authors (Giovinazzi and Lagomarsino, 2004), who provided some equations which relate the damage threshold with the previously obtained yield and ultimate displacement. This study has adopted a different set of criteria to set the limit states, based on the capacity curves generated from the numerical models. Figure 7.17 illustrates the four damage states that are defined from a typical pushover capacity curve obtained numerically.

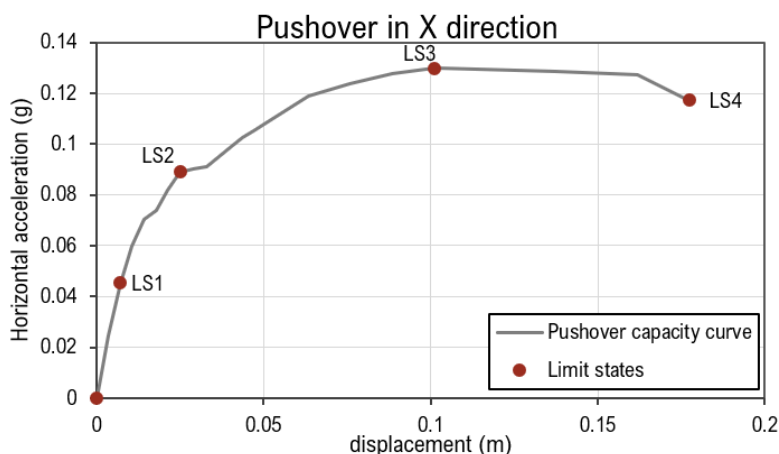


Figure 7.17 - Definition of four limit states on the pushover capacity curve in X direction of Model 20.

The first limit state LS1 is related with the appearance of the first cracks on the structure and can be defined at the end of the linear elastic range. The second limit state LS2 is linked to the cracking development on the load-bearing masonry walls. More specifically, this limit is caused by the appearance of shear cracks in the masonry piers located at the building's ground floor and it is normally associated with the first change in stiffness in the pushover curve. This behaviour has been confirmed in all the analysed numerical models, in X direction, due to the soft-storey response typically predicted for the buildings investigated (see Chapter 6, section 6.2.2). The third limit state LS3 corresponds to the maximum capacity of the building (maximum resisted acceleration) at which the structure shows a significant damage. The fourth limit state LS4 is the ultimate limit state, which is correlated with the near collapse of the building. This point has been chosen at the end of the pushover curve, which normally appears at a displacement corresponding to about 80% decrease of the maximum capacity according to the Italian seismic standards (MIT Ministero delle Infrastrutture e del Trasporti, 2019).

Furthermore, the standard deviation β_{ds} corresponding to each mean spectral damage threshold S_{ds} is estimated. Assuming that the probability of each damage state in its mean spectral displacement is 50% and that the probability of the other damage states follows a Beta distribution,

it is possible to calculate the standard deviation corresponding to each damage state (Giovinazzi, 2005).

In order to obtain the discrete probability distribution corresponding to the four damage states, the Continuous Beta Probability Distribution Function (PDF) is used. The Beta distribution is defined as follows (Giovinazzi, 2005):

$$PDF = p_{\beta}(x) = \frac{\Gamma(t)}{\Gamma(r)\Gamma(t-r)} \frac{(x-a)^{r-1}(b-x)^{t-r-1}}{(b-a)^{t-1}} \quad a \leq x < b \quad (7.15)$$

Where a , b , t , and r are the parameters of the distribution and Γ is the Gamma function. The bounds of the distribution are fixed as $a = 0$ and $b = 6$, and $t = 8$ is used as the value that makes this distribution fit well to a binomial distribution. The parameter r is a function of both parameters t and μ_D and is defined by the following Equation (7.16) (Giovinazzi, 2005):

$$r = t \cdot (0.007\mu_D^3 - 0.0525\mu_D^2 + 0.2875\mu_D) \quad (7.16)$$

The four mean damage values μ_D are calculated, by considering that the probability of each damage state is equal to 50% (see Table 7.29), see Equation (7.17).

$$p_{\beta}(k) = 0.5 \quad \text{for damage state } k = 1, 2, 3, \text{ and } 4 \quad (7.17)$$

The probability that the damage could be smaller or equal to one damage state is obtained by integrating the PDF function, equation (7.15), between a and the corresponding damage state x (see Equation (7.18):

$$P_{\beta}(x) = \int_a^x p_{\beta}(y) dy \quad (7.18)$$

The fragility curves define the probability of reaching or exceeding each damage grade D_k ($k=0 \div 5$) and are obtained directly from the beta cumulative probability density function (Giovinazzi, 2005), as indicated by Equation (7.19):

$$P[D_k] = 1 - P_{\beta}(k) \quad (7.19)$$

The fragility curves can be used to calculate the probability of occurrence of each state of damage and to create damage probability matrices. The damage probability matrices are derived using the performance point (which is related to the seismic demand and the capacity of the structure) and the corresponding fragility curves. Therefore, by entering the fragility curves with the parameter representing the structural response (in this case, the spectral displacement S_d), the probabilities corresponding to each damage state can be obtained according to Equation (7.20):

$$p_k = P_{\beta}(k+1) - P_{\beta}(k) = P_{\beta}[D_k] - P_{\beta}[D_{k+1}] \quad (7.20)$$

7.3.5.1. Tentative application to a subset of numerical models from the *Eixample* district

The previously described approach for construction of fragility curves has been used in a preliminary example of application to a subset of 13 numerical models of representative *Eixample* buildings. The models of this subset have all 5 storeys over the ground floor, and differ by a single variation of one structural attribute, i.e. the material property, the type of horizontal diaphragm, the size of the façade openings, the thickness of the wall, and the presence of patios. Although this considered subset of models is clearly unable of representing the entire complexity of the *Eixample*'s buildings, it constitutes an example of application derived from a reasonable number of detailed numerical computations.

Due to the limited number of numerical models considered in this tentative study, the construction of the fragility curves through Equation (7.13) is conducted by using a weighted mean $\overline{S_{d,ds}}^*$, which depends on the relative frequency of a specific instance related to a structural attribute, instead of considering the median value of numerical models' spectral displacements $\overline{S_{d,ds}}$. Given the impossibility of evaluating exactly the relative frequencies of each specific instance within all possible for a structural attribute, as this would require a comprehensive statistical study supported by a detailed survey of a large sample of buildings, the relative frequencies have been estimated based on expert judgment, as shown in Table 7.26. Such relative frequencies could be more accurately determined based on future studies based on a wider database of buildings of the *Eixample* district. Table 7.27 indicates the derived frequencies for the 13 numerical models, evaluated as the product of the assumed relative frequencies corresponding to the relevant instances of the considered structural attributes. Such frequencies are necessary to calculate the weighted means of spectral displacements corresponding to a given damage state $\overline{S_{d,ds}}^*$ of Table 7.28, and they provide a tentative criterion to weight the contribution of each model pertaining to the subset while evaluating the fragility curves. The spectral displacements for each of the numerical models have been estimated with the application of the N2 method (Fajfar, 2000), by transforming the Multi Degree Of Freedom (MDOF) model to an equivalent Single Degree Of Freedom (SDOF) system (see Chapter 6).

It is worth noticing that this proposed procedure is not conventional and it was adopted due to the lack of a greater amount of data resulting from various numerical models. As many buildings with varying structural characteristics coexist in the *Eixample* district, a more rigorous procedure would require the use of a high number of numerical models with numerous combinations of different instances of structural attributes. These limitations can be overcome by having a greater number of numerical models, by varying more than one structural attribute. In this way, the median value of numerical models' spectral displacements $\overline{S_{d,ds}}$ would be obtained more precisely from relative frequencies of a greater number of numerical models with more realistic variation of different structural attributes.

Table 7.26 - Tentative values of relative frequencies of instances for considered structural attributes in a subset of numerical models from the Eixample district based on expert judgement: a) material properties; b) horizontal diaphragms; c) façade openings; d) wall thickness; and e) presence of patios.

a)	Material	5 MPa	4 MPa	3 MPa	2 MPa
	Frequency	10%	60%	20%	10%
b)	Horizontal diaphragms	Rigid	Semi-flexible (steel beams)	Semi-flexible (timber beams)	Flexible
	Frequency	10%	45%	40%	5%
	Frequency	10%	60%	20%	10%
c)	Façade openings	Small openings	Reference openings	Big openings	
	Frequency	20%	60%	20%	
d)	Wall thickness	30 and 15 cm	45 and 15 cm		
	Frequency	60%	40%		
e)	Presence of patios	Narrow (without patios)	Lateral patios	Wide (two semi-patios)	Narrow (lateral patio)
	Frequency	40%	45%	5%	10%

Table 7.27 - Tentative evaluation of the frequencies of the assumed subset of numerical models based on expert judgement.

Models	Material	Horizontal diaphragms	Façade openings	Wall thickness	Presence of patios	Frequency
Model 1	0.6	0.45	0.6	0.6	0.45	0.18
Model 10	0.1	0.45	0.6	0.6	0.45	0.03
Model 11	0.2	0.45	0.6	0.6	0.45	0.06
Model 12	0.1	0.45	0.6	0.6	0.45	0.03
Model 14	0.6	0.1	0.6	0.6	0.45	0.04
Model 15	0.6	0.4	0.6	0.6	0.45	0.16
Model 16	0.6	0.05	0.6	0.6	0.45	0.02
Model 18	0.6	0.45	0.2	0.6	0.45	0.06
Model 19	0.6	0.45	0.2	0.6	0.45	0.06
Model 13	0.6	0.45	0.6	0.4	0.45	0.12
Model 20	0.6	0.45	0.6	0.6	0.4	0.16
Model 21	0.6	0.45	0.6	0.6	0.05	0.02
Model 22	0.6	0.45	0.6	0.6	0.1	0.04

Table 7.28 - Weighted means
 $\overline{S_{d,ds}}$ * of spectral displacements for each damage threshold.

Models	S _{d1}	S _{d2}	S _{d3}	S _{d4}
Model 1	0.34	0.68	6.39	9.1
Model 10	0.67	0.96	3.57	10.46
Model 11	0.7	1.05	4.88	5.58
Model 12	0.19	0.23	1.73	3.65
Model 14	0.28	0.55	2.12	3.5
Model 15	0.28	0.82	5.89	12.99
Model 16	0.28	0.8	1.53	13.11
Model 18	0.18	0.88	4.32	4.32
Model 19	0.23	0.92	3.27	6.31
Model 13	0.28	1.28	5.47	6.78
Model 20	0.49	0.98	7.01	12.3
Model 21	0.47	0.93	5.97	5.97
Model 22	0.38	0.85	7.03	10.58
<i>Weighted mean</i>	0.36	0.88	5.40	9.02
$\overline{S_{d,ds}}$ *				

Table 7.29 presents the values obtained for the mean damage μ_D with the probabilities of the expected damage state, when the probability of each damage state (slight, moderate, extensive and complete) is fixed at 50%.

Table 7.29 - Probability distribution of the expected damage states when fixing a 50% probability for each damage state: (1) slight, (2) moderate, (3) extensive and (4) complete, according to Giovinazzi (2005).

Condition	μ_d	$P_\beta(1)$	$P_\beta(2)$	$P_\beta(3)$	$P_\beta(4)$
$P_\beta(1) = 0.50$	0.767	0.500	0.850	0.973	0.998
$P_\beta(2) = 0.50$	1.556	0.132	0.500	0.822	0.969
$P_\beta(3) = 0.50$	2.499	0.018	0.174	0.500	0.827
$P_\beta(4) = 0.50$	3.443	0.001	0.031	0.178	0.500

The parameter β_{ds} is estimated by applying the least-square method criterion of the lognormal distribution function Equation (7.13) to pass closely to the probabilities obtained from the Beta distribution, presented in Table 7.29. Figure 7.18 illustrates an example of fragility curves construction using the methodology described.

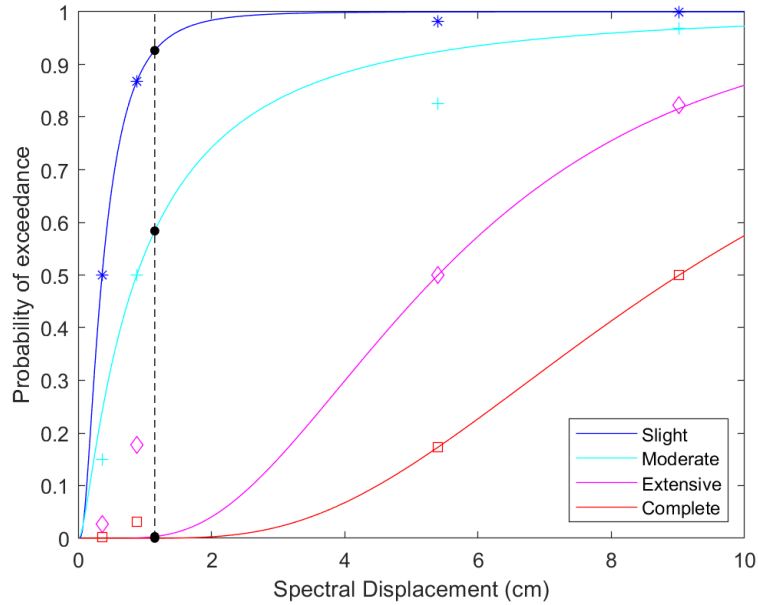


Figure 7.18 - Example of fragility curves for the subset of existing masonry buildings in the Eixample district for four different damage states (slight, moderate, extensive and complete), by plotting the spectral displacement for the reference model.

Table 7.30 shows the parameters used for the generation of the fragility curves for the selected numerical models, such as the estimated mean spectral displacements values and the standard deviation for each damage state.

Table 7.30 - Parameters characterising the fragility curves for the selected subset of numerical models of the existing URM buildings.

S_{d1}	S_{d2}	S_{d3}	S_{d4}	β_1	β_2	β_3	β_4
0.36	0.88	5.40	9.02	0.80	1.27	0.57	0.54

The mean damage grade can be defined following a discrete damage distribution by using Equation (2.6). Table 7.31 presents an example of the obtained damage probability matrix for URM buildings with six storeys (GF+5) with different material properties located in the Eixample district for the probabilistic hazard scenario for the city of Barcelona reported in Chapter 3 (Irizarry, 2004). As expected, the model with the highest masonry compression strength (Model 10, with compressive strength of 5 MPa) has the lowest mean damage grade of 1.47 and the model with the lowest compressive strength of 2 MPa (Model 12) has a higher damage grade of 1.58. However, the values of the mean damage grade for the selected numerical models by varying the masonry’s compressive strength are very close and their estimation could be influenced by uncertainties regarding the definition of the damage thresholds, the demand spectral parameters, and the structural parameters obtained from the numerical models (Bonett Díaz, 2003).

Table 7.31 - Damage probability matrix for URM existing building in Eixample district for the performance point (PP) obtained for a probabilistic hazard scenario for the city of Barcelona.

Models	PP	0	1	2	3	4	μ_D
Model 1	1.15	0.07	0.34	0.58	0	0	1.50
Model 10	1.13	0.08	0.35	0.55	0	0	1.47
Model 11	1.21	0.07	0.34	0.6	0	0	1.54
Model 12	1.27	0.06	0.33	0.61	0.01	0	1.58

7.4. EXAMPLES OF APPLICATION OF THE PROPOSED METHODOLOGY

The new proposed methodology has been applied to two cases: (1) a large number of existing masonry buildings reported by Cornadó Bardón (2015) and (2) a typical urban block considering the aggregate effect. This has been considered as a test study for the application of the previously proposed methodology for the seismic vulnerability assessment of masonry building with specific characteristics, by considering parameters which have been calibrated and applied for different building typologies. Each of the vulnerability parameters can contribute for the decrease or increase of the vulnerability depending on the definition of the appropriate classes.

7.4.1. Application to a sample of buildings from the *Eixample* district

The sample of 70 building typologies provided by Cornadó Bardón (2015), as presented in Chapter 4 (see section 4.3), is considered for the application of the new proposed methodology for evaluating the seismic vulnerability to individual existing URM buildings. The new proposed VIM forms for the X and Y loading directions have been applied to the building stock, without considering the aggregate effect, in order to evaluate, as a first approach, their seismic vulnerability as individual buildings. Hence, for the X direction only the parameters 1 to 9 (the seven calibrated parameters and the two parameters from the original VIM forms) have been considered (see Table 7.23). The estimated vulnerability index (I_V) can be within the range $0 \leq I_V \leq 362.25$ for the X and Y direction, according to the assigned calibrated weights for the new proposed vulnerability parameters. However, both indices have been normalised to be within the range of $0 \leq I_V \leq 100$, where if $I_V = 0$ indicates that the building has no seismic vulnerability and if $I_V = 100$ presents the maximum seismic vulnerability.

Figure 7.19 shows a frequency distribution of the values estimated for the vulnerability index for X and Y directions of the analysed building typologies. As expected and obtained previously with the nonlinear static analysis of the numerical building models, the seismic vulnerability is much higher in the X loading direction (parallel to the façade) than the Y direction (perpendicular to the façade). The biggest influence in the determination of the vulnerability index has the first parameter regarding the calculation of the seismic coefficient, which considers the building's geometrical configuration, structural system and the material properties. Moreover, the number of storeys, which is normally between 6 and 8, including the vertical extensions, has a significant effect in both directions.

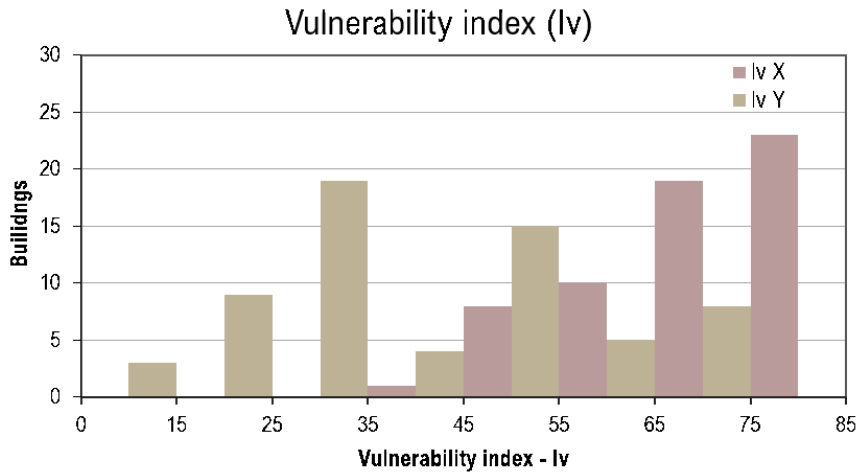


Figure 7.19 - Vulnerability index distribution for both X and Y directions of the analysed building typologies in the Eixample district.

Figure 7.20a presents the obtained results for the vulnerability index calculated for the X direction, by indicating that 5% of the buildings have a vulnerability index between 41 and 50, which is regarded as low to medium vulnerability, 11% are between 51 and 60, 27% are between 61 and 70, 48% are between 71 and 80 and only 9% surpass a seismic vulnerability of 80, which corresponds to medium, medium-high and high levels of vulnerability, respectively. Regarding the lv for the Y direction (see Figure 7.20b), a higher percentage of buildings have a low to medium vulnerability (14% below 20 and 31% for a range between 21 and 40, 29% for a range between 41 and 60, and 22% for a range between 51 and 70) and only 4% of the buildings show a higher level of seismic vulnerability.

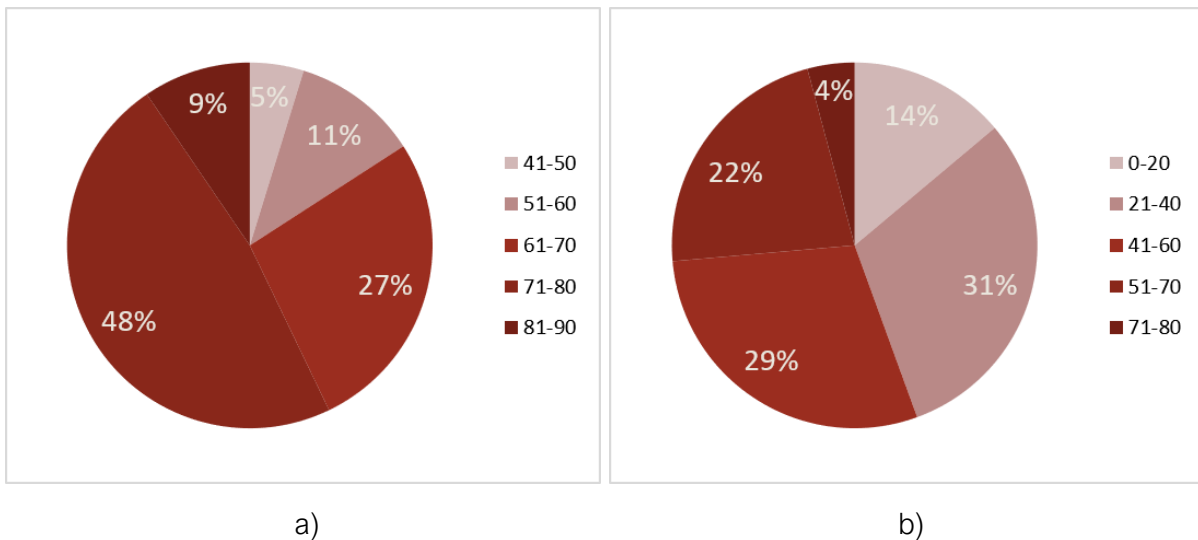


Figure 7.20 - Frequency of calculated vulnerability index values: a) lv for X direction and b) lv for Y direction.

The mean damage grade has been evaluated using the previously explained equations (2.3) and (2.4) in Chapter 2 proposed by Lagomarsino and Giovinazzi (2006) and later improved by Bernardini et al. (2007) for the macroseismic vulnerability method. This equation correlates the

seismic hazard in terms of macroseismic intensity I_{EMS-98} ($0 \leq I_{EMS-98} \leq 12$), the building's vulnerability (V) and the ductility (Q). The analytical correlation (Equation (2.5) between the macroseismic vulnerability index (V) and the vulnerability index (I_v) proposed by Vicente et al. (2011) has been used. Subsequently, vulnerability curves have been plotted considering the mean values of the estimated mean damage grade, as well as by adding or subtracting their standard deviation ($I_{v,mean}+STD$; $I_{v,mean}-STD$), as shown in Figure 7.21. The mean damage grade for an intensity I_{EMS-98} between VI and VII falls between 1 and 2.5, which is similar to the mean damage grade obtained from the numerical models, equal to 1.5 (in a scale from 0 to 4), as presented in section 7.3.5.

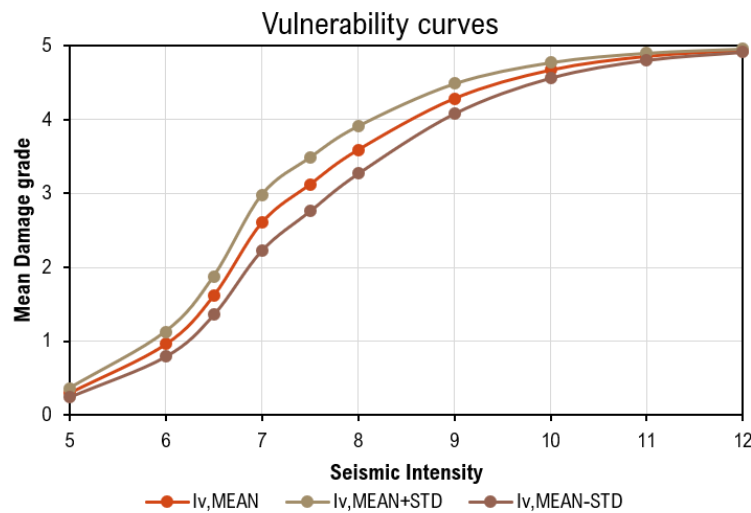


Figure 7.21 - Vulnerability curves for the analysed building stock in the Eixample district.

Figure 7.22 shows the generated fragility curves for the mean vulnerability index for the X seismic loading direction obtained for the analysed building sample for different I_{EMS-98} intensities (from V to XII). The fragility curves defining the probability of reaching or exceeding each damage grade D_k ($k = 0 \div 5$) are determined directly from the beta cumulative density function, by using the Equation (7.19).

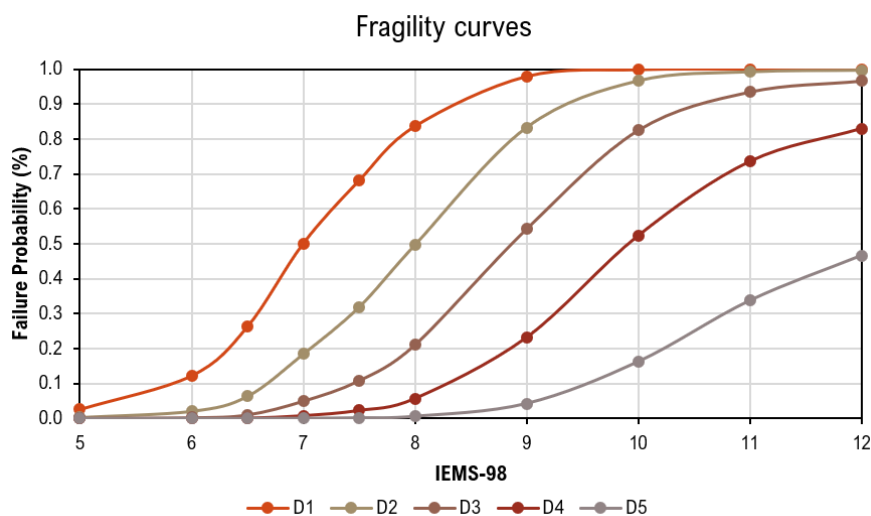


Figure 7.22 - Fragility curves obtained for the mean vulnerability index of the analysed building stock.

As previously mentioned in Chapter 2, the expected seismic intensity in Barcelona is between the grades VI and VII according to the European Macroseismic Scale EMS-98 intensity, corresponding with the demand spectra curves for the deterministic and the probabilistic approach (Alex H. Barbat et al., 2006; Irizarry, 2004). Figure 7.23 shows the histogram of probability of damage occurrence for six damage grades by considering the null damage (D_0 , D_1 , D_2 , D_3 , D_4 and D_5) for a possible earthquake with a I_{EMS-98} intensity of VI and VII. These probability histograms of a certain damage grade, $P(D_k)$, are derived from the difference of cumulative probabilities as presented in Equation (7.20).

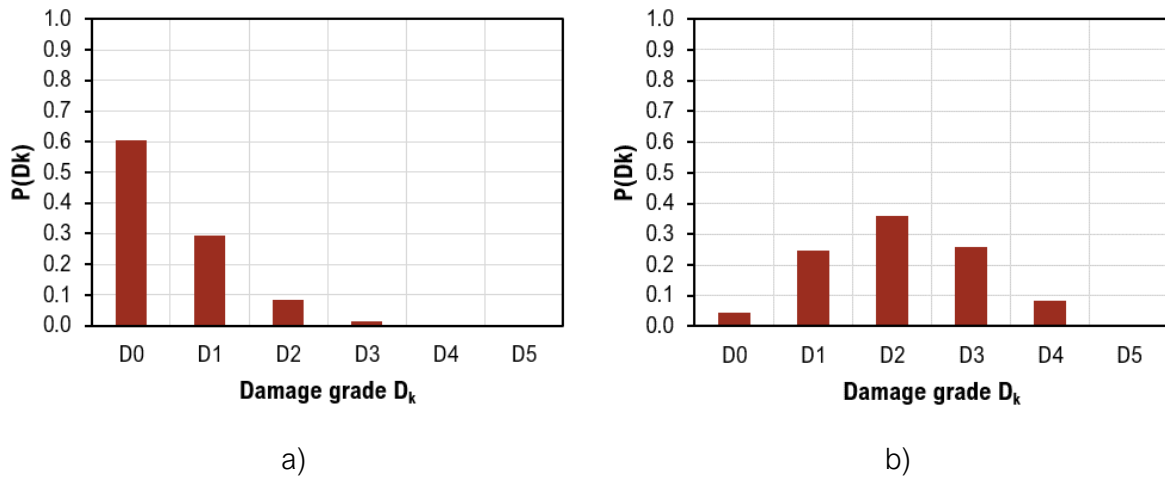


Figure 7.23 - Discrete damage distribution histograms for the mean I_v value of the analysed building stock: a) $I_{EMS-98} = VI$; b) $I_{EMS-98} = VII$.

7.4.2. Specific urban block of the *Eixample* district

The second example consists of a test study of a specific urban block of the *Eixample* district, by considering the aggregate effect for the seismic vulnerability assessment of the existing masonry buildings. It should be noted that the vulnerability parameters related to the influence of the adjacent buildings in the seismic performance and vulnerability of the *Eixample*'s buildings have not been recalibrated, following the approach proposed by Formisano et al. (2015) as part of the proposed methodology. Hence, there is need of further investigation with detailed numerical models in order to determine the influence of each of the new parameters regarding the aggregate effect.

The selected block has been chosen from the area of the *Eixample* district with the greatest proportion of unreinforced masonry buildings, as reported and previously investigated by (Rago, 2022). The block is located in *La Dreta de l'Eixample* neighbourhood, between the following streets: *Gran Via de les Corts Catalanes*, *Carrer de Roger de Llúria*, *Carrer de Casp* and *Carrer de Pau Claris*. This urban block consists of 15 URM residential existing buildings, one reinforced concrete building and a church. The last two buildings have not been considered as part of the study. Figure 7.24 shows a geometrical configuration of the selected urban block with the buildings' main façades elevations. The buildings are identified as B1 to B17. Figure 7.25 shows a 3D representation of the urban block. Architectural plans of some of the buildings have been found from previous studies (Ajuntament de Barcelona, 1987; Cornadó Bardón, 2015).

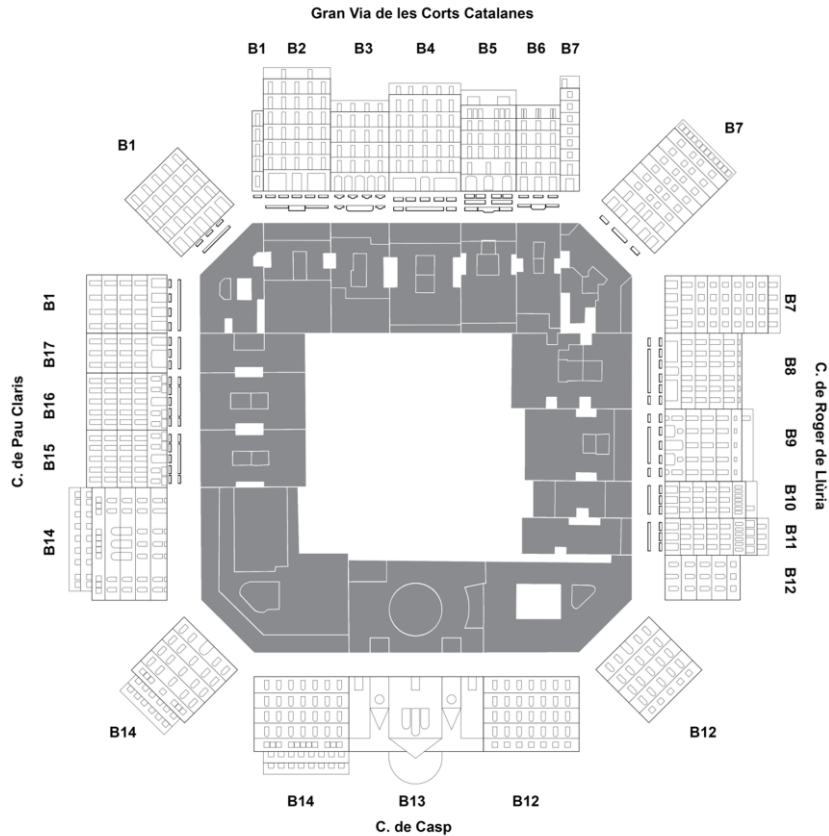


Figure 7.24 - Geometrical configuration of the specific urban block with the main façade elevations of the existing buildings (Rago, 2022).

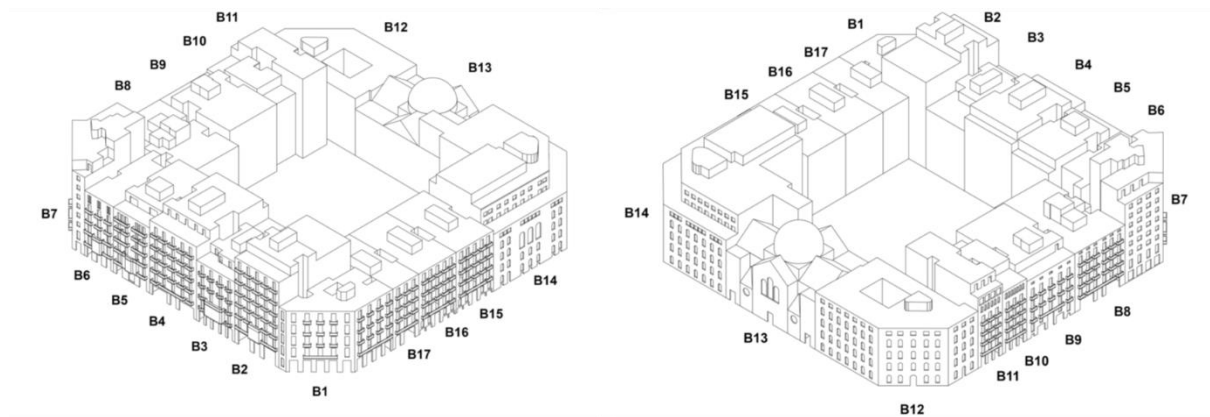


Figure 7.25 - 3D representation of the urban block (Rago, 2022).

The new proposed VIM forms have been adopted in order to consider the aggregate effect in X direction (parallel to the façade) including the five parameters proposed by Formisano et al. (2015). The data collection was done by carrying out a preliminary visual inspection and by compiling a checklist in order to identify and classify the necessary information (position of buildings, number of floors, number of openings, presence of vertical extensions etc.). Additionally, the information regarding the vulnerability parameters related to the aggregate effect (height difference of adjacent buildings, presence of staggered floors, the presence of in structural

or typological heterogeneity, and difference in percentage of openings between adjacent buildings) have been evaluated by on-site survey and also using Google Earth satellite view (Rago, 2022).

Table 7.32 shows the information of the buildings' characteristics (including position and location in the urban block, the date of construction, the type of material, the number of storeys, the geometrical configuration - width and depth of the building, the presence of patios and the existence of vertical extensions).

Table 7.32 - Summary information of the buildings' characteristics of the studied urban block (the buildings highlighted in grey are not evaluated) (Rago, 2022).

Nº	Position	Street name	Construction Date	Material	Nº of storeys	Width (m)	Depth (m)	Patios	Remuntes
B1	Corner	Pau Claris 96	1881	M	5	15.43	17	1	0
B2	Row	Gran Via 652	1890	M	8	17.75	23	1	1
B3	Row	Gran Via 654	1904	M	6	15.50	29	1	1
B4	Row	Gran Via 656	1880	M	7	18.90	29	1	1
B5	Row	Gran Via 658	1871	M	8	14.65	29	1	1
B6	Row	Gran Via 660	1890	M	6	11.60	29	1	0
B7	Corner	Roger de Llúria 23	1946	RC	10	15.00	19	1	1
B8	Row	Roger de Llúria 21	1872	M	5	20.00	32	2	0
B9	Row	Roger de Llúria 19	1872	M	6	19.10	28	1	1
B10	Row	Roger de Llúria 17	1900	M	7	9.70	26	1	1
B11	Row	Roger de Llúria 15	1884	M	8	9.70	29	1	2
B12	Corner	Roger de Llúria 13	1883	M	5	25.23	26	0	1
B13	Row	Casp 27 (Church)	1883	M	1	35.50	26	0	0
B14	Corner	Casp 25-29	1884	M	8	25.00	26	0	3
B15	Row	Pau Claris 90	1883	M	5	15.20	28	1	0
B16	Row	Pau Claris 92	1883	M	5	15.10	28	1	0
B17	Row	Pau Claris 94	1883	M	5	10.50	28	1	0

The oldest URM building (B5) was constructed in 1871, while the reinforced building B7 is the most recent one, dated from 1946. Since all of the URM buildings were built before the adoption of the first Spanish Seismic Code (1969), it can be concluded that they were designed with no seismic design requirements. However, it is unknown whether any structural reinforcement has been implemented. Almost all of the buildings have a similar resisting structural system consisting of load-bearing walls with one-way semi-flexible floor slab (steel or timber beams and tile vaults). The number of storeys varies from 5 to 8 including vertical extensions when present. In terms of geometry, the facades' widths range from 9.7 m for the narrowest (B7) to 35.5 m for the widest (B13). The buildings' plan has an average depth of 27 m, ranging from 17 m (B1) to 32 m (B8). The most typical geometrical configuration is the one with central staircase and interior patios in the central core, with lateral patios that interrupt the continuity of the longitudinal masonry walls between adjacent buildings.

After applying the new proposed VIM forms for both directions, the vulnerability indices have been estimated by assigning the class scores C_{vi} and weights w_i to the all the vulnerability parameters referring to the structural features of an existing masonry building by considering the aggregate effect (see Table 7.23 and Table 7.24) shows a summary of the calculated vulnerability indices normalised from 0 to 100 for the existing URM buildings considering the aggregate effect in X direction, which is the direction parallel to the buildings' façades. The vulnerability in X direction for a single building varies between 26 and 75, and it decreases to values between 9 and 57, with an average value of 32, when the aggregate effect is considered. As it can be seen, even if the aggregate effect is considered, a low to moderate vulnerability is obtained for the buildings of the typical urban block in the X direction. The I_v in the Y direction ranges between 12 and 64, with average value of 32, which can be considered as a medium vulnerability level.

Table 7.33 - Vulnerability index calculated for X and Y direction for the existing buildings from the specific urban block, with and without the aggregate effect.

Nº	Position	I_v (X)	I_v (X) with aggregate effect	I_v (Y)
B1	Corner	54	29	22
B2	Row	59	32	48
B3	Row	60	34	28
B4	Row	56	40	36
B5	Row	66	39	49
B6	Row	59	44	24
B8	Row	50	27	15
B9	Row	53	33	36
B10	Row	60	37	28
B11	Row	75	57	47
B12	Corner	26	23	21
B14	Corner	64	46	64
B15	Row	36	18	36
B16	Row	36	10	12
B17	Row	34	9	12

The most vulnerable building for the X direction is one with the highest number of storeys and presence of vertical extensions (B11). As for the seismic vulnerability in the Y direction, the highest vulnerability index appears for the corner building, with 8 storeys of which the last two are *remuntes*. Figure 7.26 illustrates a vulnerability map for the urban block with the vulnerability index distribution for both seismic loading directions (X and Y).

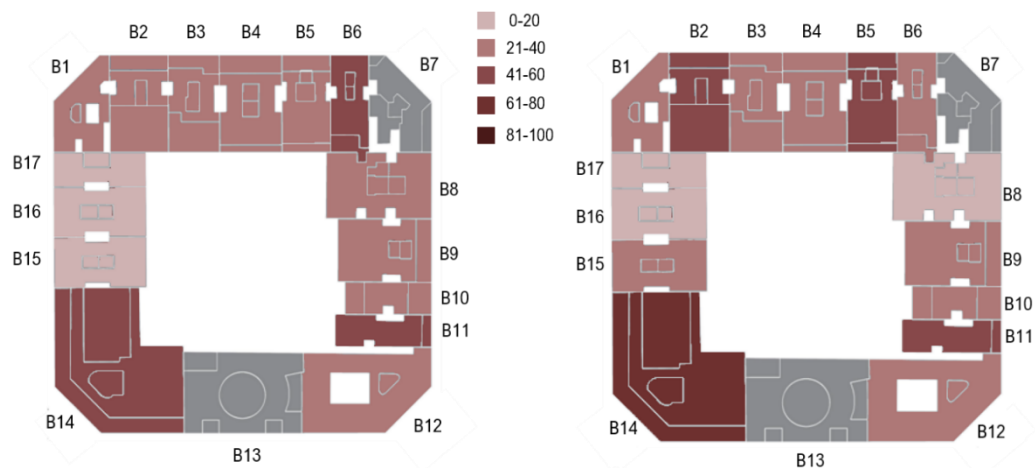


Figure 7.26 - Vulnerability index map for the urban block for both loading directions X considering the aggregate effect (left) and Y (right) (adapted from Rago 2022).

In conclusion, the aggregate effect parameters have shown to significantly affect the building's vulnerability in X direction (parallel to the façade), and without changing it for the Y direction (perpendicular to the façade). The seismic vulnerability in the X direction has resulted to be much lower than that previously calculated for the individual building without the aggregate effect.

7.5. SUMMARY

This chapter presents a methodology for the seismic vulnerability assessment of URM buildings in the *Eixample* district of Barcelona. Since there are no data of post-earthquake observed damage in the city, the suggested method involves the calibration of a new vulnerability index form based on a parametric analysis derived from numerical simulations. The purpose of the updated VIM forms is to assess the seismic vulnerability in the urban area of the *Eixample* district. This methodology is constructed in such a way that could be easily adapted and applied to other particular building typologies from different urban centres.

An overview of the vulnerability parameters selected for the new proposed VIM form is provided. These parameters have been adopted based on the detailed building taxonomy for the building typologies from the *Eixample* district (see Chapter 4), following the considerations of the VIM. Additionally, the definition of the vulnerability classes for each parameter is explained in accordance with the parametric studies carried out on the detailed numerical FE models, with the variations of the selected vulnerability parameters. The weights assigned for each parameter, which consider their relative influence on the structures' seismic behaviour, have been defined using the Analytical Hierarchy Process (AHP). Although this procedure was performed by collecting information from experts' opinions in previous research by other authors, this thesis considers the variation of the maximum strength capacity obtained from the numerical models for

quantifying the relative significance of the parameters. The obtained weights for each of the analysed parameters have been normalised in accordance to the sum of weights used in the original VIM form. Additionally, the vulnerability index for each numerical model is calculated and used to further calculate the mean damage grade. For the representative building typologies, fragility curves have been developed that correspond to the spectral displacements obtained from the application of the N2 method as a variable that characterises the seismic action.

The last part of this chapter presents the application of the proposed VIM forms to the chosen case study, the *Eixample* district of Barcelona. The seismic vulnerability of a disperse sample of 70 existing masonry buildings from the *Eixample* building stock has been evaluated, followed by an estimation of the mean damage grade for these building typologies. These results show the different percentages of buildings in specific ranges of seismic vulnerability. Moreover, the mean damage grades for possible earthquakes of seismic intensity of 6 and 7 have been presented. Additionally, a particular urban block from the *Eixample* district neighbourhood with the highest concentration of URM buildings has been chosen for the vulnerability evaluation taking the influence of the aggregate effect into account. The new proposed forms have been applied in order to evaluate the seismic vulnerability for both main seismic loading directions. The obtained results have confirmed that the influence of the aggregate decreases the seismic vulnerability in X direction (parallel to the façade). However, it is worth noticing that these vulnerability parameters concerning the aggregate effect have been evaluated following the approach proposed by Formisano et al. (2015) for Italian buildings. Further detailed numerical simulations should be considered for proper evaluation of the aggregate effect for the analysed case study of the *Eixample* district.

CHAPTER 8. CONCLUSIONS

8.1. SUMMARY

The devastating damage caused by major earthquakes in populated urban areas due to the collapse of existing buildings has prompted increasing concern in the scientific community on the seismic risk assessment at urban level. Different methods have been developed for the evaluation of the buildings' seismic vulnerability as their capacity to sustain damage due to a possible seismic event. However, seismic vulnerability assessment is still a challenging aim. Further scientific contributions are necessary, in specific, to evaluate the performance of existing masonry buildings, which can present high vulnerability due to their specific structural characteristic. Among these characteristics are the limited resistant capacity of the material, the presence of very slender load-bearing walls, and the, in some cases, remarkable buildings' height. A better understanding of the seismic behaviour of masonry structures requires, as a fundamental first step, the elaboration of a building taxonomy with a proper classification of the structural types of specific urban or geographical environment. This taxonomy must identify the structural features and constructive characteristics that are relevant to the buildings' seismic behaviour.

The research has presented a methodology contributing to the seismic vulnerability assessment of existing masonry buildings in urban centres with low to medium seismic hazard. The study has allowed the calibration of Vulnerability Index Method (VIM) forms for the *Eixample* district of Barcelona, by using detailed numerical simulations to quantify the expected damage in case of different earthquake intensities.

This chapter summarises the conclusions drawn from the presented research work. First, a general description is given of the work developed in each of this thesis chapters, followed by the enumeration of the most relevant contributions and some suggestions for future work.

Chapter 2 has presented an overview of the available methods used to evaluate seismic risk at a large urban scale. Special focus has been given to the seismic vulnerability approaches, since they are a key component of the risk assessment studies. From the manifold methods presented, the Vulnerability Index Method (VIM) and the macroseismic approach have been emphasised, as the mostly used tools for the buildings' vulnerability assessment. Lastly, this section has presented an overview of the available building taxonomies, given their critical role in seismic vulnerability assessments.

Chapter 3 has provided a detailed description of the existing unreinforced masonry (URM) buildings in the *Eixample* district, one of the Barcelona's most representative urban areas that has been selected as the case study for this doctoral thesis. The first part of this chapter has provided a historical overview and urban evolution of Barcelona, in order to better understand the development of the *Eixample* district. The chapter has also presented the experimental characterisation of the masonry's mechanical properties of the existing URM buildings, in an attempt of identifying reliable reference parameters for the FE numerical models. The available

data regarding the seismic hazard have been used as a starting point for the vulnerability assessment of the *Eixample* district.

Chapter 4 has proposed a specific building taxonomy as a fundamental first step in the seismic vulnerability assessment at large scale. The classification scheme has employed specific characteristics, such as load-bearing resisting system, materials used, height, geometrical configuration, different structural and non-structural elements, which have a significant influence on the buildings' seismic vulnerability. The most common existing buildings have been identified and selected from the detailed building taxonomy, by using available statistical data. The selected buildings have been used for developing detailed numerical models for a better understanding of their global seismic behaviour.

Chapter 5 has described the FE numerical simulations of the representative building typologies in order to evaluate their seismic response. The reference model has been developed according to the most recurrent building typology, considering two different structural systems, i.e. the homogeneous and the hybrid ones. Moreover, various models have been generated by varying the parameters that mostly affect the buildings' seismic performance and vulnerability, i.e. number of storeys, presence of vertical extensions, material properties, wall thickness variation, horizontal diaphragms, façade openings, and plan configuration.

Chapter 6 has elaborated the results from the nonlinear static pushover analyses performed on the FE models of the representative *Eixample* buildings. These seismic analyses have allowed for the evaluation of the seismic performance of these existing URM buildings and understanding the impact of the different structural attributes on the buildings' capacity and vulnerability. Additionally, the seismic performance of the buildings has been evaluated using the N2 Method by obtaining the performance point for two different seismic demand spectra, deterministic and probabilistic.

Chapter 7 has focused on the description of the general methodology suggested for large-scale evaluation of the seismic vulnerability of existing masonry buildings in the *Eixample* district, characterised by specific structural features and located in low to medium seismic hazard areas. New forms based on the Vulnerability Index Method (VIM) have been proposed and calibrated, by implementing specific vulnerability parameters relevant for the seismic behaviour of the analysed buildings. The chapter presents the application of the proposed VIM forms to the chosen case study, the *Eixample* district of Barcelona, by analysing a large number of individual existing masonry buildings and a typical urban block considering the aggregate effect.

8.2. MAIN CONCLUSIONS AND CONTRIBUTIONS

This section includes an outline of the main conclusions and contributions reached during the present research, outlined in accordance with this research's specific objectives:

- The construction of a detailed building taxonomy for existing masonry structures in urban areas is an essential tool for the seismic vulnerability assessment at large scale. It must be oriented to categorise various construction types based on their specific attributes (structural systems, materials, geometry, etc.), as well as on their heterogeneities, singularities, and seismic vulnerability sources. The careful definition of a catalogue

reporting different existing masonry buildings with similar structural features, based on their expected performance and similar vulnerability, is necessary for the identification and selection of representative building typologies. In the frame of a seismic assessment at urban scale based on computational simulation, the availability of such taxonomy can contribute to reduce the amount of required numerical modelling and computational effort. In this work, a detailed building taxonomy has been defined and created for the specific case of the *Example* district by characterising all the different structural attributes that affect the buildings' seismic performance and vulnerability. Such parameters have been grouped into the following sections: general building information, structural building system, structural elements and connections, configuration and irregularities, conservation state of the building, and behaviour of the building within a block. Furthermore, a new methodology has been developed for the selection of a set of representative buildings to be numerically analysed. The following primary tasks have been envisaged for this purpose: i) definition of a detailed building taxonomy; ii) statistical distribution analysis regarding the geometrical and structural morphology of the buildings; iii) selection of the most representative building typologies, which have been then considered for the numerical modelling.

- Sophisticated numerical models using the continuum FE method can be satisfactorily used for an accurate numerical simulation of the global seismic response of existing URM building under seismic actions. They can be combined with simpler empirical and expert judgment methods for large-scale applications, in the frame of the so-called hybrid seismic vulnerability approaches, to carry out seismic vulnerability studies in cases lacking proper databases on post-earthquake observed damage. In this research, detailed numerical models of the selected URM buildings have been developed using the Finite Element Method in order to realistically simulate their global seismic response. A reference model has been prepared according to the most recurrent building typologies. Two different structural systems have been considered for this purpose, i.e. the homogeneous system with slender URM walls, and a hybrid one involving a combination of steel members at the ground floor and unreinforced masonry walls on the upper floor levels. Moreover, additional models have been generated by considering the variation of different parameters considered in the detailed building taxonomy, such as the number of storeys, presence of vertical extensions, material properties, change of walls' thickness, horizontal diaphragms, different plan configurations, and façade openings.
- The flexibility of the horizontal diaphragms can play an important role in the seismic performance of URM buildings and thus, their in-plane stiffness should be estimated in a realistic way for the buildings' seismic assessment. In this research, a numerical procedure has been proposed for the simplified and efficient modelling of jack arch one-way floors with tile vaults combined with steel or timber beams, which are the recurrent floor system in the existing *Example* buildings. This procedure has been based on the modelling of the floor slabs by means of 2D shell elements with an equivalent orthotropic elastic homogeneous material. To properly model the behaviour of the jack arch floors, a detailed 3D solid FE model and a simplified 2D shell FE model have been created and compared. The equivalent elastic orthotropic properties of the composite floor system have been

determined through an iterative procedure based on matching the effective stiffness of the 3D and 2D models.

- Nonlinear static (pushover) analyses on the FE models have enabled the identification of different vulnerabilities in the *Example's* existing buildings. The results from the pushover analyses in both main directions have offered a satisfactory understanding of the global seismic behaviour of the analysed masonry structures. The adopted modelling approach has allowed a successful characterisation of the capacity curves and a realistic identification of the failure mechanisms. The different seismic response of the existing *Example's* buildings has been characterised along two loading directions X and Y (parallel and perpendicular to the street façade). The collapse mechanism in the X direction has been connected to the appearance of the soft-story effect at ground level, whereas the collapse mechanism in the other Y direction has been linked to the local in-plane shear failure of the lateral masonry walls. Moreover, the parametric analysis carried out has provided a detailed understanding of the impact of the variation of the different parameters as possible sources of vulnerability in the *Example's* buildings. The application of the N2 method has allowed a proper evaluation of the seismic performance of the existing buildings against the different seismic hazard scenarios considered (deterministic and probabilistic).
- The results from the pushover capacity curves of the FE models have been used for the definition of the corresponding new vulnerability parameters to be considered in an adapted VIM form. In specific, it has been possible to use the numerical models for the calibration of the classes and weights of such parameters. The proposed methodology has allowed an adaptation of the existing vulnerability index method for this specific building typologies, by defining and calibrating the classes and weights of the vulnerability parameters for the new VIM forms for both main directions through numerical analysis. The steps of this methodology can be used as guidelines for the application of this seismic assessment methodology to several building typologies located in different urban centres.
- The application of the new VIM forms has allowed to estimate a moderate to high vulnerability for the X loading direction (parallel to the façade), by analysing the existing URM buildings as isolated. A lower vulnerability has been estimated for the Y loading direction (perpendicular to the façade). Moreover, it has been established that the aggregate effect could significantly affect the building's vulnerability in the direction parallel to the façade. In this case, a better seismic behaviour of the buildings for the X direction has been obtained by lowering the vulnerability from high to moderate.

8.3. SUGGESTIONS FOR FUTURE WORK

This section includes some suggestions for future work on the seismic vulnerability assessment of existing masonry buildings in large urban centres.

Building a comprehensive building taxonomy for a region or a specific urban area is essential task in the seismic vulnerability assessment in order to classify the different building typologies and to identify their most recurrent attributes, as sources of seismic vulnerability. For this purpose,

a large statistical data is required for the selection of the most representative building typologies, which will be used for a large-scale vulnerability assessment. As data collection is a very time-consuming process, there is a substantial need of implementing some systematic and extensive survey strategies.

The connection between horizontal diaphragms and load-bearing masonry walls is in need of a more accurate characterisation and a more detailed and realistic simulation in the numerical models. Moreover, the quality of the wall-to-floor slab connection, as a structural attribute, should be included in the VIM form, as it can influence the structure's seismic performance.

The effect of the incidence direction of the horizontal seismic forces on the buildings should be studied into larger detail. Multi-directional pushover analyses can produce more accurate results regarding the seismic vulnerability of existing buildings, according to recent research by Kalkbrenner, Pelà, and Sandoval (2019). This more detailed analysis is of large importance for buildings with irregular plan configurations, such as the chamfer buildings of the *Eixample* district (with pentagonal shape), in which the structure is asymmetrical along the considered main directions X and Y.

Pushover analyses have been chosen for this study because they require less computation than other procedures, such as nonlinear dynamic (time-history) analysis. Nevertheless, it may also be advised to conduct nonlinear dynamic analyses in order to verify the validity of the adopted pushover technique.

A thorough numerical analysis to determine the impact of the aggregate configuration on the seismic performance of buildings in the *Eixample* district is deemed necessary, as it could contribute to characterise the beneficial effect of such configuration on the seismic response of the structural units. In this thesis, only detailed numerical models of individual buildings have been developed due to the high computational time and cost required by the analyses. For this reason, the parameters characterising the aggregate effect as proposed by Formisano et al. (2015) have been applied without any specific recalibration. For future research, the aggregate configurations could be analysed by means of more simplified numerical modelling techniques such as the Equivalent Frame Method (EFM). Using the numerical results obtained from the modelling of the aggregate effect, the classes and weights of the aggregate-related five additional parameters proposed by Formisano et al. (2015) could be calibrated specifically for the building blocks of the *Eixample* district.

The analytical expressions proposed for the correlation of vulnerability index and the mean damage grade could be calibrated to better represent the seismic behaviour observed in the buildings of the *Eixample* district. Several authors have used the theoretical basis of the previously proposed expert judgment methods (VIM and macroseismic method) to calibrate proper correlations for various building typologies (Basaglia et al., 2018; Ferreira et al., 2020; Giovinazzi and Lagomarsino, 2004; Ortega, 2018; Vicente, 2008). Normally, the correlations are done by comparing post-earthquake damage data with the damage estimated with such methods. However, due to the lack of damage evidence in specific regions, a sufficient amount of detailed numerical simulations could be used for an improved calibration of the previously proposed analytical equations.

The VIM forms could be updated in order to account for some strengthening strategies which could be implemented to improve the seismic performance and decrease the seismic vulnerability of the existing masonry buildings. The implementation of some strengthening techniques such as the application of Textile Reinforced Mortar (TRM) would significantly influence the first parameter of the VIM form, concerning the estimation of the seismic coefficient. It could be also recommended to assess the effectiveness of proposed seismic strengthening strategies by applying and managing cost-effective mitigation strategies. The regional impact of such strategies could be assessed by updating the estimated vulnerability indices for the studied existing buildings, followed by the assessment of the expected damage grade in the urban centre for various levels of seismic hazard.

A probabilistic procedure for studying the seismic vulnerability at the urban level could be implemented based on an analysis of seismic response at various scales, incorporating the behaviour of individual buildings and aggregates, as well as their inherent relationship within the urban layout. Under the conditions of a seismic emergency, the response of urban neighbourhoods should be carefully investigated in order to ensure the functionality of critical roadways allowing access to strategic buildings, such as hospitals and fire stations, as a continuation of the work done by Cara et al. (2018). This could allow envisaging mitigation measures to ensure the minimum functionality required by the Emergency Limit Condition (ELC) in the event of future seismic events. By extending the concept of ELC with the definition of higher performance levels for the urban system, the proposed approach could be useful in improving civil protection plans, leading to potentially higher levels of resilience.

Also, past debatable structural interventions should be considered as another significant parameter for the VIM, which could be further numerically evaluated. The substitution of some construction and structural elements with others can have significantly impacted the building's seismic vulnerability. It is important to identify the most typical structural modifications that can be often found in the existing masonry buildings in the *Eixample* district, e.g. replacing the semi-flexible one-way floor slab systems with rigid concrete slabs, adding an additional layer of concrete over the previous floor system, replacing some load-bearing masonry walls with steel beams and pillars in order to have more open space, increasing the size of some openings, etc.

The developed methodology used for the evaluation of the seismic performance and vulnerability of existing URM buildings could be used, with the necessary modifications, for future researches on the vulnerability of different urban centres, where there is lack of post-earthquake damage data. Continuing these research lines is crucial, since the seismic vulnerability assessment can contribute to reduce the possible damage and, more importantly, the loss of people caused by earthquakes.

BIBLIOGRAPHY

- Adam, J. M., and Ivorra, S. (2007). Behaviour of axially loaded RC columns strengthened by steel angles and strips. *Steel. Compos. Struct.*, 7(5), 405–419. <https://doi.org/10.12989/scs.2007.7.5.405>
- Aguilar-Meléndez, A. García-Elías, A., Pujades, L. G., Barbat, A. H., Lantada, N., and Ordaz, M. G. (2012). Probabilistic assessment of the seismic risk of Barcelona. *12th World Conference on Earthquake Engineering (WCEE)*.
- Aguilar, A., Pujades, L. G., Barbat, A., and Lantada, N. (2009). A probabilistic model for seismic risk assessment of buildings. *8th International Workshop on Seismic Microzoning Risk Reduction*.
- Aguilar Meléndez, A. (2011). *Evaluación probabilista del riesgo sísmico de edificios en zonas urbanas*. Universitat Politècnica de Catalunya.
- Aira, J. R., Arriaga, F., Íñiguez-González, G., and Crespo, J. (2014). Static and kinetic friction coefficients of Scots pine (*Pinus sylvestris* L.), parallel and perpendicular to grain direction. *Materiales de Construcción*, 64(315), e030. <https://doi.org/10.3989/mc.2014.03913>
- Ajuntament de Barcelona. (1987). *Catàleg del patrimoni arquitectònic històric-artístic de la ciutat de Barcelona*. Ajuntament de Barcelona. Àrea d'Urbanisme i Obres Públiques. Servei de Protecció del Patrimoni Monumental.
- Ajuntament de Barcelona. (1993). *Els Colors de l'Eixample*. Ajuntament de Barcelona, Districte de l'Eixample.
- Ajuntament de Barcelona. (2005). *Anuari Estadístic de la Ciutat de Barcelona*.
- Ajuntament de Barcelona. (2011). *Estadística i Difusió de Dades - Estadístiques urbanístiques*.
- Ajuntament de Barcelona. (2021). *Anuari Estadístic de la Ciutat de Barcelona*.
- Ajuntament de Barcelona. (2022). *La població de Barcelona*.
- Ambraseys, N. N., Simpson, K. A., and Bommer, J. J. (1996). Prediction of horizontal response spectra in Europe. *Earthquake Engineering and Structural Dynamics*, 25, 375–400.
- ASCE/SEI 41-17. (2017). *Seismic Evaluation and Retrofit of Existing Buildings*. Reston, Virginia: American Society of Civil Engineers: Structural Engineering Institute.
- Aşıkoğlu, A., Vasconcelos, G., Lourenço, P. B., and Pantò, B. (2020). Pushover analysis of unreinforced irregular masonry buildings: Lessons from different modeling approaches. *Engineering Structures*, 218(November 2019). <https://doi.org/10.1016/j.engstruct.2020.110830>
- ATC-13. (1985). *Earthquake damage evaluation data for California, ATC-13*.
- ATC-13. (1987). *Earthquake damage evaluation data for California*.
- ATC 40. (1996). *Seismic evaluation and retrofit of concrete buildings*.
- Augenti, N., and Parisi, F. (2010). New Tools for Non-Linear Analysis of Masonry Buildings. *14th European Conference of Earthquake Engineering*.

- Avila-Haro, Jorge A., González-Drigo, J. R., Vargas-Alzate, Y. F., Pujades, L. G., and Barbat, A. H. (2012). Seismic performance of unreinforced masonry buildings : application to Barcelona, Spain. *15th World Conference on Earthquake Engineering - WCEE*, 10.
- Avila-Haro, Jorge Arturo. (2021). *Análisis estructural probabilista orientado a evaluación del daño sísmico de edificios de mampostería no reforzada: aplicación a edificios aislados y agregados del distrito del ensanche de Barcelona*. Universitat Politècnica de Catalunya.
- Avila-Haro, Jorge Arturo, and Máca, J. (2015). A comparison between methodologies in the seismic assessment of URM buildings. *13th International Conference on New Trends in Statics and Dynamics of Buildings*.
- Azizi-bondarabadi, H., Mendes, N., and Lourenço, P. B. (2021). Higher Mode Effects in Pushover Analysis of Irregular Masonry Buildings Higher Mode Effects in Pushover Analysis of Irregular Masonry. *Journal of Earthquake Engineering*, 25(8), 1459–1493. <https://doi.org/10.1080/13632469.2019.1579770>
- Baggio, C., Bernardini, A., Colozza, R., Corazza, L., Bella, M. Della, Pasquale, G. Di, Dolce, M., Goretti, A., Martinelli, A., Orsini, G., Papa, F., and Zuccaro, G. (2007). *Field manual for post-earthquake damage and safety assessment and short-term countermeasures (AeDES)*.
- Barbat, A., Canas, J., and Yépez, F. (2010). Riesgo, peligrosidad y vulnerabilidad sísmica de edificios. In *Monografías de Ingeniería Sísmica* (p. 296). <http://www.cimne.com/tiendaCIMNE/free/MIS12.pdf>
- Barbat, Á. H., Yépez Moya, F., and Canas, J. A. (1996). Damage Scenarios Simulation for Seismic Risk Assessment in Urban Zones. *Earthquake Spectra*, 12(3), 371–394.
- Barbat, A.H., Mena, U., and Yépez, F. (1998). Evaluación probabilista del riesgo sísmico en zonas urbanas. *Revista Internacional de Métodos Numéricos Para Cálculo y Diseño En Ingeniería*.
- Barbat, Alex H., Carreño, M. L., Pujades, L. G., Lantada, N., Cardona, O. D., and Marulanda, M. C. (2010). Seismic vulnerability and risk evaluation methods for urban areas. A review with application to a pilot area. *Structure and Infrastructure Engineering*, 6(1–2), 17–38. <https://doi.org/10.1080/15732470802663763>
- Barbat, Alex H., Pujades, L. G., and Lantada, N. (2006). Performance of buildings under earthquakes in Barcelona, Spain. *Computer-Aided Civil and Infrastructure Engineering*, 21(8), 573–593. <https://doi.org/10.1111/j.1467-8667.2006.00450.x>
- Barbat, Alex H., Pujades, L. G., and Lantada, N. (2008). Seismic damage evaluation in urban areas using the capacity spectrum method: Application to Barcelona. *Soil Dynamics and Earthquake Engineering*, 28(10–11), 851–865. <https://doi.org/10.1016/j.soildyn.2007.10.006>
- Barcelona City Council. (1991). *Ordenança sobre obres i instal·lacions de serveis en el domini públic municipal [1991]*.
- Basaglia, A., Aprile, A., Spacone, E., and Pelà, L. (2020). Assessing community resilience, housing recovery and impact of mitigation strategies at the urban scale: a case study after the 2012 Northern Italy Earthquake. *Bulletin of Earthquake Engineering*, 18(13), 6039–6074. <https://doi.org/10.1007/s10518-020-00919-8>
- Basaglia, A., Aprile, A., Spacone, E., and Pilla, F. (2018). Performance-based Seismic Risk

- Assessment of Urban Systems. *International Journal of Architectural Heritage*, 12(7–8), 1131–1149. <https://doi.org/10.1080/15583058.2018.1503371>
- Benedetti, D., and Petrini, V. (1984). Sulla vulnerabilità sismica di edifici in muratura: Un metodo di valutazione (in Italian). *L'Industria Delle Costruzioni*, 149(18), 66–78.
- Bernardini, A., Giovinazzi, S., Lagomarsino, S., and Parodi, S. (2007). Vulnerabilità e previsione di danno a scala territoriale secondo una metodologia macrosismica coerente con la scala EMS-98. *ANIDIS, XII Convegno Nazionale l'ingegneria Sismica in Italia, 10 a 14 Giugno, Pisa, November 2015*. <http://ir.canterbury.ac.nz/handle/10092/4060>
- Bernardini, A, Gori, R., and Modena, C. (1990). Application of Coupled Analytical Models and Experimental Knowledge to Seismic Vulnerability Analyses of Masonry Buildings. *Eng Damage Eval Vulnerability Anal Build Struct*.
- Bernardini, Alberto, Giovinazzi, S., Lagomarsino, S., and Parodi, S. (2007). The vulnerability assessment of current buildings by a macroseismic approach derived from the EMS-98 scale. *Asociación Española de Ingeniería Sísmica Girona, 8-11 Mayo 2007, April 2017*, 1–15.
- Betti, M., Galano, L., and Vignoli, A. (2015). Finite element modelling for seismic assessment of historic masonry buildings. *Earthquakes and Their Impact on Society*, 377–415. https://doi.org/10.1007/978-3-319-21753-6_14
- Bonett Díaz, R. L. (2003). Curvas de fragilidad y matrices de probabilidad de daño. *Vulnerabilidad y Riesgo Sísmico de Edificios, Aplicación a Entornos Urbanos En Zonas de Amenaza Alta y Moderada. Tesis Doctor En Ingeniería*, 99–130.
- Bonett Díaz, R. L. (2003). *Vulnerabilidad y riesgo sísmico de edificios aplicación a entornos urbanos en zonas de amenaza alta i moderada* [Universitat Politècnica de Catalunya]. <https://upcommons.upc.edu/handle/2117/93542>
- Braga, F., Dolce, M., and Liberatore, D. (1982). A statistical study on damaged buildings and an ensuing review of the M.S.K76 scale. *Proc. of the 7th European Conference on Earthquake Engineering*.
- Brignola, A., Pampanin, S., and Podestà, S. (2009). Evaluation and control of the in-plane stiffness of timber floors for the performance-based retrofit of URM buildings. *Bulletin of the New Zealand Society for Earthquake Engineering*, 42(3), 204–221. <https://doi.org/10.5459/bnzsee.42.3.204-221>
- Brzev, S., Scawthorn, C., Charleson, A. W., Allen, L., Greene, M., Jaiswal, K., and Silva, V. (2013). GEM Building Taxonomy (Version 2.0). In *GEM Technical Report (Version 1.)*. <http://pubs.er.usgs.gov/publication/70058718>
- Cabané, A., Pelà, L., and Roca, P. (2022). Anisotropy and compressive strength evaluation of solid fired clay bricks by testing small specimens. *Construction and Building Materials*, 344(June). <https://doi.org/10.1016/j.conbuildmat.2022.128195>
- Caicedo, C., Barbat, A. H., Canas, J. A., and Aguiar, R. (1994). Vulnerabilidad sísmica de edificios. In *Monografías de Ingeniería Sísmica. CIMNE-IS-6* (p. 106). <https://doi.org/10.13140/2.1.4142.6244>
- Calderini, C., Cattari, S., and Lagomarsino, S. (2009). In-plane strength of unreinforced masonry

piers. *Earthquake Engineering and Structural Dynamics*, 38(2), 243–267. <https://doi.org/10.1002/eqe.860>

Calvi, G. M. (1999). A displacement-based approach for vulnerability evaluation of classes of buildings. *Journal of Earthquake Engineering*, 3(3), 411–438.

Calvi, G. M., Pinho, R., Mgabes, G., Bommer, J. J., Restrepo-Vélez, L. F., and Crowley, H. (2006). Development of seismic vulnerability assessment methodologies over the past 30 years. *ISET Journal of Earthquake Technology*, 43(472), 75–104.

Campione, G., Cavaleri, L., Di Trapani, F., and Ferrotto, M. F. (2017). Frictional Effects in Structural Behavior of No-End-Connected Steel-Jacketed RC Columns: Experimental Results and New Approaches to Model Numerical and Analytical Response. *Journal of Structural Engineering*, 143(8). [https://doi.org/10.1061/\(ASCE\)ST.1943-541X.0001796](https://doi.org/10.1061/(ASCE)ST.1943-541X.0001796)

Cara, S., Aprile, A., Pelà, L., and Roca, P. (2018). Seismic Risk Assessment and Mitigation at Emergency Limit Condition of Historical Buildings along Strategic Urban Roadways. Application to the “Antiga Esquerra de L’Eixample” Neighborhood of Barcelona. *International Journal of Architectural Heritage*, 12(7–8), 1055–1075. <https://doi.org/10.1080/15583058.2018.1503376>

Cardona, O. D. (2001). *Estimación holística del riesgo sísmico utilizando sistemas dinámicos complejos* [Universitat Politècnica de Catalunya]. <http://www.tesisenred.net/handle/10803/6219>

Casanovas, X., Graus i Rovira, R., and Rosell, J. R. (1993). *Manual de diagnosi i intervenció en sostres unidireccionals de formigó i ceràmics*. Col·legi d’Aparelladors i Arquitectes Tècnics.

Castilla Marne, J. (2010). *Catalogación y levantamiento gráfico de fachadas de las manzanas del Eixample*. Universitat Politècnica de Catalunya.

Cerdá, I. (1860). *Reforma y Ensanche de Barcelona*.

Chieffo, N., Mosoarca, M., Formisano, A., Lourenço, P. B., and Milani, G. (2021). The effect of ground motion vertical component on the seismic response of historical masonry buildings: The case study of the Banloc Castle in Romania. *Engineering Structures*, 249, 113346. <https://doi.org/10.1016/j.engstruct.2021.113346>

Cid, J. (1998). *Zonación sísmica de la ciudad de Barcelona basada en métodos de simulación numérica de efectos locales*. Universitat Politècnica de Catalunya.

Cid, J., Susagna, T., Goula, X., Chavarria, L., Figueras, S., Fleta, J., Casas, A., and Roca, A. (2001). Seismic zonation of Barcelona based on numerical simulation of site effects. *Pure and Applied Geophysics*, 158(12), 2559–2577. <https://doi.org/10.1007/PL00001186>

Coburn, A., and Spence, R. (1992). *Earthquake Protection*. John Wiley and Sons Ltd., Chichester, England.

Coburn, A., and Spence, R. (2002). *Earthquake Protection*. Wiley. https://books.google.es/books?id=MjUdkHJ%5C_wHcC

Colom, E. (2014). *Classificació i anàlisi tipològica de les remuntes en edificis residencials històrics de l’Eixample de Barcelona*. Universitat Politècnica de Catalunya.

Colom, E., Cornadó Bardón, C., and Díaz, C. (2016). Caracterización sintética de las actuaciones de adición de plantas en los edificios históricos del ensanche de Barcelona. *Rehabend*, 2016-

- May(May), 93–100. <https://doi.org/10.13140/RG.2.1.5149.4004>
- Colom, E., Cornadó, C., and Díaz, C. (2016). Caracterización sintética de las actuaciones de adición de plantas en los edificios históricos del ensanche de Barcelona. *Rehabend*, 2016-May(May), 93–100. <https://doi.org/10.13140/RG.2.1.5149.4004>
- Cornadó Bardón, C. (2015). *Comportament mecànic-estructural dels edificis històrics de murs d'obra de fàbrica de maó de l'Eixample de Barcelona* [Universitat Politècnica de Catalunya]. <http://hdl.handle.net/2117/95802>
- Corominas i Ayala, M. (2002). *Los orígenes del Ensanche de Barcelona : suelo, técnica e iniciativa* (Edicions U).
- Corsanego, A., and Petrini, V. (1994). Evaluation criteria of seismic vulnerability of the existing building patrimony on the national territory. *Seismic Engineering*, 1, 16–24.
- CTE_DB-SE-AE. (2009). *Documento Básico SE-AE Seguridad Estructural: Acciones en la edificación*.
- CTE-DB-SE-M. Código Técnico de la Edificación. (2007). *Documento Básico SE-M Seguridad Estructural: Madera*.
- D'Altri, A. M., Sarhosis, V., Milani, G., Rots, J., Cattari, S., Lagomarsino, S., Sacco, E., Tralli, A., Castellazzi, G., and de Miranda, S. (2019). A review of numerical models for masonry structures. In *Numerical Modeling of Masonry and Historical Structures: From Theory to Application* (pp. 3–53). Elsevier. <https://doi.org/10.1016/B978-0-08-102439-3.00001-4>
- D'Altri, A.M., Sarhosis, V., Milani, G., Rots, J., Cattari, S., Lagomarsino, S., Sacco, E., Tralli, A., Castellazzi, G., and de Miranda, S. (2019). A review of numerical models for masonry structures. In *Numerical Modeling of Masonry and Historical Structures*. Elsevier Ltd. <https://doi.org/10.1016/b978-0-08-102439-3.00001-4>
- D'Altri, Antonio Maria, Sarhosis, V., Milani, G., Rots, J., Cattari, S., Lagomarsino, S., Sacco, E., Tralli, A., Castellazzi, G., and de Miranda, S. (2020). Modeling Strategies for the Computational Analysis of Unreinforced Masonry Structures: Review and Classification. *Archives of Computational Methods in Engineering*, 27(4), 1153–1185. <https://doi.org/10.1007/s11831-019-09351-x>
- D'Ayala, D. F., and Speranza, E. (2004). Un criterio per la formulazione e la calibrazione di curve di fragilità e scenari di danno: il caso di Nocera Umbra (PG). In *Proceedings of the 11th Conference of the Italian National Association of Earthquake Engineering - ANIDIS, December 2017*, 12.
- D'Ayala, D., and Speranza, E. (2003). Definition of Collapse Mechanisms and Seismic Vulnerability of Historic Masonry Buildings. *Earthquake Spectra*, 19(3), 479–509. <https://doi.org/10.1193/1.1599896>
- D'Ayala, Dina, Meslem, A., Vamvatsikos, D., Porter, K., Rossetto, T., Crowley, H., and Silva, V. (2014). GEM Guidelines for Analytical Vulnerability Assessment of Low/Mid-rise Buildings. In *Vulnerability Global Component project*.
- de la Fuente-Leon, J., Lafuente-Jimenez, E., Hermosilla, D., Broto-Cartagena, M., and Gasco, A. (2014). Physico-mechanical properties of Spanish juniper wood considering the effect of

heartwood formation and the presence of defects and imperfections. *Forest Systems*, 23(1), 64–71. <https://doi.org/10.5424/fs/2014231-03671>

Diaferio, M., Foti, D., Giannoccaro, N. I., and Ivorra, S. (2014). Optimal model through identified frequencies of a masonry building structure with wooden floors. *International Journal of Mechanics*, 8(1), 282–288.

DIANA FEA BV. (2020). *Displacement method ANALyser (DIANA FEA) User's Manual release 10.4*.

Diana, L., Thirirot, J., Reuland, Y., and Lestuzzi, P. (2019). Application of association rules to determine building typological classes for seismic damage predictions at regional scale: The case study of basel. *Frontiers in Built Environment*, 5(April), 1–17. <https://doi.org/10.3389/fbuil.2019.00051>

Dimovska, S., Saloustros, S., Pelà, L., and Roca, P. (2022). Modelling of in-plane seismic behaviour of one-way steel or timber jack arch floors in existing buildings. Application to the Eixample district of Barcelona. *Engineering Structures*, 262, 114343. <https://doi.org/10.1016/j.engstruct.2022.114343>

Diodato, M, Macchioni, N., Brunetti, M., Pizzo, B., Nocetti, M., Burato, P., Sozzi, L., Pecoraro, E., Vegas López-Manzanares, F., and Mileto, C. (2015). Understanding Spanish Timber Jack Arch Floors : Examples of Assessment and Conservation Issues Understanding Spanish Timber Jack Arch Floors : Examples of Assessment and Conservation Issues. *International Journal of Architectural Heritage*, 9(6), 641–654. <https://doi.org/10.1080/15583058.2015.1041193>

Diodato, Maria, Macchioni, N., Brunetti, M., Pizzo, B., Nocetti, M., Burato, P., Sozzi, L., Pecoraro, E., Vegas López-Manzanares, F., and Mileto, C. (2013). A Peculiar Spanish Timber Floor, the “Revoltón”: A Diagnostic Example at the “Palacio del Marqués de Benicarló.” *Advanced Materials Research*, 778(June 2014), 1064–1071. <https://doi.org/10.4028/www.scientific.net/AMR.778.1064>

Dolce, M., Zuccaro, G., Kappos, A., and Coburn, A. (1994). Report of the EAEE Working Group 3: Vulnerability and risk analysis. *Proc. of 10th European Conference on Earthquake Engineering*, 3049–3077.

Drougkas, A., Roca, P., and Molins, C. (2016). Compressive strength and elasticity of pure lime mortar masonry. *Materials and Structures*, 49(3), 983–999. <https://doi.org/10.1617/s11527-015-0553-2>

Dubois, D., and Parade, H. (1980). *Fuzzy Sets and Systems*. Academic Press.

Dumova-Jovanoska, E. (2000). Fragility curves for reinforced concrete structures in Skopje (Macedonia) region. *Soil Dynamics and Earthquake Engineering*, 19(6), 455–466. [https://doi.org/10.1016/S0267-7261\(00\)00017-8](https://doi.org/10.1016/S0267-7261(00)00017-8)

EERI Committee. (1986). Glossary of terms for probabilistic seismic-risk and hazard analysis. *Bulletin of the New Zealand Society for Earthquake Engineering*, 19(3 SE-Articles), 155–157. <https://doi.org/10.5459/bnzsee.19.3.155-157>

EN 1998-1. (2004). *Eurocode 8: Design of structures for earthquake resistance - Part 1: General rules, seismic actions and rules for buildings*.

- Endo, Y. (2015). *Modelling and Structural analysis of historical masonry systems including vaulted structure* [Universitat Politècnica de Catalunya]. <http://hdl.handle.net/2117/95728>
- Endo, Y., Llorens, M. S., Roca, P., and Pelà, L. (2017). Dynamic Identification and Static Loading Tests of Timbrel Vaults: Application to a Modernist 20th Century Heritage Structure. *International Journal of Architectural Heritage*, 11(4), 607–620. <https://doi.org/10.1080/15583058.2016.1277566>
- Endo, Y., Pelà, L., and Roca, P. (2017a). Review of Different Pushover Analysis Methods Applied to Masonry Buildings and Comparison with Nonlinear Dynamic Analysis. *Journal of Earthquake Engineering*, 21(8), 1234–1255. <https://doi.org/10.1080/13632469.2016.1210055>
- Endo, Y., Pelà, L., and Roca, P. (2017b). Review of Different Pushover Analysis Methods Applied to Masonry Buildings and Comparison with Nonlinear Dynamic Analysis. *Journal of Earthquake Engineering*, 21(8), 1234–1255. <https://doi.org/10.1080/13632469.2016.1210055>
- Fajfar, P. (2000). A Nonlinear Analysis Method for Performance-Based Seismic Design. *Earthquake Spectra*, 16(3), 573–592. <https://doi.org/10.1193/1.1586128>
- Federal Emergency Management Agency (FEMA). (2003). HAZUS-MH MR4 Technical Manual. *National Institute of Building Sciences and Federal Emergency Management Agency (NIBS and FEMA)*.
- FEMA. (1988). *Rapid visual screening of buildings for potential seismic hazards: A handbook*.
- FEMA. (2003). *Multi-hazard Loss Estimation Methodology Earthquake Model HAZUS-MH MR4 Technical Manual*. http://www.civil.ist.utl.pt/~mlopes/conteudos/DamageStates/hazus_mr4_earthquake_tech_manual.pdf
- FEMA. (2015). *Rapid Visual Screening of Buildings for Potential Seismic Hazards: A Handbook (FEMA P-154)*. <https://doi.org/10.4231/D3M90238>
- FEMA 356. (2000). *Prestandard and commentary for the seismic rehabilitation of buildings* (Issue November). Federal Emergency Management Agency.
- Ferreira, T. M., Vicente, R., and Varum, H. (2014). Seismic vulnerability assessment of masonry facade walls: development, application and validation of a new scoring method. *Structural Engineering and Mechanics*, 50(4), 541–561. <https://doi.org/10.12989/SEM.2014.50.4.541>
- Ferreira, T., Vicente, R., and Varum, H. (2012). *Vulnerability assessment of building aggregates: A macroseismic approach*.
- Ferreira, Tiago Miguel, Costa, A. A., Vicente, R., and Varum, H. (2015). A simplified four-branch model for the analytical study of the out-of-plane performance of regular stone URM walls. *Engineering Structures*, 83, 140–153. <https://doi.org/10.1016/j.engstruct.2014.10.048>
- Ferreira, Tiago Miguel, Maio, R., and Vicente, R. (2017). Seismic vulnerability assessment of the old city centre of Horta, Azores: calibration and application of a seismic vulnerability index method. *Bulletin of Earthquake Engineering*, 15(7), 2879–2899. <https://doi.org/10.1007/s10518-016-0071-9>
- Ferreira, Tiago Miguel, Rodrigues, H., and Vicente, R. (2020). Seismic Vulnerability Assessment

of Existing Reinforced Concrete Buildings in Urban Centers. *Sustainability*, 12(5). <https://doi.org/10.3390/su12051996>

Formisano, A, Florio, G., Landolfo, R., and Mazzolani, F, M. (2011). Un metodo per la valutazione su larga scala della vulnerabilità sismica degli aggregati storici. *XV Convegno ANDIS - L'Ingegneria Sismica in Italia*.

Formisano, A, Marzo, A., and Indirli, M. (2013). Analisi comparativa tra metodi di valutazione della vulnerabilità sismica degli edifici murari di Arsita (TE). *XV Convegno ANIDIS 2013, Padova*.

Formisano, Antonio, Florio, G., Landolfo, R., and Mazzolani, F. M. (2015). Numerical calibration of an easy method for seismic behaviour assessment on large scale of masonry building aggregates. *Advances in Engineering Software*, 80(C), 116–138. <https://doi.org/10.1016/j.advengsoft.2014.09.013>

Freeman. (1998). The Capacity Spectrum Method as a Tool for Seismic Design. *Proceedings of the 11th European Conference on Earthquake Engineering*, 6–11.

Galasco, A., Lagomarsino, S., and Penna, A. (2007). Non linear macro-element dynamic analysis of masonry buildings. *ECCOMAS Thematic Conference on Computational Methods in Structural Dynamics and Earthquake Engineering*.

Giongo, I. (2013). *Role of the timber diaphragms in the seismic response of unreinforced masonry (URM) buildings*. University of Trento.

Giovinazzi, S. (2005). *The vulnerability assessment and the damage scenario in seismic risk analysis*. Technical University Carolo-Wilhelmina at Braunschweig and University of Florence.

Giovinazzi, S., and Lagomarsino, S. (2004). A macroseismic method for the vulnerability assessment of buildings. *13th World Conference on Earthquake Engineering*.

GNDT. (1986). *Istruzioni per la Compilazione della Scheda di Relivamento Esposizione e Vulnerabilità Sismica Degli Edifici, Gruppo Nazionale per la Difesa dai Terremoti, 'Tegione Emilia Romagna y Regione Toscana, Italy*.

GNDT. (1993). Rischio Sismico Di Edifici Pubblici, Parte I: Aspetti Metodologici. *Proceedings of CNR-Gruppo Nazionale per La Difesa Dai Terremoti, Roma, Italy*.

GNDT. (2007). *Manuale per Il Rilevamento Della Vulnerabilità Sismica Degli Edifici. Istruzione per La Compilazione Della Scheda Di 2° Livello*.

Gonzalez-Drigo, R., Avila-Haro, A., Barbat, A. H., Pujades, L. G., Vargas, Y. F., Lagomarsino, S., and Cattari, S. (2015). Modernist unreinforced masonry (URM) buildings of barcelona: Seismic vulnerability and risk assessment. *International Journal of Architectural Heritage*, 9(3), 214–230. <https://doi.org/10.1080/15583058.2013.766779>

González, R. M., and Bairán, J. M. (2015). Performance of Existing Modernist Buildings in Barcelona. *Journal of Performance of Constructed Facilities*, 29(4), 04014091. [https://doi.org/10.1061/\(ASCE\)CF.1943-5509.0000501](https://doi.org/10.1061/(ASCE)CF.1943-5509.0000501)

Grünthal, G. (1998). European Macroseismic Scale 1998. In Centre Européen de éodynamique et de Séismologie, Luxembourg. Vol. 15.

Guagenti, E., and Petrini, V. (1989). Il caso delle vecchie costruzioni: verso una nuova legge danni-

- intensità. *Proc. of 4th Italian Conference on Earthquake Engineering*, 145–153.
- Gupta, I. D. (2002). The state of the art in seismic hazard analysis. *ISSET Journal of Earthquake Technology*, 39(4), 311–346.
- HAZUS. (1999). *Earthquake Loss Estimation Methodology - Technical and User Manuals*.
- Hendry, A. W. (1998). *Structural Masonry*. Macmillan Education UK. <https://doi.org/10.1007/978-1-349-14827-1>
- Herrera, G. R., Vielma, J. C., Barbat, A. H., and Pujades, L. (2013). Estado del conocimiento sobre metodologías de evaluación de vulnerabilidad sísmica de edificios. *Ingeniería Y Sociedad Uc.*, 8, 7–28.
- Irizarry, J., Lantada, N., Pujades, L. G., Barbat, A. H., Goula, X., Susagna, T., and Roca, A. (2011). Ground-shaking scenarios and urban risk evaluation of Barcelona using the Risk-UE capacity spectrum based method. *Bulletin of Earthquake Engineering*, 9(2), 441–466. <https://doi.org/10.1007/s10518-010-9222-6>
- Irizarry, J. (2004). *An advanced approach to seismic risk assessment. Application to the cultural heritage and the urban system of Barcelona*. Universitat Politècnica de Catalunya.
- ITEC. (1994). *Norma reglamentària d'edificació sobre accions en l'edificació en les obres de rehabilitació estructural dels sostres d'edificis d'habitatges. NRE-AEOR-93*. Institut de Tecnologia de la Construcció de Catalunya - ITEC.
- Jaiswal, K. S., and Wald, D. J. (2008). *Creating a Global Building Inventory for Survey, Earthquake Loss Assessment and Risk Management*.
- Jaiswal, K., Wald, D., and D'Ayala, D. (2011). Developing Empirical Collapse Fragility Functions for Global Building Types. *Earthquake Spectra*, 27(3), 775–795. <https://doi.org/10.1193/1.3606398>
- Jiménez-Pacheco, J. (2016). *Evaluación sísmica de edificios de mampostería no reforzada típicos de Barcelona: modelización y revisión de la aplicación del Método del Espectro de Capacidad* [Universitat Politècnica de Catalunya]. <http://hdl.handle.net/2117/111235>
- Jiménez-Pacheco, J., González-Drigo, R., Pujades Beneit, L. G., Barbat, A. H., and Calderón-Brito, J. (2020). Traditional High-rise Unreinforced Masonry Buildings: Modeling and Influence of Floor System Stiffening on Their Overall Seismic Response. *International Journal of Architectural Heritage*. <https://doi.org/10.1080/15583058.2019.1709582>
- Jiménez, B., Pelà, L., and Hurtado, M. (2018). Building survey forms for heterogeneous urban areas in seismically hazardous zones. Application to the historical center of Valparaíso, Chile. *International Journal of Architectural Heritage*, 12(7–8), 1076–1111. <https://doi.org/10.1080/15583058.2018.1503370>
- Jiménez, B., Saloustros, S., and Pelà, L. (2021). Seismic vulnerability index method for hybrid timber–masonry structures. Numerical calibration and application to the city of Valparaíso, Chile. *Journal of Building Engineering*, 44, 103185. <https://doi.org/10.1016/j.job.2021.103185>
- Kalkbrenner, P., Pelà, L., and Sandoval, C. (2019). Multi directional pushover analysis of irregular masonry buildings without box behavior. *Engineering Structures*, 201, 109534.

<https://doi.org/https://doi.org/10.1016/j.engstruct.2019.109534>

Kappos, A. J. (2016). An overview of the development of the hybrid method for seismic vulnerability assessment of buildings. *Structure and Infrastructure Engineering*, 12(12), 1573–1584. <https://doi.org/10.1080/15732479.2016.1151448>

Kappos, A. J., Panagopoulos, G., Panagiotopoulos, C., and Penelis, G. (2006). A hybrid method for the vulnerability assessment of R/C and URM buildings. *Bulletin of Earthquake Engineering*, 4(4), 391–413. <https://doi.org/10.1007/s10518-006-9023-0>

Kassem, M. M., Mohamed Nazri, F., and Noroozinejad Farsangi, E. (2020). The seismic vulnerability assessment methodologies: A state-of-the-art review. *Ain Shams Engineering Journal*, 11(4), 849–864. <https://doi.org/10.1016/j.asej.2020.04.001>

Kircher, C., Whitman, R. V., and Holmes, W. T. (2006). HAZUS Earthquake Loss Estimation Methods. *Natural Hazards Review*, 7(2), 45–59. [https://doi.org/10.1061/\(ASCE\)1527-6988\(2006\)7:2\(45\)](https://doi.org/10.1061/(ASCE)1527-6988(2006)7:2(45))

Lagomarsino, S., and Cattari, S. (2015). PERPETUATE guidelines for seismic performance-based assessment of cultural heritage masonry structures. *Bulletin of Earthquake Engineering*, 13(1), 13–47. <https://doi.org/10.1007/s10518-014-9674-1>

Lagomarsino, S., and Giovinazzi, S. (2006). Macro seismic and mechanical models for the vulnerability and damage assessment of current buildings. *Bulletin of Earthquake Engineering*, 4(4), 415–443. <https://doi.org/10.1007/s10518-006-9024-z>

Lagomarsino, S., Penna, A., Galasco, A., and Cattari, S. (2013). TREMURI program: An equivalent frame model for the nonlinear seismic analysis of masonry buildings. *Engineering Structures*, 56, 1787–1799. <https://doi.org/10.1016/j.engstruct.2013.08.002>

Lang, K. (2002). *Seismic vulnerability of existing buildings*. Institute of Structural Engineering Swiss Federal Institute of Technology.

Lantada, N., Irizarry, J., Barbat, A. H., Goula, X., Roca, A., Susagna, T., and Pujades, L. G. (2010). Seismic hazard and risk scenarios for Barcelona, Spain, using the Risk-UE vulnerability index method. *Bulletin of Earthquake Engineering*, 8(2), 201–229. <https://doi.org/10.1007/s10518-009-9148-z>

Lantada, N., Pujades, L., and Barbat, A. H. (2004). Seismic risk scenarios for Barcelona, Spain. *Computational Civil Engineering 2004, January*, 22–34.

Lantada, Nieves. (2007). *Evaluación del riesgo sísmico mediante métodos avanzados y técnicas GIS. Aplicación a la ciudad de Barcelona* (Issue Volumen I) [Universitat Politècnica de Catalunya]. <http://www.tdx.cat/handle/10803/6259>

LEMPRIERE, B. M. (1968). Poisson's ratio in orthotropic materials. *AIAA Journal*, 6(11), 2226–2227. <https://doi.org/10.2514/3.4974>

Lourenço, P. B. (2002). Computations on historic masonry structures. *Progress in Structural Engineering and Materials*, 4, 301–319.

Lourenço, P. B. (2009). Recent advances in masonry modelling: micromodelling and homogenisation. *Multiscale Model. Solid Mech. Comput. Approaches*, 3, 251–294.

https://doi.org/10.1142/9781848163089_0006

Lourenço, P. B., Mendes, N., Ramos, L. F., and Oliveira, D. V. (2011). Analysis of masonry structures without box behavior. *International Journal of Architectural Heritage*, 5(4–5), 369–382. <https://doi.org/10.1080/15583058.2010.528824>

Magenes, G., and Calvi, G. (1997). In-plane seismic response of brick masonry walls. *Earthq Eng Struct Dyn*, 26(11), 1091–1112.

Maheri, M R, and Rahmani, H. (2003). Seismic evaluation and design of jack arch slabs. *Engineering Structures*, 25, 1639–1654.

Maheri, Mahmoud R, and Rahmani, H. (2004). Static and seismic design of one-way and two-way jack arch masonry slabs. *Proceedings of the 13th World Conference on Earthquake Engineering, Vancouver, Canada, 1-6 August 2004*, 25, 1639–1654. [https://doi.org/10.1016/S0141-0296\(03\)00143-3](https://doi.org/10.1016/S0141-0296(03)00143-3)

Maio, R., Estêvão, J. M. C., Ferreira, T. M., and Vicente, R. (2020). Casting a new light on the seismic risk assessment of stone masonry buildings located within historic centres. *Structures*, 25(December 2019), 578–592. <https://doi.org/10.1016/j.istruc.2020.03.008>

Maio, R., Vicente, R., Formisano, A., and Varum, H. (2015). Seismic vulnerability of building aggregates through hybrid and indirect assessment techniques. *Bulletin of Earthquake Engineering*, 13(10), 2995–3014. <https://doi.org/10.1007/s10518-015-9747-9>

Makoond, N., Pelà, L., and Molins, C. (2021). A Risk Index for the Structural Diagnosis of Masonry Heritage (RISDiMaH). *Construction and Building Materials*, 284, 122433. <https://doi.org/10.1016/j.conbuildmat.2021.122433>

Maps, B. (2021). *Bing Maps*.

Marafini, F., Dimovska, S., Saloustros, S., Cornadó, C., and Roca, P. (2022). Historical Development and Seismic Performance of Unreinforced Masonry Buildings with Vertical Extensions in the City Centre of Barcelona Historical Development and Seismic Performance of Unreinforced Masonry Buildings with Vertical Extensions in the City. *International Journal of Architectural Heritage*, 00(00), 1–24. <https://doi.org/10.1080/15583058.2022.2096513>

Marino, S., Cattari, S., and Lagomarsino, S. (2019). Are the nonlinear static procedures feasible for the seismic assessment of irregular existing masonry buildings? *Engineering Structures*, 200(January), 109700. <https://doi.org/10.1016/j.engstruct.2019.109700>

Masi, A. (2003). Seismic vulnerability assessment of gravity load designed R/C frames. *Bulletin of Earthquake Engineering*, 1(3), 371–395. <https://doi.org/10.1023/B:BEEE.0000021426.31223.60>

McGuire, R. . (2004). *Seismic hazard and risk analysis*. Earthquake Engineering Research Institute.

Mena, U. (2002). *Evaluación del Riesgo Sísmico en Zonas Urbanas*. Universitat Politècnica de Catalunya.

Mendes, N., and Lourenço, P. B. (2014). Sensitivity analysis of the seismic performance of existing masonry buildings. *Engineering Structures*, 80, 137–146. <https://doi.org/10.1016/j.engstruct.2014.09.005>

Milutinovic, Z. V, and Trendafiloski, G. S. (2003). WP4: Vulnerability of Current Buildings. *RISK-UE Project Handbook*, 111.

MIT Ministero delle Infrastrutture e dei Trasporti. (2019). Circolare del ministero delle infrastrutture e dei trasporti, n.7 del 21 Gennaio 2019: "Istruzioni per l'applicazione dell'aggiornamento delle Norme tecniche per le costruzioni di cui al D.M. 17 gennaio 2018. In *Consiglio superiore dei lavori pubblici. G.U. n.35 del 11.02.2019*. Cons. Super. Dei Lav. Pubblici. G.U. n.35 Del 11.02.2019.

Modrego Casquero, N. (2011). *Collapse mechanisms due to earthquake in urban buildings application to Barcelona 's Eixample typical buildings*. Technical University of Catalonia.

Molins i Borrell, C. (1996). *Un Model per a l'anàlisi del comportament resistent de construccions de maçoneria* [Universitat Politècnica de Catalunya]. <http://hdl.handle.net/2117/93468>

Monteiro, R., Ceresa, P., Cerchiello, V., Dabeek, J., Di Meo, A., and Borzi, B. (2016). Towards Integrated Seismic Risk Assessment in Palestine. Application to the City of Nablus. *VII European Congress on Computational Methods in Applied Sciences and Engineering*. <https://doi.org/10.7712/100016.2235.12031>

Moreno-González, R., and Bairán, J. M. (2011). Análisis del comportamiento sísmico de los edificios de obra de fábrica, típicos del distrito Eixample de Barcelona. *Informes de La Construcción*, 63(524), 21–32. <https://doi.org/10.3989/ic.10.045>

Moreno-González, R., Pujades, L. G., Barbat, Á. H., and Lagomarsino, S. (2008). Seismic risk of traditional unreinforced masonry buildings of Barcelona, Spain. *International Seminar On Seismic Risk And Rehabilitation Of Stone Masonry Housing*.

Moreno González, R., and Bairán García, J. M. (2012). Evaluación sísmica de los edificios de mampostería típicos de Barcelona aplicando la metodología Risk-UE. *Revista Internacional de Metodos Numericos Para Calculo y Diseno En Ingenieria*, 28(3), 161–169. <https://doi.org/10.1016/j.rimni.2012.03.007>

Munari, M., Valluzzi, M., and Modena, C. (2009). Classificazioni di vulnerabilità sismica dal calcolo limite per macroelementi: applicazione ad aggregati edilizi in muratura in alcuni centri storici umbri. In: *XIII Convegno ANIDIS "L'Ingegneria Sismica in Italia."* Bologna.

Najam, F. A. (2018). *Nonlinear Static Analysis Procedures for Seismic Performance Evaluation of Existing Buildings – Evolution and Issues* (pp. 180–198). https://doi.org/10.1007/978-3-319-61914-9_15

NCSE-02. (2002). *Norma de Construcción Sismorresistente: Parte general y edificación (NCSE-02)* (Vol. 53, Issue 9). <https://doi.org/10.1017/CBO9781107415324.004>

Nicodemo, G., Pittore, M., Masi, A., and Manfredi, V. (2020). Modelling exposure and vulnerability from post-earthquake survey data with risk-oriented taxonomies: AeDES form, GEM taxonomy and EMS-98 typologies. *International Journal of Disaster Risk Reduction*, 50(September), 101894. <https://doi.org/10.1016/j.ijdr.2020.101894>

Novelli, V. I., D'Ayala, D., Makhloufi, N., Benouar, D., and Zekagh, A. (2015). A procedure for the identification of the seismic vulnerability at territorial scale. Application to the Casbah of Algiers. *Bulletin of Earthquake Engineering*, 13(1), 177–202. <https://doi.org/10.1007/s10518-014-9666-1>

- NZSEE. (2006). *Assessment and improvement of the structural performance of buildings in earthquakes: prioritisation, initial evaluation, detailed assessment, improvement measures: recommendations of a NZSEE study group on earthquake risk buildings*. New Zealand Society for Earthquake Engineering Wellington, New Zealand.
- Ortega, J. (2018). *Reduction of the seismic vulnerability of vernacular architecture with traditional strengthening solutions*. University of Minho.
- Ortega, J., Saloustros, S., and Roca, P. (2021). Seismic vulnerability assessment method for vernacular architecture considering uncertainty. In Pere Roca, L. Pelà, and C. Molins (Eds.), *Int. Conf. Struct. Anal. Hist. Constr., International Centre for Numerical Methods in Engineering*. CIMNE.
- Ortega, J., Vasconcelos, G., Rodrigues, H., Correia, M., and Miguel, T. (2019). Use of post-earthquake damage data to calibrate, validate and compare two seismic vulnerability assessment methods for vernacular architecture. *International Journal of Disaster Risk Reduction*, 39(February), 101242. <https://doi.org/10.1016/j.ijdr.2019.101242>
- Page, A. W. (1983). The strength of brick masonry under biaxial tension-compression. *Int. J. Mason. Constr*, 3, 26–31.
- Page, A. W. (1981). The biaxial compressive strength of brick masonry. *Proceedings of the Institution of Civil Engineers*, 893–906. <https://doi.org/https://doi.org/10.1680/iicep.1981.1825>
- Palazzi, N. C., Barrientos, M., Sandoval, C., and de la Llera, J. C. (2022). Seismic Vulnerability Assessment of the Yungay's Historic Urban Center in Santiago, Chile. *Journal of Earthquake Engineering*, 1–28. <https://doi.org/10.1080/13632469.2022.2087793>
- Panagiotis, G., and Vagelis, P. (2015). Handbook of Research on Seismic Assessment and Rehabilitation of Historic Structures. In P. G. Asteris and V. Plevris (Eds.), *Handbook of Research on Seismic Assessment and Rehabilitation of Historic Structures* (Issue July). IGI Global. <https://doi.org/10.4018/978-1-4666-8286-3>
- Paricio Casademunt, A. (2001). *Secrets d'un sistema constructiu: l'Eixample* (Edicions U). Edicions de la Universitat Politècnica de Catalunya.
- Pavić, G., Hadzima-Nyarko, M., Bulajić, B., and Jurković, Ž. (2020). Development of Seismic Vulnerability and Exposure Models—A Case Study of Croatia. *Sustainability*, 12(3). <https://doi.org/10.3390/su12030973>
- PCI Industry Handbook Committee. (2004). *PCI Design Handbook: Precast and Prestressed Concrete*.
- Pelà, L., Aprile, A., and Benedetti, A. (2009). Seismic assessment of masonry arch bridges. *Engineering Structures*, 31(8), 1777–1788. <https://doi.org/10.1016/j.engstruct.2009.02.012>
- Pelà, L., Canella, E., Aprile, A., and Roca, P. (2016). Compression test of masonry core samples extracted from existing brickwork. *Construction and Building Materials*, 119, 230–240. <https://doi.org/10.1016/j.conbuildmat.2016.05.057>
- Pelà, L., Kasioumi, K., and Roca, P. (2017). Experimental evaluation of the shear strength of aerial lime mortar brickwork by standard tests on triplets and non-standard tests on core samples. *Engineering Structures*, 136, 441–453.

<https://doi.org/https://doi.org/10.1016/j.engstruct.2017.01.028>

Pelà, L., Roca, P., and Aprile, A. (2018). Combined In-Situ and Laboratory Minor Destructive Testing of Historical Mortars. *International Journal of Architectural Heritage*, 12(3), 334–349. <https://doi.org/10.1080/15583058.2017.1323247>

Pelà, L., Roca, P., and Benedetti, A. (2016). Mechanical Characterization of Historical Masonry by Core Drilling and Testing of Cylindrical Samples. *International Journal of Architectural Heritage*, 10(2–3), 360–374. <https://doi.org/10.1080/15583058.2015.1077906>

Pereira, J. M., Correia, A. A., and Lourenço, P. B. (2021). In-plane behaviour of rubble stone masonry walls: Experimental, numerical and analytical approach. *Construction and Building Materials*, 271. <https://doi.org/10.1016/j.conbuildmat.2020.121548>

Petracca, M., Pelà, L., Rossi, R., Oller, S., Camata, G., and Spacone, E. (2016). Regularization of first order computational homogenization for multiscale analysis of masonry structures. *Computational Mechanics*, 57(2), 257–276.

Piazza, M., Baldessari, C., and Tomasi, R. (2008). The role in-plane floor stiffness in the seismic behaviour of traditional buildings. *Proceedings of the 14th World Conference on Earthquake Engineering, Beijing, China, 12-17 October*.

Pitilakis, K., Franchin, P., Khazai, B., and Wenzel, H. (2014). *SYNER-G: Systemic Seismic Vulnerability and Risk Assessment of Complex Urban, Utility, Lifeline Systems and Critical Facilities* (K. Pitilakis, P. Franchin, B. Khazai, and H. Wenzel (eds.); Vol. 31). Springer Netherlands. <https://doi.org/10.1007/978-94-017-8835-9>

Pittore, M., Haas, M., and Megalooikonomou, K. G. (2018). Risk-Oriented, Bottom-Up Modeling of Building Portfolios With Faceted Taxonomies . In *Frontiers in Built Environment* (Vol. 4). <https://www.frontiersin.org/articles/10.3389/fbuil.2018.00041>

Pujades, L. G., Barbat, A. H., González-Drigo, R., Avila, J., and Lagomarsino, S. (2012). Seismic performance of a block of buildings representative of the typical construction in the Eixample district in Barcelona (Spain). *Bulletin of Earthquake Engineering*, 10(1), 331–349. <https://doi.org/10.1007/s10518-010-9207-5>

Pujades, L. G., Canas, J. A., Mena, U., Espinoza, F., Alfaro, A., and Caselles, J. (2000). Seismic Risk Evaluation in Barcelona, Spain. *On Earthquake Engineering (WCEE)*.

Rago, M. (2022). *Study of the seismic vulnerability of masonry building aggregates in the city of Barcelona*. Universitat Politècnica de Catalunya University of Minho.

Rigalt i Farriols, L. (1857). *Album enciclopédico-pintoresco de los industriales: colección de dibujos geométricos*. Barcelona: Litografía de la Unión de Francisco Campañá, 1857-1859.

RISK-UE. (2004). *An advanced approach to earthquake risk scenarios with applications to different European towns. WP08-Application to Barcelona*.

Roca, P., Cervera, M., Gariup, G., and Pelà, L. (2010). Structural Analysis of Masonry Historical Constructions. Classical and Advanced Approaches. *Archives of Computational Methods in Engineering*, 17(3), 299–325.

Roca, P., Lourenço, P. B., and Gaetani, A. (2019). *Historic construction and conservation*.

Materials, systems and damage. Routledge.

Roca, Pere, Cervera, M., Pelà, L., Clemente, R., and Chiumenti, M. (2013). Continuum FE models for the analysis of Mallorca Cathedral. *Engineering Structures*, 46, 653–670. <https://doi.org/10.1016/j.engstruct.2012.08.005>

Romis, F. (2020). *Development of innovative methods for the seismic risk classification of masonry aggregates*. University of Minho and University of Florence in.

Romis, F., Caprili, S., Ferreira, T. M., and Lourenco, P. B. (2021). *An Improved Seismic Vulnerability Assessment Approach for Historical Urban applied sciences An Improved Seismic Vulnerability Assessment Approach for Historical Urban Centres : The Case Study of Campi Alto di. January*. <https://doi.org/10.3390/app11020849>

Rossetto, T., and Elnashai, A. (2005). A new analytical procedure for the derivation of displacement-based vulnerability curves for populations of RC structures. *Engineering Structures*, 27(3), 397–409. <https://doi.org/10.1016/j.engstruct.2004.11.002>

Saaty, R. W. (1987). The analytic hierarchy process-what it is and how it is used. *Mathematical Modelling*, 9(3–5), 161–176. [https://doi.org/10.1016/0270-0255\(87\)90473-8](https://doi.org/10.1016/0270-0255(87)90473-8)

Saloustros, S. (2017). *Tracking Localized Cracks in the Computational Analysis of Masonry Structures*. Universitat Politècnica de Catalunya.

Saloustros, S., Pelà, L., Contrafatto, F. R., Roca, P., and Petromichelakis, I. (2019). Analytical Derivation of Seismic Fragility Curves for Historical Masonry Structures Based on Stochastic Analysis of Uncertain Material Parameters. *International Journal of Architectural Heritage*, 13(7), 1142–1164. <https://doi.org/10.1080/15583058.2019.1638992>

Saloustros, S., Pelà, L., and Roca, P. (2020). Nonlinear Numerical Modeling of Complex Masonry Heritage Structures Considering History-Related Phenomena in Staged Construction Analysis and Material Uncertainty in Seismic Assessment. *Journal of Performance of Constructed Facilities*, 34(5), 04020096. [https://doi.org/10.1061/\(ASCE\)CF.1943-5509.0001494](https://doi.org/10.1061/(ASCE)CF.1943-5509.0001494)

Saloustros, S., Pelà, L., Roca, P., and Portal, J. (2015). Numerical analysis of structural damage in the church of the Poblet Monastery. *Engineering Failure Analysis*, 48, 41–61. <https://doi.org/https://doi.org/10.1016/j.engfailanal.2014.10.015>

Secanell, R. (1999). *Avaluació de la perillositat sísmica a Catalunya: anàlisi de sensibilitat per a diferents models d'ocurrència i paràmetres sísmics*. Universitat Politècnica de Catalunya.

Secanell, R., Goula, X., Susagna, T., Fleta, J., and Roca, A. (2004). Seismic hazard zonation of Catalonia, Spain, integrating uncertainties. *Journal of Seismology*, 8, 24–40.

Segura Domingo, J. (2020). *Laboratory experimental procedures for the compression and shear characterisation of historical brick masonry*. Universitat Politècnica de Catalunya.

Segura, J., Bernat, E., Mendizábal, V., Pelà, L., Roca, P., and Gil, L. (2021). Experimental comparison of two testing setups for characterizing the shear mechanical properties of masonry. *Journal of Building Engineering*, 44(April). <https://doi.org/10.1016/j.jobbe.2021.103277>

Segura, J., Pelà, L., and Roca, P. (2018). Monotonic and cyclic testing of clay brick and lime mortar masonry in compression. *Construction and Building Materials*, 193, 453–466.

<https://doi.org/10.1016/j.conbuildmat.2018.10.198>

Segura, J., Pelà, L., Roca, P., and Cabané, A. (2019). Experimental analysis of the size effect on the compressive behaviour of cylindrical samples core-drilled from existing brick masonry. *Construction and Building Materials*, 228, 116759. <https://doi.org/10.1016/j.conbuildmat.2019.116759>

Segura, J., Pelà, L., Saloustros, S., and Roca, P. (2021). Experimental and numerical insights on the diagonal compression test for the shear characterisation of masonry. *Construction and Building Materials*, 287, 122964. <https://doi.org/10.1016/j.conbuildmat.2021.122964>

Senaldi, I. E., Guerrini, G., Comini, P., Graziotti, F., Penna, A., Beyer, K., and Magenes, G. (2020). Experimental seismic performance of a half-scale stone masonry building aggregate. *Bulletin of Earthquake Engineering*, 18(2), 609–643. <https://doi.org/10.1007/s10518-019-00631-2>

Senaldi, I., Magenes, G., Penna, A., Galasco, A., and Rota, M. (2014). The Effect of Stiffened Floor and Roof Diaphragms on the Experimental Seismic Response of a Full-Scale Unreinforced Stone Masonry Building. *Journal of Earthquake Engineering*, 18(3), 407–443. <https://doi.org/10.1080/13632469.2013.876946>

Shakib, H., Mirjalili, A., Dardaei, S., and Mazroei, A. (2015). Experimental Investigation of the Seismic Performance of Retrofitted Masonry Flat Arch Diaphragms. *Journal of Performance of Constructed Facilities*, 29(4), 04014115. [https://doi.org/10.1061/\(asce\)cf.1943-5509.0000611](https://doi.org/10.1061/(asce)cf.1943-5509.0000611)

Silva, V., Brzev, S., Scawthorn, C., Yepes, C., Dabbeek, J., and Crowley, H. (2022). A Building Classification System for Multi-hazard Risk Assessment. *International Journal of Disaster Risk Science*, 13(2), 161–177. <https://doi.org/10.1007/s13753-022-00400-x>

Stepinac, M., Lourenço, P. B., Atalić, J., Kišiček, T., Uroš, M., Baniček, M., and Šavor Novak, M. (2021). Damage classification of residential buildings in historical downtown after the ML5.5 earthquake in Zagreb, Croatia in 2020. *International Journal of Disaster Risk Reduction*, 56. <https://doi.org/10.1016/j.ijdr.2021.102140>

Tomažević, M., Weiss, P., and Velechovsky, T. (1991). The Influence of Rigidity of Floors on the Seismic Behaviour of Old Stone-Masonry Buildings. *European Earthquake Engineering*, 5(3), 28–41.

Tomažević, Miha. (1999). *Earthquake-resistant design of masonry building*. Imperial College Press.

Torner, F. M. (2009). El Ensanche de Barcelona y la modernidad de las teorías urbanísticas de Cerdà. *I.T. Nº 88, January 2009*, 68–75. <https://www.researchgate.net/publication/42365247>

Turnsek, V., and Sheppard, P. (1980). The shear and flexural resistance of masonry walls. *Proc. Research Conference on Earthquake Eng.*

Tzitzikas, Y. (2009). *Faceted Taxonomy-Based Sources BT - Dynamic Taxonomies and Faceted Search: Theory, Practice, and Experience* (G. M. Sacco and Y. Tzitzikas (eds.); pp. 19–34). Springer Berlin Heidelberg. https://doi.org/10.1007/978-3-642-02359-0_2

Valluzzi, M, Garbin, E., Benetta, M. D., and Modena, C. (2010). In-plane strengthening of timber floors for the seismic improvement of masonry buildings. *Proceedings of the 11th World Conference on Timber Engineering WCTE, Trentino, Italy, 20 – 24 June*.

- Valluzzi, MR, Munari, M., Cardani, G., and Binda, L. (2009). Aggiornamento della vulnerabilità sismica del centro storico di Campi Alto di Norcia (PG). *ANIDIS 2009, Bologna*.
- Vicente, R, Parodi, S., Lagomarsino, S., Varum, H., and Silva, J. A. R. M. (2008). *SEISMIC VULNERABILITY ASSESSMENT , DAMAGE SCENARIOS AND LOSS ESTIMATION Case study of the old city centre of Coimbra , Portugal*.
- Vicente, Romeu. (2008). *Estratégias e metodologias para intervenções de reabilitação urbana. Avaliação da vulnerabilidade e do risco sísmico do edificado da Baixa de Coimbra*. University of Aveiro.
- Vicente, Romeu, Ferreira, T., Maio, R., Varum, H., Costa, A., Costa, A., Oliveira, C. S., and Estêvão, J. (2014). Seismic Vulnerability Assessment of Existing Masonry Buildings : Case Study of the Old City Centre of Faro , Portugal. *2th European Conference on Earthquake Engineering and Seismology*, 1–9. <https://doi.org/10.1007/s10518-013-9447-2.2>
- Vicente, Romeu, Parodi, S., Lagomarsino, S., Varum, H., and Silva, J. A. R. M. (2011). Seismic vulnerability and risk assessment: Case study of the historic city centre of Coimbra, Portugal. *Bulletin of Earthquake Engineering*, 9(4), 1067–1096. <https://doi.org/10.1007/s10518-010-9233-3>
- Vila, J. (Vila R. (1989). *La Casa original del ensanche a Barcelona : 1860-1864 : los parámetros formales y métricos de la unidad residencial de la manzana Cerdà*. Universitat Politècnica de Catalunya.
- Vintzileou, E., Mouzakis, C., Adami, C.-E., and Karapitta, L. (2015). Seismic behavior of three-leaf stone masonry buildings before and after interventions: Shaking table tests on a two-storey masonry model. *Bulletin of Earthquake Engineering*, 13(10), 3107–3133. <https://doi.org/10.1007/s10518-015-9746-x>
- Whitman, R. V., Reed, J. W., and Hong, S. T. (1973). Earthquake Damage Probability Matrices. *5th European Conference on Earthquake Engineering*, 2531.
- Yépez, F., Barbat, A. H., and Canas, J. A. (1996). Simulación de escenarios de daño sísmico en zonas urbanas. *Revista Internacional de Métodos Numéricos Para Cálculo y Diseño En Ingeniería*.
- Yepez, F. (1996). *Metodología para la evaluación de la vulnerabilidad y riesgo sísmico de estructuras aplicando técnicas de simulación*. Universitat Politècnica de Catalunya.
- Yepez, Fabricio, Barbat, A. H., and Canas, J. A. (1996). Simulación de Escenarios de Daño Sísmico en Zonas Urbanas. *Revista Internacional de Métodos y Cálculo y Diseño En Ingeniería*, 12(3), 331–358.
- Zahrai, S M, Zahraei, S. A., and Edalat Manesh, R. (2006). Evaluation of retrofitting methods for flexible floor slab. *Proceedings of the First European Conference on Earthquake Engineering and Seismol-Ogy, Geneva, Switzerland, 3-8 September*.
- Zahrai, Seyed Mehdi. (2015). Experimental study of typical and retrofitted jack arch slabs in a single story 3D steel building. *International Journal of Civil Engineering*, 13(3).

APPENDIX A

This appendix presents the statistical data obtained for the different recurrent building typologies: 'C' – band building with central patios and staircase and without and with lateral patios; 'L' - narrow buildings with lateral staircase and patios and 'V' - corner buildings), with the frequency distributions of all the general geometrical characteristics. The information is complimentary to the previously presented statistical data in Chapter 4 (section 4.3).

- Statistical data for the building typology C21AB

According to the statistical data obtained by Cornadó Bardón (2015) the building typology C21AB is a rectangular band building with a central staircase and one patio, as well as lateral patios on each side of the longitudinal walls (see Figure 4.20). Figure A.1 and Figure A.2 illustrate the frequency distributions of the band buildings' width and length, respectively.

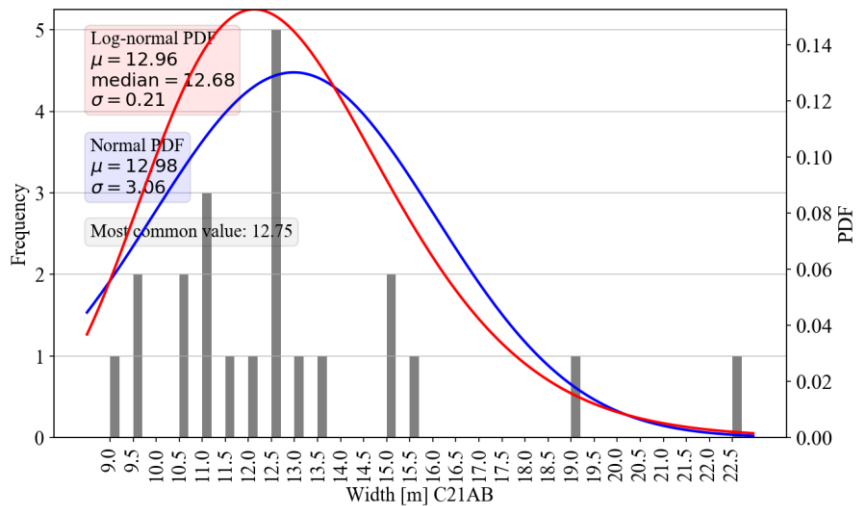


Figure A.1 - Frequency of width of the band building's façades - type C21AB.

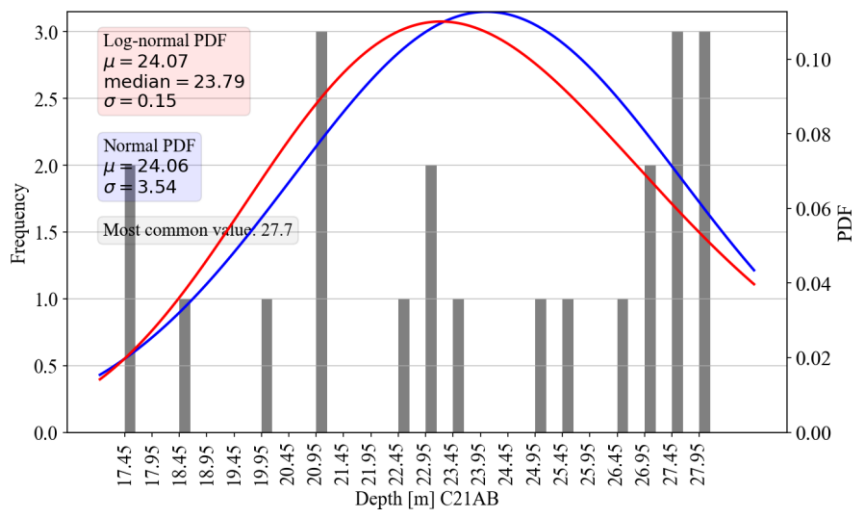


Figure A.2 - Frequency distribution of building's plot depth -type C21AB.

Moreover, Figure A.3 shows the frequency distribution of the total number of floors, without or with vertical extensions (*remuntes*).

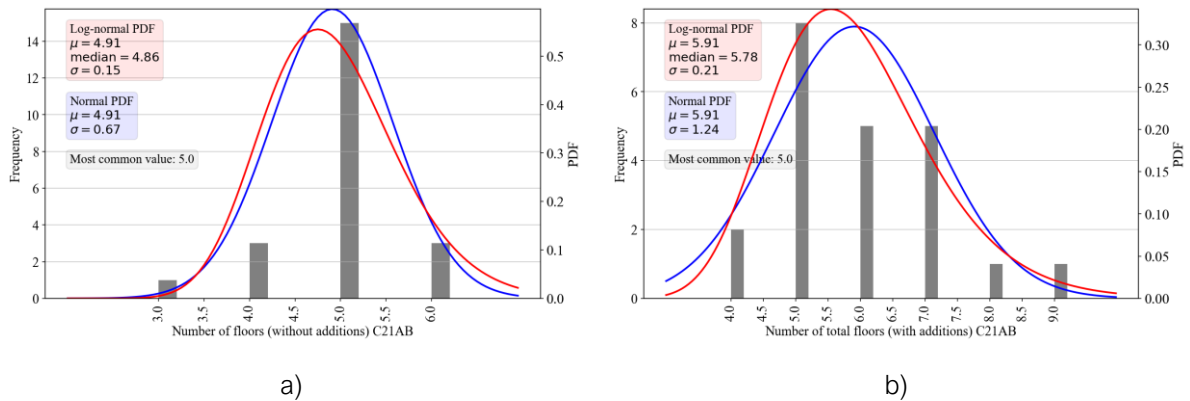


Figure A.3 - Frequency distribution of the total number of floors for the band building typology -type C21AB: a) without vertical additions (*remuntes*) and b) with vertical additions (*remuntes*).

Figure A.4 represents the distances between the load bearing walls parallel to the *façades* (see Figure 4.21 for the proper nomenclature of the walls and distances).

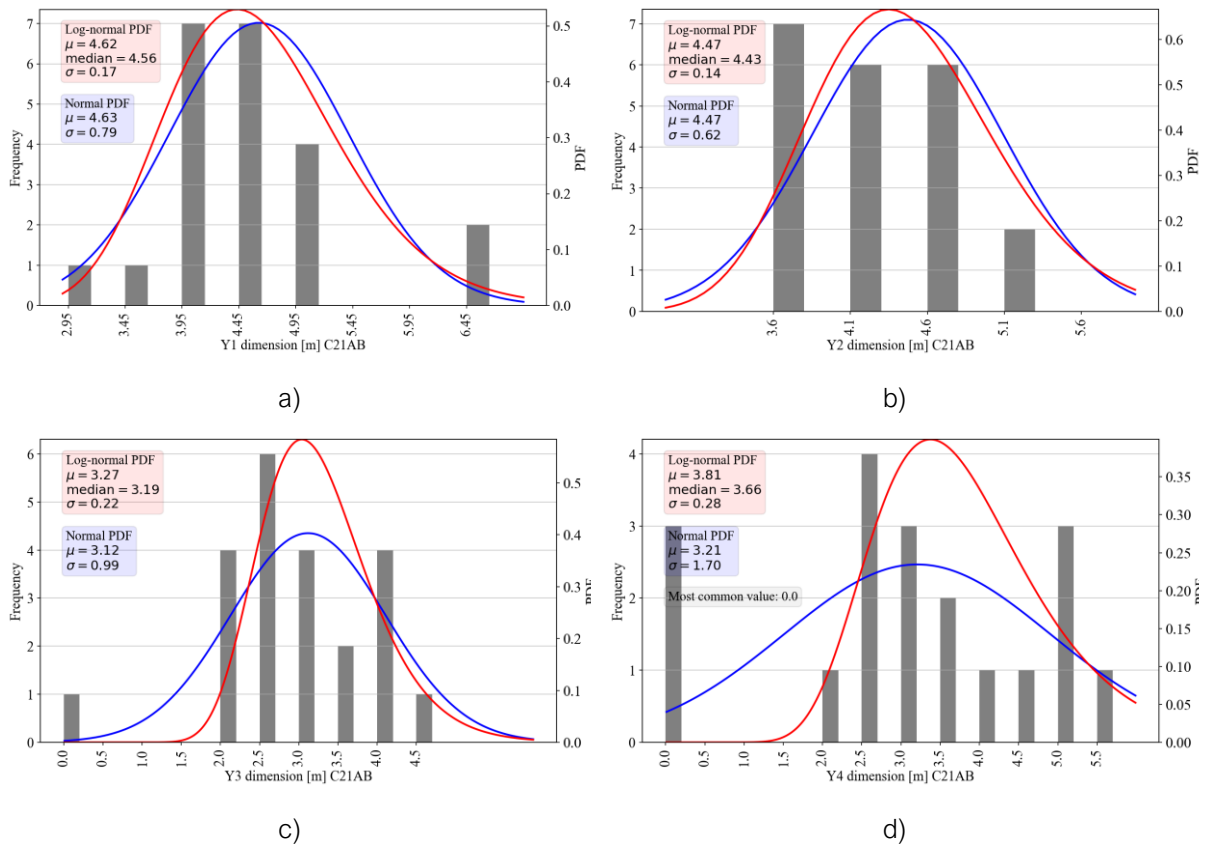


Figure A.4 - Frequency distribution of the following wall distances for the band building typology -type C21AB: a) Y1 distance between the front *façade* wall (W1) and the parallel interior wall (W5); b) Y2 distance between the back *façade* wall (W2) and the parallel interior wall (W6); c) Y3 distance between the interior walls W3 and W5 of the bay situated in front of the central part; d) Y4 distance between the interior walls W4 and W6 of the bay situated after the central part.

Figure A.5 shows the frequency distribution of the number of openings and the number of flats per floor level in this building typology.

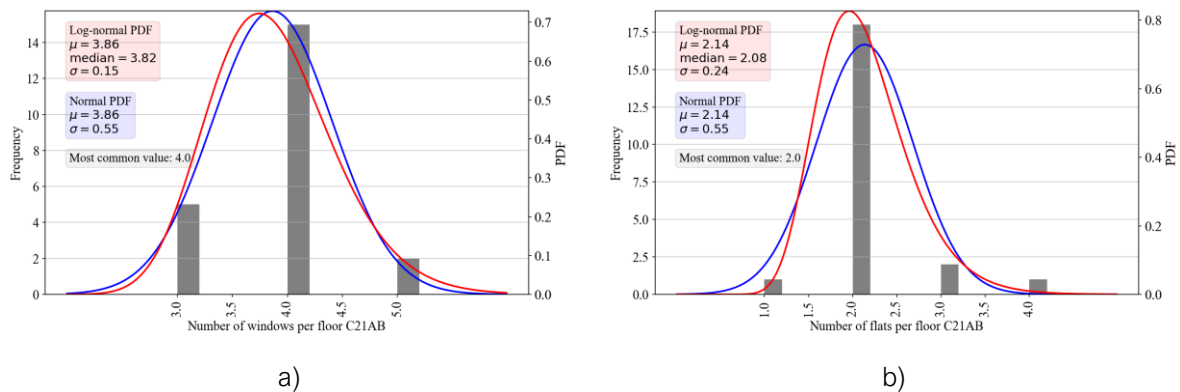


Figure A.5 - Frequency distribution of the number of façade openings (a) and number of flats per floor (b).

- Statistical data for the building typology C12AB

The building typology C12AB is a rectangular band building with a central staircase and patio, and with continuous lateral walls, without any lateral patios (see Figure 4.20). According to the type of central part configuration (see Figure 4.22), the type 1a is the second most frequent typology by representing around 48% of the total sample of analysed buildings with a central staircase. Figure A.1, Figure A.6 and Figure A.7 illustrate the frequency distributions of the band buildings' width and length, respectively.

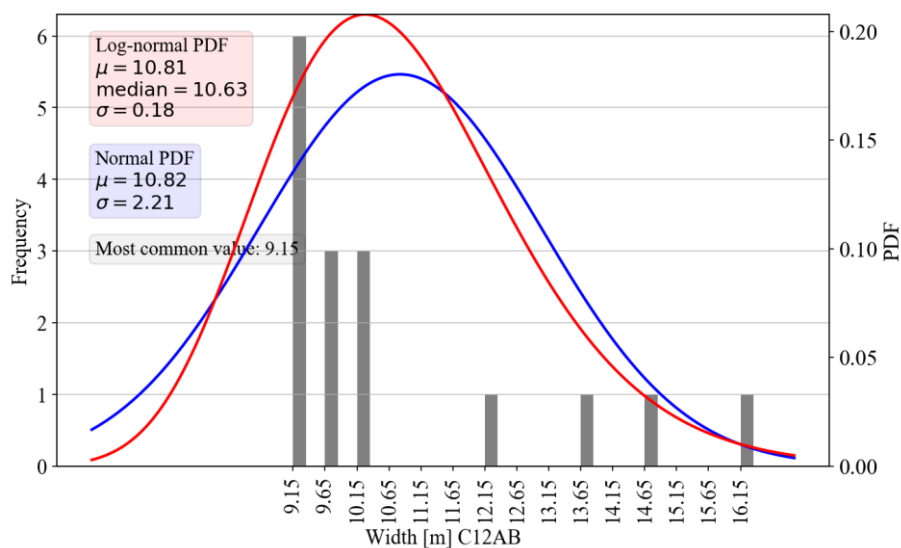


Figure A.6 - Frequency of width of the most representative band building's façades - type C12AB.

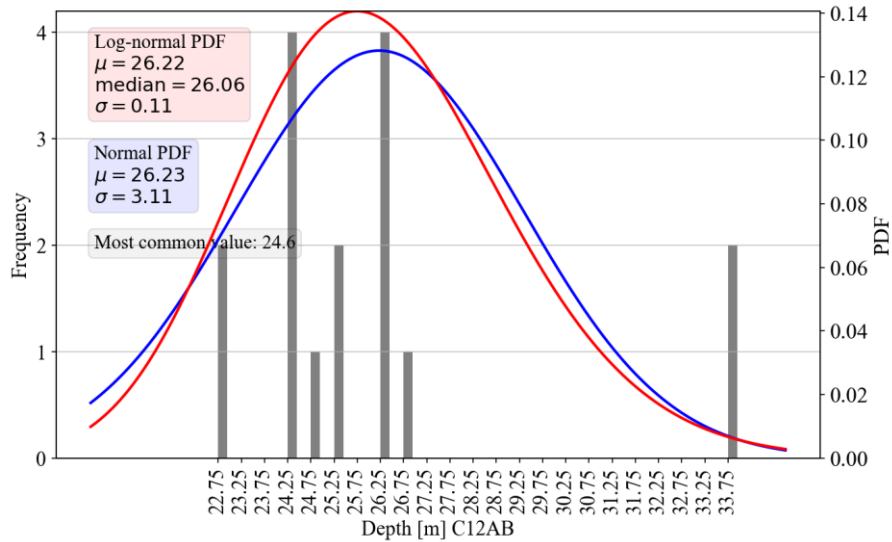


Figure A.7 - Frequency distribution of building's plot depth - type C12AB.

The following Figure A.8, Figure A.9 and Figure A.10 illustrate the obtained frequency distribution for the different parameters that vary in the *Example* existing building typologies, by representing number of floors (with and without *remuntes*), the distances between walls parallel to the façade, and the number of façade openings and number of flats per floor level, respectively.

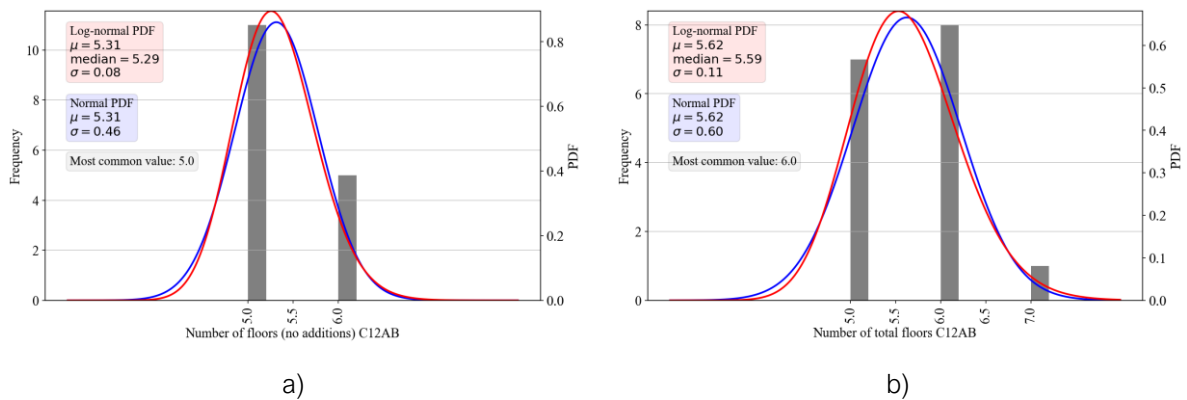


Figure A.8 - Frequency distribution of the total number of floors for the band building typology - type C12AB: a) without vertical additions (*remuntes*) and b) with vertical additions (*remuntes*).

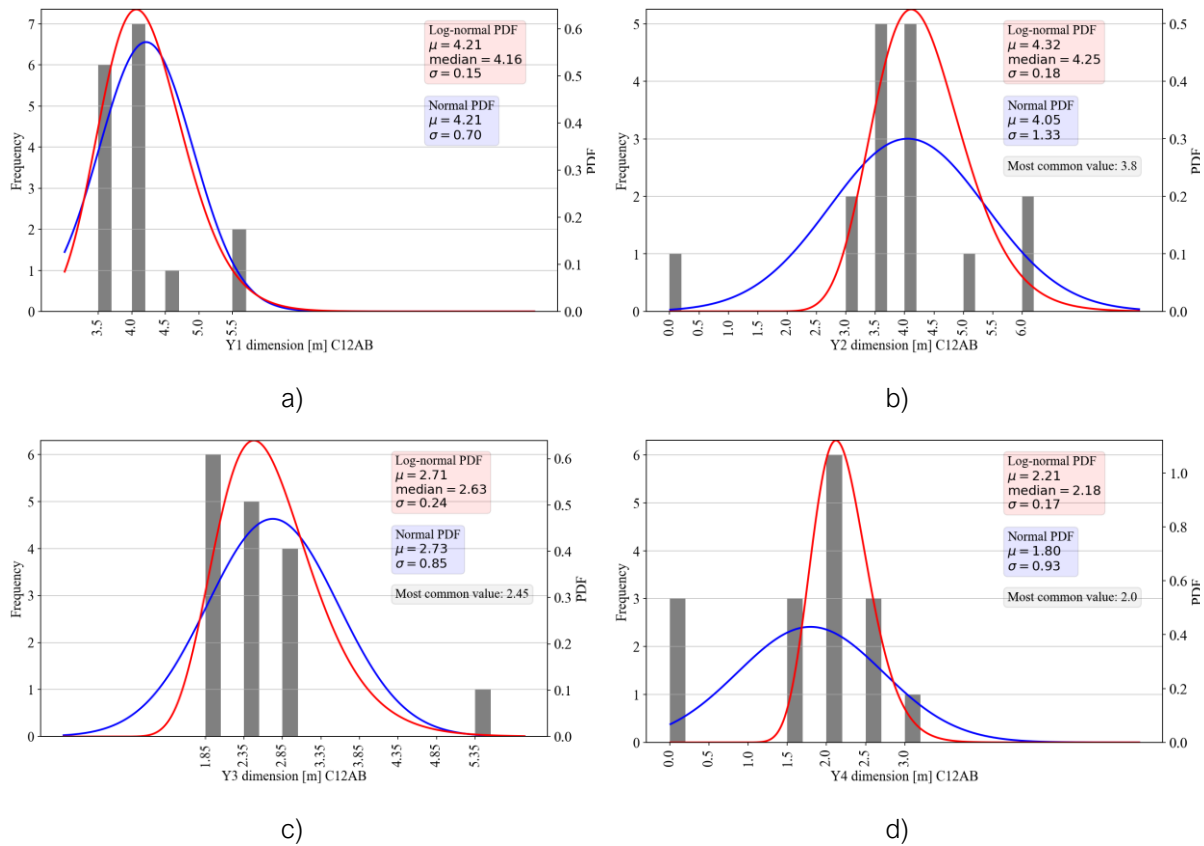


Figure A.9 - Frequency distribution of the following wall distances for the band building typology - type C12AB: a) Y1 distance between the front façade wall (W1) and the parallel interior wall (W5); b) Y2 distance between the back façade wall (W2) and the parallel interior wall (W6); c) Y3 distance between the interior walls W3 and W5 of the bay situated in front of the central part; d) Y4 distance between the interior walls W4 and W6 of the bay situated after the central part (see Figure 4.21 for the proper nomenclature of the walls and distances).

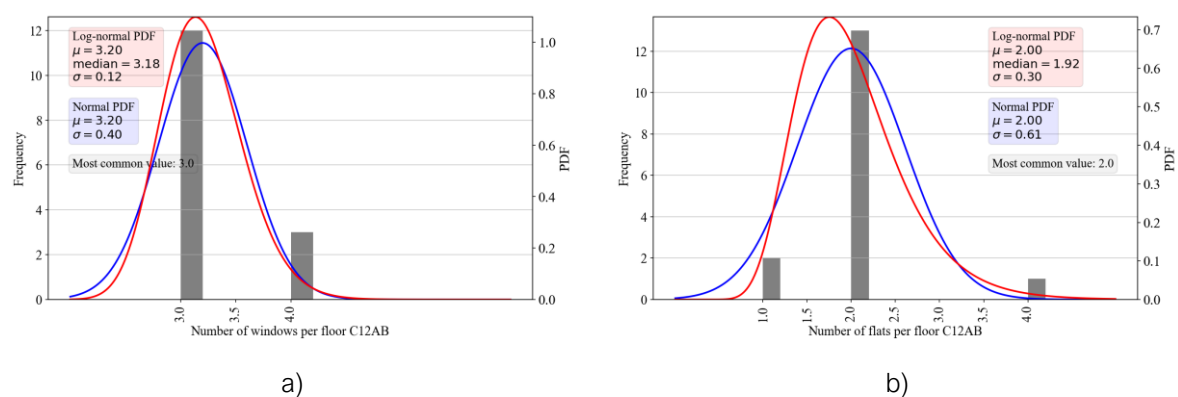


Figure A.10 - Frequency distribution of the number of façade openings (a) and number of flats per floor (b).

- Statistical data for the building typologies with lateral staircase

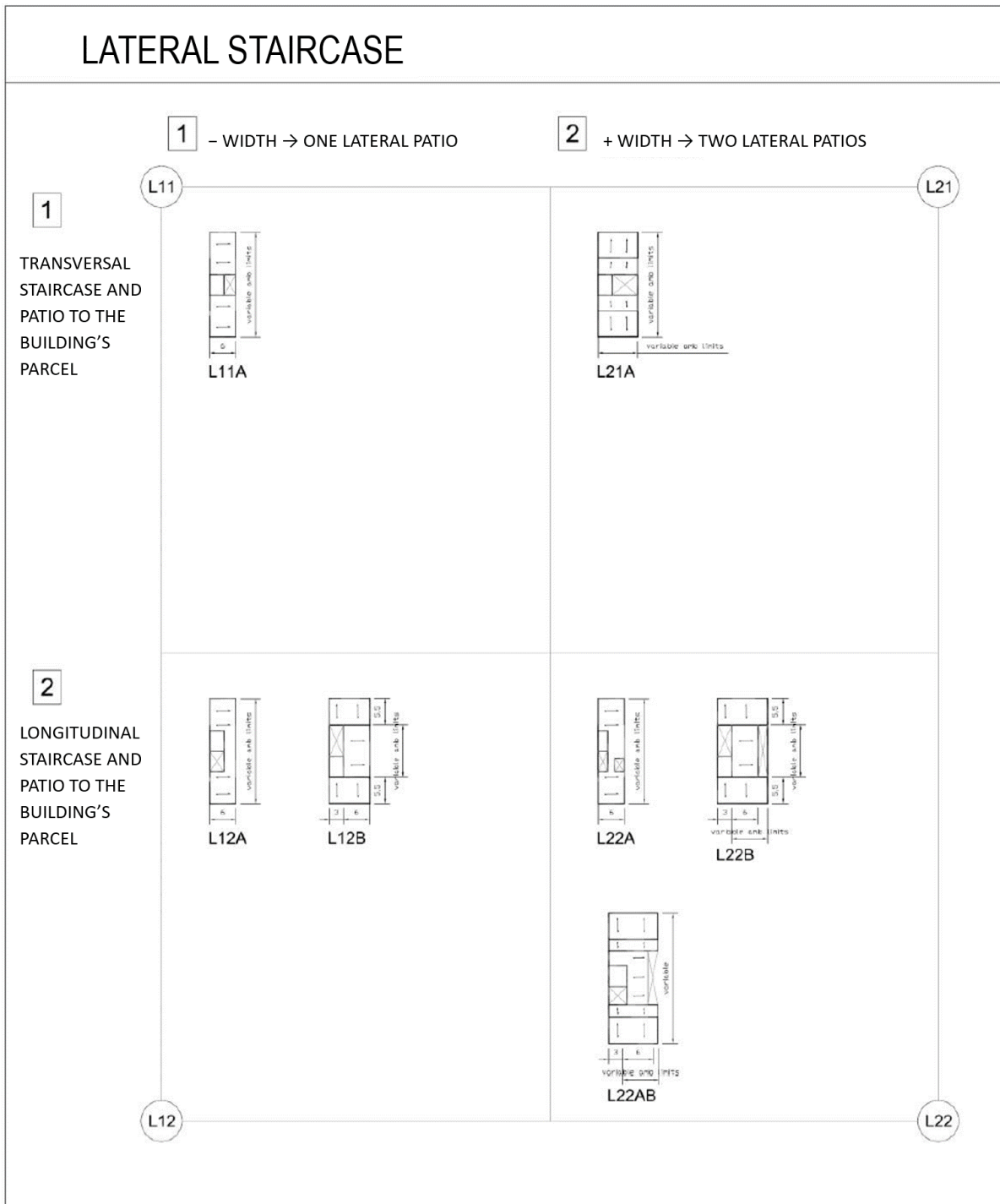


Figure A.11 - Schematisation of subtypes for the building typology with lateral staircase 'L' (adapted from Cornadó Bardón 2015).

According to the statistical data presented in Chapter 4 (see section 4.4), the most common narrow building typologies with lateral staircase are the types L22AB and L11A (see Figure 4.32). These building typologies represent a smaller percentage of the representative *Example* buildings

and typically, they consist of a lateral staircase with patio, which can be placed transversal (type L11A) or longitudinal towards the building's plot (type L22AB).

Figure A.12 and Figure A.13 illustrate the frequency distributions of the narrow band buildings' width and length, respectively for the type L22AB.

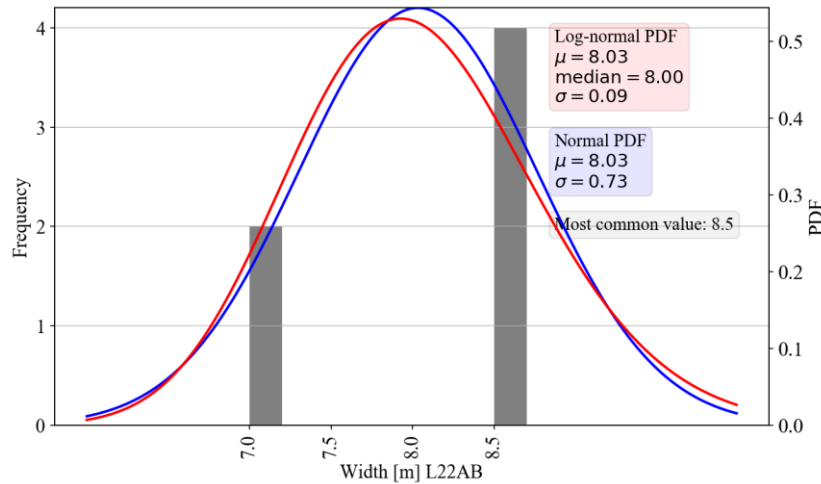


Figure A.12 - Frequency of width of the most representative band building's façades for the narrow band building typology - type L22AB.

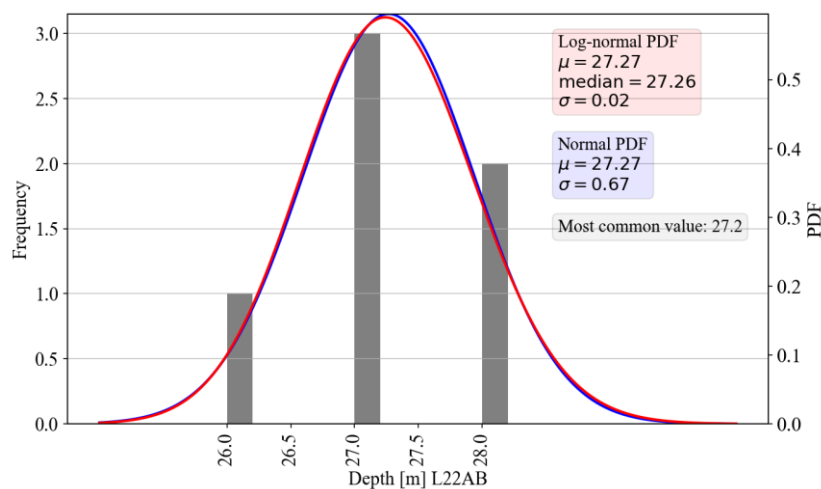


Figure A.13 - Frequency distribution of building's plot depth for the narrow band building typology - type L22AB.

The following figures (Figure A.14, Figure A.15 and Figure A.16) illustrate the frequency distributions regarding the total number of floors, wall distances and the number of flats per floor level for narrow building with lateral staircase - type L22AB.

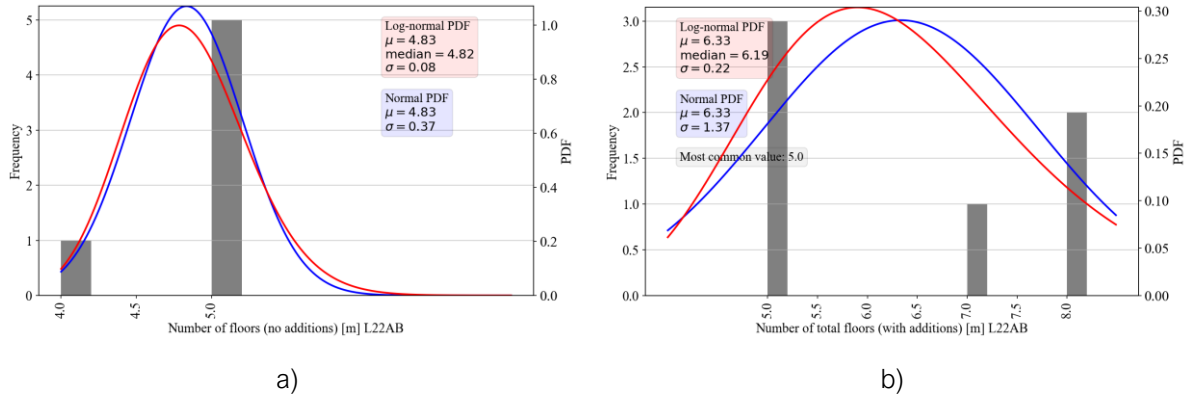


Figure A.14 - Frequency distribution of the total number of floors for the narrow band building typology - type L22AB: a) without vertical additions (remuntes) and b) with vertical additions (remuntes).

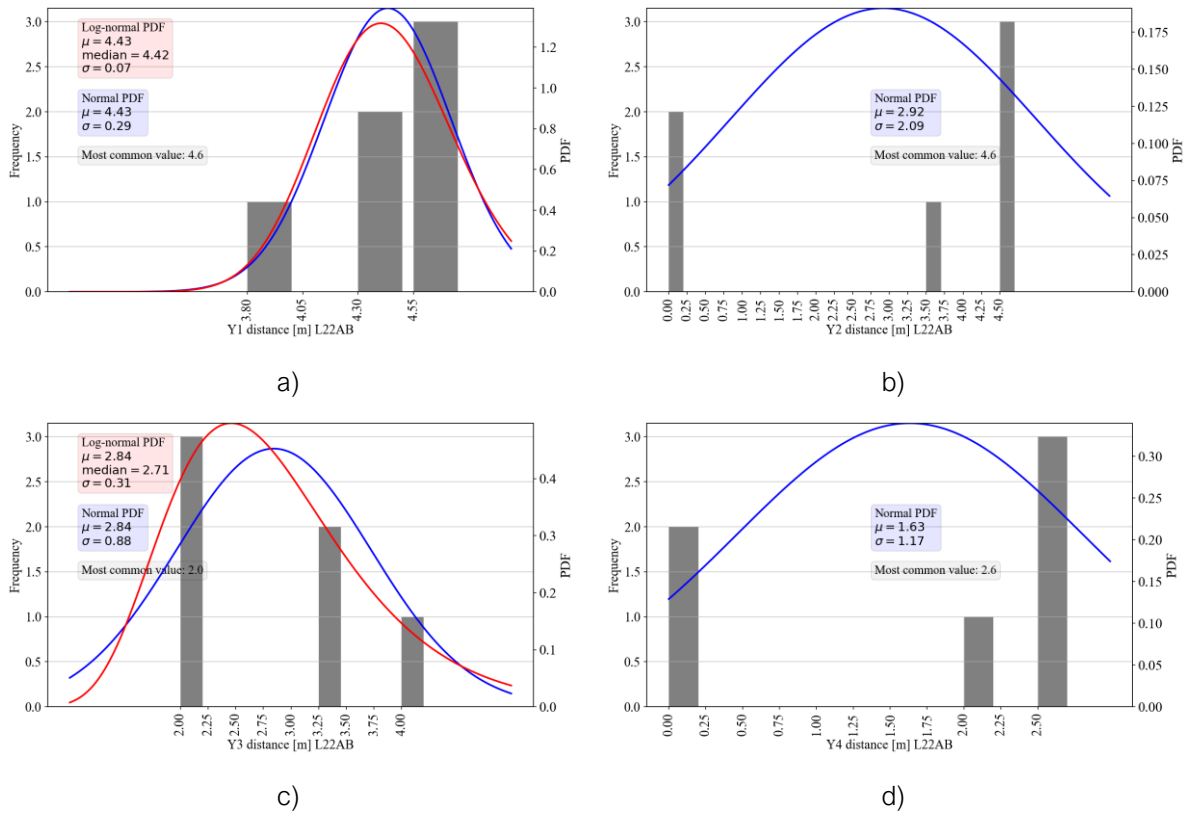


Figure A.15 - Frequency distribution of the following wall distances for the narrow band building typology - type L22AB: a) Y1 distance between the front façade wall (W1) and the parallel interior wall (W5); b) Y2 distance between the back façade wall (W2) and the parallel interior wall (W6); c) Y3 distance between the interior walls W3 and W5 of the bay situated in front of the central part; d) Y4 distance between the interior walls W4 and W6 of the bay situated after the central part (see Figure 4.21 for the proper nomenclature of the walls and distances).

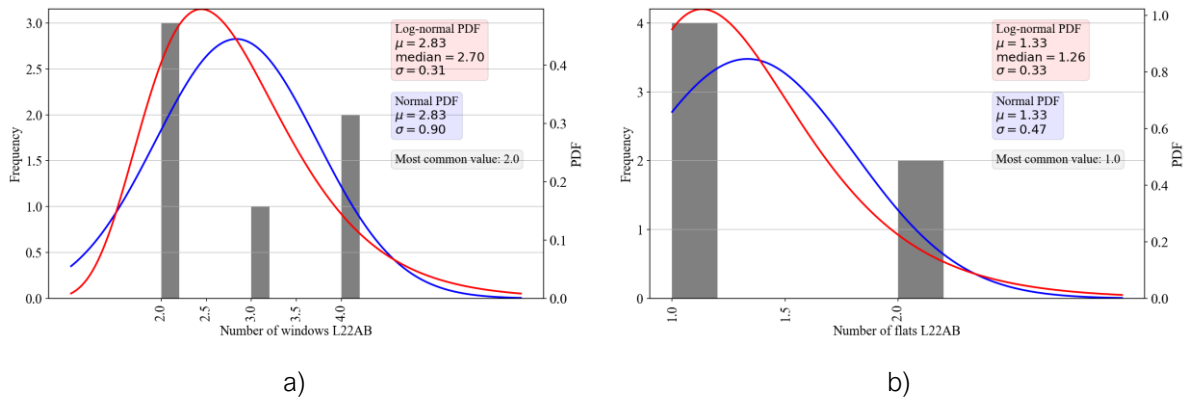


Figure A.16 - Frequency distribution of the number of façade openings (a) and number of flats per floor.

Figure A.17 and Figure A.18 Figure A.13 illustrate the frequency distributions of the narrow band buildings' width and length, respectively for the type L22AB.

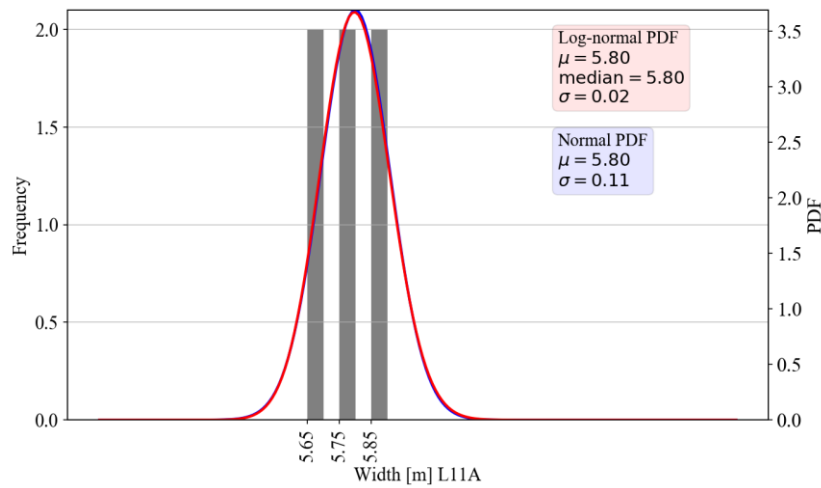


Figure A.17 - Frequency of width of the most representative band building's façades for the narrow band building typology - type L11A.

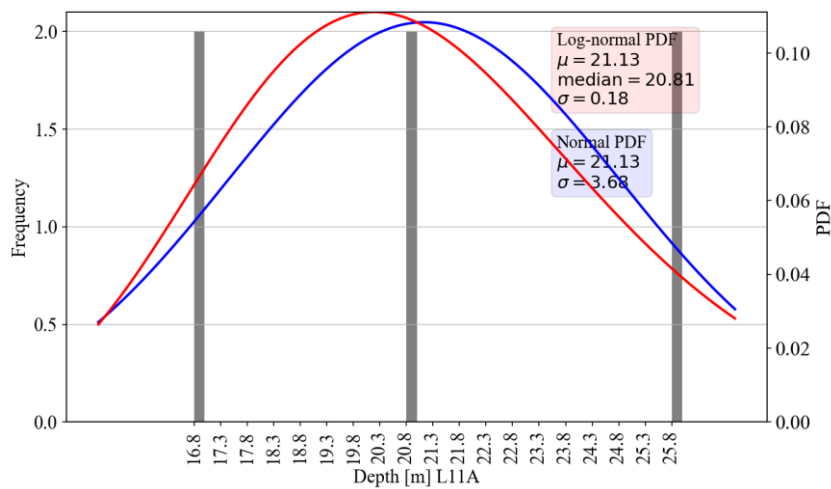


Figure A.18 - Frequency distribution of building's plot depth for the narrow band building typology - type L11A.

Moreover, Figure A.19 shows the number of floors for the narrow band building typology - type L11A with vertical additions (*remuntes*).

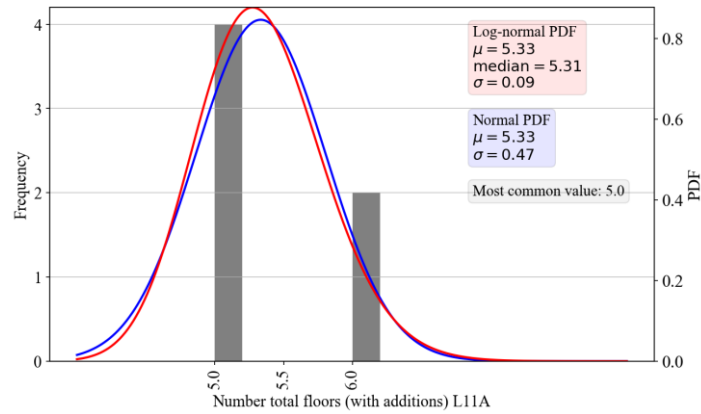


Figure A.19 - Frequency distribution of the total number of floors for the narrow band building typology - type L11A with vertical additions (*remuntes*).

- Statistical data for the corner building typologies 'V'

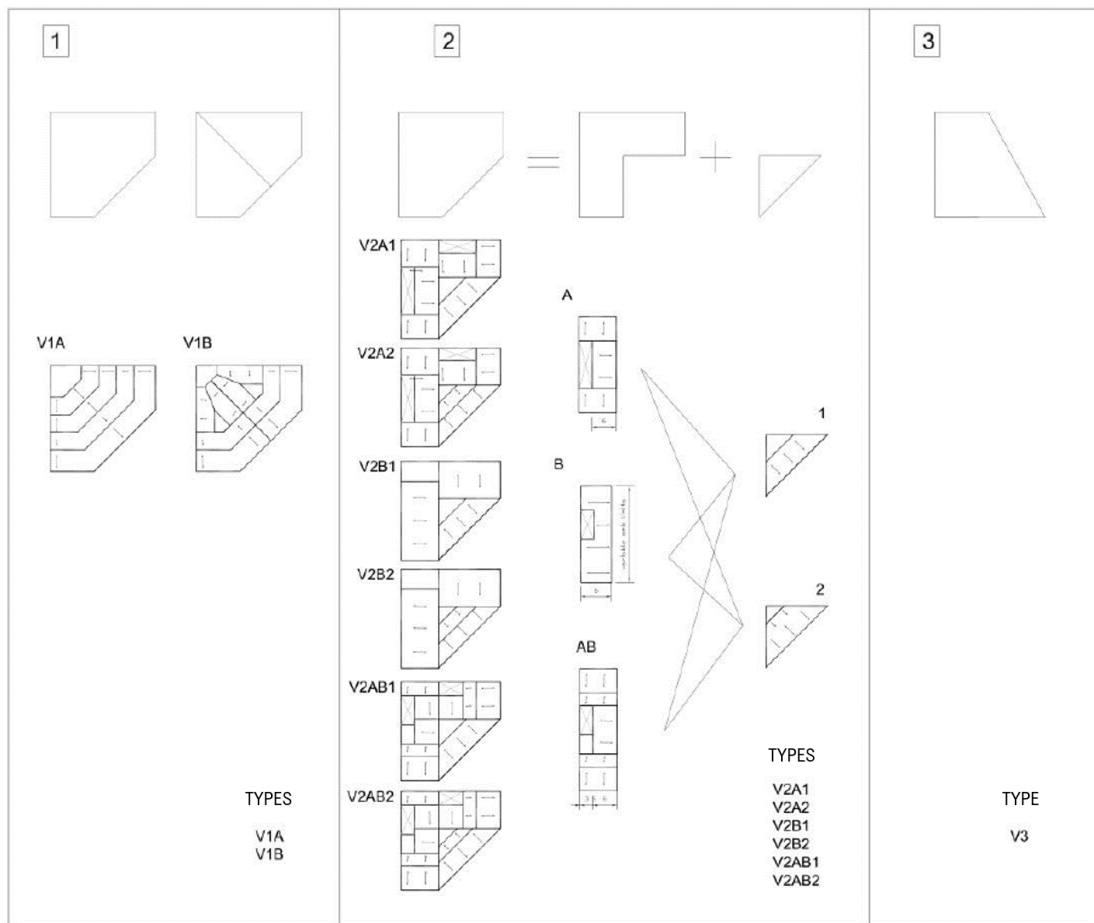


Figure A.20 - Schematisation of subtypes for the corner building typology 'V' (adapted from Cornadó Bardón 2015).

According to the statistical data presented in Chapter 4 (see section 4.4), the most common corner building typologies are the types V1A and V3 (see Figure 4.33). The following figures (Figure A.21 to Figure A.24) illustrate the frequency distributions regarding the total number of floors and the corresponding wall distances for each type.

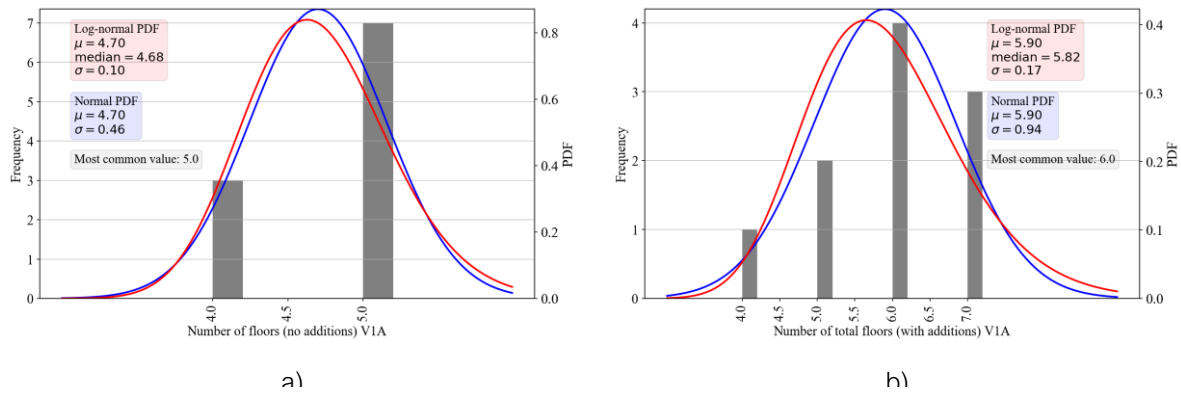


Figure A.21 - Frequency distribution of the total number of floors for the corner building typology - type V1A: a) without vertical additions (remuntes) and b) with vertical additions (remuntes).

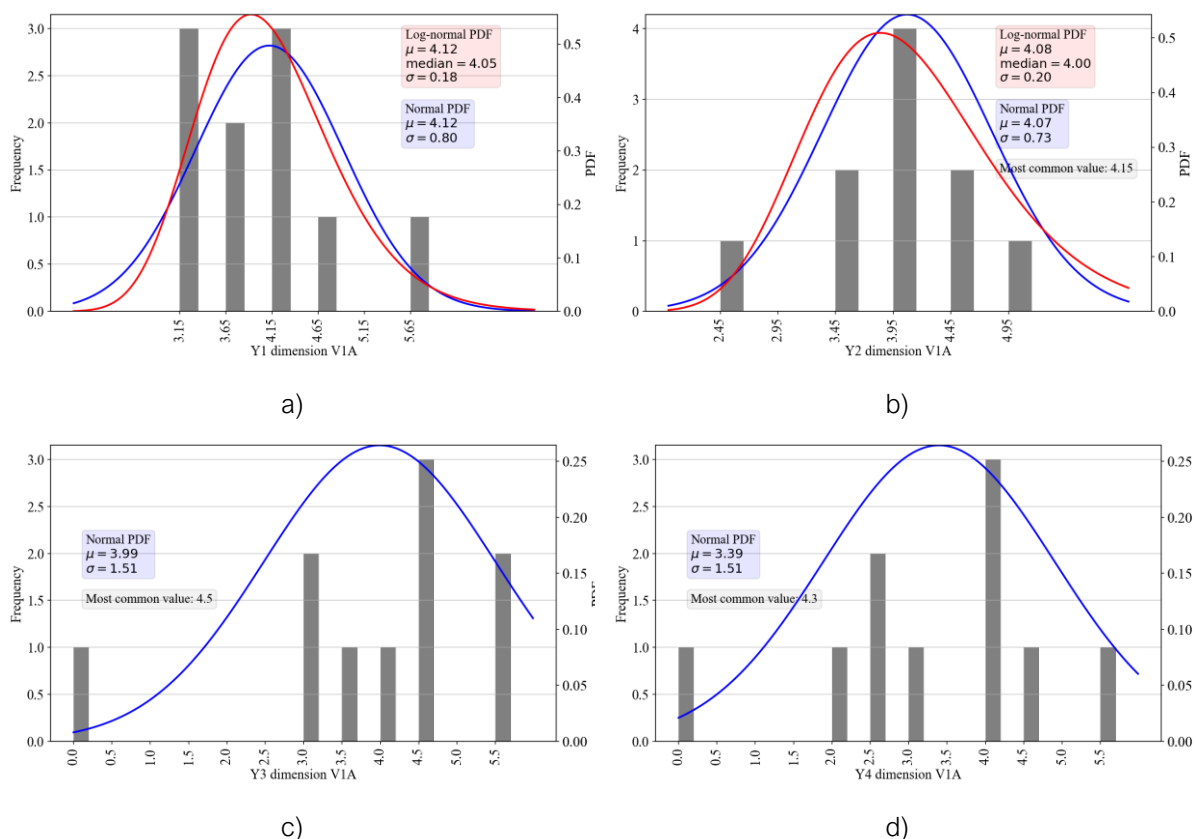


Figure A.22 - Frequency distribution of the following wall distances for the corner building typology - type V1A: a) Y1 distance between the front façade wall (W1) and the parallel interior wall (W5); b) Y2 distance between the back façade wall (W2) and the parallel interior wall (W6); c) Y3 distance between the interior walls W3 and W5 of the bay situated in front of the central part; d) Y4 distance between the interior walls W4 and W6 of the bay situated after the central part (see Figure 4.21 for the proper nomenclature of the walls and distances).

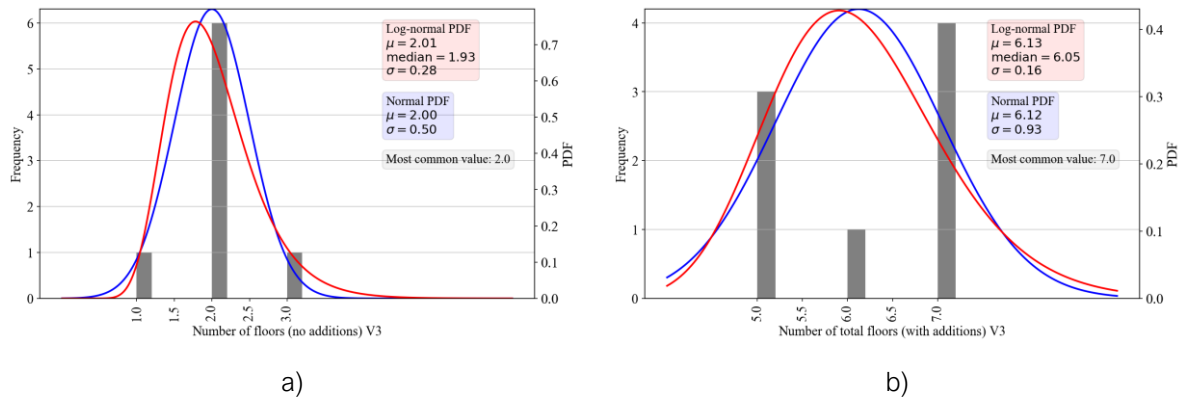


Figure A.23 - Frequency distribution of the total number of floors for the corner building typology - type V3: a) without vertical additions (remuntes) and b) with vertical additions (remuntes).

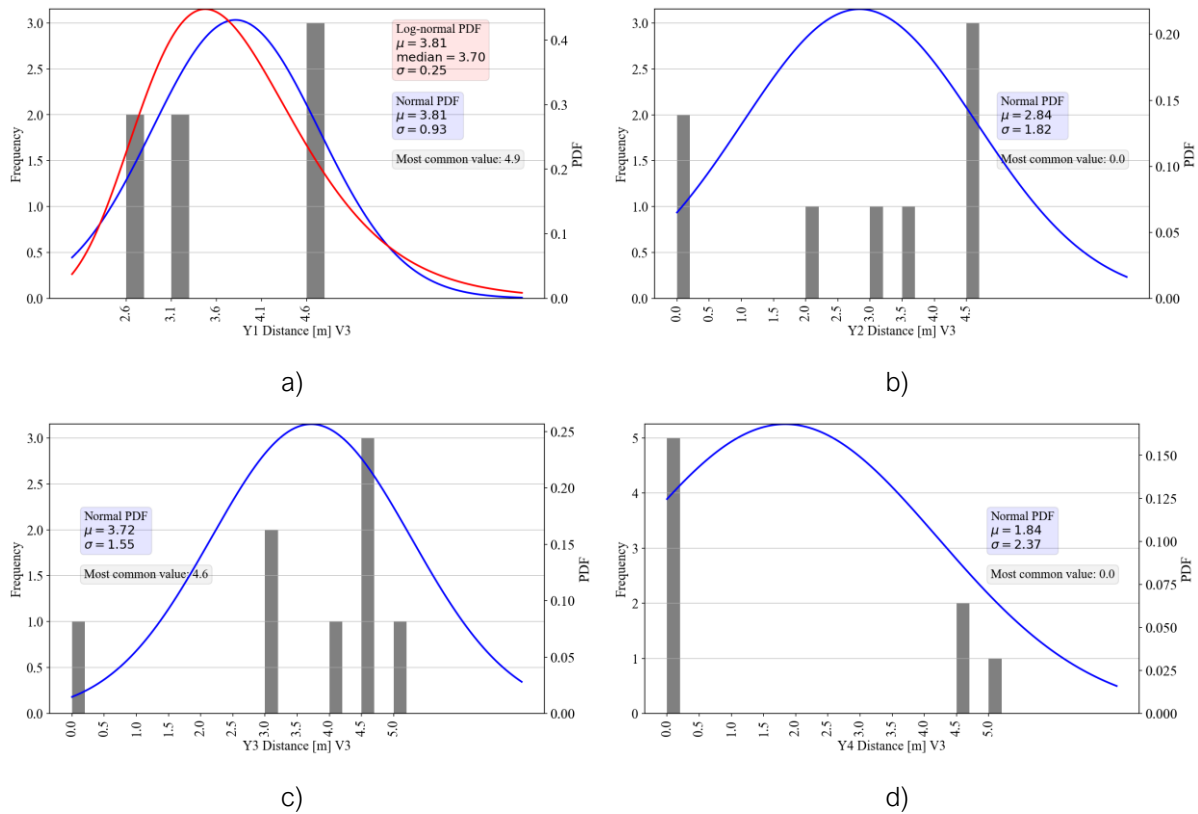


Figure A.24 - Frequency distribution of the following wall distances for the corner building typology - type V3: a) Y1 distance between the front façade wall (W1) and the parallel interior wall (W5); b) Y2 distance between the back façade wall (W2) and the parallel interior wall (W6); c) Y3 distance between the interior walls W3 and W5 of the bay situated in front of the central part; d) Y4 distance between the interior walls W4 and W6 of the bay situated after the central part (see Figure 4.21 for the proper nomenclature of the walls and distances).

APPENDIX B

The information provided in Appendix B is complementary to the numerical procedure for the simplified modelling of the in-plane stiffness of the one-way floor slab systems with shell elements in 3D FE models of URM buildings, as part of the research paper Dimovska et al. (2022). As previously explained in Chapter 5 (see section 5.2.3.1), the evaluation of the Young's and shear moduli of the orthotropic material for the floor slabs has been obtained through a comparison of the in-plane response under uniaxial and shear loading of the 3D solid model of the floors and 2D shell model of each floor type with elastic orthotropic properties.

Figure B.1 presents the force-displacement curves obtained from these analyses for the two floor systems. For load applied perpendicular to the beams, the capacity curves present a first linear range followed by a hardening branch. This behaviour is observed for the slabs with either steel or timber beams. For loading parallel to the beams, the force-displacement curves present a linear elastic behaviour up to a displacement of 3 mm. The differences between the two analyses reveal the orthotropic behaviour of the floor. As expected, the stiffness is higher for a loading parallel to the longitudinal axis of the floor beams, due to the higher contribution of the beam stiffness to the total stiffness of the floors. On the contrary, the lower stiffness of the floor in a direction perpendicular to the longitudinal axis of the beams results in a higher deformation of the masonry vaults and subsequently their damage. This drop in the global stiffness due to the damage in the vaults is illustrated by the nonlinear force displacement response shown in Figure B.1 (left).

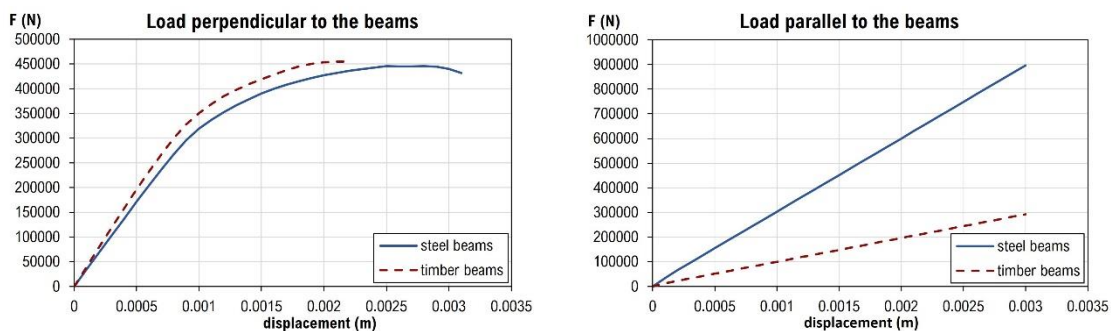


Figure B.1 - Load-displacement curves derived from a compression test of the 3D solid floor models in X direction (perpendicular to the beams, left) and in Y direction (parallel to the beams, right).

The initial values for the Young's moduli in the two directions of orthotropy have been chosen such that the axial stiffness of the 2D shell models is equal to the initial (elastic) axial stiffness of the 3D solid floor models, see Table 5.8.

Once the elastic modulus has been calibrated, a simple shear configuration has been used for the estimation of the shear modulus by considering the same boundary conditions that these one-way floors have in the existing building. This configuration has been previously verified by means of a simple elastic analysis comparing the states of simple shear and pure shear. The shear modulus G_{xy} of the 2D shell models has been computed by matching the elastic shear stiffness of

the 3D solid floor models. Thus, two analyses have been performed using the 3D solid model for each floor system inducing a shear deformation of the floor, by applying a horizontal displacement at one end of the floor (restraining the vertical displacement) and keeping the opposite end fixed. The displacement is orthogonal to the longitudinal axis of the beams in the first analysis, in order to obtain the shear modulus of a floor with beams orthogonal to the seismic load ($G_{xy\perp}$), and parallel to them in the second one for obtaining the shear modulus of a floor with beams parallel to the loading direction ($G_{xy\parallel}$). It is worth noticing that the parameters $G_{xy\perp}$ and $G_{xy\parallel}$ have been artificially introduced to distinguish the two different loading procedures assumed to evaluate the shear modulus G_{xy} . Figure B.2 and Figure B.3 present the contour of the horizontal displacements of the floor for a loading of 0.5 mm in the X direction (orthogonal to the beams) and in the Y direction (parallel to the beams), respectively.

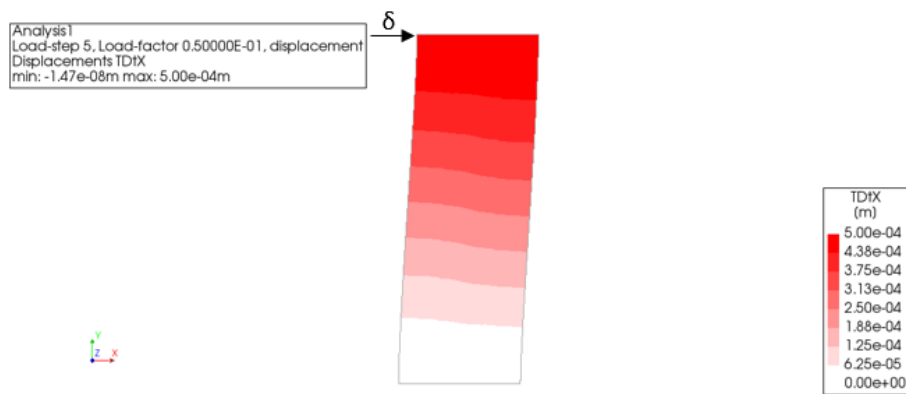


Figure B.2 - Displacements in X direction of the 3D solid floor model with steel beams from a displacement load of 0.5 mm applied orthogonal to the beams.

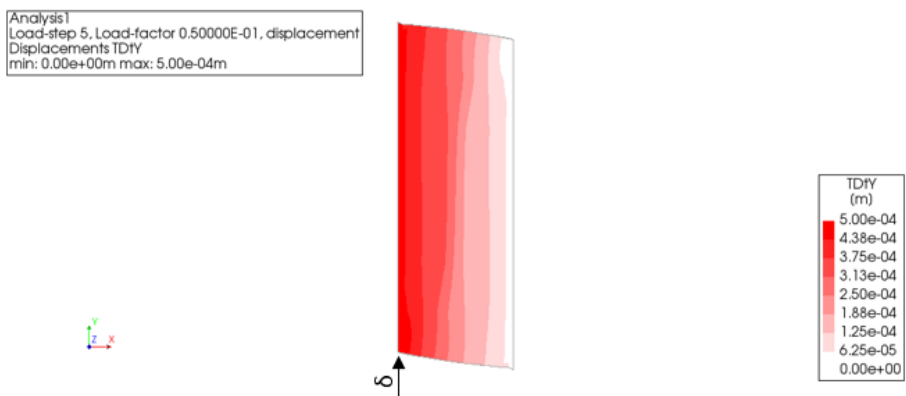


Figure B.3 - Displacements in Y direction of the 3D solid floor model with steel beams from displacement load of 0.5 mm applied parallel to the beams.

Figure B.4 shows the force-displacement capacity curves obtained from the in-plane shear analyses of these 3D solid floor models for the two loading directions. The capacity curves, obtained from the loading applied perpendicular to the beams, present a similar nonlinear behaviour for both types of floor. For this loading direction, the floor with steel beams is stiffer and shows higher capacity than the one with timber beams. The first branch of the curves obtained for loading parallel to the beams is similar for the two types of floor slabs investigated. However, the floor slab with timber beams reaches a lower ultimate strength than the one with steel beams for

the investigated levels of displacements. In both cases, the nonlinear response is due to shear cracking at the masonry vaults and sliding at the masonry-beam interface.

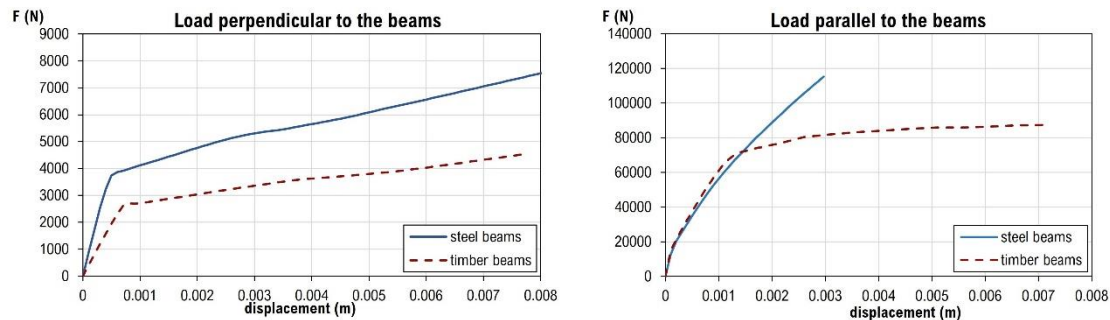


Figure B.4 - Load-displacement capacity curves obtained from in-plane shear tests of the 3D solid floor models in X direction (perpendicular to the beams, left) and in Y direction (parallel to the beams, right).

Similar to the case of the Young's moduli, the initial assumptions on the values of the G_{xy} of the 2D shell models are such that the shear stiffness of those is equal to the initial (elastic) shear stiffness of the 3D solid floor models (Figure B.5 and Figure B.6).

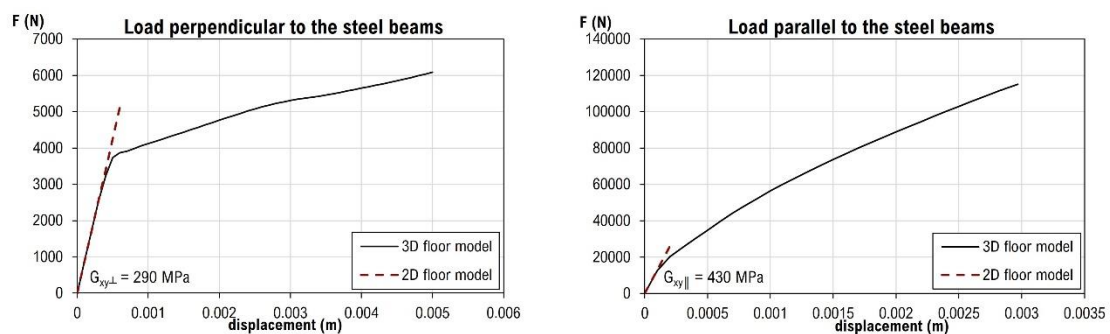


Figure B.5 - Calibration of the elastic shear stiffness based on the comparison of the 3D solid and 2D shell floor models with steel beams (for both loading directions).

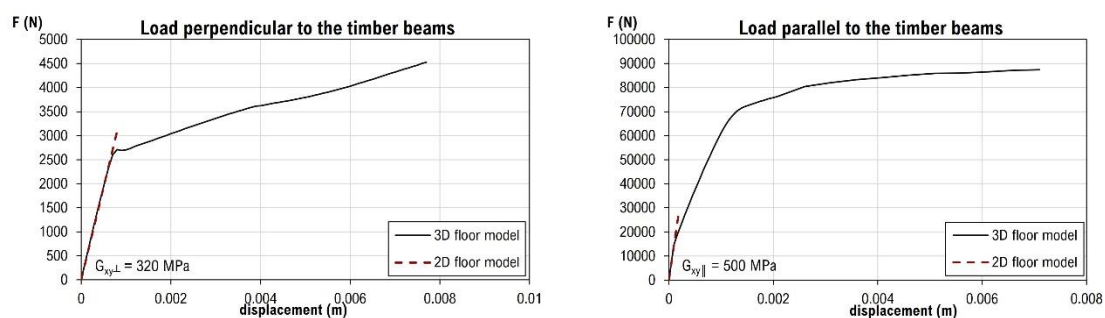


Figure B.6 - Calibration of the elastic shear stiffness based on the comparison of the 3D solid and 2D shell floor models with timber beams (for both loading directions).

The elastic orthotropic properties obtained from the floor models are different in both floor systems depending on the loading direction. There is a difference of around 65% for the Young's moduli E_y , due to the different material used for the beams in the floor systems and a smaller difference of 10% between the values of the Young's moduli in the direction perpendicular to the beams (E_x), due to the different geometry of the masonry vaults and the material of the beams.

The values of the shear moduli $G_{xy\perp}$ and $G_{xy\parallel}$ for the jack arch floor with timber beams are 10% and 16% higher than the ones of the one-way floor system with steel beams.

The numerical procedure used to compute the values of the shear moduli of the jack arch floors, as explained in Chapter 5, is iterative, by simulating nonlinear pushover analysis of the URM building model (see Figure 5.12). The analysis includes two steps, the first corresponding to the application of the self-weight and the second to the horizontal loading of the structure with a force pattern proportional to the distribution of the mass. After performing pushover analyses in X and Y directions, the longitudinal and shear deformations have been computed considering the displacements at the end sides of the top floors of the model. The pushover analysis in X direction provokes a torsional movement of the building (Figure B.7a). This is anticipated due to the non-symmetrical distribution of the walls in the front and rear façades, which result in an eccentricity between the centre of mass and the centre of stiffness of the building. The building is symmetrical in the Y direction and it does not exhibit a torsional response when loaded parallel to it (Figure B.7b). Thus, the floor deformations of the building model have been estimated only from the pushover in X direction as this constitutes the only case producing shear deformation to the floors due to the torsional response of the building.

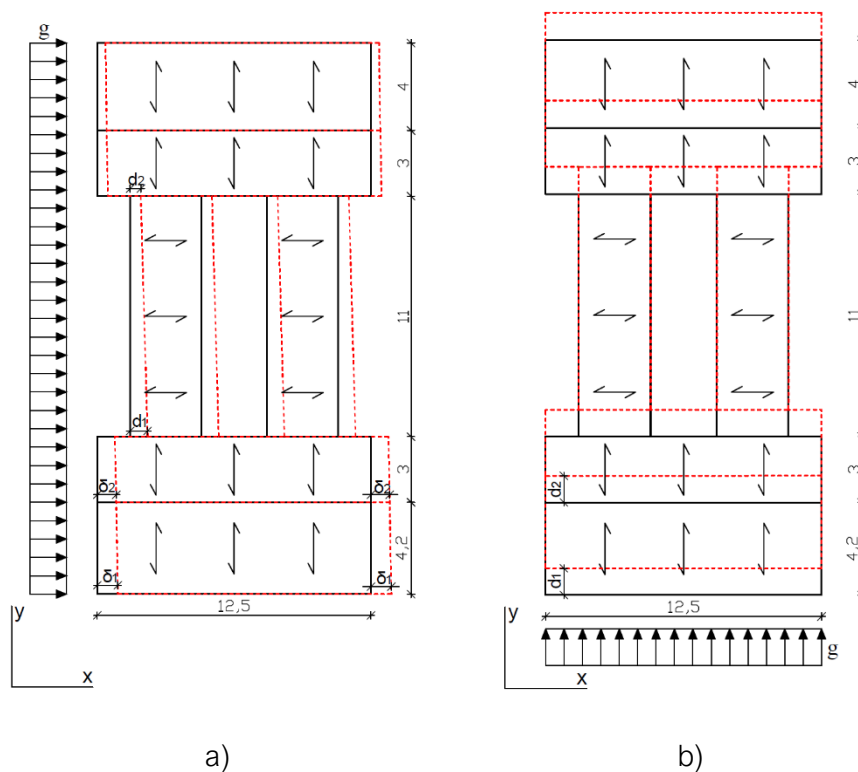


Figure B.7 - a) Displacements of the floors in the FEM building model from pushover in X direction; b) Displacements of the floors in the building model from pushover in Y direction (dimensions in meters). Red dashed lines illustrate the deformed shape at the maximum load capacity of the pushover analysis (deformation multiplied by 10).

The longitudinal and shear deformations have been used to compare the level of deformations experienced by the 2D shell floors in the global FEM model of the building with those of the 3D solid models of the isolated floors. The analysis stage used as reference for computing these deformations in the models of the building is the one corresponding to the maximum load capacity.

The different levels of the displacements can be visualized in the capacity curves in the Figure B.10 for each case. The longitudinal deformation of a floor along the loading direction corresponds to the change in the length of the floor parallel to the loading direction (i.e. its contraction) over the original length (see Figure B.8a and Figure B.8c). The shear deformation has been computed as the angular distortion of the originally orthogonal floor, see equation (11), as shown in Figure B.8b, and Figure B.8d. The average values for the displacements of both sides of the floors (marked as ① and ② in Figure B.7a) have been considered for the calculation of the longitudinal and shear deformation, as they present the maximum deformation during the performed analyses. With reference to Figure B.8a and Figure B.8b, longitudinal and shear deformations of the floors in the models of the building from the pushover in X direction have been computed using the equations (B.1) and (B.2).

$$\Delta u = \frac{u_1 - u_2}{H_1} \quad (\text{B.1})$$

$$\theta = \frac{\delta_1 - \delta_2}{L_1} \quad (\text{B.2})$$

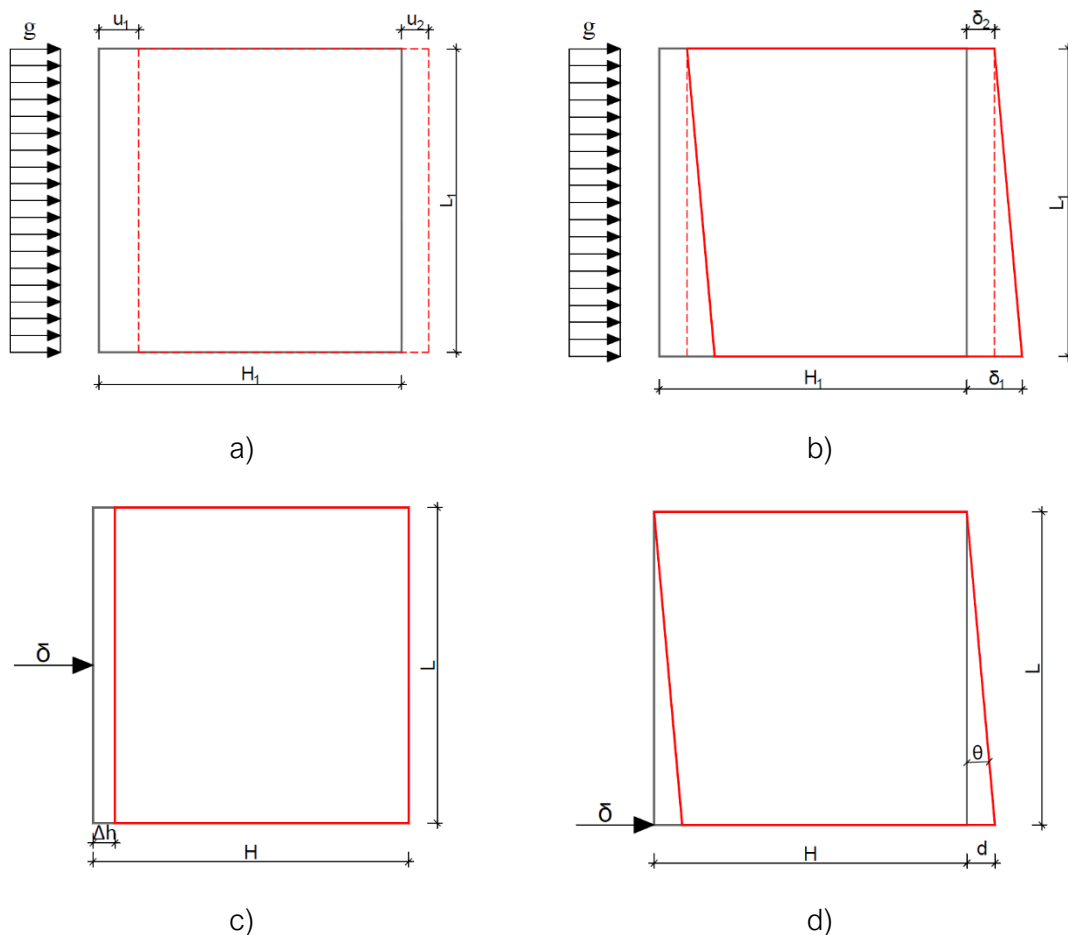


Figure B.8 - Longitudinal and shear deformation modes: a) longitudinal deformation in X direction of the floors in the FEM building model; b) shear deformation of the floors in the FEM building model; c) longitudinal deformation in X direction of the 3D solid floor model; d) shear deformation of the 3D solid floor model.

These deformations have been compared to the ones of the 3D solid models of the floors, which have been computed using the equations (B.3) and (B.4), see Figure B.8c and Figure B.8d. The relative displacements from the floors with maximum deformation of the building model have been calculated according to the equations (B.5) and (B.6).

$$\Delta u = \frac{\Delta h}{H} \tag{B.3}$$

$$\theta = \frac{d}{L} \tag{B.4}$$

$$\Delta h = \left(\frac{u_1 - u_2}{H_1} \right) \cdot H [m] \tag{B.5}$$

$$d = \left(\frac{\delta_1 - \delta_2}{L_1} \right) \cdot L [m] \tag{B.6}$$

With regard to the longitudinal deformations, the values computed for all the floor types and for both pushover directions fall within the linear range of the capacity curves of the 3D solid floor slab model. Therefore, the Young’s moduli in both directions of the floor systems have been considered equal to the values shown in Table 5.8.

Contrary to the longitudinal deformations, the shear ones experienced by the 2D shell floors of the building models fall beyond the elastic range of shear deformations as computed by the 3D solid floor slab models. This implies that the floors in the FEM model of the building present an excessive in-plane shear stiffness that should be reduced in order to satisfy the shear-strain admissibility derived from the previous nonlinear analyses of the 3D solid floor models. Hence, the shear modulus computed for the 2D shell floor models has been reduced and an “effective” shear stiffness has been adopted instead of the elastic one of the 3D solid floor models.

Figure B.9a and Figure B.9b show the effective stiffness values of the 2D shell floor models obtained from the procedure for the floors with steel beams parallel and orthogonal to the loading direction, respectively. Convergence of the two monitored parameters, i.e. maximum force capacity and local relative displacements of the floors, was achieved after four iterations.

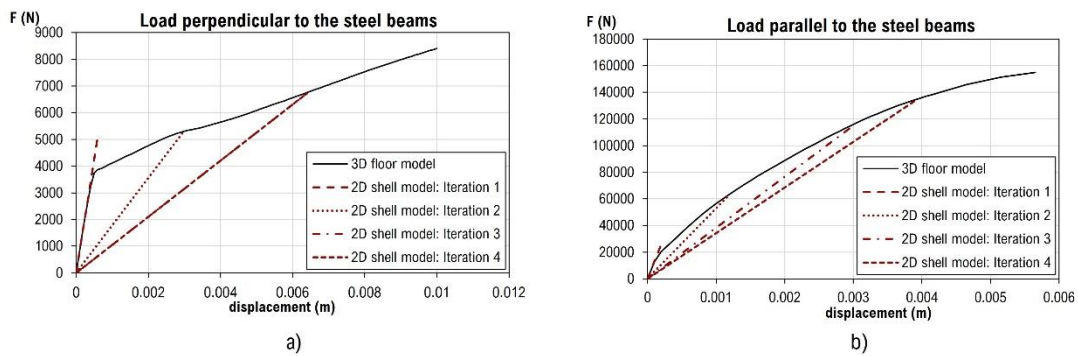


Figure B.9 - Calibration of the effective shear stiffness of the 2D shell model in the 3D building model: a) floors with steel beams parallel to the loading direction; b) floors with steel beams perpendicular to the loading direction.

Figure B.10 presents the capacity curves of the building with steel and timber beam floors for the different iterations. These pushover (acceleration-displacement) curves in X direction indicate

differences in both capacity and ductility of the building model after modifying the elastic properties of the floors at each iteration. The building model with elastic properties of the 2D shell floors equal to those of the 3D solid model (first iteration) has the highest maximum capacity and lowest ductility. There is a drop of 8% for the maximum capacity of the building model after the second iteration. On the contrary, the ductility of the building increases with the change of the elastic properties in the 2D shell floors obtained by assuming the secant stiffness of the 3D solid floor model corresponding to the computed shear deformations of the floors of the building model. This result confirms the important influence of the in-plane stiffness of the one-way floors in the global behaviour of the URM building.

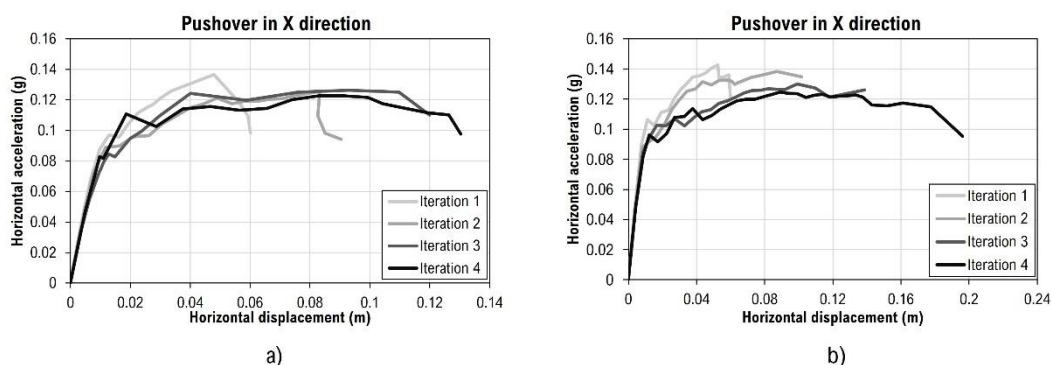


Figure B.10 - Capacity curves from pushover analyses in X direction with different shear moduli for the one-way flexible floors: a) floors with steel beams; b) floors with timber beams.

The graphs in Figure B.11 show the convergence of the values of the shear modulus when the load is perpendicular ($G_{xy\perp}$) and parallel ($G_{xy\parallel}$) to the longitudinal axis of the beams. The difference for the maximum capacity between the third and fourth iteration is less than 3%.

The differences in the control values of the maximum capacity and relative displacement of the floors with beams perpendicular to the loading direction are 2.4% and 6%, respectively. The converged values of $G_{xy\perp}$ and $G_{xy\parallel}$ are 9.3% and 25.6% of the elastic ones considered in the first iteration (see Table 5.9).

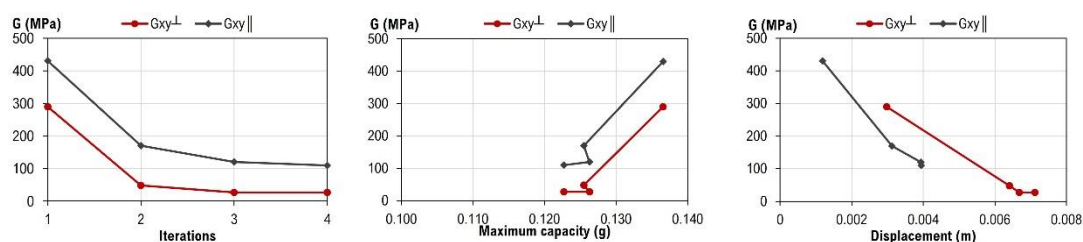


Figure B.11 - Convergence of the values of the shear moduli of the 2D shell floors with steel beams.

The same methodology has been applied for the calculation of the shear moduli of the one-way floors with timber beams and ceramic tile vaults. The pushover capacity curves of the building with timber beam floors are presented in Figure B.10b. The model with the orthotropic properties of the 2D shell floors estimated from the initial elastic stiffness of the 3D solid floors has the highest maximum capacity of 0.143g and presents the lowest ductile behaviour. The ductility of the building increases by updating the elastic properties of the floors in the following iterations. Figure

B.12 presents the different iterations that have been done in order to obtain the final values of the shear modulus for both floor directions ($G_{xy\perp}$ and $G_{xy\parallel}$).

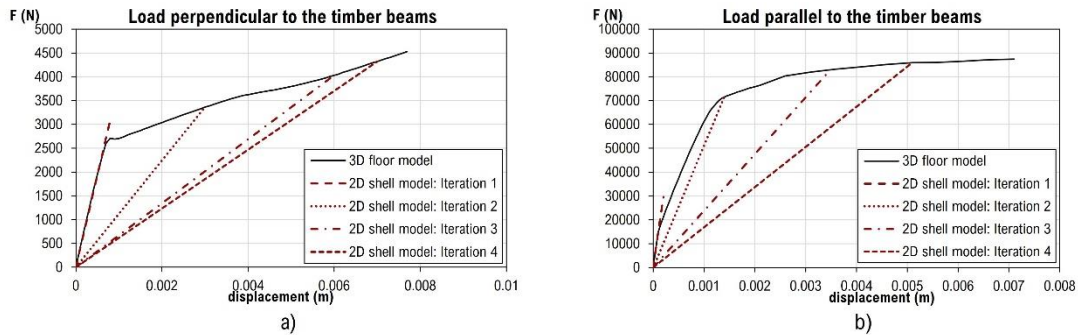


Figure B.12 - Calibration of the effective shear stiffness of the 2D elastic shell model in the 3D building model: a) floors with timber beams parallel to the loading direction; b) floors with timber beams perpendicular to the loading direction.

Figure B.13 shows the convergence of the values of the shear modulus for the floors with timber beams and ceramic tile vaults. Table B.1 presents the values of the shear moduli, the maximum load capacity and corresponding relative displacements for the case of the timber beam floors. Again, the difference of the maximum capacity between the third and fourth iteration is smaller than 5%. The difference for the relative displacements of the floors with timber beams perpendicular to the loading direction is 12%. This confirms the convergence of the values of the orthotropic properties for the floors. The converged values of $G_{xy\perp}$ and $G_{xy\parallel}$ are 8.4% and 9.2% of the elastic ones considered in the first iteration.

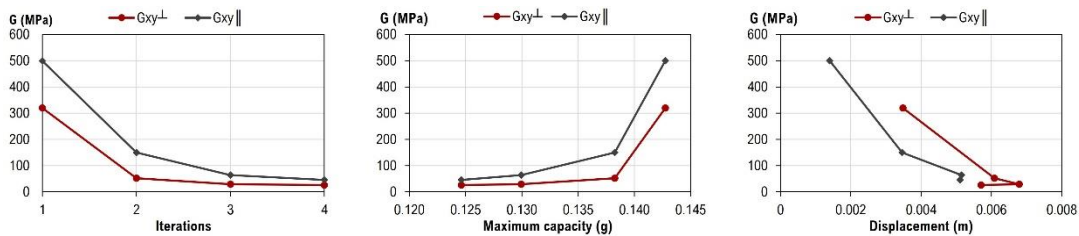


Figure B.13 - Convergence of the values for the shear moduli of the 2D shell floors with timber beams.

Table B.1 - Values obtained of the shear properties of the floor system with timber beams after the proposed iterative procedure.

Convergence of the shear properties for the floors with timber beams				
Properties	Iteration 1	Iteration 2	Iteration 3	Iteration 4
$G_{xy\perp}$ (MPa)	320	53	30	27
$G_{xy\parallel}$ (MPa)	500	150	65	46
Maximum capacity (g)	0.143	0.138	0.13	0.125
Displacement \perp (m)	0.003	0.0061	0.0068	0.0057
Displacement \parallel (m)	0.0014	0.0035	0.0051	0.0051

APPENDIX C

This appendix presents the capacity curves obtained from the nonlinear static (pushover) analysis for both pushover loading X and Y directions (parallel and perpendicular to the façade), by plotting the horizontal acceleration against the top horizontal displacements. As previously discussed in Chapter 6, the behaviour of these URM existing buildings differs in both directions, by being more flexible in the direction parallel to the façade, due to the presence of large façade openings and the lack of interior masonry walls at the ground floor in this loading direction. On the contrary, these buildings present greater stiffness in the direction perpendicular to the façade due to the presence of lateral load bearing walls, which act as shear walls. Figure C.1 to Figure C.5 illustrate the pushover curves of the FE numerical models with the variations of the different parameters in the reference model (Model 1) such as the material properties, the wall thickness, the horizontal diaphragms, the façade openings on the ground floor, and the different geometrical configurations. The information regarding the geometrical and structural configurations of all the numerical models, as well as the denomination of each numerical model was summarized and presented in Chapter 5 (see Table 5.15).

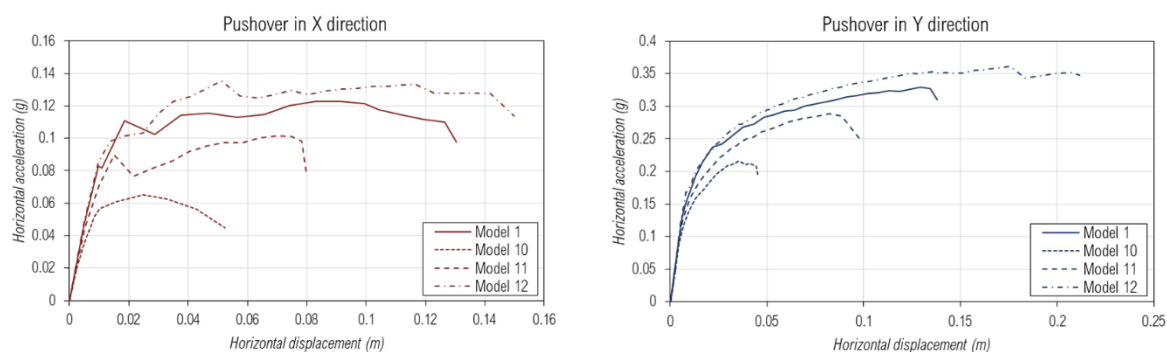


Figure C.1 - Pushover capacity curves of the FE numerical models with the variation of the material properties: pushover in X direction (left) and pushover in Y direction (right).

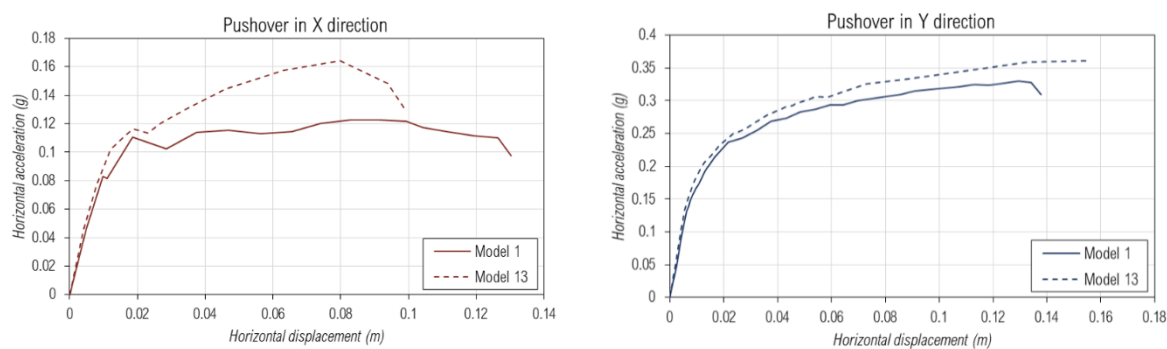


Figure C.2 - Pushover capacity curves of the FE numerical models with the variation of the wall thickness: pushover in X direction (left) and pushover in Y direction (right).

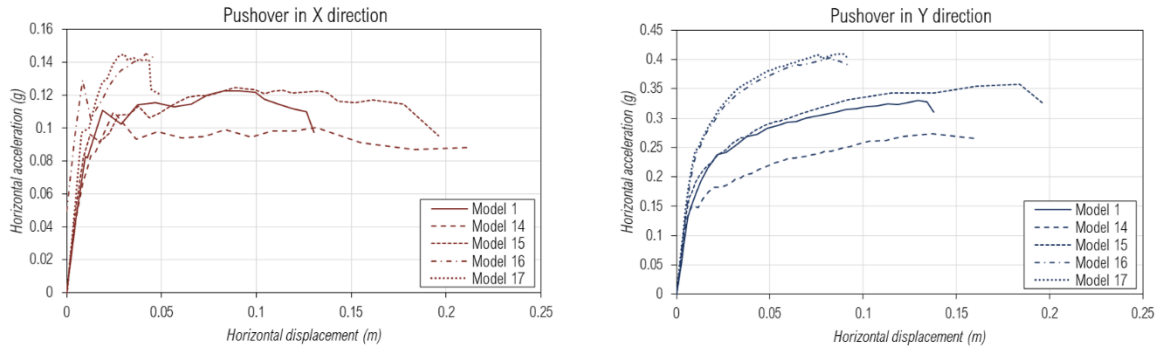


Figure C.3 - Pushover capacity curves of the FE numerical models with the variation of the different horizontal diaphragms: pushover in X direction (left) and pushover in Y direction (right).

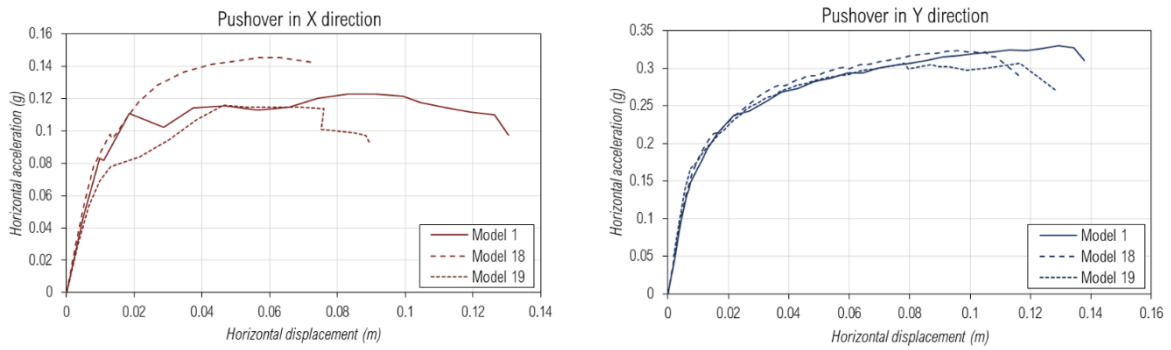


Figure C.4 - Pushover capacity curves of the FE numerical models with the variation of the façade openings on the ground floor: pushover in X direction (left) and pushover in Y direction (right).

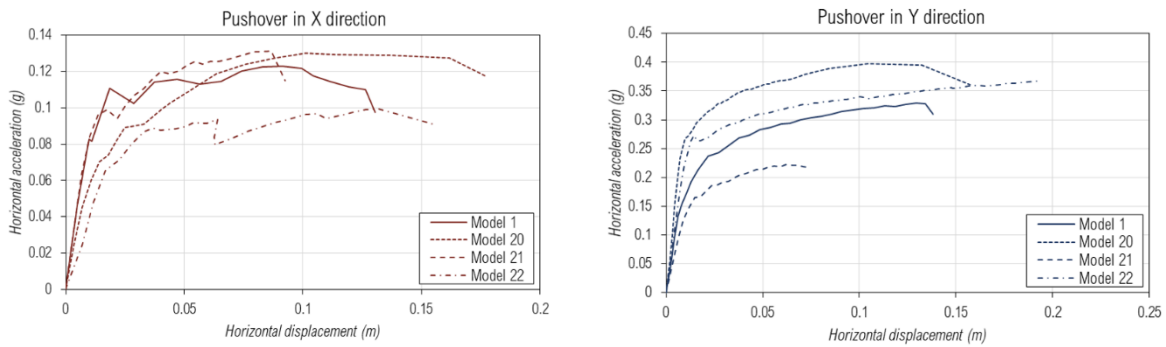


Figure C.5 - Pushover capacity of the FE numerical models with the different geometrical configurations: pushover in X direction (left) and pushover in Y direction (right).

Moreover, a summary of the characteristics of the equivalent SDOF system and the results obtained from the application of the N2 method to all the FE numerical models is presented in Table C.1. The procedure for the transformation of the capacity curve of the MDOF system to an equivalent idealised SDOF system was described in Chapter 6 (section 6.3.1). The N2 method has been applied for obtaining the performance point (spectral displacement), by crossing the demand spectra and capacity curve (see Figure 6.18). The values of the spectral displacements for the performance points of the SDOF systems are obtained for the both loading directions (X and Y) and for the two seismic scenarios (deterministic and probabilistic demand spectra).

Table C.1 - Summary information of the characteristics of the SDOF systems of all the numerical models and the spectral displacements (PP) obtained with the application of the N2 method for both deterministic and probabilistic spectra.

Model	Pushover direction	F _y [kN]	d _y [m]	F _u [kN]	d _u [m]	Γ	Deterministic spectra (PP) [m]	Probabilistic spectra (PP) [m]
Model 1	+ X	1281.71	0.0113	1281.71	0.084	1.43	0.0072	0.0122
	+ Y	3154.35	0.0137	3154.35	0.091	1.46	0.0057	0.0091
Model 2	+ X	1112.48	0.0106	1112.48	0.065	1.38	0.0076	0.0130
	+ Y	3369.77	0.0161	3369.77	0.085	1.44	0.0060	0.0097
Model 3	+ X	1064.47	0.0055	1064.47	0.086	1.44	0.0056	0.0086
	+ Y	2714.48	0.0085	2714.48	0.098	1.52	0.0046	0.0070
Model 4	+ X	1157.81	0.0070	1157.81	0.088	1.43	0.0061	0.0100
	+ Y	1157.81	0.0070	1157.81	0.088	1.43	0.0061	0.0100
Model 5	+ X	1244.30	0.0121	1244.30	0.075	1.36	0.0078	0.0139
	+ Y	3179.22	0.0171	3179.22	0.086	1.38	0.0065	0.0108
Model 6	+ X	1454.18	0.0068	1454.18	0.007	1.44	0.0059	0.0095
	+ Y	2565.24	0.0132	2565.24	0.075	1.48	0.0059	0.0095
Model 7	+ X	1416.69	0.0084	1416.69	0.033	1.44	0.0065	0.0110
	+ Y	2699.03	0.0165	2699.03	0.077	1.45	0.0065	0.0110
Model 8	+ X	1398.05	0.0108	1398.05	0.030	1.50	0.0071	0.0122
	+ Y	2496.79	0.0179	2496.79	0.069	1.51	0.0070	0.0118
Model 9	+ X	1371.76	0.0134	1371.76	0.033	1.51	0.0078	0.0134
	+ Y	2363.77	0.0187	2363.77	0.068	1.54	0.0073	0.0124
Model 10	+ X	635.24	0.0061	635.24	0.037	1.43	0.0073	0.0127
	+ Y	2088.73	0.0088	2088.73	0.031	1.46	0.0057	0.0091
Model 11	+ X	990.50	0.0086	990.50	0.056	1.43	0.0071	0.0121
	+ Y	2786.97	0.0137	2786.97	0.067	1.46	0.0059	0.0095
Model 12	+ X	1346.42	0.0098	1346.42	0.105	1.43	0.0068	0.0113
	+ Y	3521.14	0.0178	3521.14	0.145	1.46	0.0060	0.0100
Model 13	+ X	1597.89	0.0116	1597.89	0.068	1.46	0.0067	0.0113
	+ Y	1597.89	0.0116	1597.89	0.068	1.46	0.0067	0.0113
Model 14	+ X	797.58	0.0075	797.58	0.131	1.61	0.0068	0.0111
	+ Y	2085.69	0.0136	2085.69	0.100	1.60	0.0060	0.0098
Model 15	+ X	1020.36	0.0078	1020.36	0.130	1.51	0.0065	0.0106
	+ Y	2967.78	0.0158	2967.78	0.132	1.48	0.0058	0.0093
Model 16	+ X	1338.28	0.0079	1338.28	0.035	1.44	0.0068	0.0113
	+ Y	3937.34	0.0118	3937.34	0.068	1.38	0.0051	0.0081
Model 17	+ X	1549.71	0.0074	1549.71	0.035	1.42	0.0062	0.0102
	+ Y	4612.05	0.0118	4612.05	0.067	1.37	0.0049	0.0077
Model 18	+ X	1422.15	0.0107	1422.15	0.043	1.46	0.0068	0.0113
	+ Y	3125.87	0.0123	3125.87	0.079	1.47	0.0056	0.0088
Model 19	+ X	1125.40	0.0105	1125.40	0.063	1.42	0.0073	0.0124
	+ Y	2985.48	0.0115	2985.48	0.088	1.47	0.0055	0.0088
Model 20	+ X	1015.10	0.0214	1015.10	0.123	1.44	0.0084	0.0149
	+ Y	2933.29	0.0077	2933.29	0.105	1.51	0.0046	0.0070
Model 21	+ X	1253.24	0.0095	1253.24	0.060	1.45	0.0068	0.0115
	+ Y	2206.90	0.0105	2206.90	0.052	1.42	0.0058	0.0095
Model 22	+ X	398.05	0.0158	398.05	0.107	1.45	0.0084	0.0148
	+ Y	1426.47	0.0090	1426.47	0.131	1.48	0.0063	0.0102